EFFECT OF PULSE-LIKE NEAR-FAULT GROUND MOTIONS ON INELASTIC RESPONSE OF STRUCTURES INCLUDING FOUNDATION FLEXIBILITY

by

Ramin Latifi

B.Sc., Isfahan University of Technology

M.Sc. Sharif University of Technology

A THESIS SUBMITTED IN PARTIAL FULFILMENT OF

THE REQUIREMENTS FOR THE DEGREE OF

DOCTOR OF PHILOSOPHY

in

The Faculty of Graduate and Postdoctoral Studies

(Civil Engineering)

THE UNIVERSITY OF BRITISH COLUMBIA

(Vancouver)

November 2013

Abstract

For the sites in close proximity to a causative fault where formation of near fault long period velocity pulses is conceivable, consideration of flexibility of the foundation system is very important. This is due to the fact that when the flexibility of the base is taken into account the period of the system is longer than the period of the same system assuming a fixed base. Depending on the depth and the stiffness of the underlying soil the period of the system approaches the period of the near fault long period pulses, hence the response of the structure could be much larger.

The purpose of this research is to study the nonlinear response of structures to pulse-like near fault ground motions with and without allowing for the foundation system flexibility.

To highlight the impact of the near fault ground motions the nonlinear responses of single degree of freedom systems (resembling fixed base structures) to the near fault ground motions are compared to the responses of the same systems to the equivalent far field ground motions.

The effects of (translational and rocking) flexibility of the foundation system is also considered using equivalent linear springs and lumped masses added to the base of the single degree of freedom systems.

A major parametric study is performed to determine which parameter has the most significant impact on the response of the structure for near fault ground motions when effect of flexibility of the foundation system is explicitly accounted for.

An efficient procedure has been developed for predicting the response of a structure with a flexible base to near fault ground motions deduced from the response of an equivalent single degree of freedom system to the equivalent far field ground motions. Validity of the proposed procedure for assessing the effects of near fault ground motions, and the influence of flexibility of the foundation system on the structures' responses is verified using different analytical models, including a full 3D analysis of a bridge structure; the results proved to be quite satisfactory.

Preface

This dissertation is original, unpublished, independent work by the author, R.Latifi.

Table of contents

List of tables

List of figures

Lists of symbols and abbreviations

Symbol / Abbreviations	Note
$2DOF$	Two degrees of freedom system
AFE	Annual frequency of exceedance
$Cov[X,Y]$	covariance of X and Y
C_y	Strength characteristic defined as ratio of $\frac{F_y}{W}$ where F_y is the yield capacity of the structure and W is the seismic weight of the structure
$C_y{}^*$	Strength characteristic of the equivalent SDOF
CV	Coefficient of variation
D_{5-95}	Significant duration; the time needed to build up between 5 and 95 percent of the total Arias intensity.
D_{CF}	Displacement correction factor
DDR	Ductility demand ratio
DOF	Degree of freedom
E_I	Input energy
EDP	Engineering demand parameter
$\mathrm{EDP}_{\mathrm{FF-GMs}}$	EDP for far-field ground motions
$\mathrm{EDP}_{\mathrm{NF-GMs}}$	EDP for near-fault ground mMotions
EDP. Ratio	Ratio of engineering demand parameters (i.e. $EDP_{NF-GMs}/EDP_{FF-GMs}$)
f_{y}	Yield strength of the system
FEM	Finite element method
FF	Far field
FFS	Flexibility of the foundation system
FN	Fault normal

Symbol / Abbreviations	Note
FP	Fault parallel
g	Acceleration of gravity
GM	Ground motion
IDA	Incremental dynamic analysis
IDDR	Inelastic displacement demand ratio
K_{e}	Elastic stiffness
k_{eq}	Equivalent stiffness of the soil–foundation–structure system
k_{f}	Equivalent stiffness of foundation accounting for both rotational stiffness and transversaltransversal stiffness
K_{s}	Secondary stiffness, indicating the stiffness of stress hardening branch of backbone curves
K_{t}	Tertiary stiffness, indicating the negative stiffness of the backbone curves
k_x	Transversal stiffness of foundation
k_θ	Rotational stiffness of foundation
LPFNF GM	Low-pass filtered near-fault ground motion
M_w	Moment magnitude
MDOF	Multi-degree of freedom Freedom system
$\mathrm{MP}_i(\mathrm{e.g.}, \mathrm{MP}_1 \ \& \ \mathrm{MP}_2)$	Modal participation ratio for the ith mode of vibration
MSE	Mean squared error
NF	Near fault (associted with long period velocity pulses)
NGA#	NGA number
NLT	Nonlinear link type
NLTHA	Nonlinear time history analysis
PGA	Peak ground acceleration
PGV	Peak ground velocity
R_{d}	Ductility reduction factor
R_{jb}	Joyner-Boore distance
R_{Rup}	Closest distance to rupture plane

Symbol / Abbreviations	Note
R_{y}	Yield-strength reduction factor
$R_{\mathrm{y}}{}^{*}$	Soil–structure–foundation system -strength reduction factor of the equivalent Single gree of freedom system
RRMF	Required response modification factor
S_{a}	Spectral acceleration
S_{d}	Spectral displacement
S_{v}	Spectral velocity
SDOF	Single degree of freedom
SFSI	Soil–foundation–structure interaction
$T-5\%\ E_I$	Time at which the input energy (for each system) reaches 5% of its total value
$T-95\%\ E_I$	Time at which the input energy (for each system) reaches 95% of its total value
T_{c}	Period separating the acceleration and velocity sensitive regions of UHRS
T_{e}	Elastic period of vibration
T_{fb}	Elastic period of vibration of the fixed-base superstructure
T_{p}	Period of the velocity pulse (Usually more than 1.2 S)
T_{sys}	Equivalent elastic period of vibration of the soil–foundation–structure system
U_{e}	Maximum elastic displacement of (equivalent) SDOF
U_{max}	Maximum inelastic displacement of (equivalent) SDOF
u_{s}	Part of total displacement due to deformation of structure
u_{total}	Total (roof/deck) displacement of a simplified 2DOF system
u_x	Part of total displacement due to transversal movement of foundation of a simplified 2DOF systems
u_θ	Part of total displacement due to rotation of foundation
UHRS	Uniform hazard response spectrum
V_{base_i}	Base shear associated with mode “i”
V_{e}	Elastic base shear

Symbol / Abbreviations	Note
V_{in}	Inelastic base shear
V_{S30}	Site shear wave velocity in the upper 30 m
V_{y}	Effective yield strength
W	Effective seismic weight, equivalent to g times the totl mass participating in seismic response of the structure
YCDR	Yield capacity demand ratio
α	Ratio of foundation mass to superstructure mass in a simplified 2DOF model
α_{YCDR}	YCDR constant
β	Ratio of foundation stiffness to superstructure's stiffness in a simplified two degree of freedom model
$(\delta_{\mathrm{in}})_{\mathrm{ExP-FN}}$	Maximum displacement demand in FN direction due to extracted long-period pulse
$(\delta_{\mathrm{in}})_{\mathrm{LPF-FN}}$	Maximum displacement demand in FN direction due to low pass filtered signals
δ_{y}	Yield displacement of the system
δ_{FF} and δ_{NF}	Maximum displacement of the system due to FF and NF GMs
Δ	Displacement
Δ_{y}	Yield displacement
ε	Number of standard deviations by which the predicted value exceeds the median
μ	Ductility ratio
μ_{Design}	Design ductility ratio
μ_R	Ductility demand ratio (equivalent to DDR)
μ_{Ttarget}	Target ductility ratio
ζ	Damping ratio (equal to the value of equivalent viscous damping normalized with the critical damping of the system)
φ	Mode shape vector
ω_i	Circular frequency of the system associated with i^{th} mode of vibration of the system

Acknowledgements

I would like to express my deepest gratitude to Dr. Carlos Ventura who helped me throughout my PhD program at The University of British Columbia and generously shared his extensive knowledge and experience with me. I am truly indebted to Dr. Ventura for his genuine consideration, guidance, encouragement, and supports; indeed, without his asistance I wouldn't have been able to finish my program.

I would also like to extend my most profound appreciation to Dr. Liam Finn for providing me with his sound and critical perspective and for being a true mentor and role model during my recent studies; many thanks for his open-minded objective thinking, and his genuine friendship. Being Dr. Finn's student has been a real pleasure and an invaluable experience for me.

Also, my special thanks go to my advisory committee member, Dr. Mahdi Taiebat, for always being there to help me, for reviewing this dissertation, for his constructive comments, and for his true friendship.

My sincere thanks go to the SFSI research team members who contributed to this work by providing great ideas and exciting intellectual challenges during our bi-weekly meetings.

My deep and greatest thanks go to my family, especially to my wife, Neda, for her incredible support and companionship, her understanding and help as I was completing this program; she was always there at every step of the way for me, with her unconditional love.

Dedication

This dissertation is dedicated to my parents, my wife "Neda", my Daughter "Maya" and my son "Benjamin". Their constant love and caring are every reason for where I am and what I am.

1. Introduction

Chapter Outline:

1. Section 1.1 presents the statement of the problem addressed and the motivations behind this project
2. Section 1.2 describes the objectives of this research project
3. Section 1.3 briefly discusses the methodology adopted to achieve the objectives outlined in 1.2
4. Section 1.4 summarizes the organization of this document

This study intends to inter-relate two important aspects of seismic analysis and design of structures located close to seismic sources; namely, the combined effects of near-fault (NF) ground motions (GMs) associated with long-period velocity pulses, and the effect of flexibility of the foundation system (FFS).

Characteristics of the NF GMs associated with long period velocity pulses are usually very different from those of ordinary far-field (FF) GMs. A significant portion of the input energy from NF GMs is carried by a few strong and coherent long period pulses. As a result of this phenomenon, the damages sustained by the structures subjected to pulse-like NF GMs are usually associated with few large cycles of nonlinear displacement. However, what is typically observed in the response of structures to the ordinary FF GMs is very different, i.e. the damages to the structures are mainly associated with many low amplitude nonlinear excursions (Bertero et al. 1978). Hence, one can expect that the particularities associated with the response of structures to the NF GMs to render the standard design procedures inappropriate for design of the structures in close proximity of the faults.

The nature of NF GMs associated with long period velocity pulses indicates that the underestimation of effective period of the structure may result in the underestimation of input energy, and the related damage/risk. This contrasts with what is expected for FF GMs and what is proposed by design codes. The omission of FFS (and its associated period elongation) as is typical in practice most likely

would not lead into a conservative design for the structures in close proximity of an active fault.[1]

The general understanding of the practicing enginees is that disregarding FFS should result in a more conservative design. This belief is mainly because of the code-prescribed design spectrum which suggests that consideration of FFS, invariably, result in reduced demands on the structures. Conversely, researchers have already shown that under certain conditions (i.e. when underlying layers of soil deposit are soft or input motions are associated with long-period pulses), period elongation due to FFS might lead to increased demands and, hence, more damage. This fundamentally contradicts what is inferred from simplified code-prescribed design spectra (Gazetas, 2000).

Similarly, nonlinear response of the structures to the NF GMs can elongate the effective period of the structure; this may render the structure more susceptible to the NF GMs as it can shift the effective period of the system to a longer period range where the energy content of the NF GMs is more condensed. The importance of consideration of period elongation due to nonlinear behaviour of the structures becomes more noticeable when one considers that the nonlinearity due to NF GMs. This usually takes place in the beginning of input motions; hence a significant amount of energy is imposed to the structure after initial yielding.

In general, simplified design procedures prescribed by current codes and design guidelines explicitly does not address the broad variability of responses due to NF GMs nor do they explicitly deal with the effects of flexibility of foundations.

1.1 Statement of problem

For the sites close to a known source of an earthquake, where formation of NF long period velocity pulses is possible, consideration of FFS could be very important. This is primarily because the presence of a flexible base is associated with

[1] While FFS, usually referred to as inertia effect of soil–foundation–structure-Interaction (SFSI), has been the subject of numerous research projects in the past, it is not well codified for seismic design of the structures, especially when effects of NF GMs are of interest.

elongation of the fundamental period of the system; and this can shift the effective period of the system into a period range that is more affected by NF long period velocity pulses.

This phenomenon is more pronounced where surface soil below the foundation amplifies the low frequency content of input ground motions (e.g. the amplitude of the long period velocity pulses associated with NF effects) travelling from the outcrop to the surface, thus making the situation worse.

Therefore, one can argue that ignoring combined effects of NF GMs and FFS can potentially result in underestimation of seismic demands and/or the associated risks.

The problem for consideration of combined effects of NF GMs and FFS for analysis and design of the structures located close to an active seismic source can be broken into two sub-issues, namely; (A) lack of knowledge and (B) practical difficulties. Below is a brief description of each of these sub-issues.

A) Lack of knowledge

Lack of knowledge in this area and ignorance of the practicing engineering community about this phenomenon are primarily due to the fact that:

- the impedance functions developed for consideration of Solid Foundation Structure Interaction (SFSI)/FFS are not suitable representatives of the real nonlinear interactions occurring between different interfaces as a result of strong GMs. This is more evident in layered soils and soils subjected to significant strains,
- the number of available strong NF GMs is very limited, and strong NF GMs are not readily available for all code-prescribed site classes (soil types),
- a comprehensive set of experimental/measured data (i.e., recorded structural responses) is not available to validate the proposed engineering design procedures resulting from numerical analysis.

B) Practical difficulties

In addition to lack of knowledge as noted above, the inclusion of combined effects of NF GMs and FFS in seismic analysis and design procedures is associated with some practical challenges, namely:

- The concurrent consideration of effects of NF GMs and FFS is a problem which requires a close integration of three different disciplines, namely,
    - Seismologists for evaluation of exposure of the structures to NF effects,
    - Geotechnical engineers for proper evaluation of soil properties/type and credible impedance functions for a specific site,
    - Structural engineers for evaluation of nonlinear response and performance of the structures,
- The seamless integration between the above-mentioned disciplines is an arduous task, as each usually practices independently from the others,
- The numerical analysis of the structure with FFS is usually computationally expensive and time consuming,
- The number of reliable recorded ground motions with long-period pulses is relatively limited,
- The uncertainties associated with soil properties and FFS modeling parameters and also the variability of properties of NF GMs are so significant that deterministic approaches are not very realistic,

As a result of the implicit language of some early codes/design recommendations, i.e., ASCE41-06 or FEMA 440, the general understanding of the practicing community is that consideration of FFS is (often) a conservative design approach. Hence, they tend to routinely ignore the effect of FFS even for soft soils and in the presence of NF GMs.

1.2 Research objectives

The objective of this research is to shed some light on effects of NF GMs on nonlinear response of simple structures supported on flexible foundations.

Thus, the primary objective of this research project is to gain quantitative knowledge about effects of pulse-like NF GM on nonlinear performance of simple structures when FFS effects are also taken into account.

The ultimate objective is to formulate a simple procedure that allows practicing engineers to approximate the magnitude and potential significance of NF GMs on

the inelastic response of structures/bridges supported on flexible foundations using the simplified procedures prescribed per current codes.

1.3 Research methodology

The method adopted for achieving the objectives of this research, as noted in previous section, can be broken down into four main task groupings, namely; (A) studying effects of NF GM on nonlinear response of the structures, (B) studying effects of FFS on nonlinear response of the structures, (C) studying combined effects of NF GMs and FFS on nonlinear response of the structures, complete with proposing a simplified procedure for accounting for these combined effects, and (D) verification of the proposed procedure.

Each of above main task groupings is further detailed below.

(A) Studying NF GMs

For the study of the effects of NF GM on nonlinear response of structures two comprehensive suites of NF GMs and their equivalent FF GMs were selected. Also, to account for variability of structural parameters a comprehensive set of simplified single degree of freedom (SDOF) mathematical models were developed.

To better understand and quantify the effects of NF GMs on nonlinear response of the fixed base structures results of Nonlinear time history analysis (NLTHA) of the SDOF systems determined for the selected NF GMs were compared with the same determined for the equivalent FF GMs. Results of studying effects of NF GM (summarized in Chapter 4) led to the production of a set of procedures/equations which allow for approximating Engineering Demand Parameters (EDPs) which are of interest due to NF GMs from the same due to FF GMs.

(B) Studying FFS effects

For the study of the effects of FFS on nonlinear response of the structures a series of simplified 2 degrees of freedom (2DOF) systems was developed to implicitly account for the effects of FFS in the analysis.

The same analysis procedure that was used in main task grouping (A) was repeated for 2DOF systems. Results of NLTHA of 2DOF systems were compared with their equivalents determined in main task grouping (A). The results of studying effects of FFS (summarized in Chapter 5) were used for formulating a simple

procedure which could assist engineers to better evaluate the effects of FFS on nonlinear response of the structures.

(C) Combined effects of NF GMs and FFS

The ultimate objective of this project is achieved by integration of the results of the main task grouping (A) and (B), into a simple, yet effective procedure which can assist practicing engineers to estimate the combined effects of NF GMs and FFS from nonlinear response of the corresponding fixed base superstructure subjected to the equivalent FF GMs. That is to say, the proposed procedure can assist practicing engineers to estimate response of a structure, supported on a flexible foundation and subjected to NF GMs, from code prescribed procedures (originally developed for fixed base structures, subjected for FF GMs).

(D) Verification

Finally, the validity of the proposed procedure was verified by different methods and against different models, including nonlinear analysis of a prototype multi-degree of freedom (MDOF) bridge system.

In summary, to achieve the objectives noted in previous section the following steps were taken:

Step#1: Two comprehensive suites of NF GMs and their equivalent FF GMs were selected.

Step#2: A comprehensive set of simplified single degree of freedom (SDOF) mathematical models were developed.

Step#3: A series of NLTHA of the SDOF systems was performed to determine the effects of NF GMs on the response of fixed-base structures.

Step#4: A series of simplified 2 degrees of freedom (2DOF) systems were developed to simulate the effects of FFS on nonlinear response of structures (essentially step 3 but repeated for 2DOF systems).

Step#5: The results of the above analysis were formulized in a simplified framework to allow for the consideration of effects of NF GMs and FFS on nonlinear response of the structures/bridges, using code provisions.

Step#6: The results of step 4 were expanded and verified against a nonlinear analysis of a prototype multi-degree of freedom (MDOF) bridge system.

1.4 Thesis organization

Chapter 1 presents a general introduction to this research project, its objectives, and the research methodology.

Chapter 2 presents a general introduction to FFS and NF GM effects.

Chapter 3 discusses mathematical models used in this research, including variation of structural parameters and selected suites of GMs used for sensitivity analysis. This chapter also discusses the monitored and reported EDPs as used in this research.

Chapter 4 summarizes the results of parametric study and sensitivity analysis of fixed base systems (SDOF models) used for understanding the effects of NF GMs on nonlinear response of simple structures.

Chapter 5 summarizes and discusses the results of parametric study and sensitivity analysis of simplified flexible base systems (2DOF models) used for characterizing the effects of flexibility and mass of the foundation system on nonlinear response of simple structures. This chapter also presents a simplified mathematical method, developed for predicting response of flexible-base structures from response of their equivalent SDOF model.

Chapter 6 discusses results of analyses of a full 3D MDOF system used to check the validity of the proposed method. In this chapter the EDPs of MDOF were calculated using a 3D general analysis program. These results were compared with the results of the equivalent system developed in chapter 5 and the results were satisfactory.

Chapter 7 presents a conclusion statement and summarizes the findings of this project, in addition, recommendation regarding potential future research projects that could supplement the findings of this project and enhance the knowledge about effects of NF GMs and FFS are presented.

2. Overview of NF and FFS effects

Chapter Outline:

1. Section 2.1 describes important aspects of NF GMs; including discussion about their properties and mathematical models for simulating forward directivity and fling-step pulses.
2. Section 2.2 discusses important aspects of effects of FFS on the response of a structure.
3. Section 2.3 briefly discusses effects of NF GMs on the response of a structure.

The following sub-sections briefly describe the main aspects NF GMs and FFS. Although the contents of the following sub-sections are very introductory to the subjects of NF GM and FFS effects, they are directly related to what will be presented in the remaining sections.

2.1 Near fault ground motions

Recorded free-field ground motions in close proximity to the causative faults might exhibit some specific characteristics that are not evident in FF GMs. These characteristics, known as NF effects, usually encompass a half-cycle or a full-cycle strong dynamic long-period velocity pulse.

The half-cycle (a one-sided) long-period velocity pulse (usually $T_{\mathrm{P}} \geq 1.2$ s) is known as the “fling-step” effect and is a function of permanent deformation of the ground caused by a tectonic event. On the other hand, the full-cycle long-period velocity pulse (a two-sided, reversing pulse) is a dynamic phenomenon attributed to (a) the fault rupture-mechanism, (b) site-to-fault orientation and distance, and (c) wave propagation characteristics (Bray and Rodriguez-Marek 2004). Forward directivity usually occurs when a fault rupture propagates toward a site with a rupture velocity close to the shear wave velocity. The forward directivity intense velocity pulses, caused by constructive interference of travelling waves toward the site, are mostly oriented in the fault-normal (FN) direction; this phenomenon is due to radiation

pattern of the shear dislocation on the fault plane (Somerville et al. 1997). Conversely, backward directivity effects, which occur when the rupture propagates away from the site, cause long-duration motion pulses that have relatively low amplitudes. Therefore, from a structural point of view, the backward directivity pulses are not as important as forward directivity pulses.

NF GMs have been the subject of many research projects in the past few decades (i.e., after the 1971 San Fernando earthquake showed some evidence of long-period pulses in its recorded NF GMs). After the 1979 Imperial Valley earthquake, Anderson and Bertero (1987) identified the intense energy associated with strong long-period velocity pulses (NF effects) as an important parameter affecting the maximum inelastic response of structures subjected to NF GMs. However, NF GM effects were not incorporated into design provisions until the 1994 Northridge and the 1995 Hyogo-Ken Nambu (Kobe) earthquakes, where NF long-period pulses were recognized as a significant cause of damage. The 1994 Northridge earthquake showed that long-period pulses associated with NF GMs can cause a single (or a few) cycle(s) of inelastic deformation, which usually imposes a high ductility demand on the structures in the near vicinity of the causative fault in the form of a biased response on one side. As a result of this observation, near-source factors were introduced in the Uniform Building Code for the first time in 1997.

2.1.1 Properties of near-fault ground motions

It has been long proven that NF GMs usually have some distinct and different characteristics from FF GMs; visual identification of these differences is much easier in the velocity and displacement seismographs (but it is not as easy to identify them in the acceleration time histories.

Bray and Rodriguez-Marek (2004) reported that in their research no particular trend was identified in the ratio of peak ground velocities in the fault-parallel (FP) and fault-normal directions with respect to varying magnitude or distance. This is somewhat similar to findings of previous researchers who claimed to find no strong coupling between forward directivity and fling-step effects irrespective of the fault mechanism (Abrahamson 2001).

It is of note that during past earthquake events, at some sites that were very close to the faults, no long-period velocity pulse is observed in the recorded GMs. This in

turn indicates that even at locations where forward directivity effects are likely, they are not certain to occur (Lervolino and Cornell 2007).

The following two subsections briefly discuss properties of typical NF pulses, namely, fling-step and directivity pulses.

2.1.1.1 Properties of fling step pulses:

A fling-step pulse is a one-sided long-period velocity pulse associated with a permanent displacement of ground due to a tectonic event. As a result, for a normal or reverse fault, a fling-step pulse is most expected to be formed in the vertical component of the GM; also, as most dip-slip reverse and normal faults (unless very high angle dipping faults) will displace in the horizontal direction, fling-step can occur in the horizontal direction as well; similar to what was observed in the Chi-Chi earthquake (Mavroeidis and Apageorgiou 2003). Bolt (1975) mathematically showed how for dip-slip earthquakes a fling velocity pulse may occur on the fault-normal component; this phenomenon can associate the fault-normal components of dip-slip earthquakes with both directivity and fling effects.

However, for a shallow strike-slip earthquake, a fling-step pulse typically occurs on the ground displacement component parallel to the slip direction, similar to what was observed in the Kocaeli and Duzce earthquakes (Kalkan et al. 2004).

Figure 2.1 depicts the normal fling in the vertical component of GM of the El Mayor-Cucapah Earthquake, 2010. Figure 2.2 depicts the normal fling in the horizontal component of GM for a shallow strike-slip fault due to permanent tectonic deformation at the surface due to the Düzce Earthquake in Kaynasli, Turkey.

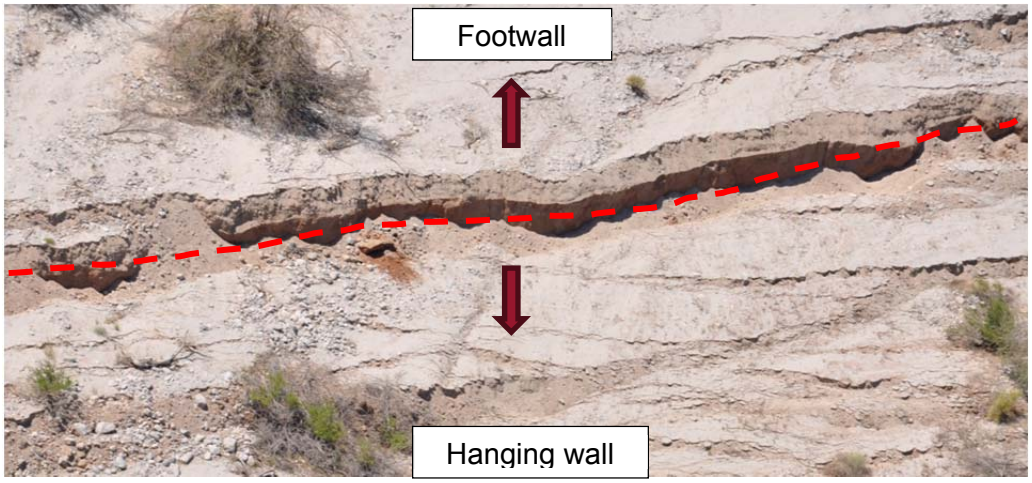

Figure 2.1: 2010 M_W 7.2 El Mayor-Cucapah Earthquake, normal fling pulse in the vertical component of GM

Figure 2.2: Shallow strike-slip fault permanent tectonic deformation at the surface, Kaynasli ,Turkey

Figure 2.3 illustrates how S-wave propagation through a fracture system can result in directivity effects in the FN GM component and fling effects in FP GM component.

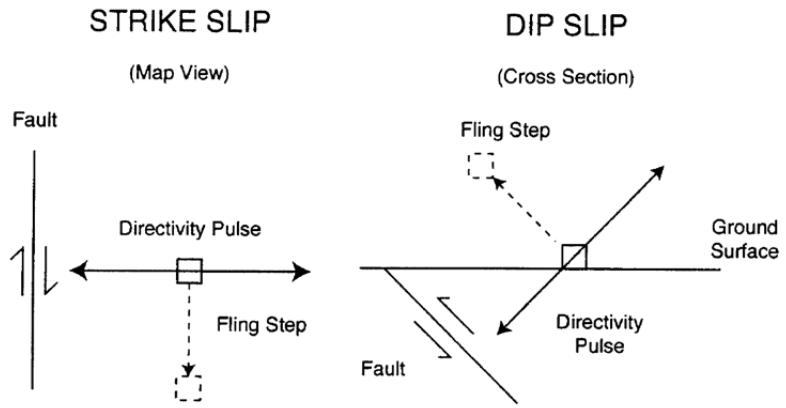

Figure 2.3: Schematic orientation of the rupture directivity pulse and fault displacement (fling step) for strike-slip (left) and dip-slip (right) faulting (after Somerville 2002)

Table 2-1 tabulates the possible scenarios for observation of NF GM effects, namely, fling-step effect and forward directivity effects in terms of the sense of slip of a fault.

Table 2-1: Possible scenarios for observations of near-field fffects

Sense of slip	Directivity	Fling
Dip-Slip	Fault-Normal	Fault-Normal
Strike-Slip	Fault-Normal	Fault-Parallel

Since bridges are usually long, with multiple supports, they are more susceptible to the differential displacements of the ground. These differential displacements may be caused by both dynamic (mainly forward directivity) and/or static (fling-step) ground displacements. However, the static ground displacements in near-fault ground motions can subject a structure/bridge crossing a fault to significant differential displacements (Somerville 2002).

It is of note that while the forward directivity effect has received a great deal of attention in past research, the fling-step effect has not yet been fully studied. This is partially because

1. Fling-step pulses carry less energy as compared with forward directivity pulses if both have the same amplitude.
2. A very limited number of reliable fling-step GMs are available that demonstrate a clean and distinct one-sided pulse.

2.1.1.2 Properties of Directivity Pulses

Interference of horizontal shear waves generated from parts of the rupture toward or away from the site causes double-sided (full-cycle) velocity pulses, recognized as directivity effects.

Directivity effects are more intese when the site is away from the epicentre and rupture propagates toward the site with a velocity close to the surface shear wave velocity in the surrounding soil matrix. In such cases, constructive interference of the traveling waves creates an intense long-period pulse known as the forward directivity pulse. Conversely, backward directivity happens when the fault ruptures away from the site, toward the other end of the fault. In this case, interference of surface shear waves creates a very long-period pulse with relatively lower amplitude than forward directivity pulse.

Figure 2.4 illustrates how forward directivity pulses occur when the fault rupture propagates with a velocity close to the shear wave velocity toward the site and how constructive interference of shear waves generated from parts of the rupture located between the site and epicentre forms the long-period strong pulses.

The radiation pattern of the shear dislocation on the fault causes these directivity pulses to be oriented in the direction perpendicular to the fault plane. This, of course, usually causes the FN component of ground motion to be more damaging than the FP component, especially at periods longer than approximately 0.5 s (Somerville 2002).

2.1.1.3 Energy content of Near-Fault Pulses

Knowing that in theory, the seismic input energy is proportional to cumulative velocity-squared values, one can simply show that NF effects cause the majority of the seismic energy to arrive in a single long-period pulse into the system(Somerville et al. 1997). Therefore, pulses like NF GMs tend to

- significantly increase the magnitude of the long-period range of the elastic acceleration response spectrum (within a narrow band of periods in the vicinity of the pulse period),
- create high demands that force the structures to dissipate the input energy with a few large displacement excursions,

- impose a high ductility demand in the form of a biased response in one direction,
- significantly increase the risk of brittle failure for poorly detailed systems.

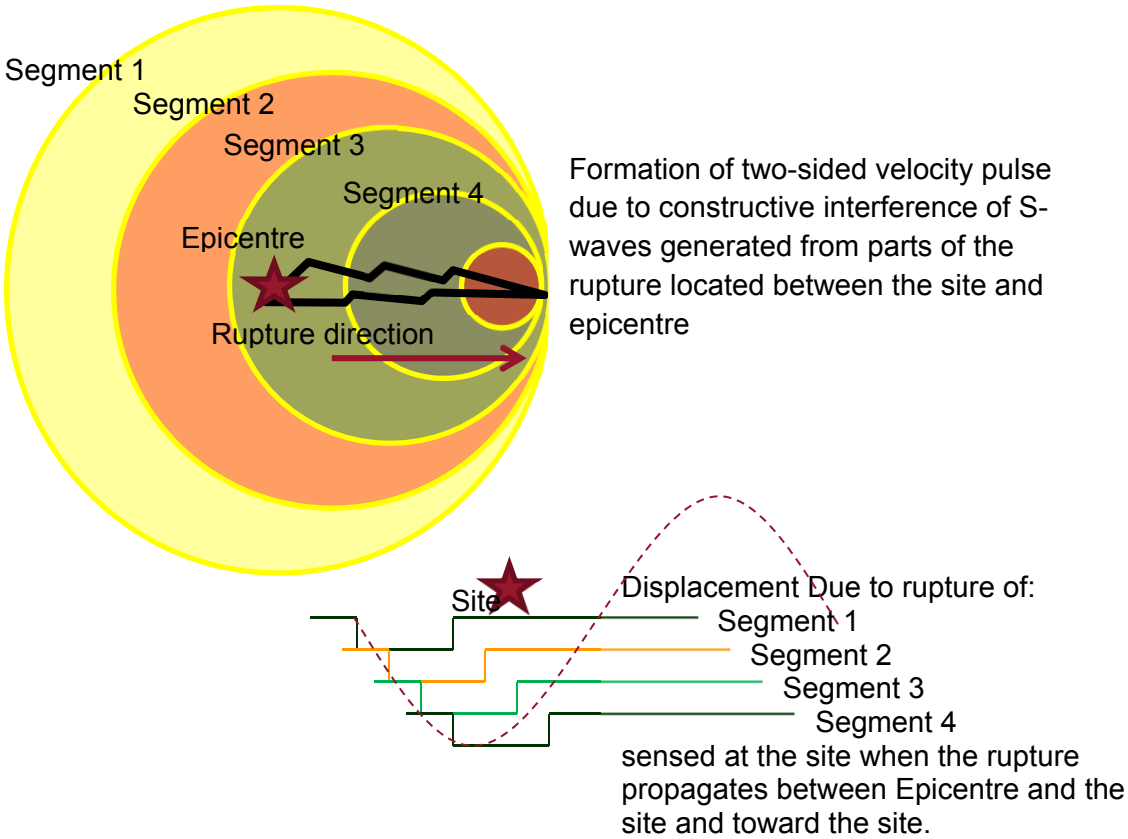

Figure 2.4: Constructive interference of a wave source moving at a speed close to the wave speed

2.1.2 Mathematical models of near-fault ground motions

The importance of assessing effects of high-amplitude pulses on structural demands and also the lack of enough reliable recorded NG GMs have led several researchers to demonstrate that NF GMs (directivity or fling-step) effects can be represented by equivalent pulses defined on the basis of a limited number of ground motion parameters.

Since the forward directivity pulses are recognized as the most damaging NF effects, the majority of these studies focused on synthesizing pulses (using

mathematical models) to simulate artificial forward directivity effects in GMs. Fortunately, NF forward directivity pulses are simple enough to be represented by simplified time histories consisting of one or a few simple time domain pulse functions.[1]

For exemple; Mavroeidis et al. (2004) defined a formulation that is a product of a harmonic oscillation and a bell-shaped function to mathematically synthesize the near-fault ground velocity pulses; also Menun and Fu (2002) proposed another mathematical model for synthesizing the forward directivity and fling pulses that uses only four parameters: the amplitude of the pulse, the period of the pulse, the time at which the pulse starts, and the shape parameter (shape function). The list goes on and on. However, amongst all those mathematical pulse modeling functions, two of them are found to be much more practical, as they represent the targeted pulses in a simple yet very comprehensive way. These are the models presented by (1) Bray and Rodriguez-Marek in 2004, and (2) Sasani and Bertero in 2000. Each of these models is briefly discussed below.

1. Bray and Rodriguez-Marek 2004, defined a simplified sine-pulse function representing velocity time histories as a function of (A) the number of equivalent half-cycle pulses, (B) the period of each half cycle, and (C) the amplitude of pulses. They also introduced a time lag parameter between the initiation of the fault-normal and fault-parallel component pulses that needs to be defined to fully model a bi-directional horizontal effect. (Please note that the latter parameter is addressed by only this model, as most of other mathematical models consider no close correlation between fault-normal and fault-parallel pulses). Figure 2.5 depicts the model proposed by Bray and Rodriguez-Marek (2004), where N is the number of equivalent half-cycles of pulse motions, $T_{v,i}$ is the period of each half-cycle, A_i is the half-cycle pulse amplitude, and t_{off} is the time lag between the pulse start time in two horizontal directions.

[1] The number of pulses is most likely related to slip-segment distributions in the causative fault and, hence, is very difficult to be predicted (Bray et al. 2004).

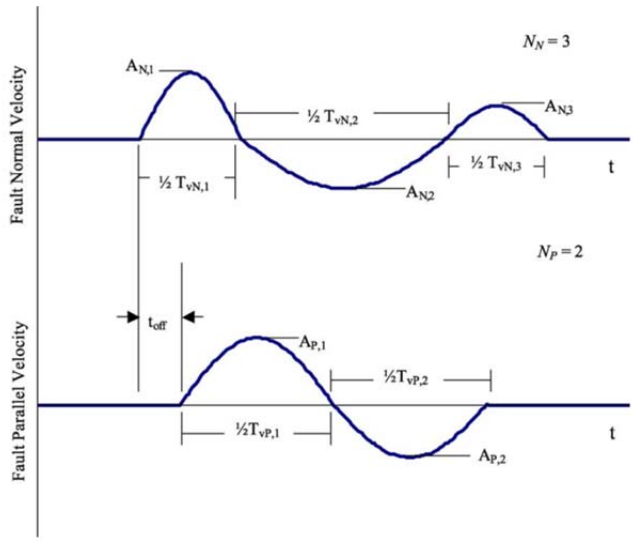

Figure 2.5: Parameters required to define the fault-normal and fault-parallel components of simplified velocity pulses (after Bray and Rodriguez-Marek (2004))

2. One of the most simplified models, which uses a simple sinusoidal function based on definition of fling-step and forward directivity pulses, was presented by Sasani and Bertero (2000). The simplified wave forms presented by Sasani and Bertero (2000) are presented in Figure 2.6.

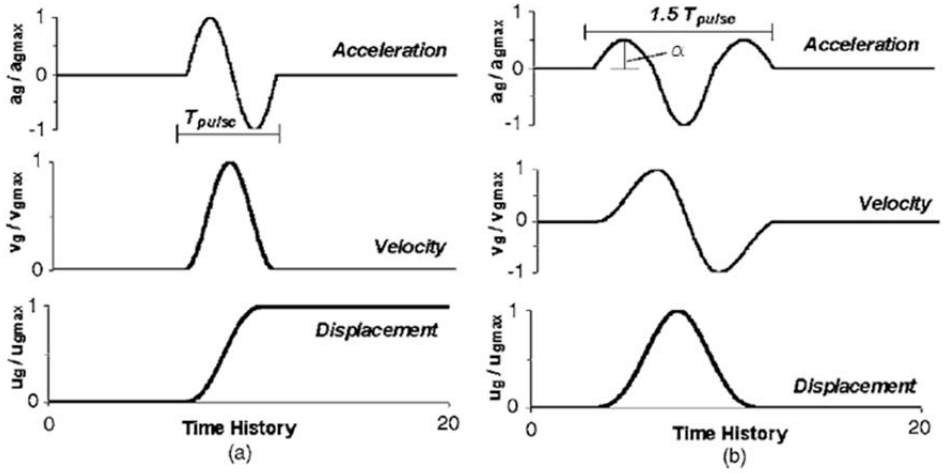

Figure 2.6: Idealized sinusoidal pulse shape functions: (a) fling step, (b) forward-directivity. Shape functions are normalized by maximum acceleration, velocity, and displacements (Sansani and Bertero 2000)

The mathematical models for the acceleration time history of the two pulse models recommended by Sasani and Bertero can be expressed as follows:

$$a(t) = \alpha \frac{2\pi D}{{T_p}^2} Sin[\frac{2\pi}{T_p}(T - T_i)] \qquad 2\text{-}1$$

where D is the maximum amplitude of the displacement obtained by double time integration of acceleration, $a(t)$, T_p is the period of the sinusoidal pulse, T_i is the pulse arrival time, and α is a scale factor that shapes the function for forward directivity and is equal to unity for fling-step functions.

Regardless of the shape of the pulse functions proposed by different researchers, all of these mathematical models have some parameters in common, namely: (1) amplitude of the (velocity) pulse, (2) period of the (velocity) pulse, and (3) arrival time of the pulse. Different equations relating the period of the pulse to the earthquake magnitude and the effective velocity of the pulse to the earthquake magnitude and distance have been developed using regression analysis (Somerville 2002). Arrival time of the pulse could be estimated based on the shear wave velocity and site to fault distance, also. The following sections briefly describe each of these parameters.[1]

2.1.2.1 Amplitude of the pulse

Amplitude of the velocity pulse - usually equal to Peak Ground Velocity (PGV) could be determined from some regression analysis that results in attenuation

[1]As opposed to all mathematical models, recently Baker and his research group developed an analytical technique which utilizes wavelet analysis to decompose the GM velocity signals and extract the long-period pulses from the seed GMs. See http://www.stanford.edu/~bakerjw/research/pulse-classification.html. Although pulses extracted by Baker's method might be contaminated with other long-period pulses resulting from sources other than NF effect (i.e. basin effects) they are considered to be representative of NF pulses and have the same effect on the structure as pure NF pulses might have. Furthermore, the extracted wavelets are more accurate in shape, function, and amplitude than any synthetic method. Hence; hence, the response of the structures to these wavelets is expected to be a better representative of the real response of structures to NF GMs.

relationships or simulated from probability distributions determined from a database of similar recorded ground motions. [1]

Different attenuation models for PGV are already developed and proposed by different researchers. For example, Somerville in 1998 proposed using a bilinear relationship between the logarithm of PGV, magnitude, and the logarithm of the distance; however, it capped the equation at a distance cut-off of 3 km. Bray et.al (2009) proposed another model similar to equation 2-2:

$$ln(PGV) = 2.05 + 0.55 \times Mw - 0.39\, ln(R^2 + 25) \qquad 2\text{-}2$$

where Mw is moment magnitude and R is rupture distance in kilometres.

It is of note that the original proposed equation by Bray et.al (2009) accounts for uncertainties as well. However, equation 2-2 is a truncated form (i.e. error terms of the original equation is omitted) which gives a good estimate of median value of PGV. Based on the regression that is made to determine equation 2-2, the standard error associated with the estimate of PGV is dependent on ground conditions and is about 0.44. Being a function of site-to-source distance, Equation 2-2 results in a nearly zero slope at close distances to the fault, and for larger distances it decreases linearly with the logarithm of distance. This is clearly evident in Figure 2.7. Figure 2.7 shows that for very close site to fault distance (<3.0 km), PGV remains almost constant. This is in close agreement with what Somerville proposed in 1998.

In general, median peak ground velocities for soil conditions are expected to be larger than median peak ground velocities for rock conditions. The amplitude is a function of wave propagation through the medium, so the difference increases as the wave traveling distance increases (Bray and Rodriguez-Marek 2004).

[1] Alavi and Krawinkler (2000) determined equivalent pulse amplitude and showed that in almost all cases, the equivalent pulse velocity lies within $\pm$20% of the PGV of the record.

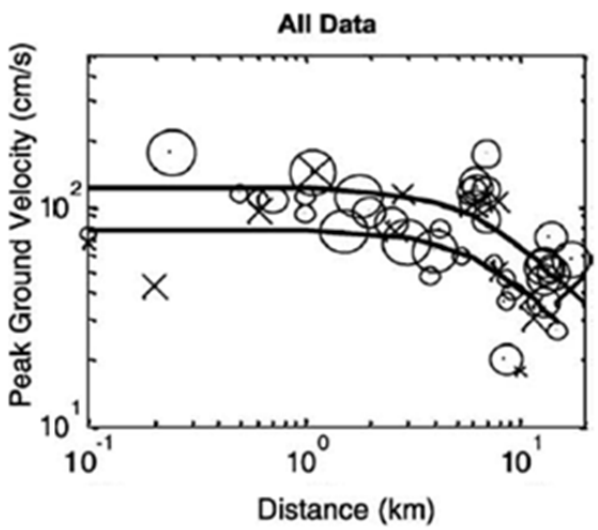

Figure 2.7: Attenuation relationship for PGV in the near-fault region (after Bray and Rodriguez-Marek 2004))

2.1.2.2 Period of the pulse

Previous researchers showed that forward directivity and fling-step pulse periods are strongly and linearly correlated with the moment magnitude of the causative earthquake. They also demonstrated that local site conditions can affect the pulse period, i.e., soil sites tend to elongate the pulse period slightly as compared with rock sites.

It is of note that the significance of the site effect on the predicted pulse period is much less than the significance of the earthquake magnitude on it, i.e., the effect of site class on NF pulse periods diminishes as the magnitude increases. That is to say, for events with *Mw* ≈ 7.5 the pulse periods at rock and soil sites are about the same (Bray and Rodriguez-Marek 2004).

Depending on the *Mw* (fault mechanism, length, and complexity of the rupture) and the site conditions, the period of the significant pulse of a NF GM may range from 0.5 to 5.0 s.

In Baker and Shahi (2011) a new linear regression analysis between $ln(T_P)$ and M_w based on the most recent set of NF GMs is spresented; namely, equation 2-3, which estimates expected T_P based on moment magnitude of a NF GMs:

$$E([ln(T_P)] = A + B \times M_w \qquad 2\text{-}3$$

The pulse period used for this regression analysis is the maximum Fourier amplitude of the extracted pulse following wavelet analysis proposed by Baker (2007). In equation 2-3 $E([ln(T_P)]$ denotes the expected value of the natural logarithm of pulse period (T_P), *A* is–5.755 ± 0.025, and *B* is about 1.05 ± 0.15. The standard deviation of the above regression or natural logarithm of the pulse period, $\sigma[ln(T_P)]$, is about 0.56. Figure 2.8 shows the observed T_P (in log scale) vs. expected M_w values.

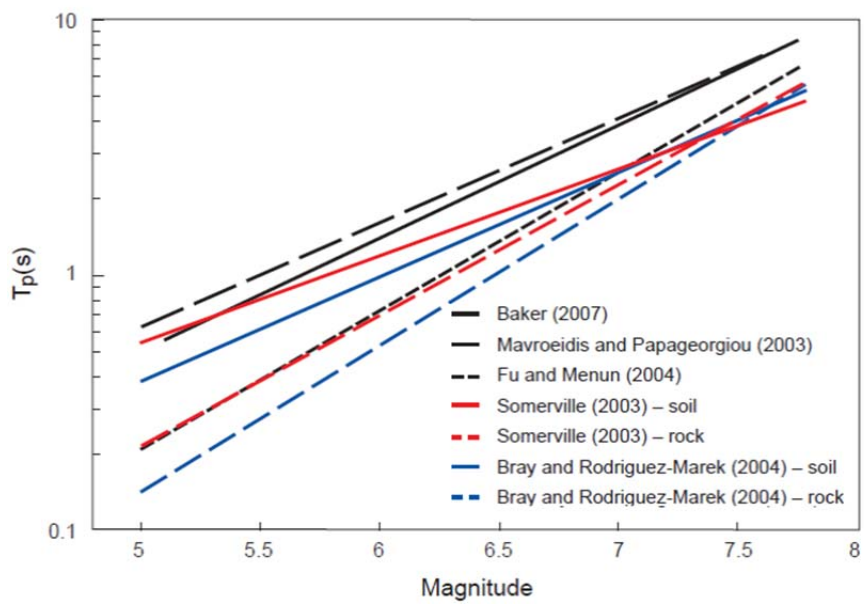

Figure 2.8: Pulse period versus earthquake magnitude for the NF GMs with forward directivity or fling-step pulses by different researchers (after PEER Ground Motion Database technical report, 2010)

Since the energy content of the forward directivity and fling-step NF GMs are concentrated in a narrow-period band centered about the pulse period, one can expect that the elastic response spectrum shows a local increase/hump in close proximity to the NF pulse period. Thus, the magnitude dependency of the pulse period indicates that this increase (hump) shifts to the higher period range as the magnitude of the earthquake increases. Hence, the amplitudes of NF GMs from moderate magnitude earthquakes may exceed those of larger magnitude earthquakes at the intermediate-period range, i.e., lower magnitude NF GMs might be more destructive to stiff structures as they tend to have more energy content in lower-period ranges (Bray and Rodriguez-Marek 2004). This is further discussed in section 2.3.1 (also see Figure 2.12).

2.1.2.3 Arrival time of the pulse

An accurate estimate of arrival time of the pulse is required only if one intends to patch a synthesized pulse to a recorded GM (usually ground velocity motions). Thus, this parameter is not required if a pulse signal is used independently to estimate the response of the structures.

Although no analytically robust and clear indication of exact arrival time of the pulse is yet identified, it is already known that long-period pulses usually arrive as soon as S-waves arrive; this is mainly because the long-period pulse is from constructive interferane of swaves, which is equivalent to coherent S-waves arriving simultaneously. The pulse does not arrive after S-waves arrive. it is the result of the major S-wave arrivals. Hence, if one is interested in patching a pulse into an already available GM, one might choose to locate the start point right before a clear S-wave in either of the horizontal components.

2.2 Flexibility of the foundation system

Although effects of FFS, considered within context of SFSI, has been the subject of many studies in the past few decades, the significance of it on the seismic performance and nonlinear behaviour of the structures is not yet clearly understood.

Traditionally, accounting for FFS has been considered important only if an effective design or an economical scheme was of concern. Thus, it has been recommended by various researchers/regulatory bodies to disregarded FFS in favour of reaching a (so-called) more conservative design.

Owing to the shape of simplified code-prescribed design response spectrum, an increase in the fundamental period of the structure due to the presence of a flexible foundation (period elongation) should always result in some reduction in seismic demands. As a result, if a simplified code-based design response spectrum is used, then FFS effects would invariably result in reduced seismic and ductility demand (or risk).

However, in reality this is not always true; i.e. in some cases FFS may have an adverse effect on the seismic demand and ductility demand of the structures or bridge piers. This is more pronounced for moderately flexible structures (Mylonakis and Gazetas 2000) subjected to NF GMs.

This inconsistency in response of structures due to consideration of FFS effects is already proven by some recorded seismic responses of instrumented structures/bridges. This is also justifiable from a pure theoretical standpoint as well, i.e., some input motions have considerable energy content in a certain period range, which in turn causes an irregular increase in elastic response amplitudes around the neighborhood of their high energy frequency content. Such a situation can happen when the structure is built on a soft layer of soil deposit and the input GMs have some low-frequency content. Obviously, this effect is more evident if the input motion has significant low-frequency content, i.e., due to the presence of NF long-period velocity pulses. Nonetheless, in such cases the code-based elastic response spectrum, driven from FF GM attenuation relationships, is not a real representative of the response of the systems to NF GMs.

To overcome this deficiency in code provisions, different researchers used different scaling functions to change the code-based (FF GM compatible) design response spectrum and to produce a NF GM compatible design response spectrum. For example, Shahi and Baker (2011) proposed a narrowband amplification function that modifies the regular code-based response spectra to account for the expected effects of NF long-period velocity pulses. The narrowband adjustments explicitly account for the expected pulse period and apply adjustments to spectral accelerations in the neighborhood of the expected pulse period. In contrast, Somerville et al. (1997) and Abrahamson (2000) proposed a broadband scaling function that amplifies a much wider range of periods to take into account the potential effects of pulses with a range of possible periods. The former approach is appropriate for adjusting a target spectrum and producing a scenario earthquake target spectrum that explicitly accounts for a certain pulse period associated with a specific moment magnitude and a specific site to source distance. Conversely, the latter approach is more appropriate for adjusting a Uniform Hazard Response Spectrum (UHRS) to account for a wide range of possible pulse periods.

Figure 2.9 shows the code-based design response spectrum (determined from FF GM attenuation relationships and usually used for analysis of fixed-based structure) in the solid blue line. In the same figure, the blue dashed line represents a possible adjusted design response spectrum to account for NF effects, i.e., the adjusted response spectrum (schematically) represents the NF compatible UHRS produced

from code-based UHRS using some hypothetical narrowband amplification factor with pulse period of approximately 2.5 s. The red solid line and the red dashed line are analogues to the blue solid line and the blue dashed line, respectively, while their ordinates are deamplified to account for 5% extra damping (to allow for 10% total viscous system damping) due to different effects of SFSI, including radiation damping, soil material hysteresis damping, wave incoherency, wave scattering, etc.

To better illustrate the possible adverse effects of FFS/SFSI on response of structures when the input motions are associated with long-period velocity pulses, a hypothetical case of a-fixed-base structure with fundamental period of some 1.8 s is considered, and reflected in Figure 2.9. For such a system, the elastic response of the first mode of vibration is approximately 0.22*g*, where *g* is the acceleration of gravity (see the blue dotted arrows on Figure 2.9). Now, if the FFS effect elongates the fundamental period of the system to some 2.65 s and equivalent effects of radiation damping and kinematic SFSI introduce 5% extra damping into the system, then one can argue that the elastic response of the first mode of vibration can be reduced to some 0.11*g*, which is equivalent to approximately 50% reduction in elastic response.[1]

However, if amplification factors due to NF GM effects are considered, the same response could be increased to some 0.25*g*. which is equivalent to approximately 15% increase in elastic response of the first mode of vibration (see the red dotted arrows on Figure 2.9). As one can easily conclude, the results of this simple example contradict the assumption that “disregarding FFS/SFSI would result in a more conservative design”. It is of note that if one considers only the effects of FFS (inertia effects of SFSI), then the response could have been increased to 0.30*g*, which is some 36% more than what code prescribes.

[1] In general, one may argue that except for deep and sizable foundation systems (i.e., caisson foundations), relatively stiff foundations in soft soils, and for large rigid shallow foundations (i.e.,. thick mat foundations), the effect of kinematic interaction on input motions is negligible. Hence, the free-field motions could be used as foundation input motions without too much loss in accuracy.

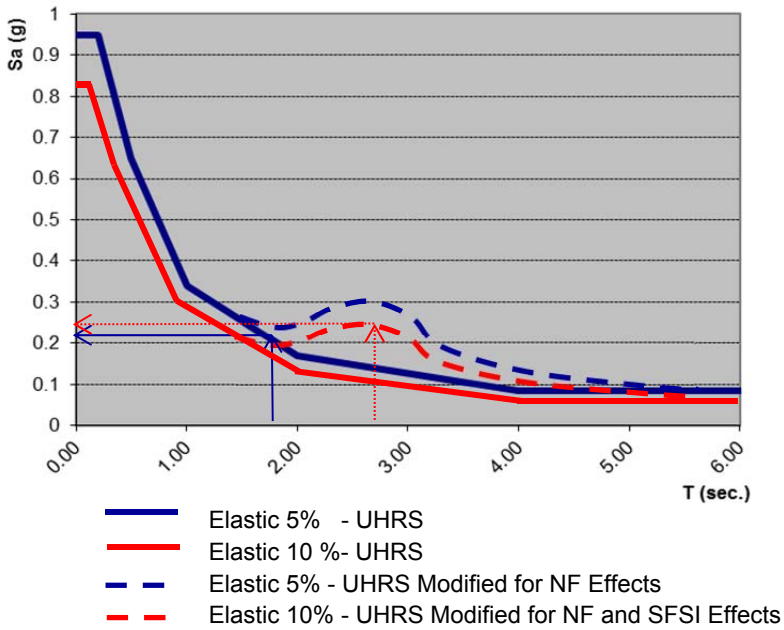

Figure 2.9: Effect of period elongation and increased damping on the elastic response of structures based on code-prescribed design response spectrum

The above example is based on the elastic response for a very simple structure that essentially has one mode of vibration (or the effect of its higher modes on the total response of the structure is insignificant). However, in reality, when the structures are subjected to strong motions neither is their response governed by only one mode of vibration nor does it remains totally elastic.[1]

2.3 Structural response to NF GMs

Many aspects of the general effects of FFS on response of structures were detailed in the previous sections. In this section, mainly linear response of structures to NF GMs with and without effects of FFS is described.

[1] Although different researchers, including Krawinkler and Alavi (1998, 2001, 2004), extensively worked on different aspects of NF GM effects on responses of MDOF systems, none of them considered the effect of base flexibility, and none of them established a generalized pattern for response variation due to the presence of NF GMs.

2.3.1 Linear response

Linear response of the structures due to input motions is the basis of almost all design codes and guidelines. That is to say that design codes and guidelines usually define the design forces as the elastic demand divided by some strength reduction factor, depending on the target ductility of the system. However, this approach is chiefly established based on the work in 1960s and 1970s with consideration of ordinary ground motions and without any specific attention of pulse-like NF GMs.

Recent studies showed that there are some fundamental differences between characteristics of NF and FF GMs, which render their elastic response spectra somewhat different. Figure 2.10 depicts the 5% damped response spectrum of an ordinary FF GM, i.e., Taft, 1952 Kern County earthquake, which matches what Newmark-Hall proposed in 1960. On the other hand, Figure 2.11 shows the 5% damped response spectrum of a NF GM, i.e., NR94rrs, which has a shape significantly different from the FF GM spectral shape.

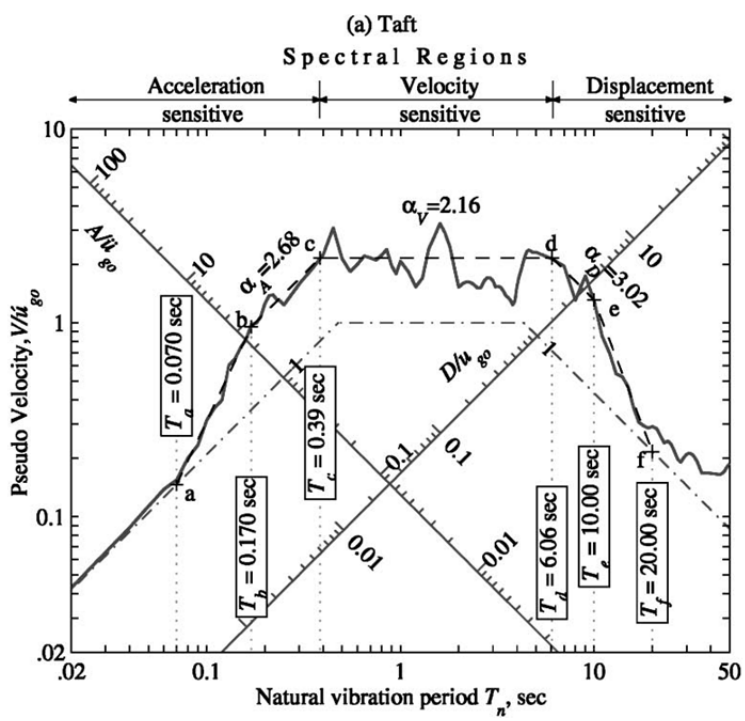

Figure 2.10: 5% damped response spectrum for the fault-formal component of a FF GM (Taft) shown by a solid line together with an idealized version shown by a dashed line (after Chopra et al. (2001))

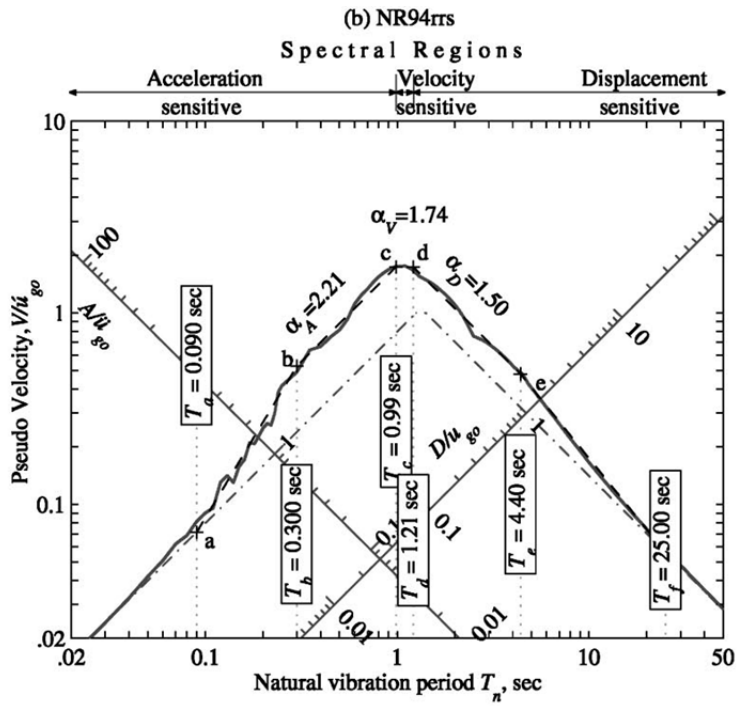

Figure 2.11: 5% damped response spectrum for the fault-normal component of a NF GM (NR94rrs), shown by a solid line together with an idealized version shown by a dashed line (after Chopra et al. (2001))

An obvious difference between response spectra of FF GMs and those of NF GMs is that the velocity-sensitive region of the response spectra of NF GMs is much narrower, and their acceleration and displacement-sensitive regions are much wider. This phenomenon is chiefly associated with the frequency content of GMs and the presence of a strong long velocity pulse in NF GMs.

Another aspect of NF GMs that can affect the response of the structures is the magnitude of the causative event. As briefly explained before, for many short- to moderate-period structures, the expected large pulse periods from a relatively large magnitude earthquake may not produce significant levels of damage. Conversely, the lower magnitude earthquakes may result in velocity pulses with periods closer to the fundamental period of the short- to moderate-period (squad/stiff) structures.

Thus, moderate[1] NF GMs might be more detrimental to the short-period structures, despite them having less energy content. Hence, ground motions recorded at NF sites for large magnitude earthquakes cannot be assumed to be "the worst-case scenarios" for the design of all structures (Bray and Rodriguez-Marek 2004). Thus, a much wider range of possible earthquake magnitudes (i.e., various scenarios), from very strong to moderate NF earthquakes, needs to be considered to account for the effect of NF GMs on different structures with different fundamental periods.

Figure 2.12 schematically illustrates what was conceptualized above regarding more damaging effects of moderate NF earthquakes on relatively short-to moderate-period structures (e.g., structures with periods of <2.0 s).

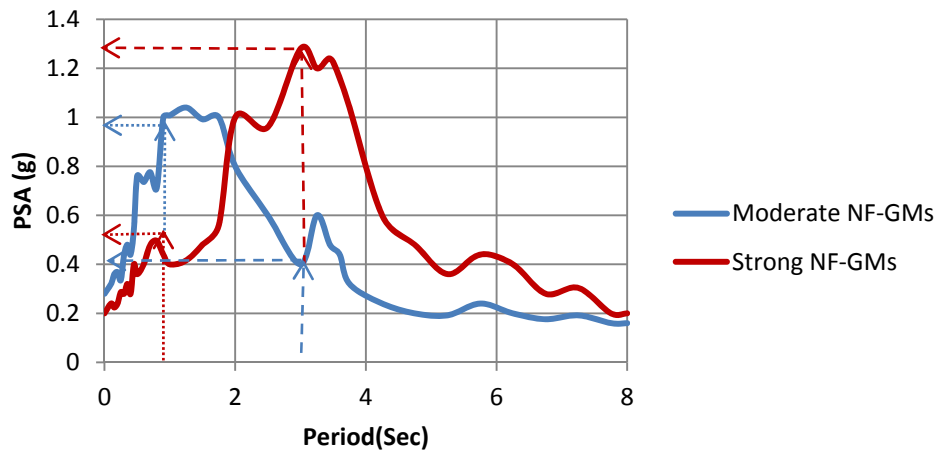

Figure 2.12: Schematic expected NF GM response spectra for two hypothetical events

It is of note that probability of a structure close to a causative fault being damaged by a NF GM is a joint probability function of (at least) three variables, namely:

a. probability of having a tectonic activity or Annual Frequency of Exceedance (AFE) of an event generated from the nearby causative fault,

[1] Previous researchers (i.e.,. Mavroeidis et al. (2004)).) grouped the seismic events into three categories: moderate (M_w ≤ =6.3), moderate to large (M_w = 6.4 to –6.7), and large (M_w ≥ =6.8) earthquakes.

b. possibility of having some long velocity pulse associated with each input motion generated from the nearby causative fault,

c. fragility of the structure.

It is of note that because the AFE of moderate NF GMs is more than the AFE of strong NF GMs, the short-period structures might be subjected to much more risk owing to the NF GMs than what traditionally was expected.

2.3.2 Nonlinear response

One of the main differences between response of the structure to strong NF GMs compare with those to strong FF GMs is that the arrival of a strong long-period velocity pulse in a NF GM causes the structure to a dissipate considerable amount of input energy in relatively few (inelastic) cycles, whereas in FF GMs the input energy is imposed gradually and within many more reversing cycles of motions. Hence, cumulative energy dissipation from increased cyclic demands is much more evident in FF GMs than in NF GMs. Furthermore, imposing some significant inelastic excursions in the very beginning of NF GMs (due to early arriving long-period pulses) makes the structures much more vulnerable to the demands attributable to the rest of the NF input motion.

Although the elastic response spectrum is extensively used for analysis and design of the structures, it is a general consensus that the response spectrum alone is not an adequate representation of NF GM characteristics because it does not adequately represent the demand for a high rate of energy absorption presented by NF pulses. This is especially applicable to the high ground motion levels that drive structures into the inelastic range, invalidating the linear elastic assumption on which the elastic response spectrum is based (Somerville (2002), with reference to the FHWA/NCEER Workshop on the National Representation of Seismic Ground Motion for New and Existing Highway Facilities, San Francisco, May 29–30, 1997). Hence, one may argue that to fully portray the response of structures to NF GMs, nonlinear time history analysis is required.

Current structural engineering practice determines the maximum inelastic demand (U_{max}) of regular and simple structures (due to FF GMs), based on the maximum elastic demands (U_e) of the structure using elastic response spectrum. This

approach is chiefly based on equal-displacement and/or equal-strain energy rules for a specific target ductility ratio (μ), as proposed by Numark-Hall (1960); where, the equal-displacement rule (i.e., $U_{max} = U_e$) governs the velocity and displacement-sensitive regions of the response spectrum, and the equal-strain energy rule (i.e., $U_{max}/U_e = \mu/\sqrt{2\mu - 1}$) governs the acceleration-sensitive region of the response spectrum.

Using the above equations, Newmark and Hall also proposed a constant-ductility design spectrum by dividing the elastic design spectrum by an appropriate ductility-dependent yield-strength reduction factor (R_y), where

$$R_y = \begin{cases} 1, & T_n < T_a \\ \sqrt{2\mu - 1} & T_b \le T_n \le T_c \\ \mu & T_n > T_a \end{cases} R_y = \begin{cases} 1, & T_n < T_a \\ \sqrt{2\mu - 1} & T_b \le T_n \le T_c \\ \mu & T_n > T_a \end{cases} \qquad 2\text{-}4$$

The Newmark-Hall's equation is based on analysis of elastoplastic response of structures due to limited number of earthquake records available in 1960s', i.e., without any specific attention to the particularities of NF GMs and substantial differences between FF and NF GM elastic response spectra.

However, as is evident from comparison of Figure 2.10 and Figure 2.11, because of substantial differences between characteristics of FF and NF GM elastic response spectra, the Numark-Hall equations (as defined originally and without any amendment) are not directly applicable to NF GMs. While this statement in principle is correct, Chopra and Chintanapakdee (2001) showed that if abscissa of elastic and inelastic response spectra of SDOF systems are normalized with respect to the period separating the acceleration and velocity-sensitive regions (T_c),) then the ratio of $\frac{U_{max}}{U_e}$ becomes very similar for the two types of motions (NF and FF GMs) over their corresponding spectral regions. Thus, they noted that the standard-design provisions for reduction factors can be used for NF GMs in way similar to that used for FF GMs, provided that normalized response spectra are used and design equations for R_y explicitly recognize the spectral regions. Based on numerical analysis, Chpora and Chintanapakdee (2001) also proposed using the T_a = 0.04 s, T_b = 0.35s and T_c = 0.79 s as partition periods for separation of different spectral

regions of the fault-normal component of NF GMs (for the purpose of normalizing abscissa of elastic and inelastic response spectra).

2.3.3 Response of the structures to NF GMs vs. equivalent pulses

Some researchers attempted to use either synthesized or extracted pulses that are equivalent to the NF GM pulses and investigate the possibility of substituting analysis of the system response due to NF GMs with analysis of several bunches of predetermined equivalent pulses.

The results of previous investigations showed that simple pulses can capture the peak response of SDOF at long periods if the system has an undamped natural period of vibration that is more than 0.75 times the period of the pulse (and less than 3.0 times the period of the pulse). At periods shorter than 0.75 times the period of the pulse, the structures response to the simple pulse significantly underestimates the response of the structure to a real NF GM, as the response of structure is also significantly dependent on the content of the GM, which does not exist in a simple long-period pulse signal. In general, one can expect that maximum displacements computed using equivalent pulses are about 70% of that computed by using actual NF GMs (provided that the natural period of vibration is more than 0.75 times the period of the pulse). This ratio tends to increase to 100% as the ratio of the natural period of the system to the pulse period increases, i.e., if the ratio of the natural period of the system to the pulse period is between 150% to 300% then the response of the structure to the equivalent pulse could be considered a very good representative of the response of the structure to the actual NF GMs (Rupakhety and Sigbjörnsson 2011).

It is of note that recent studies of MDOF systems showed that response of MDOF systems to an equivalent simple pulse cannot be a good representative of those to full NF GMs unless the first mode of the vibration is a very good representative of the dynamic response of the structure to base excitations. Again, this is because pulse models (either synthesized or extracted) lack high frequencies and, hence, cannot capture the response of higher modes of vibration (Krawinkler and Alavi 2004). Nonetheless, effects of higher modes on the response of MDOF to NF GMs are mainly determined from some linear analysis. However, one should note that

development of nonlinearity through structure, in the course of response to the actual NF GM, might significantly change the characteristics of the structure. This is because the effective modal periods constantly change in a nonlinear system going through a transient loading, and so-called higher-mode periods also shift as the building moves into the inelastic range. Hence, above statement should be taken with a grain of salt when MDOF systems undergo substantial inelastic response due to input NF GMs.

2.3.4 Vertical component of NF GMs

The magnitude of the vertical component of NF GMs could be much more than the magnitude of vertical component of FF GMs. This phenomenon is irrespective of orientation and presence of a long velocity pulse in the input GM.

Figure 2.13 shows the ratio of vertical to horizontal response spectrum for a suite of NF GMs as well as the same for a comparable suite of FF GMs, when

$$\text{Vertical to horizontal response spectrum} = \frac{\text{Averaged spectral acceleration of vertical components}}{\text{Averaged spectral acceleration of geometric mean of two horizontal components}}\overline{\overline{av}}$$

It is of note that Figure 2.13 is developed using a suite of Peak Ground Acceleration (PGA) matched GMs, as detailed in Appendix F.2.

Figure 2.13 indicates that unlike ordinary FF GMs, the impact of the vertical component of NF GMs on the nonlinear response of structures might be of great importance. Therefore, inclusion of the vertical component of NF GMs in analysis and design should be accounted for somehow.

Despite knowing the importance of the effect of the vertical component of NF GMs on the response of the structures in close proximity to an active fault, only a few research studies are available that account for the effects of the vertical component of NF GMs on the response of structures. Papazoglou and Elnashai (1996) presented comprehensive field evidence, complete with results of some dynamic analysis, which together shows the susceptibility of structures to strong vertical ground motion.

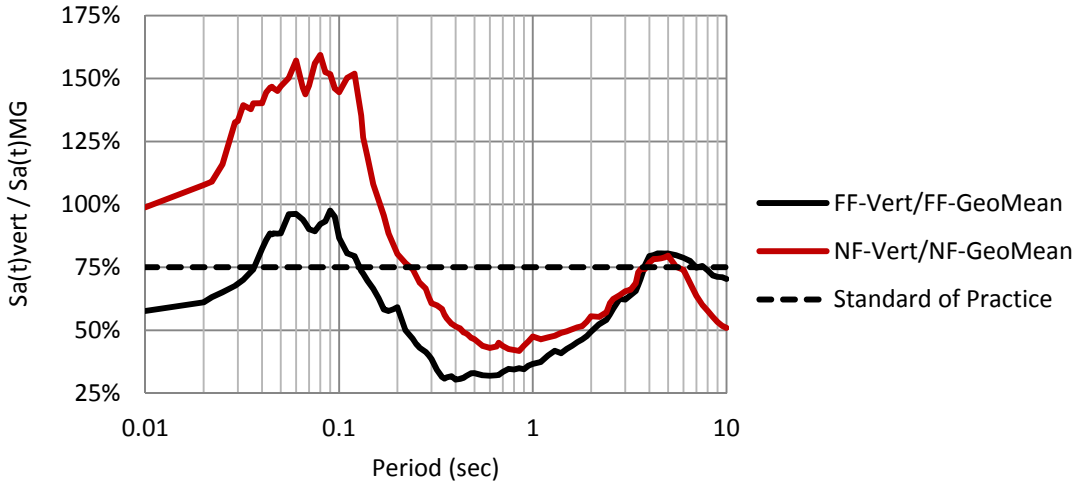

Figure 2.13: Ratioratio of vertical to horizontal response spectrum for 40 x PGA- matched matched GM

3. Introduction to mathematical modeling

Chapter Outline:

1. Section 3.2 gives an overview of the mathematical models used in this research project
2. Section 3.3 describes types and ranges of parameters used for parametric study and sensitivity analysis
3. Section 3.4 itemizes monitored and reported responses and relates them to some practical problems

---

This chapter briefly discusses computer models, parametric studies, and monitored EDPs used in this research to gain some general knowledge about parallel (or independent) effects of NF GMs and FFS on the nonlinear response of different structures.

3.1.1.1 Method of analysis

Proper evaluation of the maximum nonlinear response of structures due to earthquake excitations can be determined only via NLTHA using a large suite of ground motions.

To evaluate the effect of NF GMs on nonlinear response of the structures, two comparable suites of GMs are needed: firstly, a suite of recorded GMs representing realistic NF GMs associated with long-period pulses (NF GMs) and, secondly, a suite of FF GMs that forms the comparable counterparts of NF GMs.

With two comparable suites of GMs it was possible to implement a series of NLTHA, extract the responses of interest for each suite, and carefully compared them to determine if NF GMs do or do not have a systematic effect on responses of structures.

3.1.1.2 Computer models

In this research, three classes of mathematical models were redeveloped and used, namely

1. Nonlinear Single Degree Of Freedom (SDOF) models: primarily used for studying the effects of NF GMs on nonlinear response of different structures,
2. 2-Degree Of Freedom (2DOF) models: an upgrade to SDOF models that allows for consideration of base flexibility, mainly used for studying combined effects of NF GMs and FFS on nonlinear response of structures,
3. a MDOF model: used for validation of a proposed simplified procedure for consideration of combined effects of NF GMs and FFS.

For the purposes of mathematical modeling, SAP2000-Nonlinear, Ver. 15, a commercially available general-purpose three-dimensional Finite Element Method (FEM) structural analysis program is used. It is of note that in this study all nonlinearity in the modeling is assumed to be due only to ductile inelastic behaviour of the structures.

3.1.1.3 Parametric studies

In a design project, to achieve reliable results for a particular structure, the idealized model should realistically represent the actual physical properties of the system, i.e., geometry, boundary conditions, gravity load, mass distribution, energy dissipation mechanisms, and nonlinear properties of all major components of the system. However, this level of complexity is neither practical nor desirable for a study project that is intends to gain some general understanding about combined effects of NF GMs and FFS on the response of simple structures. Thus, to extend the applicability of the results of this research, an extensive parametric study was conducted to account for a range of important properties, which may need to be accounted for if a real project is modeled. These are variabilities associated with

- input GMs, and GM intensities
- elastic period of vibration of the superstructure,
- strength characteristics of the superstructure,
- hysteresis behaviour of the systems,
- equivalent damping of the system,
- foundation flexibility,
- foundation mass.

Figure 3.1 shows the logic tree and range of parameters used in NLTHA of SDOF and 2DOF models.

3.1.1.4 Monitored EDPS

In general the modeling and nonlinear analysis procedures described in this chapter were primarily intended to predict the expected displacements and system ductility demands (in a probabilistic context) with no special attention paid to any specific GM or to any particular structural system. Nonetheless, in addition to expected displacements and system ductility demands, some other EDPs are also studied in this research. Please refer to section 3.4.

The following subsections briefly explain the mathematical models, modeling assumptions, range of modeling parameters, and sensitivity analysis that used in this research. A further description of each model can be found in Chapters 4 to 6.

3.2 Mathematical models used in this study

As mentioned in the previous section, to evaluate and compare nonlinear response of the structures to the selected NF and FF GMs, with and without FFS, three series of mathematical models were developed and used; these are:

1. Nonlinear SDOF models

SDOFs are the most simplified models of a fixed-base structure, used for sensitivity analysis and response identification. Stiffness and associated mass of each SDOF system is set to allow for a wide range of elastic natural vibration periods, ranging from 0.20 to 2.4 s. The nonlinearity and hysteretic behaviour of the systems are idealized using five different discrete plastic hinge models assigned to the base of SDOF systems. A wide range of yield thresholds (strength characteristic), ranging from 5% of effective seismic weight (W refer to “Lists of symbols and abbreviations”) to 50% W, is assigned to each selected period of vibration (ranging from 0.20 to 2.4 s).

The analyses were run for two different levels of system damping, 2% and 5%. The analysis were run for two different sets of NF GMs, FF GMs, and their corresponding extracted pulses and the residual pulses as detailed in section 3.3.1.

The analyses were also run for five different levels of input motions using five different amplification factors applied to input GMs.

Table 3-1 summarizes the different analyses performed on SDOF systems to account for various permutations of the above parameters.

Table 3-1: Summary: summary of NLTHA of SDOF models

Elastic periods of vibration			12
Strength characteristics			11
Backbone curves			5
System damping ratios			2
GM set "1"			280
FN component	NF GM	40	
	FF GM	40	
	Filtered pulse*	40	
	Extracted pulse using wavelet analysis*	40	
	Residual pulse*	40	
FP component	NF GM	40	
	FF GM	40	
GM set "2"			120
FN component	NF GM	30	
	FF GM	30	
FP component	NF GM	30	
	FF GM	30	
Earthquake intensity level			5
Total number of SDOF analyses			2 640 000

*For definition of filtered pulse, extracted pulse, and residual pulse refer to section 3.3.1.

Details of mathematical models of inelastic discrete link elements used for NLTHA of SDOF systems are presented in section 3.3.6.1.

Results of NLTHA of SDOF systems are presented in Chapter 4.

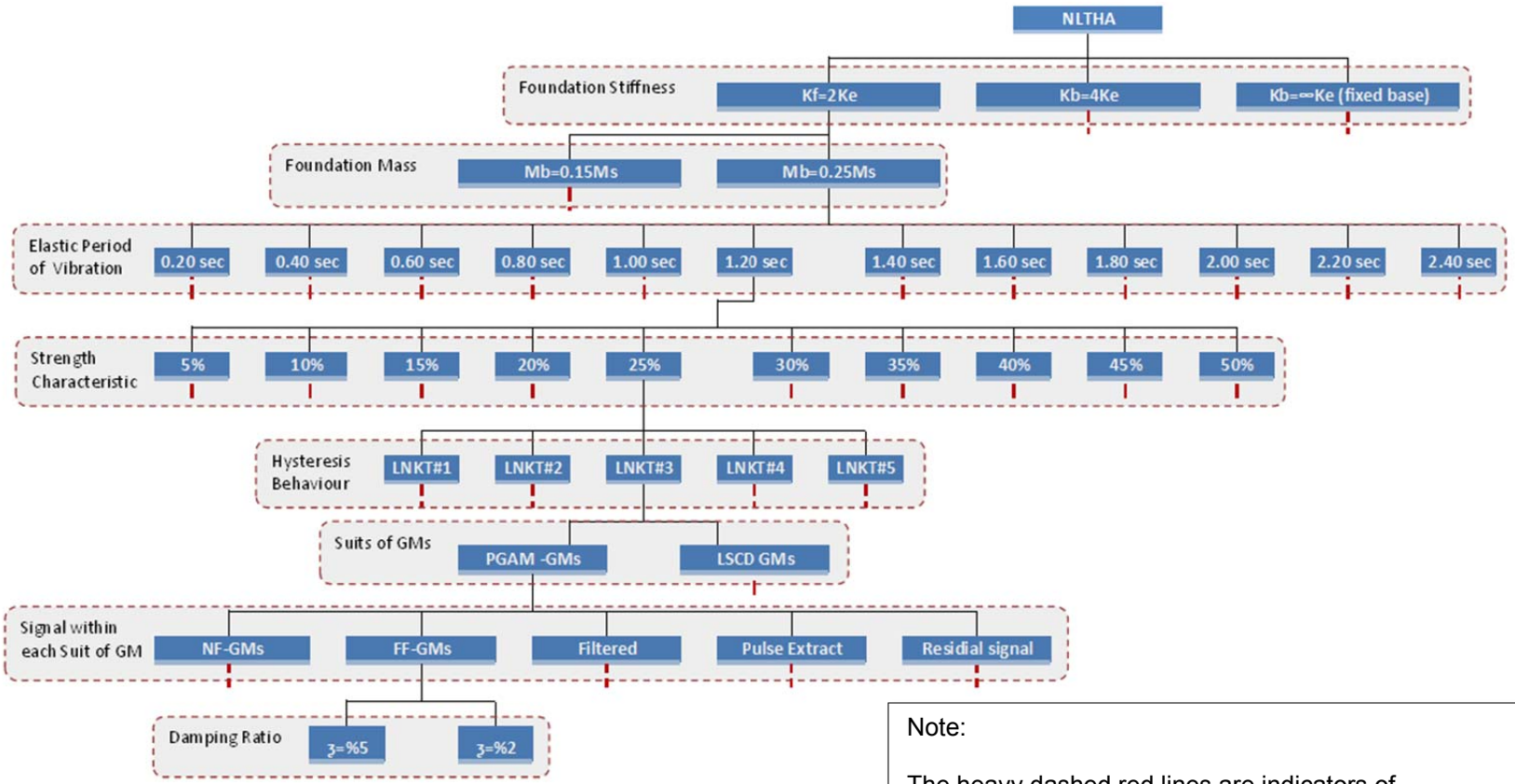

Note:

The heavy dashed red lines are indicators of assemblies of cells that are similar to the parallel assemblies indicated by solid black lines; deleted for brevity.

Figure 3.1: Logic tree of analysis/parametric study performed for each level of intensity of input motions

2. Nonlinear 2DOF models

These are the most simplified models of a flexible-base structure, used for sensitivity analysis and response identification. All basic parameters associated with modeling of the superstructures are similar to those of SDOF models, as noted above, except that NLTHAs were done only for the PGA-matched set of GMs (as detailed in section 3.3.1), and only one backbone curve was examined.

Effects of FFS were modeled using some linear springs at the base of 2DOF systems in each horizontal direction. Two levels of relative stiffness of the base to the stiffness of the superstructure were considered; namely, 200% and 400%. Also, two different values for foundation to superstructure mass ratios were considered to account for the mass of the foundation and mass of the soil that moves in phase with the foundation/pile group, at the bases of the structure. These were foundation to superstructure mass ratios of 15% and 25%. The analyses were run for five different levels of input motions using five different amplitude scale factors applied to input GMs. Table 3-2 summarizes different analyses performed on 2DOF systems, accounting for various permutations of above-mentioned parameters.

Table 3-2: Summary of 2DOFmodels NLTHA

<table>
<tr><td colspan="3">Elastic period of vibrations</td><td>12</td></tr>
<tr><td colspan="3">Strength characteristic</td><td>11</td></tr>
<tr><td colspan="3">Backbone curves</td><td>1</td></tr>
<tr><td colspan="3">System damping ratio</td><td>1</td></tr>
<tr><td colspan="3">GM set "1"</td><td rowspan="7">280</td></tr>
<tr><td rowspan="5">FN component</td><td>NF GM</td><td>40</td></tr>
<tr><td>FF GM</td><td>40</td></tr>
<tr><td>Filtered pulse*</td><td>40</td></tr>
<tr><td>Extracted pulses *</td><td>40</td></tr>
<tr><td>Residual pulse*</td><td>40</td></tr>
<tr><td rowspan="2">FP component</td><td>NF GM</td><td>40</td></tr>
<tr><td>FF GM</td><td>40</td></tr>
<tr><td colspan="3">Foundation stiffness ratio</td><td>2</td></tr>
<tr><td colspan="3">Foundation mass ratio</td><td>3</td></tr>
<tr><td colspan="3">Earthquake intensity level</td><td>4</td></tr>
<tr><td colspan="3">Number of 2DOF total analyses</td><td>887 040</td></tr>
</table>

*For definition of filtered pulse, extracted pulse using wavelet analysis, and residual pulse, refer to section 3.3.1.

Results of NLTHA of 2DOF systems are presented in Chapter 5.

3. Nonlinear 3D-MDOF model

A comprehensive three-dimensional (3D) MDOF model of a bridge structure supported on pile groups is used to validate a simplified method proposed for consideration of combined effects of NF GMs and FFS. The nonlinearity and hysteretic behaviour of the system is again idealized using discrete hinge models.

Details of the MDOF mathematical model and its NLTHA results are presented in Chapter 6.

3.3 Parametric study and sensitivity analysis

To determine the effect of variability of important seismic parameters on nonlinear responses of structures subjected to combined effects of NF GMs and FFS, an extensive parametric study and sensitivity analysis was conducted. The parametric studies and sensitivity analysis were performed over a practical range of important seismic parameters to account for variability of

- Input motions
- Intensity of input motions
- Elastic period of vibration
- Strength characteristic
- Damping ratio
- Hysteresis behaviour

General results of these parametric studies and sensitivity analysis are available in Chapters 4 and 5.

The following subsections briefly explain the selected range of each parameter considered in various NLTHAs.

3.3.1 Input motions

Some aspects of selected NF GMs and their FF GM counterparts are summarized below

1. all GMs are selected from verified recorded strong motion databases, (i.e., no synthetic GM)
2. special attention was given to unique properties of each NF GM (and also to the selection of their FF GM counterparts to make sure the frequency content of the input motions and their dominant pulse period remains unchanged
3. all NF GMs are associated with forward directivity pulses, originated form crustal earthquakes

Since the quality of the results of all NLTHA conducted throughout the course of this study is directly related to the quality of the selected input motions, special care was exercised to select a comprehensive set of GMs that can reasonably represent the generic properties of NF GMs (and their FF GM counterparts) for moderate to strong earthquakes.

In general, the time history GMs to be used for analysis and design of any type of structure need to be selected with consideration of tectonic environment, fault mechanism, earthquake magnitude, source to site distance, and soil conditions. Consideration of all these parameters for selection of design ground motions, even for a specific site, is not always practical. This is partly attributed to the complexity of a model that can account for all the above parameters and partly to the limited number of NF GMs.

Amongst the above parameters, site class, magnitude of earthquake, and site to source (or fault) distance were recognized as the most important parameters that should be considered in selection of input GMs for this project. These parameters are selected because they tend to have more effect on the frequency content, shape of the response spectrum, duration of the strong shaking, and NF GM characteristics of the input motions.

3.3.1.1 Pairing techniques

To study the effect of NF GMs on inelastic response of the structures, a comparable baseline is required. This baseline may consist of inelastic responses of the same structures to some compatible FF GMs. Thus, the challenge of selecting a suite of reliable NF GMs that can reasonably represent the generic properties of a wide variety of NF GMs is also coupled with the challenge of selecting a suite of compatible FF GMs that can be properly paired with the selected suite of NF GMs.

To address this issue, two different pairing techniques have been adopted, namely,

1. Pairing in a way to have each member of selected NF GMs matched with one (and only one) member of the selected FF GMs, or
2. Pairing in a way to have a general agreement between averaged properties of the selected NF GMs with those of the selected FF GMs.

Indeed, each of these pairing techniques has their own pros and cons. Therefore, to minimize the uncertainties associated with selection of compatible NF and FF GMs, two groups of GMs were selected in a way that the selection criteria for each group falls in line with one of the above-mentioned pairing techniques.

In general, the criteria for selection of the first group of GMs, hereafter called “PGA - matched GMs”, was set in a way that each selected NF GM has a counterpart FF GM that is originated from the same event that the NF GM is originated from and has a very close PGA to the PGA of its NF GM pair. Details of selection criteria and selected PGA-matched GMs are presented in Appendix F.

On the other hand, the general criteria for selection of the second group of GMs, hereafter called “linearly scaled GMs”, was set to have the geometric mean of response spectra of each suite of (linearly scaled) NF GMs and (linearly scaled) FF GMs closely match a target response spectra (i.e., the NBCC2010 response spectrum of Vancouver, BC; Site Class “C”), for the period range of 0.15 to 2.0 s. Details of selection criteria and selected linearly scaled GMs are presented in Appendix G.

3.3.1.2 Signal processing (modified near-fault GMs)

As an interim objective, it was decided to study the effect of long period velocity pulses on nonlinear response of the structures and see if the NF effects on nonlinear response of the structures are mainly associated with the long period velocity pulses, or if residual signal (NF GMs minus their pulses) have some distinguishable effect on nonlinear response of structures as well. To achieve this goal, all PGA-Matched NF GMs were processed and each NF GM was decomposed into two components, namely, (1) a pulse signal and (2) a residual signal.

Comparison of results of NLTHA of original NF GMs, their extracted pulses, and their residual signals with results of NLTHA of FF GMs reveals how much of response amplifications associated with NF GMs is attributed to long-period pulses and how much of it is attributed to (the nature, amplitude, and frequency content of NF GMs that remains) the residual signals.

To extract the long-period velocity pulses from the recorded NF GMs, two different approaches were adopted: (1) frequency domain filtering and (2) wavelet analysis.

Frequency domain filtering is a rudimentary process for extracting long-period pulses. This process uses standard filtering techniques based on Fourier transform functions of input motions to reach a series of harmonic signals. The Butterworth low-frequency pass filter function was used for processing the signals and for extracting the low-frequency content of the NF GMs. Details of the filtering procedure and filtered NF GMs are presented in Appendix H. This set of GMs is called Low-Pass Frequency NF GMs (LPFNF GMs), see Figure 3.2.

Wavelet analysis is a much more refined process in comparison with the filtering process. Wavelet analysis is based on wavelet signal decomposition of input motions using the Baker (2007) algorithm allowing for identification and extraction of pulselike features from NF GMs. The Mathlab subscript offered on Jack Baker's research group website (see http://www.stanford.edu/~bakerjw/pulse-classification_old.html) was used to allow for implementation of Baker's proposed wavelet signal analysis method.

Figure 3.2 depicts the extracted pulse acceleration signals for the FN component of the 1979 Imperial Valley earthquake (NGA#171), using wavelet analysis and also standard Butterworth low-frequency pass filtering techniques.

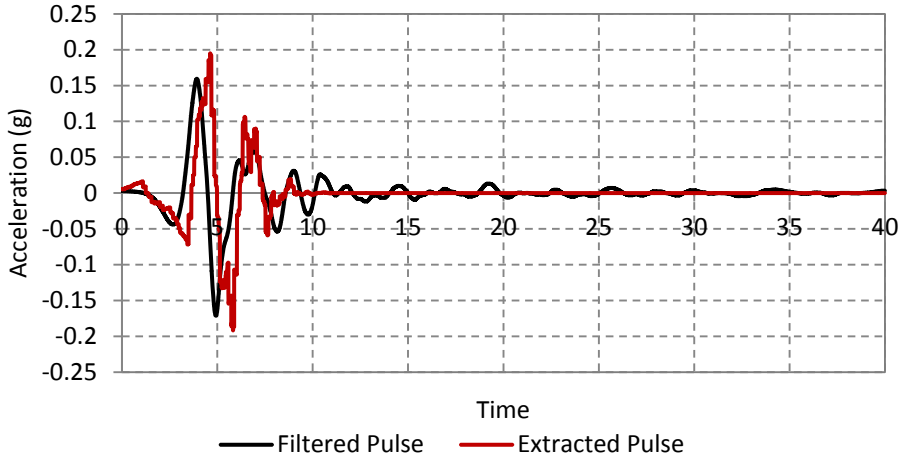

Figure 3.2: NF GM pulse for 1979 Imperial Valley earthquake (NGA# 171, M_w = 6.53). Red curve: the extracted pulse using wavelet analysis technique calculated through the Mathlab subscript prepared by the Baker research group. Black curve: the extracted low-frequency content of acceleration GMs using a standard Butterworth low-frequency pass filter.

3.3.2 Intensity of input motions

To have a better understanding of the effect of different intensity levels of input ground motion on displacement demands (and similarly on ductility demands), a series of Incremental Dynamic Analyses (IDA) were performed, where the input ground motions were amplitude scaled from 1.0 to 5.0.

The larger scale factors were used to assure development of the nonlinear response of long-period systems. (Note: As mentioned in section 2.1.2.2, the periods of NF GM pulses are strongly correlated with the moment magnitude of the causative events, i.e. the expected value of the natural logarithm of the pulse period is linearly dependent on Mw, see equation 2 3. That is to say, if the magnitude of an event increases, both the amplitude of the peak response spectrum and the pulse period are expected to be increased. However, in this IDA, only linear scaling was used to scale the amplitude of an event up or down, without making any change to the pulse period. Hence, although these IDAs can shed some light on the possible inelastic response of the structures to different magnitudes of selected input

motions, their results for NF GMs should be taken with cautious, as no pulse period adjustment is considered.)

3.3.3 Elastic period of vibration

The primary elastic period range of SDOF systems is set from 0.2 to 2.4 s. Hence, idealized models were generated for 12 discreet values with 0.2 s intervals.

While the effect of NF GMs on response of very long-period structures might be of paramount importance, yet it was decided to opt out investigation of those systems in this study because

a) Long-period structures are usually important structures whose design requires extensive analysis with special attention to particularities of the site and the structure.
b) Estimation of the nonlinear response of long-period structures (due to material nonlinearities) could be approximated by standard linear analysis procedures without losing that much of accuracy.
c) FFS has much less (if any) effect on long-period structures.
d) The effect of higher modes on response of long-period structures to input motions and especially to (NF GMs) is important.

It is of note that Sasani and Bertero (2000) also indicated that unlike what is inferred by the near-source amplification factor introduced by the UBC-97, the effect of NF GMs on short- and medium-period structures may be as critical as on long-period structures.

3.3.4 Strength characteristic

To investigate the effect of yield level (strength characteristic, C_y) on nonlinear response of the systems subjected to NF GMs, the idealized systems were modeled using 10 different values of C_y, ranging from 5.0% to 45% with 5.0% intervals.

While the lower bound of selected strength characteristics is substantially less than the values recommended by the codes, they are deemed to be representative of

some old constructions which were built with less attention to seismic demands or whose capacity has deteriorated over time.

3.3.5 Viscous damping

The most common sources of damping in ordinary structures are Coulomb damping, foundation damping, and hysteretic damping. Since explicit modeling of nonlinear hinges in this project directly accounts for the effect of hysteretic damping, the variation of this type of damping is expected to be captured using different backbone curves (hysteresis behaviour), as detailed in section 3.3.6.

However, to account for variation of the compound effects of foundation damping and Coulomb/friction damping, two levels of equivalent viscous system damping ratios were considered and used in all NLTHA of this project; namely: $\zeta = 2\%$ and $\zeta = 5\%$.

3.3.6 Hysteretic behaviour of the structure and ductility consideration

Hysteretic behaviour of the systems is modeled using discrete nonlinear link/hinge elements at the base of the SDOF, 2DOF, and MDOF models.

The following subsections briefly describe different hysteresis models used in FEM models during the course of this research project.

3.3.6.1 Inelastic discrete links used for simplified SDOF and 2DOF models

To evaluate the effect of hysteretic behaviour of inelastic models on the response of the structures subjected to NF GMs, a series of sensitivity analyses using five different sets of inelastic discrete link models was performed. While each set of selected inelastic discrete link models demonstrates different unloading patterns and degradation regimes, they all have similar backbone curves, which in general follow the very basic principles of idealization of a system nonlinear behaviour as depicted in Figure 3-3.

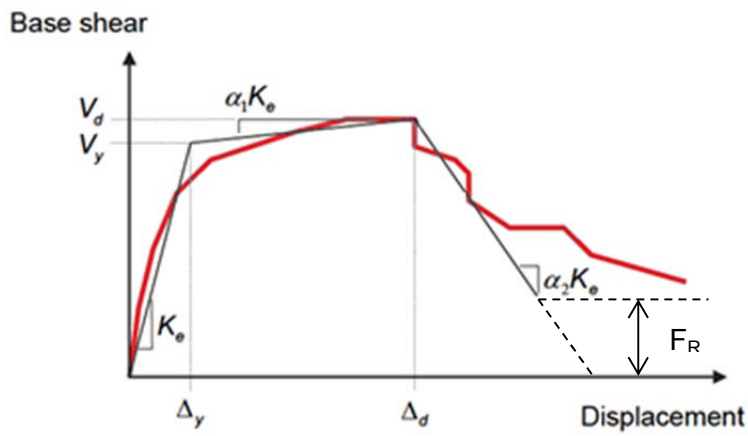

Figure 3-3: Idealized force-displacement/Backbone curve

As shown in Figure 3-3, in general an idealized backbone curve needs to account for the effective elastic lateral stiffness (K_e), effective yield strength (V_y), the effective post-yield positive (α_1) and/or negative (α_2) stiffnesses, and the residual strength capacity (F_R).

The effective post-yield positive stiffness (α_1) accounts for strain hardening after yield onset. In this project, for all five sets of inelastic discrete link models, a value of 10% is assigned to α_1.

The post-yield negative stiffness (α_2) accounts for strength and stiffness-degrading behavior of structures in which lateral stiffness and lateral strength decrease when a system is subjected to cyclic reversals. Typically, α_2 should be set to account for two different phenomena:

a) P-Δ effects (using some apparent negative stiffness)

b) Stiffness and strength degradation due to material deterioration because of cyclic damage under high inelastic demands

It is of note that P-Δ effects are equivalent to a type of strength degradation that occurs in every cycle of motion. Hence, they should be modeled using in-cycle stiffness degradation routines.

Conversely, cyclic degradation of the stiffness and strength needs to be accounted for in every subsequent cycle. Thus, strain-related stiffness and strength degradation should be modeled using cyclic degradation routines.

In this project, and for all five sets of inelastic discrete link models, a value of (–5%) is assigned to α_2.

Table 3-3 lists the inelastic discrete link models used in this research, and it also briefly highlights important features of each inelastic discrete link model.

Table 3-3: Summary of inelastic discrete links used for simplified SDOF and 2DOF models

Inelastic discrete links models	Properties
Nonlinear Link Type #1 (NLT#1)	• Bilinear lumped plasticity model o K_e = Elastic stiffness o K_s = post yield stiffness = 10% K_e • With coupled properties in two horizontal directions
Nonlinear Link Type #2 (NLT#2)	• Tri-linear lumped plasticity model o K_e = Elastic stiffness o K_s = 10% K_e (1) o K_t = –5% K_e (2) o $\Delta_d = 6\Delta_y$ • Uncoupled properties • Complete with in-cycle stiffness and strength degradation but NO cyclic degradation
Nonlinear Link Type #3 (NLT#3)	• Tri-linear lumped plasticity model o K_e = Elastic stiffness o K_s = 10% K_e (1) o K_t = – 5% K_e (2) o $\Delta_d = 6\Delta_y$ • Uncoupled properties • Complete with both in-cycle and cyclic stiffness and strength degradation

Inelastic discrete links models	Properties
Nonlinear Link Type #4 (NLT#4)	• Quadri-linear lumped plasticity model o K_e = Elastic stiffness o K_s = 10% K_e (1) o K_t = –5% K_e (2) o $\Delta_d = 3\Delta_y$ o $F_R = 0.25\ F_y$ (3) • Uncoupled properties • Complete with in-cycle stiffness and strength degradation but NO cyclic degradation
Nonlinear Link Type #5 (NLT#5)	• Quadri -linear lumped plasticity model o K_e = Elastic stiffness o K_s = 10% K_e (1) o K_t = –5% K_e (2) o $\Delta_d = 3\Delta_y$ o $F_R = 0.25F_y$ (3) • Uncoupled properties • Complete with both "in-cycle" and "cyclic" stiffness and strength degradation

(1) Post-yield stiffness
(2) Apparent negative stiffness starting at Δ_d
(2) Residual strength

Ideally each of these five sets of nonlinear link elements should be able to capture the salient hysteretic behaviour and nonlinear characteristics of a system that is typically available in practice, although none of them is an exact resemblance of any one specific material or structural system.

For details of nonlinear dynamic properties of each inelastic discrete link model, as named above, refer to Appendix E.

3.4 Monitored and reported engineering design parameters

Monitored (and calculated) engineering design parameters in this research are mainly selected based on the key EDPs (i.e., maximum displacement demands)

required for performance design or performance evaluations of a structure. Results of analysis are reported in two main categories, namely,

1. Category #1: median and standard deviation values for maximum EDPs of interest; for example median and standard deviation of maximum displacements due to NF GMs and FF GMs; and
2. Category #2: mean and standard deviation values of $\mathrm{EDP.Ratios}$, where $\mathrm{EDP.Ratio}$ is defined as

$$\mathrm{EDP.Ratio} = \left[\frac{\mathrm{EDP\ due\ to\ NF-GM}}{\mathrm{EDP\ due\ to\ a\ compatible\ FF-GM}}\right] \qquad 3\text{-}1$$

While results of category #1 outputs can improve our understanding of nonlinear response of different structures due to NF and FF GMs, they cannot be directly used for practical design purposes.

Conversely, results of category #2 outputs are expected to assist design engineers to readily assess the effect of NF GMs on EDPs of interest, based on EDPs due to FF GMs.

That is to say, one would be able to closely approximate an EDP of interest due to NF GMs from those due to FF GMs (determined from code provisions), if one knew what statistical relationship is in effect between those two parameters, i.e., if one knows the distribution parameters of the EDP Ratio of interest.

Determining distribution parameters of the EDP Ratio of interest is a trivial task if each member of the suite of NF GMs has one and only one counterpart in the suite of FF GMs, which is the case for the suite of PGA-matched GMs in this project. Thus, for the suite of PGA-matched GMs, the ratio of EDPs of interest due to NF GMs to those due to FF GMs was directly determined for each pair of NF and FF GMs, and a proper distribution was fitted over the data. To find the best distribution fit and distribution parameters, the EDP Ratio of interest for the suite of PGA-matched GMs, several sets of results of NLTHA were fed into “@RISK” software, a commercially available risk analysis and simulation program. Results of analysis by @RISK showed that the log-normal distribution is one the best fits over the entire range of input data.

However, calculation of distribution parameters of the EDP.Ratio of interest for linearly scaled GMs was not a trivial task because for linearly scaled GMs a one-to-

one relationship between members of the suite of NF GMs and members of the suite of FF GMs does not exist. For this case, as equation 3-1 indicates, EDP.Ratio is a function of two random variables, namely, EDP due to NF GMs and EDP due to its compatible FF GMs. Therefore, to determine the distribution parameters of the EDP.Ratio for a suite of linearly scaled GMs, one needs to know the best distribution model that fits EDPs due to NF GMs from those due to FF GMs. Again, to find the best distribution fit and distribution parameters of EDPs of interest, "@RISK" software was used. Results of analysis of @RISK again showed that the log-normal distribution is one the best fits over the entire range of EDPs of interest (both for NF GMs and FF GMs). For example, Figure 3-4 shows results of @Risk distribution fitting for maximum displacement demand of a system subjected to Fault-Normal components of FF-GMs when elastic period of the system is 0.6 Sec, strength characteristic of the system is %20, and the nonlinearity of the system is modeled with LNK#4.

Knowing the distribution of input random variables, one may use the following procedure, developed mainly based on Taylor multivariable expansion series, to approximate the EDP.Ratio, as defined in equation 3-1.

$$Z_{\text{EDP.Ratio}} = \frac{X}{Y} \qquad \text{3-2}$$

where X is the EDP due to NF GMs and Y is the EDP due to FF GMs (both are log-normally distributed random variables).

Now if one applies the Taylor second-order expansion series about the point, (μ_x, μ_y), where μ_X is the expected value of EDP due to NF GMs and μ_Y is the expected value of EDP due to FF GMs, to the right side of equation 3-2, one gets:

$$Z_{\text{EDP.Ratio}} \approx \frac{\mu_x}{\mu_y} + \frac{(X-\mu_x)}{\mu_y} - \frac{\mu_x}{{\mu_y}^2}(Y-\mu_y) + \frac{1}{2}\left[(X-\mu_x)^2 \times \frac{0}{\mu_y} - \frac{2(X-\mu_x)(Y-\mu_y)}{{\mu_y}^2} + \frac{2\mu_x(Y-\mu_y)^2}{{\mu_y}^3}\right] \qquad \text{3-3}$$

Taking the expectation of both sides of equation 3-3, one can calculate

$$E(Z_{\text{EDP.Ratio}}) \approx \frac{\mu_x}{\mu_y} + \frac{E[X-\mu_x]}{\mu_y} - \frac{\mu_x}{{\mu_y}^2} E\left[Y-\mu_y\right] + -\frac{E\left[(X-\mu_x)(Y-\mu_y)\right]}{{\mu_y}^2} + \frac{\mu_x E\left[\left(Y-\mu_y\right)^2\right]}{{\mu_y}^3} \quad \text{3-4}$$

Knowing that

$$E[X-\mu_x] = E\left[Y-\mu_y\right] = 0 \quad \text{3-5}$$

$$E\left[(X-\mu_x)(Y-\mu_y)\right] = Cov(X,Y) \quad \text{3-6}$$

$$E\left[\left(Y-\mu_y\right)^2\right] = VAR(Y) \quad \text{3-7}$$

where $VAR[X]$ is variance of x and $Cov(X,Y)$ denotes covariance of X and Y. Thus, one may rewrite equation 3-4 as:

$$E(Z_{EDP.Ratio}) = E\left(\frac{X}{Y}\right) \cong \frac{E(X)}{E(Y)} - \frac{Cov[X,Y]}{E(Y)^2} + \frac{E(X)}{E(Y)^3} \times VAR[Y] \quad \text{3-8}$$

Similarly, using the multivariate Taylor expansions procedure, the variance of the probability ratio of $[X/Y]$ can be approximated as

$$VAR(Z_{EDP.Ratio}) \cong \left(\frac{\partial E(X/Y)}{\partial X}\right)^2_{\mu_x} \times VAR(X) + \left(\frac{\partial E(X/Y)}{\partial Y}\right)^2_{\mu_y} VAR(Y) + 2\left(\frac{\partial E(X/Y)}{\partial X}\right)_{\mu_x} \left(\frac{\partial E\left(\frac{X}{Y}\right)}{\partial y}\right)_{\mu_y} \times Cov(X,Y) \quad \text{3-9}$$

$$VAR(Z_{EDP.Ratio}) \cong \frac{1}{{\mu_y}^2} \times VAR(X) + \frac{{\mu_x}^2}{{\mu_y}^4} \times VAR(Y) - 2\frac{\mu_x}{{\mu_y}^3} \times Cov(X,Y) \quad \text{3-10}$$

$${\sigma_{Z_{EDP.Ratio}}}^2 \cong \left(\frac{\mu_x}{\mu_y}\right)^2 \left[(CV[X])^2 + (CV[Y])^2 - \frac{2 \times Cov[X,Y]}{\mu_x \times \mu_y}\right] \quad \text{3-11}$$

$$\sigma_{Z_{EDP.Ratio}} \cong \frac{\mu_x}{\mu_y} \times \sqrt{\left[(CV[X])^2 + (CV[Y])^2 - \frac{2 \times Cov[X,Y]}{\mu_x \times \mu_y}\right]} \quad \text{3-12}$$

where, $CV[x]$ denotes coefficient of variation of random variable x and $\sigma_{Z_{EDP.Ratio}}$ denotes the standard deviation of the EDP.Ratio.

Up to this point, the mean and variance of the EDP.Ratio, $E[Z_{EDP.Ratio}]$ and $VAR(Z_{EDP.Ratio})$, respectively, have been determined from

equations 3-8 and 3-11. Now, to be able to determine the EDP.Ratio as defined in equation 3-1, it is necessary to determine the median value of $[X/Y]$, $M[Z_{EDP.Ratio}]$.

Knowing that EDPs of interest due to NF GMs and FF GMs (*X* and *Y*) are log-normally distributed, using central limit theorem, one can show that ($Z_{EDP.Ratio}$) is also log-normally distributed. Thus,

$$E(Z_{EDP.Ratio}) = e^{\mu+\sigma^2/2} \qquad 3\text{-}13$$

$$VAR(Z_{EDP.Ratio}) = \left(e^{\sigma^2} - 1\right)\left(e^{2\mu+\sigma^2}\right) = \left(e^{\sigma^2} - 1\right) \times \left[E(Z_{EDP.Ratio})\right]^2 \qquad 3\text{-}14$$

where μ and σ are the mean and standard deviation of $\mathrm{Ln}(Z_{EDP.Ratio})$ and $Ln(\ldots)$ denotes the function of the natural logarithm.

Using equations 3-13 and 3-14, one would be able to determine μ and σ in terms of the known median and variance of $Z_{EDP.Ratio}$, namely:

$$\sigma^2 = ln\left(\frac{VAR(Z_{EDP.Ratio})}{E[Z_{EDP.Ratio}]^2} + 1\right) \qquad 3\text{-}15$$

$$\mu = ln(E[Z_{EDP.Ratio}]) - \frac{\sigma^2}{2} = ln\left(\frac{E[Z_{EDP.Ratio}]^2}{\sqrt{VAR(Z_{EDP.Ratio}) + E[Z_{EDP.Ratio}]^2}}\right) \qquad 3\text{-}16$$

Thus, the median of $Z_{EDP.Ratio}$ could be determined as

$$M[Z_{EDP.Ratio}] = e^{\mu} = \frac{E[Z_{EDP.Ratio}]^2}{\sqrt{VAR(Z_{EDP.Ratio}) + E[Z_{EDP.Ratio}]^2}} \qquad 3\text{-}17$$

From distribution, mean, median, and variance of $[X/Y]$, one would be able to estimate the EDP of interest due to NF GMs from the same due to FF GMs for any desired level of confidence (i.e., probability of not exceeding).

Problem example #3-1 shows how distribution properties of ductility and displacement ratios can assist practicing engineers to estimate the effect of NF GMs on the response of a given structure.

Problem example #3-1:
Maximum roof displacement and maximum ductility demand of a structure, designed based on current code provisions, is required to be estimated considering adverse effects of a probable NF GM.
Assumptions*:*
1. System properties, including, elastic period of vibration (T_e), target ductility (μ_{Target}) *or* (μ_{design}) and strength characteristics $(C_y = \left[\frac{Capacity\ of\ the\ structure}{Seismic\ weight}\right] \cong \left[\frac{Design\ Base\ Shear}{Seismic\ weight}\right])$ of the structure are known (i.e., one can determine them from the code or from the design standard procedures)
2. Median and variance of the Inelastic Displacement Demand Ratio (IDDR), M_{δ_R} and σ_{δ_R}, are both available from results of this research 3. Similarly, median and standard deviation of Ductility Demand Ratio (DDR), M_{μ_R} and σ_{μ_R} are both available from results of this research Note: M_{δ_R} , σ_{δ_R} , M_{μ_R}, and σ_{μ_R} are all functions of $(T_e$ &and $C_y)$ and/or $(T_e$ and $\mu_{design})$. See the following chapters.
Solution:
1. Determine expected maximum roof displacement for FF GMs, δ_{FF-GMs}, using a code-based simplified method. *Let's call this* δ_{FF-GMs} 2. Determine M_{δ_R} , σ_{δ_R} , M_{μ_R}, and σ_{μ_R} values based on either $(T_e$ and $\mu_{design})$ or $(T_e$ and $C_y)$ from results of this research. 3. Approximate the expected maximum roof displacement demands for the target NF GMs, as below: $$\delta_{NF-GMs} = \delta_{FF-GMs} \times M_{\delta_R}$$ 4. Approximate the expected ductility demands for the target NF GMs, as below: $$\mu_{NF-GMs} = \mu_{design} \times M_{\mu_R}$$
Note*:*

Problem example #3-1:
Estimated EDPs in steps 3 and 4 are based on median values of IDDR or DDR; hence there is ~50% chance that M_{δ_R} or M_{μ_R} underestimate δ_{NF-GMs} and μ_{NF-GMs}, respectively. To have more confidence in estimated δ_{NF-GMs} one may select a given confidence level for estimation of maximum roof displacement due to NF GMs, denoted *P* (when *P* is a number between 0.00% and 100%). Then, the variance of the natural logarithm of IDDR is calculted using equation 3-15, as below: $$\sigma^2 \cong ln\left(\frac{\sigma_{\delta_R}{}^2}{\mu_{\delta_R}{}^2}+1\right)$$ Now, having σ available, one may estimate δ_{NF-GMs} for a target quantile as below: $$\delta_{NF-GMs} \cong \delta_{FF-GMs} \times M_{\delta_R} \times e^{[\sigma \times \Phi^{-1}(P)]}$$ where Φ^{-1} is the quantile function, i.e., the inverse cumulative distribution function of a standard normal distribution. In the same manner, one may also calculate the expected ductility demands due to NF GMs for a target quantile by calculating the standard deviation of natural logarithm of the ductility demand ratios and following the same procedure as was used above.

Table 3-4 gives a list of monitored EDPs and EDP Ratios reported in Chapters 4 and 5.

Table 3-4: Summary of reported EDP and EDP.Ratios

Item #	Description
1	"Maximum Displacement Demands" and "Inelastic Displacement Demand Ratio" (IDDR) See section 3.4.1.
2	"Maximum Ductility Demand" and "Ductility Demand Ratio" (DDR) in Terms of strength See section 3.4.2.
3	"Yield Capacity Demand" and "Yield Capacity Demand Ratio" (YCDR) See section 3.4.3.
4	"Maximum Inelastic to Elastic Displacement Demand" and "Maximum Inelastic to Elastic Displacement Demand Ratio" see section 3.4.4

Also, sections 3.4.1 to 3.4.4 briefly explain each of these EDP or EDP Ratios, and describe the motivation behind choosing each of them by explaining how they might be used in an actual design procedure.

(A)

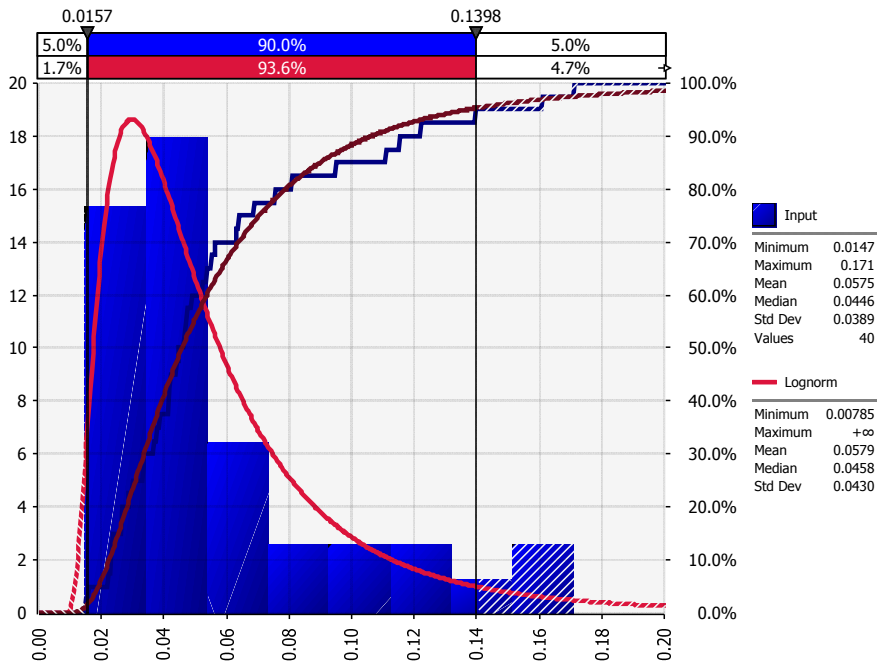

(B)

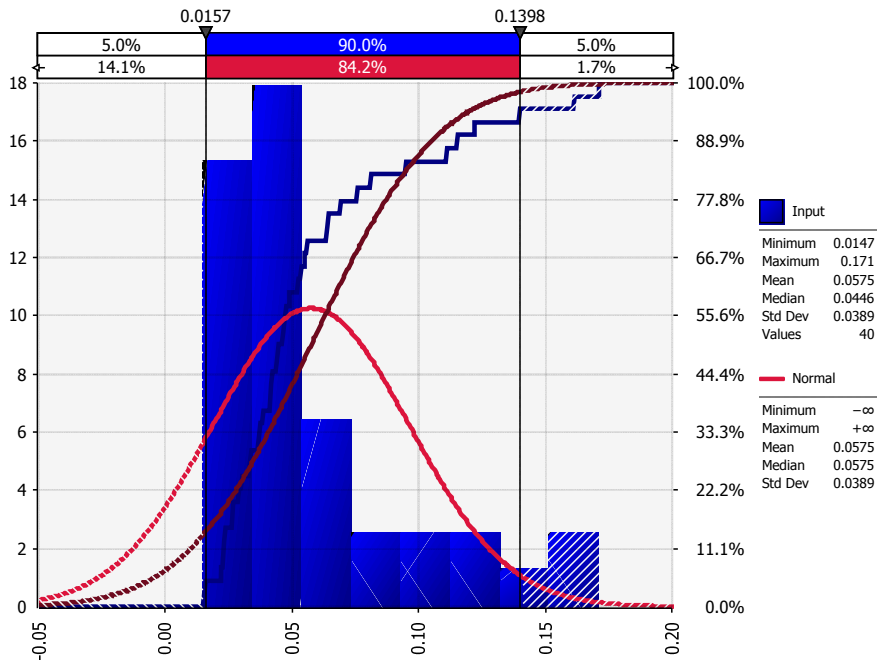

Figure 3-4: Distribution fitting for LNK#4 | FF-FN | Te=0.6 & Cy=0.2 | Figure (A): Log-Normal Distribution & Figure(B): Normal Distribution

3.4.1 Displacement demands

Maximum displacement demand is a key parameter in both analysis and design of the structures. For example, this parameter is required for the following:

- displacement controlled pushover analysis
- displacement-based and performance-based seismic design of the structures
- evaluation of displacement serviceability and/or ultimate limit states, considered at local and global levels, as required by most codified stress-based design approaches, etc.

Thus, the median and variance values for both NF and FF GMs are reported for the entire range of parameters considered, as detailed in sections 3.2 and 3.3.

Similarly the ratio of maximum displacement demand due to NF GMs to maximum displacement demand due to FF GMs is defined as IDDR, and its median and variance values are determined and reported; i.e., analogous to equation 3-1, IDDR is denoted as δ_R, and defined as

$$\delta_R = \left[\frac{\delta_{NF-GMs}}{\delta_{FF-GMs}}\right] \qquad 3\text{-}18$$

Knowing the distribution model and distribution parameters of IDDR, one would be able to simply prorate the maximum displacement demands determined for the FF GMs and approximate the maximum displacement demand due to NF GMs.

A practical example of using IDDR distribution (and its distribution parameters) is when one wants to evaluate the effect of NF GMs on the maximum displacement demand of an existing structure which:

a. is designed based on the current (or a specific) code procedures and has a fundamental period of T_e,
b. has an ultimate capacity of $R_y \times S_a \times W$; when R_y is defined as the code-based yield-strength reduction factor and S_a is an equivalent

spectral response acceleration (accounting for response of all important modes of vibration of the structure),[1]

c. is expected to have a maximum displacement demand of δ_{FF-GMs} based on the code design displacement response spectra (developed based on FF GMs).[2]

A simple solution to this problem is similar to the proposed solution of the Problem Example #3-1, i.e., δ_{NF-GMs} could be estimated as

$$\delta_{NF-GMs} = \delta_{FF-GMs} \times \text{Median}(\delta_R) \times e^{[\sigma_\delta \times \Phi^{-1}(P)]} \qquad 3\text{-}19$$

where

$$\sigma_\delta = ln\left(\frac{{\sigma_{\delta_R}}^2}{[\text{Median}(\delta_R)]^2} + 1\right) \qquad 3\text{-}20$$

It is of note that $\text{Median}(\delta_R)$ and σ_{δ_R} are scalar values, which are extracted from results presented in Chapters 4 and 5 and are functions of T_e and C_y of the system (properties of the existing structure).

3.4.2 Ductility demands

Based on target performance of the structures, usually design criteria either (implicitly or explicitly) limit the expected damage by means of limiting the maximum ductility demand or the maximum displacement/inter-story drift of the structures.

Generally speaking, a satisfactory seismic design needs to allow for some local and/or global ductility capacities that exceed the expected maximum ductility demands.

---

[1] For simple structures where the first mode of vibration governs the response, S_a is the code specified elastic spectral acceleration at the first mode of vibration in the direction of interest.

[2] For standard structures with reasonable elastic periods of vibration, (usually) constant displacement rule governs; thus, δ_{FF-GMs} can be approximated with the elastic displacement of the system, determined as $\delta_{FF-GMs} \cong S_a \times g \times (T/2\pi)^2$

While ductility capacity is a function of section/system properties, which could be easily tested or numerically evaluated for a given section, the - expected maximum ductility demand is a function of input motions, which vastly depends on the type of input GMs, i.e., NF or FF.

Thus, variation of maximum ductility demand due to NF GMs compared with those due to FF GMs is recognized as another key parameter to be reported in this research.

To determine the maximum ductility demand, the maximum displacement demand of each system (as discussed in the previous section) was normalized by yield displacement of the system, when yield displacement (δ_y, – determined from equation 3-22) is defined as the ratio of the strength characteristic of the system to the elastic stiffness of the system. Elastic stiffness of the system is determined from equation 3-21:

$$K_e = \left(\frac{2\pi}{T_e}\right)^2 \times \frac{W}{g} \qquad \text{3-21}$$

$$\delta_y = \frac{C_y \times W}{K_e} = \left(\frac{T_e}{2\pi}\right)^2 \times C_y \times g \qquad \text{3-22}$$

The ratio of maximum ductility demand due to NF GMs (μ_{NF-GMs}) to maximum ductility demand due to FF GMs (μ_{FF-GMs}) is defined as DDR and denoted as μ_R:

$$\mu_R = \left[\frac{\mu_{NF-GMs}}{\mu_{FF-GMs}}\right] \qquad \text{3-23}$$

A practical example of using $Median(\mu_R)$ and σ_{μ_R} is when one wants to know the effect of NF GMs on the maximum ductility demand of an existing structure with some known properties, including its T_e , C_y and μ_{FF-GMs} The procedure of determining μ_{NF-GMs} from μ_{FF-GMs} is similar to what is described in the practical example # 3-1 detailed in section 3.4.

3.4.3 Capacity demand

Yield capacity demand is defined as minimum yield capacity required for limiting the ductility ratio of a structure, subjected to certain input motions, to a specific ductility level, e.g.,. $\mu_{Target} = 2$.)

From the definition of yield capacity demand one can infer that the minimum required capacity demand is essentially dependent on three different factors as quoted above, namely:

1. Target ductility ratio, i.e., μ_{Target}
2. Structural properties, e.g., T_e
3. Inputinput motions, e.g., NF vs. FF GMs

Thus, in Chapters 4 and 5, minimum yield capacities (strength characteristics), required for limiting ductility demand ratios to some certain levels are presented for both NF and FF GMs (and for a wide variety of structural parameters as detailed in section 3.3).

If one wants to design a structure and size its members for a maximum ductility ratio of μ_{Target}, he may use the constant-ductility design spectrum as originally proposed by Newmark-Hall to determine the minimum yield capacity demands (refer to section 2.3.2). However, in this situation, if one decides to do so he should be aware that

1. The Newmark-Hall proposed relationship between R_y and μ_{Target} (see equation 2-4), widely adopted by codes and design guidelines for developing constant-ductility design spectrum, is primarily developed for FF GMs, and is not readily applicable to the nonlinear response of the structures subjected to NF GMs.[1]

[1] See, section 2.3.2 for the solution for extending applicability of Newmark-Hall equation to NF GMs, using normalized response spectra, proposed by Chopra and Chintanapakdee (2001).

2. Code-based design response spectrum is developed only based only on FF GMs. Hence, they cannot be used for NF GMs unless one changes their properties using one of the methods mentioned in section 2.3.2.

Thus, if one wants to use a code-based approach to calculate the minimum required yield capacity for a structure located in close proximity of an active fault (i.e., subjected to NF GMs) for a specific μ_{Target} , one may need to follow one of the approaches below.

Approach #1: Using a modified code-prescribed constant ductility design spectrum. Modifications to a code-prescribed constant ductility design spectrum need to be applied in the following order:

Step 1: Modify the code specified response spectrum to generate a new UHRS that accounts for NF GMs (based on Somerville or Baker's proposed methods). Here, this is, called NF-compatible UHRS."

Step 2: Normalize the period axes of NF-compatible-UHRS with respect to T_c, where T_c is the period separating the acceleration and velocity sensitive regions of UHRS, as proposed by Chopra and Chintanapakdee (2001), this will be called normalized NF-compatible UHRS.

Step 3: Use the Newmark-Hall method to generate a constant-ductility design spectrum from the normalizedNormalized NF-compatible UHRS",

Approach #2: alternatively one may elect to take a shortcut and prorate the minimum yield capacity demand calculated based on the code requirements (i.e., $F_{y_{FF-GMs}}$) to determine the minimum yield capacity demand for NF GMs (i.e., $F_{y_{NF-GMs}}$).

To take the latter approach one needs to use YCDR which is defined as the ratio of the minimum yield capacity demand due to NF GMs, $(Cy_{NF-GMs} \times W)$, to the minimum yield capacity demand due to FF GMs, $\left(Cy_{FF-GMs} \times W\right)$, for a given structure with some specific T_e and μ_{design} . Thus:

$$\text{YCDR} = \frac{F_{y_{NF-GMs}}}{F_{y_{FF-GMs}}} = \frac{Cy_{NF-GMs} \times W}{Cy_{FF-GMs} \times W} = \frac{Cy_{NF-GMs}}{Cy_{FF-GMs}} \qquad 3\text{-}24$$

The method of using YCDR to approximate the minimum required yield capacity due to NF GMs from that due to FF GMs is similar to what is used in the solution of Problem Example #3-1, for determining δ_{NF-GMs} from δ_{FF-GMs}.

For more information refer to 4.2.3.

3.4.4 Maximum inelastic to elastic displacement demand

Another interesting parameter, which can become handy in some performance evaluation, is the ratio of maximum inelastic to elastic displacement demand, $(\frac{\delta_{inelastic}}{\delta_{elastic}})$.

$(\frac{\delta_{inelastic}}{\delta_{elastic}})$ is an indicator of how well elastic analysis can approximate the maximum displacement response of a structure.

Most of design codes and guidelines introduce factors that explicitly take into account the ratio $(\frac{\delta_{inelastic}}{\delta_{elastic}})$, to estimate maximum inelastic displacements from elastic analyses. However, it seems that all these code-specified factors are produced using FF GMs with no specific attention to the particularities associated with NF GMs.

Thus, in this research, the ratio $(\frac{\delta_{inelastic}}{\delta_{elastic}})$ is reported for a wide range of structural parameters and for both NF and FF GMs.

Hence, now, one may simply prorate the code-specified maximum inelastic displacement response of a structure due to FF GMs with the ratio of $\left(\frac{\delta_{inelastic}}{\delta_{elastic}}\right)_{NF} \Big/ \left(\frac{\delta_{inelastic}}{\delta_{elastic}}\right)_{FF}$ to estimate maximum inelastic displacement response of a structure due to NF GMs. For more information refer to section 4.2.4.

4. Nonlinear response of simple structures to NF GMs

Chapter Outline:

1. Section 4.1 details the implemented procedure and important aspects of the parametric analysis conducted.
2. Section 4.2 discusses observations made through all NLTHA with various parameters considered
3. Section 4.3 discusses the results of NLTHA of processed signals, i.e., extracted pulses, residual pulses
4. Section 4.3.1 summarizes some salient findings of this chapter

---

As mentioned in past sections, to gain some insight into basic characteristics of the nonlinear response of simple structures to NF GMs, a range of fundamental parametric analysis of the dynamic nonlinear response of SDOF systems is performed. For the list and details of chosen parameters, please refer to section 3.3.

For the purpose of parametric analysis of the dynamic response of SDOF systems, a range of idealized (lollipop-shaped) SDOF models, corresponding to a typical column bent bridge section, with a fixed base and a lumped mass at the top, is generated, and used.

SDOF systems are modeled to account for nonlinearity of the systems using some discrete nonlinear hinge models at their bases. See Figure 4.1.

The effects of long-period velocity pulses on nonlinear response of the structures have been investigated by computing required strength, displacement demands, ductility demands, etc., for NF GMs and comparing them with the same for FF GMs.

The procedure implemented for analysis of SDOF systems is briefly discussed in section 4.1.

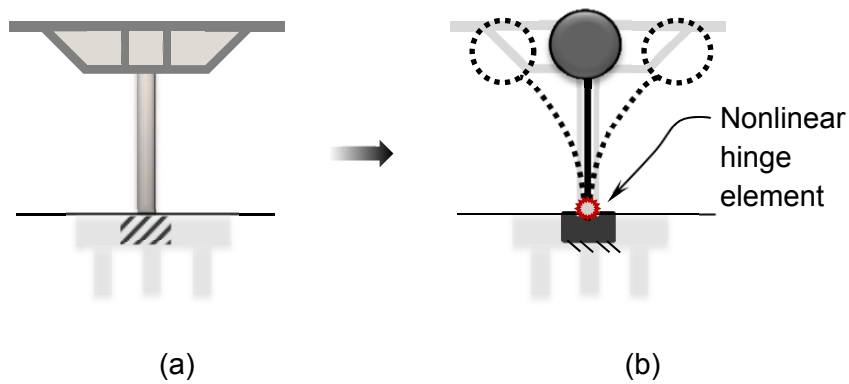

Figure 4.1: (a) Comprehensive model, (b) simplified SDOF system complete with a discreet nonlinear hinge element at its base

To allow for better understanding of the implemented procedure and the nature of monitored EDPs (and their variability), results of analysis of a representative SDOF system subjected to a representative NF GM (and its FF GM counterpart) are presented in Appendix C.

Also, to account for variability of monitored EDPs due to the full range of parameters adopted in this study, results of analysis of all SDOF models are presented in a generalized probabilistic context (as detailed in section 3.4). See section 4.2.

It is worthwhile to reiterate that having distribution parameters of EDP_{FF-GMs} and $EDP.Ratio$ would assist practicing engineers in prorating EDP_{NF-GMs} from EDP_{FF-GMs}., One may use equation 4-1 for such a purpose.

$$EDP_{NF-GMs} \cong EDP_{FF-GMs} \times M_{EDP.Ratio} \times e^{[\sigma_{EDP.Ratio} \times \Phi^{-1}(P)]} \qquad 4\text{-}1$$

4.1 Implemented procedure

Investigation of the effect of pulse-like NF GMs on performance of SDOF systems consisted of a comprehensive parametric analysis accounting for variation of input motions (i.e., NF vs. FF GMs), elastic period of vibrations, strength characteristic, system damping, and inelastic/hysteretic behavior (i.e., such as cyclic versus in-cycle degradation and/or non-degrading inelastic models). For details of each selected parameter please refer to section 3.3.

The procedure implemented for performing (the above-mentioned) parametric study is summarized below.

First, a range of SDOF mass-spring systems was developed. Developed models consist of 12 elastic and 120 inelastic systems using an NLT#1 inelastic model, as detailed in Appendix E.1, featuring

1. twelve different elastic periods of vibrations ranging from 0.2 to 2.4 s with 0.2 s intervals
2. ten different strength characteristics ranging from %5.0*W* to %50*W* with %5*W* intervals,

The same suite of SDOF systems described above was reproduced four more times to allow for consideration of NLT#2 to NLT#5 (as detailed in Appendix E.2 to Appendix E.3).

Table 4-1 summarizes different permutations of 12 different elastic periods of vibration and 10 different strength characteristics that are used in each suite of SDOF systems (EL denotes elastic SDOF models and NL denotes inelastic models – produced five times for NLT#1 to NLT#5).

Table 4-1: Details of 132 SDOF systems

		Elastic Periods (s)											
		0.2	0.4	0.6	0.8	1	1.2	1.4	1.6	1.8	2	2.2	2.4
$C_y = F_y/W$	∞	EL-121	EL-122	EL-123	EL-124	EL-125	EL-126	EL-127	EL-128	EL-129	EL-130	EL-131	EL-132
	0.5	NL-109	NL-110	NL-111	NL-112	NL-113	NL-114	NL-115	NL-116	NL-117	NL-118	NL-119	NL-120
	0.45	NL-97	NL-98	NL-99	NL-100	NL-101	NL-102	NL-103	NL-104	NL-105	NL-106	NL-107	NL-108
	0.4	NL-85	NL-86	NL-87	NL-88	NL-89	NL-90	NL-91	NL-92	NL-93	NL-94	NL-95	NL-96
	0.35	NL-73	NL-74	NL-75	NL-76	NL-77	NL-78	NL-79	NL-80	NL-81	NL-82	NL-83	NL-84
	0.3	NL-61	NL-62	NL-63	NL-64	NL-65	NL-66	NL-67	NL-68	NL-69	NL-70	NL-71	NL-72
	0.25	NL-49	NL-50	NL-51	NL-52	NL-53	NL-54	NL-55	NL-56	NL-57	NL-58	NL-59	NL-60
	0.2	NL-37	NL-38	NL-39	NL-40	NL-41	NL-42	NL-43	NL-44	NL-45	NL-46	NL-47	NL-48
	0.15	NL-25	NL-26	NL-27	NL-28	NL-29	NL-30	NL-31	NL-32	NL-33	NL-34	NL-35	NL-36
	0.1	NL-13	NL-14	NL-15	NL-16	NL-17	NL-18	NL-19	NL-20	NL-21	NL-22	NL-23	NL-24
	0.05	NL-1	NL-2	NL-3	NL-4	NL-5	NL-6	NL-7	NL-8	NL-9	NL-10	NL-11	NL-12

A series of NLTHA was performed using the SAP2000 program for:

a. two different suites of GMs as detailed in section 3.3.1

b. two different levels of system damping, namely 2% and 5%. See section 3.3.5
c. five different intensity levels for input motions (IDA) ranging from 100% to 500%.

In total over 2.6 million SDOF analysis were performed. Results of analysis for NF GMs were compared with results of analysis for FF GMs for a wide variety of EDPs.

A summary of observations made is presented in the following sections.

4.2 Statistical representation of results of comprehensive parametric analysis of SDOF systems

This section summarizes results of more than 2.6 million NLTHA performed on a series of SDOF systems, as described in section 3.2.

The results are presented in terms of

1. Maximum displacement demand spectra and IDDR
2. Maximum ductility demand spectra and DDR
3. Yield capacity demand (strength spectra) for a specific target ductility and YCDR
4. Maximum inelastic to elastic displacement demand ratio.

Description of each of monitored engineering design parameter is presented in section 3.4.

In the following sections, the observations made with respect to each of the monitored EDP and EDP Ratios are briefly discussed. A set of practical examples illustrate how the results of this study can be implemented in real projects.

4.2.1 Maximum displacement demand spectra and IDDR

Median value and dispersion of maximum displacement demand for each nonlinear model and in each horizontal direction (i.e., FN and FP) were determined for all permutations of important seismic parameters, as detailed in section 3.3.

A suite of representative results of the parametric analysis, in the form of figures, is presented in Appendix A for reference. The comprehensive results will be available,

in the form of a database, on the website of the projects at http://ssi-civil.sites.olt.ubc.ca/ in the near future.

The following subsections discuss observations made through investigation of median value and dispersion of maximum displacement demand spectra due to NF GMs and those due to FF GMs as well as the ratio of these two spectra in each horizontal direction.

4.2.1.1 Analysis of results in the FN direction

Figure 4.2 shows variation of median values of maximum displacement demand in the FN direction for both NF and FF GMs, when nonlinearity of the system is modeled using NLT#4, as described in Appendix E.4.

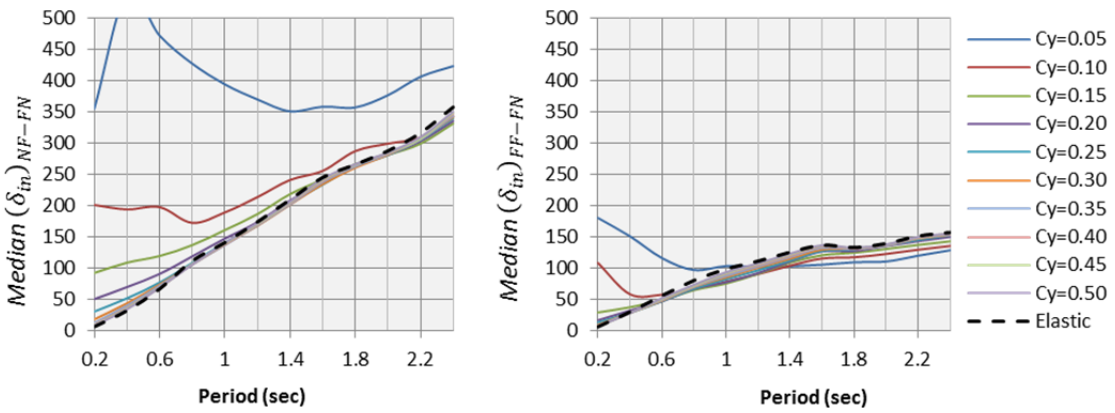

Figure 4.2: SDOF maximum displacement demand spectra in the FN direction: nonlinear model = NLT#4, Damping ratio ζ = 2%. Left figure, NF GMs, right figure, FF GMs

From Figure 4.2 it is evident that the maximum displacement demand due to NF GMs are, in general, more than those due to their corresponding FF GMs. To have a better quantitative measure of the influence of NF GMs on the maximum displacement demand, the median values of maximum displacement demand due to NF GMs in the FN direction were normalized to their corresponding values determined for FF GMs. The result, i.e., IDDR, is presented in Figure 4.3.

Figure 4.3 shows that IDDR is invariably more than 1.0, and increases as the elastic period of vibration of the system increases.

Figure 4.4 shows dispersion of IDDR in the FN direction in terms of the modified coefficient of variation, when modified coefficient of variation is defined as standard deviation of IDDR normalized with the median value of IDDR.

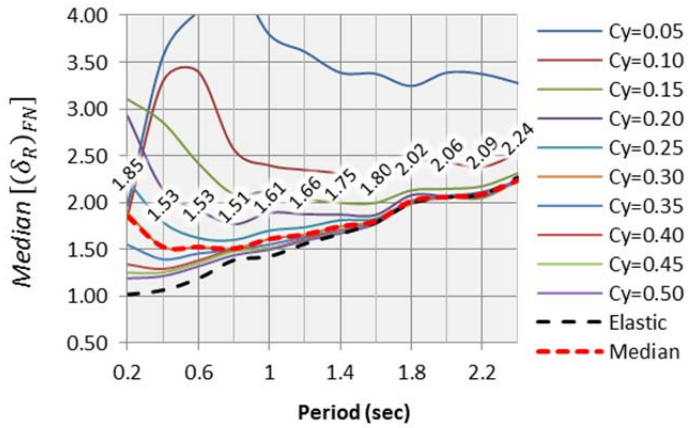

Figure 4.3: IDDR in the FN direction, nonlinear model = NLT#4, damping ratio ζ=2%

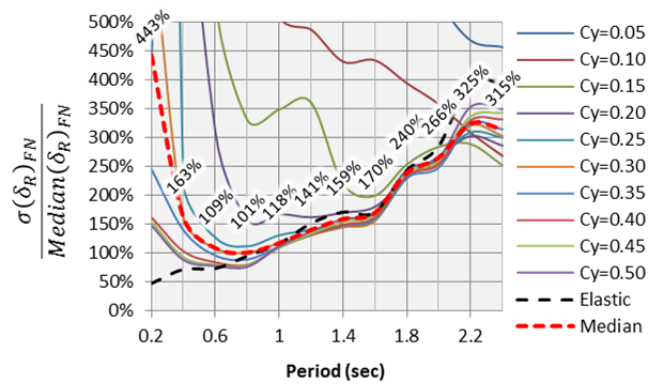

Figure 4.4: SDOF modified CV of IDDR in the FN direction: nonlinear model = NLT#4, damping ratio ζ = 2%

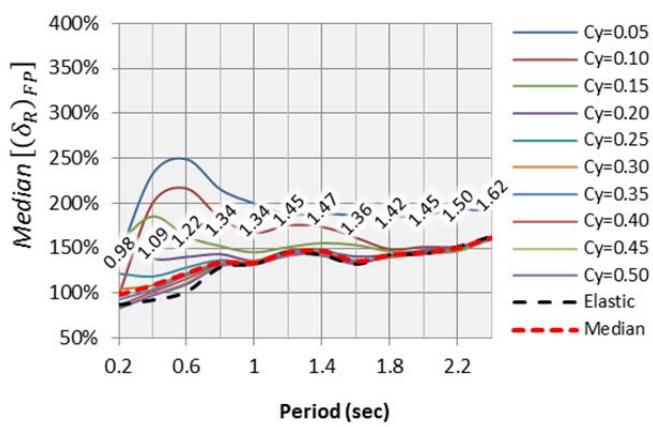

Figure 4.5: SDOF IDDR in the FP direction, nonlinear model = NLT#4, damping ratio ζ = 2%

From Figure 4.2 to Figure 4.5 (and their equivalent figures for other nonlinear models, presented in Appendix A), one can infer that:

- For the structures with $C_y \geq 20\%$ (which is almost the practical range of the strength characteristic for newly designed structures) the inelastic behaviour of the system has minimal effect on maximum displacement demand (see Figure 4.3),
- Effect of degradation is of paramount importance for the structures with small capacity (Cy ≤ 20%), especially in the short-period range, e.g., Te ≤ 1.0 s. This is mainly due to early yielding of the system, which causes significant stiffness and strength degradation. After the initial yielding takes place, equivalent period of the system is significantly increased. Hence, as properties of the system are changed, considerable deformation may take place due to the portion of the input motion which arrives after initial yielding. In reality, such a weak system most possibly would not be able to sustain the earthquake loads and would see extensive damage or become unstable owing to excessive deformations. Nonetheless, if those weak systems (hypothetically) could have sustained infinite displacements, then NF GMs would have imposed much greater displacement demands than FF GMs.
- From Figure 4.4 one can infer that dispersion of IDDR in the FN direction is almost linear for Cy ≥ 20% and T1 ≥ 0.6 s. However, for Cy ≤ 20% or T1 ≤0.6 s no clear pattern for data dispersion is evident; in general one may say for smaller Cy values the data is much more scattered.
- For the structures with Cy ≥ 20% the IDDR in the FN direction has almost a linear trend with respect to the elastic period of vibration. This trend is very similar to the maximum displacement demand ratio trend determined for elastic structures.

Traces of IDDR in the FN direction for systems with $C_y \geq 20\%$ and their fitted curve (red dashed line) is shown in Figure 4.6. A simplified equation for the proposed fitted curve is presented in equation 4-2:

$$\delta_R = \begin{cases} 1.4 & T_e < 0.6 \text{ sec} \\ 1.1 + 0.50T_e & T_e \geq 0.6\, sec \end{cases} \qquad 4\text{-}2$$

where δ_R denotes IDDR in the direction of interest.

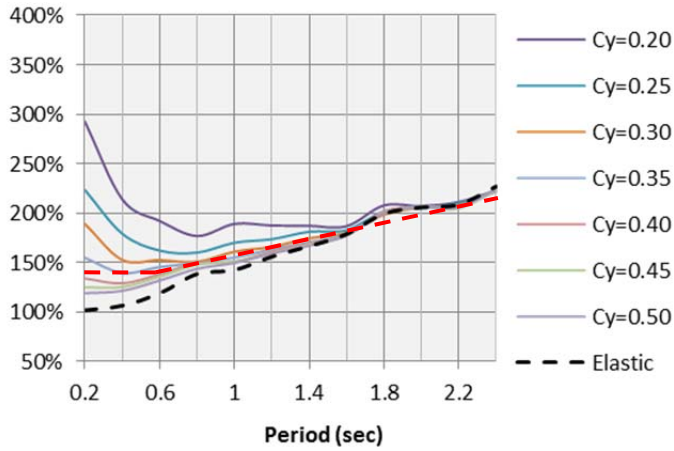

Figure 4.6: SDOF IDDR in the FN direction, nonlinear model = NLT#4, damping ratio ζ = 2%

Also, the modified CV of IDDR in the FN direction for systems with $C_y \geq 20\%$ could be approximated as

$$\frac{\sigma(\delta_R)_{FN}}{\text{Median}(\delta_R)_{FN}} = 1.2T_e + \left(\frac{1.4}{e^{T_e}}\right)^8 \qquad 4\text{-}3$$

Figure 4.7 shows how well the proposed equation for estimation of modified CV of IDDR in FN direction matches the analysis results.

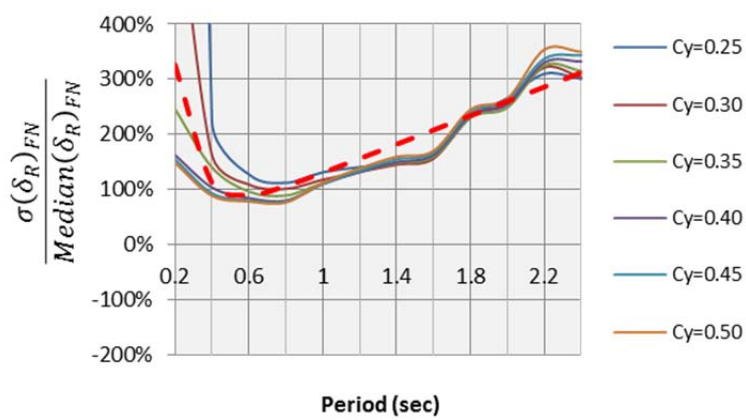

Figure 4.7: SDOF modified CV of IDDR in the FN direction nonlinear model = NLT#4, damping ratio ζ = 2%

It is of note that the second term of equation 4-2 alone can fairly accurately estimate IDDR. Thus, with consideration of second terms of equations 4-2, 4-3, and 3-19; one may estimate the NF nonlinear response of a system (with NLT#4 nonlinear

model and 2% damping ratio) in the FN direction from the FF response of the system, i.e., equation 4-4

$$(\delta_{in})_{NF-FN} = (\delta_{in})_{FF-FN} \times (1.1 + 0.5T_e) \times Exp\left\{Ln\left(\left[\frac{1.2T_e + \left(\frac{1.4}{e^{T_e}}\right)^8}{1.1 + 0.5T_e}\right]^2 + 1\right) \times \Phi^{-1}(P)\right\} \quad 4\text{-}4$$

If only the mean value of IDDR is of interest, then equation 4-4 would be simplified to equation 4-5.

$$(\delta_{in})_{NF-FN} = (\delta_{in})_{FF-FN} \times (1.1 + 0.5T_e) \quad 4\text{-}5$$

Note: equations 4-4 and 4-5 are applicable only to structures with $C_y \geq 20\%$. For structures with $C_y < 20\%$, one should use appropriate figures from Appendix A to determine the statistics of IDDR for their respective C_y.

4.2.1.2 Analysis of results in the FP direction

In this section, similar results to those developed for the FN component of input motions (as presented in section 4.2.1.1) are replicated for the FP component of input motions. Figure 4.8 shows the variation of median values of maximum displacement demand in the FP direction for both NF and FF GMs. Nonlinearity of the system is modeled using NLT#4, and a modal damping of 2% is also accounted for. Also, Figure 4.9 and Figure 4.10 show median and dispersion values of IDDR in the FP direction respectively.

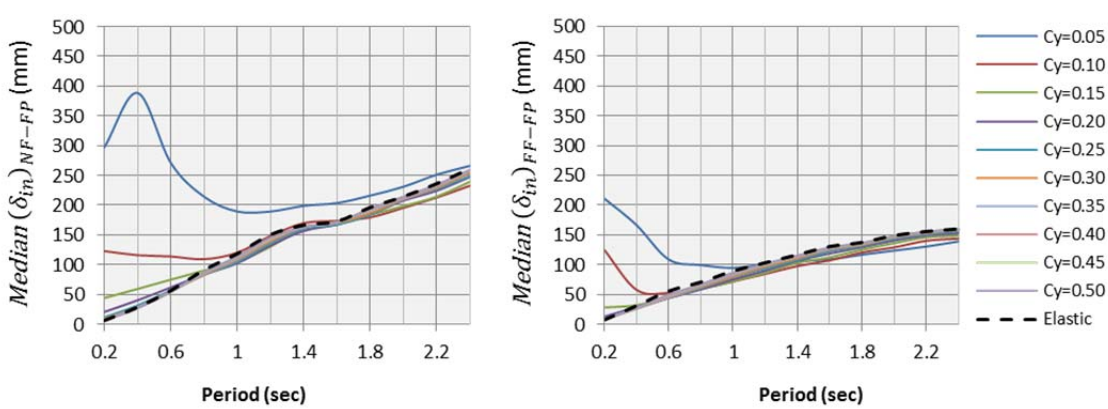

Figure 4.8: SDOF maximum displacement demand spectra in the FP direction: nonlinear model = NLT#4, damping ratio, ζ=2%. Right figure, FF GMs, Left figure, NF GMs

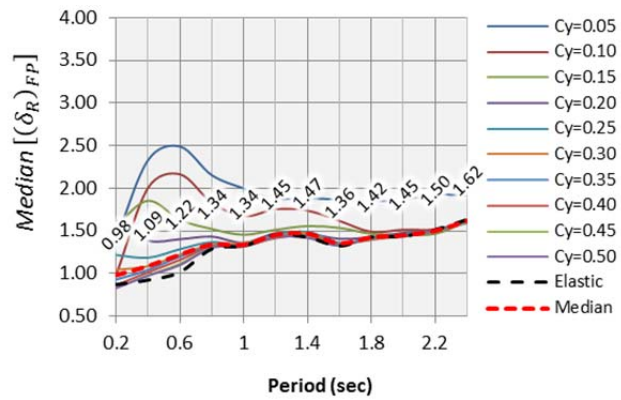

Figure 4.9: IDDR in the FP direction: nonlinear model = NLT#4, damping ratio ζ= 2%

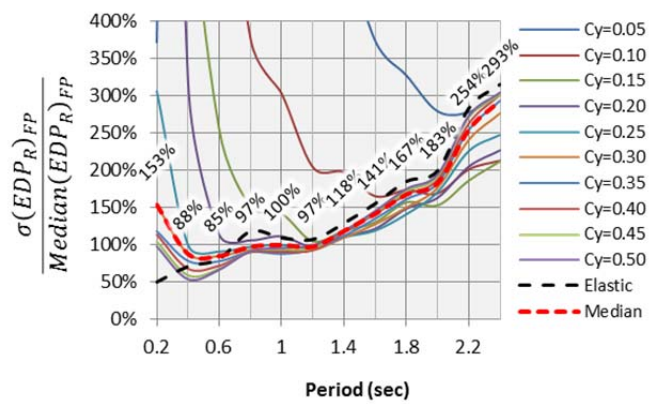

Figure 4.10: SDOF modified CV of IDDR in the FP direction: nonlinear model = NLT#4, damping ratio ζ= 2%

General observations (for FP responses):

- Since demand in the FP direction is generally much less than that in the FN direction, the weak structures are less affected by degradation behaviour of nonlinear elements.
- Also, owing to less input energy in the FP direction (vs. input energy in the FN direction), structures experience less nonlinearity in the FP direction. Thus, one may argue that maximum displacement demand is mainly governed by elasticity of the system if $C_y > 0.1$
- Similarly, for the structures with $C_y > 0.1$, IDDR in the FP direction has almost a linear trend with respect to the elastic period of vibration. A simplified equation for the proposed fitted line is presented in equation 4-6:

$$(\delta_R)_{FP} = 0.2T_e + 1 \qquad 4\text{-}6$$

Dispersion of IDDR in the FP direction is very much alike that in the FN direction. Hence, a simplified model for modified CV of IDDR in the FN direction could be used for the FP direction as well (see equation 4-3). Nonetheless, equation 4-3 slightly overestimates the modified CV of IDDR in the FP direction. However, its order of accuracy is deemed to be sufficient for engineering purposes. If one wants to use a much more accurate estimate of dispersion of IDDR in FP direction, one may use equation 4-7.

$$\frac{\sigma(\delta_R)_{FP}}{\mathrm{Median}(\delta_R)_{FP}} = 0.8{T_e}^{1.5} + \left(\frac{1.4}{\mathrm{e}^{T_e}}\right)^8 \qquad \text{4-7}$$

Again, with consideration of equations 4-6, 4-3, and 3-19, one may estimate the NF nonlinear response of a system (with NLT#4 nonlinear model and 2% damping ratio) in the FP direction from the FF response of the same system in the same direction using equation 4-8.

$$\begin{aligned}(\delta_{in})_{NF-FP} = \ & (\delta_{in})_{FF-FP} \times (0.2T_e + 1) \\ & \times Exp\left\{ln\left(\left[\frac{0.8{T_e}^{1.5} + (1.4/\mathrm{e}^{T_e})^8}{0.2T_e + 1}\right]^2 + 1\right)\right. \\ & \left.\times \Phi^{-1}(P)\right\}\left\{ln\left(\left[\frac{0.8{T_e}^{1.5} + \left(\frac{1.4}{\mathrm{e}^{T_e}}\right)^8}{0.2T_e + 1}\right]^2 + 1\right) \times \Phi^{-1}(P)\right\}\end{aligned} \qquad \text{4-8}$$

Again, if the mean value of IDDR is of interest, then equation 4-8 could be simplified to

$$(\delta_{in})_{NF-FP} = (\delta_{in})_{FF-FP} \times (0.2T_e + 1) \qquad \text{4-9}$$

Note that: when one considers combined effects of FN and FP components, the above results for short- and moderate-period ranges are very much in line with Caltrans seismic design criteria provisions.

4.2.1.3 Sensitivity analysis for maximum displacement demand spectra and IDDR

Table 4-2 summarises the results of a qualitative sensitivity analysis performed for maximum displacement demand spectra and IDDR.

Table 4-2: Qualitative results for sensitivity analysis of maximum displacement demand spectra and IDDR

Parameter of interest	Fault Normal			Fault Parallel		
	$(\delta_{in})_{NF}$	$(\delta_{in})_{FF}$	$\sigma(\delta_R)$	$(\delta_{in})_{NF}$	$(\delta_{in})_{FF}$	$\sigma(\delta_R)$
Hysteretic behaviour	Insignificant	Insignificant	Nominal	Insignificant	Insignificant	Nominal
Viscous damping	Moderate	Moderate	Nominal	Moderate	Moderate	Nominal
Pairing technique	Moderate	Moderate	Nominal	Moderate	Moderate	Nominal
Intensity of input motions	Significant	Significant	Significant	Significant	Significant	Significant

A more detailed discussion about variation of results of sensitivity analysis performed on maximum displacement demand spectra and IDDR with respect to variation of important parameters, as noted in section 3.3, is presented in Appendix C.2.

4.2.1.4 Observations

- IDDR is always more than unity in both FN and PF directions; irrespective of the elastic period of vibration.
- Unlike maximum expected displacement due to FF and NF GMs, IDDR is almost independent of the backbone curve and load reversal model, system damping, and pairing techniques.
- Dispersion of IDDR increases with an increasing degree of degradation and decreasing residual strength value.

4.2.2 Maximum ductility demand spectra spectra and DDR

Similar to the results of previous section, the median value of maximum ductility demands for each nonlinear system in each horizontal direction due to various system parameters were determined.

To determine maximum ductility demands, the expected maximum displacement demands of each system were normalized by its own Δ_y, when Δ_y denotes yield

displacement of the system (refer to Appendix E.3 for more details). The maximum ductility demand was set to one if it was less than unity.

The following subsections briefly discuss our observations with respect to maximum ductility demand determined for different systems.

4.2.2.1 Analysis of results in the FN direction

Figure 4.11 shows the variation of median values of maximum ductility demand in the FN direction for both NF and FF GMs, with respect to the variation of fundamental period of vibration of the structure as well as strength characteristics of a system, when inelastic behaviour is modeled using NLT#4 as described in Appendix E.4.

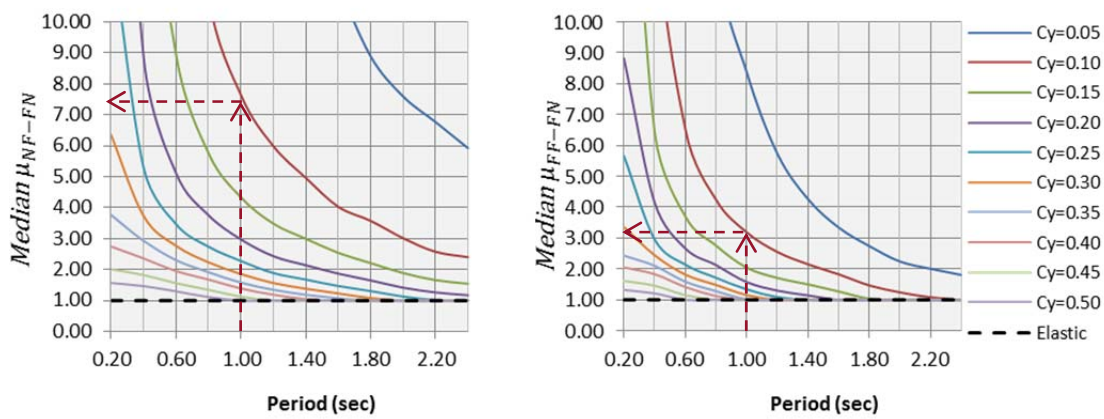

Figure 4.11: SDOF maximum ductility demand spectra in the FN direction: nonlinear model = NLT#4, damping ratio, $\zeta = 2\%$. Left figure, FF GMs, right figure, NF GMs

As one may expect the magnitude of maximum ductility demand increases as the elastic period of vibration of the system and/or strength characteristic of the system decreases.

To have a better quantitative measure of the influence of NF GMs on maximum ductility demand, the median values of maximum ductility demand due to NF GMs in the FN direction are normalized to that due to FF GMs in each horizontal direction. The result, DDR as defined in section 3.4.2, is presented in Figure 4.12.

Dashed-line arrows in Figure 4.11 show how the DDR for a structure with an elastic period of vibration of 1.0 s and a strength characteristic of 10% is determined. For ease of reference, the same point is marked on Figure 4.12.

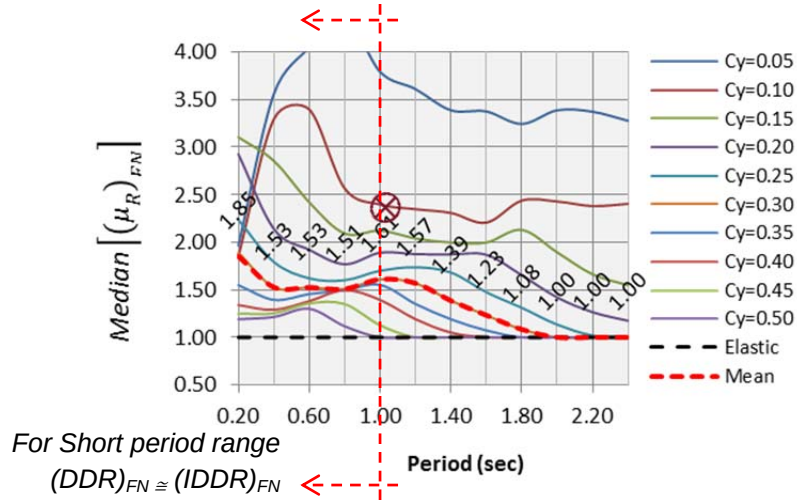

Figure 4.12: SDOF DDR in the FN direction: nonlinear model = NLT#4, damping ratio ζ= 2%

The black dashed line in Figure 4.11 shows the threshold where structures remain elastic. It is of note that the values of DDR are (almost) equal to values of IDDR for moderate short-period structures, but start to approach unity as median values of maximum ductility demand for both FF GMs and NF GMs approach one.

It is also evident from Figure 4.12 that DDR in the FN direction is always more than 1.00; this in turn indicates that in FN direction, NF GMs always impose more nonlinear demand than their FF counterparts.

From Figure 4.11 one may infer that for relatively strong structures ($C_y \geq$ ~20%) DDR has an almost constant value for the short-period range that quickly tapers off to unity with almost a linear trend. The maximum DDR for a structure with $C_y \geq$ ~20% can be calculated using equation 4-10.

$$\mu_R(\text{in FN direction for } C_y \geq 20\%) = \begin{cases} 2.3 - 2.0\,C_y & 0.4\text{ s} \leq T_e \leq 2.2 - 3.2C_y \\ 1 & \text{for } T_e \geq 3.5 - 5C_y \end{cases} \quad \text{4-10}$$

where μ_R is DDR.

μ_R would be linearly interpolated if $(2.2 - 3.2C_y) < T_e < (3.5 - 5C_y)$.

Figure 4.13 shows how well equation 4-10 approximates the values of Figure 4.12.

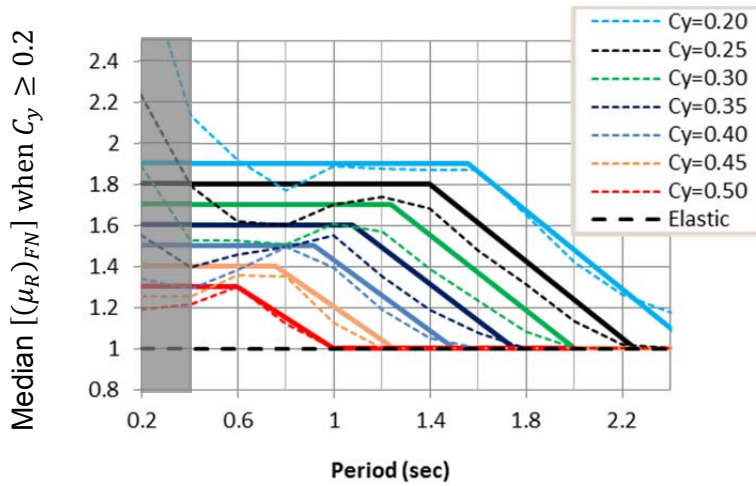

Figure 4.13: SDOF approximation of DDR in FN direction as a function of strength characteristic: nonlinear model = NLT#4, damping ratio ζ = 2%, $C_y \geq \sim 20\%$

Since maximum ductility demands are essentially maximum displacement demands normalized by yield displacements, the modified CV of maximum ductility demands are very similar to those of maximum displacement demands in both the FN and FP directions. Hence, the modified CV of DDR (for short-period structures) can be represented by equation 4-3. Thus, with consideration of equations 4-10, 4-3, and equation 3-19, one may approximately determine the ductility demand of a system (with the NTL#4 nonlinear model 2% damping ratio, and $C_y \geq \sim\%20\%$) in the FN direction from the FF ductility demand of the system using equation 4-1.

$$\mu_{NF-FN} = \mu_{FF-FN} \times \begin{pmatrix} (2.3 - 2.0\,C_y) \times Exp\left\{ ln\left(\left[\frac{0.8{T_e}^{1.5} + (1.4/e^{T_e})^8}{0.2T_e + 1} \right]^2 + 1 \right) \times \Phi^{-1}(P) \right\} & 0.4\,\mathrm{s} \leq T_e \leq 2.2 - 3.2C_y \\ 1 & T_e \geq 3.5 - 5C_y \end{pmatrix} \quad \text{4-11}$$

For median values of DDR, equation 4-11 is simplified to

$$\mu_{NF-FN} = \mu_{FF-FN} \begin{pmatrix} 2.3 - 2.0\,C_y & 0.4\,\mathrm{s} \leq T_e \leq 2.2 - 3.2C_y \\ 1 & \text{for } T_e \geq 3.5 - 5C_y \end{pmatrix} \quad \text{4-12}$$

4.2.2.2 Analysis of results in the FP direction

Similar results as noted for the FN component can be replicated for the FP component of input motions. Figure 4.14 shows the variation of median values of maximum ductility demand in the FP direction for both NF and FF- GMs, for a system with the NLT#4 nonlinear model and modal damping of 2%.

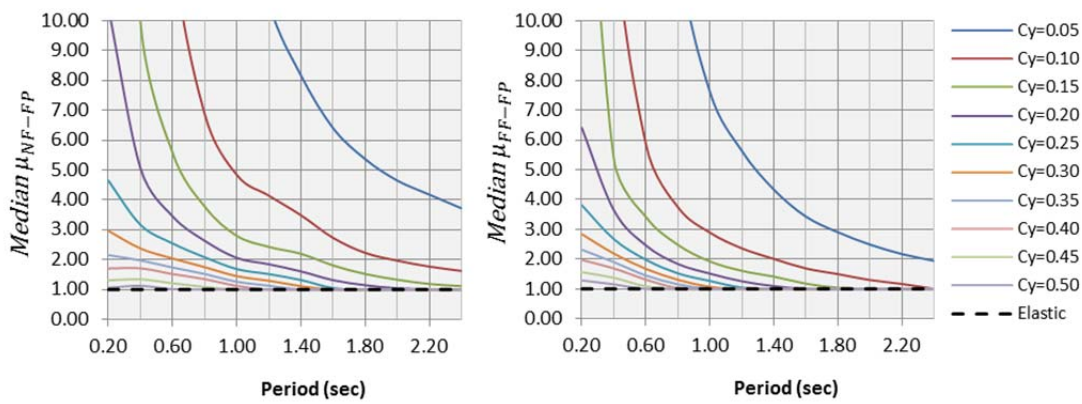

Figure 4.14: SDOF maximum ductility demand spectra in the FP direction: nonlinear model = NLT#4, dDamping ratio $\zeta = 2\%$. Right figure, FF GMs, Left figure, NF GMs

Analogous to what was presented in the previous section, Figure 4.15 shows DDR in the FP direction for a system with the NLT#4 nonlinear model and modal damping of 2%.

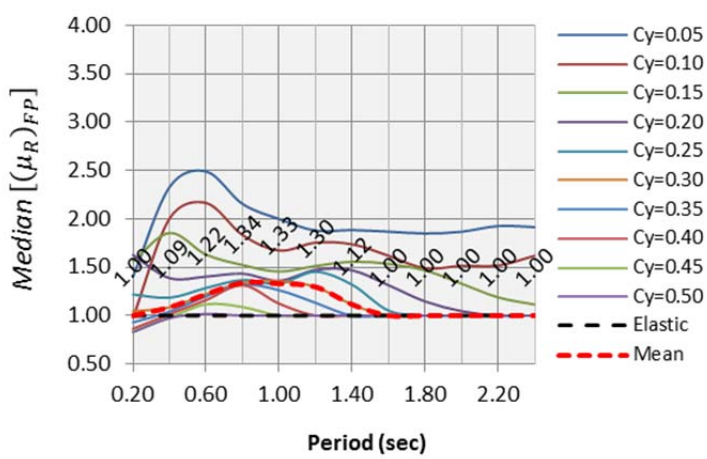

Figure 4.15: SDOF DDR in the FN direction: nonlinear model = NLT#4, damping ratio, $\zeta = 2\%$

Figure 4.15 is the counterpart of Figure 4.14 but in the FP direction. By comparing Figure 4.14 and Figure 4.15, one may conclude that

a) DDR in the FP direction is less than that in FN direction,

b) Due to development of less nonlinearity in the FP direction the shape/values of DDR in the FP direction are not similar to shape/values of IDDR in the FP direction (for any period range),

c) unlike DDR in the FN direction, which showed an almost constant value in short-period ranges (for the structures with $C_y \geq \sim 20\%$), DDR in the FP direction does not show a regular pattern,

d) unlike DDR in the FN direction, which shows more than unity value for all period ranges, DDR for some structures in the FP direction results in slightly less than unity values in short-period ranges (this means that although μ_{NF-FP} is mainly limited to one, μ_{FF-FP} ,is more than one in the short-period range)

e) For reasonably designed structures ($C_y \geq \sim 20\%$), DDR in the FP direction could be conservatively estimated as

$$\mu_R(\text{in FP direction for } C_y \geq 20\%) = \begin{cases} 2.0 - 1.9\,C_y & T_e \leq 1.9 - 2.7C_y \\ 1 & \text{for } T_e \geq 3.0 - 4.5C_y \end{cases} \qquad 4\text{-}13$$

Figure 4.16 shows how well equation 4-13 approximates the DDR values of Figure 4.15 for a system with the NLT#4 model and damping ratio of 2% when $C_y \geq \sim \%20$.

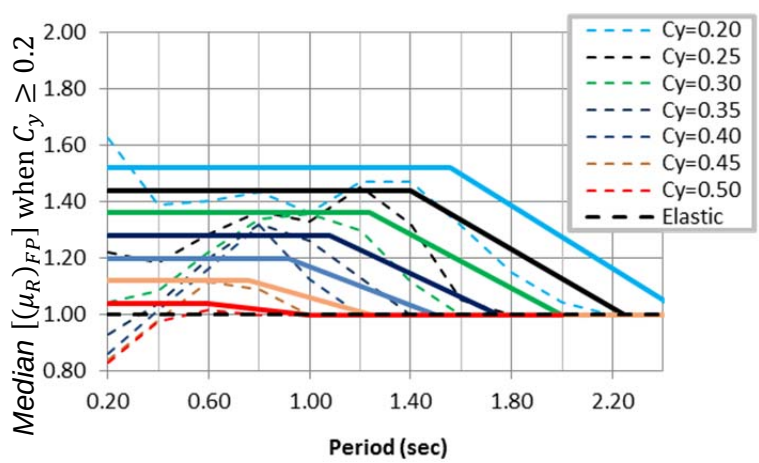

Figure 4.16: SDOF DDR in the FP direction: nonlinear model = NLT#4, damping ratio ζ= 2

As mentioned in section 4.2.2.1, dispersion of DDR in the FP direction could be represented by equation 4-8. Hence, one may approximately determine the ductility

demand of a system in the FP direction from the FF ductility demand of the system using equation 4-14.

$$\mu_{NF-FN} = \begin{cases} \mu_{FF-FN} \times (2.0 - 1.9\,C_y) \times \mathrm{Exp}\left\{ ln\left(\left[\frac{1.2T_e + \left(\frac{1.4}{e^{T_e}}\right)^8}{1.1 + 0.5T_e} \right]^2 + 1 \right) \times \Phi^{-1}(P) \right\} & T_e \leq 0.9 - 2.7C_y \\ 1 & T_e \geq 3.0 - 4.5C_y \end{cases} \mu_{NF-FN} \quad \text{4-14}$$

Again, for median values of DDR, equation 4-14 could be simplified as

$$\mu_{NF-FN} = \mu_{FF-FN} \times \begin{pmatrix} 2.0 - 1.9\,C_y & T_e \leq 0.9 - 2.7C_y \\ 1 & \text{for } T_e \geq 3.0 - 4.5C_y \end{pmatrix} \quad \text{4-15}$$

4.2.2.3 Sensitivity analysis for maximum ductility demand spectra and DDR

Table 4-3 summarises results of a qualitative sensitivity analysis performed for ductility demand spectra and DDR.

A more detailed discussion about variation of results of sensitivity analysis performed on ductility demand spectra and DDR with respect to variation of important parameters, as noted in section 3.3, is presented in Appendix C.3.

Table 4-3: Qualitative results for sensitivity analysis of maximum displacement demand spectra and IDDR

Parameter of interest	Fault Normal			Fault Parallel		
	$C_y(\mu)_{FF}$	$C_y(\mu)_{NF}$	$\boldsymbol{\sigma}(YCDR)_{\boldsymbol{FN}}$	$C_y(\mu)_{FF}$	$C_y(\mu)_{NF}$	$\boldsymbol{\sigma}(YCDR)_{\boldsymbol{FP}}$
Hysteretic behaviour	Insignificant	Insignificant	Insignificant	Insignificant	Insignificant	Insignificant
Viscous damping	Moderate	Moderate	Nominal	Moderate	Moderate	Nominal
Pairing technique	Moderate	Moderate	Nominal	Moderate	Moderate	Nominal
Intensity of input motions	Significant	Significant	Significant	Significant	Significant	Significant

4.2.2.4 Observations

- DDR for NF and FF GMs follow the same shape/trend for all strength characteristic levels and for all intensity levels,
- DDR is (almost) always more than one in the FN direction,
- DDR is almost equivalent to IDDR in the FN direction, for short-period structures,
- DDR approaches unity for higher-period ranges.

4.2.3 Yield capacity demand for constant ductility (strength spectra) and YCDR

To limit the risk associated with excessive nonlinear behaviour (undesired response) of the structure, simplified design procedures usually require limiting maximum ductility demands to some certain levels.

The code-specified permissible ductility demand thresholds are usually determined based on the performance objectives of the structure and the structural systems, for which special design and detailing measures are taken in the critical zones of the structural elements.

Thus, from a design point of view, constant ductility strength spectra can greatly assist design engineers to easily determine the strength required for limiting the ductility demand of a structure to some target value.

To develop constant ductility strength spectra for both NF and FF GMs in this project, an interpolation process was used. Figure 4-17 and Figure 4-18 show constant ductility strength spectra for a system with the nonlinear model of NLT#4 and a damping ratio of 2% in the FN and FP directions, respectively.

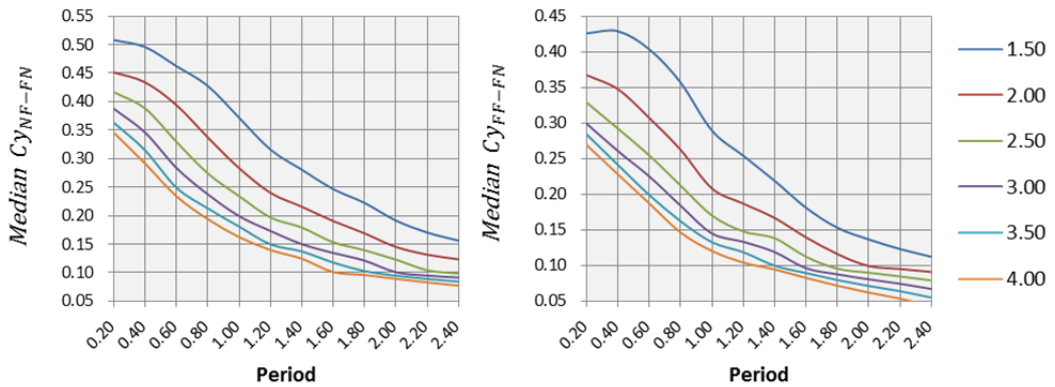

Figure 4-17: SDOF yield capacity demand (strength spectra), for a system with nonlinear model = NLT#4, damping ratio $\zeta = 2\%$ for NF and FF GMs in the FN direction

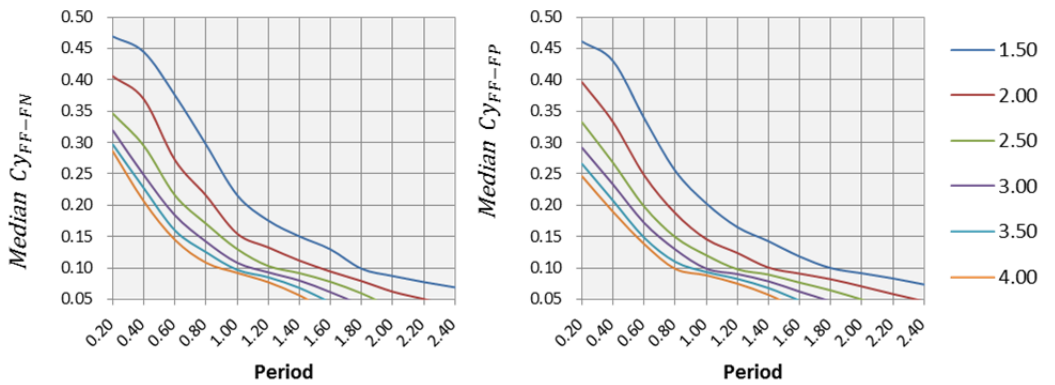

Figure 4-18: SDOF yield capacity demand (strength spectra) for a system with nonlinear model = NLT#4, damping ratio $\zeta = 2\%$ for NF and FF GMs in the FP direction

To have a better understanding of effect of NF GMs on the strength required to meet some specific target ductility, the values of strength spectra due to NF GM in each horizontal direction (Figure 4-18) are normalized by their corresponding values due to FF GMs (Figure 4-17). The results are called YCDR and are presented in Figure 4-19.

The yield capacity demand ratio can assist practicing engineers to estimate the required base shear of the structure to limit the ductility ratio imposed by NF GMs to some target ductility value. That is to say, one can prorate the base shear required for designing a structure for NF GMs from the code-specified base shear (which is

essentially developed for FF GMs), when the ductility needs to be limited to some target value.[1]

It is of note that the above-mentioned approach, i.e., scaling demand ratio of FF GMs by YCDR, is substantially different from what current code and design guidelines (like Caltrans seismic design criteria) propose for considerations of NF effects in their design procedure. Namely, current codes and design guidelines apply a narrowband or a broadband amplification factor to the UHRS, to account for effects of NF GM on the response of structures. Obviously, this approach pays no explicit attention to particularities of nonlinear response of the structures and the high flux of energy imposed by NF GMs to the structures. Conversely, in this approach, the base shear amplification factor (YCDR) is a direct function of expected ductility demand of the structure determined based on the nonlinear response of an equivalent system for both NF and FF GMs.

Figure 4-19 shows YCDR for a system with the nonlinear model of NLT#4 and a damping ratio of 2% in the FN and FP directions. As is evident from Figure 4-19, the traces are truncated for long-period ranges; this is mainly due to data unavailable in those ranges for the earthquake level of interest (i.e., if one increases the input motion intensity by a factor of 2 so all systems experience some level of nonlinearity, then the figures become complete). Figure 4-20 is equivalent to Figure 4-19, except it is developed for an input intensity level of 2 (input motions are amplified by a factor of 2). It is of note that YCDR is almost independent of the input intensity level (see Appendix C.4.3). Hence, the missing values of YCDR for earthquake level one can be easily substituted by their corresponding values from other intensity levels and be used in practice.

[1] The upper bound of target ductility is usually implicitly prescribed by the codes, in the form of some ductility related load reduction factors, R_d. R_d is usually a function of the lateral load resisting system and/or the design measures taken in the critical zones of the structural elements.

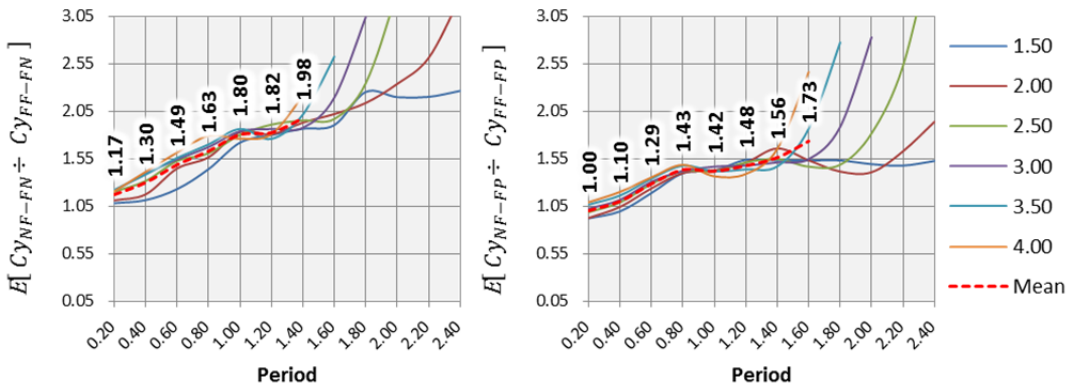

Figure 4-19: SDOF YCDR for a system with nonlinear m = NLT#4, damping ratio ζ = 2% for NF and FF GMs in the FP direction, EQ Level = 1. Left figure, YCDR in the FN direction; right figure, YCDR in the FP direction

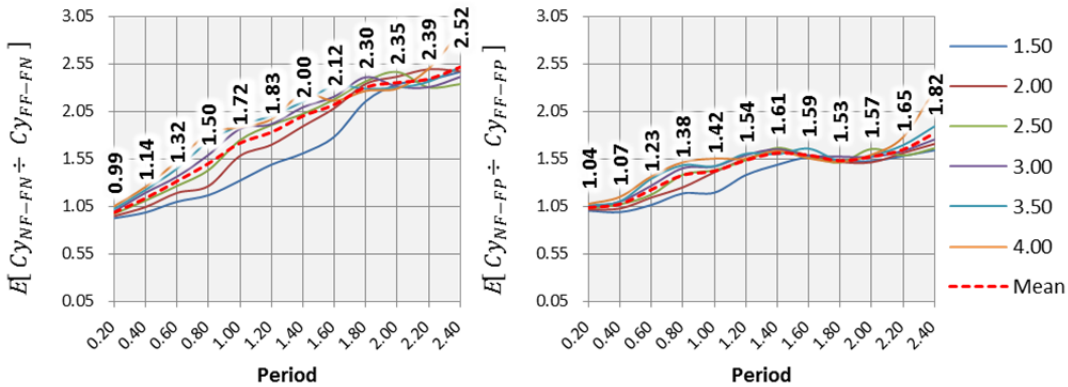

Figure 4-20: SDOF YCDR for a system with Nonlinear model = NLT#4, damping ratio ζ = 2% for NF and FF GMs in the FP direction, EQ Level = 2. Left figure, YCDR in the FN direction; right figure, shows YCDR in the FP direction

The YCDR in the FN and FP directions could be simply estimated using a linear trend line similar to equation 4-16:

$$\mathrm{YCDR} = 1 + \alpha_{\mathrm{YCDR}}\, T_e \qquad 4\text{-}16$$

when α_{YCDR} is 0.65 for the FN direction and 0.30 for the FP direction.

Thus, one may use equation 4-17 to estimate the required strength of a system to withstand NF GMs, and yet meet the target ductility level, from the strength demand of the same system designed to meet the same ductility level due to FF GMs:

$$C_{y_{NF}} = C_{y_{FF}} \times (1 + \alpha_{\mathrm{YCDR}}\, T_e) \qquad 4\text{-}17$$

4.2.3.1 Sensitivity analysis for strength spectra and YCDR

Table 4-4 summarises results of a qualitative sensitivity analysis performed for the strength spectra in both the FN and FP directions and YCDR.

A more detailed discussion about variation of results of sensitivity analysis performed on ductility demand spectra and DDR with respect to variation of important parameters, as noted in section 3.3, is presented in Appendix C.4.

Table 4-4: Qualitative results for sensitivity analysis of maximum displacement demand spectra and IDDR

Parameter of interest	Fault Normal			Fault Parallel		
	$C_y(\mu)_{FF}$	$C_y(\mu)_{NF}$	$\sigma(YC$	$C_y(\mu)_{FF}$	$C_y(\mu)_{NF}$	$\sigma(YCDR)_{FP}$
Hysteretic behaviour	Insignificant	Insignificant	Insignificant	Insignificant	Insignificant	Insignificant
Viscous damping	Moderate	Moderate	Insignificant	Moderate	Moderate	Insignificant
Pairing technique	Moderate	Moderate	Moderate	Moderate	Moderate	Moderate
Intensity of input motions	Significant	Significant	Insignificant	Significant	Significant	Insignificant

4.2.3.2 Observations

- Capacity demand due to NF GMs for a specific target ductility could be estimated from the same due to FF GMs, using YCDR.
- YCDR is
  - always more than unity in both the FN and FP directions. However, it is much more pronounced in the FN direction,
  - almost independent to backbone curve and load reversal model, intensity of input motions, and system damping
- Pairing technique can affect the value of YCDR.

- YCDR is a very robust and stable parameter that can be incorporated easily into design procedure and allow for an easy and accurate estimate of required capacity to meet some target ductility ratio, when a structure is subjected to NF GMs.

4.2.4 Maximum inelastic to elastic displacement demand and maximum inelastic to elastic displacement demand ratio ratio

While seismic design provisions of current codes and design guidelines allow structures to respond inelastically to strong ground motions, yet the simplified design procedures are based on linear elastic analyses of the system. The results of such linear analysis are usually used to indirectly estimate the maximum inelastic displacement response of the structures.

The basis for estimation of the maximum displacement demand of inelastic systems from the maximum displacement demand of linear elastic systems goes back to the 1970s, to the work of Veletsos, Newmark, and Hall work, which was based on analysis of the SDOF system using elastic-perfectly -plastic models. The result of the work of Veletsos, Newmark, and Hall, which is still the backbone of seismic provisions of many codes and design standards, indicates that in the high-period ranges, the maximum deformation of the inelastic and corresponding elastic systems are almost the same (equal displacement rule). It also indicates that in the low-period (and moderately low-period) ranges, the inelastic displacements are significantly higher than their elastic counterparts.

It is of note that all past research by Veletsos, Newmark, and Hall was based on estimating maximum displacement demand of inelastic systems from the maximum displacement demand of linear elastic systems using some ordinary GMs, with no specific attention to the effect of long-period pulses associated with NF GMs. To address this shortcoming, Miranda et al. (2000), performed an extensive study to estimate the maximum displacement demand of inelastic systems from the maximum displacement demand of linear elastic systems $\delta_{inelastic}/\delta_{elastic}$ subjected to NF GMs. Results of their study showed that, in general, $\delta_{inelastic}/\delta_{elastic}$ determined for NF GMs are more than those determined for FF

GMs. They also studied the influence of several parameters on $\delta_{inelastic}/\delta_{elastic}$ and concluded that

- for sites with average shear wave velocities of 180 m/s or more, the influence of soil conditions is negligible
- for systems with periods of vibration of 1.0 s or more, the influence of elastic period of vibration is also negligible.

During course of this project, the Miranda et al. (2000) study was extended and the variation of $\delta_{inelastic}/\delta_{elastic}$ for a range of parameters not accounted for or addressed in previous studies was investigated. The aforementioned parametric analyses were performed for both NF and FF GMs, and results were compared to allow for evaluation of effect of NF GMs on $\delta_{inelastic}/\delta_{elastic}$ with respect to various parameters.

It is of note that previous studies presented the ratio of $\delta_{inelastic}/\delta_{elastic}$ as mainly a function of the ductility ratio. However, in real practice the ductility ratio is not readily available. That is because, in practice, engineers usually assume a target ductility ratio, and based on that they determine the strength demand of the structure. Then, they design their structures in a way that the capacity of the structure is more than the strength demand. Hence, although the actual strength is readily available, actual ductility may not be equal to the initially assumed target ductility. This is simply because the final design might allow for a system with a capacity that exceeds the strength demand, initially determined based on the target ductility ratio.

Thus, in this project, a parametric study was used to investigate the effect of NF GMs on the ratio $\delta_{inelastic}/\delta_{elastic}$ and the results were presented in terms of (A) strength characteristic of the structures and (B) target ductilities.

The following sections briefly discuss results, findings, and observations regarding variation of $\delta_{inelastic}/\delta_{elastic}$ with respect to variation parameters, as noted in section 3.3.

4.2.4.1 Analysis of results in the FN and FP directions

Figure 4-21 shows the variation of median values of $\delta_{inelastic}/\delta_{elastic}$ in the FN and FP directions, for both NF and FF- GMs, as a function of the elastic period of the

system and with respect to variation of strength characteristics for a system with the NLT#4 nonlinear model (as described in Appendix E.4).

Figure 4-22 is similar to Figure 4-21. However, median values of $\delta_{inelastic}/\delta_{elastic}$ are presented with respect to variation of the target ductility.

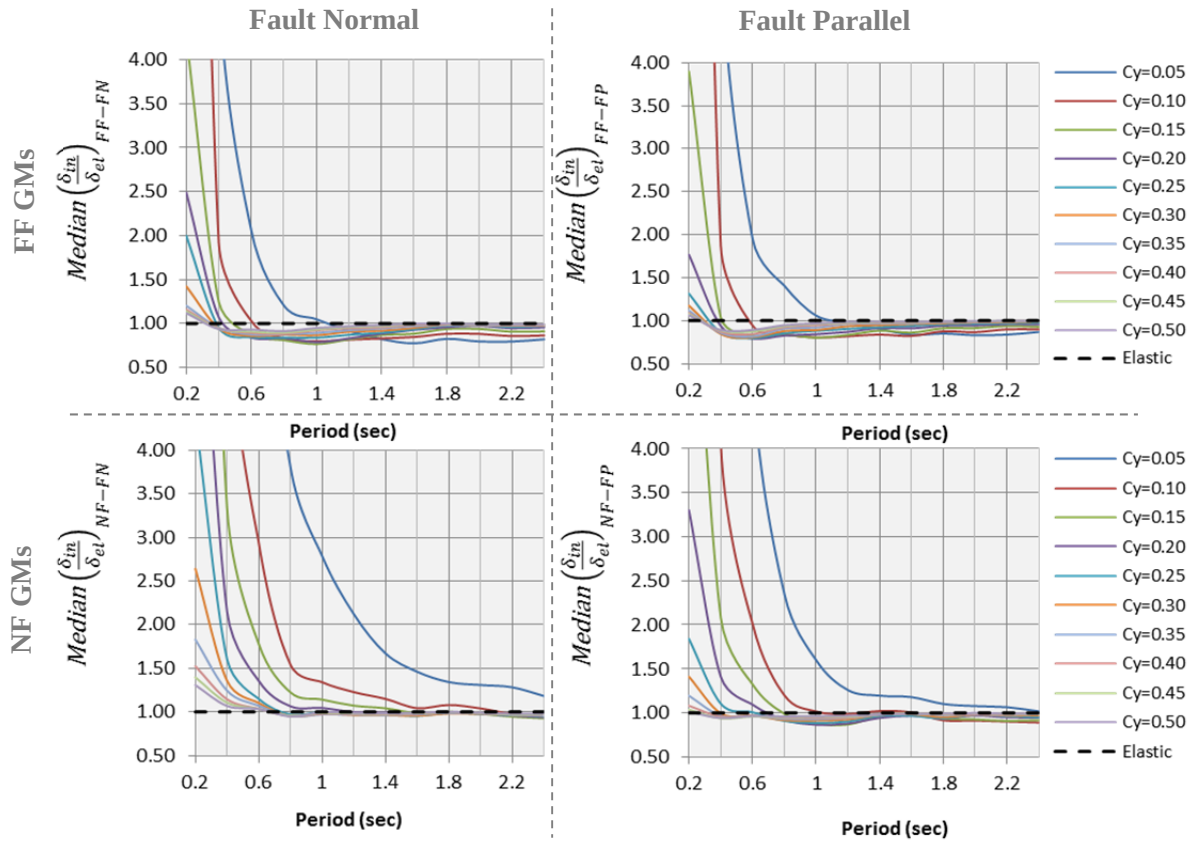

Figure 4-21: SDOF median ratio of maximum displacement demand of inelastic systems to the maximum displacement demand of linear elastic systems: nonlinear model = NLT#4, damping ratio $\zeta = 2\%$. Top left: FF GMs in Fault-Normal direction, top right: FF GMs in Fault-Parallel direction, bottom left: NF GMs in Fault-Normal direction, bottom right NF GMs in Fault-Parallel direction

From both Figure 4-21 and Figure 4-23 one can infer that the trend of $\delta_{inelastic}/\delta_{elastic}$ is very similar to what is noted in FEMA 440, i.e., $\delta_{inelastic}/\delta_{elastic}$ for both NF and FF GMs in short-period ranges become almost unbounded and for the medium- to long-period ranged approaches unity, as reported by Miranda et al. (2000).

Also, one may infer that if the elastic period of the structure is not within short-period ranges, then almost invariably, median values of $\delta_{inelastic}/\delta_{elastic}$ for FF GMs in both the FN and FP directions are slightly less than unity. This phenomenon

can be justified with consideration of significant energy dissipation that numerous low amplitude nonlinear excursions can provide while the structure is subjected to FF GMs. Obviously, the same is not expected for pulse-like NF GMs, as the energy input rate does not allow the structure to gradually dissipate the energy through hysteretic response. Thus, for NF GMs the median value of $\delta_{inelastic}/\delta_{elastic}$ either exceeds unity or is very close to unity.

The same results are also evident in Figure 4-22, i.e., Figure 4-22 shows that

- median value of $\delta_{inelastic}/\delta_{elastic}$ is unbounded for short-period structures,
- for mid to long periods (e.g., $T_e \geq 0.6$ s), $\delta_{inelastic}/\delta_{elastic}$:
    - is always less than one for FF GMs
    - is usually more than one for NF GMs

These results are irrespective to their target ductility values.

To find the effect of NF GMs on the ratio of maximum displacement demand of inelastic systems to the maximum displacement demand of linear elastic systems, the lower row figures of Figure 4-21 are normalized to the top row figures of Figure 4-21, respectively, (i.e., $\delta_{inelastic}/\delta_{elastic}$. for NF GMs is normalized to its counterpart for FF GMs). The results are presented in Figure 4-23.

From Figure 4-21 and Figure 4-23, one can infer that for the practical ranges of strength characteristics for newly designed structures (e.g., $C_y \geq 20\%$) and for elastic period of vibrations more than 0.6~0.8 s, the ratio of $\delta_{inelastic}/\delta_{elastic}$ for FF GMs and $\delta_{inlastic}/\delta_{elastic}$ for NF GMs are both approximately unity.

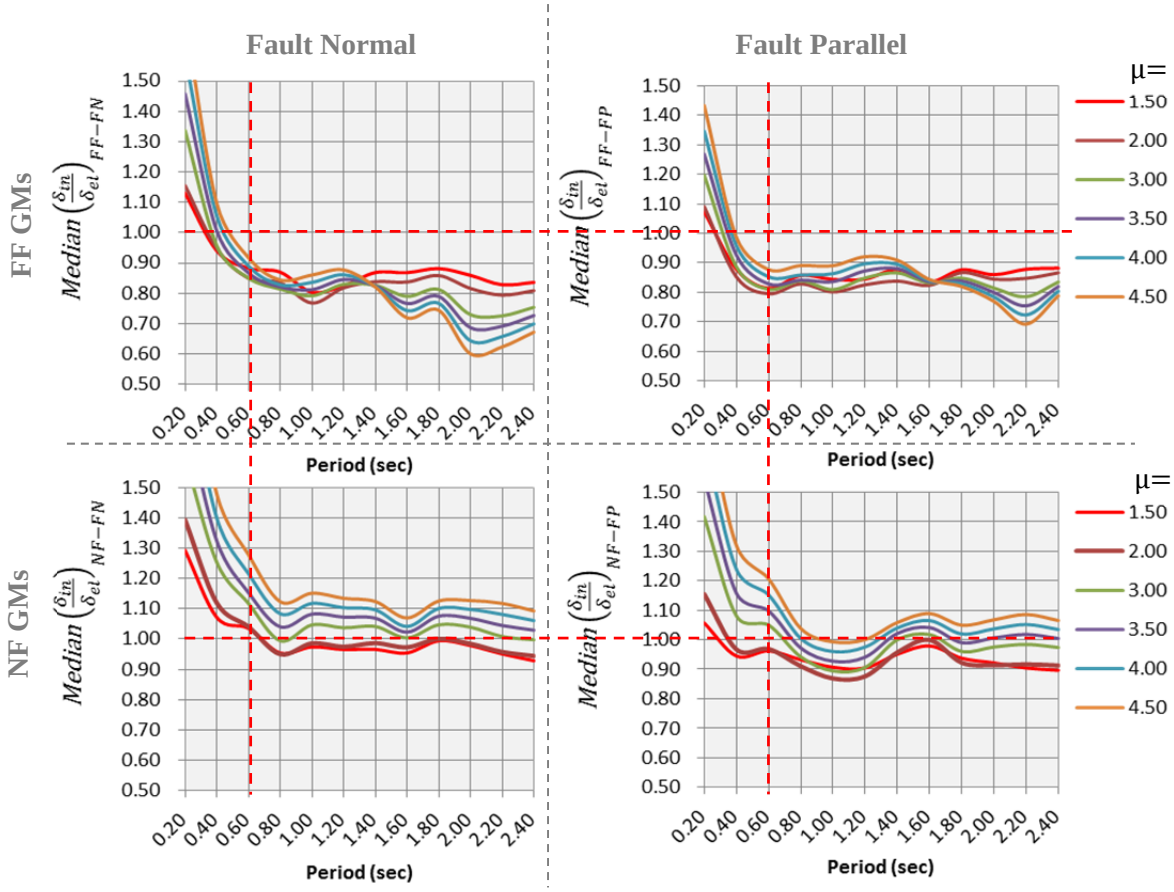

Figure 4-22: SDOF median ratio of maximum displacement demand of inelastic systems to the maximum displacement demand of linear elastic systems: nonlinear model = NLT#4, damping ratio ζ = 2%. Top left: FF GMs in Fault-Normal direction, top right: FF GMs in Fault-Parallel direction, bottom left: NF GMs in Fault-Normal direction, bottom right NF GMs in Fault-Parallel direction

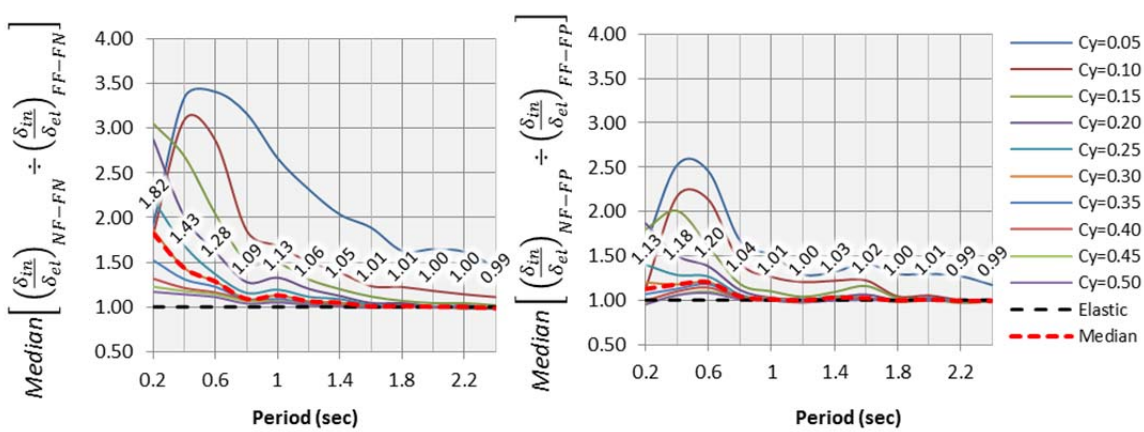

Figure 4-23: SDOF ratio of $(\delta_{inelastic}/\delta_{elastic})$ for NF GMs to $(\delta_{inelastic}/\delta_{elastic})$ for FF GMs: nonlinear model = NLT#4, damping ratio ζ = 2%. Left figure is for Fault- Normal direction and right figure is for Fault-Parallel direction

For the short-period ranges of Figure 4-23 (e.g., $T_e \leq 0.6$ s), the results in the FN direction show a different trend compared with those in the FP direction; i.e., in the FN direction $\delta_{inelastic}/\delta_{elastic}$ for FF GMs underestimates $\delta_{inelastic}/\delta_{elastic}$ for NF GMs.

It is of note that the results above for the FN direction are well in line with what Miranada et al. (2000) and Chopra et al. (2003) found.

For a brief description of sensitivity analysis of maximum inelastic to elastic displacement demand and maximum inelastic to elastic displacement demand ratio refer to Appendix C.5.

4.2.4.2 Observations

- Results show that structures subjected to NF GMs may experience larger $\delta_{inelastic}/\delta_{elastic}$ than those subjected to FF GMs, especially for structures with an elastic period of 0.8 s or less and C_y of 20% or less.
- The elastic results can be used as a good estimation of the maximum inelastic displacement for period ranges beyond 0.6~0.8 s, invariably for NF and FF GMs, and in both FN and FP directions.
- For short-period structures (e.g., with elastic period of vibration less than 0.6 s), the effect of system (viscous) damping can play an pivotal role in estimation of maximum inelastic response/instability of the structure.

4.3 Nonlinear time history analysis of processed signals

Historically, most of irregularities observed in the response of the structures due to NF GMs were related to their velocity long-period pulses. However, the work of Krawinkler and Alavi (1998) on the response of the structure to the simplified equivalent long-period pulses showed that a significant part of the response of the structures to the NF GMs could be associated with other aspects of the NF GMs.

Thus, for analysis and design purposes a simplified equivalent long-period pulse in general cannot represent the entire NF GMs or reproduce the expected response of the structure. However, if one can find a signal that in combination with an

equivalent simplified long period pulse (please refer to section 2.1.2) approximates the effect of NF GMs then they can synthesize the NF GMs in a novel way.

To investigate such a possibility we decomposed the NF GMs into their pulse signal content and their residual signal content and evaluate the response of the structures to each of these two parts. The pulse signals were extracted using wavelet analysis as proposed by Baker et al. (2011), and the residual signal was obtained from subtraction of the pulse signal from the original NF GM. Another set of pulse signals was also generated from low-pass filtering of the NF GMs with a conjectured threshold frequency of 0.5 Hz. The latter set was produced only to see if a simple filtering process can result in a signal that produces the same effect that extracted signals can produce.

The responses of the structures due to residual signals of NF GMs were compared with their FF GM counterparts to see if the residual parts can be approximated by their FF GM counterparts. Finally a simple procedure was proposed for synthesizing NF GMs for an event for which the FF GM is recorded but the NF GM is unavailable (see section 4.3.1.3).

4.3.1 Results of analysis of pulses, residual and original signals

The following subsections show comparison of results of NLTHA for (a) original NF GMs, (b) their corresponding extracted pulse signals (using wavelet analysis and simple filtering), (c) their corresponding residual signals, and (d) their FF GMs counterparts.

The objective of this comparison is to see how much of response amplification associated with NF GMs is attributed to long-period pulses and how much of it is attributed to nature, amplitude, and frequency content of NF GMs (which remains in residual signals).

The results of these analyses and comparisons are intended to answer some of the questions regarding the equivalent pulses, the equivalent residual signals, and new synthesized NF GM, for instance, how well can the extracted pulses represent all NF-effects? How well can the filtered signals represent the extracted NF-pulses

(using wavelet analysis)? How comparable is the residual signal to its FF GM counterparts?

Note: All results in this subsection are presented for GMs in only the FN direction. This is mainly because the forward directivity effect is most evident in the FN component of selected NF GMs.

4.3.1.1 How well can the extracted pulses represent the whole NF-effects?

Figure 4-24 shows the median of maximum displacement demand in the FN direction for the original NF GMs and their corresponding extracted signal using the routine proposed/developed by the Baker research group.

Figure 4-24 shows that amplitudes of extracted signal are markedly less than those of the original GM. This is partially because the period range selected for this project (typical period of simple structures) is much less than the median value of periods of selected FN GM pulses (See Appendix F.5. The median value of periods of FN pulses is about 4.11 s, with an average of 5.35 s). Thus, according to previous researchers, in such cases the response of the system is not expected to be well determined by an equivalent pulse (extracted or synthesized).

To better illustrate this phenomenon, the values of $\text{Median}\,(\delta_{in})_{ExP-FN}$ are normalized to their corresponding values of $\text{Median}\,(\delta_{in})_{ORIG-FN}$; results are presented in Figure 4-25.

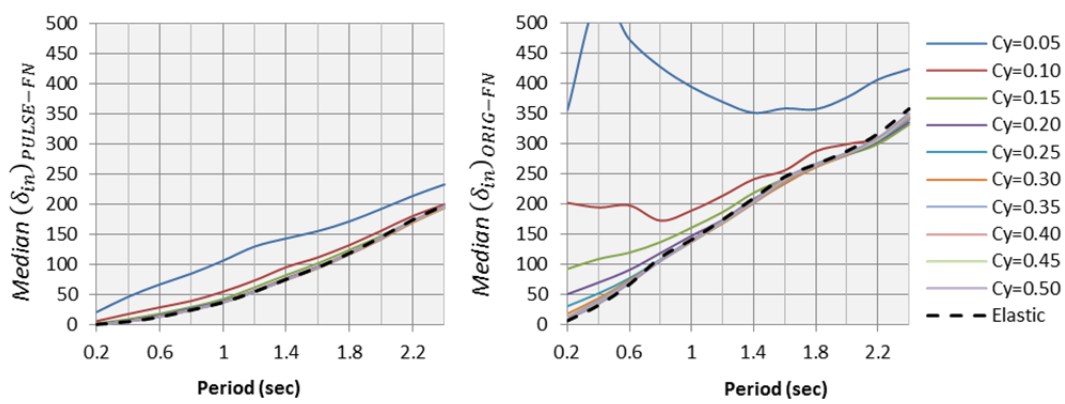

Figure 4-24: SDOF median of maximum displacement demand in the FN direction: nonlinear model = NLT#4, damping ratio $\zeta = 2\%$. Right figure, original NF GM; left figure, the extracted pulse signal

Figure 4-25 shows that the median value of maximum displacement demand due to extracted pulses excessively and systematically underestimates the same due to the original FN record. Nonetheless, the trend of Figure 4-25 suggests that the ratio of $\text{Median}\ (\delta_{in})_{ExP-FN}/\text{Median}\ (\delta_{in})_{FF-FN}$ approaches unity as the elastic period of vibration of the system tends to higher values.

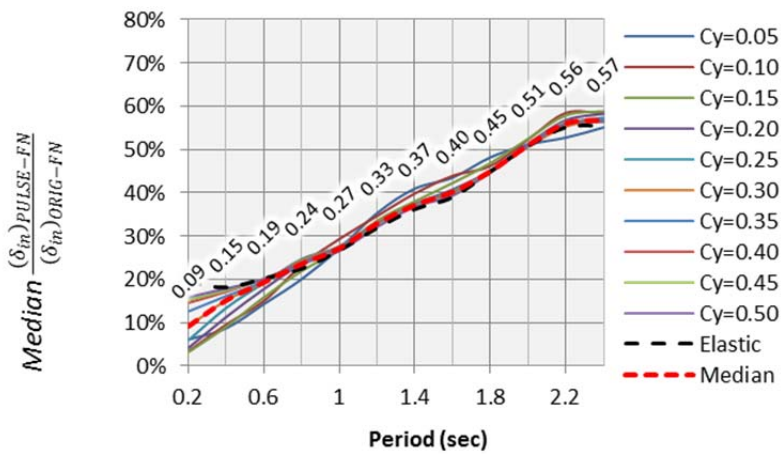

Figure 4-25: SDOF ratio of median of maximum displacement demand in the FN direction due to original NF GM to the same due to the extracted pulse signal: nonlinear model = NLT#4, damping ratio $\zeta = 2\%$

4.3.1.2 How well can the filtered signals represent the extracted NF pulses?

Figure 4-26 shows the ratio of the median of maximum displacement demand for the extracted signal using low-pass filtered NF GMs, to the median of maximum displacement demand for the extracted signal using wavelet analysis in the FN direction, i.e., $(\delta_{in})_{\text{Filtered-PULSE-FN}}/(\delta_{in})_{\text{Wavelet-PULSE-FN}}$.

As Figure 4-26 indicates, the response of the structures due to filtered signals tends to over-predict the response of the structures due to extracted signals, for short-period structures (Te $<$ 0.6 s) and does the opposite for the structures with longer periods. This phenomenon is partially related to the shape of the filter function employed and its frequency pass threshold.

Thus, from Figure 4-26, one may conclude that using a filtering process to extract the pulse might be a good starting point in design but it cannot closely reproduce the median of maximum displacement demand due to extracted pulses.

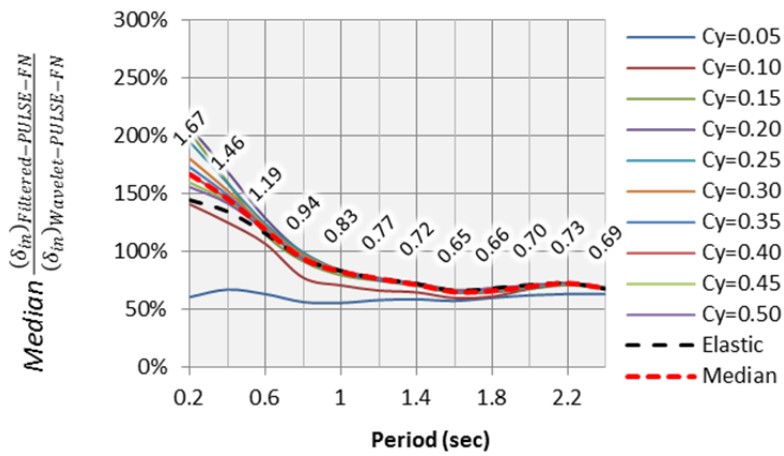

Figure 4-26: SDOF ratio of median of maximum displacement demand in the FN direction due to low-pass filtered signal to the same due to the extracted pulse signal: Nonlinear model = NLT#4, damping ratio $\zeta = 2\%$

4.3.1.3 How comparable is the residual signal to the FF GMs?

Figure 4-27 shows the median of maximum displacement demand in the FN direction for the residual signal of NF GMs after long-period velocity pulse is extracted from the original NF GM using Baker's proposed method.

Figure 4-27 indicates that the trends of response for both FF GMs and residual signals are very similar. However, the amplitudes of the responses of residual signals are somewhat higher than those due to their FF GM counterparts.

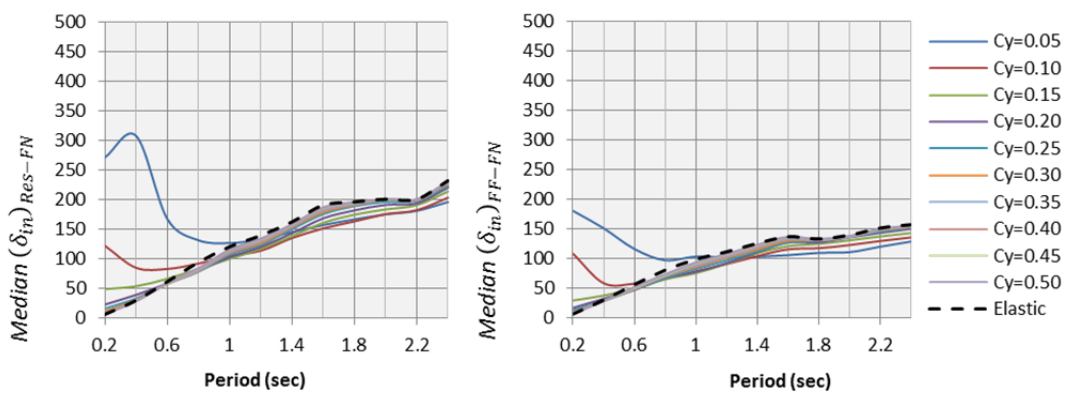

Figure 4-27: SDOF median of maximum displacement demand in the FN direction: nonlinear model = NLT#4, damping ratio $\zeta = 2\%$. Left figure, residual signal of NF GMs; right figure, the same for the FF GMs (compatible to the original NF GMs)

To better estimate the similarities between residual signals and their FF GM counterparts, the median of maximum displacement demand due to residual signals

is normalized to those due to their FF GM counterparts. Results are presented in Figure 4-28, which shows that for elastic periods of vibration of less than 1.0 s the compatible FF GMs can reasonably approximate the response of the residual signals. However, FF GMs tend to underestimate the response of residual signals as the elastic period of the system increases.

It is of note that the response is mainly governed by elasticity of the system. Hence, effects of yield characteristics or different nonlinear models on the results presented in Figure 4-28 are negligible.

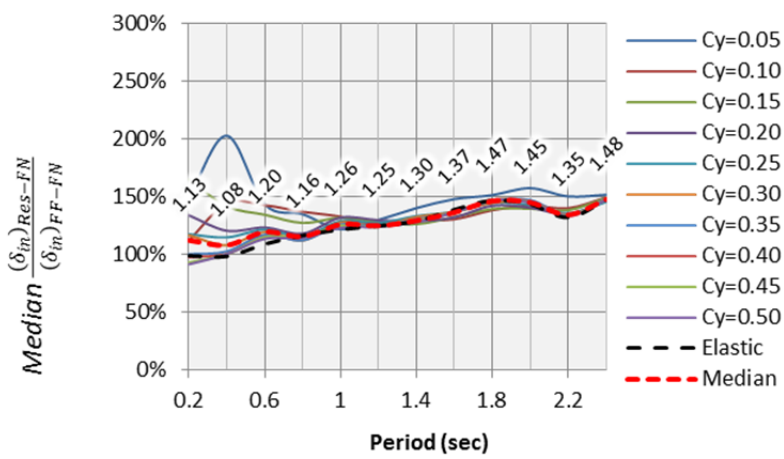

Figure 4-28: SDOF ratio of median of maximum displacement demand in the FN direction due to residual signal of NF GMs to the same due to the FF GMs: nonlinear model = NLT#4, damping ratio $\zeta = 2\%$

From Figure 4-28 one can infer that nonlinear responses of structures due to residual signals are within $\pm$20% of those due to 1.2 × FF GMs (when 1.2 x FF GMs denotes 120% amplified FF GMs). Hence, one might argue that by compiling extracted pulses (or synthesized pulses) with 1.2 × FF GMs one can produce a semi-realistic NF GM for an event for which the FF GM is recorded but the NF GM is unavailable. The same technique can be used to compile synthesized pulsed with available FF GMs and generate some new semi-realistic NF GMs. These compiled semi-realistic NF GMs might be considered as a substitute to entirely synthesized NF GM for design purposes. It is of note that synthesizing a signal pulse as a function of M_w, distance, and fault mechanism is a very well formulated procedure, and is a fairly trivial task.

This is a simple yet novel way for synthesizing NF GMs, and an answer to the hypothesis that was discussed in section 4.3.

4.4 Discussion

In this chapter effects of NF GMs on various EDPs of interest were investigated and a simplified method to prorate the EDPs of interest for NF GMs from the same for FF GMs was proposed. For example, with the proposed simplified method one can approximate the expected maximum displacement of a structure due to NF GMs from the maximum displacement of the structure determined based on the code-proposed procedures.

Results of analysis of NF GMs and their FF counterparts show that

- response of structures to FF GMs usually shows significant numbers of excursion with relatively small displacement amplitudes. Conversely, response of the structure to NF GMs shows a few excursions. However, all are associated with relatively large displacement amplitudes.
- the effect of strength and stiffness degradation is much more pronounced when the system is subjected to NF GMs. This is mainly due to early yielding of the structure, which in turn results in a reduced equivalent period of the system in response to the remainder of the NF input motion,
- the rate of input energy (input energy per second) of NF GMs is generally considerably more than that of FF GMs.
- nonlinear backbone curves/model and reversal loading pattern have a small effect on maximum displacement demand and maximum ductility demands, especially for structures with $C_y \geq 20\%$ or moderate- and long-period systems,
- YCDR is a very stable and robust parameter that can be used for estimating the required strength of a structure subjected to NF GMs for limiting ductility ratio of a structure to some target ductility value. The YCDR in the FN and FP directions can be estimated from
- $\text{YCDR} = \begin{cases} 1 + 0.65T_e & \text{in the FN direction} \\ 1 + 0.30T_e & \text{in the FP direction} \end{cases}$

- the ratio of $\delta_{inelastic}/\delta_{elastic}$ is approximately one for both NF and FF GMs (nonetheless, $\delta_{inelastic}/\delta_{elastic}$ for NF GMs general supersedes those for FF GMs).
- The following table summarizes the proposed procedure for determining EDP of interest due to NF GMs from the same due to FF GMs. The same procedure is summarized in Flowchart # 4-1 as well.

Table 4-5: Step-by-step procedure for determining EP of interest due to NF GMs from the same due to FF GMs

Use code provisions to:
1. Determine T_e, period of vibration at first significant mode in direction of interest: Either from code provisions/empirical equations or from simple linear analysis for the fixed-base structure 2. Determine $S_a(T_e)$, spectral acceleration response Use code-prescribed response spectrum (developed based on FF GMs) or from site specific response spectrum (without consideration of any near-fault effect adjustments) 3. Determine V_e, elastic base shear $$\mathrm{V_e = S_a(T_e) \times W}$$ 4. Determine R_y Use code-prescribed yield-strength reduction factor, representing the capability of a structure to dissipate energy through reversed cyclic inelastic behaviour (a function of structural system)
Analyse the system:
5. Decide if a linear analysis or a nonlinear analysis is preferable; go to step 5.b to do a nonlinear analysis a. A) Linear analysis: i. Determine C_y when $C_y = \frac{F_y}{W} \cong \frac{V_{in}}{W} \cong \frac{S_a(T_e)}{R_y}$ and $S_a(T_e)$ and R_y are determined from steps 2 and 3, respectively

Use code provisions to:
ii. Determine EDP_{FF} For example, δ_{FF} is the maximum inelastic displacement for FF GMs that can be estimated as $U_{max} \cong U_e \times R_y$ when U_e denotes elastic displacement. iii. Go to step 6 b. B) Nonlinear analysis: i. Determine $\mathrm{C_y}$ from nonlinear analysis ii. Determine $\mathrm{EDP_{FF}}$ from nonlinear analysis
Prorating $\mathbf{EDP_{NF-GMs}}$ from $\mathbf{EDP_{FF-GMs}}$
6. Use C_y from step#7.a or 6.a and T_e from step#1 to approximate/interpolate $M_{EDP.Ratio}$ and $\sigma_{EDP.Ratio}$ from the content of Appendix A or Chapter 4 7. Prorate EDP_{NF} from $$EDP_{NF-GMs} \cong EDP_{FF-GMs} \times M_{EDP.Ratio} \times e^{[\sigma_{EDP.Ratio} \times \Phi^{-1}(P)]}$$

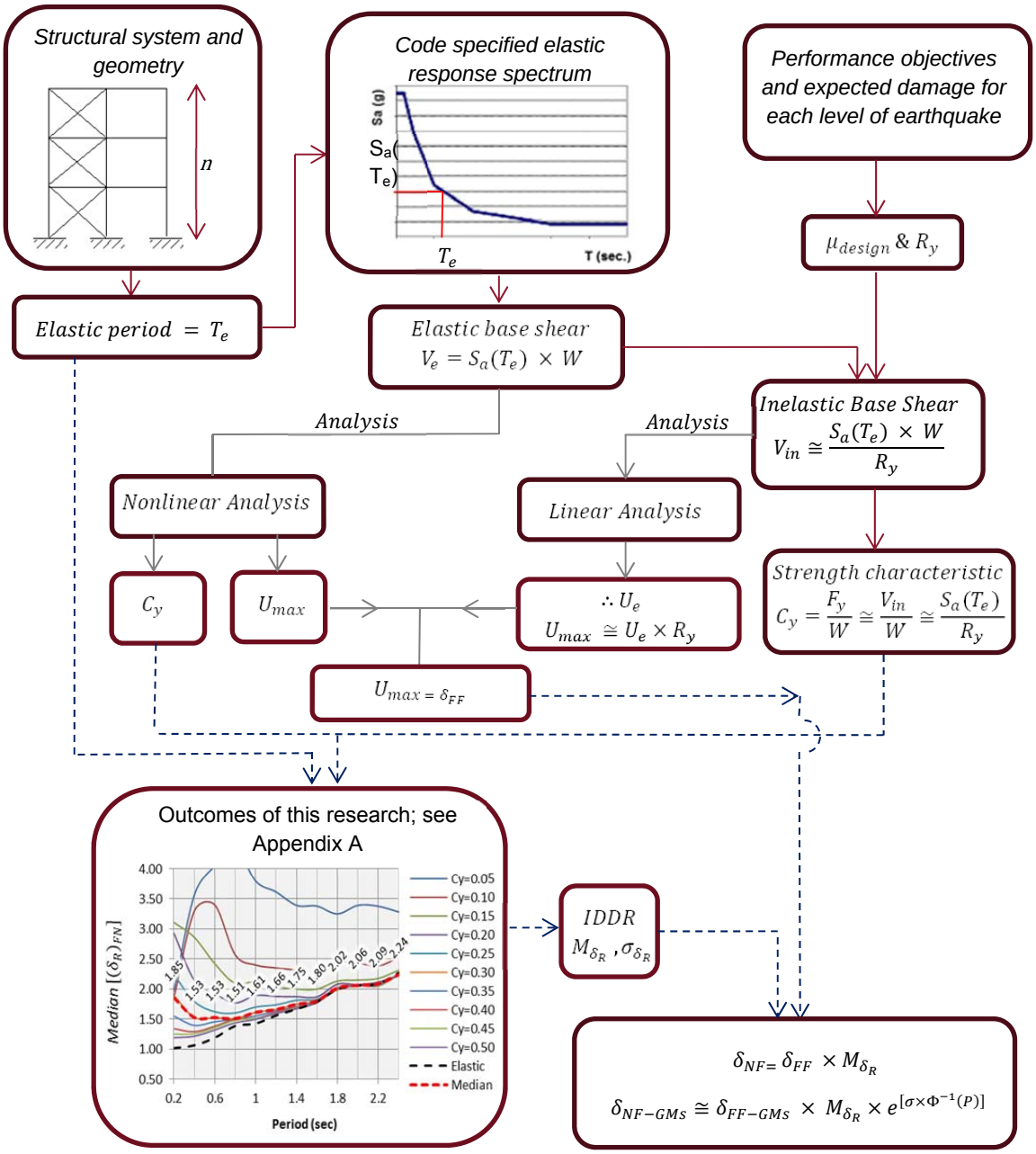

Flowchart # 4-1: Proposed procedure for determining δ_{NF-GMs} from δ_{FF-GMs} (e.g., determined based on code-prescribed method. Note: a similar approach is applicable to other EDPs of interest, too)

5. A simplified method for predicting response of flexible-base structures from response of their equivalent fixed-base models

Chapter Outline:

1. Section 5.1 details a proposed mathematical equivalent 2DOF model for consideration of FFS effects
2. Section 5.2 briefly discusses nonlinear behaviour of a representative 2DOF system analysed for a variety parameters.
3. Section 5.3 details a proposed method for evaluation of effects of FFS using an equivalent nonlinear SDOF system
4. Section 5.4 presents a practical example to show how content of sections 5.2 and 5.3 might be used in practice.
5. Section 5.5 presents a summary of this chapter

In the previous chapter the nonlinear response of a variety of fixed-base structures due to NF GMs were discussed and their responses compared with the same due to FF GMs. In the previous chapter a simplified procedure to approximate EDPs of interest for NF GMs from the same determined for their FF GM counterparts was also proposed.

In this chapter, effects of FFS on the response of the structures due to NF and FF GMs; will be studied, i.e., first the same results of Chapter 4 will be replicated when the structure is supported on a flexible base. That is to say, the effects of NF GMs on the nonlinear response of the same structures studied in Chapter 4 will be evaluated when FFS is explicitly factored into the modeling to allow for consideration of combined effects of NF GMs and FFS. To achieve this goal a simplified 2DOF model that accounts for the effects of flexibility and mass of the foundations is introduced.

Following the NLTHA of 2DOF systems, as described above, a simplified mathematical procedure that can accurately and efficiently estimate EDPs of interest for a simple structure on a flexible base (i.e., 2DOF) from the same EDPs of interest determined for an equivalent fixed-base structure (i.e., SDOF) will be formulated. This should assist engineers to indirectly account for FFS by determining an equivalent SDOF system; the behaviour of this system due to NF GMs has already been studied/formulated in Chapter 4.

5.1 Proposed simplified 2DOF model for consideration of FFS effects

Figure 5-1 shows a simplified model that is widely accepted and used by the industry for preliminary evaluation of effects of FFS on the nonlinear response of structures. This model was used in many studies since the 1970s. For example, Veletsos and Meek (1974) calculated the period of the flexible-base system subject to horizontal excitations, and Veletsos and Nair (1975) determined a closed-form expression for damping of the flexible-base system (as a function of the elongated period of the system and foundation damping consisting of hysteretic and radiation damping).

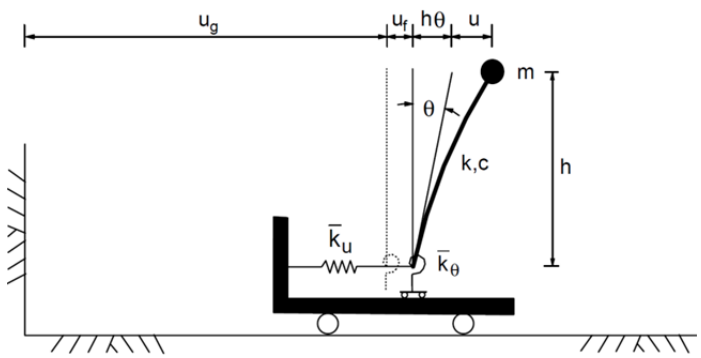

Figure 5-1: Simplified oscillator model for analysis of inertial interaction under lateral excitation (after Bozorgnia and Bertero (2004)

While the simplified model presented in Figure 5-1 was very well studied in past, almost invariably all researchers assumed a massless foundation in their analysis. However, this assumption is not conclusive; for example, in situation when the foundation is massive or when a considerable amount of soil attached to the foundation moves in phase with the foundation. An example of the latter case is

dense pile groups, where closely spaced piles can confine a significant amount of soil between them. The effect of soil moving in phase with the foundations could be treated as an added mass to the foundation.

From what has been stated above, one can easily envisage many other real cases where the simplified model presented in Figure 5-1 does not adequately simulate real behaviour. A quick remedy to the above model is to consider some translational and rotational masses at the base of the model.

A new simplified model, which in general is in line with what is presented in Figure 5-1, is proposed below. However, the new proposed model:

a. Also allows for modeling of the transversal mass of the foundation[1]
b. Merges the rotational and the transversal springs into one equivalent horizontal spring (which accounts for effect of both transitional and rotational springs, while it produces the same effect as if they were modeled individually).

Thus; the equivalent horizontal base spring is modeled in a way such that, because of a horizontal unit load applied to the top of the model, the system produces the same lateral displacement as the assembly of rotational and transversal base springs could have produced if they had been modeled individually; i.e.,

$$u_{total} = u_s + u_x + u_\theta \qquad 5\text{-}1$$

where

u_{total} is total displacement due to a unit load at the tip of the model

u_s is the part of the total displacement due to deformation of the superstructure (above foundation)

1 Note: in this research, it was judged that the effect of the rotational mass of the foundation (whether in the case of massive rafts or pile groups with their associated confined soil) is not significant. Hence, rotational foundation mass is ignored in the following subsections.

u_x the part of the total displacement due to transversal movement of foundation

u_θ the part of the total displacement due to rotation of foundation

Equation 5-1 can be rewritten in terms of the stiffness values of the system:

$$\frac{1}{k_{eq}} = \frac{1}{k_s} + \left(\frac{h^2}{k_\theta} + \frac{1}{k_x}\right) \qquad 5\text{-}2$$

where h is the effective height of the elevated mass (above the foundation).

Since the last two terms of equation 5-2 collectively represent the equivalent stiffness of the foundation (both rotational and transversal), if one substitutes them with an equivalent transversal foundation stiffness,k_f, then one would have

$$\left(\frac{h^2}{k_\theta} + \frac{1}{k_x}\right) = \frac{1}{k_f} \qquad 5\text{-}3$$

$$\frac{1}{k_{eq}} = \frac{1}{k_s} + \frac{1}{k_f} \qquad 5\text{-}4$$

Equation 5-4 indicates that the equivalent stiffness of the system could be represented with two springs assembled in series, namely, k_s and k_f.

Figure 5-2 shows how a real structure can be modeled using the proposed 2DOF system when the foundation stiffness, K_f, is modeled with an equivalent transversal spring and foundation transversal mass, M_f, is accounted for explicitly.

To further simplify the model and reduce the number of variables, M_f and K_f would be also represented in Terms of the mass of the superstructure, M_s and stiffness, K_s, respectively. That us to say,

$$M_f = \alpha M_s \qquad \text{and} \qquad k_f = \beta k_s \qquad 5\text{-}5$$

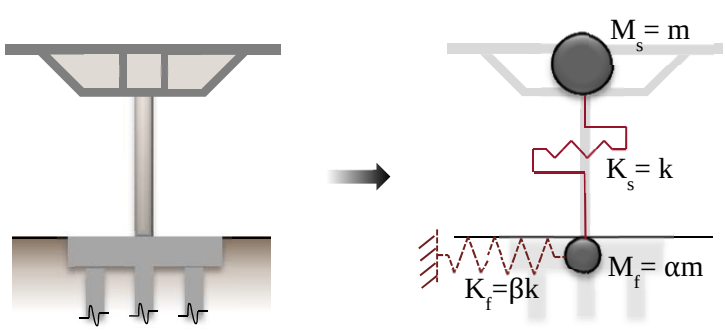

Figure 5-2: Proposed 2DOF simplified equivalent system, for consideration of FFS when foundation mass is explicitly factored into the modeling

To account for combined effects of FFS and NF GMs, a series of simplified models using the proposed 2DOF systems were developed, analysed, and studied. To achieve this goal, the effect of FFS was factored into the mathematical models used in section 4 by adding transversal springs and foundation added masses to the base of the SDOF systems in each horizontal directions. Foundation stiffness ratio, mass ratio, and nonlinearity model used for the analysis of 2DOF systems are listed below:

- System #1: $\alpha = 0.15$ and $\beta = 2.0$; complete with LNK#4 nonlinear model
- System #2: $\alpha = 0.15$ and $\beta = 4.0$; complete with LNK#4 nonlinear model
- System #3: $\alpha = 0.25$ and $\beta = 4.0$; complete with LNK#4 nonlinear model

The procedure implemented for NLTHA of the 2DOFs is exactly the same as that described in section 4.1 for SDOF systems.

Similar to what was used in the previous chapter, to allow for better understanding of the implemented procedure, results of the analysis of a representative SDOF system subjected to a representative NF GM (and its FF GM counterpart) are presented in Appendix D.

Also, to account for variability of monitored EDPs of the flexible-base structures due to the full range of parameters adopted in this study, results of the analysis of different 2DOF models (with different permutations of system parameters as noted above) are presented in a generalized probabilistic context. Please see the following section.

5.2 Statistical representation of results of comprehensive parametric analysis of 2DOF systems

This section summarizes the results of NLTHA performed on a series of 2DOF systems, as detailed in Table 3-2.

Similar results to those presented in section 4.2 for fixed-base systems are presented in this section for 2DOF systems, as detailed in Table 3-2. Results are presented in Terms of

1. Maximum displacement demand spectra and IDDR*
2. Maximum ductility demand spectra and DDR*
3. Maximum inelastic to elastic displacement demand ratio

The following sections briefly discuss the observations made with respect to each of above-mentioned items.

5.2.1 Maximum displacement demand spectra and IDDR* for 2DOF systems

The following subsections discuss observations made through investigation of median and dispersion values of maximum displacement demand spectra due to NF GMs as well as those due to FF GMs for the 2DOF models detailed in section 3.2.

For reference, a complete set of results of the parametric analysis of the 2DOF systems studied are presented in Appendix B.

5.2.1.1 Analysis of maximum displacement demand spectra and IDDR* in the FN direction

Figure 5-3 shows the variation of median values of the maximum displacement demand of the superstructure in the FN direction for both NF and FF GMs with respect to variation of the fundamental period of vibration as well as strength characteristics of the superstructure for system #3, as defined in section 3.

It is of note that Figure 5-3 is the counterpart of Figure 4.2; i.e., Figure 4.2 shows the maximum displacement demand spectra of a system with a fixed-base boundary condition, while Figure 5-3 shows the same when effects of FFS are accounted for using α = 0.25 and β = 4.0.

In general, the trend of maximum displacement demand spectra in FN direction for 2DOF systems is similar to what was presented in section 4.2.1.1 for SDOF

systems. However, comparing Figure 5-3 with Figure 4.2 shows that consideration of FFS has dual effects on both NF and FF GMs.

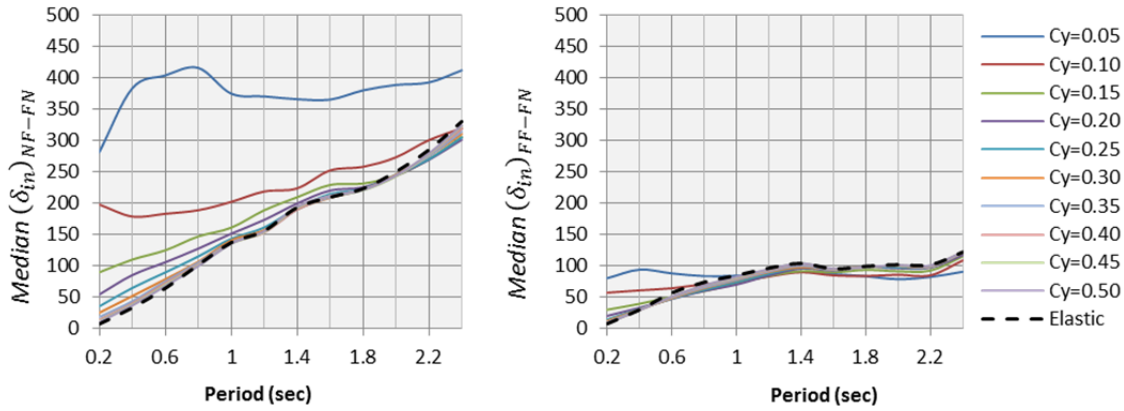

Figure 5-3: 2DOF maximum displacement demand spectra in the FN direction: nonlinear model = NLT#4, α = 0.25,| β = 4.0, ζ = 2%. Left figure, NF GMs; right figure, FF GMs

To better illustrate this dual effect, Figure 5-4 provides a general trend comparison by presenting maximum displacement demand spectra of flexible-base system #3 for the FN component of NF GMs, normalized by their fixed-base counterparts (i.e., values of Figure 5-3 FN components are divided by the same values of Figure 4.2).

Figure 5-4 shows that the maximum displacement response of flexible-base system is generally within ±20% of those determined for its fixed-base counterpart when the system is subjected to the FN components of NF GMs.

Figure 5-5 is similar to Figure 5-4, except that it is for the FN component of FF GMs.

Comparison of Figure 5-5 and Figure 5-4 shows that FFS have similar trends on maximum displacement response of structures due to both NF and FF GMs, however with different amplitudes. That is to say, FFS causes more displacement (amplification) in the short-period range, and less displacement (deamplification) in moderate- to long-period ranges for NF GMs than those for FF GMs.

(Note: the values in the shaded zones of both Figure 5-5 and Figure 5-4 should be used with caution, as the response of structures become unbounded for short-period structures.)

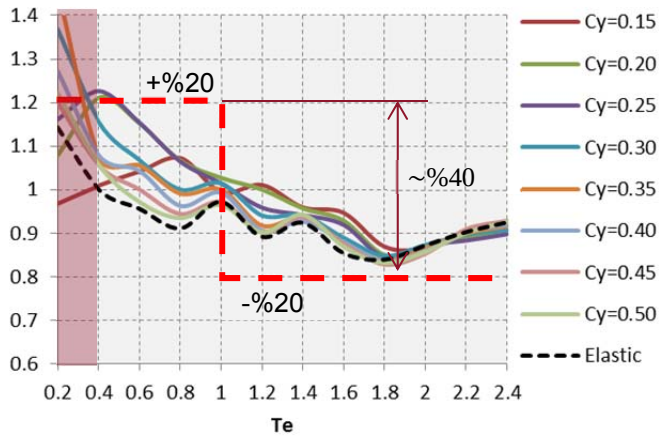

Figure 5-4: 2DOF, System#3 maximum displacement demand spectra due to the FN component of NF GMs normalized to its fixed-base counterparts

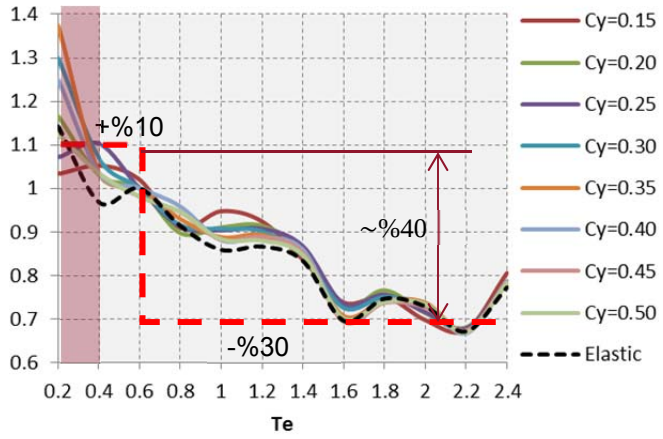

Figure 5-5: 2DOF, System#3 maximum displacement demand spectra due to FN component of FF GMs normalized to its fixed-base counterparts

To have a better quantitative measure of the influence of NF GMs on the maximum displacement demand of a flexible-base system, IDDR* was defined as the median values of the maximum displacement demand of the superstructure due to NF GMs in the FN direction normalized by the same due to FF GMs. Figure 5-6 shows IDDR* for a system with α = 0.25 and β = 4.0 (system #3). Figure 5-6 is also a counterpart of Figure 4.4; the former one is developed for a flexible-base system using α = 0.25 and β = 4.0, and the latter one is developed for the same system, except with fixed-base boundary conditions.

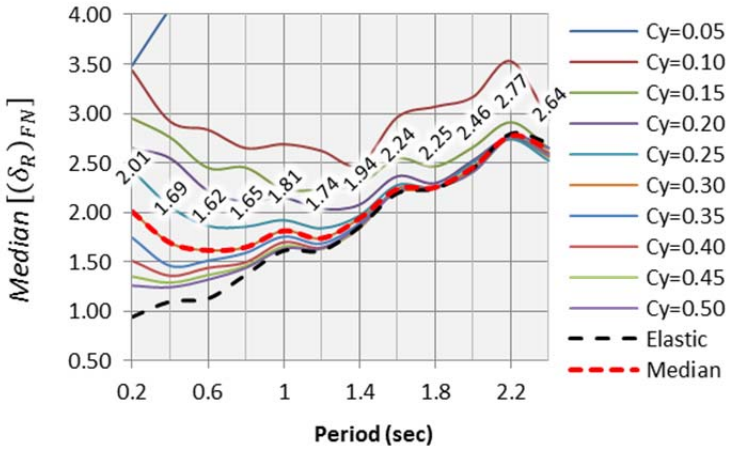

Figure 5-6: 2DOF IDDR* in the FN direction: nonlinear model = NLT#4, α = 0.25, β=4.0, ζ = 2%

Comparison of Figure 5-6 with its counterpart, Figure 4.4, shows that values of IDDR* exceeds those of IDDR.

Results of Figure 5-6 reinforce the hypothesis made in section 0.

Figure 5-7 provides a general trend comparison between IDDR* and IDDR in the FN direction when **α** = 0.25 and **β** = 4.0:

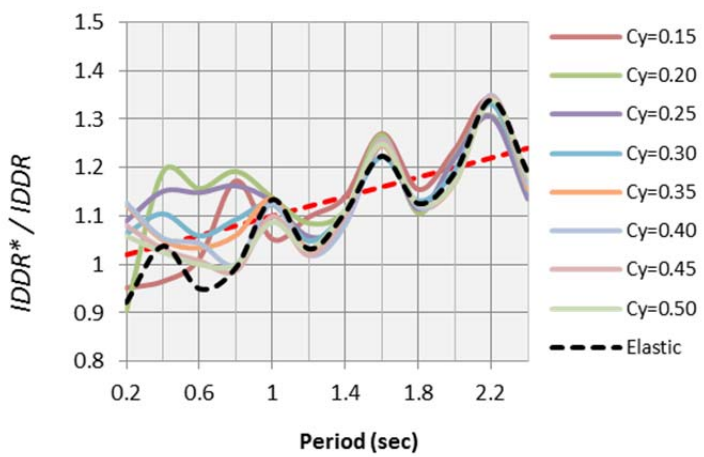

Figure 5-7: $IDDR^*/IDDR$ in the FN direction: nonlinear model = NLT#4, α = 0.25, β = 4.0, ζ = 2%

Figure 5-7 shows that consideration of FFS, in general, can result in higher values of inelastic displacement demand ratios. This phenomenon can be justified by considering the elongated period of flexible-base systems (in comparison with their fixed-base counterparts). To be precise, FFS causes period elongation, which in

turn results, in more susceptibility of the system to input motions with long-period pulses.

The red dashed line in Figure 5-7 shows the proposed trace of the ratio of IDDR* to IDDR. This fitted curve is evident for all three systems that are defined in section 3, namely, Systems #1 to #3. Equation 5-6, which results from regression analysis of all three systems, represents the fitted curve of $IDDR^*/IDDR$ in fault normal direction:

$$\frac{IDDR^*{}_{FN-Direction}}{IDDR_{FN-Direction}} = 0.5\left(\frac{\alpha^3}{\beta}\right)^{0.2} T_e + 0.93 \qquad 5\text{-}6$$

5.2.1.2 Analysis of maximum displacement demand spectra and IDDR* in the FP direction

Figure 5-8 depicts the variation of median values of maximum displacement demand of the superstructure in the FP direction for both NF and FF GMs with respect to variation of T_e and C_y.

Figure 5-8 is the counterpart of Figure 4.8; i.e., Figure 4.8 shows maximum displacement demand spectra of a system with a fixed-base boundary condition, and Figure 5-8 shows the same for system #3, as described in section 3.

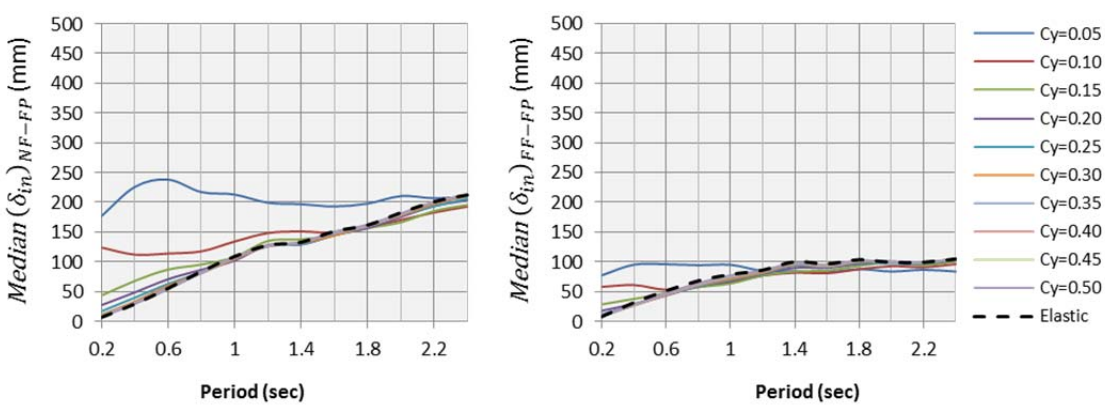

Figure 5-8: 2DOF maximum displacement demand spectra in the FP direction: nonlinear model = NLT#4, α = 0.25, β = 4.0, ζ = 2%. Left figure, NF GMs; right figure, FF GMs

In general, the same observations that were reported in section 5.2.1.1 for FN components (of input motions) are valid for FP components as well. Figure 5-9 illustrates maximum displacement demand spectra of flexible-base systems #3 for

FP component of NF GMs, normalized by their fixed-base counterparts (i.e., Figure 5-8 values are divided by Figure 4.8 values). Figure 5-9 shows a similar trend as was observed in the FN direction; namely, Figure 5-9 is very much like Figure 5-4.

A similar observation as that reported for normalized maximum displacement spectra due to the FP component of NF GMs is valid for the FP component of FF GMs.

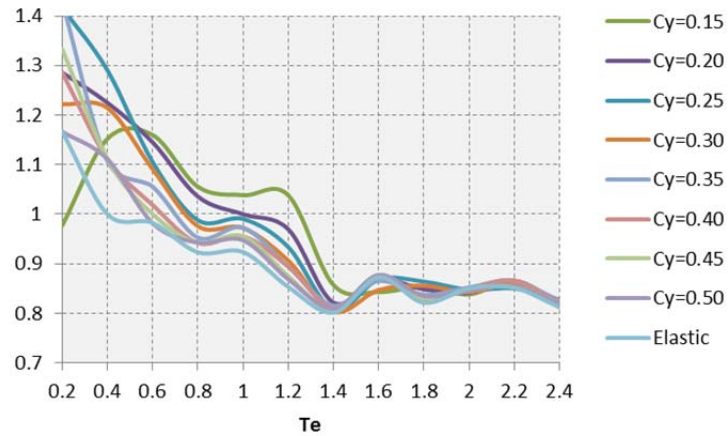

Figure 5-9: 2DOF System#3 maximum displacement demand spectra due to the FP component of NF GMs normalized to its fixed-base counterparts

IDDR* in the FP direction is determined and presented in Figure 5-10. Figure 5-10 is also a counterpart of Figure 4.9, while the former figure is developed for flexible-base system #3 as detailed in section 3 and the latter one is developed for the same system but with a fixed-base boundary condition

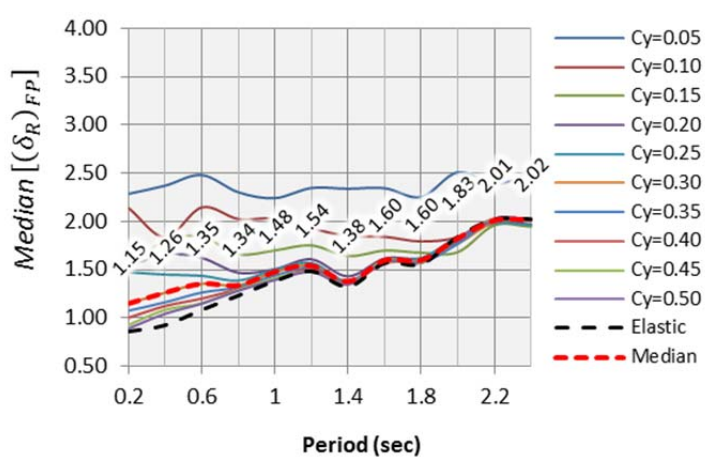

Figure 5-10: 2DOF IDDR* in the FN direction: nonlinear model = NLT#4, α = 0.25. β = 4.0, ζ = 2%

By comparing Figure 5-10 with its counterpart, Figure 4.9, one can infer that IDDR* in the FP direction is more than IDDR in the FP direction. This observation matches what was observed in the FN direction and is another proof for the basic hypothesis stated in section 0.

Figure 5-11 provides a general trend comparison between IDDR* and IDDR in the FP direction for system #3 (i.e., α = 0.25 and β = 4.0):

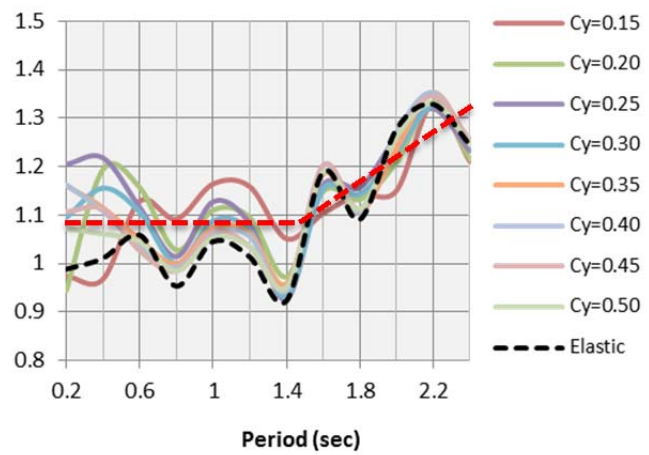

Figure 5-11: $IDDR^*/IDDR$ in the FP direction: nonlinear model = NLT#4, α = 0.25, β = 4.0, $\zeta = 2\%$

Unlike the trend of $IDDR^*/IDDR$ in the FN direction, fitting a simple curve over $IDDR^*/IDDR$ in the FP direction which accurately can estimate the original results might not be very practicable (Figure 5-11); yet one may use the red dashed line as a fair estimate of $IDDR^*/IDDR$ in the FP direction.

Generally speaking, Figure 5-11 shows that consideration of FFS typically results in higher values for IDDR; this is again chiefly due to period elongation of flexible-base systems.

5.2.2 Maximum ductility demand and DDR*

This section is very similar to what was presented in section 5.2.1, except the instead of the maximum displacements, the maximum ductility demands are considered and determined. The following subsections briefly discuss the observations with respect to maximum ductility demand due to NF GMs when the structure is supported on a flexible-base system.

5.2.2.1 Analysis of maximum ductility demand and DDR* in the FN direction

The trends of variation of median values of maximum ductility demand of the structures supported on flexible bases are very similar to those when fixed-base boundary conditions are assumed for the structures. However, since the amplitude of the maximum displacement demand of the superstructure varies by variation of the flexibility of the base, one can expect that ductility demand amplitudes also vary with variation of flexibility of the bases. This phenomenon is depicted in Figure 5-12, which shows the maximum ductility demand spectra in the FN direction for a flexible-base system with α = 0.25 and β=4.0 and subjected to NF GMs normalized to the same when the boundary condition of the systems is assumed to be fixed. As is evident from comparison of Figure 5-12 and Figure 5-4, the trend and amplitude variation of maximum ductility demand due to effects of FFS is very much like the trend and amplitude variation of the maximum displacement response of the superstructure.

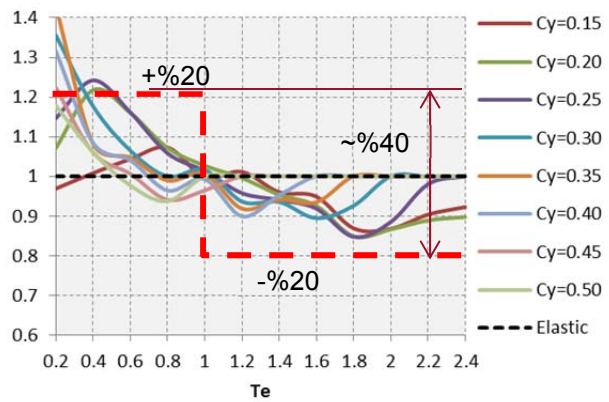

Figure 5-12: 2DOF, system#3, maximum ductility demand spectra due to the FN component of NF GMs normalized to its fixed-base counterparts

Figure 5-13 shows similar information to that presented in Figure 5-12 for the FN component of FF GMs. Again, the general trend and amplitude of the effects of FFS on ductility demand is very similar to those to maximum displacement demand, except that for long-period range, ductility of both fixed- and flexible-base systems approaches unity as the system remains elastic.

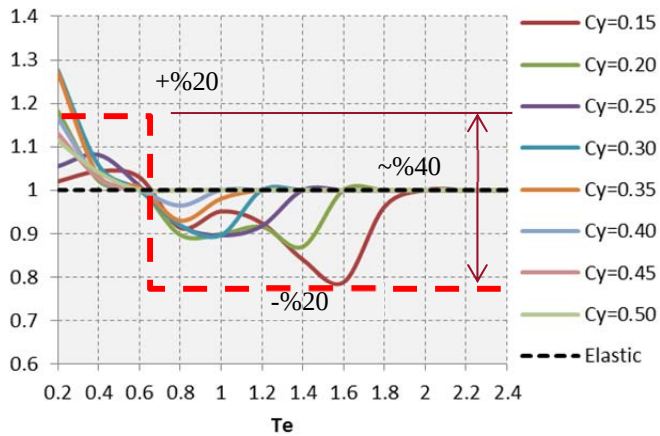

Figure 5-13: 2DOF, system#3, maximum ductility demand spectra due to the FP component of NF GMs normalized to its fixed-base counterparts

To have a better quantitative measure of the influence of NF GMs on the maximum ductility demand of a flexible-base system, the median values of maximum ductility demand due to NF GMs in the FN direction were normalized to those due to FF GMs in the same direction, i.e., for a system with α = 0.25 and β = 4.0. The result, DDR*, is presented in Figure 5-14.

Figure 5-14, developed for system #3 as detailed in section 3, is the counterpart of Figure 4.12 developed for the same system but with a fixed-base boundary condition.

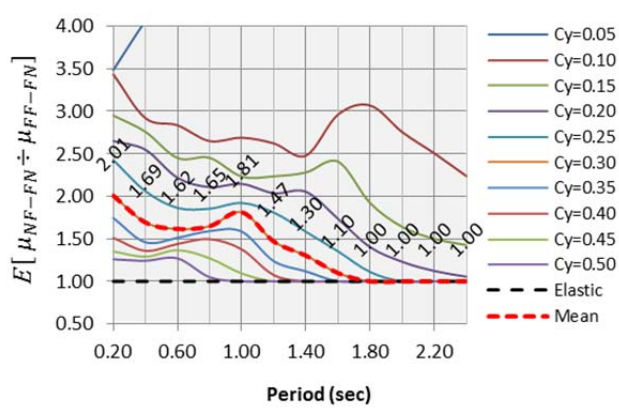

Figure 5-14: 2DOF DDR* in FN direction: nonlinear model = NLT#4, α = 0.25, β = 4.0, ζ = 2%

Comparison of Figure 5-14 with its counterpart, Figure 4.4 shows that the DDR* trend is very similar to the DDR trend, except that

a) short-period structures experience more ductility demand, and moderate to long-period structures experience less ductility demand,

b) weak structures (e.g., C_y < 0.15) may have a much higher ductility ratio

c) the ratio of DDR* to DDR varies from 1.2 for short-period structures to 0.8 for long-period structures (if/when the long-period systems yield)

5.2.2.2 Analysis of maximum ductility demand and DDR* in the FP direction

The trend of variation of median values of the maximum ductility demand of structures supported on a flexible-base due to input motions in the FP direction are quite similar to what was observed due to input motions in the FN direction (as detailed in the previous subsection). Hence, for brevity, details are omitted in this subsection, and the reader is referred to section 5.2.2.1 (and Appendix B) for more information.

5.2.3 Maximum inelastic to elastic displacement demand and maximum inelastic to elastic displacement demand ratio

When one considers the trend of the variation of maximum displacement demand, as detailed in section 5.2.1, one may expect the effects of FFS will result in

a) maximum inelastic to elastic displacement demand ratio for short-period structures increases as flexibility of the base increases,

b) maximum inelastic to elastic displacement demand ratio for moderate- and long-period structures decreases/approaches unity as flexibility of the base increases.

Figure 5-15 shows the ratio of ($\delta_{inelastic}/\delta_{elastic}$) for system #3 as detailed in section 3 to ($\delta_{inelastic}/\delta_{elastic}$) for the same system when the base of the system is fixed.

It is of note that similar observations are made for both FP component of NF GMs, and FP and FN components of FF GM. Please refer to Appendix B for information.

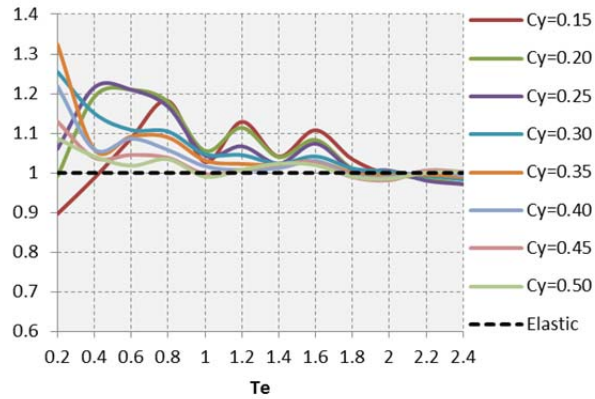

Figure 5-15: ($\delta_{inelastic}/\delta_{elastic}$) in the FN direction for system #3 normalized to the same as when boundary condition of the system is set to full fixity: nonlinear model = NLT#4, damping ratio $\zeta = 2\%$

5.3 A simplified mathematical method for predicting the response of flexible-base structures from the response of their equivalent fixed-base models

The seismic response of a variety of SDOF systems due to a range of selected NF and FF GMs was addressed in Chapter 4. Also, in the previous section, FEM was used to study the seismic response when the structures were supported on flexible-base systems (complete with foundation mass and soil added masses).

In this section, a simplified mathematical approach is used to formulate a simple procedure which assists design engineers to evaluate effects of FFS on the response of structures using results of analysis of an equivalent SDOF system. The proposed method is highly efficient and requires no sophisticated analysis or computer modeling.

The proposed equivalent SDOF system is an outcome of a two-stage simplification of a soil–foundation–structure comprehensive model, namely,

c) Stage-1 simplification: allows for simplifying the comprehensive system to an equivalent 2DOF model, which accounts for elasticity of the foundation and foundation mass (see section 5.1),

d) Stage-2 simplification: allows for substituting the simplified 2DOF model by an equivalent SDOF system.

Using structural parameters of the above-mentioned equivalent SDOF system, one may use either the code specified nonlinear response spectra (displacement, ductility, etc.), or any rudimentary routine to perform a NLTHA of the equivalent SDOF system and evaluate EDPs of interest, when inertia effects of SFSI are implicitly accounted for.

The following sections briefly describe the proposed procedure and evaluate its validity using results of Chapter 4 and section 5.2.

5.3.1 Conversion of properties of flexible-base systems to properties of their equivalent SDOF systems

A new mathematical model which allows for condensing rotational and the transversal base springs into one equivalent horizontal base spring, which produces the same effect as if both transitional and rotational springs are modeled individually, was proposed in section 5.1. See Figure 5-2 and equations 5-1 to 5-4.

Since the proposed system is a 2DOFmodel, its equation of motion can be formulated as per equation 5-7:

$$[M]\{\ddot{u}\} + [C]\{\dot{u}\} + [K]\{u\} = [M] \times \{i\} \times \ddot{u}_g \qquad 5\text{-}7$$

where

$$[M] = \begin{bmatrix} M_f & 0 \\ 0 & M_s \end{bmatrix} = \begin{bmatrix} \alpha M_s & 0 \\ 0 & M_s \end{bmatrix} = M_s \begin{bmatrix} \alpha & 0 \\ 0 & 1.0 \end{bmatrix} \qquad 5\text{-}8$$

$$[K] = \begin{bmatrix} K_f + K_s & -K_s \\ -K_s & K_s \end{bmatrix} = \begin{bmatrix} \beta K_s + K_s & -K_s \\ -K_s & K_s \end{bmatrix} = K_s \begin{bmatrix} 1.0 + \beta & -1.0 \\ -1.0 & 1.0 \end{bmatrix} \qquad 5\text{-}9$$

$$[C] = \begin{bmatrix} C_f + C_s & -C_s \\ -C_s & C_s \end{bmatrix} \qquad 5\text{-}10$$

$$\{i\} = \begin{Bmatrix} 1.0 \\ 1.0 \end{Bmatrix} \qquad 5\text{-}11$$

The classic general solution of equation 5-7 is represented in equation 5-12:

$$\begin{Bmatrix} u_1 \\ u_2 \end{Bmatrix} = \begin{Bmatrix} \phi_1 \\ \phi_2 \end{Bmatrix} \sin(\omega_{sys} t - \theta) \qquad 5\text{-}12$$

Substituting equation 5-12 in equation 5-7 results in the characteristic equation of motion, as presented in equation 5-13.

$$\begin{bmatrix} (K_f + K_s - m_1\omega_{sys}{}^2) & -Ks \\ -K_s & (K_s - m_2\omega_{sys}{}^2) \end{bmatrix} \begin{Bmatrix} \phi_1 \\ \phi_2 \end{Bmatrix} = \begin{Bmatrix} 0 \\ 0 \end{Bmatrix} \qquad 5\text{-}13$$

Hence, solution of the Eigenvalues problem of equation 5-13 results in the characteristic polynomial of equation of motion as noted in equation 5-14:

$$\omega_{sys}{}^4 - \left(\frac{K_f + K_s}{M_f} + \frac{K_s}{M_s} \right) \omega_{sys}{}^2 + \frac{K_f K_s}{M_f M_s} = 0 \qquad 5\text{-}14$$

$$\omega_{sys}{}^2 = \frac{1}{2} \left\{ \left[\frac{K_f + K_s}{M_f} + \frac{K_s}{M_s} \right] \pm \left[\left(\frac{K_f + K_s}{M_f} + \frac{K_s}{M_s} \right)^2 - \frac{K_f K_s}{M_f M_s} \right]^{1/2} \right\} \qquad 5\text{-}15$$

Now, substituting M_f with αM_s and k_f with βk_s gives

$$\omega_{sys}{}^2 = \frac{\omega_{fb}{}^2}{2} \times \left(\frac{\alpha + \beta + 1}{\alpha} \mp \sqrt{\left(\frac{\alpha + \beta + 1}{\alpha} \right)^2 - 4\frac{\beta}{\alpha}} \right) \qquad 5\text{-}16$$

To simplify equation 5-16 and derive the next few equations, which describe the dynamic properties of the equivalent SDOF system, the following five system constants, which are all functions of α and β, have been defined. These are *A*, *B*, *C*, *D*1, and *D*2 and are formulated in equations 5-17 to 5-21

$$A = \left(\frac{\alpha + \beta + 1}{2\alpha} \right) \qquad 5\text{-}17$$

$$B = \sqrt{\mathrm{A}^2 - \frac{\beta}{\alpha}} \qquad 5\text{-}18$$

$$C = \mathrm{A} - \frac{\beta + 1}{\alpha} \qquad 5\text{-}19$$

$$D1 = \frac{(\alpha(B + C) + 1)^2}{\alpha(B + C)^2 + 1} \qquad 5\text{-}20$$

$$D2 = \frac{(\alpha(B - C) - 1)^2}{\alpha(B - C)^2 + 1} \qquad 5\text{-}21$$

Now, substituting *A* and *B* in Equation 5-16, results in

$$\omega_{sys}{}^2 = \omega_{fb}{}^2 \times (A \pm B) \qquad 5\text{-}22$$

Thus, ratio of the period of the first mode of vibration of a soil–foundation–structure system (equivalent 2DOF) to the period of vibration of its fixed-base superstructure (SDOF) can be determined as

$$\frac{T_{sys}}{T_{fb}} = \frac{1}{\sqrt{A - B}} \qquad 5\text{-}23$$

where the T_{sys}/T_{fb} period is the elongating ratio.

Similarly, the first mode shape of the equivalent 2DOF can be determined from

$$\varphi = \begin{Bmatrix} C + B \\ 1 \end{Bmatrix} \qquad 5\text{-}24$$

Also, to estimate the significance of the first mode in the total response of the system, the base shear modal participation ratio for the first and the second modes of vibration could be determined from

$$MP1 = \frac{D1}{D1 + D2} \qquad 5\text{-}25$$

$$MP2 = 1 - MP1 \qquad 5\text{-}26$$

Up to this point, all linear properties of the flexible-base system are determined in terms of the dynamic properties of the fixed-base superstructure, α and β. The linear properties determined for the flexible-base system can assist in the development of an equivalent elastic SDOF model based on properties of the first mode of vibration of the simplified 2DOF system in the direction of interest.[1]

However, to be able to account for nonlinearity of the structure and extend the results of Chapter 4 to the flexible-base systems, it is necessary to assign some realistic nonlinear properties to the equivalent elastic SDOF model. This will produce an equivalent nonlinear SDOF model which can reasonably approximate total response of its associated 2DOF system.

To achieve this goal, a simple procedure is defined that allows for estimating nonlinearity of equivalent SDOF systems from nonlinearity of their associated superstructures. To be precise, a procedure to determine the adjusted strength

[1] Assuming that first mode of vibration of equivalent 2DOF is dominant and governs the responses.

characteristics of the equivalent SDOF ($C_y{}^*$) from the dynamic properties and strength characteristic of its relative superstructure (C_y) was defined.

The process of adjusting C_y for producing $C_y{}^*$ is a two-step procedure:

1. Step#1: adjustment due to new load distribution (associated with the first mode of vibration of 2DOF). This adjustment accounts for the new mass/new lateral load distribution.
2. Step#2: adjustment due to new stiffness of equivalent SDOF (at first mode of vibration). This adjustment allows for modifying C_y to allow for a backbone curve that matches the family of backbone curves used for evaluation of response of the superstructure.

The concurrent effects of the two-step adjustment allows for a modified strength characteristic ($C_y{}^*$), which can be used in modeling of an equivalent SDOF system to fairly accurately predict the response of a 2DOF system (the simplified model of the structure with consideration of its FFS effects).

Determining the step#1 adjustment:

The step#1 adjustment can be determined by calculating the base shear of the system for the condition that the system vibrates in its fundamental modes of vibration and the superstructure reaches its ultimate elastic state. This will be referred to as base shear V_{base_1}. Now, dividing V_{base_1} by the entire mass of the system (assuming that almost the entire mass participates in the first mode of vibration) results in a new strength characteristic of the system, $C_{y1}{}^*$. The step#1 adjustment value is determined by dividing $C_{y1}{}^*$by C_y.

Now, if it is assumed that a structure vibrates in its first mode of vibration, then the maximum equivalent static force on the top node and on the foundation node could be determined using equations 5-27 and 5-28, respectively.

$$F_{2,1} = m \times D(t) \times \varphi_{2,1} \times \omega_{sys)1}{}^2 \qquad 5\text{-}27$$

$$F_{1,1} = \alpha m \times D(t) \times \varphi_{1,1} \times \omega_{sys)1}{}^2 \qquad 5\text{-}28$$

where $D(t)$ is the response of a system with unit mass and circular frequency of $\omega_{sys)1}$. Thus, the ratio of base shear of the superstructure to base shear of the system (below the foundation level) could be determined as

$$\frac{F_{2,1}}{V_{base_1}} = \frac{\varphi_{2,1}}{\varphi_{21i} + \alpha\varphi_{1,1}} = \frac{1}{1 + \alpha(C + B)} \qquad 5\text{-}29$$

Now, if the top spring is pushed to its ultimate elastic capacity, then $F_{2,1}$ = $C_y \times m \times g$. By substituting this value in equation 5-29, one can estimate ${C_{y1}}^*$; see equations 5-30 and 5-31.

$$\frac{C_y \times m \times g}{{C_{y1}}^* \times (1 + \alpha)m \times g} = \frac{1}{1 + \alpha(C + B)} \qquad 5\text{-}30$$

$$Adj\#1 = \frac{{C_{y1}}^*}{C_y} = \frac{1 + \alpha(C + B)}{1 + \alpha} \qquad 5\text{-}31$$

where $Adj\#1$ is the step#1 adjustment factor for correcting the strength characteristic to allow for new load distribution.

Determining step#2 adjustment:

The step#2 adjustment allows for a modified inelastic load-displacement pattern that accounts for the stiffness of the equivalent SDOF and an equivalent backbone curve that is consistent with the family of backbone curves used for analysis of superstructure/SDOF system. To apply this adjustment, one should prorate C_y with the ratio K_2/K_1.[1]

$$Adj\#2 = \frac{{C_{y2}}^*}{C_y} = \frac{K_2}{K_1} = \frac{(1 + \alpha)m}{{T_{sys}}^2} \times \frac{{T_{fb}}^2}{m} \qquad 5\text{-}32$$

$$Adj\#2 = (1 + \alpha) \times \left(\frac{T_{fb}}{T_{sys}}\right)^2 = (1 + \alpha) \times (A - B) \qquad 5\text{-}33$$

Thus, total adjustment of the strength characteristic of the SFSI system can be approximated by $Adj\#1 \times Adj\#2$, that is to say,

$$Adj.Factor = Adj\#1 \times Adj\#2 = [1 + \alpha(C + B)] \times (A - B) \qquad 5\text{-}34$$

$${C_y}^* = [1 + \alpha(C + B)] \times (A - B) \times C_y \qquad 5\text{-}35$$

[1] This adjustment is more easily comprehended, when one considers that response of a SDOF with K, m, and C_y to an input GM is equivalent to response of a system with αK, αm, and αC_y to the same input motion.

where $C_y{}^*$ is the strength characteristic of the equivalent SDOF.[1]

Summary:

To determine EDPs of interest for a simple structure when FFS needs to be accounted for, one may combine properties of the superstructure with properties of the foundation (i.e., foundation stiffness and mass ratio) to determine properties of an equivalent SDOF system. Then, with the properties of the equivalent SDOF system, one can use standard nonlinear (displacement, ductility, etc.) response spectra to determine EDPs of interest for the equivalent SDOF system, which indirectly accounts for the effects of FFS as well.

It is of note that displacements determined from this approach are total displacements, i.e., displacement of superstructure plus displacement of foundation. Now, if one is only interested in determining displacement of the superstructure, then the calculated displacements needs to be corrected. A rough remedy for this problem is to assume that displacement of the system at the maximum displacement state of the superstructure has almost the same shape as the shape of the first mode of vibration of the system. From this assumption one may calculate a displacement correction factor (D_{CF}) as per equation 5-36

$$D_{CF} = 1 - (C + B) \qquad \text{5-36}$$

Although this is a very rudimentary correction, it provides fairly accurate estimates of the superstructures displacement.

The validity of this approach is examined in section 5.3.2.

[1] Although the modified strength characteristics could be mathematically determined for the second mode of vibration as well, since the response of simple structures (subject of this research) is mainly governed by the first mode of vibration, they are physically meaningless. It is of note that this method is only an estimate for the strength characteristics of the entire soil–foundation–structure system when soil remains entirely elastic.

5.3.1.1 Practical applications of proposed 2DOF system for evaluation of combined effects of NF GMs and SFSI

Using the simplified approach detailed in section 5.3, one should be able to estimate the period shift and the strength characteristic of a system with a flexible base from properties of its corresponding fixed-base superstructure.

With the new period and the new strength characteristic for the equivalent soil–foundation–structure system, it should be possible to use results of section 4 to estimate the effect of the NF GM on the response of the superstructure when FFS is implicitly accounted for.

Problem example #5-1 is devised to assist clarifying the proposed method within the context of a hypothetical case resembling a practical problem.

Problem example #5-1:

Assume a bridge with the properties below:

$T_e = 1\ \text{s},\ C_y = 0.2,\ \alpha = 0.3,\ \beta = 4\ ,\ \zeta = 2\%$ and NLT#4 model

The bridge is designed based on current design standards, using a design response spectrum that accounts for only FF GMs.

Maximum deck drift due to design earthquake is determined to be approximately 5%.

Determine the maximum drift of the structure due to a compatible NF GM for two cases, namely, (A) a fixed-base system and (B) a flexible-base system (with consideration of foundation mass and stiffness).

- For case (A), one can use Figure 4.3 to determine IDDR in the FN direction for the fixed-base system, namely, $IDDR_{FN} \cong 1.8$. Thus, maximum drift due to NF GMs would be in the order of 9%.
- For case (B), first one needs to estimate T_{sys} and $C_y{}^*$ for the equivalent SDOF system, and then use Figure 4.3 to determine IDDR in the FN direction for the flexible-base system. Therefore, from equation 5-17 to 5-19:

  A = 8.833

  B = 8.043

  C = (–7.833)

  and from equation 5-23:

$$\frac{T_{sys}}{T_{fb}} = \frac{1}{\sqrt{A-B}} = 1.13 \qquad \rightarrow \qquad T_{sys} = 1.13\ \text{s}$$

Problem example #5-1:
and $C_y{}^* = [1 + \alpha(C + B)] \times (A - B) \times C_y = 0.13$ Now, from the equivalent SDOF properties $T_{sys} = 1.13$ s and $C_y{}^* = 0.13$, and also with consideration of Figure 4.3, one can determine $IDDR_{FN \text{ and } FFS} \cong 2.25$. Thus, total deck displacement due to combined effects of NF GMs and FFS would be in the order of 11%. However, the total drift (within the superstructure) is a product of total deck displacement and D_{CF} when $D_{CF} = 1 - (C + B) = 0.8$. Thus the maximum drift of the superstructure is in the order of 8%. Note: the cumbersome calculations detailed above are not required for standard designs, as all required parameters are simplified in the form of graphs and tables in the following subsection; see Figure 5-16 to Figure 5-19.

Amongst all simplifications used for development of this approach, there are two major underlying assumptions that readers should be aware of:

a) the behaviour of the foundation (including behaviour of the soil) is assumed to be totally elastic,

b) the soil–foundation–structure system response is mainly governed by the response of the first mode of vibration.

Thus, if the second mode of vibration contributes significantly to the response of interest, then the estimated equivalent strength characteristic ($C_y{}^*$) is not an accurate estimate of the yield threshold of the structure, and results of section 4 might not be directly usable for this approach.

To simplify the proposed method and eliminated the tedious calculations required for determining equivalent properties of the systems (as detailed in the previous subsection), a series of figures and tables are prepared for a wide range of foundation mass and stiffness ratios (α and β).

- Figure 5-16 is graphical representation of equation 5-23, to be used for estimation of the period of the first mode of vibration of the soil–foundation–structure system from the period of vibration of its fixed-base superstructure.

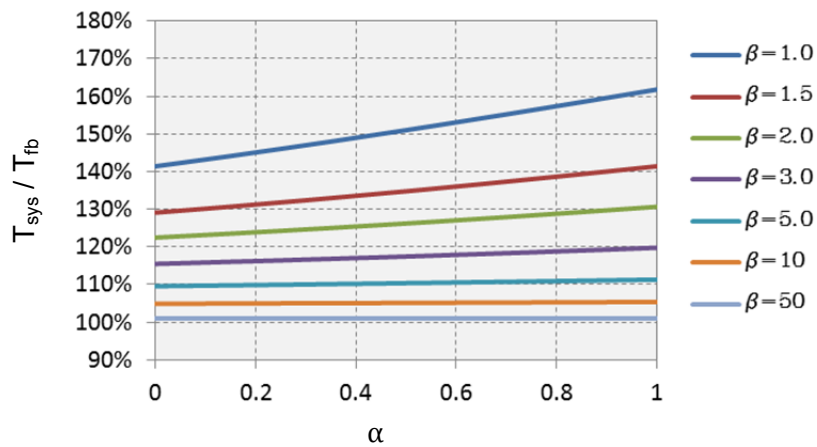

Figure 5-16: Period elongation ratio (ratio of period of the first mode of vibration of the system to the fundamental period of the fixed-base SDOF)

Note: As one can infer from Figure 5-16, except for very soft soils (small values of β), period elongation is almost insensitive to variation of foundation mass.

- Figure 5-17 is graphical representation of equation 5-35, to be used for estimation of the strength characteristic of the equivalent SDOF system from the strength characteristic of its fixed-base superstructure.

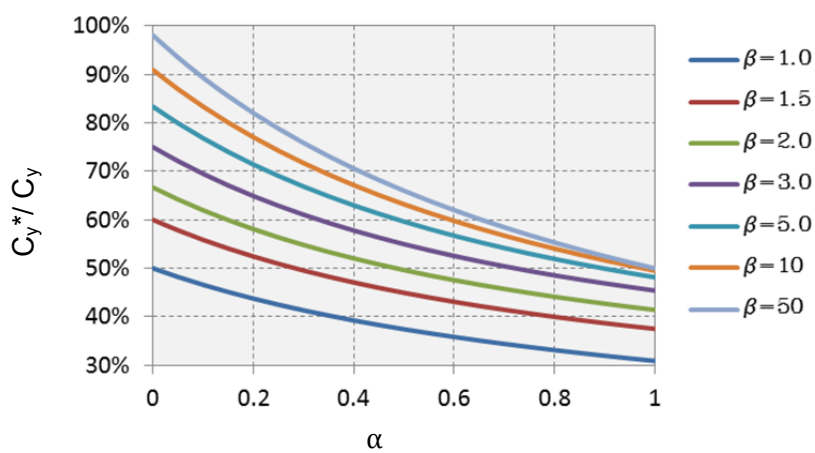

Figure 5-17: Strength characteristic correction factor

Notes:

a. Strength characteristic correction factor is always less than one.

b. Corrected strength characteristic is reduced as foundation flexibility increases.

- Figure 5-18 is graphical representation of equation 5-36, showing the displacement correction factor.

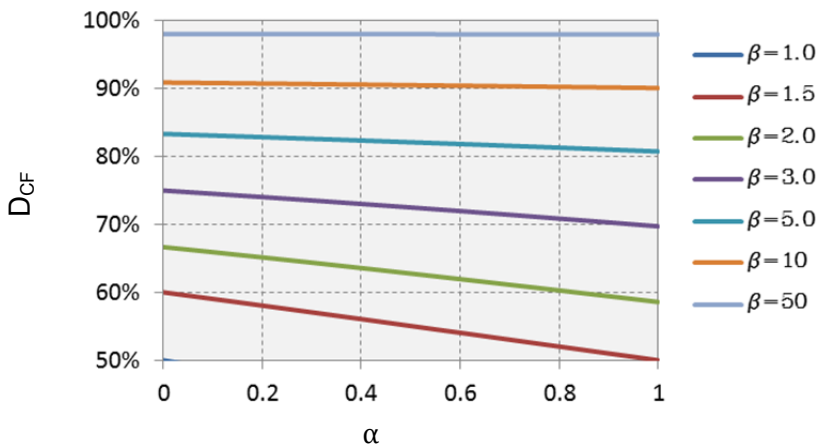

Figure 5-18: Displacement correction factor

Notes: The displacement correction factor

a. approaches unity as flexibility of foundation reduces,

b. is highly dependent on β, with almost no effect from α for practical ranges of β.

- Figure 5-19 is graphical representation of equation 5-25, to be used for estimation of the effectiveness of the first mode of vibration for determination of modified strength characteristics.

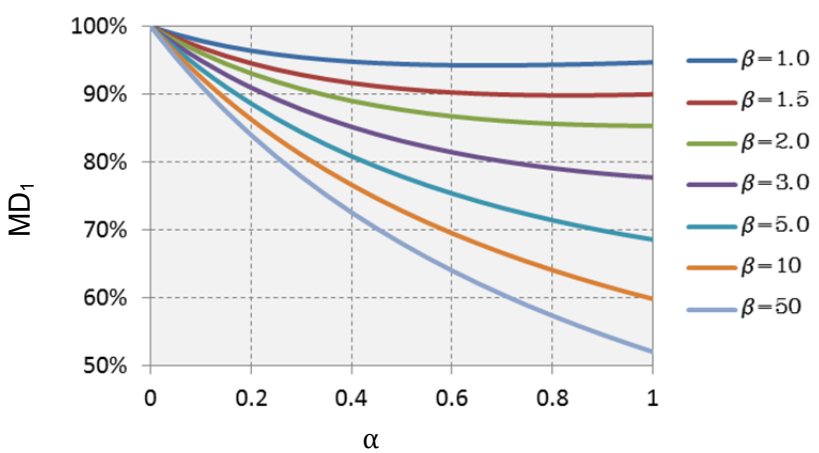

Figure 5-19: First mode participation in base shear of the system

Note: participation of the second mode of vibration increases as the foundation stiffness decreases and/or the foundation mass increases.

For example, values of Table 5-1 are extracted from Figure 5-16 to Figure 5-19, and detail the first mode period elongation ratio, first mode participation ratio in base shear, displacement correction factor and equivalent strength characteristic ratio for three different combinations of α and β, which are used for analysis of 2DOF systems in section 5.2.

Table 5-1: System parameters for different permutations of α and β based on the fixed-base structure dynamic properties

	α = 0.15 and β = 2	α = 0.15 and β = 4	α = 0.25 and β = 4
First mode period elongation ratio	1.235	1.121	1.124
$C_y{}^*/C_y$	60%	71%	67%
D_{cf}	0.655	0.795	0.792
First mode participation ratio	0.940	0.918	0.876

5.3.2 Verification of proposed simplified method for consideration of FFS effects using NLTHA of an equivalent SDOF system

In following subsections, an attempt will be made to verify validity of the simplified method proposed in section 5.3 for predicting the response of flexible-base structures from the response of their equivalent SDOF models. To do so, results of FEM analysis of a range of 2DOF systems will be compared with results of NLTHA of their simplified equivalent SDOF systems.

To achieve this goal results of FEM analysis of three 2DOF systems presented in section 5.2 were compared with results of their equivalent SDOF systems, determined based on content of Chapter 4.

5.3.2.1 Comparison of results of FEM analysis of 2DOF systems with results of NLTHA of their equivalent SDOF:

<u>Properties of 2DOF system:</u> For detailed definition of 2DOF systems used in this chapter, refer to section 3.2 and section 5.3. Table 5-2 and

Table 5-3 summarize the structural properties of the 2DOF systems used in this study project:

Table 5-2: Properties of the superstructure

	Properties of the superstructure's				
System ID	K_e (kN/m)	m (t)	T_e	C_y	Nonlinearity model
System #1	32000	810	1.0	0.2	NLK#4
System #2	32000	810	1.0	0.2	NLK#4
System #3	32000	810	1.0	0.2	NLK#4

Table 5-3: Properties of the foundation system systems

	Foundation Properties			
System ID	α	M_f (t)	β	K_f (kN/m)
System #1	0.15	121.5	2	64000
System #2	0.15	121.5	4	128000
System #3	0.25	202.5	4	128000

<u>Properties of equivalent SDOF system:</u> Using Figure 5-16 to Figure 5-19, one can easily extract parameters required for development of equivalent SDOF system parameters, namely, ratios of T_{sys}/T_{fb}, D_{CF}, and the ratio of $C_y{}^*/C_y$.

Values of ratio T_{sys}/T_{fb}, ratio of $C_y{}^*/C_y$, and D_{CF} as well as equivalent SDOF system parameters are summarized in Table 5-4.

Table 5-4: Determined properties of the equivalent SDOF system

	Properties of equivalent SDOF				
System ID	T_{sys}/T_{fb}	T_{sys}	$C_y{}^*/C_y$	$C_y{}^*$	D_{CF}
System #1	1.235	1.235	60%	0.120	0.655
System #2	1.121	1.121	71%	0.143	0.795
System #3	1.124	1.124	67%	0.133	0.792

<u>2DOF superstructure's maximum displacement demands and IDDR* determined from FEM analysis:</u> For the purpose of this verification, results of FEM analysis of 2DOF systems as described in section 5.2 and presented in Appendix B were used.

That is the maximum displacement demands and IDDR* for System #1 to system #3 for the superstructure are extracted from Figure B5-1 to Figure B5-3 of Appendix B, respectively. For example, Figure 5-20 shows the process of extrapolation of the median value of maximum displacement demand of the superstructure of system #3 due to NF GMs in the FN direction.

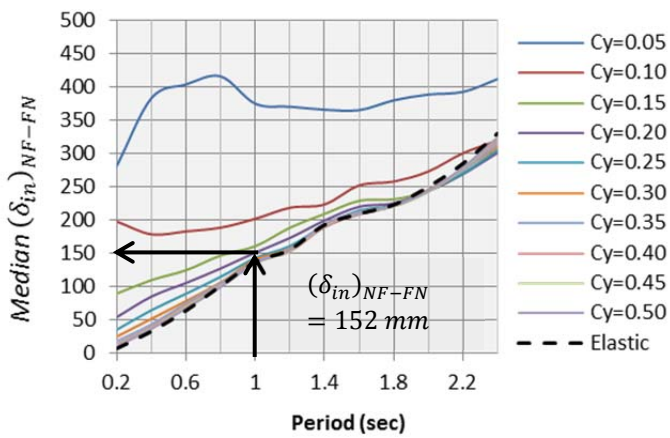

Figure 5-20: 2DOF system #3 maximum displacement demand spectra in the FN direction: nonlinear model = NLT#4, α = 0.25, β=2.0, ζ = 2%

A complete list of extracted median values of maximum displacement demands for NF and FF GMs in both FN and FP directions for all three 2DOF systems are detailed in Table 5-5. Similarly, median values of IDDR* for NF and FF GMs in both FN and FP directions are extracted from their respective figures in Appendix B and are tabulated in

Table 5-6.

Table 5-5: Median value of maximum displacements of superstructure determined from NLTHA of 2DOF with explicit consideration of foundation stiffness and mass parameters

	Results of FEM analysis of 2DOF systems			
System ID	$(\delta_{in})_{NF-FN}$ (mm)	$(\delta_{in})_{FF-FN}$ (mm)	$(\delta_{in})_{FF-FN}$ (mm)	$(\delta_{in})_{FF-FP}$ (mm)
System #1	144	67	104	66
System #2	152	72	104	70
System #3	152	71	102	68

Table 5-6: IDDR^* determined fr m NLTHA of 2DOF with explicit consideration of foundation stiffness and mass parameters

	$IDDR^* of\ 2DOF\ systems$	
System ID	$IDDR^*{}_{FN}$	$IDDR^*{}_{FP}$
System #1	217%	158%
System #2	211%	149%
System #3	215%	151%

<u>Maximum displacement demands and IDDR values for equivalent SDOF system:</u> Median value of maximum displacement demands and IDDR values for the equivalent SDOF system (as detailed per Table 5-4) are determined from results of analysis presented in section 6 (see Appendix A).

For example, Figure 5-21 shows the process of extrapolation of the median value of maximum displacement demand of the equivalent SDOF system #3 (with $T_{fb} = 1.235\ s$ and $\mathrm{C}_y{}^* = 1.20$) due to NF GMs in the FN direction. It is of note that displacement extrapolated values represent the maximum total displacement of the system (i.e., displacement of foundation plus relative displacement of superstructure to the foundation). Thus, as mentioned in section 5.3, to account for only relative displacement of the superstructure to the foundation, the extracted values need to be corrected using the factor D_{CF}.

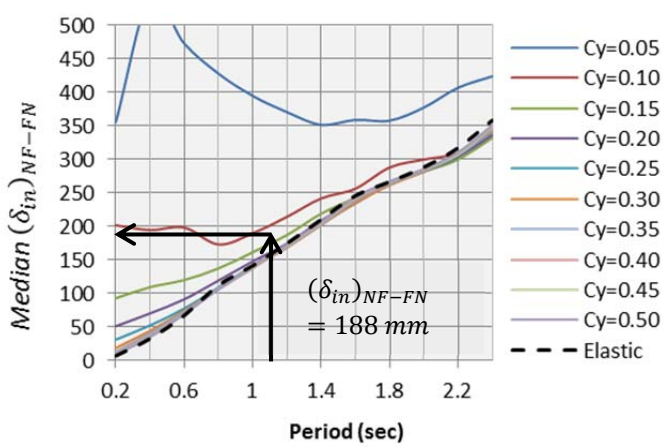

Figure 5-21: Equivalent SDOF #3 maximum displacement demand spectra in the FN direction: nonlinear model = NLT#4, α = 0.25, β = 2.0, ζ = 2%

A complete list of extracted median values of total maximum displacement demands (including foundation deformation) for NF and FF GMs in both FN and FP directions for all three equivalent SDOF systems are presented in Table 5-7.

As previously mentioned, displacements reported in Table 5-7 are total displacements (including foundation displacement). However, this study is focused on the displacement of the superstructure relative to the foundation. Thus, as mentioned in section 5.3, a simple remedy to this problem is using D_{CF} factors to approximate relative displacement of the superstructure from the total displacement determined from NLTHA of the equivalent SDOF systems.

Table 5-7: Total maximum displacement demands (including foundation deformation) determined from NLTHA of equivalent SDOF systems with implicit consideration of SFSI effects

	Total maximum displacement demands					
System ID	Tsys	Cy*	$(\delta_{in})_{NF-FN}$ (mm)	$(\delta_{in})_{FF-FN}$ (mm)	$(\delta_{in})_{FF-FN}$ (mm)	$(\delta_{in})_{FF-FP}$ (mm)
Equivalent SDOF #1	1.235	0.120	210	95	145	88
Equivalent SDOF #2	1.121	0.143	182	86	123	81
Equivalent SDOF #3	1.124	0.133	188	86	126	81

Table 5-8 shows superstructure's maximum displacement demands determined from multiplying D_{CF} factors, as presented in Table 5-4, by total maximum displacement demands, as presented in Table 5-7.

Table 5-8: Mmaximum displacement demands of the superstructure determined from NLTHA of equivalent SDOF systems with implicit consideration of SFSI effects

	Maximum displacement demands of the superstructure				
System ID	D_{CF}	$(\delta_{in})_{NF-FN}$ (mm)	$(\delta_{in})_{FF-FN}$ (mm)	$(\delta_{in})_{FF-FN}$ (mm)	$(\delta_{in})_{FF-FP})$ (mm)
Equivalent SDOF #1	0.655	138	62	95	58
Equivalent SDOF #2	0.795	145	68	98	64
Equivalent SDOF #3	0.792	149	68	100	64

Similarly, Figure 5-22 shows the process of extrapolation of IDDR of the equivalent SDOF system #3, due to NF GMs in the FN direction.

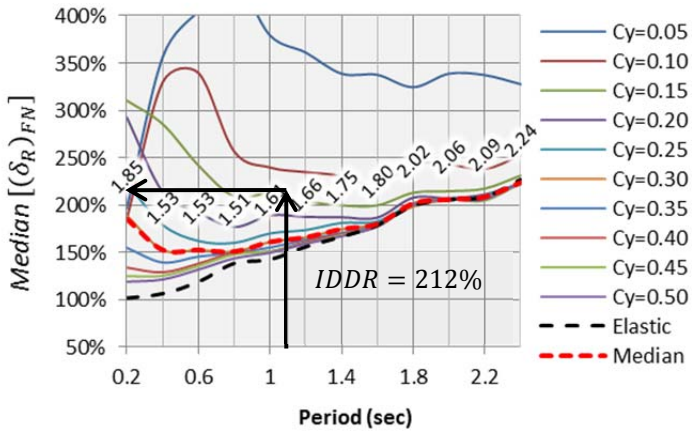

Figure 5-22: Equivalent SDOF #3 IDDR in the FN direction: nonlinear model = NLT#4, α = 0.25, β=2.0

Also, a complete list of extracted median values of IDDR for NF and FF GMs in both FN and FP directions for all three equivalent SDOF systems are presented in Table 5-9.

Table 5-9: IDDR of the superstructure determined for equivalent SDOF systems

	$IDDR^*$of equivalent SDOF	
System ID	$IDDR^*{}_{FN}$	$IDDR^*{}_{FP}$
Equivalent SDOF #1	222%	164%
Equivalent SDOF #2	212%	152%
Equivalent SDOF #3	218%	156%

<u>Comparison of results:</u> To validate the proposed simplified method, results of the maximum displacement demand and IDDR of the superstructure were determined from two independent sets of analysis and compared below.

To evaluate the accuracy of the proposed simplified method, the estimated maximum displacement demand of the superstructure when FFS is implicitly accounted for (using equivalent SDOF) is compared with those when FFS is explicitly accounted for (using 2DOF).That is, the contents of Table 5-5 are compared with the contents of Table 5-8, and the summary of this comparison is presented in Table 5-10. As one can infer from the content of Table 5-10, the

proposed simplified method can very accurately estimate the maximum displacement demand of the superstructure.

Table 5-10: Error associated with proposed simplified method for approximation of maximum displacement demand of the superstructure

	Error values			
System ID	$(\delta_{\mathrm{in}})_{\mathrm{NF-FN}}$	$(\delta_{\mathrm{in}})_{\mathrm{FF-FN}}$	$(\delta_{in})_{FF-FN}$	$(\delta_{in})_{FF-FP}$
System #1	4%	8%	9%	13%
System #2	5%	5%	6%	8%
System #3	2%	4%	2%	6%

The same procedure that was used for validation of the proposed method for estimation of maximum displacement demand of the superstructure is used for validation of $IDDR^*$. The contents of

Table 5-6 were compared with the contents of Table 5-9, and the results are presented in Table 5-11.

Table 5-11: Error associated with proposed simplified method for approximation of $IDDR^*$

	Error values	
System ID	$IDDR^*{}_{FN}$	$IDDR^*{}_{FP}$
Equivalent SDOF #1	2%	4%
Equivalent SDOF #2	0%	2%
Equivalent SDOF #3	1%	3%

Again, results of Table 5-11 indicate that the proposed simplified method can fairly accurately estimate $IDDR^*$ of the system.

5.4 Practical examples

Up to this point it has been demonstrated that

3. using EDP.Ratio values as presented in Appendix B, one can estimate EDPs of interest due to NF GMs from EDPs of interest due to FF GMs (see Chapter 4).

4. using the simplified method as proposed in this chapter, one may account for the effects of FFS, using NLTHA of an equivalent SDOF that implicitly accounts for FFS.

Problem example #5-2:

A simple concrete bridge is already designed and built based on the current code provisions, using a 5% damped UHRS, as shown in Figure G-1. See Appendix G. Now, due to some geotechnical investigations, a client found out that an active fault is located in close proximity to the structure, and he wants to know how much displacement the structure may experience in response to a pulse-like GM that may occur in the future.

Based on the geometry of the bridge and the final design drawings we know that the superstructure of the bridge can be simplified as a SDOF system with

$$T_e = 0.6 \text{ s}$$

$$\frac{\text{Design base shear}}{\text{W}} = C_y = 0.15$$

$$\alpha = 0.3$$

$$\beta = 4$$

$$\zeta = 2\%$$

Also, nonlinearity of the bridge can be modeled with a lumped plastic hinge at the base of the pier using a Takeda model (NLT#4 model).

Based on the above information, one may be able to estimate the design displacement of the structure from the response spectrum, namely,

$$S_d(0.6 \text{ s}) = S_a(0.6 \text{ s}) \times \frac{{T_e}^2}{4\pi^2}$$

$$S_d(0.6 \text{ s}) \cong 57 \text{ mm}$$

Obviously $S_d(0.6 \text{ s})$ is only due to FF GMs as it is based on the code UHRS.

Now one can use Figure A-4 of Appendix A to estimate the appropriate IDDR:

$$IDDR\big(T_e = 0.6 \text{ and } C_y = 0.15\big) \cong 2.4$$

Now, he may prorate the determined displacement demand of the superstructure due to FF GMs by determined IDDR to estimate displacement demand of the superstructure due to NF GMs:

$$\delta_{\mathrm{NF-FN}} \cong 2.4\ \delta_{\mathrm{FF}} = 0.137\ m$$

It is of note that δ_{NF} as calculated above is based on a fixed-base model.

<u>Problem example #5-3:</u>

Knowing that the δ_{NF} determined in problem example #5-2 exceeds displacement capacity of the system, a client asked the engineer to account for inertia effects of SFSI and see if that can help reducing δ_{NF} to some acceptable level. To do so the design engineer may choose to use the proposed simplified method (before entering into any sophisticated SFSI analysis). A summary of a possible solution using the proposed simplified method is below.

Knowing $\alpha = 0.3 \text{ and } \beta = 4.0$ from Figure 5-16 gives

$$\frac{T_{sys}}{T_{fb}} = 1.13$$

Thus,

$$T_{sys} = 0.68 \text{ s}$$

Also from Figure 5-17:

$$\frac{{C_y}^*}{C_y} = 0.65$$

$${C_y}^* = 0.1$$

and from Figure 5-18:

$$D_{CF} = 0.79$$

Now using the same procedure as noted in problem example #5-2 , the engineer may determine displacement of the equivalent SDOF system due to FF GMs, that is to say,

$$S_{d-eq}(0.68 \text{ s}) = S_a(0.68 \text{ s}) \times \frac{{T_e}^2}{4\pi^2} \times D_{CF}$$

$$S_{d-eq}(0.68 \text{ s}) \cong 45 \text{ mm}$$

Up to this point, analysis shows that the displacement demand for FF GMs of the structure could be reduced to 45 mm (vs. 57 mm determined for a fixed-base structure).

Now, to account for effects of NF GMs, one must multiply S_{d-eq} by the IDDR*, when IDDR* is extracted from the same figure that IDDR was extracted from, namely Figure 4 of Appendix A, this time for ${C_y}^*$ and T_{sys}. Thus,

$$IDDR^* = 2.8$$

Hence,

$$\delta_{NF-FN} \cong 2.8\,\delta_{FF} = 2.8\ \times 0.045 = 123\ \mathrm{mm}$$

In the above examples, one readily determined separate and combined effects of FFS and NF GMs on the maximum displacement demand of the structure without performing any NLTHA or any sophisticated modeling.

5.5 Comments

In this chapter:

- it was shown that the simplified method proposed in section 5.3 can fairly accurately estimate the maximum displacement demand of a complete soil–foundation–structure system from analysis of an equivalent nonlinear SDOF system,
- it was shown that the proposed method is very accurate in estimation of IDDR of a complete soil–foundation–structure system from IDDR of a simple nonlinear SDOF system (as presented in Chapter 4),
- the validity of the proposed method was verified against results of NLTHA developed in Chapter 4 and 5,

- A simple methodology that can assist practicing engineers to evaluate inertia effects of FFS on response of structures, using results of analysis of an equivalent SDOF system, is detailed and proposed. Table 5-12 summarizes the proposed procedure for determining the EDP of interest when combined effects of FFS and NF GMs are considered, from the same EDP determined for a fixed-base superstructure subjected to FF GMs. This procedure is also summarized in Flowchart # 5-1 and Flowchart # 5-2.

Table 5-12: Step by step procedure for determining EDP of interest when combined effects of FFS and NF GMs are considered from the same EDP determined for a fixed-base superstructure subjected to FF GMs

	Consideration of FFS effect:
1.	Determine ratio of the foundation mass to the superstructure mass
2.	Determine ratio of the foundation stiffness to the superstructure stiffness
3.	Use results of this study to determine ratio of $\mathrm{T_{sys}/T_e}$ and $\mathrm{C_y}^*/\mathrm{C_y}$ and the value of $\mathrm{D_{cf}}$ If effects of FFS are not of interest then, $D_{cf} = T_{sys}/T_e = C_y{}^*/C_y = 1$; otherwise see Figure 5-16 to Figure 5-19
	Use code provisions to:
4.	Determine T_e, the period of vibration at first significant mode in direction of interest: Either from code provisions/empirical equations or from simple linear analysis for the fixed-base structure
5.	Determine T_{sys} when T_{sys}/T_e is determined from step#3 and T_e is determined from step #4
6.	Determine $S_a(T_e)$, spectral acceleration response Use code-prescribed response spectrum (developed based on FF GMs) or from site specific response spectrum (without consideration of any near-fault effect adjustments)
7.	Determine V_e , elastic base shear $$V_e = S_a(T_e) \times W$$
8.	Determine R_y

Consideration of FFS effect:

Use code-prescribed yield-strength reduction factor, representing the capability of a structure to dissipate energy through reversed cyclic inelastic behaviour (a function of the structural system)

Analyse the system:

9. Decide if a linear analysis or a nonlinear analysis is preferred; go to step 9.b to do a nonlinear analysis

   a. A) Linear analysis:

      i. Determine C_y

when $C_y = \frac{F_y}{W} \cong \frac{V_{in}}{W} \cong \frac{S_a(T_e)}{R_y}$, and $S_a(T_e)$ are determined from step 6, and R_y is determined from step 8

      ii. Determine EDP_{FF}

For linear analysis, EDP of interest might be approximated as below:	
Maximum displacement:	$\delta_{FF-GM}{}^{*} = \frac{S_a(T_{sys}) \times g \times T_{sys}{}^2}{4\pi^2} \times D_{cf}$
Maximum ductility demand:	$\mu^{*} = \left[\frac{S_a(T_{sys})}{S_a(T_e)} \times \left(\frac{T_{sys}}{T_e}\right)^2 \times D_{cf} \times \mu\right] \geq 1$ *when μ is determined using Newmark and Hall relationship (equation 2.4) for $R = R_y$*
Yield capacity demand:	$C_y \times W$
Maximum inelastic to elastic displacement: demand	*≈1*

      iii. Go to step 10

   b. B) Nonlinear analysis:

      i. Determine C_y from nonlinear analysis1

      ii. Determine EDP_{FF} from nonlinear analysis

10. Determine $C_y{}^{*}$

when $C_y{}^{*}/C_y$ is determined from step#3 and C_y is determined from step #9

Consideration of FFS effect:
Prorating $\boldsymbol{EDP_{NF-GMs}}$ from $\boldsymbol{EDP_{FF-GMs}}$
11. Use $C_y{}^*$ from step#10 and T_{sys} from step#5 to interpolate/estimate $M_{EDP.Ratio}$ and $\sigma_{EDP.Rati}$ from the content of Appendix A or Chapter 4
12. Prorate EDP_{NF} from $$EDP_{NF-GMs} \cong EDP_{FF-GMs} \times M_{EDP.Ratio} \times e^{[\sigma_{EDP.Ratio} \times \Phi^{-1}(P)]}$$

Also in general one may say:

- FFS has an adverse effect on expected maximum displacement demand of the short-period structures subjected to NF GMs; conversely, the effect of FFS on expected maximum displacement demand of the medium- to long-period structures is advantageous. The main adverse effect of FFS on the displacement demand of the structures due to NF GMs is manifested in a big excursion associated with response of the structure to the long-period pulse of NF GMs. This effect can be interpreted as imposing more damage to the superstructure.
- Consideration of FFS effect increases the inelastic displacement demand ratio of the superstructures. This effect increases as the elastic period of vibration of the system increases (see equation 5-6).
- The effects of FFS on ductility demand and ductility demand ratio of the structures subjected to NF GMs are similar to what is noted for expected maximum displacement demands and maximum displacement demand ratios.
- FFS has almost no effect on input energy due to NF GMs; however, it can moderately increase the magnitude of input energy due to FF GMs. Thus, ignoring FFS in analysis can result in underestimation of accumulative damage (proportional to input energy) due to FF GMs.

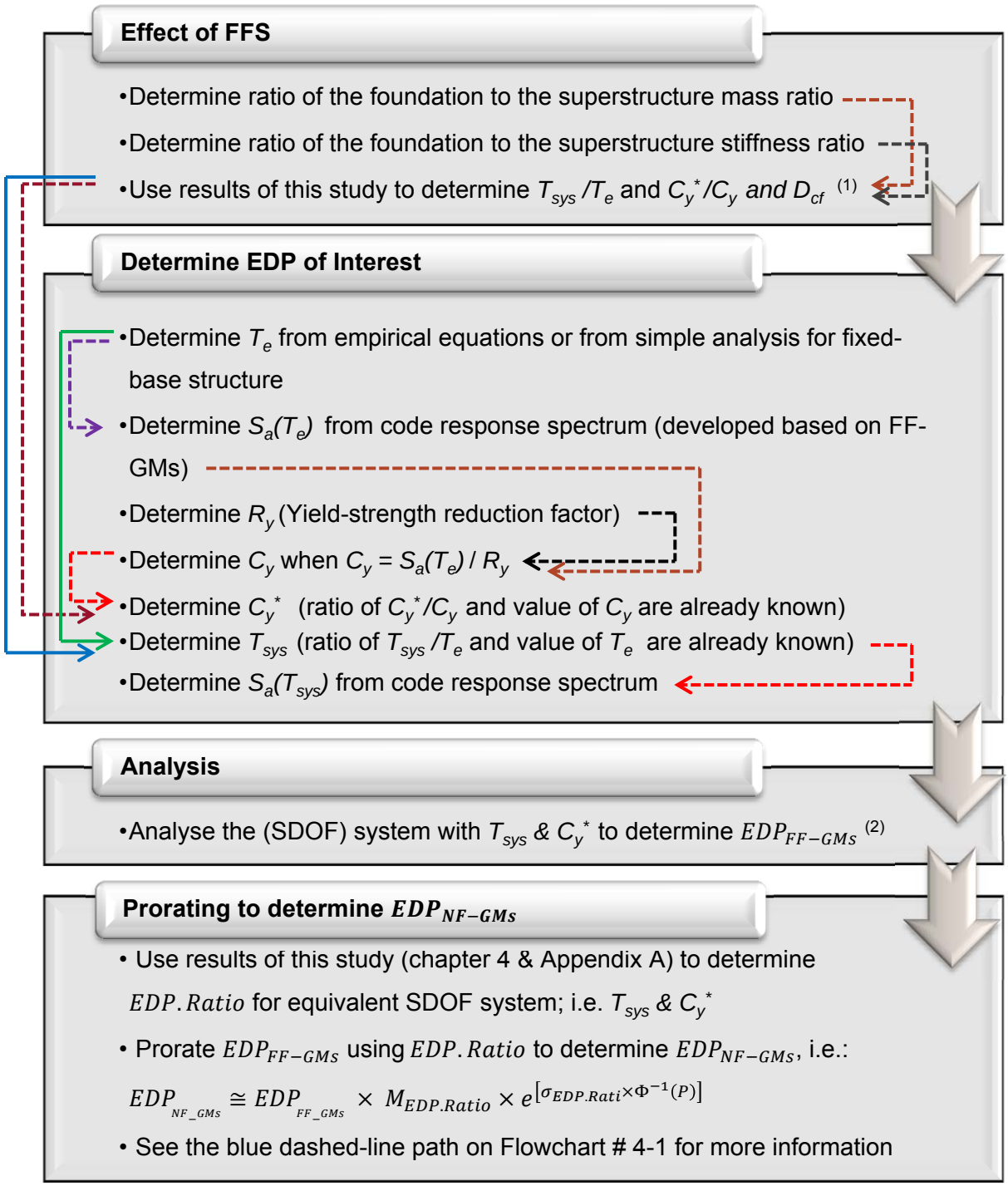

Flowchart # 5-1: Proposed procedure for consideration of combined effects of FFS and NF GMs on the nonlinear response of structures

Notes:

1. If effects of FFS are not of interest, then $D_{CF} = T_{sys} / T_e = C_y^*/C_y = 1$; *see* Figure 5-16 to Figure 5-19
2. For simple structures, each EDP_{FF-GMs} of interest could be approximated as

Maximum displacement:	$\delta_{FF-GM}{}^* = \frac{S_a(T_{sys}) \times g \times T_{sys}{}^2}{4\pi^2} \times D_{cf}$
Maximum ductility demand:	$\mu^* = \left[\frac{S_a(T_{sys})}{S_a(T_e)} \times \left(\frac{T_{sys}}{T_e}\right)^2 \times D_{cf} \times \mu\right] \geq 1$ when μ is determined using Newmark and Hall relationship (equation 2.4) for $R = R_y$
Yield capacity demand:	$C_y \times W$
Maximum inelastic to elastic displacement: demand	≈1

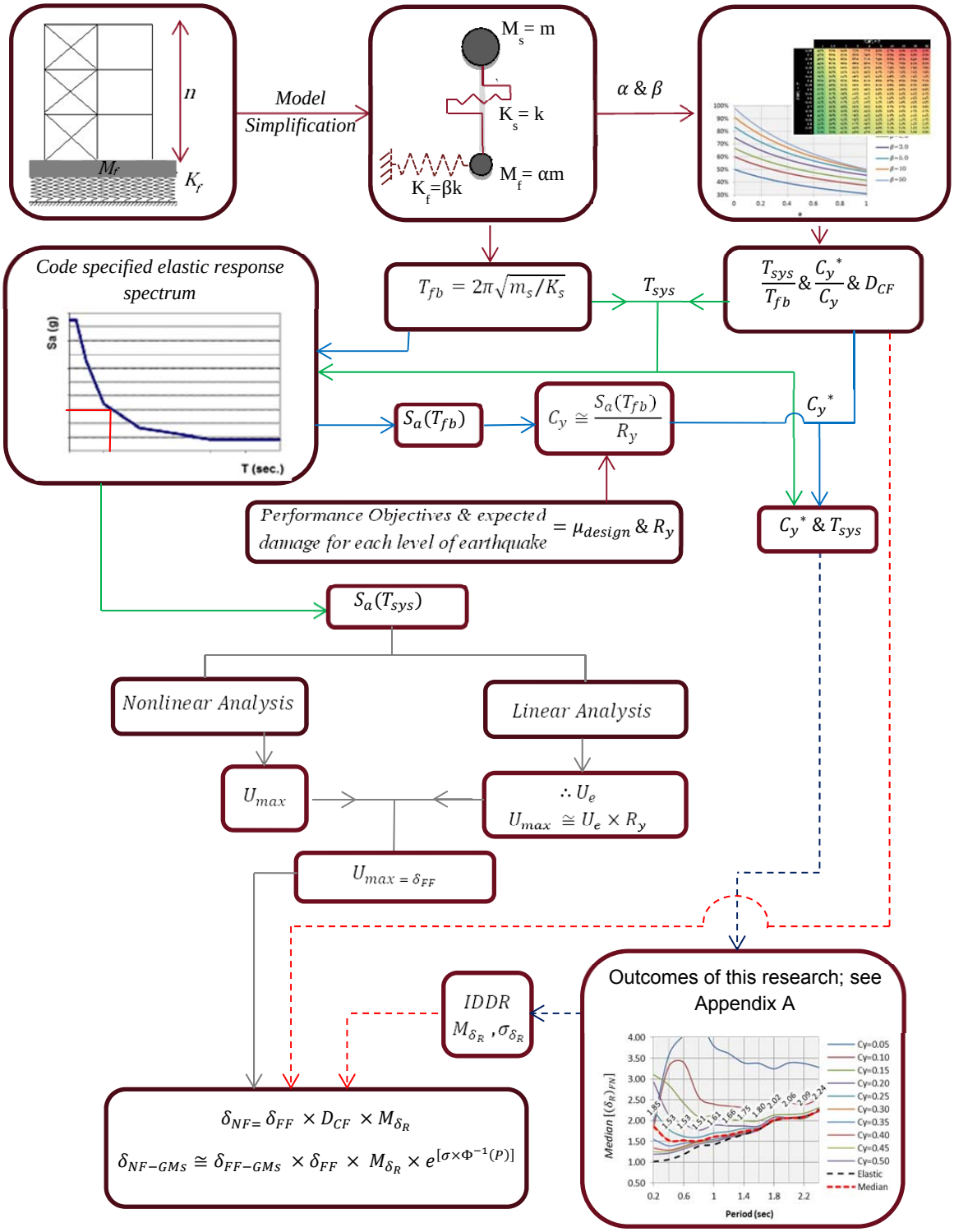

Flowchart # 5-2: Proposed procedure for consideration of combined effects of FFS and NF GMs on maximum displacement of the structures

6. MDOF systems

Chapter Outline:

1. Section 6.1 details geometry and properties of the prototype MDOF system used for numerical modeling.
2. Section 6.2 details dynamic properties of the prototype MDOF system.
3. Section 6.3 presents overview of response of the prototype MDOF system for a representative NF GM and its equivalent FF GM.
4. Section 6.4 estimates EDPs of interest based on results of past chapters and compare them with results of analysis of the MDOF system.
5. Section 6.5 presents a summary of this chapter.

In Chapter 4, effects of NF GMs on the response of simplified structural systems, i.e., SDOF systems, were extensively studied. Also, in section 5.3, an efficient procedure for considering inertia effects of SFSI using a simple method, formulized based on response of 2DOFs and their equivalent SDOF systems, was proposed. Obviously, all research presented in previous chapters is based on analysis of simplified models.

While studying these simplified models can shed light on some salient aspects of the response of the structures to strong input motions, they may or may not be very good representatives of the real structure (especially when effects of NF and SFSI add to the complexity of the nonlinear response of the system).

To be able to generalize and extend results of simplified systems (studied in the past few chapters) to MDOF systems, one needs t:

a) verify validity and accuracy of results of simplified, i.e., SDOF, systems against more comprehensive/realistic models (e.g., MDOF systems),

b) consider effects of higher modes on responses of interest,

c) make sure important aspects of responses of interest are generally captured.

Thus, in this chapter responses of a comprehensive model of a four-span pier-supported bridge structure, which explicitly account for inertia effects of SFSI and effects of NF GMs on response of the structure are investigated, and results of this study are compared with results of simplified systems, as detailed in past few chapters. Results of this comparison should assist in evaluating how well the proposed simplified models can estimate results of NLTHA of more complex and more realistic systems.[1]

6.1 System properties and numerical modeling

For the mathematical modeling, SAP2000-Nonlinear, a commercially available general purpose three-dimensional FEM structural analysis program, is used to model a four-span bridge supported on pile clusters complete with concrete pile caps as described below:

System geometry:

Total length: 150 m

Number of spans: 4

Length of spans: mid spans = 50000 mm and end spans = 25000 mm

Deck width, edge-to-edge: 12000 mm

Skew angle: none

Bridge deck material: precast/pretensioned concrete continuous beam

Boundary conditions:

Middle supports of the deck are single column pier fully integrated into the deck:

- Diameter of pier : 1800 mm

[1] The content of this chapter does not aim to represent the state of the art required for modeling a real structure for larger earthquake acceleration amplitudes. Rather, it aims to verify results of simplified models presented in the previous chapters against a MDOF model that more realistically accounts for and addresses different aspects of a real structure.

- Height of pier : 8000 mm

End supports of the deck: vertically supported at two end abutments (roller bearings)

The foundation is a 3 x 3 grid of piles spaced at 1800 mm complete with a 1500 mm thick pile cap complete with 510 mm (20 inch) diameter expanded base concrete piles (12×25M bars, assumed to behave elastically)

Figure 6-1 shows geometric properties of the MDOF bridge structure modeled in SAP2000.

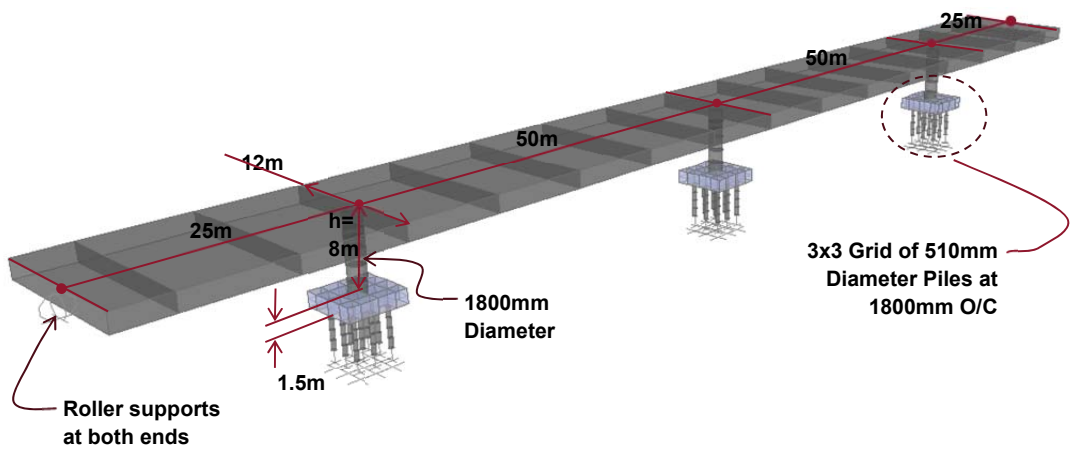

Figure 6-1: Geometry of MDOF bridge Structure

<u>Frame section properties:</u>

Structural framing elements of the bridge, namely, the piers and the deck, are modeled using linear-elastic beam-column members with material properties corresponding to the properties of cracked reinforced concrete as detailed in Table 6-1:

Table 6-1: Frame section properties

Section	Area mm^2	J (Tors.Const) mm^4	I33 mm^4	I22 mm^4	AS2 mm^2	AS3 mm^2
Pier	2.63E+06	1.10E+12	5.50E+11	5.50E+11	2.37E+06	2.37E+06
Deck	7.00E+06	1.50E+13	5.70E+12	7.65E+13	2.40E+06	3.70E+06

The effect of cracking on the stiffness of the element was considered using section property modifiers as listed in Table 6-2.

Table 6-2: Frame section properties modification factors

Section	Area Modifier	J Modifier	I33 Modifier	I22 Modifier	A2 Modifier	A3 Modifier
Pier	0.80	0.20	0.35	0.35	1.00	1.00
Deck	1.00	1.00	0.75	0.75	1.00	1.00

Nonlinearity of superstructure's framing elements:

Inelastic properties of frame elements and behaviour of the plastic hinges are captured using discrete non-linear link elements.

Formation of plastic hinges is assumed to be at the end of lower segment of the piers near the point of fixity of the column, immediately above the pile caps; see Figure 4.1.

The discrete inelastic element used to model the plastic hinge at the base of the superstructure is similar to LNK#4, as introduced in section 3.3.6.1.

Figure 6-2 shows the family of backbone curves used for modeling of the plastic hinge at the base of the pier, as depicted in Figure 4.1, and with respect to specific properties of the system as noted above.

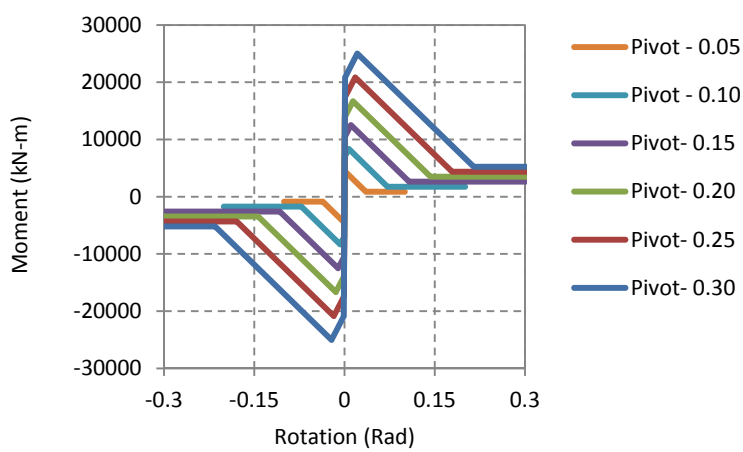

Figure 6-2: Family of backbone curves used for modeling of the plastic hinge at the base of the pier

It is of note that the MDOF bridge model plastic hinge used in the following sections is calibrated to allow for $C_y = 0.15$.

Consideration of flexibility of foundation system

To allow for consideration of FFS on nonlinear response of the structure, two different sets of boundary conditions were modeled, namely:

a) Flexible-base boundary condition, using the pile group arrangement as described in section 6.1,

b) Fixed boundary condition, using restraints at all degrees of freedom (three translational and three rotational DOFs), at the base of each pier (i.e., fixed-base systems).

<u>Modeling of flexible-base boundary conditions/pile group :</u>

For modeling of flexible-base boundary conditions, the whole foundation system is modeled using a detailed wrinkle model of the piles, as shown in Figure 6-3 and as detailed below.

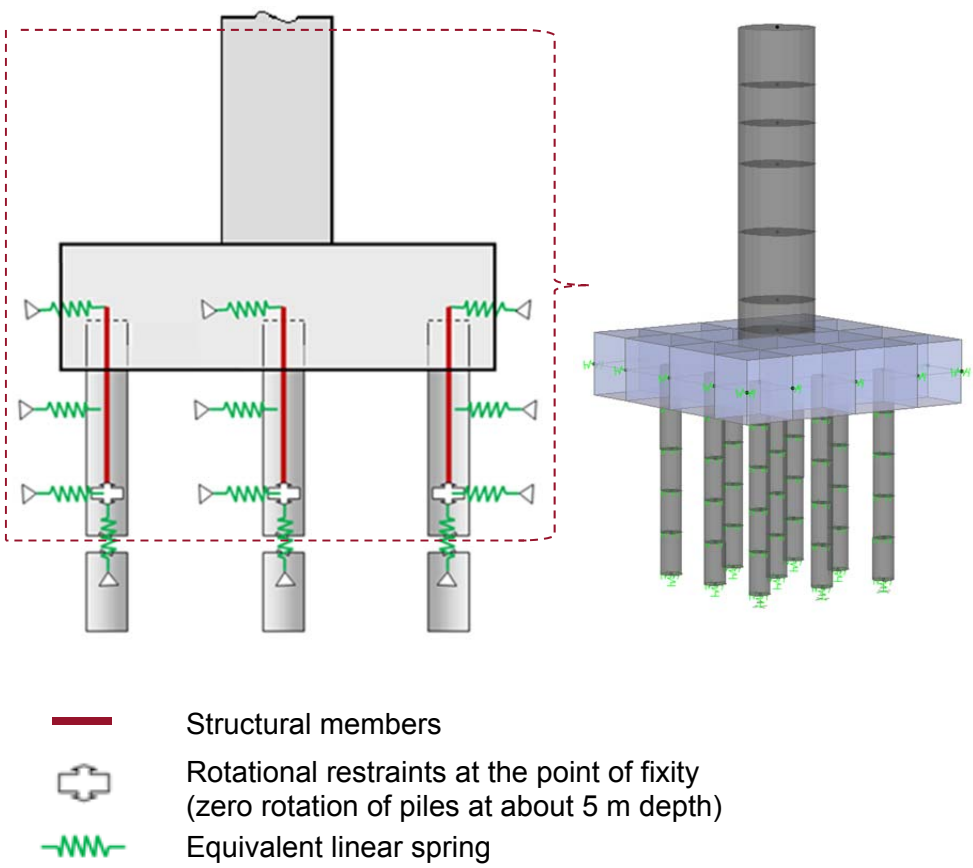

Figure 6-3: Pile group linear modeling scheme used in this study: left figure, concept model; right figure, FEM model

FFS was considered using modeling of uncoupled lateral linear Winkler springs over top 5 m length of the piles (almost point of fixity/zero rotation), complete with a vertical linear springs at the tip of each pile.

For more information about the point of fixity determined in this project, see Figure 6-4, showing the nonlinear response of a 510 mm diameter expanded base concrete pile to a displacement controlled loading applied to the top node of the pile at the grade level.

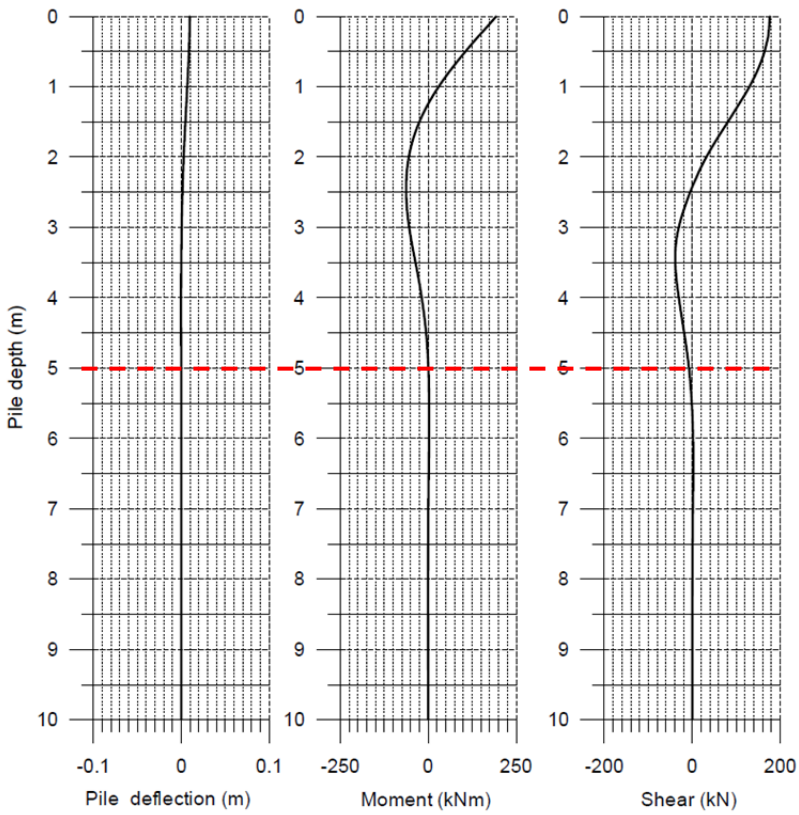

Figure 6-4: Lateral loading response of a 510 mm diameter, fixed head, expanded base concrete pile

Lateral soil springs are assumed at 1.0 m intervals along the height of the modeled segment of the pile. Effective stiffness of different lateral springs per length of the piles used for modeling are listed below:

- $K_{eff\text{-}lat}$ (2 m) = 12.5 MN/m^2 for displacements up to 30 mm
- $K_{eff\text{-}lat}$ (3 m) = 21.0 MN/m^2 for displacements up to 30 mm

- $K_{eff\text{-}lat}$ (4 m) = 7.50 MN/m^2 for displacements up to 30 mm[1]
- $K_{eff\text{-}lat}$ (5 m) = 21.0 MN/m^2 for displacements up to 10 mm

For more information refer to Figure 6-5 and Table 6-3.

Table 6-3: *p-y* curves of the 510 mm diameter piles

Depth = 2 m		Depth = 3 m		Depth = 4 m		Depth = 5 m	
y (mm)	p (kN/m)	y (mm)	p (kN/m)	y (mm)	p (kN/m)	y (mm)	p (kN/m)
0	0	0	0	0	0	0	0
1	64	1	80	1	27	2	115
2	92	2	122	2	42	5	164
3	114	3	156	3	53	7	191
4	132	4	186	4	63	9	207
5	148	5	213	5	73	11	219
6	164	6	239	6	81	14	227
7	177	7	263	7	89	16	233
9	189	9	284	9	97	18	234
10	201	10	306	10	104	21	236
11	213	11	326	11	111	23	234
12	224	12	345	12	117	25	231
13	234	13	363	13	124	28	227
29	387	29	641	29	218	46	164
794	387	794	641	794	218	64	100
1560	387	1560	641	1560	218	83	37
2325	387	2325	641	2325	218	918	37

[1] Reduced $K_{eff\text{-}lat}$ at 4 m depth is an indication of the presence of a weak layer of soil at that depth.

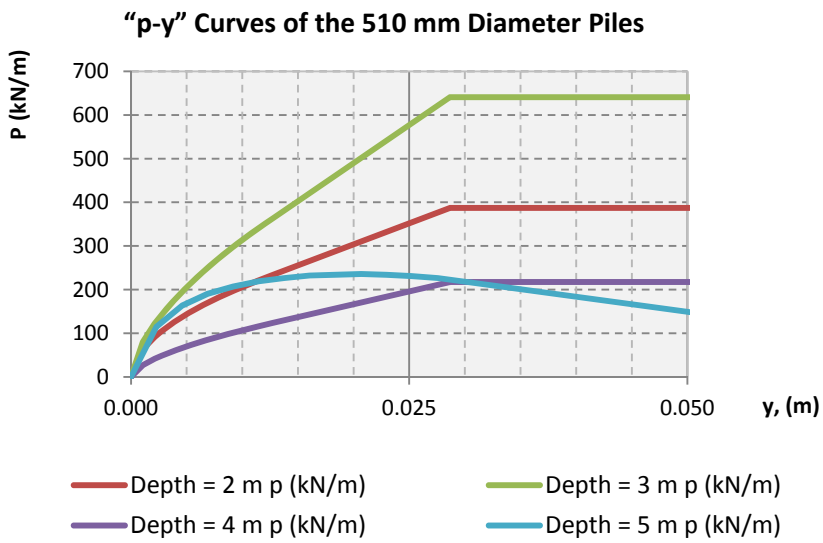

Figure 6-5: p-y curves used for determining effective stiffness of wrinklier springs

Vertical linear springs modeled using a vertical stiffness of ($K_{eff\text{-}Vert}$) 220 MN/m at the tip of the piles, determined from axial load and settlement relationship, as shown in Figure 6-6.

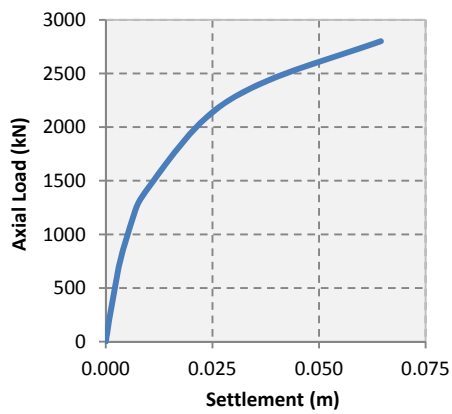

510 mm diameter pile	
Axial Load (kN)	Settlement (m)
0	0.0000
173	0.0007
260	0.0011
624	0.0027
775	0.0035
1170	0.0065
1370	0.0088
2050	0.0225
2420	0.0372
2800	0.0645

Figure 6-6: Axial load and settlement relationship

Pile caps were explicitly modeled using shell elements. Connection of piles to pile cap was considered as fixed (i.e., piles are assumed to be fixed-head piles). Resistance from earth pressure against movement of the pile caps is added to the lateral resistance of the model using linear springs modeled on the perimeter of the pile caps (edge nodes of shell elements). Figure 6-7 provides the relationship between passive resistance and horizontal movement of the pile caps, when H is the embedded height of pile caps measured in metres. Thus, the effective so-called

lateral module of reaction for passive pressure on pile caps is estimated to be approximately 2.5H MN/m^3.

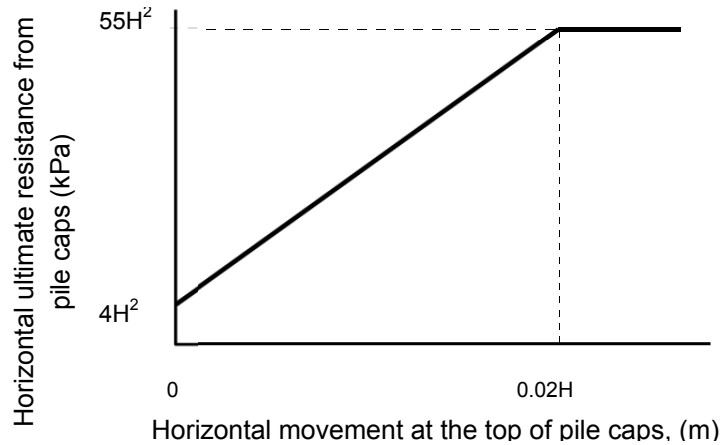

Figure 6-7: Relationship between earth pressure and movement of pile caps

Seismic mass:

To account for more realistic distribution of the seismic masses:

- each pier section is divided into six segments,
- each section of the middle span deck is divided into five segments
- each section of the end span deck is divided into three segments

Translational mass: in translational directions all nodal masses are automatically calculated by the program in three orthogonal directions and applied as lumped masses at each node. The nodal masses are determined based on tributary lengths/areas associated with each node.

Rotational mass: mass moment of inertia of the deck about the longitudinal axis of the bridge is manually calculated applied at each node of the deck. Mass moment of inertia of the deck is determined to be approximately 220 kN m s^2/m.

6.2 Dynamic properties of the structural system

The following subsections detail dynamic properties of the assembled model.

Dynamic properties of the system are listed for four scenarios:

1. Flexible-base model complete with the deck rotational inertia.

2. Flexible-base model with NO deck rotational inertia.
3. Fixed-base model complete with the deck rotational inertia.
4. Fixed-base model with “NO” deck rotational inertia.

The reason for considering two scenarios related to the deck rotational-inertia, for each boundary condition, is that the deck rotational inertia has great influence on triggering the contribution of higher modes in response of the superstructure in transversal direction.

In a sense, models complete with the deck rotational inertia are representatives of MDOF systems for which the response of their first mode alone is not a very good representative of the response of the whole system, and models with no deck rotational inertia are representatives of MDOF systems for which the response of their first mode is a very good representative of the response of the whole system. See Figure 6-8.

Details of system properties of the flexible-base system are listed below:

a) Foundation mass:
   - 3 x (pile cap mass plus 1.5 m top section of pile): 444 t
   - 3 x (pile cap mass plus 2.5 m top section of pile): 457 t

b) Assembled transversal mass of the superstructure = 2660 t

c) $\alpha_t \approx 7\%$, where α_t is the foundation mass ratio in transversal direction, as defined in Chapter 5

d) $K_f \approx 200\ 000$ kN/m (determined from applying unit load to the center of the pile cap)

e) $\beta_t \approx 6$, where β_t is the foundation stiffness ratio in the transversal direction, as defined in Chapter 5

f) $C_y = 0.15$, where C_y is the strength characteristic of the fixed-base superstructure.

Dynamic properties of flexible-base system:

The summaries of modal properties of the flexible-base system in transversal direction for two scenarios of with deck rotational inertia and without deck rotational inertia are tabulated in Table 6-4.

Table 6-4: Response of the system in transversal direction for a flexible base

	Without deck rotational inertia	With deck rotational inertia
K_{eff}	32 000 kN/m	32 000 kN/m
T_1	1.48 s	1.66 s
MP_1	86%	67%
T_2	0.168 s	0.387 s
MP_2	12%	26%

MP_1 and MP_2 are mass participation ratios for mode one and mode two in the transversal direction of the bridge, respectively. As is evident from the right column of Table 6-4, the influence of deck rotational inertia on the contribution of higher modes of vibration in total response of the structure is significant. Figure 6-8 shows the first two mode shapes of the flexible-base models in the transversal direction.

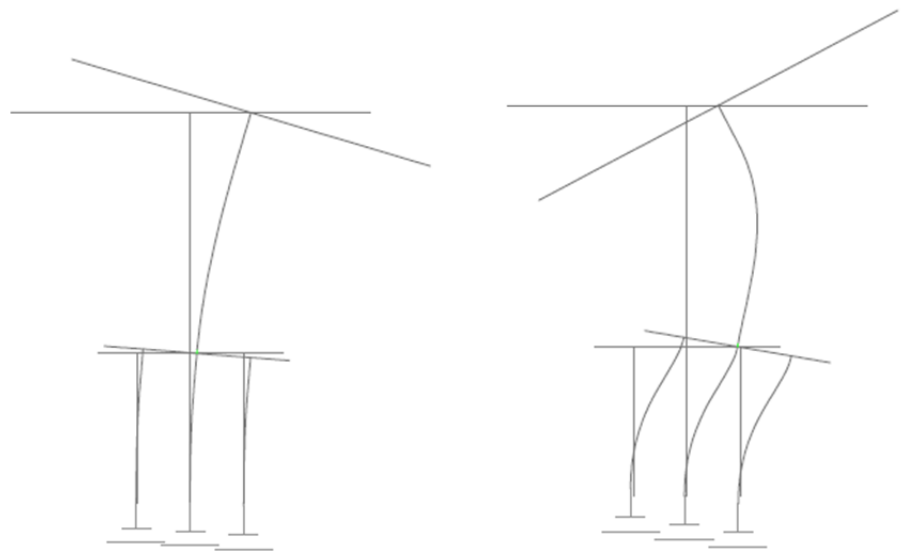

T_1=1.66 sec

MP_1= 67%

T_2=0.387 sec

MP_2=26%

Figure 6-8: Left figure, first mode shape of the flexible-base model with deck rotational inertia in transversal direction; right figure: second mode shape of the flexible-base model with deck rotational inertia in transversal direction

Dynamic properties of fixed-base system:

Summaries of modal properties of the fixed-base system in transversal direction for two scenarios of with deck rotational inertia and without deck rotational inertia are tabulated in Table 6-5.

Table 6-5: Response of the system in transversal direction for a fixed-base system (fixed boundary is located at the base of pier)

	Without deck rotational inertia	With deck rotational inertia
K_{eff}	32 000 kN/m	32 000 kN/m
T_1	1.08 s	1.29 s
MP_1	95%	66%
T_2	N/A	0.265 s
MP_2	N/A	30%

The first two mode shapes of the fixed-base systems in transversal direction are very similar to those of flexible-base systems, as depicted in Figure 6-8.

6.3 Overview of response of selected MDOF system due to Imperial Valley-06, 1979 earthquake NF and FF PGA matched records

Responses of SDOF and 2DOF systems due to the Imperial Valley-06, 1979 earthquake for a selected NF GM (NGA#0169) and its FF GM counterpart (NGA#0171) were studied in Appendix C.1 and Appendix D.1, respectively. In this section, the response of the selected MDOF as detailed in previous section 6.2 will be examined. It is of note that while SDOF and 2DOF represented in Appendix C.1 and Appendix D.1, respectively, are comparable, they cannot be considered as simplified models of the structure that is used in this chapter for studying the MDOF model, as their corresponding C_y and T_e are significantly different from C_y and T_e of the selected MDOF model.

Time history displacement response of mid-point of the deck

Figure 6-9 depicts the time history displacement response of MDOF bridge structure as described in previous sections due to NGA#171 and NGA#169 (Imperial Valley-06, 1979), except that

- displacement results are presented for equivalent LNK#4 nonlinear model while C_y is set to 5%. A different value for strength characteristic was used in Figure 6-9 to magnify the nonlinear behaviour of the structure (e.g., the residual displacements),
- the system is assumed to be fixed at the base of the piers (i.e., foundation flexibility is not considered),
- rotational mass is included.

Observations:

- Despite all differences between C_y, T_e, rotational mass, etc., the trend of response observed in Figure 6-9 is very similar to its corresponding one, Figure C-1.
- Maximum displacement demand due to FF GMs in Figure 6-9 is much less jagged than its corresponding one in Figure C-1; this is mainly due to (A) longer elastic period of vibration of MDOF system and (B) less strength characteristic used in Figure 6-9.

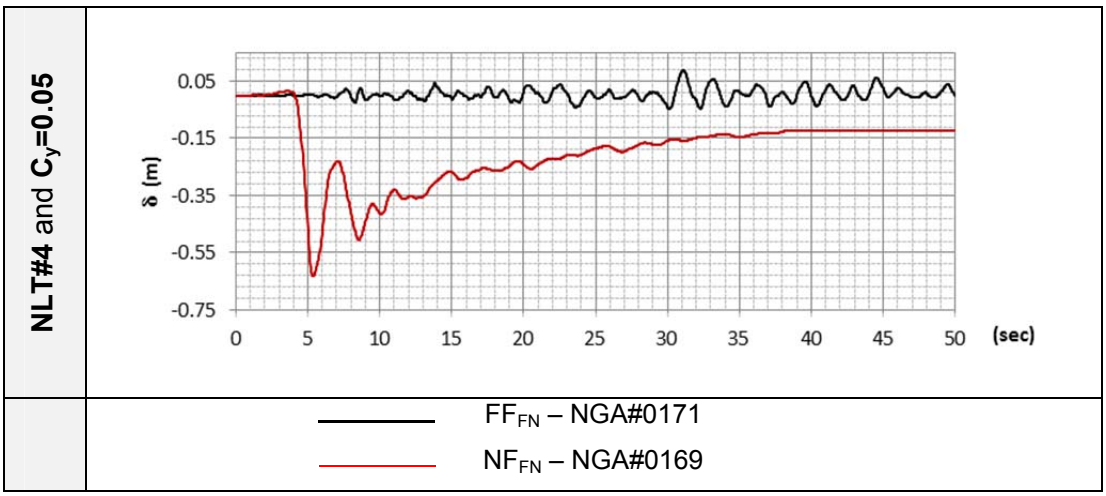

Figure 6-9: Displacement time history in the transversal direction of the fixed-base MDOF (bridge) system due to the FN component of NGA#171 and NGA#169, Imperial Valley-06, 1979 earthquake

Hysteresis response of the nonlinear hinge at the base of the middle pier

Figure 6-10 shows the moment-rotation (kN m vs. Rad) hysteresis behaviour of the nonlinear hinge at the base of the middle pier of the bridge.

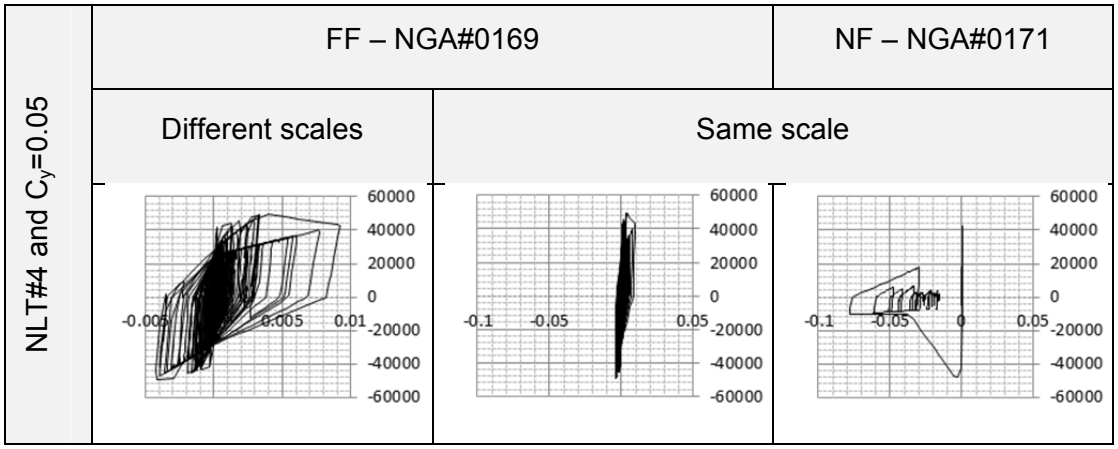

Figure 6-10: Moment-rotation (kN.m vs. Rad) hysteresis response of the nonlinear hinge at the base of the middle pier in transversal direction of fixed-base MDOF (bridge) system due to theFN component of NGA#171 and NGA#169, Imperial Valley-06, 1979 earthquake

Observations:

- Again, despite all differences between C_y, T_e, rotational mass, etc., the trend of hysteresis behaviour of the plastic hinge at the base of the pier of the fixed-base MDOF system is very similar to the trend of the hysteresis behaviour of SDOF, as depicted in Figure C-2 for LNK#4 model,
- Similar to what was observed for SDOFs, hysteresis behaviour of the nonlinear hinge at the base of the mid-pier shows:
    - relatively few numbers of excursions due to NF – NGA#0171; however, all are associated with relatively large rotations,
    - a significant number of excursions due to FF – NGA#0169; however, all are associated with relatively small rotations.

6.4 Statistical representation of results of NLTHA of MDOF (bridge) systems subjected PGA matched GMs

Results of analysis of the MDOF system for four cases, as described in section 6.2, are summarized in Table 6-6 in terms of the maximum displacement demand of the

mid-point of the deck in the transversal direction, due to the FN component of FF and NF GMs.

Table 6-6 also summarizes the same data for a 2DOF system with the NLT#4 nonlinear model, C_y = 0.15, $\alpha = 4$, and β = 15%. Results of 2DOF are presented for reference only.

It is noted that the α and β used for analysis of 2DOF are only close estimates of the α and β used for analysis of MDOF system.

Despite the fact that α and β of selected 2DOF are slightly different from those of MDOF, and the contribution of the first mode of the system is not significant in this structure (see Table 6-4), yet the 2DOF system fairly accurately estimated expected maximum displacement of the system.

Table 6-6: Summary of analysis of MDOF models in terms of maximum expected displacement of the mid-point of the deck for four different scenarios along with similar results from analysis of SDOF and 2DOF systems

		Fixed base		Flexible base	
		Without deck rotational inertia	With deck rotational inertia	Without deck rotational inertia	With deck rotational inertia
NLTHA of MDOF	T_e	1.08 s	1.29 s	1.48 s	1.66 s
	$\delta_{max})_{NF-FN}$	160 mm	140.76 mm	222 mm	195.5 mm
	$\delta_{max})_{FF-FN}$	79.21	69.0 mm	110 mm	95.85 mm
	IDDR	202%	204%	203%	204%
NLTHA of 2DOF with α=4 and β=%15	T_e			1.48 s	1.66 s
	$\delta_{max})_{NF-FN}$			214 mm	222 mm
	$\delta_{max})_{FF-FN}$			97.5 mm	99 mm
	IDDR			219%	224%

6.4.1 Validation of applicability of a simplified proposed method for consideration of effects of SFSI and NF GMs on response of MDOF systems

In this section, there will be an attempt to predict the combined effects of FFS and NF GMs on the maximum displacement response of a selected MDOF system (i.e.,

maximum displacement of the mid-point of the deck as detailed in section 6.1) using simplified method, procedures, and data presented in previous chapters (Chapter 4 and section 5.3).

Thus, to evaluate applicability of the proposed method for consideration of effects of SFSI and NF GMs on the response of MDOF systems, predicted displacement demands, determined based on the equivalent SDOF model, will be compared with results of NLTHA of MDOF system.

Predicting maximum displacement demand of the mid-point of the deck in the transversal direction, using equivalent SDOF

As mentioned before, the foundation mass ratio in the transversal direction (α_t) is approximately 17%, and the foundation stiffness ratio in transversal direction (β_t) is some 6.0. Thus, using Figure 5-16 to Figure 5-18, one can easily extract parameters required for developing system properties of an equivalent SDOF model, namely, ratio T_{sys}/T_{fb}, D_{CF}, and ratio $C_y{}^*/C_y$.

Table 6-7 summarizes parameters extracted from Figure 5-16 to Figure 5-19 for our MDOF system.

Table 6-7: Determined properties of the equivalent SDOF system

	Properties of equivalent SDOF					
	T_{FB}	$T_{Equ.SDOF}/T_{FB}$	$T_{Equ.SDOF}$	$C_y{}^*/C_y$	$C_y{}^*$	D_{CF}
System without deck rotational inertia	1.48 s	~109%	1.60 s	75%	11%	0.84
System with deck rotational inertia	1.66 s	~109%	1.80 s	75%	11%	0.84

Now, using content of Table 6-7, one should be able to use the data presented in Appendix A to predict the median value of maximum displacement demands and IDDR values for the equivalent SDOF system. For example, Figure 6-11 shows the process of extrapolation of the median value of maximum displacement demand of the equivalent SDOF system from results of analysis presented in Chapter 4 for PGA-matched FF GMs in the FN direction.

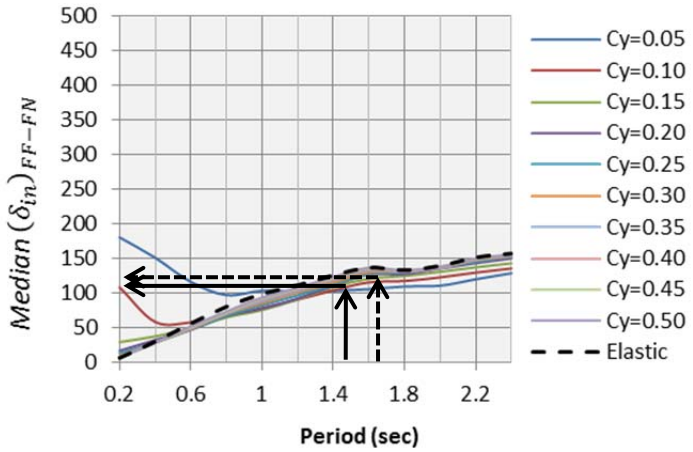

Equivalent system with consideration of Rotational Mass

Equivalent system without consideration of Rotational Mass

Figure 6-11: Equivalent SDOF maximum displacement demand spectra in the FN direction: nonlinear model = NLT#4, α = 0.17, β = 6.0, ζ = 2%

Similarly, Figure 6-12 shows the process of extrapolation of IDDR of the equivalent SDOF, due to NF GMs in the FN direction.

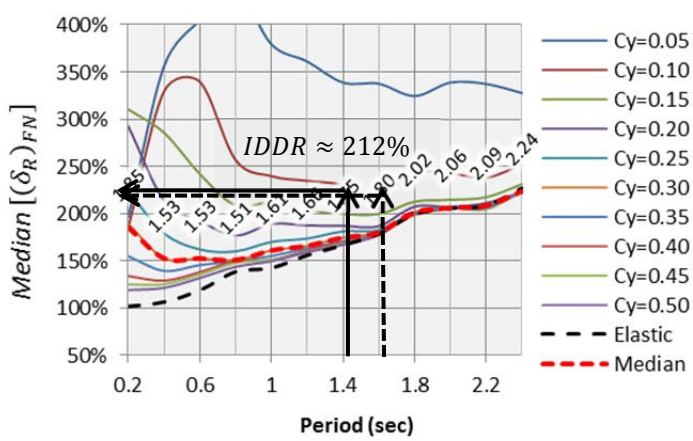

Equivalent system with consideration of Rotational Mass

Equivalent system without consideration of Rotational Mass

Figure 6-12: Equivalent SDOF IDDR in the FN direction: nonlinear model = NLT#4, α = 0.17, β = 6.0, ζ = 2%

It is of note that displacement extrapolated values represent the maximum total displacement of the system (i.e., displacement of foundation plus relative

displacement of superstructure to the foundation). Thus, the extracted values need to be corrected using the D_{CF} factor as determined in Table 6-7 to account for only the relative displacement of the superstructure to the foundation.

Based on extrapolated data from Figure 6-11 and Figure 6-12, one can predict the expected displacement demand of the superstructure when effects of SFSI are indirectly accounted for, namely,

a) Predicted displacement demand when rotational mass is disregarded,

$$\delta_{FF-FN} = 115 \text{ mm } \times \ 0.84 = 112 \text{ mm}$$

$$\delta_{NF-FN} = \delta_{FF-FN} \times IDDR = 112 \text{ mm } \times 2.12 = 205 \text{ mm}$$

b) Predicted displacement demand when rotational mass is accounted for,

$$\delta_{FF-FN} = 120mm \ \times \ 0.84 = 101mm$$

$$\delta_{NF-FN} = \delta_{FF-FN} \times IDDR = 101mm \ \times 2.12 = 213mm$$

It is of note that these displacements were good estimates of expected maximum displacement, if almost full mass participated in the first mode of vibration. Now, to account for any lower participation mass, one may choose to make a correction.

Table 6-8 summarizes the comparison of predicted maximum displacement demand of mid-point of the deck in the transversal direction, using equivalent SDOF, with results of NLTHA.

Table 6-8: Comparison of predicted maximum displacement demand using equivalent SDOF models with results of NLTHA of MDOF system in the FN direction

	$(\delta_{in})_{NF-FN}$		
	Equivalent SDOF	NLTHA	Error
With Rot. Mass	205	222	- 8%
Without Rot. Mass	212	195.5	+8%

6.5 Discussion

- In this chapter a selected MDOF bridge structure, which could be assumed as a good representative of typical highway concrete bridges, was analysed. In such bridges, the first mode of vibration governs their response in the transversal direction.
- Responses of the considered bridge structure due to NF GMs were determined when FFS is explicitly accounted for by using linear springs developed based on *p–y* curves
- Results of analysis of the selected MDOF bridge structure indicated that the proposed method for predicting the response of flexible-base structures from the response of their equivalent SDOF models is a valid approach and is applicable to (this) comprehensive MDOF model(s).
- Results of analysis of MDOF and comparison of those results with results of the proposed simplified method (for consideration of combined effects of NF GMs and FFS) showed that the proposed simplified method is reasonably accurate.

7. Summary and conclusions

Chapter Outline:

1. Section 7.1 details a summary of the work done in this study, and how the objectives of this project are met.
2. Section 7.2 summarizes the important findings of this study.
3. Section 7.3 briefly discusses the impact of this research on engineering practice.
4. Section 7.4 recommends work for future which could further our understanding of this subject

---

The following sub-sections briefly describe how well the project objectives were met and what are the conclusions and the salient findings of this study.

7.1 Summary

During course of this work, effects of the near fault ground motions with and without effects of flexibility of the foundation system on nonlinear response of the structures were investigated.

To achieve the objective of this research, results of numerous nonlinear time history analyses of a range of fixed base systems, and their equivalent flexible base systems were studied, compared, and formulated into a probabilistic framework. The proposed probabilistic framework/relationships allow for the prorating of the response of the structures due to near fault ground motions from the same responses due to their equivalent far field ground motions.

To account for the effects of the flexibility of the foundation system on the nonlinear response of the structures, a mathematical procedure was developed and proposed. The proposed procedure simplifies a structural system (including its foundation) into an equivalent single degree of freedom system. The structural properties of the equivalent single degree of freedom system is used in the proposed probabilistic equations (as noted above) to indirectly estimate the

combined effects of near fault ground motions and flexibility of the foundation system on engineering demand parameters of interest. The validity of the proposed procedure is verified against various methods and models.

Therefore in summary, one can say that all objectives of this project (as defined in chapter 1), were fully met.

7.2 Conclusions

In this section, the important conclusions and findings of this study are summarized. The conclusions are presented under three main topics, namely,

1. The effect of near fault ground motions on the nonlinear response of fixed base structures;
2. The effect of near fault ground motions on the nonlinear response of structures supported on flexible foundation systems;
3. A simplified method for consideration of combined effects of near fault ground motions and flexibility of the foundation system on the nonlinear response of the structures.

1. Effect of near fault ground motions on nonlinear response of structures

Input energy: A parametric study of a series of nonlinear time history analyses of various single degree of freedom systems showed that rate of input energy for near fault ground motions is (generally) considerably more than that for far field ground motions. As a result, the input energy of near fault ground motions must be dissipated in a relatively short period of time; this results in much larger nonlinear displacements to allow for dissipation of a large flux of energy in a relatively few cycles of motion. Disregarding this phenomenon in seismic design/evaluation of structures can result in underestimation of the seismic demands, and the risks to which structures in close proximity of a fault might be exposed.

Stiffness and strength degradation: Because the long period velocity pulses are generally in the beginning of the near fault ground motions[1], they tend to cause some large nonlinear excursions at the early stages of responding to the input near

[1] That is to say, the long-period pulses usually start before arrival of shear waves.

fault ground motions. This causes some early stiffness and strength degradation. Early stiffness degradation results in a softer system with longer effective period. The period elongation makes the structure more susceptible to the near fault ground motions as the effective period of the system becomes closer to the period of the near fault velocity pulse. Similarly, early strength degradation results in a weaker system which may experience more inelastic cycles while it responds to the remainder of the input motion, after initial yielding takes place.

Displacement demands: The results of nonlinear time history analysis of various single degree of freedom systems showed that the residual displacements of the structures are highly dependent on the backbone curve and the reversal load patterns. However, comparison of the maximum inelastic displacements for near fault ground motions with the same for their far field ground motion counterparts showed that

a) the inelastic displacement demand ratio is almost independent to the backbone curve and the reversal load patterns,

b) the inelastic displacement demand ratio is always more than one in fault normal direction, for the entire range of parameters,

c) the inelastic displacement demand ratio is slightly more than one in fault parallel direction, for the entire range of parameters (this is mainly due to the fact that some of the FP component of selected pulse-like NF-GMs are associated with long period pulses - refer to Appendix F.2),

d) the inelastic displacement demand ratio in the fault normal direction is more than that in the fault parallel direction.

In general inelastic displacement demand ratio in the fault normal direction is about 1.4 ($\pm$ 20%) for the structures with elastic period of vibration of 0.6 s or less; this value linearly increases, to 2.3 as elastic period of vibration of the system increases to 2.4 s. The inelastic displacement demand ratio in fault parallel direction has also a linear relationship with elastic period of vibration of the system; i.e. the inelastic displacement demand ratio in fault parallel direction has a value of about 1.0 for the structures with elastic period of 0.2 s, and a value of about 1.6 for the structures with elastic period of about 2.4 s.

Ductility demands: For short-period structures the values of ductility demand ratios are very similar to those of inelastic displacement demand ratio, except ductility demand ratio linearly approaches unity as the period of vibration of the system increases and the response of the system approaches elastic response (i.e., ductility ratio of one for both NF and far field ground motions). For example the value of ductility demand ratio in fault normal direction for a system with strength characteristic of 0.30 and period of vibration of less than 1.25 s is about 1.7; this value is one for the systems with the same yield level and elastic period of vibration of 1.9 s or more. Similar results are also applicable to the ductility demand ratios in fault parallel direction.

Yield capacity demand ratio: Yield capacity demand ratio is defined as the ratio of the capacity of the structure required to limit the duality demand to a certain limit for the near fault ground motions to the same for far field ground motions. The value of yield capacity demand ratio in fault normal direction is approximately unity for the structures with an elastic period of vibration of 0.2 s or less. This value increases linearly from 1.0 to 2.5 as elastic period of vibration increases from 0.2 s to 2.4 s. The value of yield capacity demand ratio in the fault parallel direction is very similar to that in fault normal direction; however, in fault parallel direction the yield capacity demand ratio increases linearly from 1.0 to 1.8, as elastic period of vibration increases from 0.2 s to 2.4 s.

Parametric analysis of various systems showed that yield capacity demand ratio is a very stable and robust parameter with very low dependency on the variation of the structural parameters used in this research. Therefore, the yield capacity demand ratio can be confidently used to approximate the minimum capacity required for limiting the ductility of the system to a certain level when the structure is subjected to the near fault ground motions from the minimum capacity required for limiting the ductility of the system to the same level when the structure is subjected the far field ground motions (e.g. from code prescribed design procedures, defined for the far field ground motions).

Maximum inelastic displacement demand to maximum elastic displacement demand: Structures subjected to near fault ground motions may experience much larger maximum inelastic to elastic displacement demand than those subjected to far field ground motions. This effect is more pronounced when the elastic period of

vibration of the system is 0.8 s or less and/or strength characteristic is 20% or less. Nonetheless, the maximum elastic displacements can be used as a good estimation of the maximum inelastic displacement for period ranges beyond 0.6~0.8 s, invariably for NF and far field ground motions, and in both fault normal and fault parallel directions.

Probabilistic relationships: Finally, all results of the analyses mentioned above were put into the probabilistic framework which can be used to approximate engineering demand parameters of interest for a structure, supported on a flexible foundation, and subjected to near fault ground motions, from analysis of an equivalent single degree of freedom system for the equivalent far field ground motions (i.e. from code prescribed procedures originally developed for fixed base structures, subjected for far field ground motions).

2. Cobined effect of near fault ground motions and the flexibility of the foundation system on nonlinear response of structures

To allow for the effect of flexibility of the foundation system on nonlinear response of the structures an equivalent nonlinear two degree of freedom system was developed. The equivalent two degree of freedom system explicitly accounted for transversal and rotation flexibility of foundation system by using an equivalent linear transversal spring at the base of a nonlinear single degree of freedom system. The mass added to the base of the system is to account for the mass of the foundation and the added mass of the soil moving in phase with the foundation.

Results of analyses showed that flexibility of the foundation system increases the maximum displacement demand of the short-period structures and reduces the maximum displacement demand of the longer period structures. For example for a representative superstructure with elastic period of vibration of 0.2 s, the maximum displacement demand in fault normal direction is approximately 20% more if flexibility of the foundation is accounted for. However, for superstructures with elastic period of vibration of 1.8 s or larger, the maximum displacement demand in fault normal direction is about 15 to 20% less, if flexibility of the foundation is accounted for.

The effect of flexibility of the foundation system on the ductility demands is very similar to the effect of flexibility of the foundation system on maximum displacement demands.

In contrast to the effects of the flexibility of the foundation system on individual engineering demand parameters, results of analyses showed that accounting for the flexibility of the foundation system invariably increases the ratios of the engineering demand parameters. The inelastic displacement demand ratio, ductility demand ratio, and ratio of inelastic displacement to elastic displacement of the superstructure are increased if flexibility of the foundation system is accounted for. It is of note that adverse effect of flexibility of the foundation system on ratios of engineering demand parameters is more pronounced as the elastic period of vibration of the system increases. For example, for the representative superstructure that is noted above, consideration of flexibility of the foundation system increases the average inelastic displacement demand ratio by a factor of 1.7 to 2.8 when the elastic period of vibration increases form 0.2 s to 2.4 s respectively.

3. Simplified method for consideration of concurrent effects of near fault ground motions and flexibility of the foundation system

To allow for the integration of the effects of near fault ground motions, and the effects of flexibility of the foundation system on engineering demand parameters of interest, a simplified procedure was developed. The proposed procedure allowed for the conversion of the entire system into an equivalent single degree of freedom system. The conversion technique is determined mathematically, based on nonlinear properties of the superstructure and the properties of the first mode of vibration of the system. The proposed procedure is formulated based on the ratio of the foundation mass to the superstructure mass and ratio of the foundation-stiffness to the superstructure-stiffness. Using this procedure one can simply approximate the ratio of engineering demand parameters of interest when the effects of flexibility of the foundation system are implicitly accounted for.

The validity of the proposed method for consideration of effects of near fault ground motions with the effects of flexibility of the foundation system was checked against

several numerical models with different levels of complexity and completeness. Results of verification analysis proved to be quite satisfactory.

7.3 Impact of this research on engineering practice

The results of analysis of single degree of freedom and two degree of freedom systems, presented in Chapters 4 and 5, respectively, can be used to readily estimate:

- the maximum displacement demand of the structures due to near fault ground motions from those due to far field ground motions,
- the maximum ductility demand of the structures due to near fault ground motions from those due to far field ground motions,
- the maximum inelastic to maximum elastic displacement demand of the structures due to near fault ground motions,
- the capacity required to limit the ductility demand of the superstructure to some target ductility ratio for near fault ground motions, based on the same for far field ground motions (useful for seismic upgrade projects).

The proposed simplified method can be used to accurately and efficiently evaluate the effects of flexibility of the foundation system on the nonlinear response of the structures.

7.4 Recommendations for future work

A. Expanding current work for a specific near fault velocity pulse period

Ground motions selected for this study did not account for any specific pulse period; however, one may decide to divide the entire range of possible pulse periods to a series of refined ranges of pulse periods and duplicate results of this study for each refined pulse period range.

Such results can assist practicing engineers to predict the dominant pulse period of the expected near fault ground motion (determined from moment magnitude of the background earthquake),and allow for more accurate estimate the effects of near fault ground motions on engineering demand parameters of interest.

B. *Investigating cumulative damage (or cyclic ductility) vs. maximum ductility demand*

Hysteretic behaviour of the structures showed that near fault ground motions can cause a few large excursions, whereas far field ground motions usually cause numerous smaller excursions. Therefore, the ductility ratio determined for near fault ground motions is much larger than that of far field ground motions.

However, although the amplitude of nonlinearity of the structure caused by far field ground motions might not result in significant damage, the cumulative effect of small cyclical damages may be an issue.

Hence, comparison of performance of structures due to near fault ground motions with the same due to far field ground motions with respect to an appropriate damaging index can be very useful.

It is worth noting that the standard detailing recommended by design codes are generally developed based on far field input motions. Therefore, the same detailing might not provide the equal level of protection/ductility for both near fault and far field ground motions.

C. *Effect of P-Δ on the nonlinear response of the structure to near fault ground motions*

In this study, P-Δ effects were considered implicitly (using negative stiffness). Further investigation into the combined effects of P-Δ and near fault ground motions in a more detailed - spatially distributed - model where the effect of P-Δ is explicitly accounted for in the solution may be of value.

D. *Effect of angle of incidence of the near fault ground motions on response of the structures*

In this research we have studied the effect of near fault ground motions on the response of the structures when the principal axes of the structure are aligned with fault normal and fault parallel directions. It may be worthwhile to extend this study to

allow for various angles of incidence and evaluate the influence of angle of incidence of near fault ground motions on the nonlinear response of structures.

References

AASHTO Guide Specifications for LRFD Seismic Bridge Design, 2nd Edition

Abrahamson, N. A. (2000). Effects of rupture directivity on probabilistic seismic hazard analysis, In Sixth International Conf. Seismic Zonation, Oakland, California. Earthquake Engineering Research Inst.

Abrahamson, N.A., and Silva, W.J., 2008, Summary of the Abrahamson & Silva NGA ground-motion relations: Earthquake Spectra, vol. 24, no. 1, pp. 67-97.

Akkar, S., Yazgan, U., and Gulkan, P., 2005, Drift estimates in frame buildings subjected to near-fault ground motions: Journal of Structural Engineering, v. 131, no. 7, pp. 1014-1024.

Alavi B., Krawinkler H. (2004). Behavior of moment-resisting frame structures subjected to near-fault ground motions. Earthq. Engrg. Struct. Dynam. 33, 687- 706.

Alavi, B., and Krawinkler, H., 2001, Effects of near-fault ground motions on frame structures: Blume Center Report #138, Stanford, California, 301 pp.

American Society of Civil Engineers (ASCE), 2006, Minimum Design Loads for Buildings and Other Structures, ASCE /SEI 7-05.

Anderson, J.C., and Bertero, V.V. (1987), Uncertainties in establishing design earthquakes, Journal of Structural Engineering, Vol.113, No.8, pp. 1709-1724.

Anderson, J.C., and Bertero, V.V., 1987, Uncertainties in establishing design earthquakes: Journal of Structural Engineering, v. 113, no. 8, pp. 1709-1724.

Applied Technology Council. (2011). ATC-58, Guidelines for Seismic Performance Assessment of Buildings, 75% Draft. Applied Technology Council, Redwood City, California.

Author, A. 2010. Title, publication details, in style permitted by your discipline. Please consult a style manual appropriate for your discipline for further details.

Author, B. 2010. Title, publication details, in style permitted by your discipline. Please consult a style manual appropriate for your discipline for further details.

Baez, J.I. and Miranda, E., ‘Amplification factors to estimate inelastic displacement demands for the design of structures in the Near-Fault’, Proceedings of the 12th World Conference on Earthquake Engineering, Auckland, New Zealand,

30 January – 4 February 2000, Paper No. 1561, New Zealand Society for Earthquake Engineering Silverstream, Upper Hutt, NZ, 2000.

Baker, J. 2013. Quantitative classification of pulse-like ground motions. http://www.stanford.edu/~bakerjw/research/pulse-classification.html. Accessed Jan-13

Baker, J.W., 2007, Quantitative classification of near-fault ground motions using wavelet analysis: Bulletin of the Seismological Society of America, v. 97, no. 5, pp. 1486-1501.

Baker, J.W., and Cornell C.A., 2005, A vector-valued ground motion intensity measure consisting of spectral acceleration and epsilon: Earthquake Engineering and Structural Dynamics, v. 34, no. 10, pp. 1193-1217.

Baker, J.W., and Cornell, C.A., 2004, Choice of a vector of ground motion intensity measures for seismic demand hazard analysis: Proceedings of the 13th World Conference on Earthquake Engineering, Vancouver, Canada, August.

Baker, J.W., and Cornell, C.A., 2006, Spectral shape, epsilon and record selection: Earthquake Engineering and Structural Dynamics, v. 35, no. 9, pp. 1077-1095.

Baker, J.W., and Cornell, C.A., 2008, Vector-valued intensity measures incorporating spectral shape for prediction of structural response: Journal of Earthquake Engineering, v. 12, Iss 4, pp. 534-554.Baker, J.W., and Jayaram, N., 2008, Correlation of spectral acceleration values from NGA ground motion models: Earthquake Spectra, vol. 24, no. 1, pp. 299-317.

Bazzurro, P., and Luco, N. 2003, Parameterization of non-stationary time series: Draft Report for Task 1G00 to PEER-Lifelines Program.

Bertero, V., Mahin S., and Herrera R., 1978, Aseismic design implications of near-fault San Fernando earthquake records: Earthquake Engineering and Structural Dynamics, v. 6, no. 1, pp. 31-42.

Bertero, V.V., Mahin, S.A., and Herrera, R.A. (1977), Problems in prescribing reliable design earthquakes, Proceedings, 6th World Conference on Earthquake Engineering, New Delhi, India, Vol. 2, pp. 1741-1746.

Boore, D.M., and Atkinson, G.M., 2008, Ground-motion prediction equations for the average horizontal component of PGA, PGV, and 5% damped PSA at spectral periods between 0.01s and 10.0s: Earthquake Spectra, vol. 24, no. 1, pp. 99-138.

Boulanger, Ross W., Christina J. Curras, Bruce L. Kutter, Daniel W. Wilson, and Abbas Abghari. Seismic soil-pile-structure interaction experiments and

analyses. Journal of Geotechnical and Geoenvironmental Engineering 125, no. 9 (1999): 750-759.

Brandenberg, S.J., Singh, P., Boulanger, R,W., Kutter B.L. (2001 – Caltrans workshop), Behaviour of piles in laterally spreading ground during earthquakes

Bray, J.D., and Rodriguez-Marek, A., 2004, Characterization of forward-directivity ground motions in the near-fault region: Soil Dynamics and Earthquake Engineering, v. 24, no. 11, pp. 815-828.

Bray, Jonathan D., Adrian Rodriguez-Marek, and Joanne L. Gillie. Design ground motions near active faults. Bulletin of the New Zealand Society for Earthquake Engineering 42.1 (2009)

Building Seismic Safety Council (BSSC), 2003, NEHRP Recommended Provisions for Seismic Regulations for New Buildings and Other Structures (FEMA 450), 2003 Edition.

Button, Martin R., Colman J. Cronin, and Ronald L. Mayes. Effect of vertical motions on seismic response of highway bridges. Journal of Structural Engineering 128.12 (2002): 1551-1564.

Caltrans' Seismic Design Criteria Version 1.6, November 2010

Campbell, K.W., and Bozorgnia, Y., 2008, NGA ground motion Model for the geometric mean horizontal component of PGA, PGV, PGD, and 5% damped linear elastic response spectra for periods ranging from 0.01s to 10.0s: Earthquake Spectra, vol. 24, no. 1, pp. 139-171.

Can simple pulses adequately represent near-fault ground motions? Rupakhety, R.; Sigbjörnsson, R. , 2011

Carbonari, S.; Dezi, F.; Leoni, G., Seismic response of bridges on pile foundations considering soil-structure interaction, Tailor Made Concrete Structures – Walraven & Stoelhorst (eds), 2008 Taylor & Francis Group, London

Ch.A. Maniatakis, I.M. Taflampas and C.C. Spyrakos , IDENTIFICATION OF NEAR-FAULT EARTHQUAKE RECORD CHARACTERISTICS , The 14th World Conference on Earthquake Engineering, 2008, China

Chioccarelli, E., and I. Iervolino (2010). Near-source seismic demand and pulse-like records: A discussion for L'Aquila earthquake, Earthquake Eng. Struct. Dynam. 39, no. 9, 1039–1062.

Chiou, B., Darragh, R., Gregor, N., and Silva, W., 2008, NGA project strong-motion database, Earthquake Spectra, vol. 24, no. 1, pp. 23-44.

Chiou, B., Power, M., Abrahamson, N., and Roblee, C., 2006, An overview of the project of next generation of ground motion attenuation models for shallow crustal earthquakes in active tectonic regions: Proceedings of the Fifth National Seismic Conference on Bridges & Highways, San Mateo, California, September.

Chiou, B.S.J. and Youngs, R.R., 2008a, Chiou-Youngs NGA ground motion relations for the geometric mean horizontal component of peak and spectral ground motion parameters, Earthquake Spectra, vol. 24, no. 1, pp. 173-215.

Chiou, B.S.J., and Youngs, R.R., 2008b, NGS model for average horizontal component of peak ground motion and response spectra, Report PEER 2008/09, Pacific Earthquake Engineering Research Center, University of California, Berkeley.

Chopra AK. Dynamics of Structures: Theory and Applications to Earthquake Engineering (2nd edn). Prentice- Hall: Upper Saddle River, NJ, 2001.

Chopra, A.; Chintanapakdee, C., Comparing response of SDF systems to near-fault and far-fault earthquake motions in the context of spectral regions, Earthquake Engineering & Structural Dynamics Volume 30, Issue 12, pages 1769–1789, December 2001

Chopra, Anil K., and Chatpan Chintanapakdee. Inelastic deformation ratios for design and evaluation of structures: Single-degree-of-freedom bilinear systems. Journal of structural engineering 130.9 (2004): 1309-1319.

Consortium of Organizations of Strong Motion Observation Systems (COSMOS), 2007, Annual Meeting Technical Session, Recommendations for Selection and Scaling of Ground Motion for Building Code and Performance-Based Earthquake Engineering (PBEE) Applications and on Evaluation of Selection and Scaling Procedures Proposed for the Next Generation of PBEE, sponsored by COSMOS and Pacific Earthquake Engineering Research Center (PEER) Berkeley, CA, November.

Consortium of Organizations of Strong Motion Systems (COSMOS), 2006, Annual Meeting Technical Session, An Evaluation of Methods for the Selection and Scaling of Ground Motion Time series for Building Code and Performance-Based Earthquake Engineering Applications, sponsored by COSMOS and Pacific Earthquake Engineering Research Center (PEER) Berkeley, CA, November.

Cordova, P.P., Mehanny, S.S.F., Deierlein, G.G., and Cornell, C.A., 2000, Development of a two-parameter seismic intensity measure and probabilistic assessment procedure: Proceedings of the Second U.S.-Japan Workshop on

Performance-Based Seismic Earthquake Engineering Methodology for Reinforced Concrete Building Structures, Sapporo, Japan, pp. 195-214.

Cornell, C.A., 2006, Should uniform hazard spectra be used for design? How should design response spectra be determined considering uniform hazard spectra from design maps and hazard deaggregation data?: Abstract and PowerPoint presentation in Preprints, Third ATC-35/USGS National Earthquake Ground Motion Mapping Workshop, San Mateo, California, December.

Dimakopoulou, V.; Fragiadakis, M.; Spyrakos, C , Seismic response of degrading SDOF systems due to near-field ground motions, ECCOMAS Thematic Conference - COMPDYN 2011: 3rd International Conference on Computational Methods in Structural Dynamics and Earthquake Engineering: An IACM Special Interest Conference, Programme, 2011

Dimakopoulou. V., Fragiadakis, M., and Spyrakos, C., Near-fault ground motions, and the response of elastic and inelastic single-degree-of-freedom (SDOF) systems

Diotallevi, P.P. and L. Landi, 2000. Effect of axial force and of the vertical ground motion component on the seismic response of R/C frames. Proceedings of the 12th World Conference on Earthquake Engineering, New Zealand, 30 January-4 February, New Zealand Society for Earthquake Engineering, pp: 1026-1026.

Elnashai, A.S. and Papazoglou, A.J. (1997). Procedure and spectra for analysis of RC structures subjected to vertical earthquake loads. Journal of Earthquake Engineering 1, 121-155.

Fu, Q., and Menun, C., 2004, Seismic-environment-based simulation of near-fault ground motions: Proceedings of the 13th World Conference on Earthquake Engineering, Vancouver, Canada, 15 pp.

Ghobarah, A. and A.S. Elnashai, 1998. Contribution of vertical ground motion to the damage of R/C buildings. Proceedings of the 11th European Conference on Earthquake Engineering, September 6-11, Balkema, Rotterdom, Paris, pp: 468-468.

GMSM Working Group, 2009, C.B. Haselton (ed.), PEER Ground Motion Selection and Modification Working Group, Evaluation of ground motion selection and modification methods: predicting median interstory drift response of buildings: PEER Report 2009/01, Pacific Earthquake Engineering Research Center, University of California, Berkeley.

Goulet, C.A., Watson-Lamprey, J., Baker, J., Haselton, C., and Luco, N., 2008, Assessment of ground motion selection and modification (GMSM) methods

for non-linear dynamic analyses of structures, Proceedings of Geotechnical Earthquake Engineering and Soil Dynamics IV Conference, Sacramento, CA, American Society of Civil Engineers, Geotechnical Special Publication No. 181, 10 pp.

Hall, J.F., Heaton, T.H., Halling, M.W. and Wald, D.J. (1995). Near-source ground motion and its effects on flexible buildings. Earthquake Spectra 11:4, 569-605.

Hall, J.F., Heaton, T.H., Halling, M.W., and Wald, D.J., 1995, Near-source ground motion and its effects on flexible buildings: Earthquake Spectra, v. 11, no. 4, pp. 569-605.

Kalkan E, Kunnath S.K., Effects of Fling-Step and Forward Directivity on the Seismic Response of Buildings. Earthquake Spectra, Vol. 22, No. 2, pp. 367-390, May 2006

Kim, S., Holub, C., and Elnashai, A. (2011). Analytical Assessment of the Effect of Vertical Earthquake Motion on RC Bridge Piers. J. Struct. Eng., 137(2), 252–260.

Krawinkler, H., and Alavi, B. Development of Improved Design Procedures for Near Fault Ground Motions (1998)

Loh, Chin-Hsiung, Shiuan Wan, and Wen-I. Liao. Effects of hysteretic model on seismic demands: consideration of near fault ground motions. The Structural Design of Tall Buildings 11.3 (2002): 155-169.

Luan X, Xueb S, and Li X , The Effect of Soil Structure Interaction on the Seismic Response of Spatial Structure Subjected to the Near Fault Ground Motion,

Mahin, S.A., Bertero, V.V., Chopra, A.K., and Collins, R.G. (1976), Response of the Olive View hospital main building during the San Fernando earthquake, Report No. UCB/EERC-76/22, Earthquake Engineering Research Center, University of California at Berkeley, Berkeley, California.

Makris, N., G. Gazetas, and E. Delis. Dynamic soil-pile-foundation-structure interaction: records and predictions. Geotechnique 46.1 (1996): 33-50.

Makris, Nicos, and George Gazetas. Dynamic pile-soil-pile interaction. Part II: Lateral and seismic response. Earthquake engineering & structural dynamics 21.2 (1992): 145-162.

Makris, Nicos, and George Gazetas. Dynamic pile□soil□pile interaction. Part II: Lateral and seismic response. Earthquake engineering & structural dynamics 21.2 (1992): 145-162.

Mavroeidis, G. and Papageorgiou, A. (2003) A mathematical representation of near-fault ground motions. Bulletin of the Seismological Society of America 93:3, 1099-1131.

Mavroeidis, G. P., Dong, G., Papageorgiou, A. S., Near-fault ground motions, and the response of elastic and inelastic single-degree-of-freedom (SDOF) systems, 2004

Mazza F., Vulcano A., Nonlinear dynamic response of r.c. framed structures subjected to near-fault ground motions, March 2010 , Springer Science+Business Media B.V. 2010

McCallen D. B., Astaneh-Asl A., Larsen S.C., and L. Hutchings J. (2009), The Response of Long-Span Bridges to Low Frequency,Near-Fault Earthquake Ground Motions

Menun, C., and Q. Fu (2002). An analytical model for near-fault ground motions and the response of SDOF systems, in Proc. 7th U.S. National Conf. Earthquake Engineering, Boston, Massachusetts, 10 pp.

Menun, Charles, and Qiang Fu. An analytical model for near-fault ground motions and the response of SDOF systems. In Proc. Seventh US Natl. Conf. Earthq. Eng., Boston, Massachusetts. 2002.

Mollaioli F., Bruno S., Decanini L., Panza G., Characterization of the Dynamic Response of Structures to Damaging Pulse-type Near-fault Ground Motions, Meccanica, v 41, n 1, p 23-46, February 2006

Mylonakis, George, and George Gazetas. Seismic soil-structure interaction: Beneficial or detrimental?. Journal of Earthquake Engineering 4.03 (2000): 277-301.

Mylonakis, George, Aspasia Nikolaou, and George Gazetas. Soil-pile-bridge seismic interaction: Kinematic and Inertial effects. Part I: soft soil. Earthquake engineering & structural dynamics 26.3 (1997): 337-359.

NIST GCR 11-917-15, Selecting and Scaling Earthquake Ground Motions for Performing Response-History Analyses - NEHRP Consultants Joint Venture, A partnership of the Applied Technology Council and the, Consortium of Universities for Research in Earthquake Engineering

Papazoglou, A.J. and A.S. Elnashai, 1996. Analytical and field evidence of the damaging effect of vertical Earthquake ground motion. J. Earthquake Eng. Struct. Dyn., 25: 1109-1137.

Porter, K., Kennedy, R., and Bachman, R. (2007). Creating Fragility Functions for Performance-Based Earthquake Engineering. Earthquake Spectra, 23(2), 471-489.

Riahi, A., Arezoumandi, M., (2008, World Conference on Earthquake Engineering)Effect of vertical motion of earthquake on RC bridge pier

Roberto Villaverde, Fundamental Concepts of Earthquake Engineering, Chapter 13, 2009 by CRC Press

Rupakhety R, Sigbjörnsson R; Can simple pulses adequately represent near-fault ground motions? Journal of Earthquake Engineering. Volume 15, Issue 8, 2011

Sasani, M., And Bertero, V. Importance of severe pulse-type ground motions in performance-based engineering: historical and critical review.

Sasani, M., and V. V. Bertero (2000). Importance of severe pulse-type ground motions in performance-based engineering: historical and critical review, in Proc. of the Twelfth World Conf. on Earthquake Engineering (12WCEE), Auckland, New Zealand, 30 January–4 February2000.

Seismic Rehabilitation of Existing Buildings (41-06) - American Society of Civil Engineers' Standard Number 41.

Seismic Retrofitting Manual for Highway Structures: Part 1 – Bridges, United States Department of Transportation - Federal Highway Administration, Publication Number: FHWA-HRT-06-032 (2006)

Seismic Retrofitting Manual for Highway Structures: Part 1 – Bridges, report FHWA-RD-94-052 of Federal Highway Administration (FHWA) publications (1995)

Shome, N., Cornell, C.A., Bazzurro, P., and Carballo, J.E., 1998, Earthquake records and nonlinear response: Earthquake Spectra, v. 14, no. 3, pp. 469-500.

Somerville, P. G. Characterizing near fault ground motion for the design and evaluation of bridges. Third National Conference and Workshop on Bridges and Highways. Portland, Oregon. 2002.

Somerville, P.G., 2003, Magnitude scaling of the near fault rupture Directivity pulse: Physics of the Earth and Planetary Interiors, v. 137, no. 1, p. 12.

Somerville, P.G., Smith, N.F., Graves, R.W., and Abrahamson, N.A., 1997, Modification of empirical strong ground motion attenuation relations to include the amplitude and duration effects of rupture Directivity: Seismological Research Letters, v. 68, no. 1, pp. 199-222.

Stewart, Jonathan P., Gregory L. Fenves, and Raymond B. Seed. Seismic soil-structure interaction in buildings. I: Analytical methods. Journal of Geotechnical and Geoenvironmental Engineering 125.1 (1999): 26-37.

Stewart, Jonathan P., Raymond B. Seed, and Gregory L. Fenves. Seismic soil-structure interaction in buildings. II: Empirical findings. Journal of geotechnical and geoenvironmental engineering 125.1 (1999): 38-48.

Tothong, P., C. A. Cornell, and J.W. Baker (2007). Explicit-directivity-pulse inclusion in probabilistic seismic hazard analysis, Earthquake Spectra 23, no. 4, 867–891.

Yi, W. and Yin, J. (2009). Discussion of Effect of Near-Fault Vertical Ground Motions on Seismic Response of Highway Overcrossings by Sashi K. Kunnath, Emrah Erduran, Y. H. Chai, and Mark Yashinsky. J. Bridge Eng., 14(5), 411–412.

Appendix A – Results of NLTHA of SDOF systems

List of selected Figures developed for SDOF systems subjected to PGA matched GMs

		NLT#1	NLT#2	NLT#3	NLT#4	NLT#5
Median values of maximum displacement demands and inelastic displacement demand ratio (IDDR) In Terms of strength characteristics	EQ Level 1	Figure A - 1	Figure A - 2	Figure A - 3	Figure A - 4	Figure A - 5
	EQ Level 2	Not presented for brevity			Figure A - 6	Figure A - 7
	EQ Level 3				Figure A - 8	Figure A - 9
	EQ Level 4				Figure A - 10	Figure A - 11
	EQ Level 5				Figure A - 12	Figure A - 13
Median values of maximum ductility demand and ductility demand ratio (DDR) in Terms of strength characteristics	EQ Level 1	Figure A - 14	Figure A - 15	Figure A - 16	Figure A - 17	Figure A - 18
	EQ Level 2	Not presented for brevity			Figure A - 19	Figure A - 20
	EQ Level 3				Figure A - 21	Figure A - 22
	EQ Level 4				Figure A - 23	Figure A - 24
	EQ Level 5				Figure A - 25	Figure A - 26
Median values of yield capacity demand and yield capacity demand ratio (YCDR) in Terms of target ductility	EQ Level 1	Figure A - 27	Figure A - 28	Figure A - 29	Figure A - 30	Figure A - 31
	EQ Level 2	Not presented for brevity			Figure A - 32	Figure A - 33
	EQ Level 3				Figure A - 34	Figure A - 35
	EQ Level 4				Figure A - 36	Figure A - 37
	EQ Level 5				Figure A - 38	Figure A - 39
Median values of maximum inelastic to elastic displacement demand and maximum inelastic to elastic displacement demand ratio in terms of strength characteristics	EQ Level 1	Figure A - 40	Figure A - 41	Figure A - 42	Figure A - 43	Figure A - 44
	EQ Level 2	Not presented for brevity			Figure A - 45	Figure A - 46
	EQ Level 3				Figure A - 47	Figure A - 48
	EQ Level 4				Figure A - 49	Figure A - 50
	EQ Level 5				Figure A - 51	Figure A - 52
Median values of maximum inelastic to elastic displacement demand and maximum inelastic to elastic displacement demand ratio in terms of ductility	EQ Level 1	Figure A - 53	Figure A - 54	Figure A - 55	Figure A - 56	Figure A - 57
	EQ Level 2	Not presented for brevity			Figure A - 58	Figure A - 59
	EQ Level 3				Figure A - 60	Figure A - 61
	EQ Level 4				Figure A - 62	Figure A - 63
	EQ Level 5				Figure A - 64	Figure A - 65
CV values of EDP and EDP.Ratio in terms of strength characteristics	EQ Level 1	Figure A - 66	Figure A - 67	Figure A - 68	Figure A - 69	Figure A - 70
	EQ Level 2	Not presented for brevity			Figure A - 71	Figure A - 72
	EQ Level 3				Figure A - 73	Figure A - 74
	EQ Level 4				Figure A - 75	Figure A - 76
	EQ Level 5				Figure A - 77	Figure A - 78

List of selected Figures developed for SDOF systems subjected to linearly scaled GMs

		NLT#1	NLT#2	NLT#3	NLT#4	NLT#5
Median values of maximum displacement demands and inelastic displacement demand ratio (IDDR) In Terms of strength characteristics	EQ Level 1	Figure A - 79	Figure A - 80	Figure A - 81	Figure A - 82	Figure A - 83
	EQ Level 2	Not presented for brevity			Figure A - 84	Figure A - 85
	EQ Level 3				Figure A - 86	Figure A - 87
	EQ Level 4				Figure A - 88	Figure A - 89
	EQ Level 5				Figure A - 90	Figure A - 91
Median values of maximum ductility demand and ductility demand ratio (DDR) in Terms of strength characteristics	EQ Level 1	Figure A - 92	Figure A - 93	Figure A - 94	Figure A - 95	Figure A - 96
	EQ Level 2	Not presented for brevity			Figure A - 97	Figure A - 98
	EQ Level 3				Figure A - 99	Figure A - 100
	EQ Level 4				Figure A - 101	Figure A - 102
	EQ Level 5				Figure A - 103	Figure A - 104
Median values of yield capacity demand and yield capacity demand ratio (YCDR) in Terms of target ductility	EQ Level 1	Figure A - 105	Figure A - 106	Figure A - 107	Figure A - 108	Figure A - 109
	EQ Level 2	Not presented for brevity			Figure A - 110	Figure A - 111
	EQ Level 3				Figure A - 112	Figure A - 113
	EQ Level 4				Figure A - 114	Figure A - 115
	EQ Level 5				Figure A - 116	Figure A - 117
Median values of maximum inelastic to elastic displacement demand and maximum inelastic to elastic displacement demand ratio in terms of strength characteristics	EQ Level 1	Figure A - 118	Figure A - 119	Figure A - 120	Figure A - 121	Figure A - 122
	EQ Level 2	Not presented for brevity			Figure A - 123	Figure A - 124
	EQ Level 3				Figure A - 125	Figure A - 126
	EQ Level 4				Figure A - 127	Figure A - 128
	EQ Level 5				Figure A - 129	Figure A - 130
Median values of maximum inelastic to elastic displacement demand and maximum inelastic to elastic displacement demand ratio in terms of ductility	EQ Level 1	Figure A - 131	Figure A - 132	Figure A - 133	Figure A - 134	Figure A - 135
	EQ Level 2	Not presented for brevity			Figure A - 136	Figure A - 137
	EQ Level 3				Figure A - 138	Figure A - 139
	EQ Level 4				Figure A - 140	Figure A - 141
	EQ Level 5				Figure A - 142	Figure A - 143
CV values of EDP and EDP.Ratio in terms of strength characteristics	EQ Level 1	Figure A - 144	Figure A - 145	Figure A - 146	Figure A - 147	Figure A - 148
	EQ Level 2	Not presented for brevity			Figure A - 149	Figure A - 150
	EQ Level 3				Figure A - 151	Figure A - 152
	EQ Level 4				Figure A - 153	Figure A - 154
	EQ Level 5				Figure A - 155	Figure A - 156

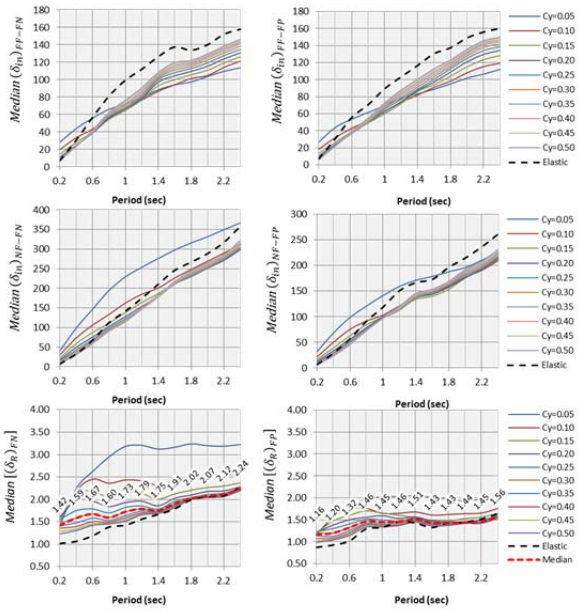

Figure A - 1: Median values of maximum displacement demands and inelastic displacement demand ratio (IDDR) In Terms of strength characteristics | Link: NLT#1| ζ=%2.0| EQ Level=1

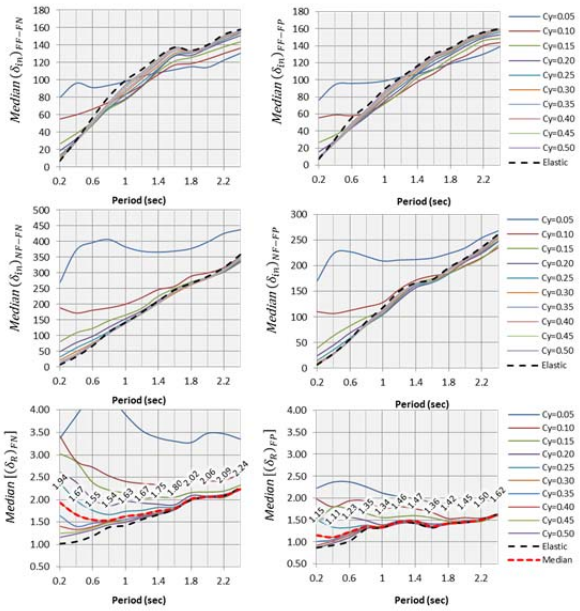

Figure A - 2: Median values of maximum displacement demands and inelastic displacement demand ratio (IDDR) In Terms of strength characteristics | Link: NLT#2| ζ=%2.0| EQ Level=1

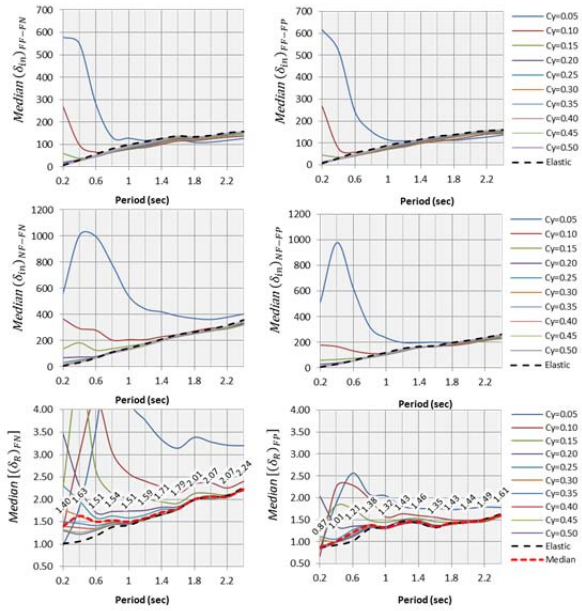

Figure A - 3: Median values of maximum displacement demands and inelastic displacement demand ratio (IDDR) In Terms of strength characteristics | Link: NLT#3| ζ=%2.0| EQ Level=1

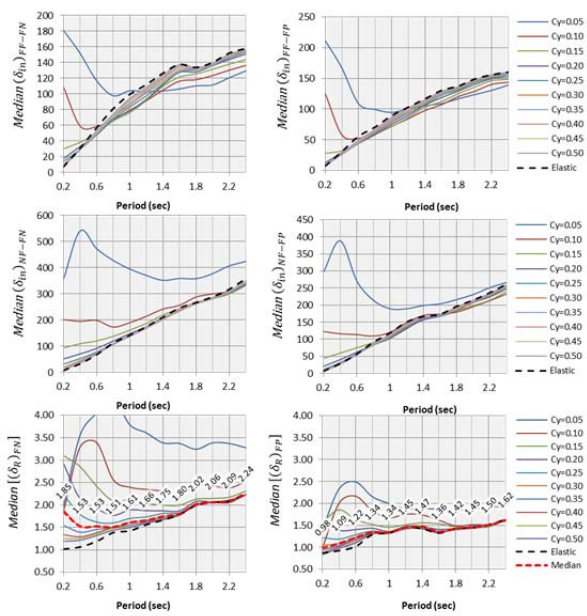

Figure A - 4: Median values of maximum displacement demands and inelastic displacement demand ratio (IDDR) In Terms of strength characteristics | Link: NLT#4| ζ=%2.0| EQ Level=1

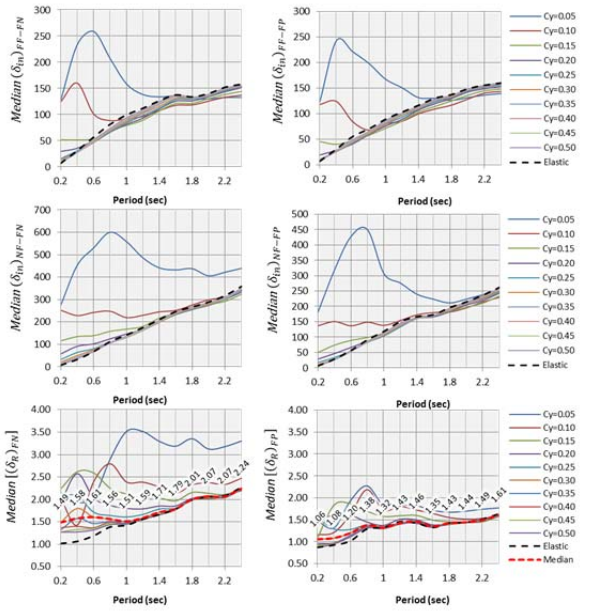

Figure A - 5: Median values of maximum displacement demands and inelastic displacement demand ratio (IDDR) In Terms of strength characteristics | Link: NLT#5| ζ=%2.0| EQ Level=1

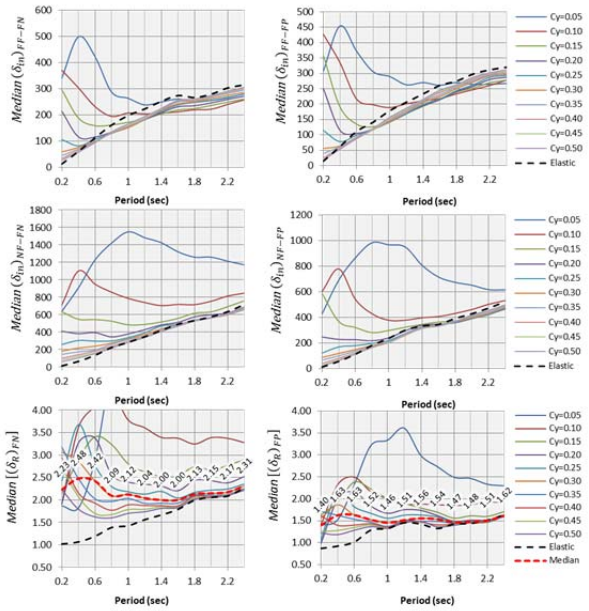

Figure A - 6: Median values of maximum displacement demands and inelastic displacement demand ratio (IDDR) In Terms of strength characteristics | Link: NLT#4| ζ=%2.0| EQ Level=2

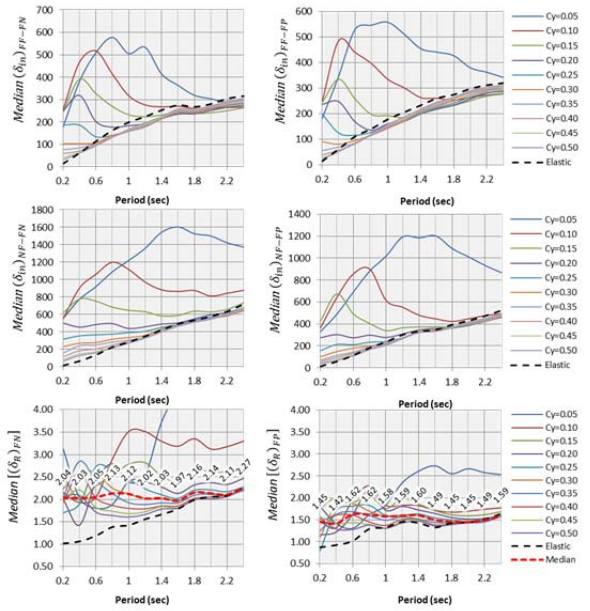

Figure A - 7: Median values of maximum displacement demands and inelastic displacement demand ratio (IDDR) In Terms of strength characteristics | Link: NLT#5| ζ=%2.0| EQ Level=2

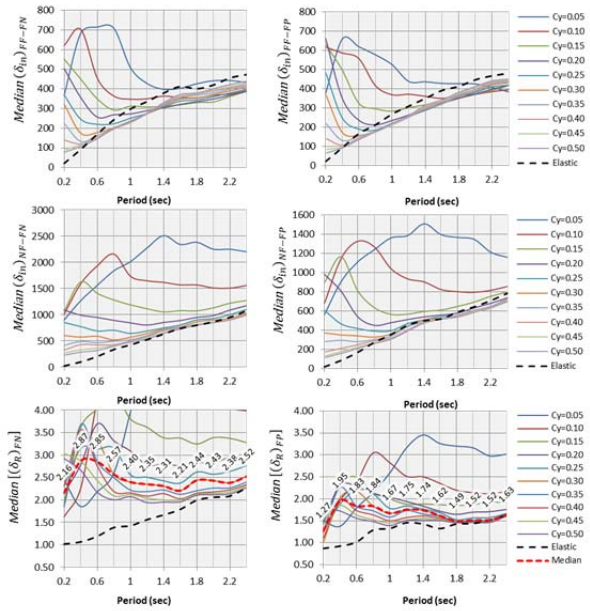

Figure A - 8: Median values of maximum displacement demands and inelastic displacement demand ratio (IDDR) In Terms of strength characteristics | Link: NLT#4| ζ=%2.0| EQ Level=3

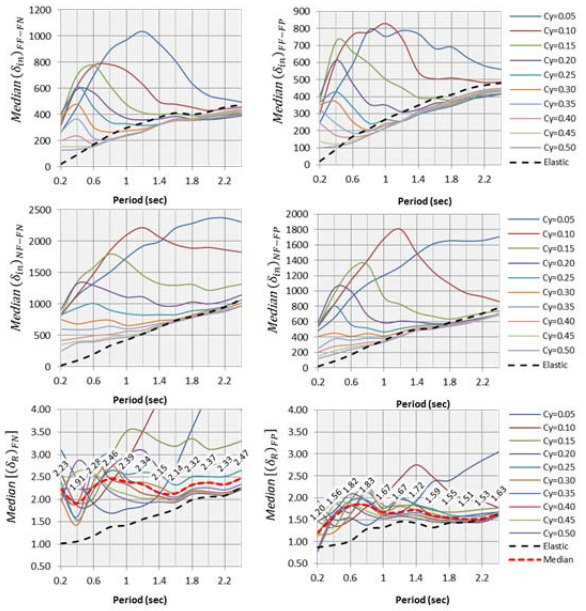

Figure A - 9: Median values of maximum displacement demands and inelastic displacement demand ratio (IDDR) In Terms of strength characteristics | Link: NLT#5| ζ=%2.0| EQ Level=3

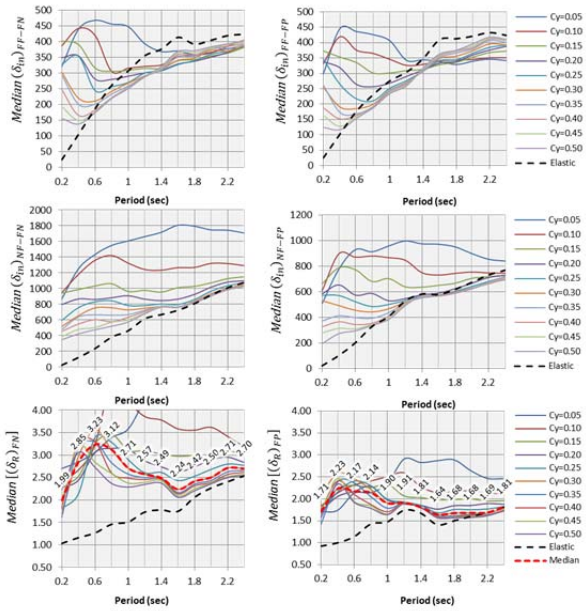

Figure A - 10: Median values of maximum displacement demands and inelastic displacement demand ratio (IDDR) In Terms of strength characteristics | Link: NLT#4| ζ=%2.0| EQ Level=4

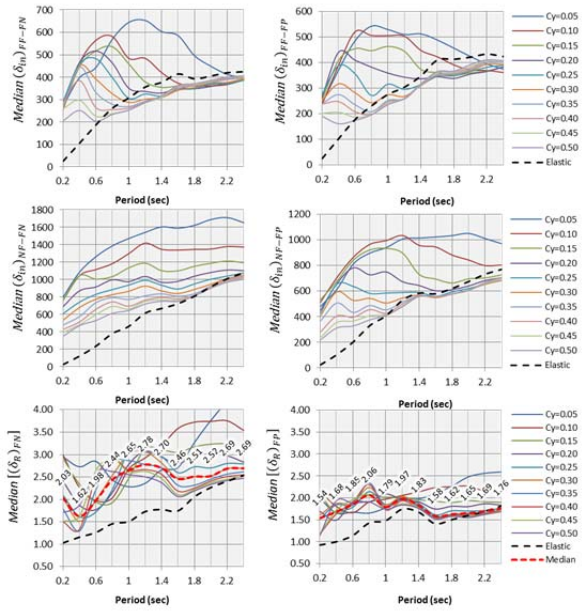

Figure A - 11: Median values of maximum displacement demands and inelastic displacement demand ratio (IDDR) In Terms of strength characteristics | Link: NLT#5| ζ=%2.0| EQ Level=4

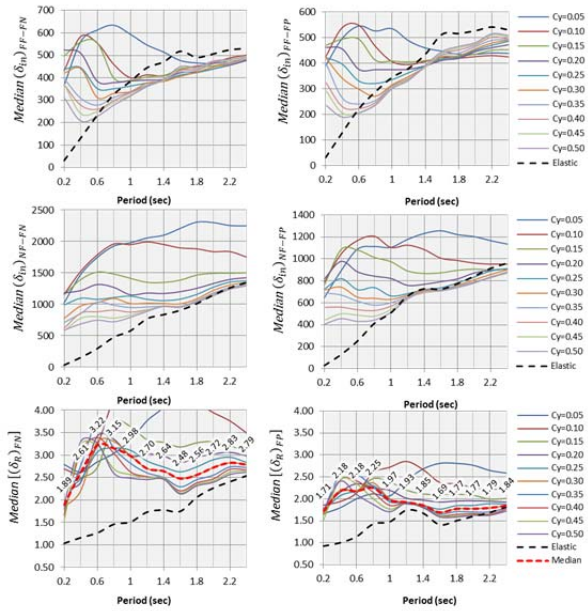

Figure A - 12: Median values of maximum displacement demands and inelastic displacement demand ratio (IDDR) In Terms of strength characteristics | Link: NLT#4| ζ=%2.0| EQ Level=5

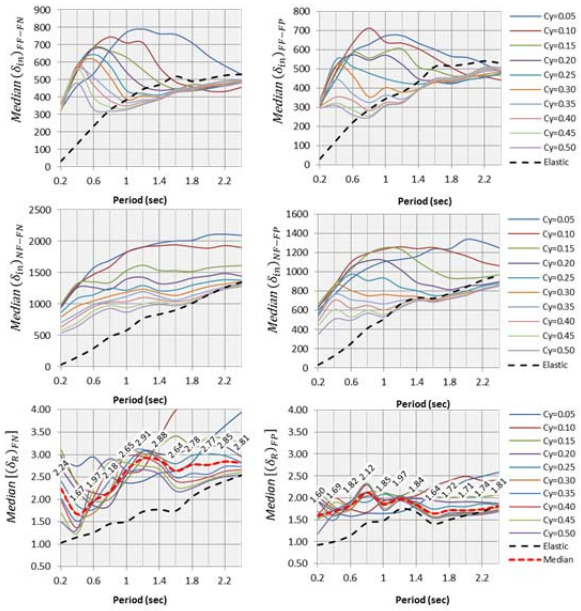

Figure A - 13: Median values of maximum displacement demands and inelastic displacement demand ratio (IDDR) In Terms of strength characteristics | Link: NLT#5| ζ=%2.0| EQ Level=5

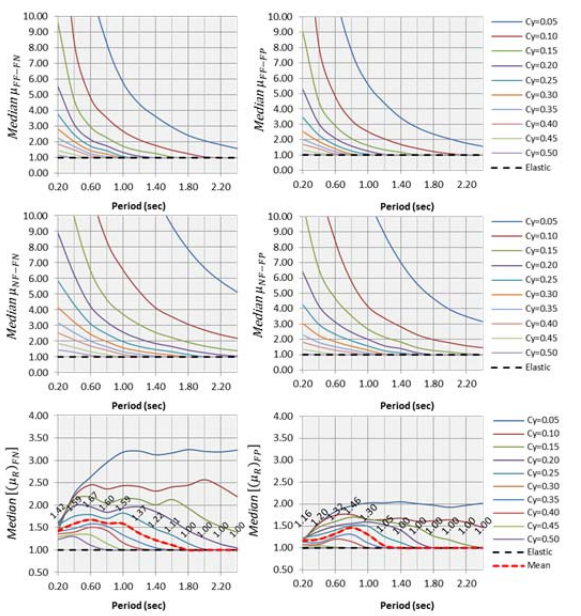

Figure A - 14: Median values of maximum ductility demand and ductility demand ratio (DDR) in Terms of strength characteristics | Link: NLT#1| ζ=%2.0| EQ Level=1

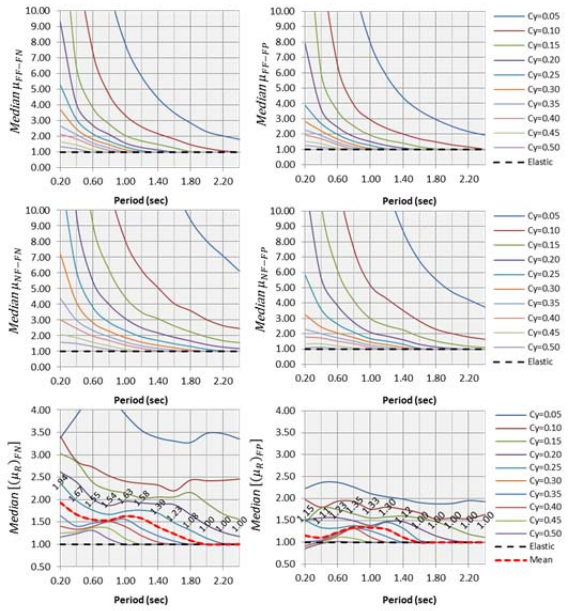

Figure A - 15: Median values of maximum ductility demand and ductility demand ratio (DDR) in Terms of strength characteristics | Link: NLT#2| ζ=%2.0| EQ Level=1

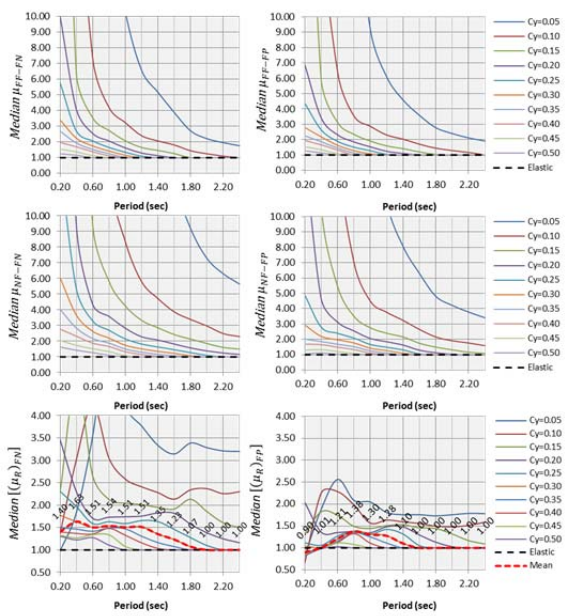

Figure A - 16: Median values of maximum ductility demand and ductility demand ratio (DDR) in Terms of strength characteristics | Link: NLT#3| ζ=%2.0| EQ Level=1

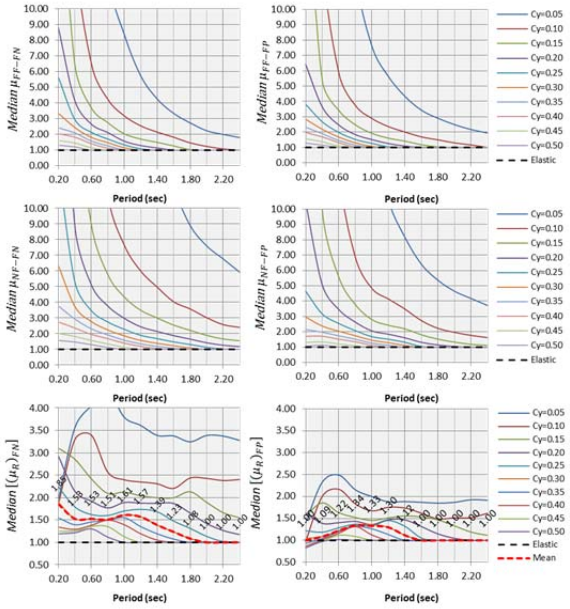

Figure A - 17: Median values of maximum ductility demand and ductility demand ratio (DDR) in Terms of strength characteristics | Link: NLT#4| ζ=%2.0| EQ Level=1

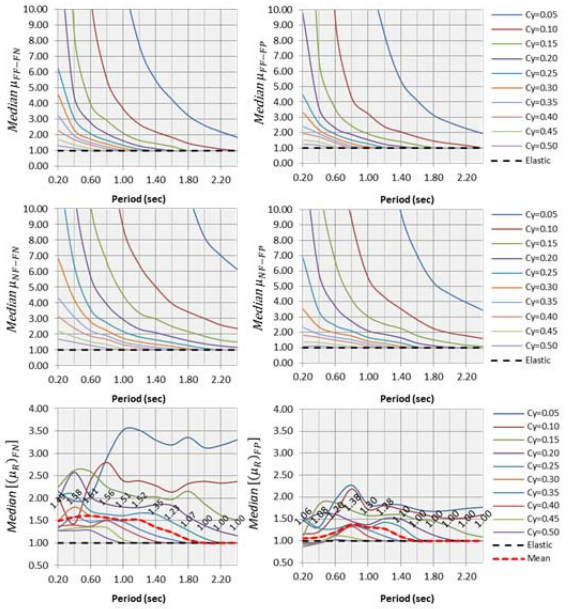

Figure A - 18: Median values of maximum ductility demand and ductility demand ratio (DDR) in Terms of strength characteristics | Link: NLT#5| ζ=%2.0| EQ Level=1

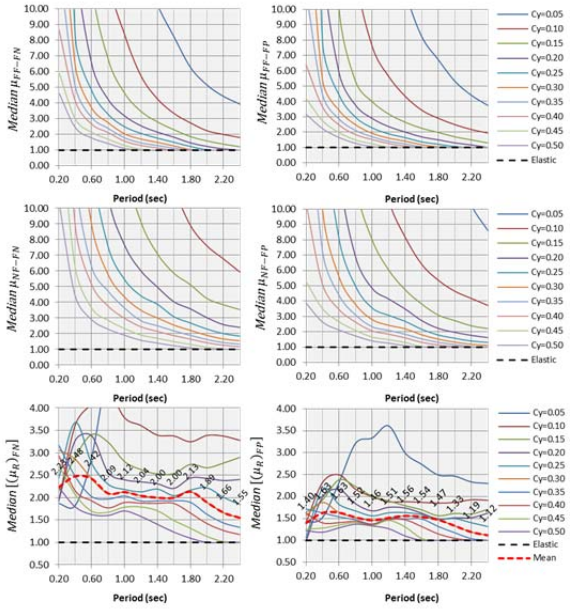

Figure A - 19: Median values of maximum ductility demand and ductility demand ratio (DDR) in Terms of strength characteristics | Link: NLT#4| ζ=%2.0| EQ Level=2

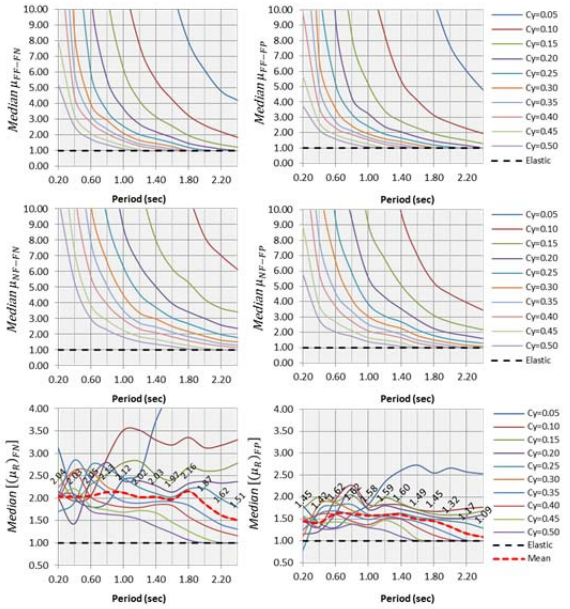

Figure A - 20: Median values of maximum ductility demand and ductility demand ratio (DDR) in Terms of strength characteristics | Link: NLT#5| ζ=%2.0| EQ Level=2

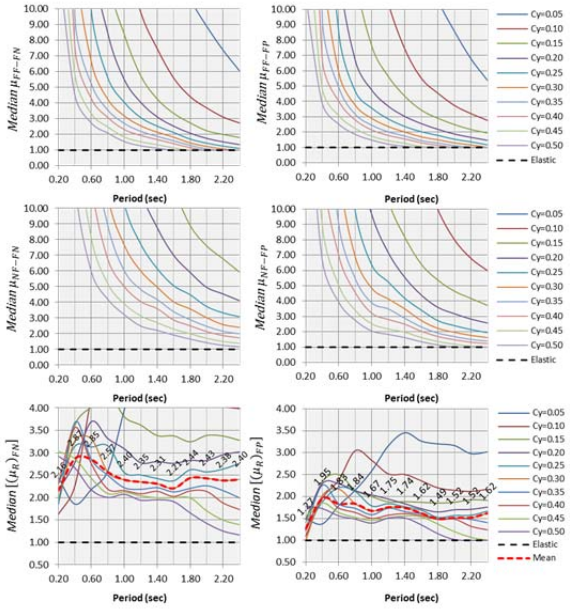

Figure A - 21: Median values of maximum ductility demand and ductility demand ratio (DDR) in Terms of strength characteristics | Link: NLT#4| ζ=%2.0| EQ Level=3

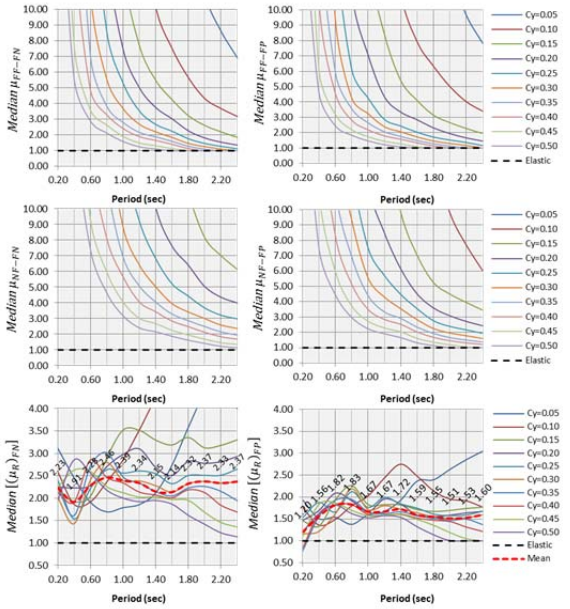

Figure A - 22: Median values of maximum ductility demand and ductility demand ratio (DDR) in Terms of strength characteristics | Link: NLT#5| ζ=%2.0| EQ Level=3

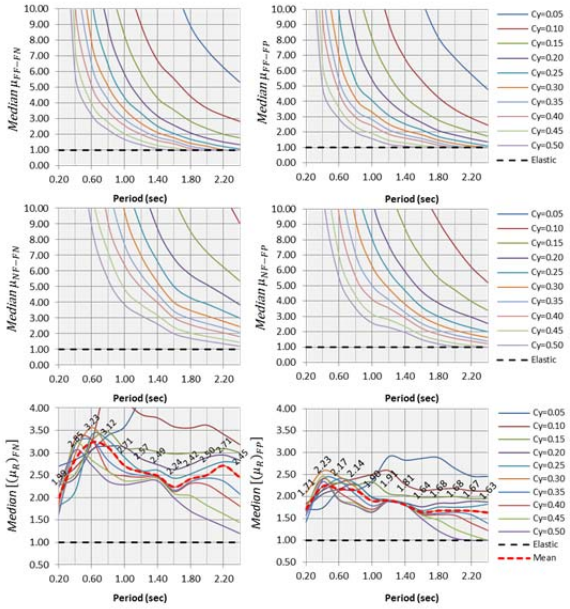

Figure A - 23: Median values of maximum ductility demand and ductility demand ratio (DDR) in Terms of strength characteristics | Link: NLT#4| ζ=%2.0| EQ Level=4

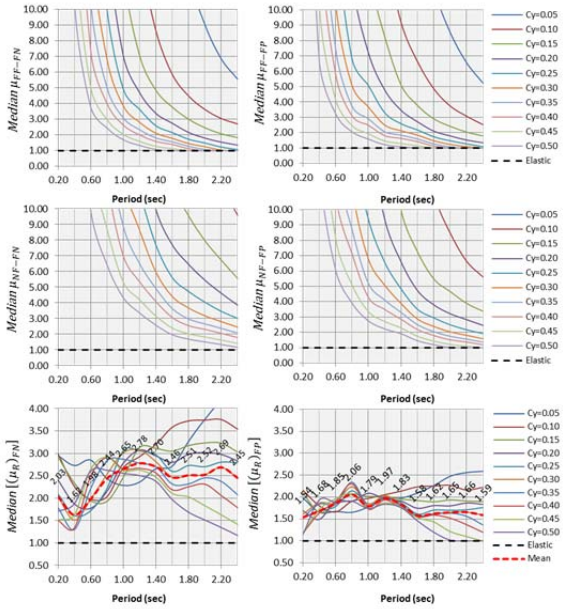

Figure A - 24: Median values of maximum ductility demand and ductility demand ratio (DDR) in Terms of strength characteristics | Link: NLT#5| ζ=%2.0| EQ Level=4

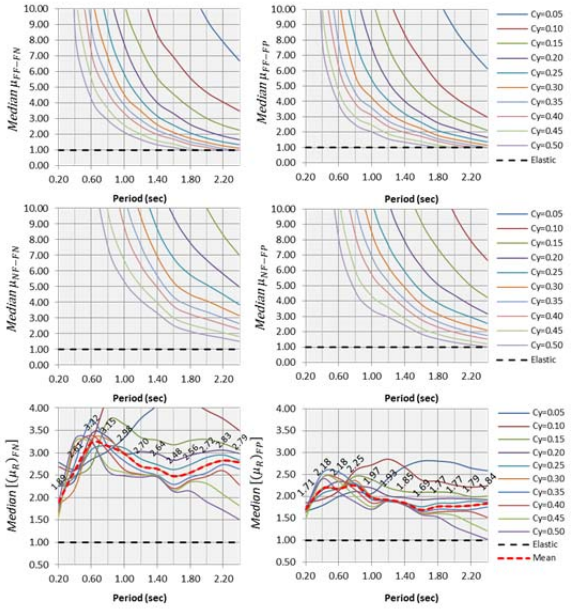

Figure A - 25: Median values of maximum ductility demand and ductility demand ratio (DDR) in Terms of strength characteristics | Link: NLT#4| ζ=%2.0| EQ Level=5

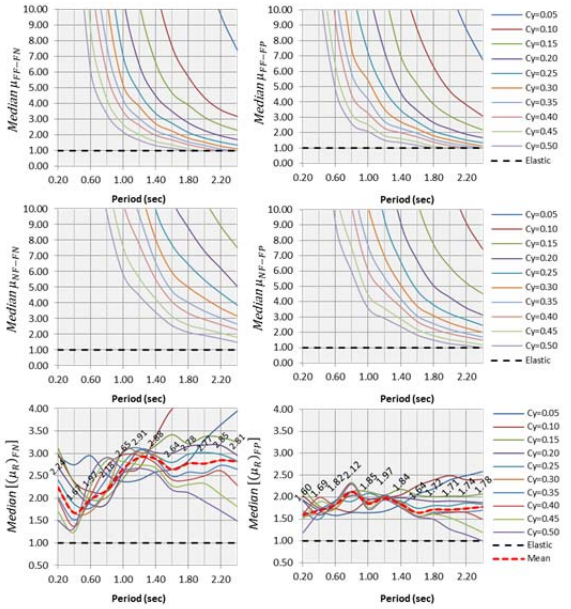

Figure A - 26: Median values of maximum ductility demand and ductility demand ratio (DDR) in Terms of strength characteristics | Link: NLT#5| ζ=%2.0| EQ Level=5

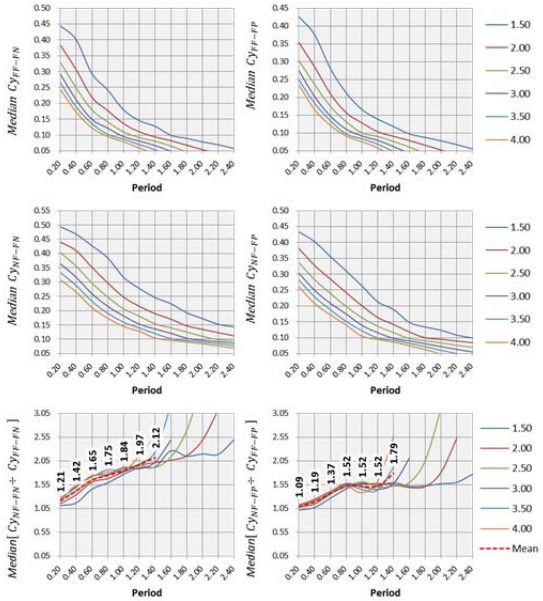

Figure A - 27: Median values of yield capacity demand and yield capacity demand ratio (YCDR) in Terms of target ductility | Link: NLT#1| ζ=%2.0| EQ Level=1

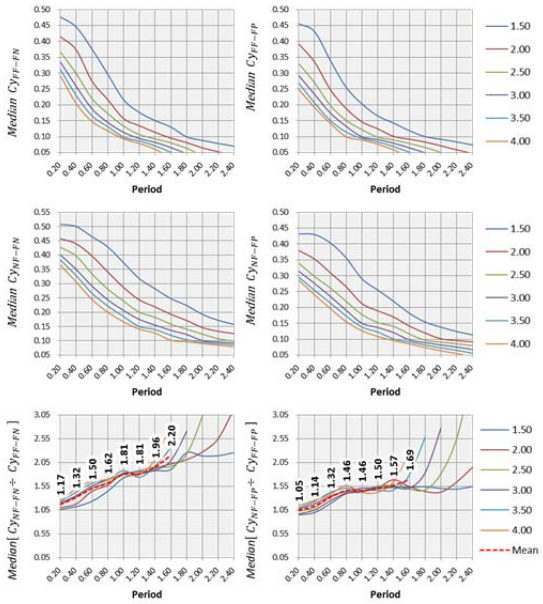

Figure A - 28: Median values of yield capacity demand and yield capacity demand ratio (YCDR) in Terms of target ductility | Link: NLT#2| ζ=%2.0| EQ Level=1

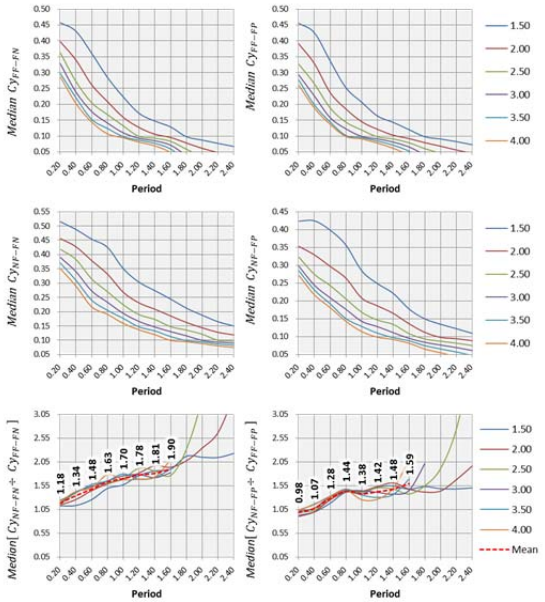

Figure A - 29: Median values of yield capacity demand and yield capacity demand ratio (YCDR) in Terms of target ductility | Link: NLT#3| ζ=%2.0| EQ Level=1

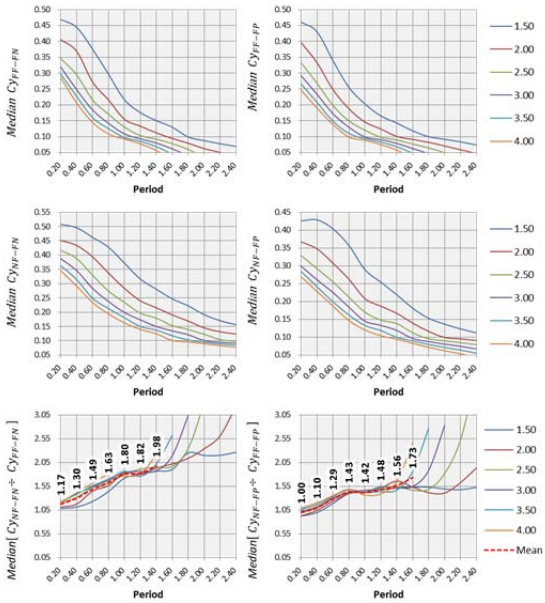

Figure A - 30: Median values of yield capacity demand and yield capacity demand ratio (YCDR) in Terms of target ductility | Link: NLT#4| ζ=%2.0| EQ Level=1

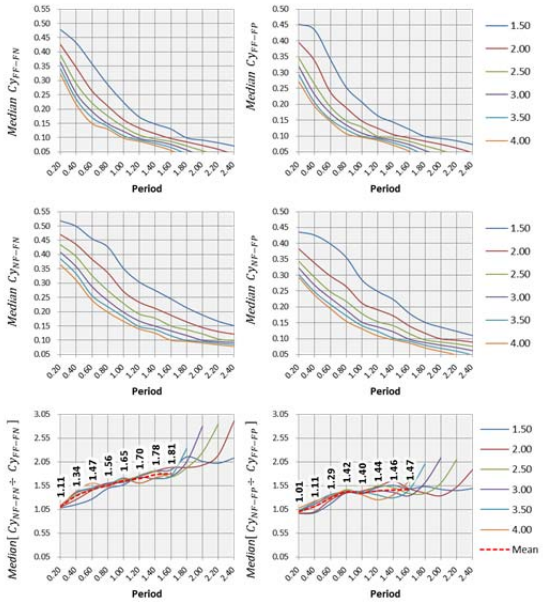

Figure A - 31: Median values of yield capacity demand and yield capacity demand ratio (YCDR) in Terms of target ductility | Link: NLT#5| ζ=%2.0| EQ Level=1

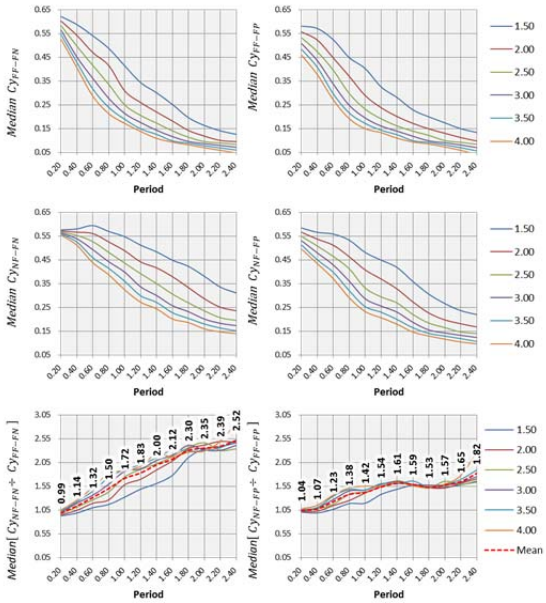

Figure A - 32: Median values of yield capacity demand and yield capacity demand ratio (YCDR) in Terms of target ductility | Link: NLT#4| ζ=%2.0| EQ Level=2

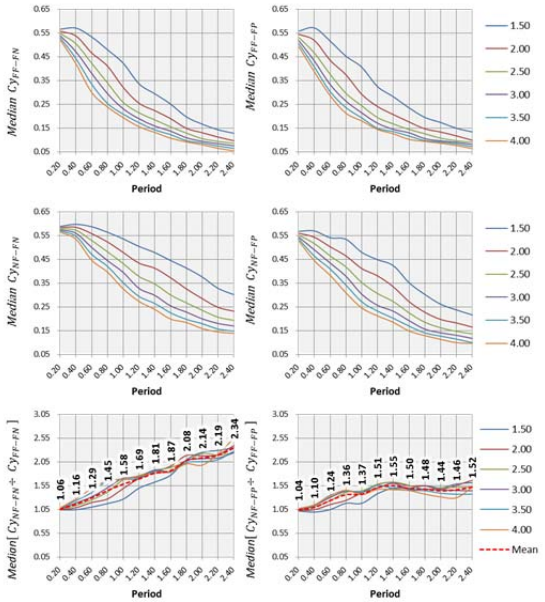

Figure A - 33: Median values of yield capacity demand and yield capacity demand ratio (YCDR) in Terms of target ductility | Link: NLT#5| ζ=%2.0| EQ Level=2

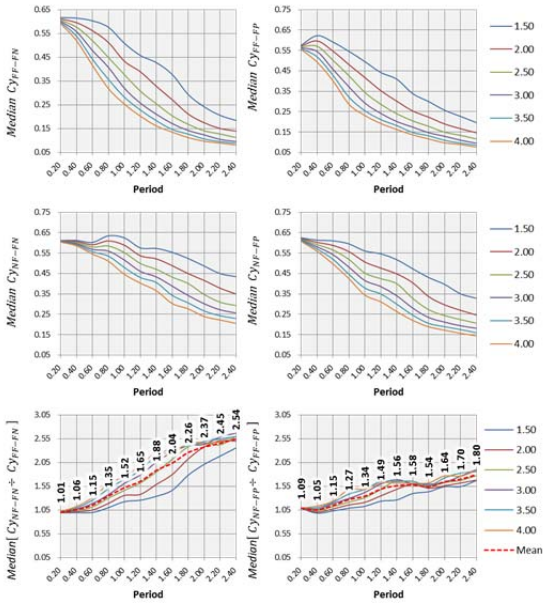

Figure A - 34: Median values of yield capacity demand and yield capacity demand ratio (YCDR) in Terms of target ductility | Link: NLT#4| ζ=%2.0| EQ Level=3

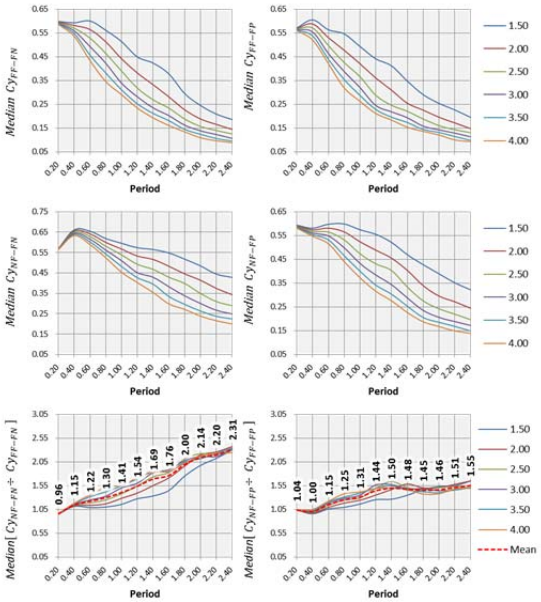

Figure A - 35: Median values of yield capacity demand and yield capacity demand ratio (YCDR) in Terms of target ductility | Link: NLT#5| ζ=%2.0| EQ Level=3

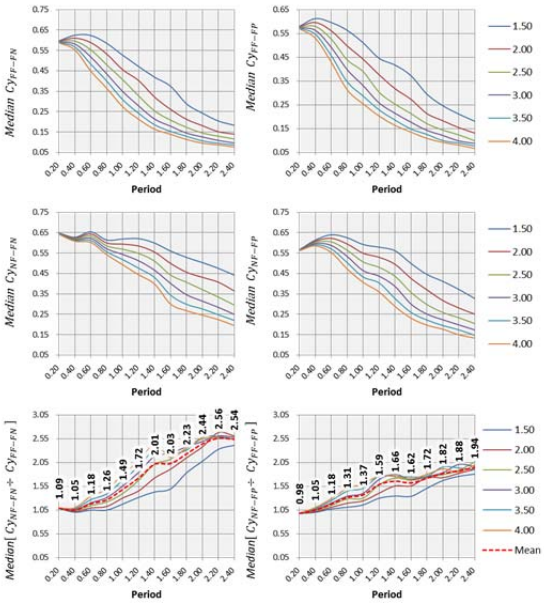

Figure A - 36: Median values of yield capacity demand and yield capacity demand ratio (YCDR) in Terms of target ductility | Link: NLT#4| ζ=%2.0| EQ Level=4

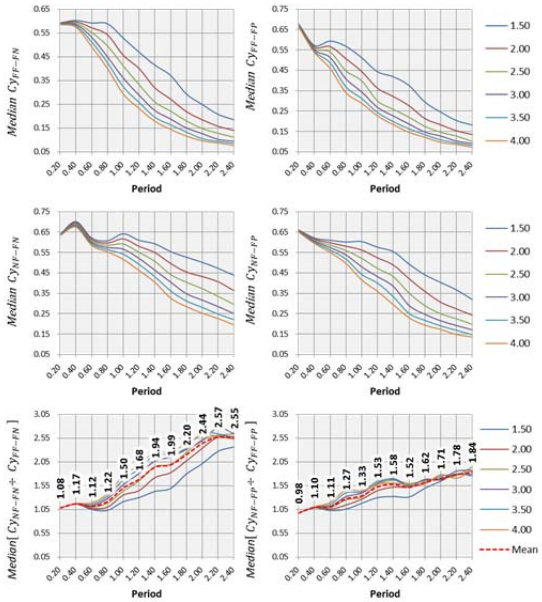

Figure A - 37: Median values of yield capacity demand and yield capacity demand ratio (YCDR) in Terms of target ductility | Link: NLT#5| ζ=%2.0| EQ Level=4

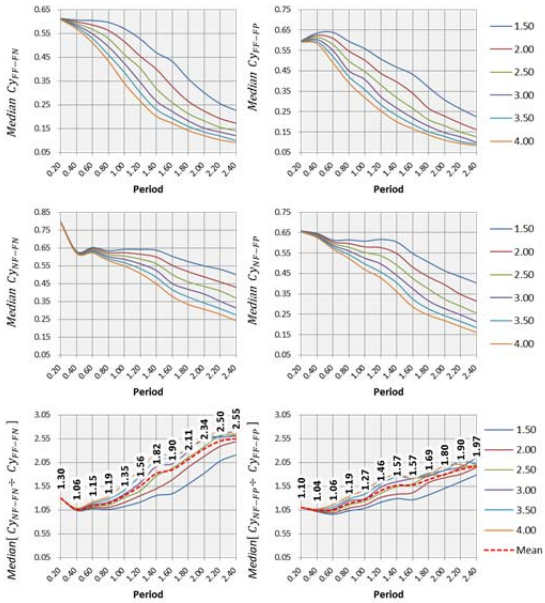

Figure A - 38: Median values of yield capacity demand and yield capacity demand ratio (YCDR) in Terms of target ductility | Link: NLT#4| ζ=%2.0| EQ Level=5

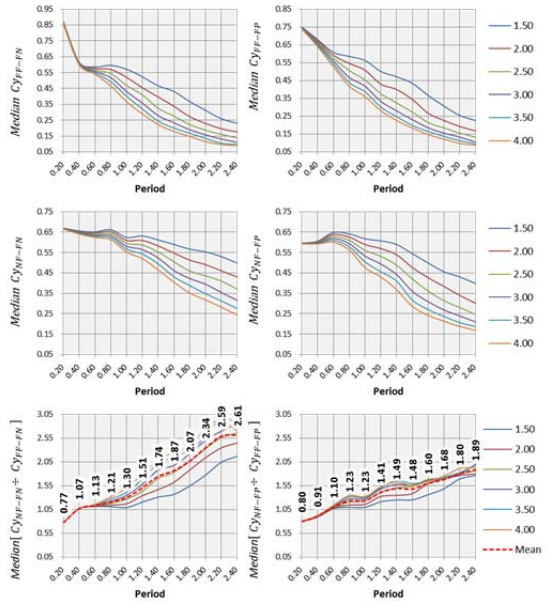

Figure A - 39: Median values of yield capacity demand and yield capacity demand ratio (YCDR) in Terms of target ductility | Link: NLT#5| ζ=%2.0| EQ Level=5

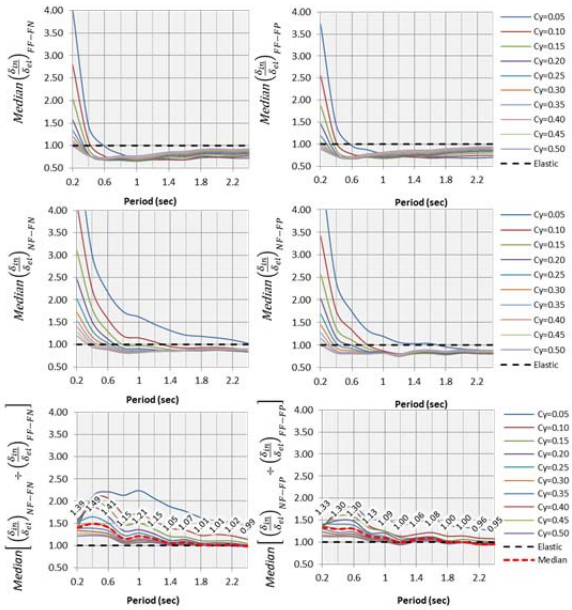

Figure A - 40: Median values of maximum inelastic to elastic displacement demand and maximum inelastic to elastic displacement demand ratio in terms of strength characteristics| Link: NLT#1| ζ=%2.0| EQ Level=1

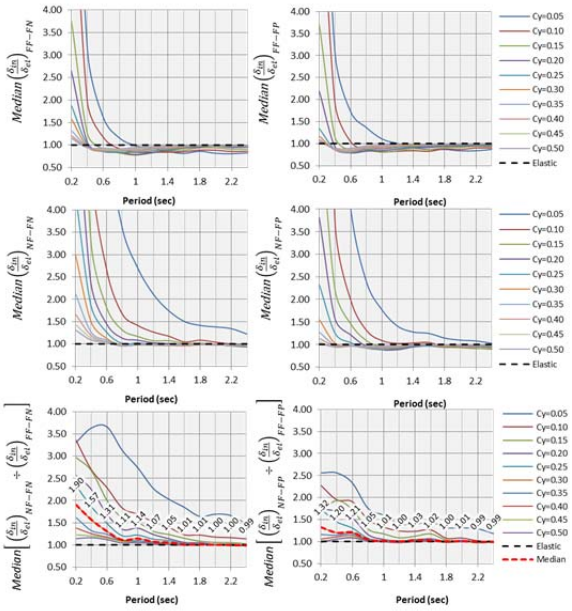

Figure A - 41: Median values of maximum inelastic to elastic displacement demand and maximum inelastic to elastic displacement demand ratio in terms of strength characteristics| Link: NLT#2| ζ=%2.0| EQ Level=1

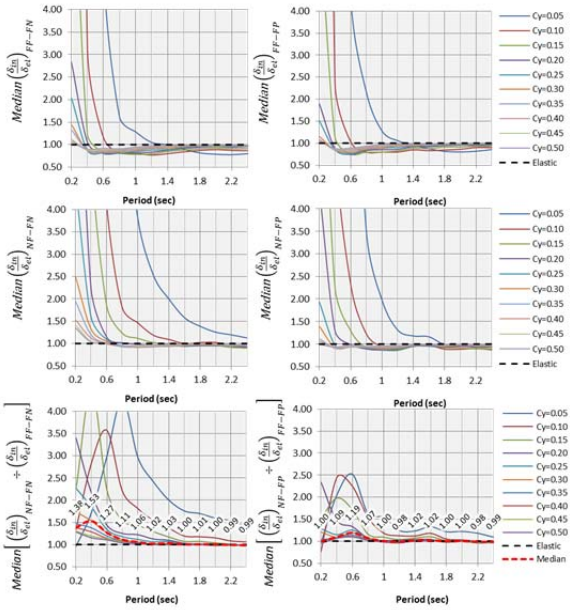

Figure A - 42: Median values of maximum inelastic to elastic displacement demand and maximum inelastic to elastic displacement demand ratio in terms of strength characteristics| Link: NLT#3| ζ=%2.0| EQ Level=1

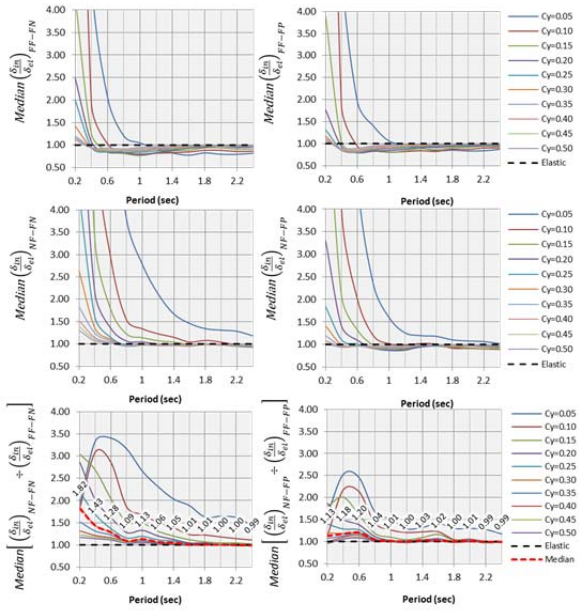

Figure A - 43: Median values of maximum inelastic to elastic displacement demand and maximum inelastic to elastic displacement demand ratio in terms of strength characteristics| Link: NLT#4| ζ=%2.0| EQ Level=1

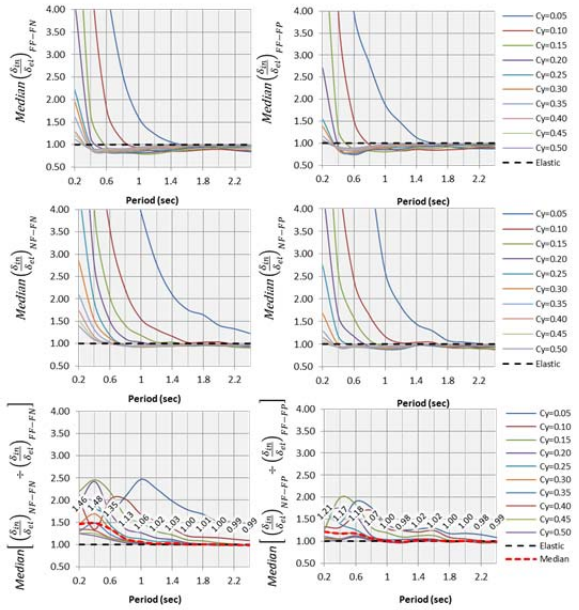

Figure A - 44: Median values of maximum inelastic to elastic displacement demand and maximum inelastic to elastic displacement demand ratio in terms of strength characteristics| Link: NLT#5| ζ=%2.0| EQ Level=1

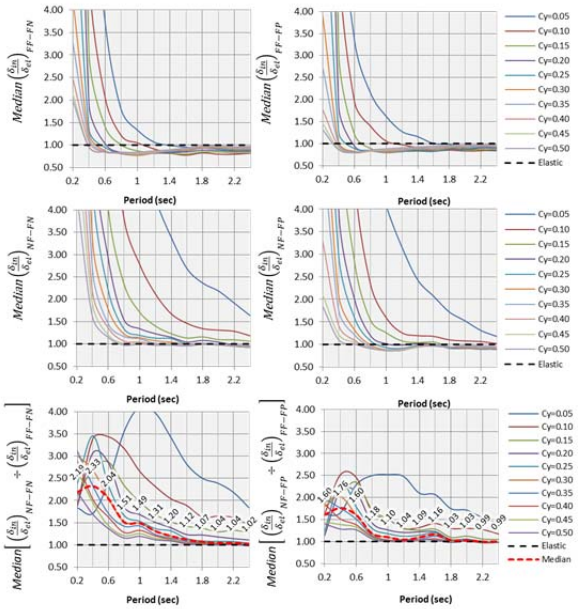

Figure A - 45: Median values of maximum inelastic to elastic displacement demand and maximum inelastic to elastic displacement demand ratio in terms of strength characteristics| Link: NLT#4| ζ=%2.0| EQ Level=2

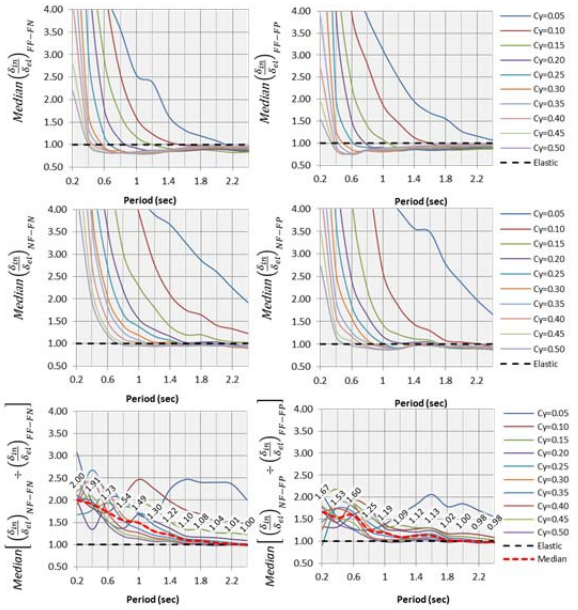

Figure A - 46: Median values of maximum inelastic to elastic displacement demand and maximum inelastic to elastic displacement demand ratio in terms of strength characteristics| Link: NLT#5| ζ=%2.0| EQ Level=2

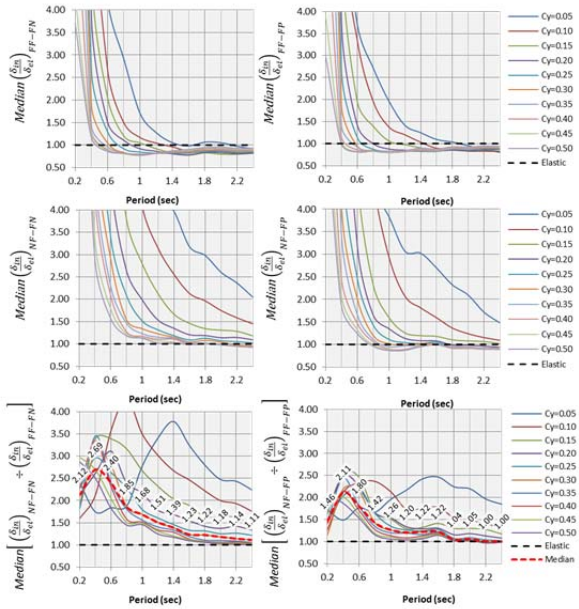

Figure A - 47: Median values of maximum inelastic to elastic displacement demand and maximum inelastic to elastic displacement demand ratio in terms of strength characteristics| Link: NLT#4| ζ=%2.0| EQ Level=3

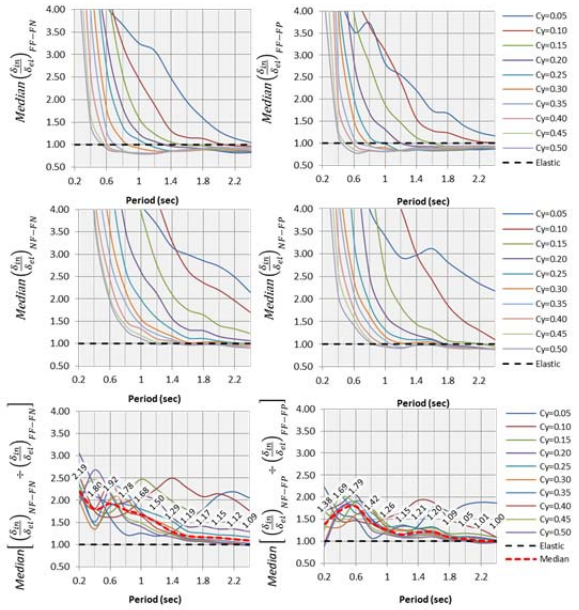

Figure A - 48: Median values of maximum inelastic to elastic displacement demand and maximum inelastic to elastic displacement demand ratio in terms of strength characteristics| Link: NLT#5| ζ=%2.0| EQ Level=3

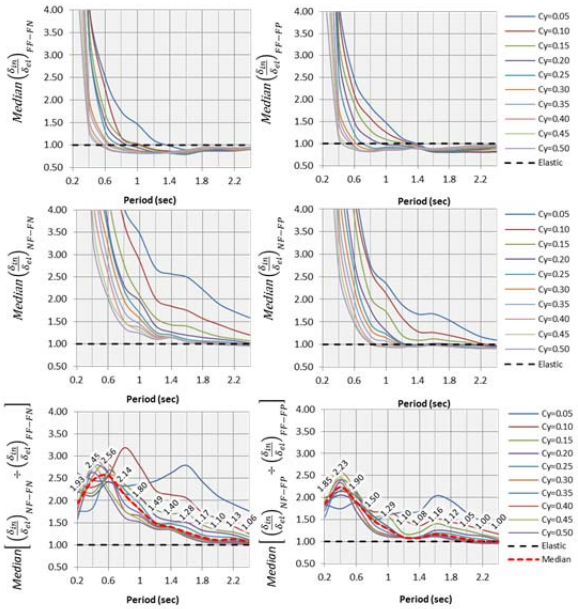

Figure A - 49: Median values of maximum inelastic to elastic displacement demand and maximum inelastic to elastic displacement demand ratio in terms of strength characteristics| Link: NLT#4| ζ=%2.0| EQ Level=4

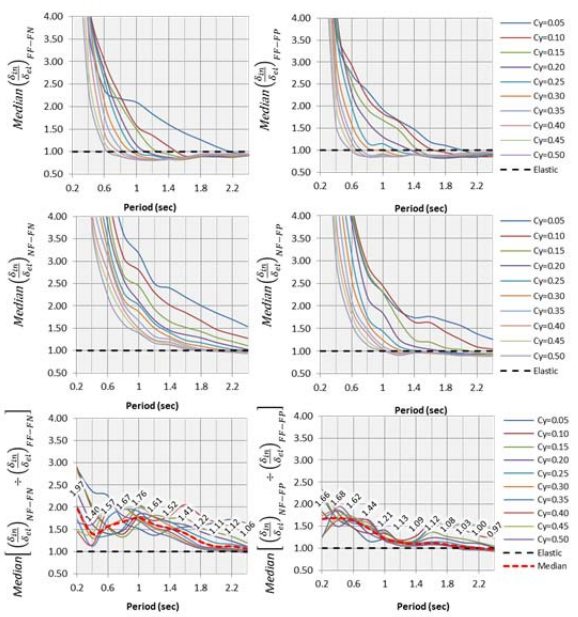

Figure A - 50: Median values of maximum inelastic to elastic displacement demand and maximum inelastic to elastic displacement demand ratio in terms of strength characteristics| Link: NLT#5| ζ=%2.0| EQ Level=4

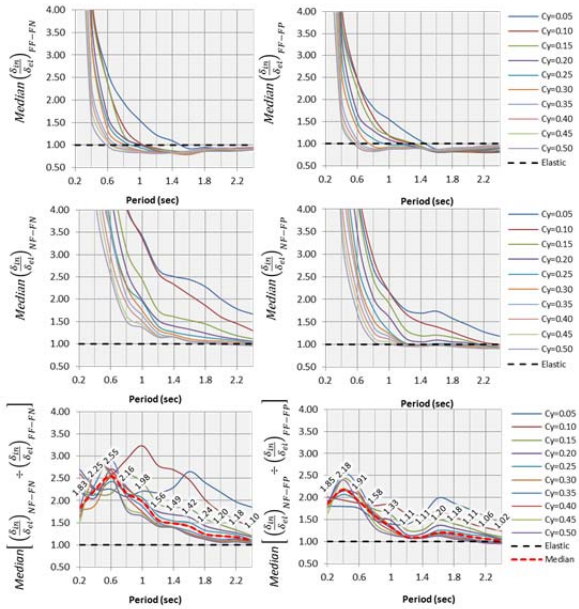

Figure A - 51: Median values of maximum inelastic to elastic displacement demand and maximum inelastic to elastic displacement demand ratio in terms of strength characteristics| Link: NLT#4| ζ=%2.0| EQ Level=5

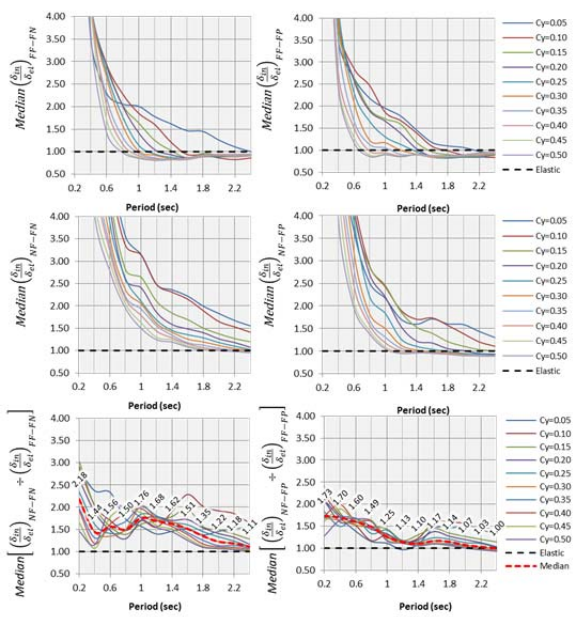

Figure A - 52: Median values of maximum inelastic to elastic displacement demand and maximum inelastic to elastic displacement demand ratio in terms of strength characteristics| Link: NLT#5| ζ=%2.0| EQ Level=5

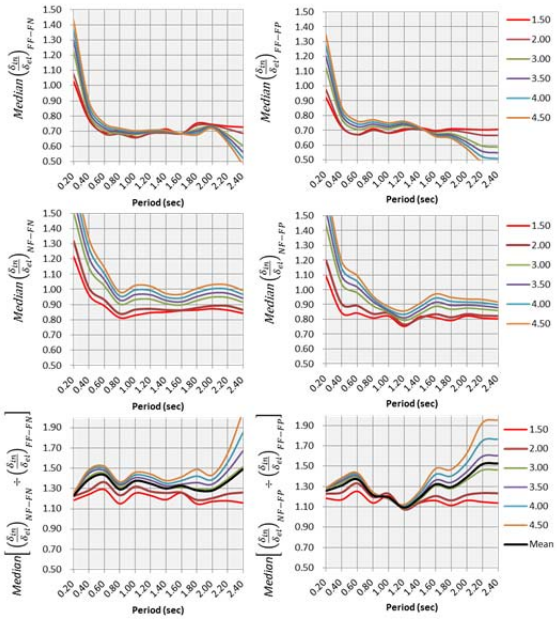

Figure A - 53: Median values of maximum inelastic to elastic displacement demand and maximum inelastic to elastic displacement demand ratio in terms of ductility | Link: NLT#1| ζ=%2.0| EQ Level=1

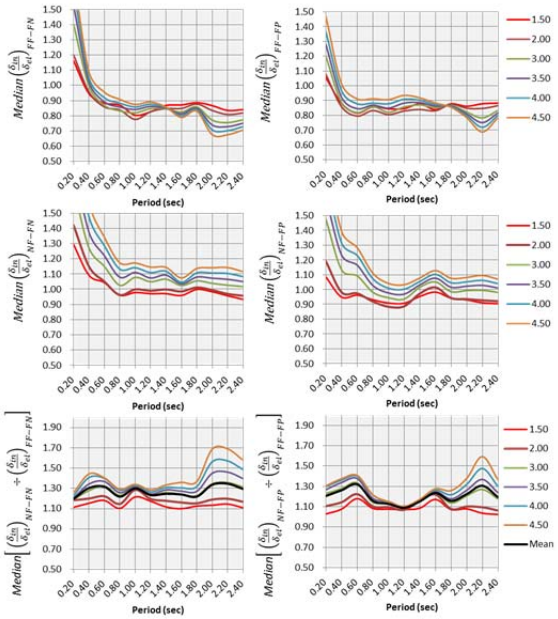

Figure A - 54: Median values of maximum inelastic to elastic displacement demand and maximum inelastic to elastic displacement demand ratio in terms of ductility | Link: NLT#2| ζ=%2.0| EQ Level=1

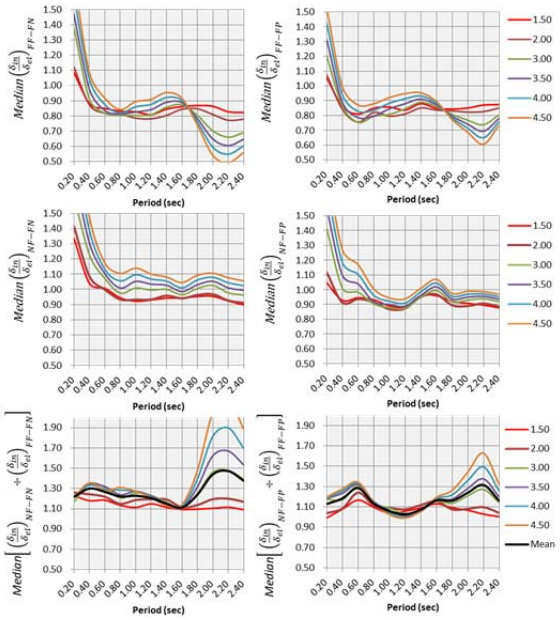

Figure A - 55: Median values of maximum inelastic to elastic displacement demand and maximum inelastic to elastic displacement demand ratio in terms of ductility | Link: NLT#3| ζ=%2.0| EQ Level=1

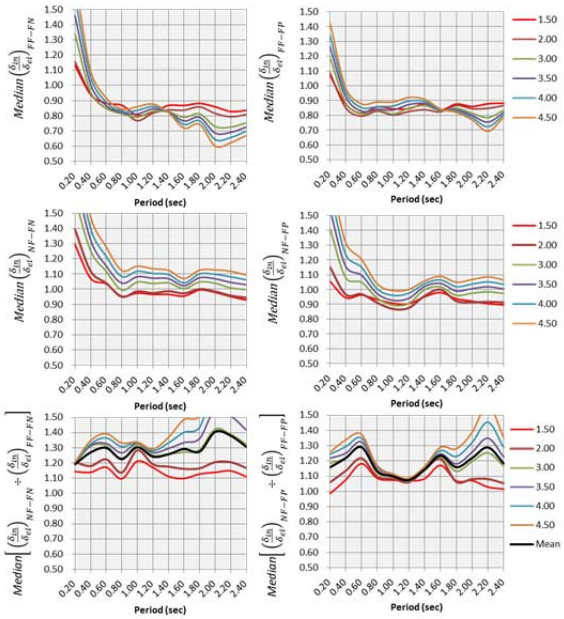

Figure A - 56: Median values of maximum inelastic to elastic displacement demand and maximum inelastic to elastic displacement demand ratio in terms of ductility | Link: NLT#4| ζ=%2.0| EQ Level=1

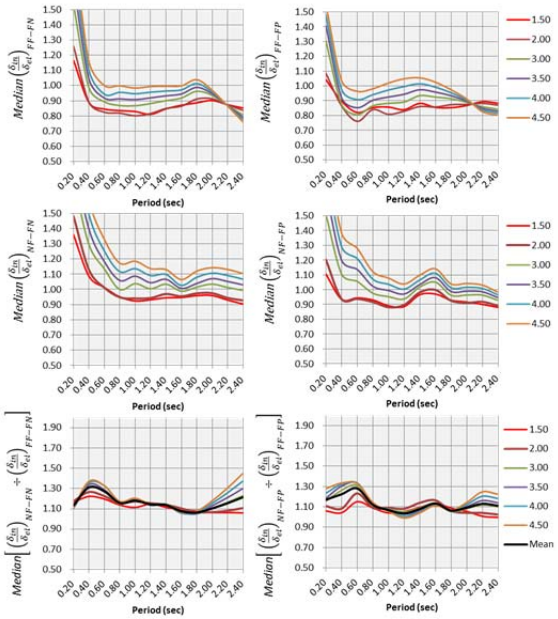

Figure A - 57: Median values of maximum inelastic to elastic displacement demand and maximum inelastic to elastic displacement demand ratio in terms of ductility | Link: NLT#5| ζ=%2.0| EQ Level=1

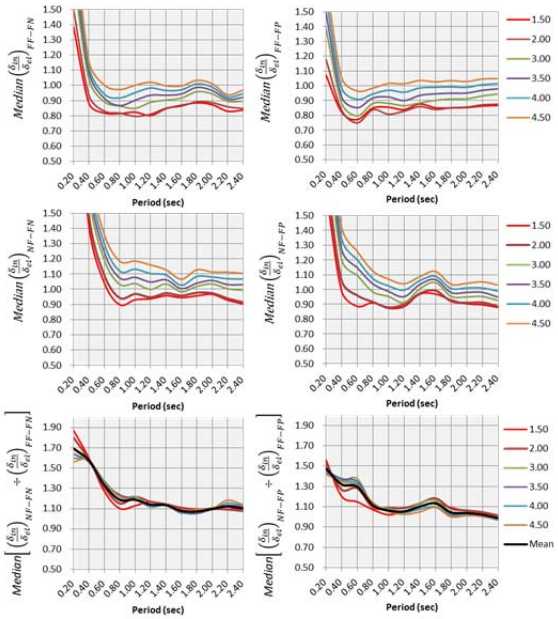

Figure A - 58: Median values of maximum inelastic to elastic displacement demand and maximum inelastic to elastic displacement demand ratio in terms of ductility | Link: NLT#4| ζ=%2.0| EQ Level=2

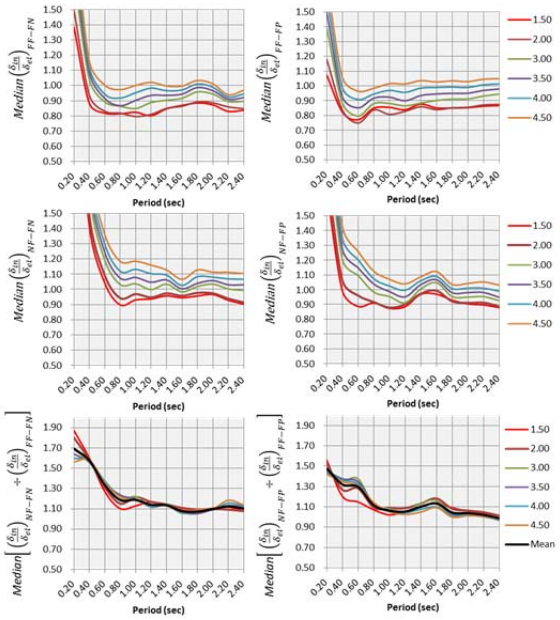

Figure A - 59: Median values of maximum inelastic to elastic displacement demand and maximum inelastic to elastic displacement demand ratio in terms of ductility | Link: NLT#5| ζ=%2.0| EQ Level=2

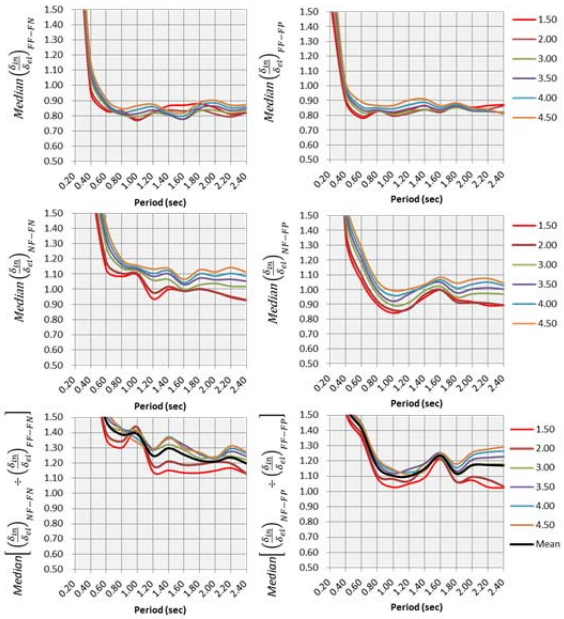

Figure A - 60: Median values of maximum inelastic to elastic displacement demand and maximum inelastic to elastic displacement demand ratio in terms of ductility | Link: NLT#4| ζ=%2.0| EQ Level=3

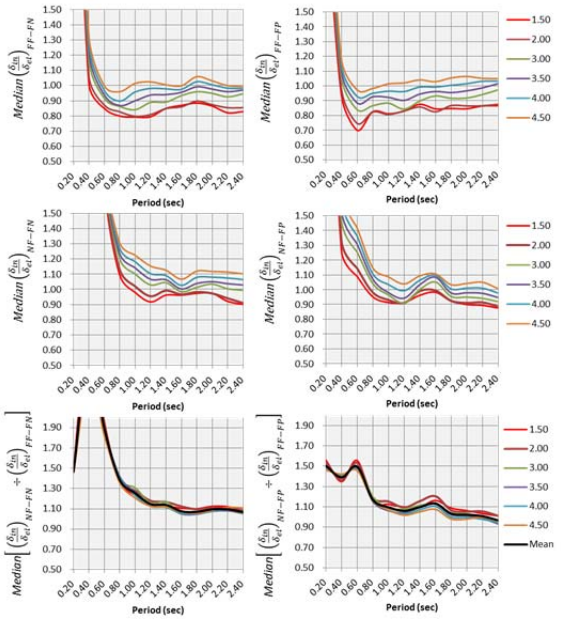

Figure A - 61: Median values of maximum inelastic to elastic displacement demand and maximum inelastic to elastic displacement demand ratio in terms of ductility | Link: NLT#5| ζ=%2.0| EQ Level=3

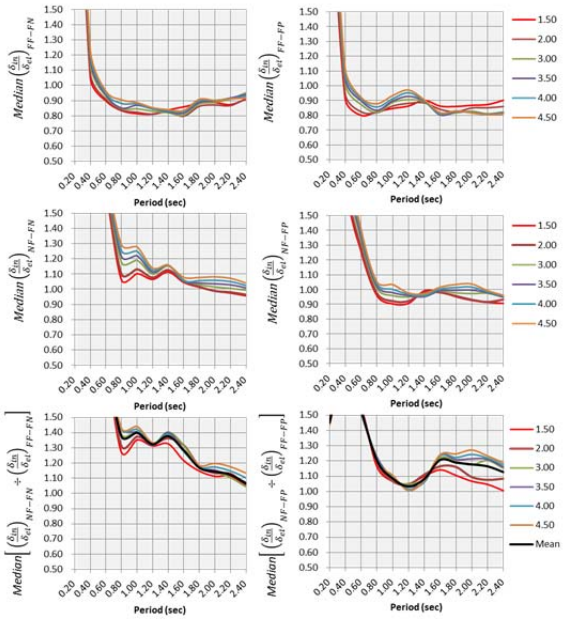

Figure A - 62: Median values of maximum inelastic to elastic displacement demand and maximum inelastic to elastic displacement demand ratio in terms of ductility | Link: NLT#4| ζ=%2.0| EQ Level=4

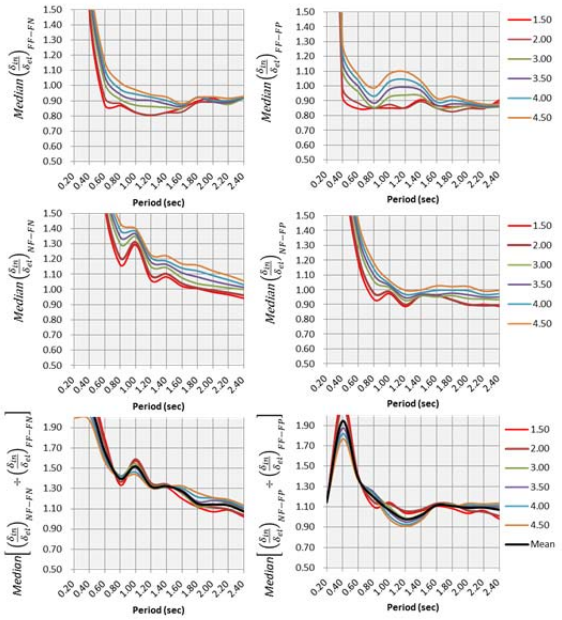

Figure A - 63: Median values of maximum inelastic to elastic displacement demand and maximum inelastic to elastic displacement demand ratio in terms of ductility | Link: NLT#5| ζ=%2.0| EQ Level=4

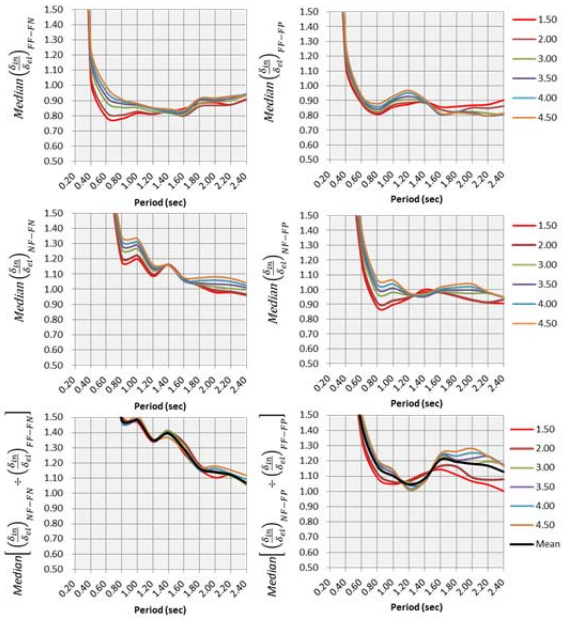

Figure A - 64: Median values of maximum inelastic to elastic displacement demand and maximum inelastic to elastic displacement demand ratio in terms of ductility | Link: NLT#4| ζ=%2.0| EQ Level=5

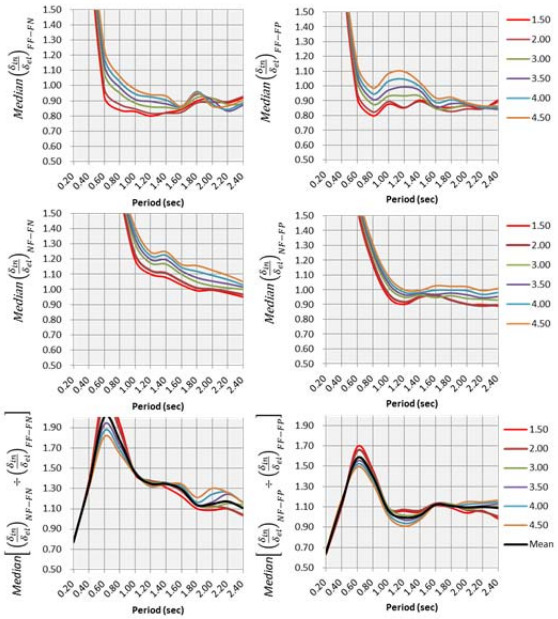

Figure A - 65: Median values of maximum inelastic to elastic displacement demand and maximum inelastic to elastic displacement demand ratio in terms of ductility | Link: NLT#5| ζ=%2.0| EQ Level=5

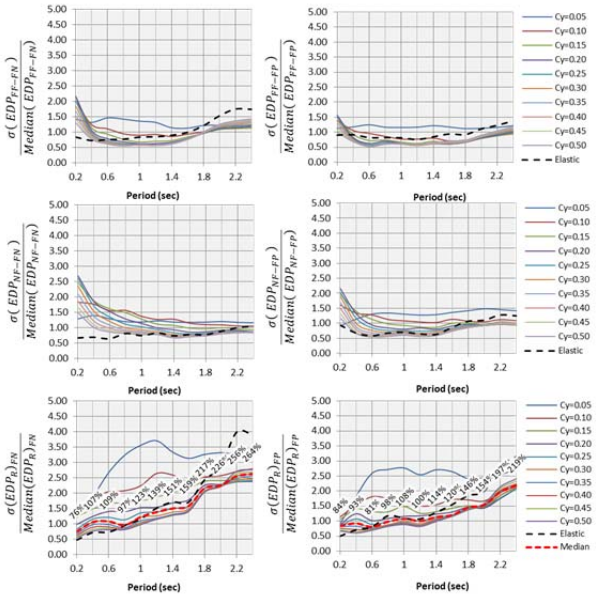

Figure A - 66: CV Values of “EDP” and “EDP Ratio” In Terms of strength characteristics | Link: NLT#1| ζ=%2.0| EQ Level=1

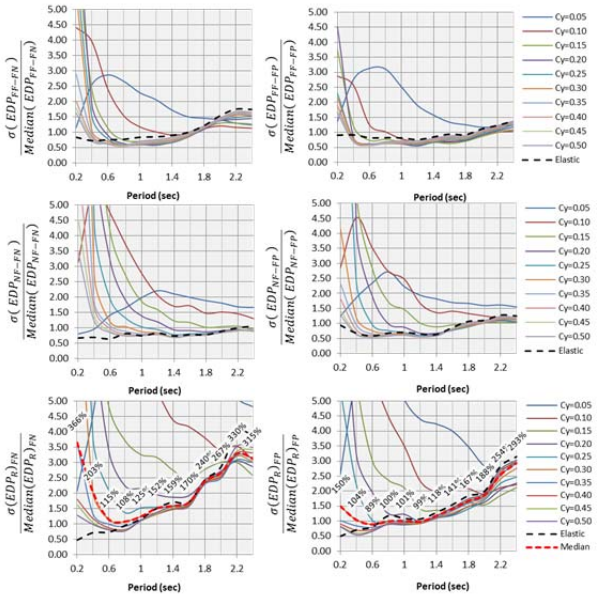

Figure A - 67: CV Values of “EDP” and “EDP Ratio” In Terms of strength characteristics | Link: NLT#2| ζ=%2.0| EQ Level=1

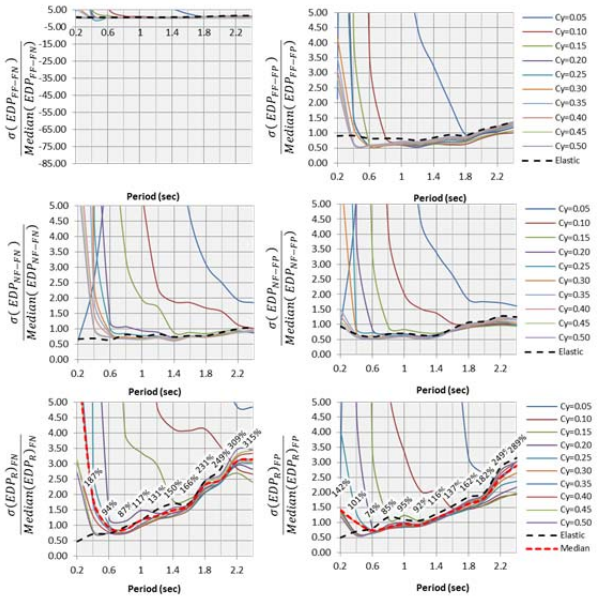

Figure A - 68: CV Values of “EDP” and “EDP Ratio” In Terms of strength characteristics | Link: NLT#3| ζ=%2.0| EQ Level=1

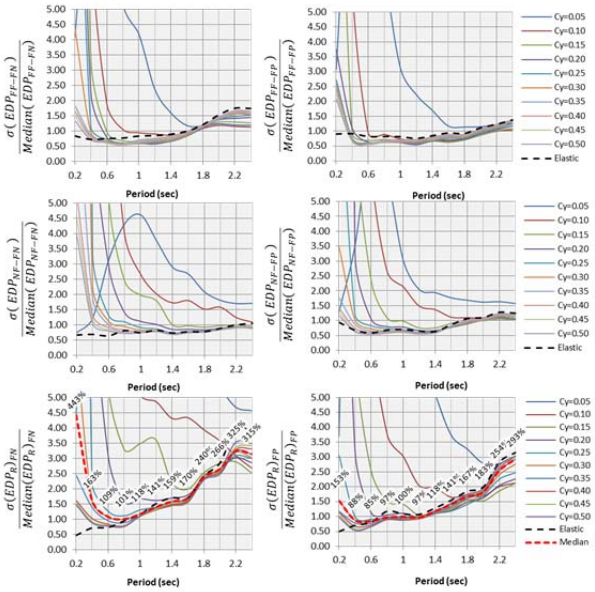

Figure A - 69: CV Values of “EDP” and “EDP Ratio” In Terms of strength characteristics | Link: NLT#4| ζ=%2.0| EQ Level=1

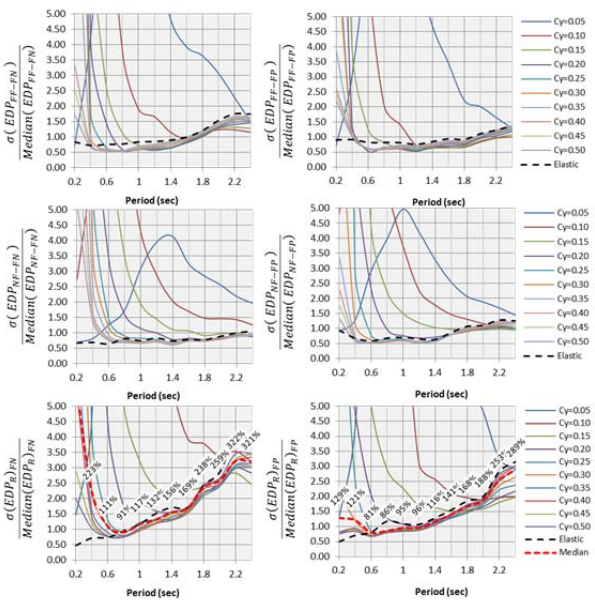

Figure A - 70: CV Values of “EDP” and “EDP Ratio” In Terms of strength characteristics | Link: NLT#5| ζ=%2.0| EQ Level=1

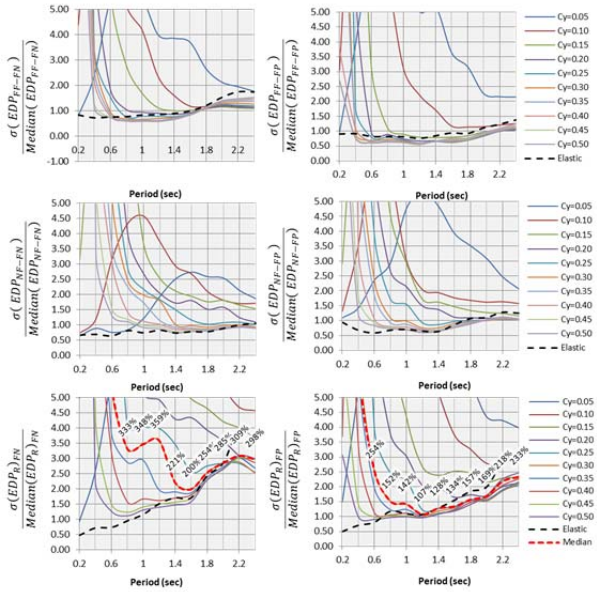

Figure A - 71: CV Values of “EDP” and “EDP Ratio” In Terms of strength characteristics | Link: NLT#4| ζ=%2.0| EQ Level=2

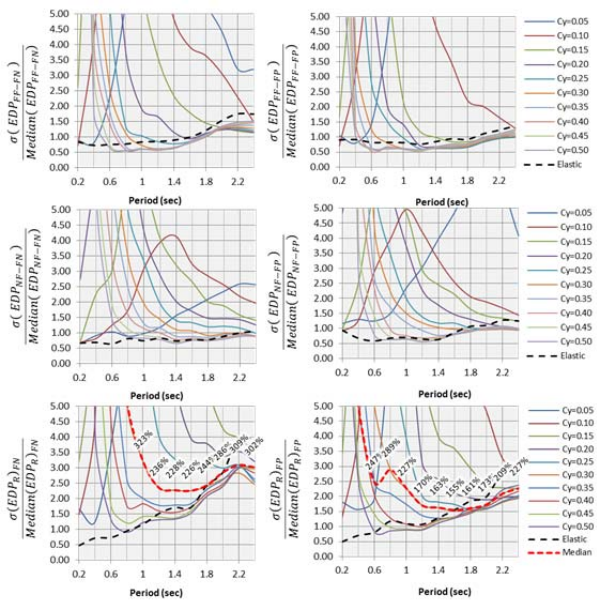

Figure A - 72: CV Values of “EDP” and “EDP Ratio” In Terms of strength characteristics | Link: NLT#5| ζ=%2.0| EQ Level=2

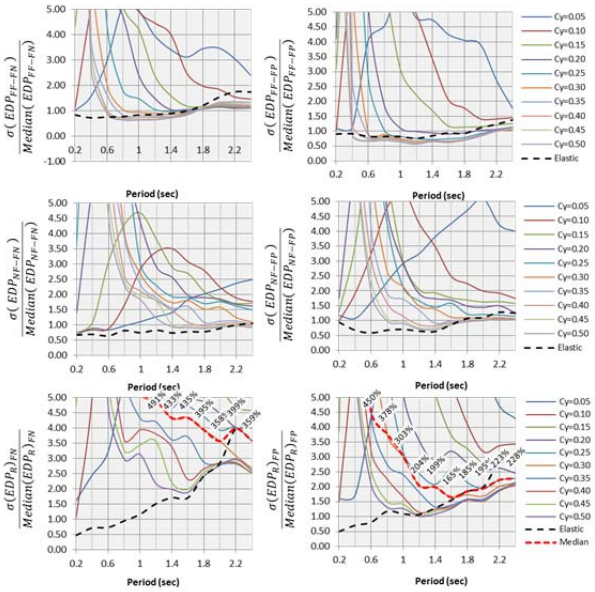

Figure A - 73: CV Values of “EDP” and “EDP Ratio” In Terms of strength characteristics | Link: NLT#4| ζ=%2.0| EQ Level=3

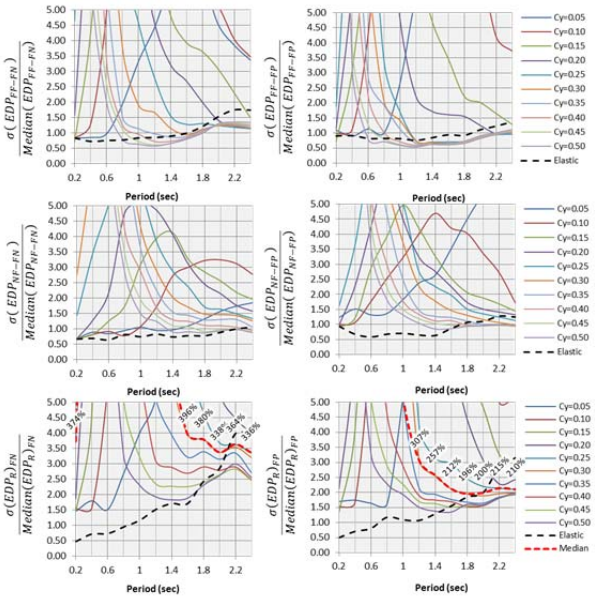

Figure A - 74: CV Values of “EDP” and “EDP Ratio” In Terms of strength characteristics | Link: NLT#5| ζ=%2.0| EQ Level=3

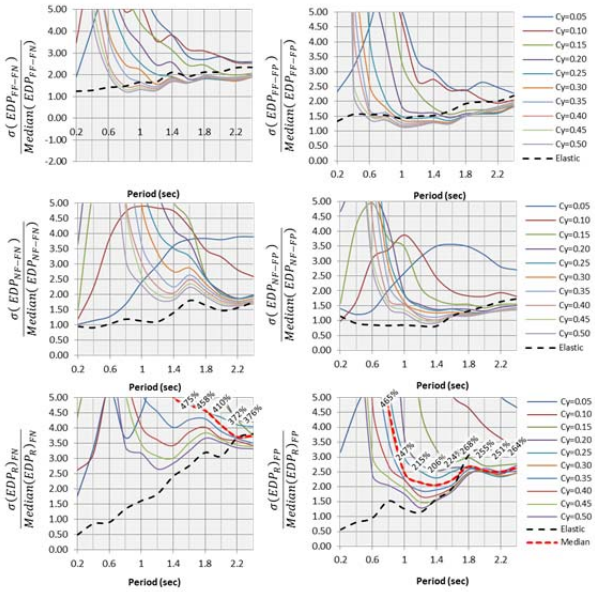

Figure A - 75: CV Values of “EDP” and “EDP Ratio” In Terms of strength characteristics | Link: NLT#4| ζ=%2.0| EQ Level=4

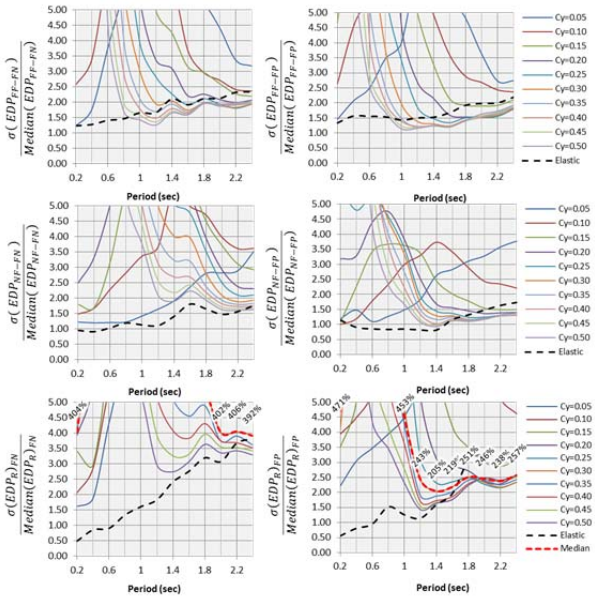

Figure A - 76: CV Values of “EDP” and “EDP Ratio” In Terms of strength characteristics | Link: NLT#5| ζ=%2.0| EQ Level=4

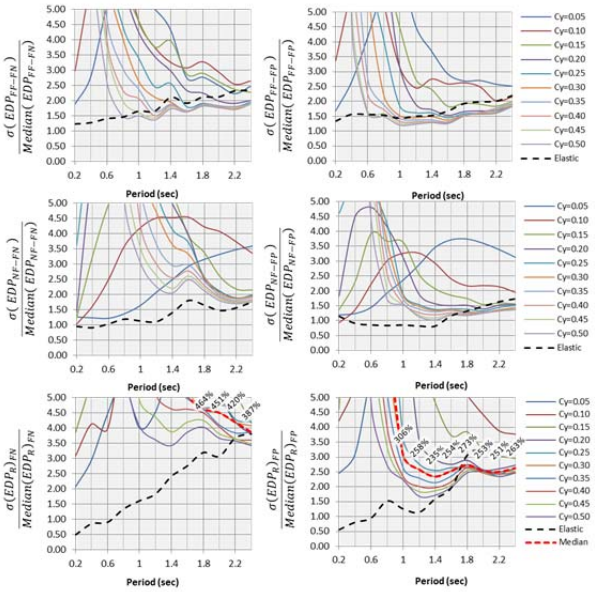

Figure A - 77: CV Values of “EDP” and “EDP Ratio” In Terms of strength characteristics | Link: NLT#4| ζ=%2.0| EQ Level=5

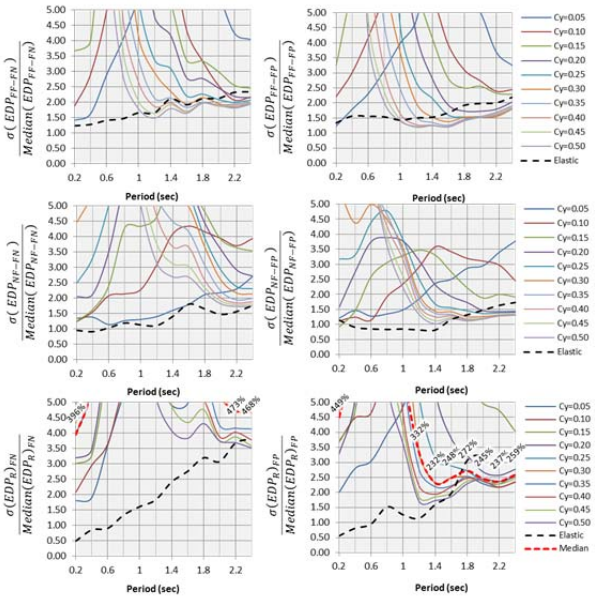

Figure A - 78: CV Values of “EDP” and “EDP Ratio” In Terms of strength characteristics | Link: NLT#5| ζ=%2.0| EQ Level=5

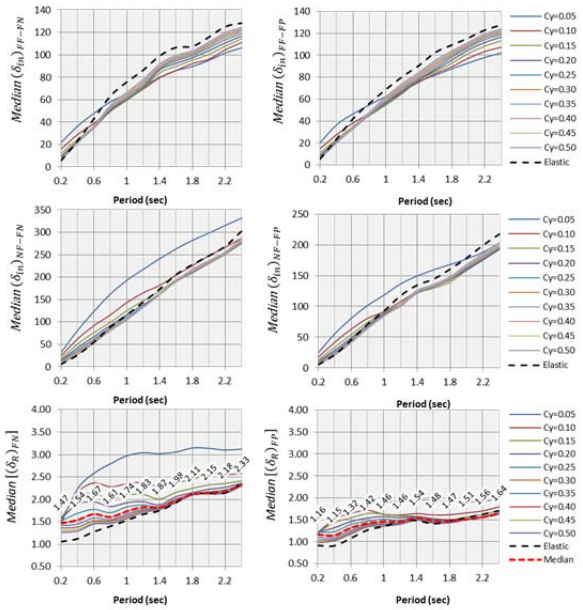

Figure A - 79: Median values of maximum displacement demands and inelastic displacement demand ratio (IDDR) In Terms of strength characteristics | Link: NLT#1| ζ=%5.0| EQ Level=1

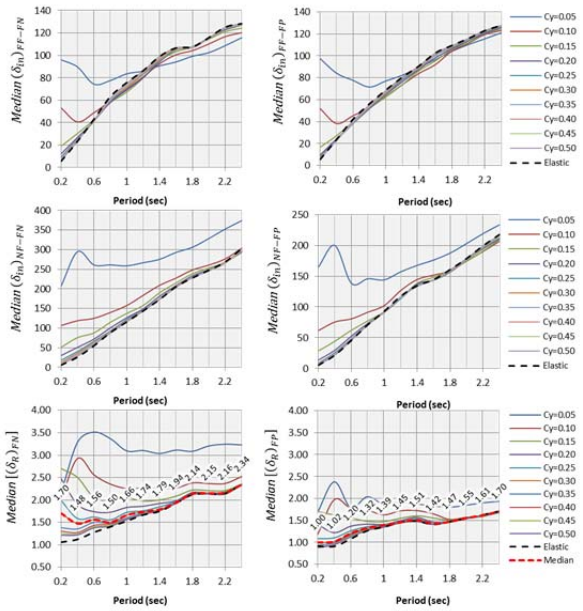

Figure A - 80: Median values of maximum displacement demands and inelastic displacement demand ratio (IDDR) In Terms of strength characteristics | Link: NLT#2| ζ=%5.0| EQ Level=1

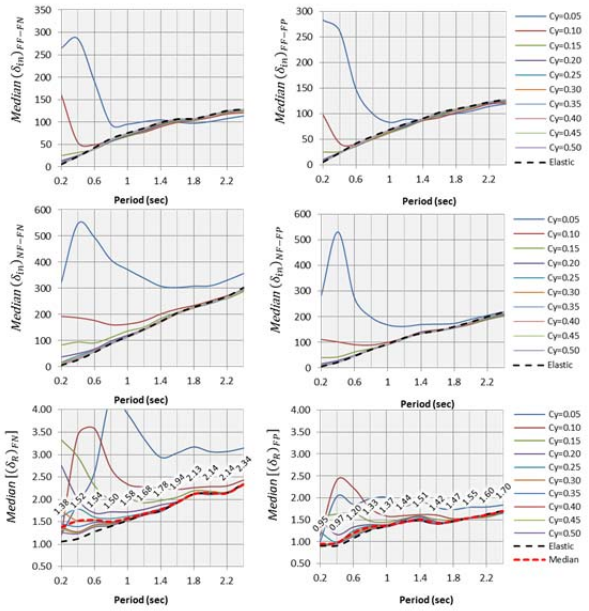

Figure A - 81: Median values of maximum displacement demands and inelastic displacement demand ratio (IDDR) In Terms of strength characteristics | Link: NLT#3| ζ=%5.0| EQ Level=1

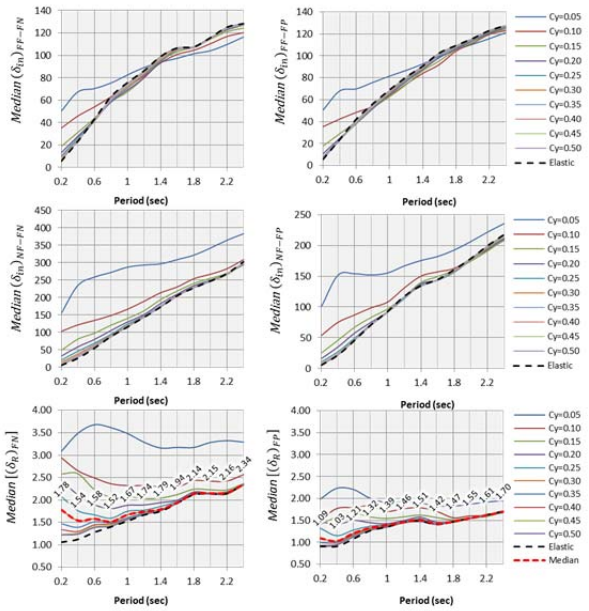

Figure A - 82: Median values of maximum displacement demands and inelastic displacement demand ratio (IDDR) In Terms of strength characteristics | Link: NLT#4| ζ=%5.0| EQ Level=1

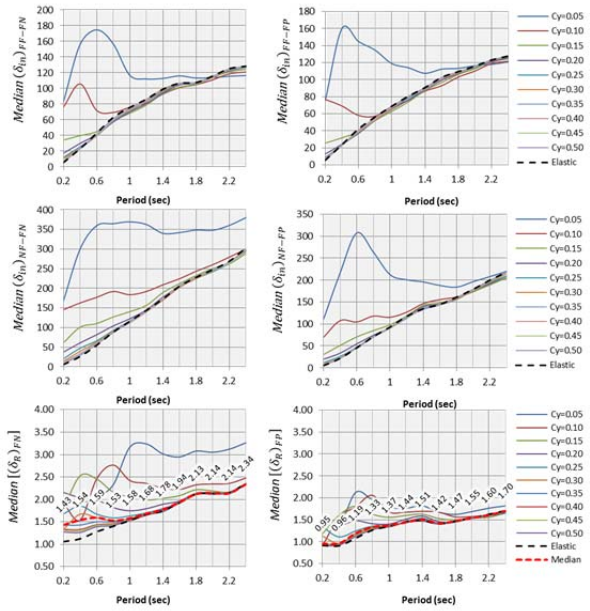

Figure A - 83: Median values of maximum displacement demands and inelastic displacement demand ratio (IDDR) In Terms of strength characteristics | Link: NLT#5| ζ=%5.0| EQ Level=1

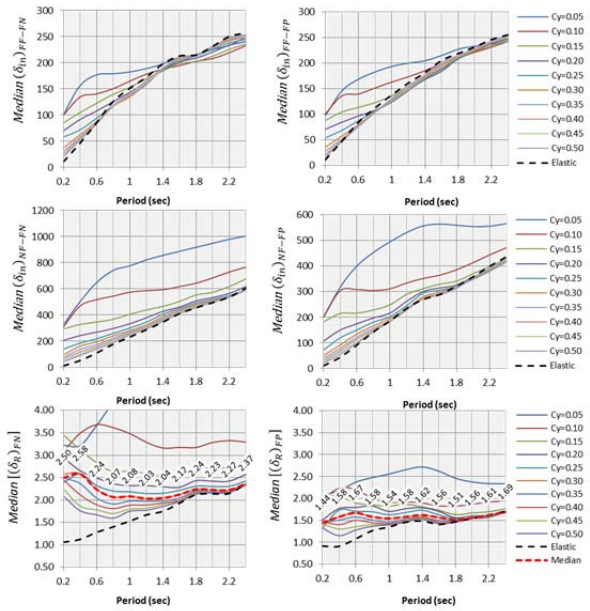

Figure A - 84: Median values of maximum displacement demands and inelastic displacement demand ratio (IDDR) In Terms of strength characteristics | Link: NLT#4| ζ=%5.0| EQ Level=2

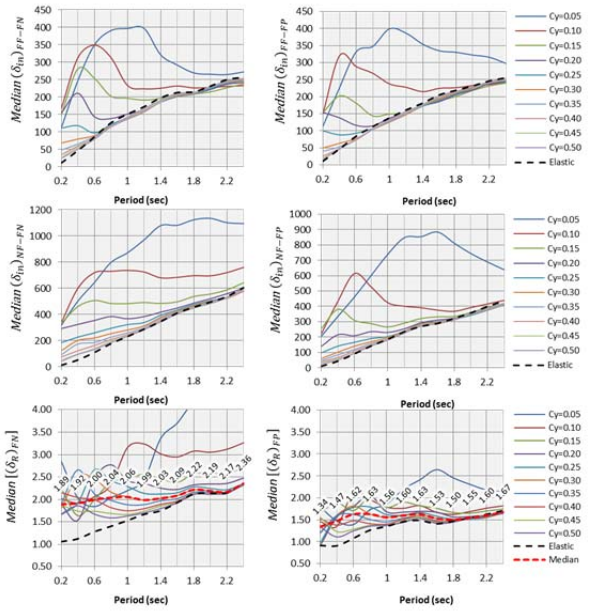

Figure A - 85: Median values of maximum displacement demands and inelastic displacement demand ratio (IDDR) In Terms of strength characteristics | Link: NLT#5| ζ=%5.0| EQ Level=2

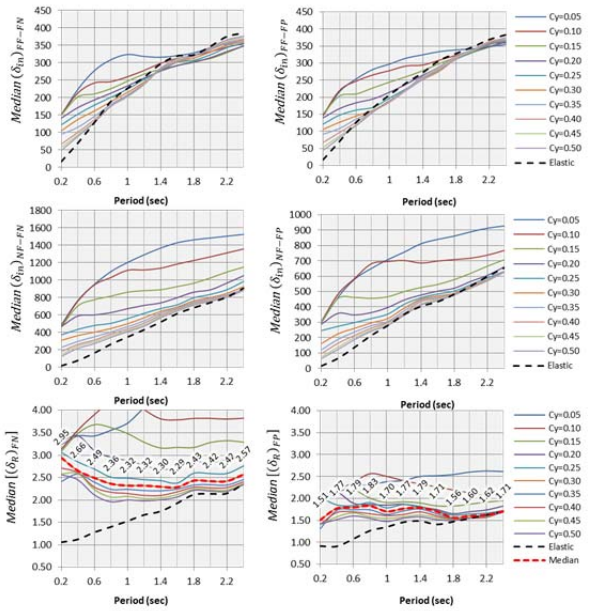

Figure A - 86: Median values of maximum displacement demands and inelastic displacement demand ratio (IDDR) In Terms of strength characteristics | Link: NLT#4| ζ=%5.0| EQ Level=3

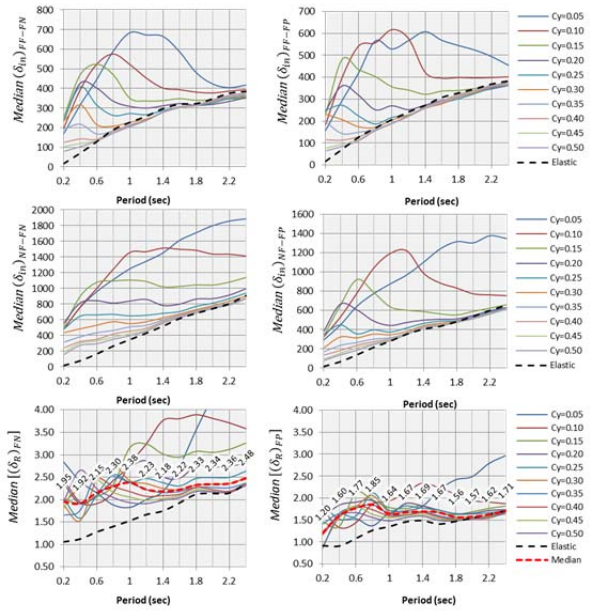

Figure A - 87: Median values of maximum displacement demands and inelastic displacement demand ratio (IDDR) In Terms of strength characteristics | Link: NLT#5| ζ=%5.0| EQ Level=3

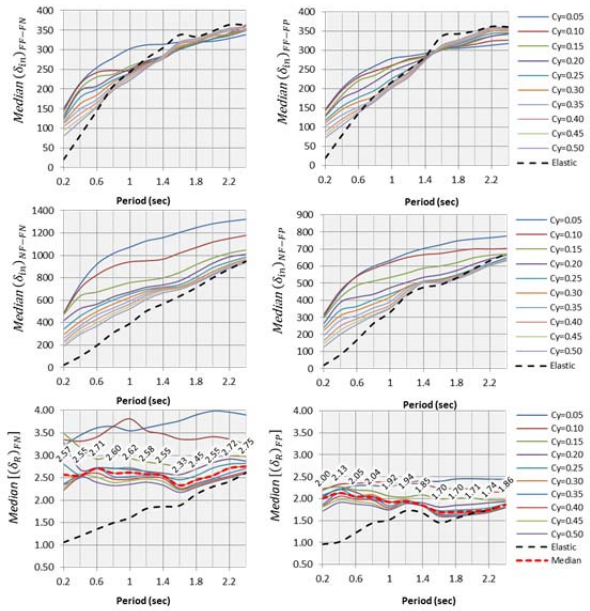

Figure A - 88: Median values of maximum displacement demands and inelastic displacement demand ratio (IDDR) In Terms of strength characteristics | Link: NLT#4| ζ=%5.0| EQ Level=4

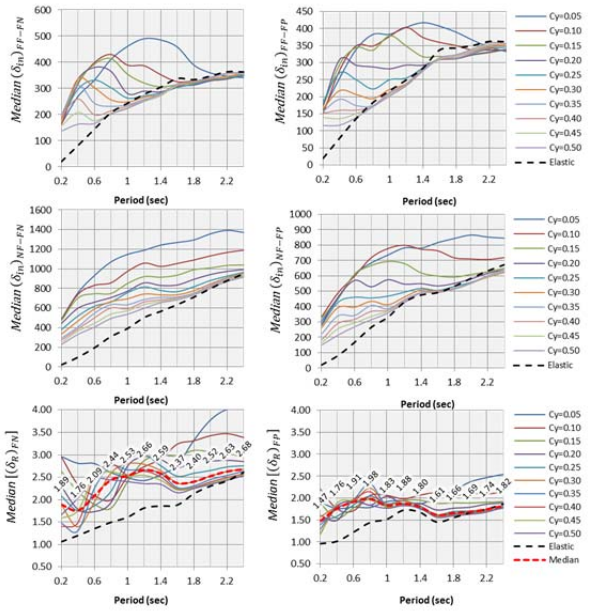

Figure A - 89: Median values of maximum displacement demands and inelastic displacement demand ratio (IDDR) In Terms of strength characteristics | Link: NLT#5| ζ=%5.0| EQ Level=4

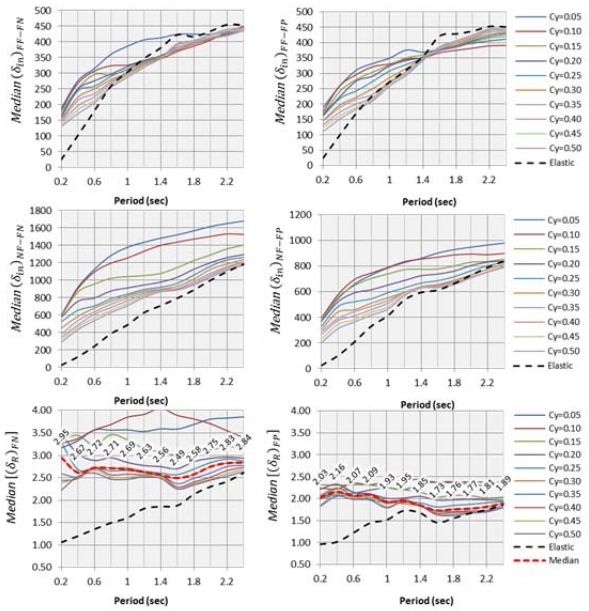

Figure A - 90: Median values of maximum displacement demands and inelastic displacement demand ratio (IDDR) In Terms of strength characteristics | Link: NLT#4| ζ=%5.0| EQ Level=5

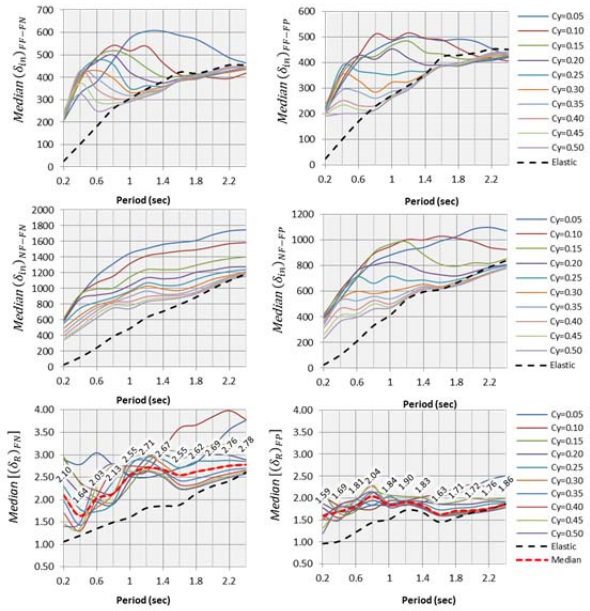

Figure A - 91: Median values of maximum displacement demands and inelastic displacement demand ratio (IDDR) In Terms of strength characteristics | Link: NLT#5| ζ=%5.0| EQ Level=5

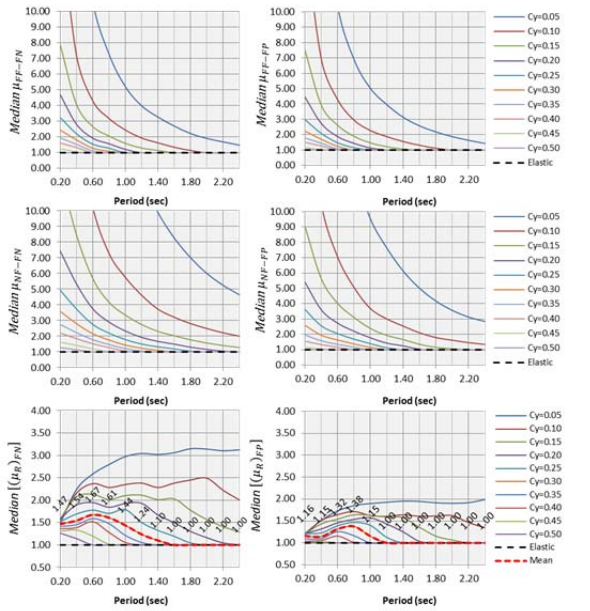

Figure A - 92: Median values of maximum ductility demand and ductility demand ratio (DDR) in Terms of strength characteristics | Link: NLT#1| ζ=%5.0| EQ Level=1

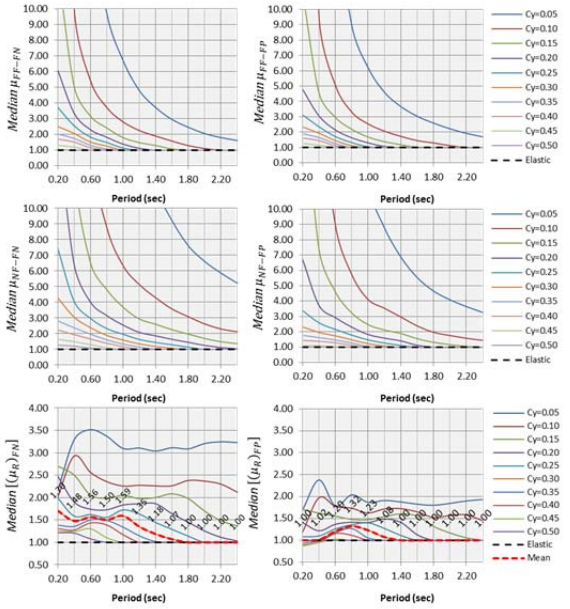

Figure A - 93: Median values of maximum ductility demand and ductility demand ratio (DDR) in Terms of strength characteristics | Link: NLT#2| ζ=%5.0| EQ Level=1

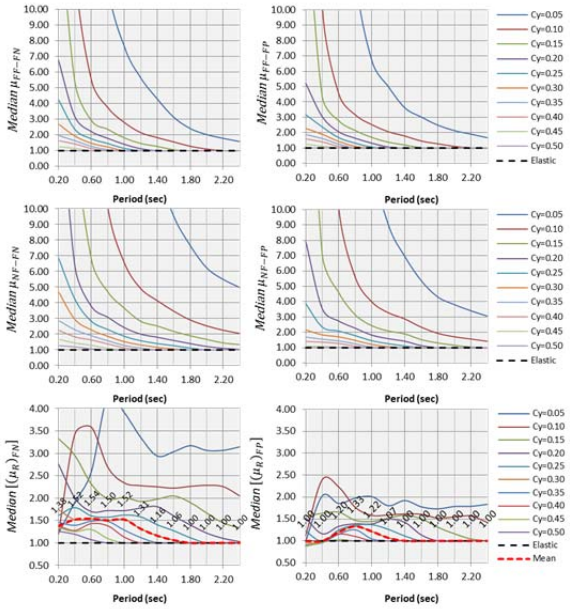

Figure A - 94: Median values of maximum ductility demand and ductility demand ratio (DDR) in Terms of strength characteristics | Link: NLT#3| ζ=%5.0| EQ Level=1

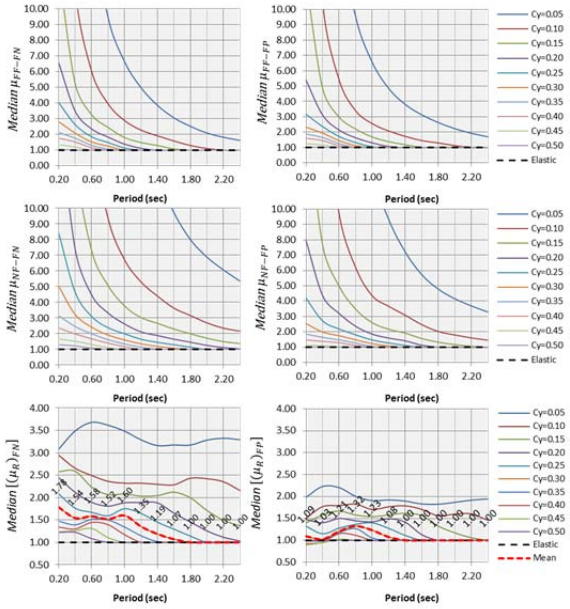

Figure A - 95: Median values of maximum ductility demand and ductility demand ratio (DDR) in Terms of strength characteristics | Link: NLT#4| ζ=%5.0| EQ Level=1

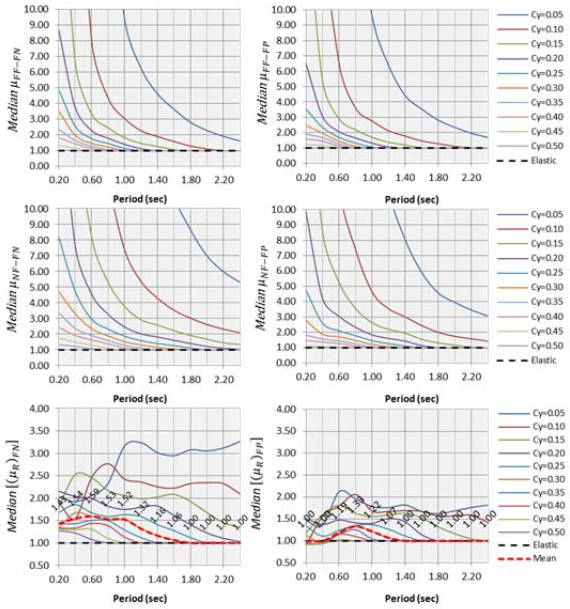

Figure A - 96: Median values of maximum ductility demand and ductility demand ratio (DDR) in Terms of strength characteristics | Link: NLT#5| ζ=%5.0| EQ Level=1

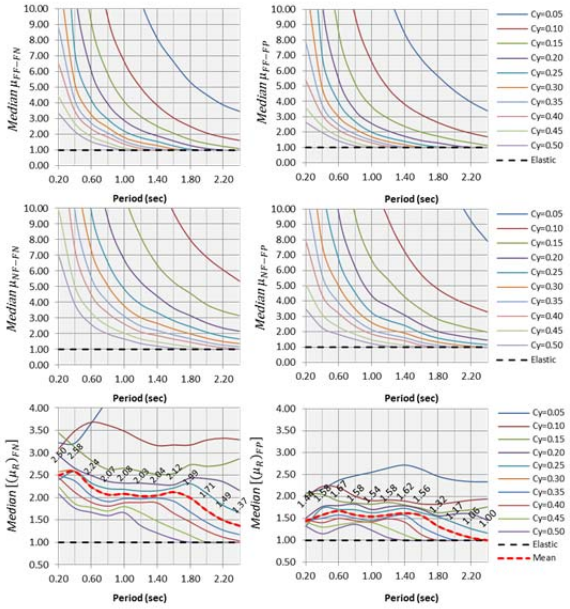

Figure A - 97: Median values of maximum ductility demand and ductility demand ratio (DDR) in Terms of strength characteristics | Link: NLT#4| ζ=%5.0| EQ Level=2

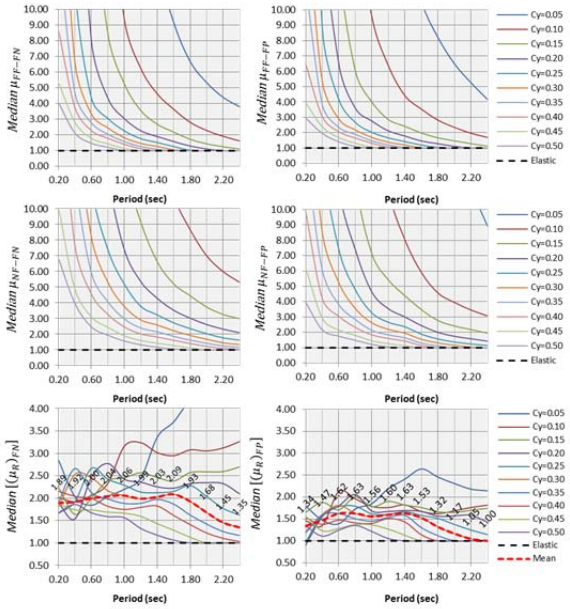

Figure A - 98: Median values of maximum ductility demand and ductility demand ratio (DDR) in Terms of strength characteristics | Link: NLT#5| ζ=%5.0| EQ Level=2

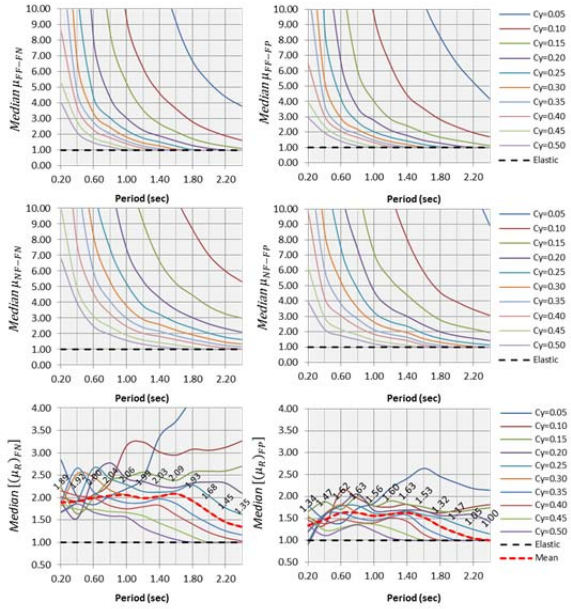

Figure A - 99: Median values of maximum ductility demand and ductility demand ratio (DDR) in Terms of strength characteristics | Link: NLT#4| ζ=%5.0| EQ Level=3

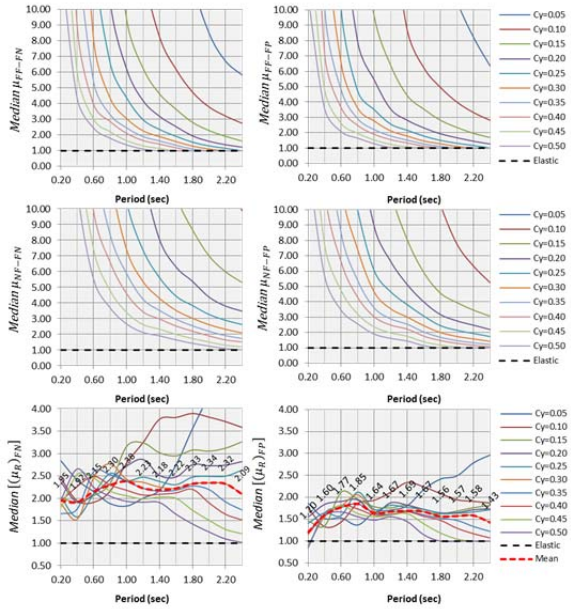

Figure A - 100: Median values of maximum ductility demand and ductility demand ratio (DDR) in Terms of strength characteristics | Link: NLT#5| ζ=%5.0| EQ Level=3

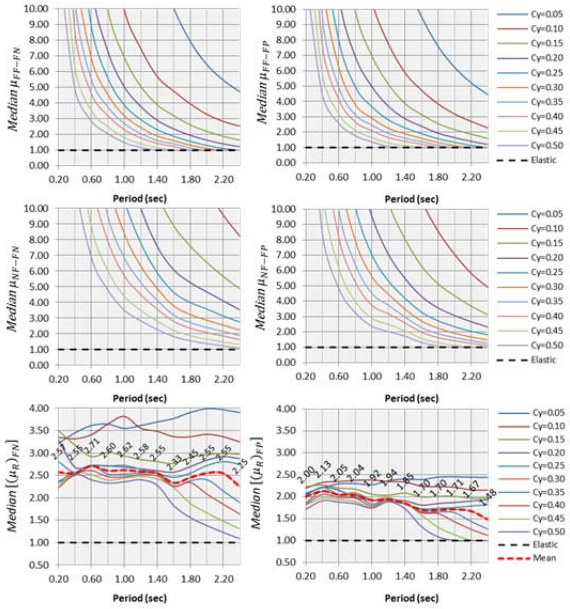

Figure A - 101: Median values of maximum ductility demand and ductility demand ratio (DDR) in Terms of strength characteristics | Link: NLT#4| ζ=%5.0| EQ Level=4

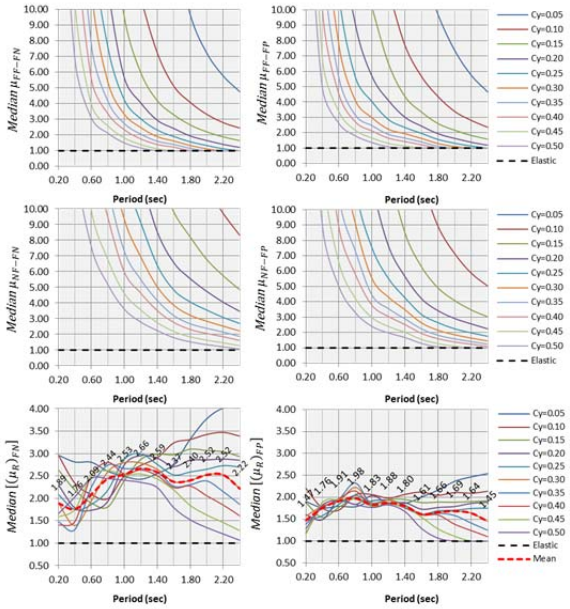

Figure A - 102: Median values of maximum ductility demand and ductility demand ratio (DDR) in Terms of strength characteristics | Link: NLT#5| ζ=%5.0| EQ Level=4

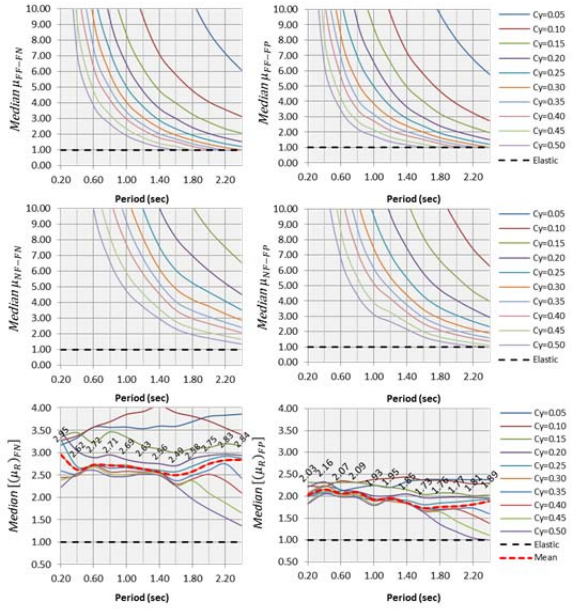

Figure A - 103: Median values of maximum ductility demand and ductility demand ratio (DDR) in Terms of strength characteristics | Link: NLT#4| ζ=%5.0| EQ Level=5

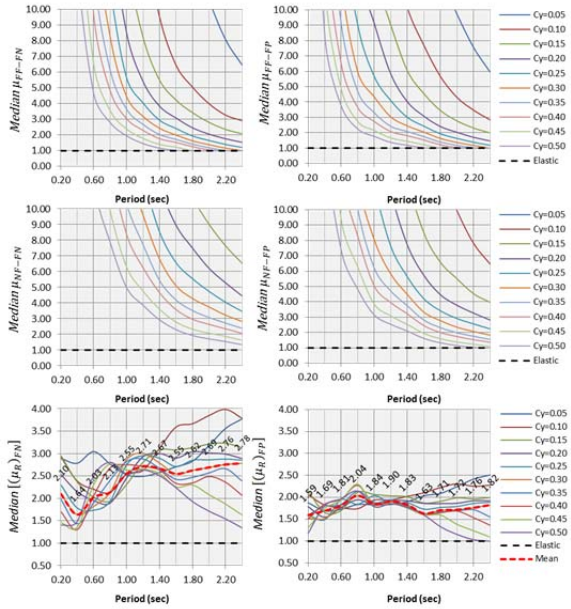

Figure A - 104: Median values of maximum ductility demand and ductility demand ratio (DDR) in Terms of strength characteristics | Link: NLT#5| ζ=%5.0| EQ Level=5

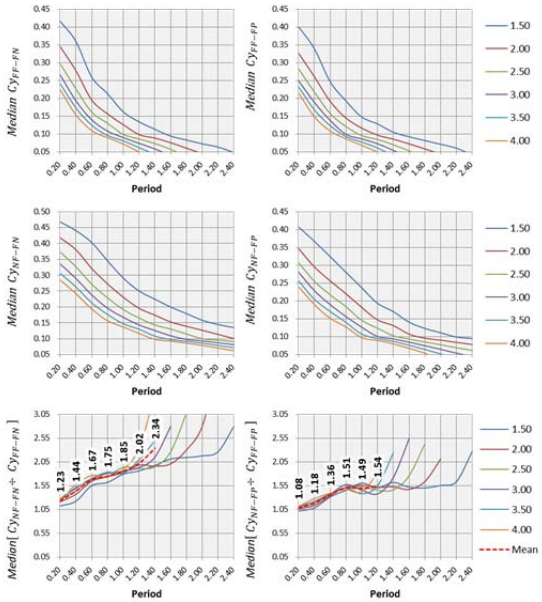

Figure A - 105: Median values of yield capacity demand and yield capacity demand ratio (YCDR) in Terms of target ductility | Link: NLT#1| ζ=%5.0| EQ Level=1

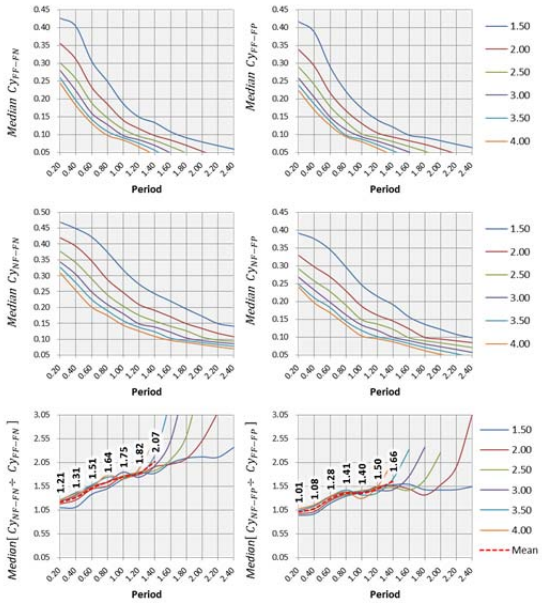

Figure A - 106: Median values of yield capacity demand and yield capacity demand ratio (YCDR) in Terms of target ductility | Link: NLT#2| ζ=%5.0| EQ Level=1

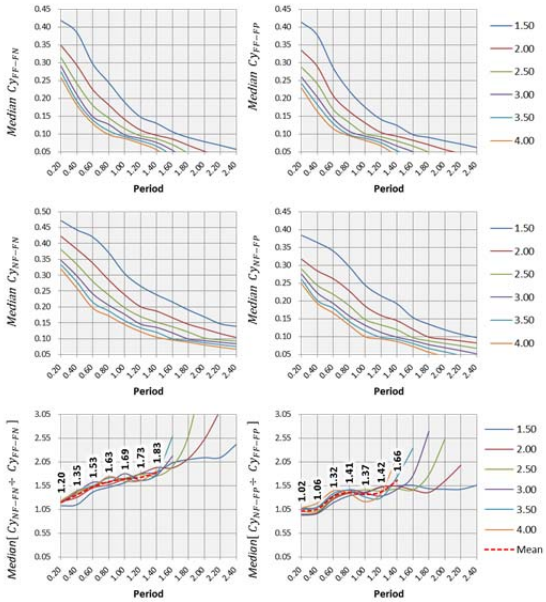

Figure A - 107: Median values of yield capacity demand and yield capacity demand ratio (YCDR) in Terms of target ductility | Link: NLT#3| ζ=%5.0| EQ Level=1

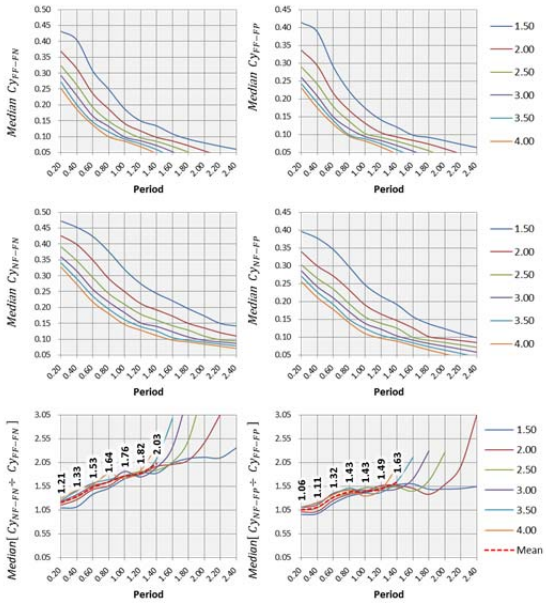

Figure A - 108: Median values of yield capacity demand and yield capacity demand ratio (YCDR) in Terms of target ductility | Link: NLT#4| ζ=%5.0| EQ Level=1

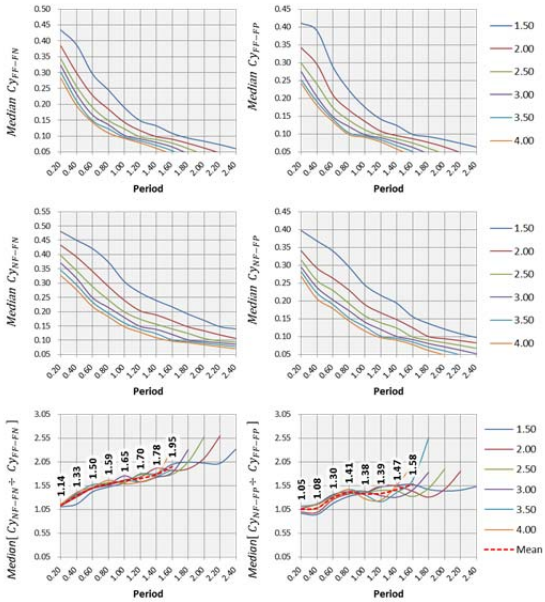

Figure A - 109: Median values of yield capacity demand and yield capacity demand ratio (YCDR) in Terms of target ductility | Link: NLT#5| ζ=%5.0| EQ Level=1

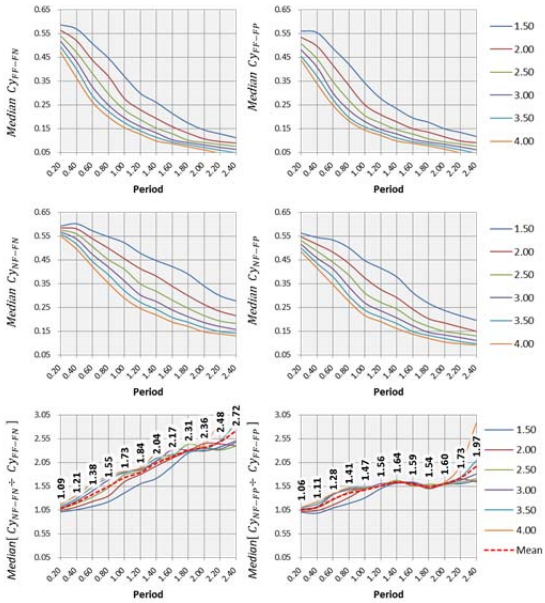

Figure A - 110: Median values of yield capacity demand and yield capacity demand ratio (YCDR) in Terms of target ductility | Link: NLT#4| ζ=%5.0| EQ Level=2

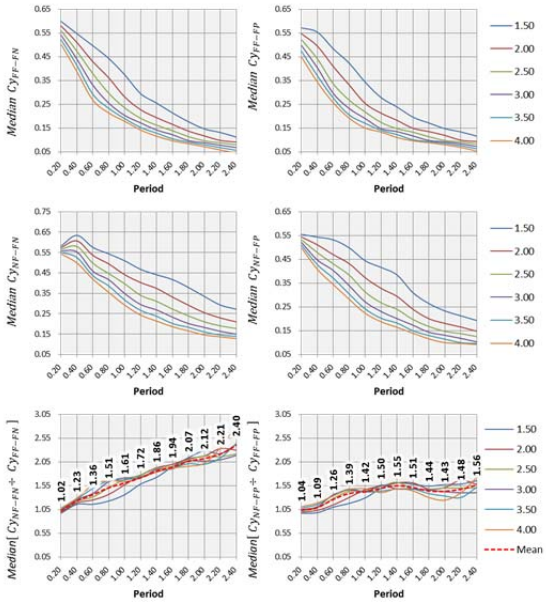

Figure A - 111: Median values of yield capacity demand and yield capacity demand ratio (YCDR) in Terms of target ductility | Link: NLT#5| ζ=%5.0| EQ Level=2

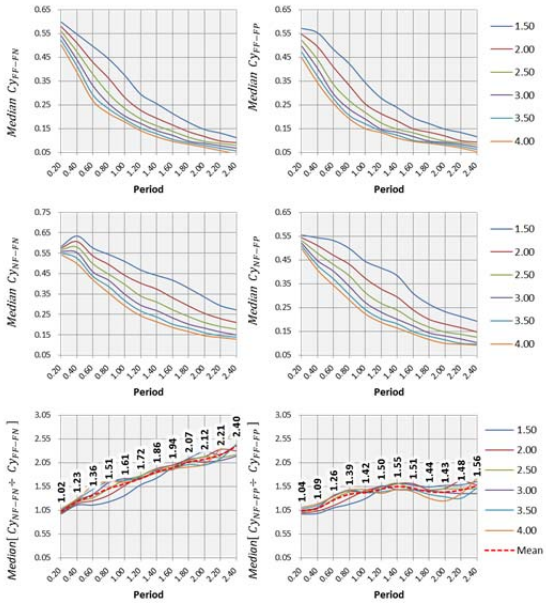

Figure A - 112: Median values of yield capacity demand and yield capacity demand ratio (YCDR) in Terms of target ductility | Link: NLT#4| ζ=%5.0| EQ Level=3

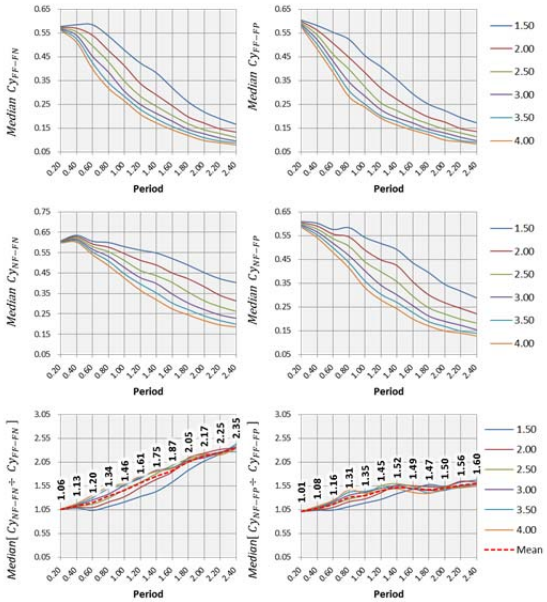

Figure A - 113: Median values of yield capacity demand and yield capacity demand ratio (YCDR) in Terms of target ductility | Link: NLT#5| ζ=%5.0| EQ Level=3

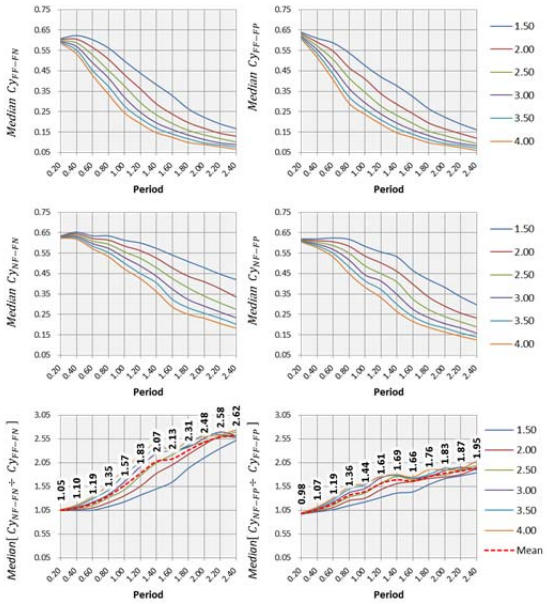

Figure A - 114: Median values of yield capacity demand and yield capacity demand ratio (YCDR) in Terms of target ductility | Link: NLT#4| ζ=%5.0| EQ Level=4

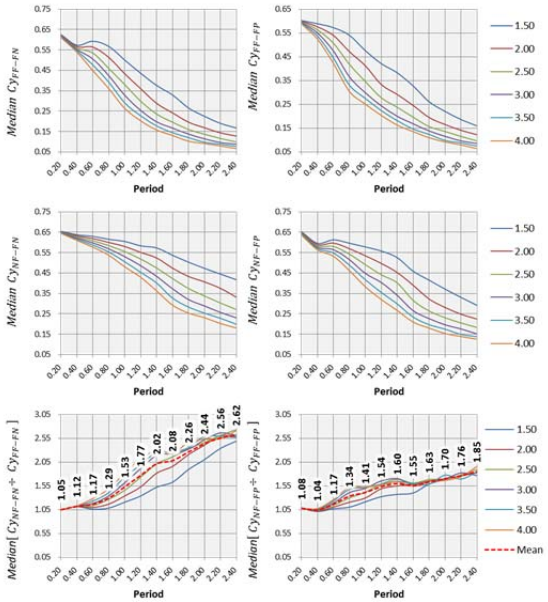

Figure A - 115: Median values of yield capacity demand and yield capacity demand ratio (YCDR) in Terms of target ductility | Link: NLT#5| ζ=%5.0| EQ Level=4

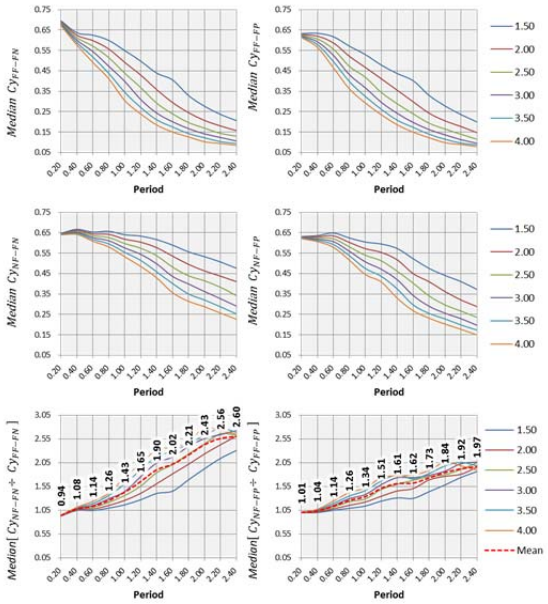

Figure A - 116: Median values of yield capacity demand and yield capacity demand ratio (YCDR) in Terms of target ductility | Link: NLT#4| ζ=%5.0| EQ Level=5

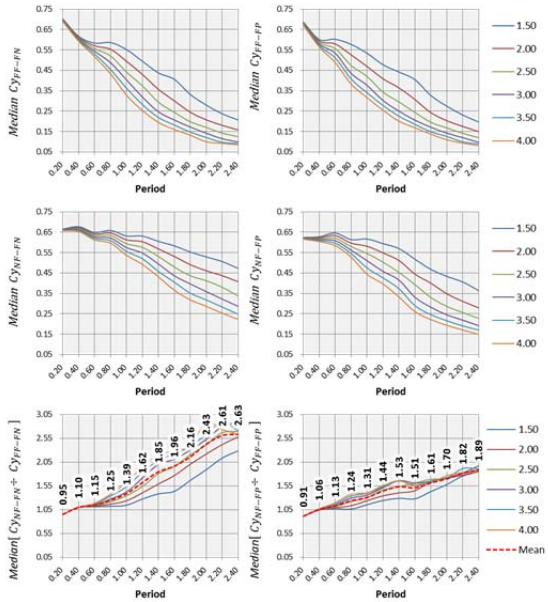

Figure A - 117: Median values of yield capacity demand and yield capacity demand ratio (YCDR) in Terms of target ductility | Link: NLT#5| ζ=%5.0| EQ Level=5

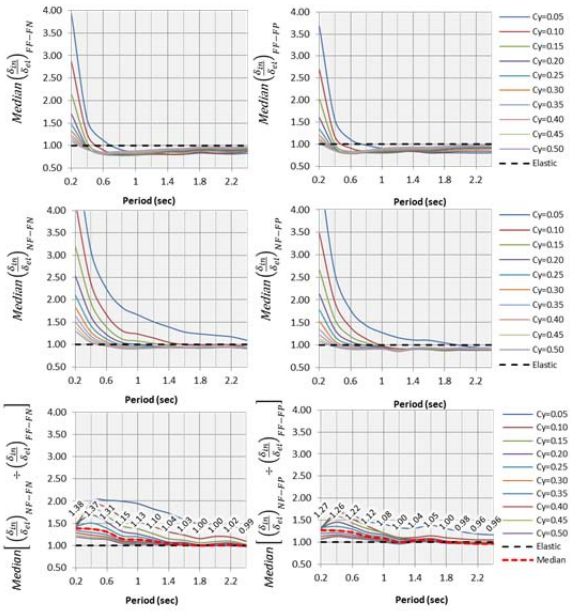

Figure A - 118: Median values of maximum inelastic to elastic displacement demand and maximum inelastic to elastic displacement demand ratio in terms of strength characteristics| Link: NLT#1| ζ=%5.0| EQ Level=1

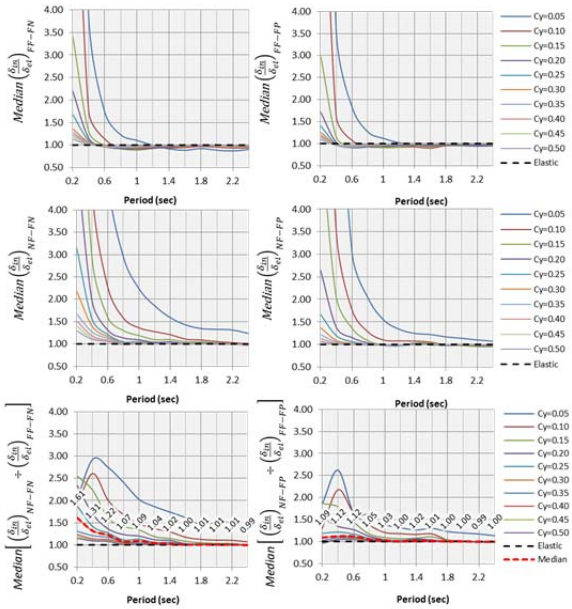

Figure A - 119: Median values of maximum inelastic to elastic displacement demand and maximum inelastic to elastic displacement demand ratio in terms of strength characteristics| Link: NLT#2| ζ=%5.0| EQ Level=1

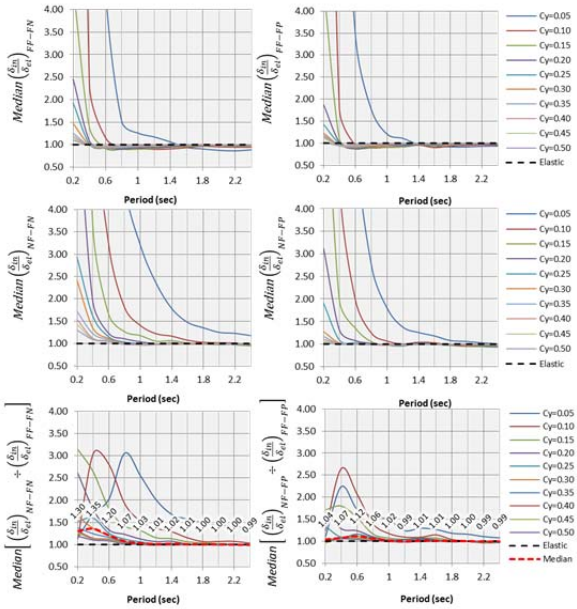

Figure A - 120: Median values of maximum inelastic to elastic displacement demand and maximum inelastic to elastic displacement demand ratio in terms of strength characteristics| Link: NLT#3| ζ=%5.0| EQ Level=1

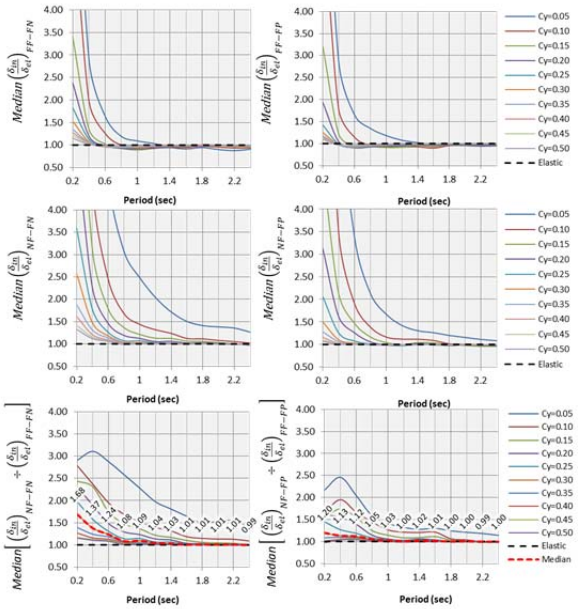

Figure A - 121: Median values of maximum inelastic to elastic displacement demand and maximum inelastic to elastic displacement demand ratio in terms of strength characteristics| Link: NLT#4| ζ=%5.0| EQ Level=1

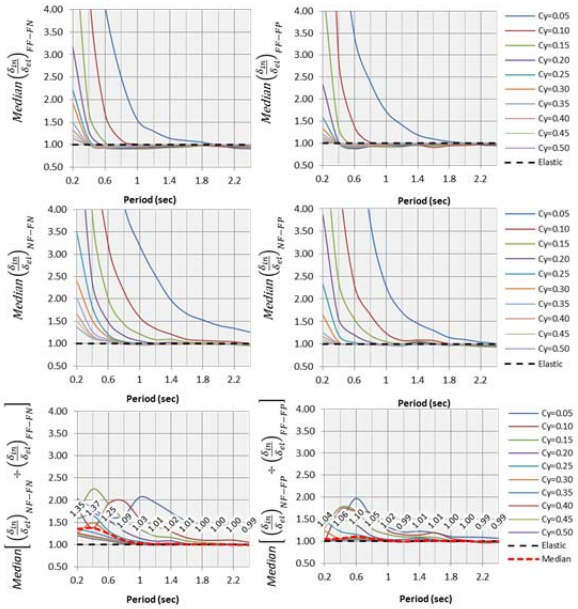

Figure A - 122: Median values of maximum inelastic to elastic displacement demand and maximum inelastic to elastic displacement demand ratio in terms of strength characteristics| Link: NLT#5| ζ=%5.0| EQ Level=1

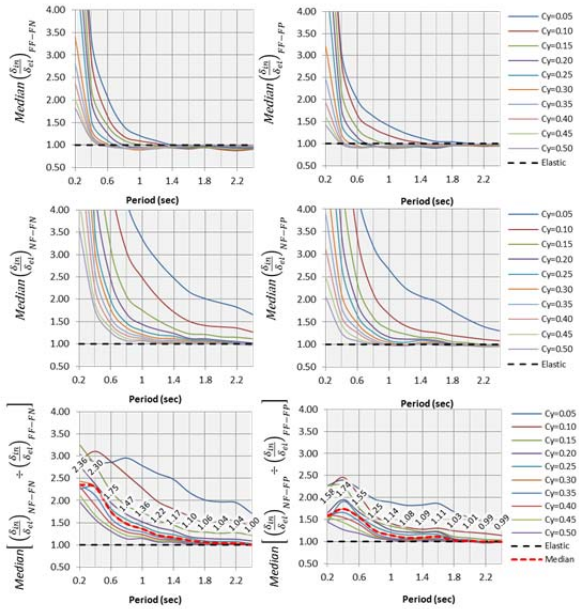

Figure A - 123: Median values of maximum inelastic to elastic displacement demand and maximum inelastic to elastic displacement demand ratio in terms of strength characteristics| Link: NLT#4| ζ=%5.0| EQ Level=2

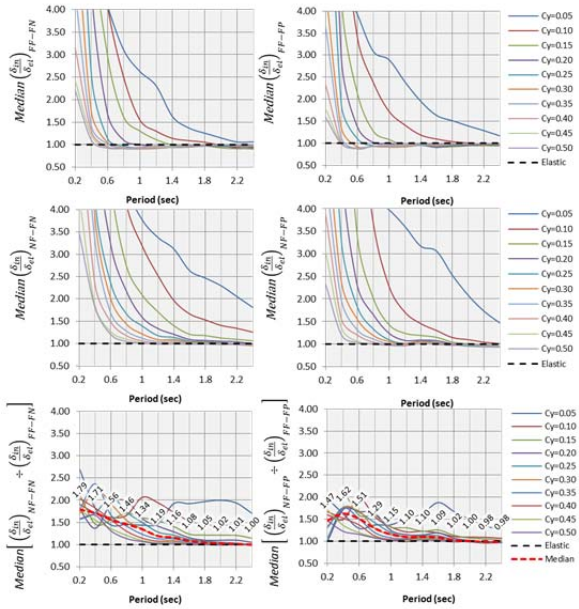

Figure A - 124: Median values of maximum inelastic to elastic displacement demand and maximum inelastic to elastic displacement demand ratio in terms of strength characteristics| Link: NLT#5| ζ=%5.0| EQ Level=2

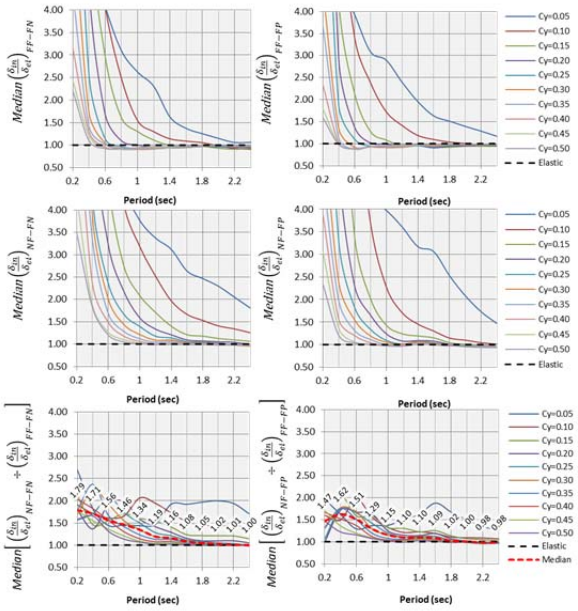

Figure A - 125: Median values of maximum inelastic to elastic displacement demand and maximum inelastic to elastic displacement demand ratio in terms of strength characteristics| Link: NLT#4| ζ=%5.0| EQ Level=3

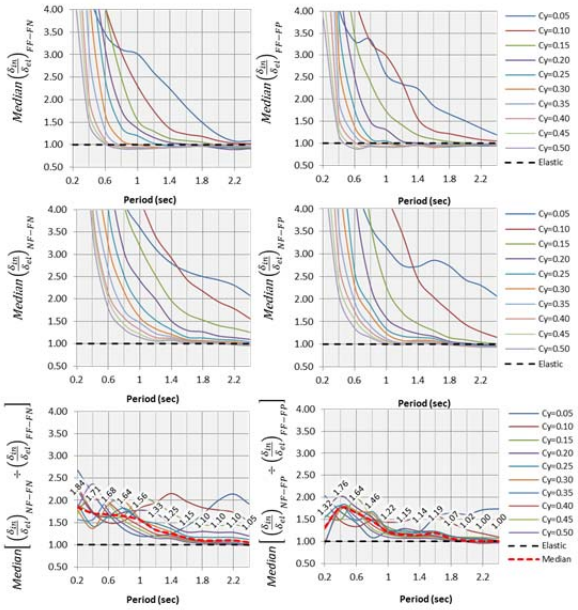

Figure A - 126: Median values of maximum inelastic to elastic displacement demand and maximum inelastic to elastic displacement demand ratio in terms of strength characteristics| Link: NLT#5| ζ=%5.0| EQ Level=3

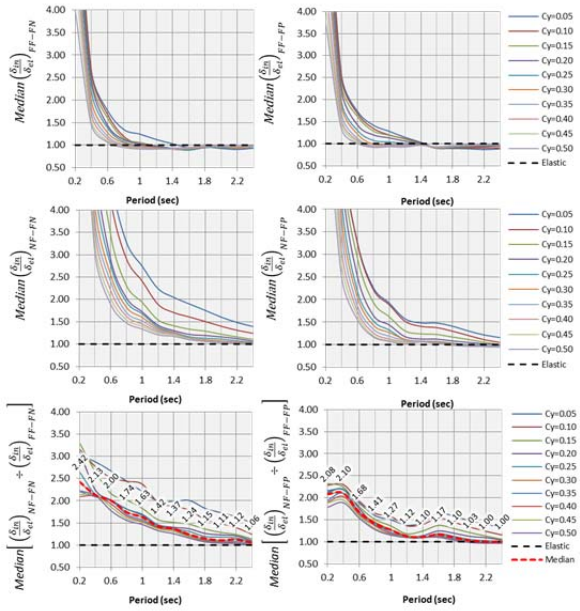

Figure A - 127: Median values of maximum inelastic to elastic displacement demand and maximum inelastic to elastic displacement demand ratio in terms of strength characteristics| Link: NLT#4| ζ=%5.0| EQ Level=4

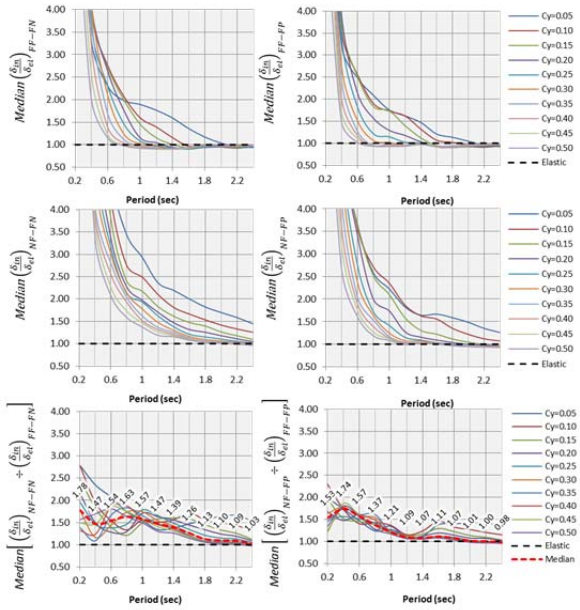

Figure A - 128: Median values of maximum inelastic to elastic displacement demand and maximum inelastic to elastic displacement demand ratio in terms of strength characteristics| Link: NLT#5| ζ=%5.0| EQ Level=4

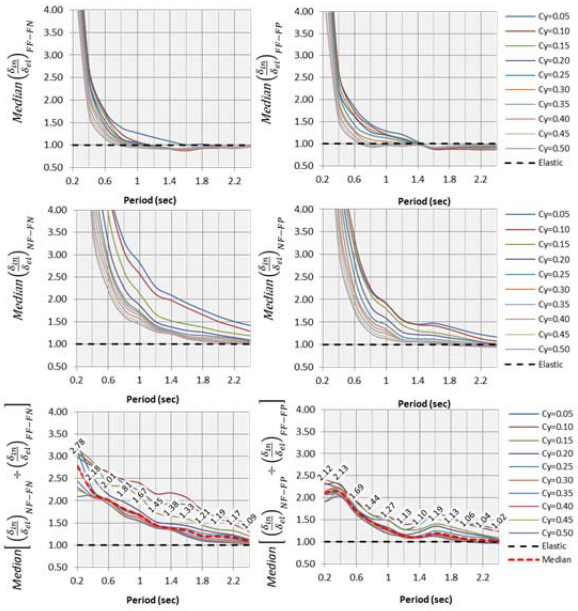

Figure A - 129: Median values of maximum inelastic to elastic displacement demand and maximum inelastic to elastic displacement demand ratio in terms of strength characteristics| Link: NLT#4| ζ=%5.0| EQ Level=5

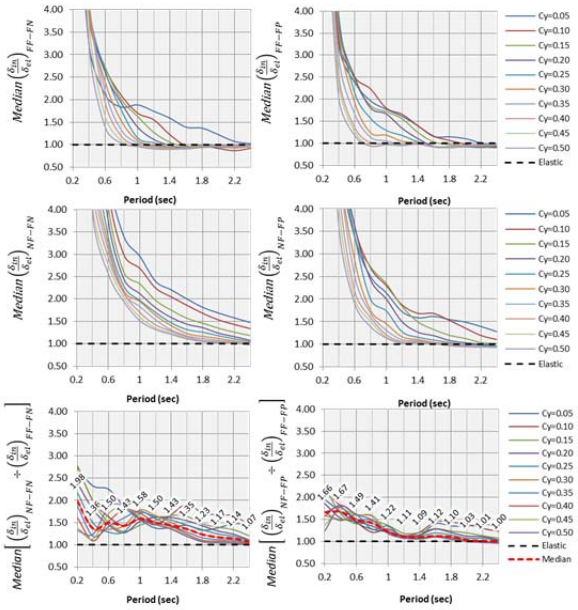

Figure A - 130: Median values of maximum inelastic to elastic displacement demand and maximum inelastic to elastic displacement demand ratio in terms of strength characteristics| Link: NLT#5| ζ=%5.0| EQ Level=5

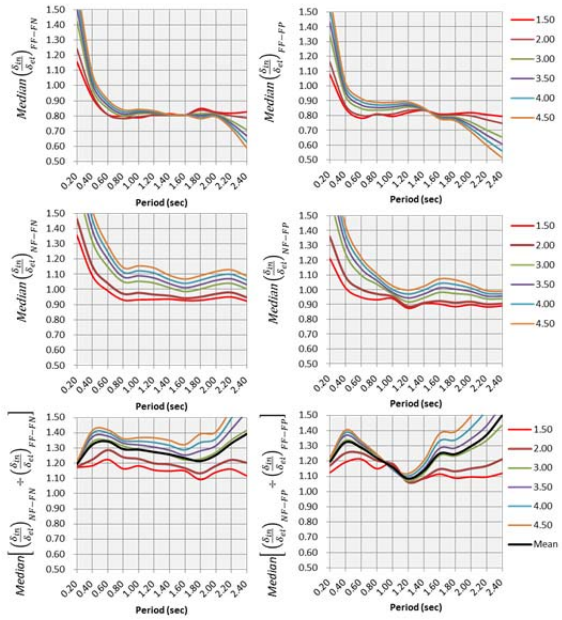

Figure A - 131: Median values of maximum inelastic to elastic displacement demand and maximum inelastic to elastic displacement demand ratio in terms of ductility | Link: NLT#1| ζ=%5.0| EQ Level=1

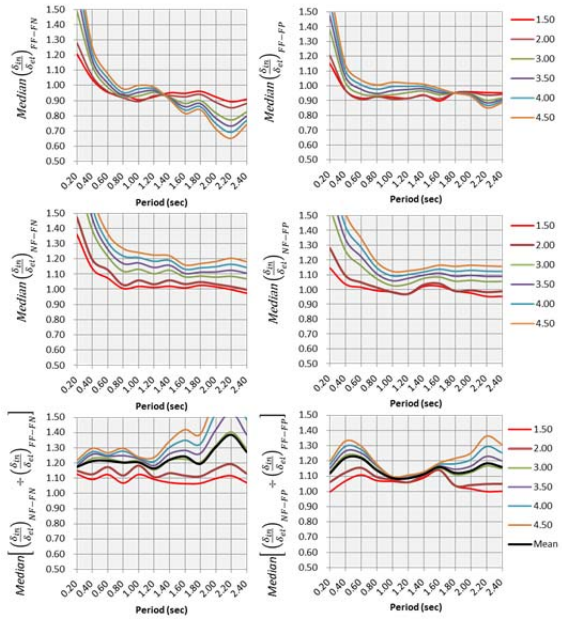

Figure A - 132: Median values of maximum inelastic to elastic displacement demand and maximum inelastic to elastic displacement demand ratio in terms of ductility | Link: NLT#2| ζ=%5.0| EQ Level=1

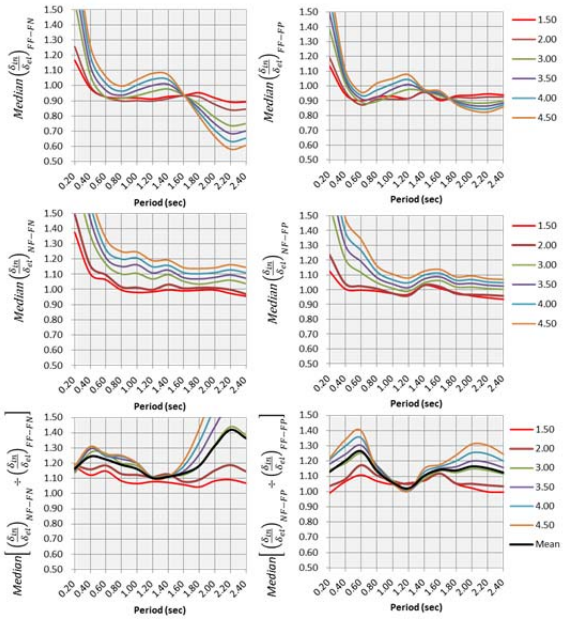

Figure A - 133: Median values of maximum inelastic to elastic displacement demand and maximum inelastic to elastic displacement demand ratio in terms of ductility | Link: NLT#3| ζ=%5.0| EQ Level=1

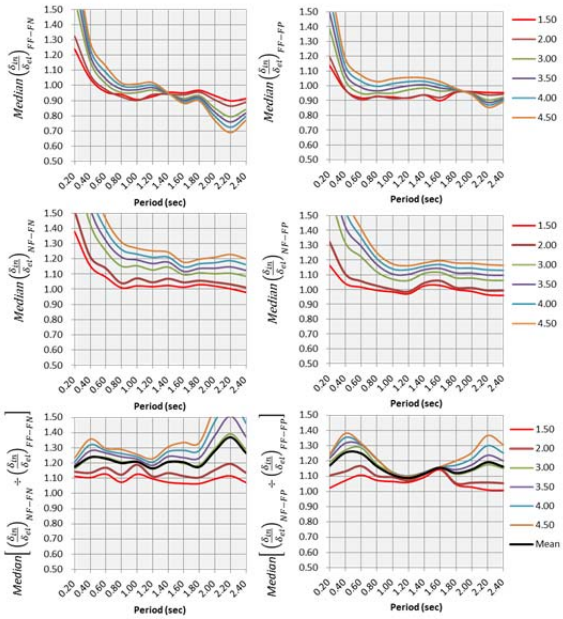

Figure A - 134: Median values of maximum inelastic to elastic displacement demand and maximum inelastic to elastic displacement demand ratio in terms of ductility | Link: NLT#4| ζ=%5.0| EQ Level=1

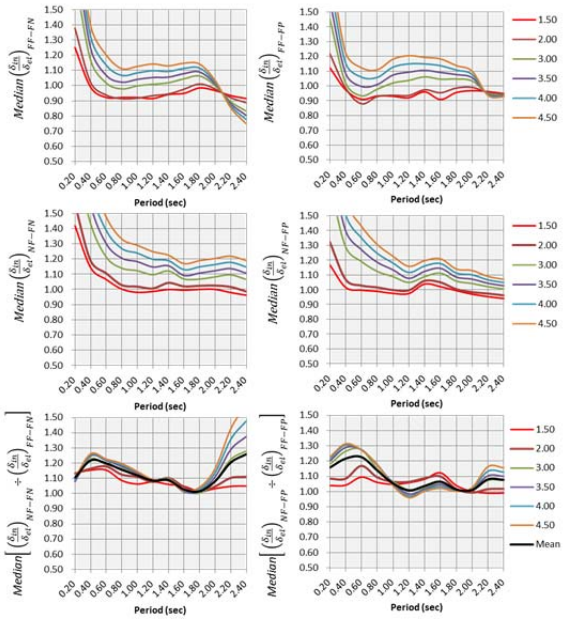

Figure A - 135: Median values of maximum inelastic to elastic displacement demand and maximum inelastic to elastic displacement demand ratio in terms of ductility | Link: NLT#5| ζ=%5.0| EQ Level=1

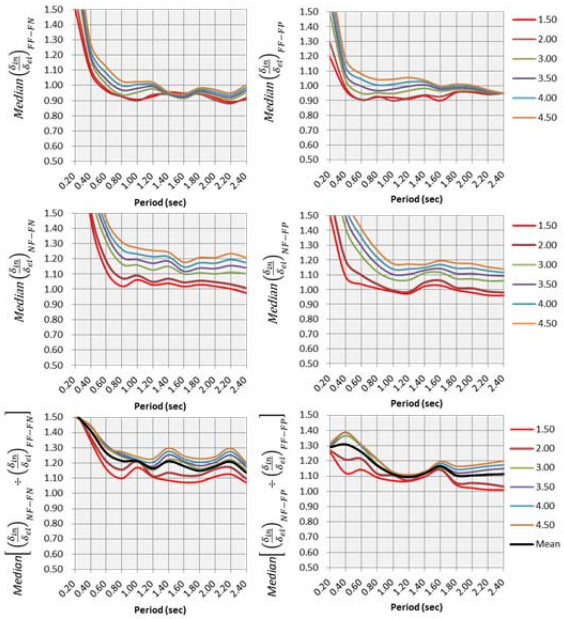

Figure A - 136: Median values of maximum inelastic to elastic displacement demand and maximum inelastic to elastic displacement demand ratio in terms of ductility | Link: NLT#4| ζ=%5.0| EQ Level=2

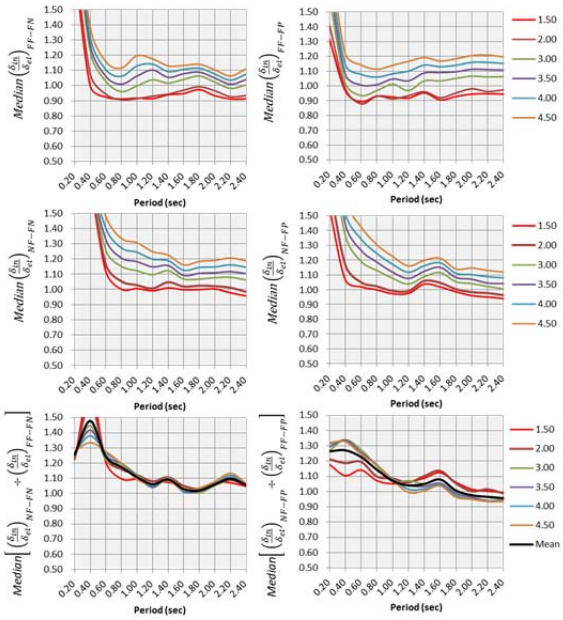

Figure A - 137: Median values of maximum inelastic to elastic displacement demand and maximum inelastic to elastic displacement demand ratio in terms of ductility | Link: NLT#5| ζ=%5.0| EQ Level=2

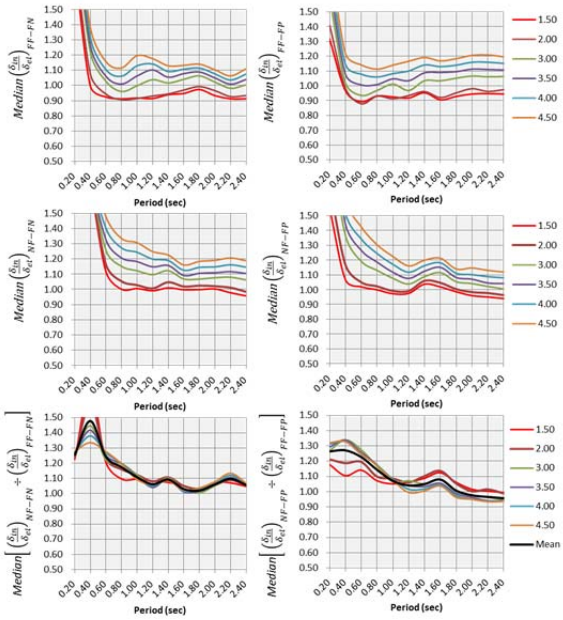

Figure A - 138: Median values of maximum inelastic to elastic displacement demand and maximum inelastic to elastic displacement demand ratio in terms of ductility | Link: NLT#4| ζ=%5.0| EQ Level=3

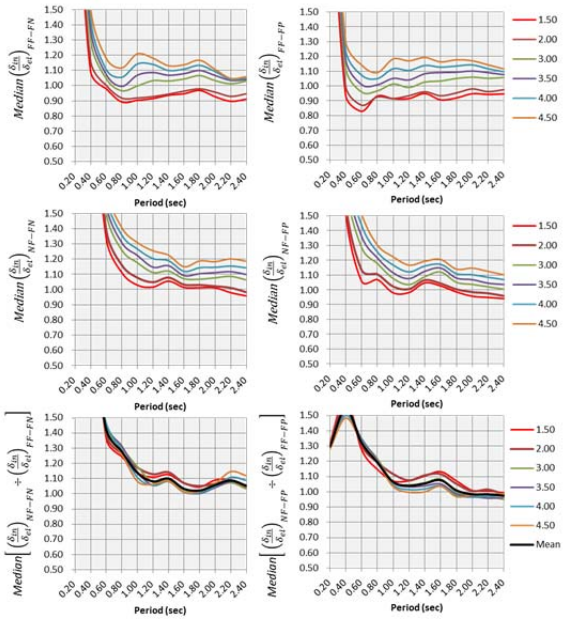

Figure A - 139: Median values of maximum inelastic to elastic displacement demand and maximum inelastic to elastic displacement demand ratio in terms of ductility | Link: NLT#5| ζ=%5.0| EQ Level=3

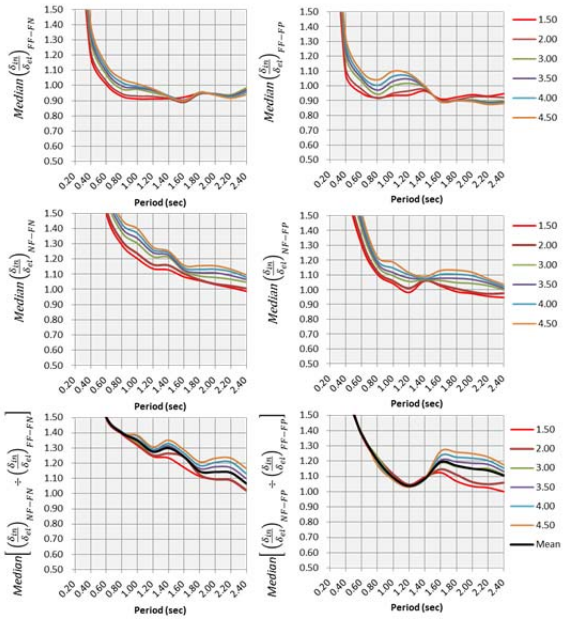

Figure A - 140: Median values of maximum inelastic to elastic displacement demand and maximum inelastic to elastic displacement demand ratio in terms of ductility | Link: NLT#4| ζ=%5.0| EQ Level=4

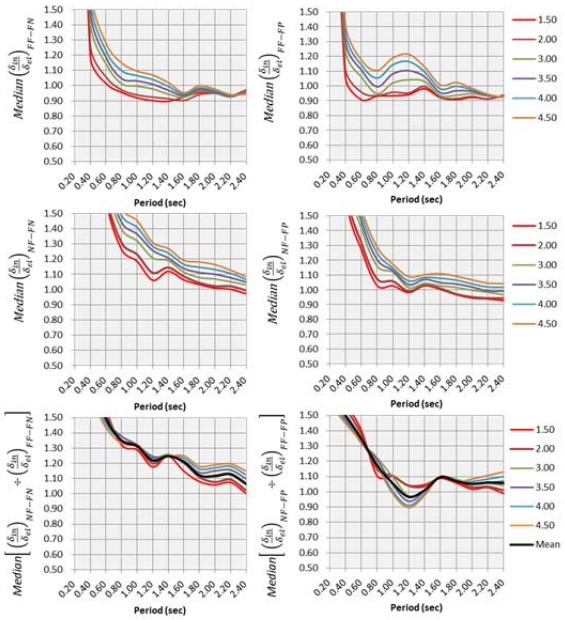

Figure A - 141: Median values of maximum inelastic to elastic displacement demand and maximum inelastic to elastic displacement demand ratio in terms of ductility | Link: NLT#5| ζ=%5.0| EQ Level=4

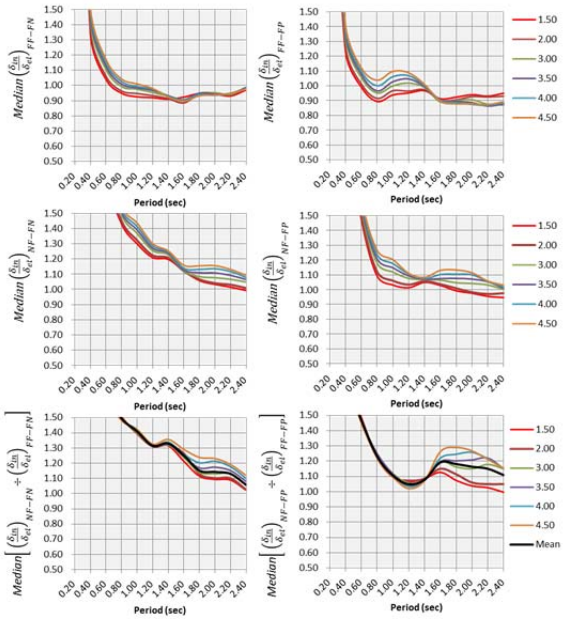

Figure A - 142: Median values of maximum inelastic to elastic displacement demand and maximum inelastic to elastic displacement demand ratio in terms of ductility | Link: NLT#4| ζ=%5.0| EQ Level=5

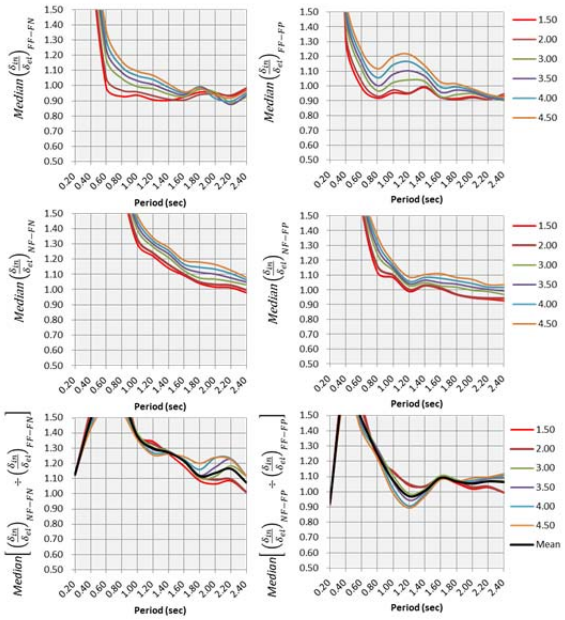

Figure A - 143: Median values of maximum inelastic to elastic displacement demand and maximum inelastic to elastic displacement demand ratio in terms of ductility | Link: NLT#5| ζ=%5.0| EQ Level=5

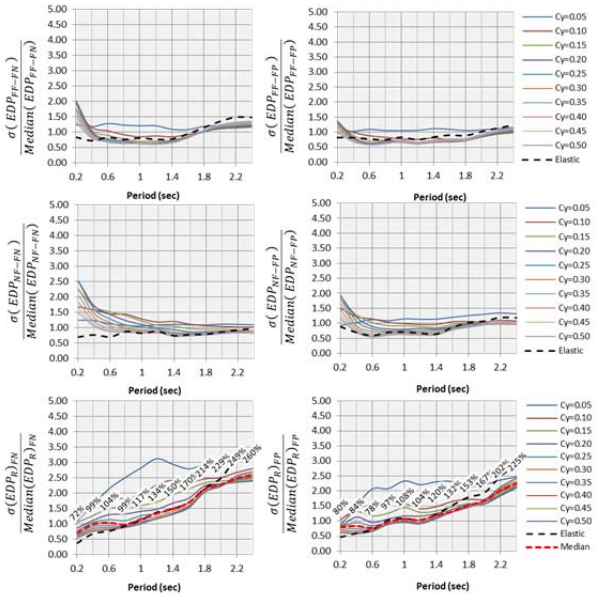

Figure A - 144: CV Values of “EDP” and “EDP Ratio” In Terms of strength characteristics | Link: NLT#1| ζ=%5.0| EQ Level=1

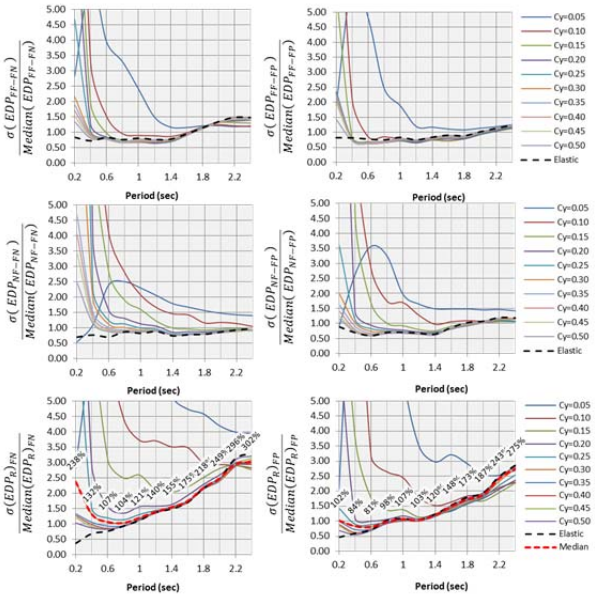

Figure A - 145: CV Values of “EDP” and “EDP Ratio” In Terms of strength characteristics | Link: NLT#2| ζ=%5.0| EQ Level=1

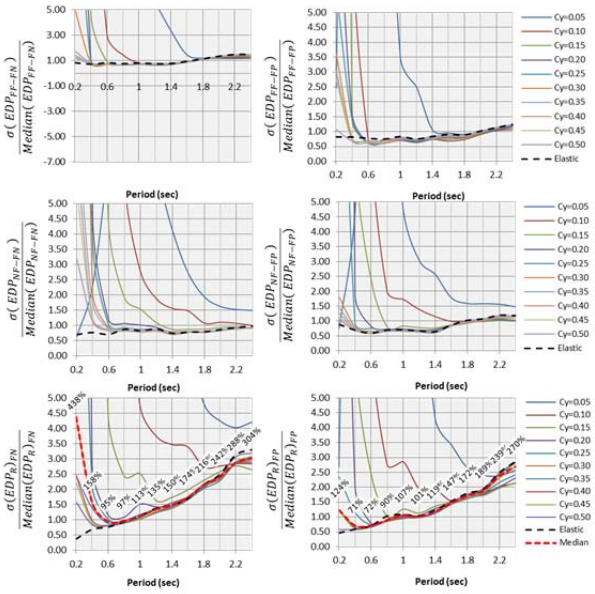

Figure A - 146: CV Values of “EDP” and “EDP Ratio” In Terms of strength characteristics | Link: NLT#3| ζ=%5.0| EQ Level=1

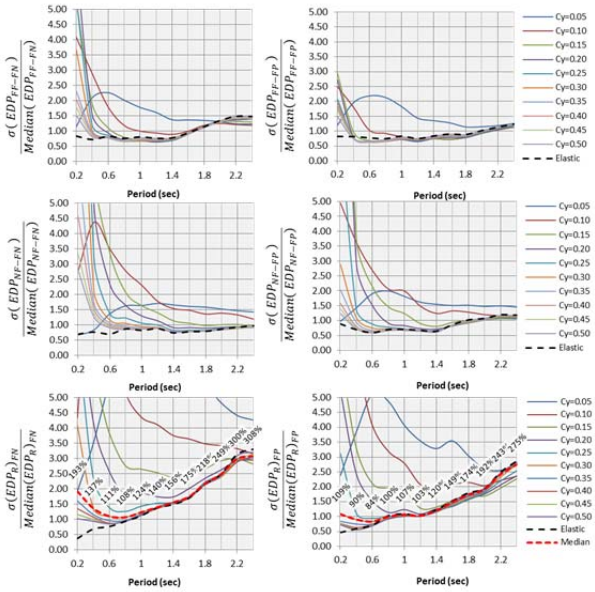

Figure A - 147: CV Values of “EDP” and “EDP Ratio” In Terms of strength characteristics | Link: NLT#4| ζ=%5.0| EQ Level=1

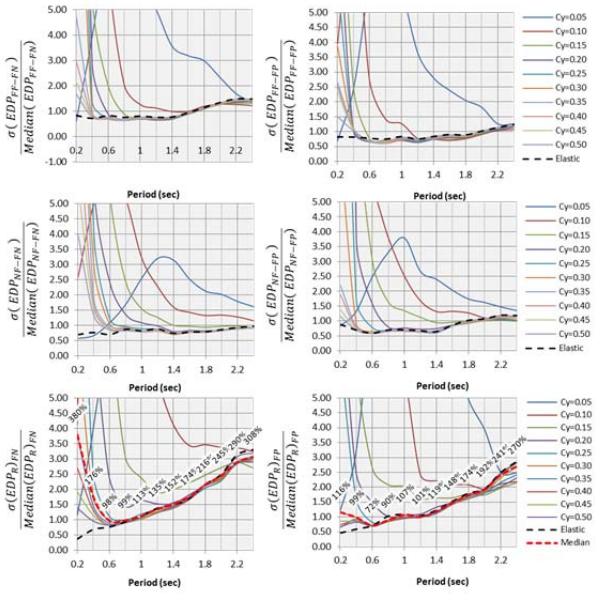

Figure A - 148: CV Values of “EDP” and “EDP Ratio” In Terms of strength characteristics | Link: NLT#5| ζ=%5.0| EQ Level=1

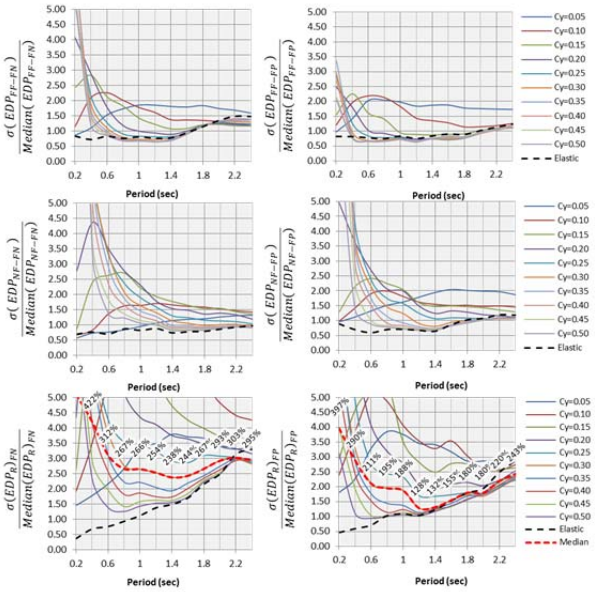

Figure A - 149: CV Values of “EDP” and “EDP Ratio” In Terms of strength characteristics | Link: NLT#4| ζ=%5.0| EQ Level=2

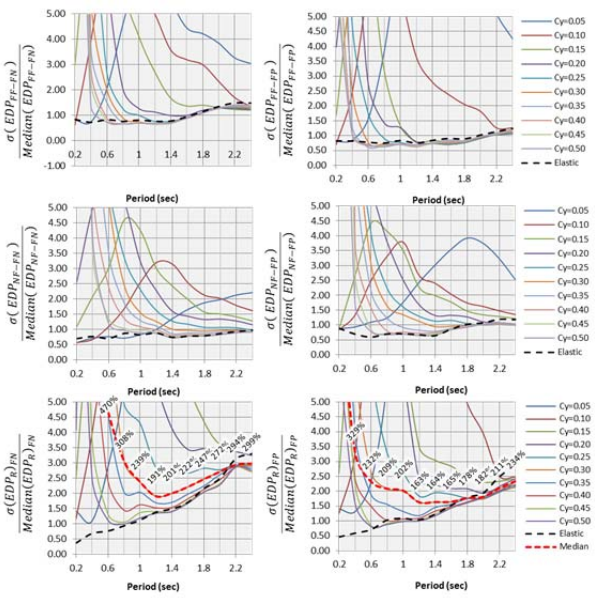

Figure A - 150: CV Values of “EDP” and “EDP Ratio” In Terms of strength characteristics | Link: NLT#5| ζ=%5.0| EQ Level=2

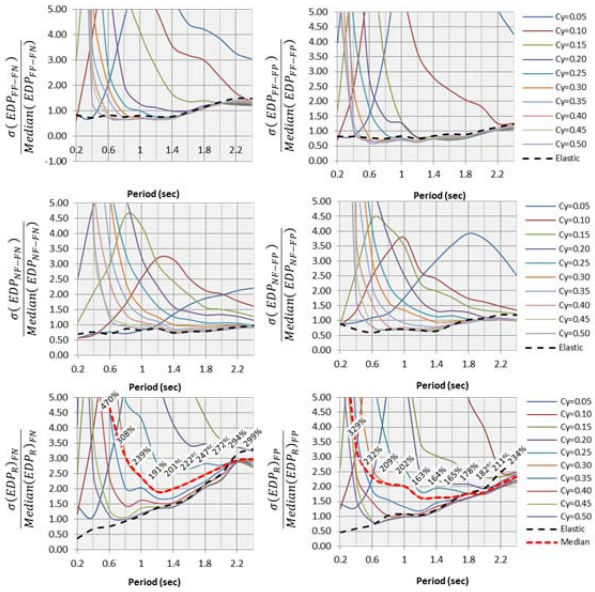

Figure A - 151: CV Values of “EDP” and “EDP Ratio” In Terms of strength characteristics | Link: NLT#4| ζ=%5.0| EQ Level=3

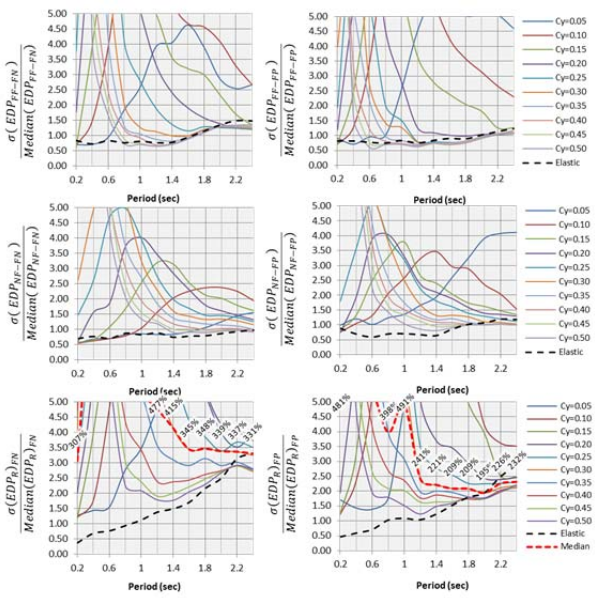

Figure A - 152: CV Values of “EDP” and “EDP Ratio” In Terms of strength characteristics | Link: NLT#5| ζ=%5.0| EQ Level=3

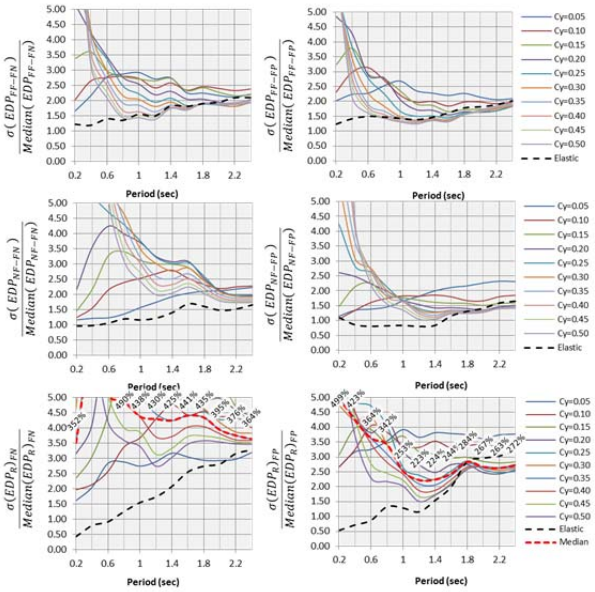

Figure A - 153: CV Values of “EDP” and “EDP Ratio” In Terms of strength characteristics | Link: NLT#4| ζ=%5.0| EQ Level=4

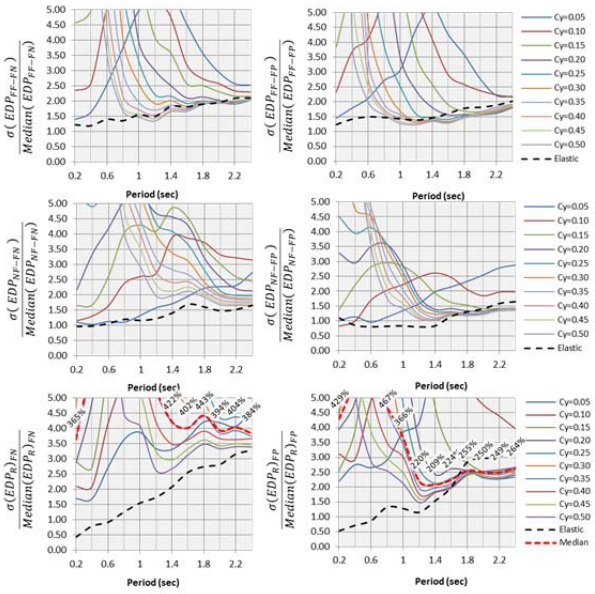

Figure A - 154: CV Values of “EDP” and “EDP Ratio” In Terms of strength characteristics | Link: NLT#5| ζ=%5.0| EQ Level=4

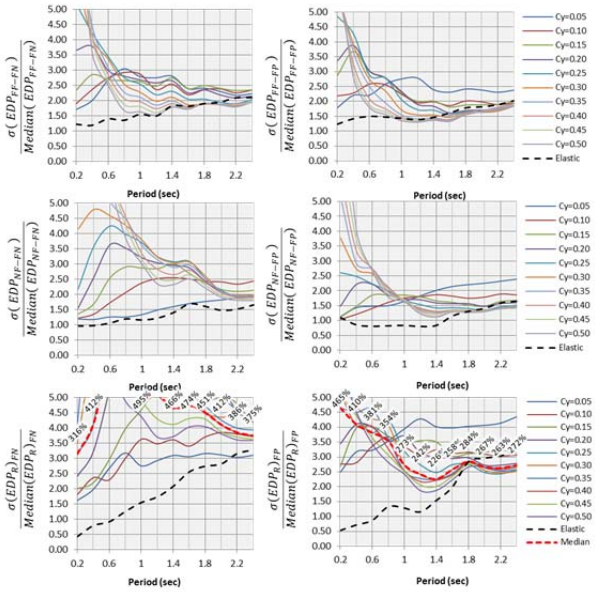

Figure A - 155: CV Values of “EDP” and “EDP Ratio” In Terms of strength characteristics | Link: NLT#4| ζ=%5.0| EQ Level=5

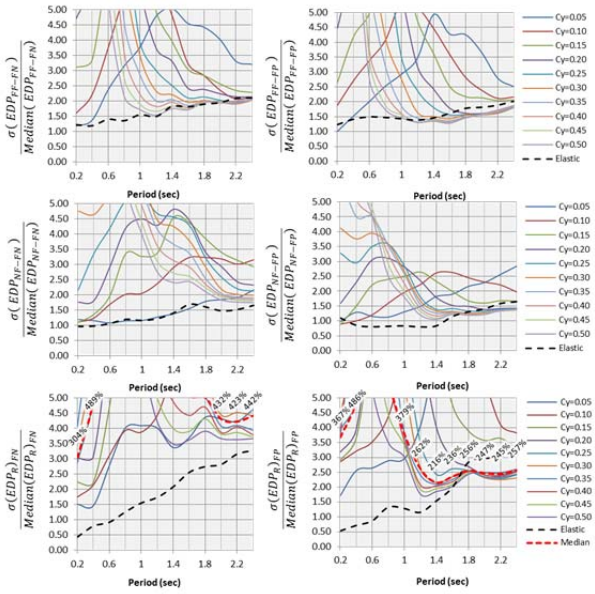

Figure A - 156: CV Values of “EDP” and “EDP Ratio” In Terms of strength characteristics | Link: NLT#5| ζ=%5.0| EQ Level=5

Appendix B – Results of NLTHA of 2DOF systems

List of selected Figures developed for 2SDOF systems subjected to PGA matched GMs

		SYS#1	SYS#2	SYS#3
	Mf/Ms	*15%*	*15%*	*25%*
	Kf/Ks	*2*	*4*	*4*
Median values of maximum displacement demands and inelastic displacement demand ratio (IDDR) In Terms of strength characteristics	EQ Level 1	Figure B - 1	Figure B - 2	Figure B - 3
	EQ Level 2	Figure B - 4	Figure B - 5	Figure B - 6
	EQ Level 3	Figure B - 7	Figure B - 8	Figure B - 9
	EQ Level 4	Figure B - 10	Figure B - 11	Figure B - 12
Median Values of “Maximum Ductility Demand” and “Ductility Demand Ratio” (DDR) in Terms of strength characteristics	EQ Level 1	Figure B - 13	Figure B - 14	Figure B - 15
	EQ Level 2	Figure B - 16	Figure B - 17	Figure B - 18
	EQ Level 3	Figure B - 19	Figure B - 20	Figure B - 21
	EQ Level 4	Figure B - 22	Figure B - 23	Figure B - 24
Median values of yield capacity demand and yield capacity demand ratio (YCDR) in Terms of target ductility	EQ Level 1	Figure B - 25	Figure B - 26	Figure B - 27
	EQ Level 2	Figure B - 28	Figure B - 29	Figure B - 30
	EQ Level 3	Figure B - 31	Figure B - 32	Figure B - 33
	EQ Level 4	Figure B - 34	Figure B - 35	Figure B - 36
Median values of maximum inelastic to elastic displacement demand and maximum inelastic to elastic displacement demand ratio in terms of strength characteristics	EQ Level 1	Figure B - 37	Figure B - 38	Figure B - 39
	EQ Level 2	Figure B - 40	Figure B - 41	Figure B - 42
	EQ Level 3	Figure B - 43	Figure B - 44	Figure B - 45
	EQ Level 4	Figure B - 46	Figure B - 47	Figure B - 48
Median values of maximum inelastic to elastic displacement demand and maximum inelastic to elastic displacement demand ratio in terms of ductility	EQ Level 1	Figure B - 49	Figure B - 50	Figure B - 51
	EQ Level 2	Figure B - 52	Figure B - 53	Figure B - 54
	EQ Level 3	Figure B - 55	Figure B - 56	Figure B - 57
	EQ Level 4	Figure B - 58	Figure B - 59	Figure B - 60
CV values of EDP and EDP.Ratio in terms of strength characteristics	EQ Level 1	Figure B - 61	Figure B - 62	Figure B - 63
	EQ Level 2	Figure B - 64	Figure B - 65	Figure B - 66
	EQ Level 3	Figure B - 67	Figure B - 68	Figure B - 69
	EQ Level 4	Figure B - 70	Figure B - 71	Figure B - 72

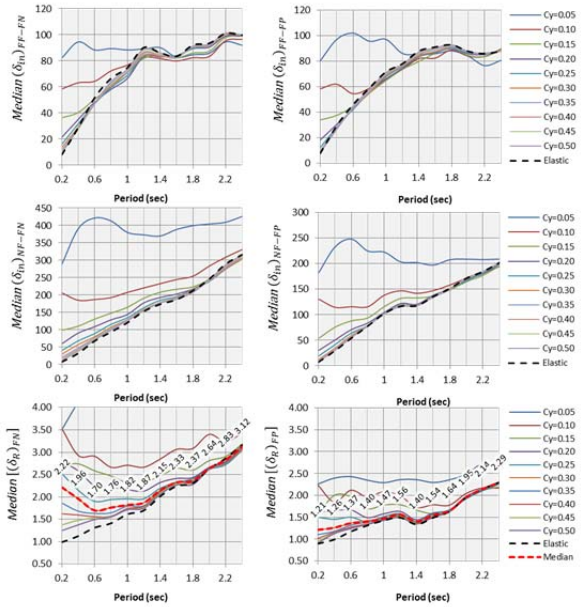

Figure B - 1: Median values of maximum displacement demands and inelastic displacement demand ratio (IDDR) In Terms of strength characteristics | Link:NLT#4 | ζ=%2.0 | EQL=1 | SYS#1 | Mf/Ms=0.15 | Kf/Ks=2

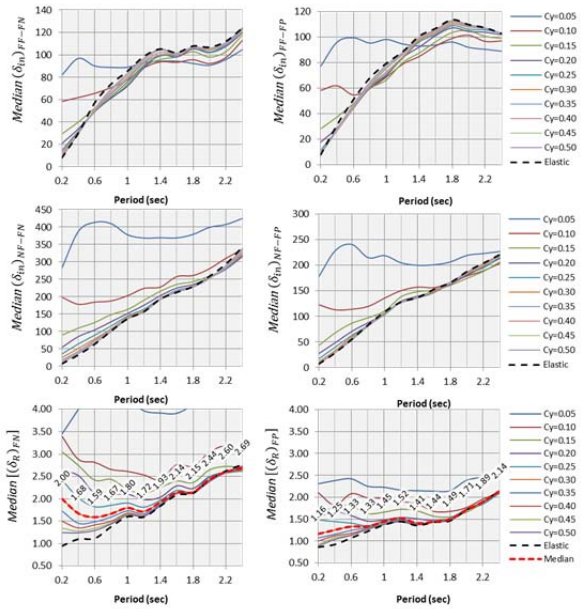

Figure B - 2: Median values of maximum displacement demands and inelastic displacement demand ratio (IDDR) In Terms of strength characteristics | Link:NLT#4 | ζ=%2.0 | EQL=1 | SYS#2 | Mf/Ms=0.15 | Kf/Ks=4

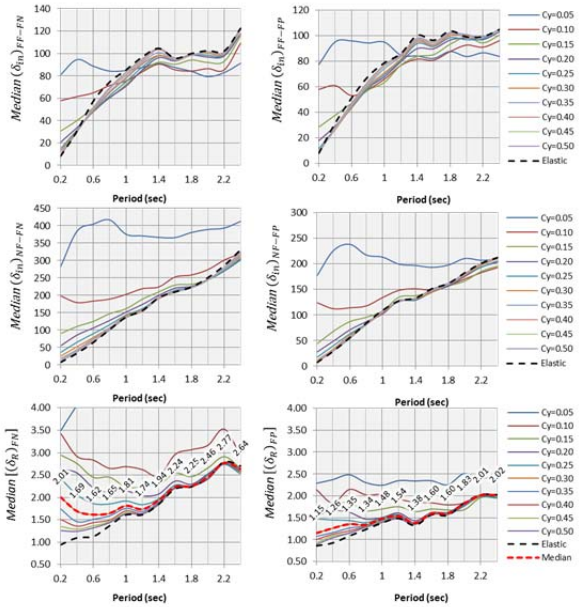

Figure B - 3: Median values of maximum displacement demands and inelastic displacement demand ratio (IDDR) In Terms of strength characteristics | Link:NLT#4 | ζ=%2.0 | EQL=1 | SYS#3 | Mf/Ms=0.25 | Kf/Ks=4

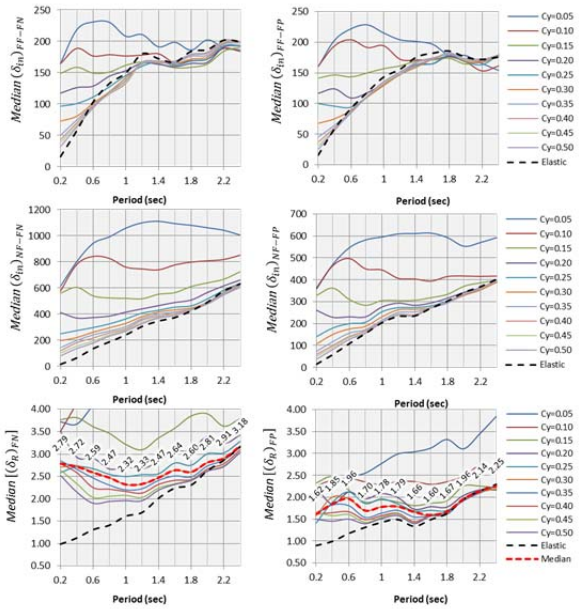

Figure B - 4: Median values of maximum displacement demands and inelastic displacement demand ratio (IDDR) In Terms of strength characteristics | Link:NLT#4 | ζ=%2.0 | EQL=2 | SYS#1 | Mf/Ms=0.15 | Kf/Ks=2

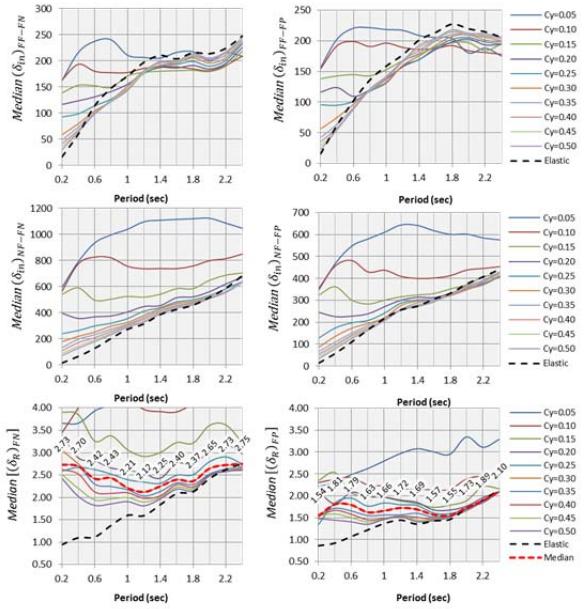

Figure B - 5: Median values of maximum displacement demands and inelastic displacement demand ratio (IDDR) In Terms of strength characteristics | Link:NLT#4 | ζ=%2.0 | EQL=2 | SYS#2 | Mf/Ms=0.15 | Kf/Ks=4

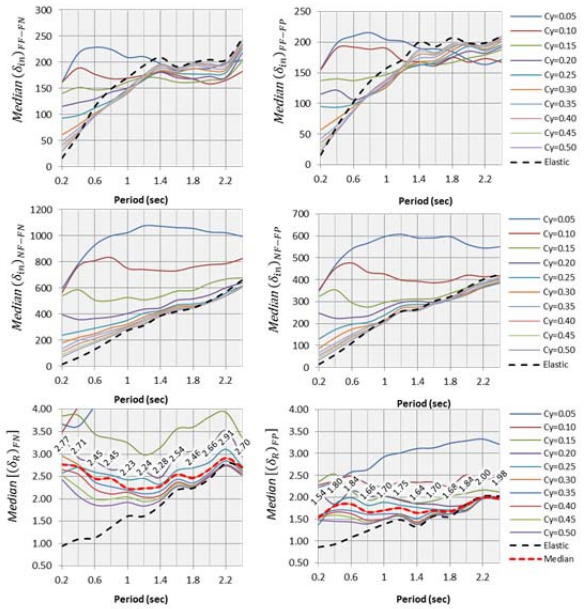

Figure B - 6: Median values of maximum displacement demands and inelastic displacement demand ratio (IDDR) In Terms of strength characteristics | Link:NLT#4 | ζ=%2.0 | EQL=2 | SYS#3 | Mf/Ms=0.25 | Kf/Ks=4

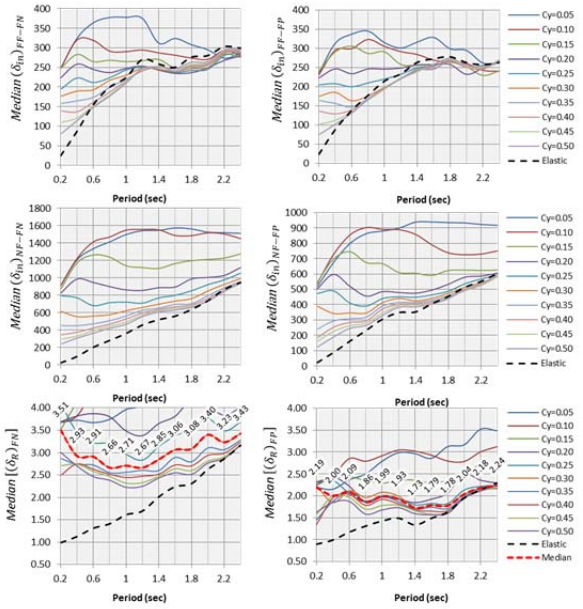

Figure B - 7: Median values of maximum displacement demands and inelastic displacement demand ratio (IDDR) In Terms of strength characteristics | Link:NLT#4 | ζ=%2.0 | EQL=3 | SYS#1 | Mf/Ms=0.15 | Kf/Ks=2

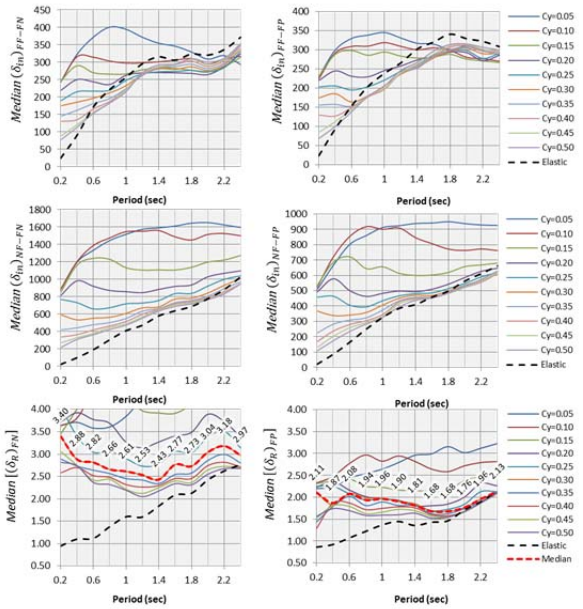

Figure B - 8: Median values of maximum displacement demands and inelastic displacement demand ratio (IDDR) In Terms of strength characteristics | Link:NLT#4 | ζ=%2.0 | EQL=3 | SYS#2 | Mf/Ms=0.15 | Kf/Ks=4

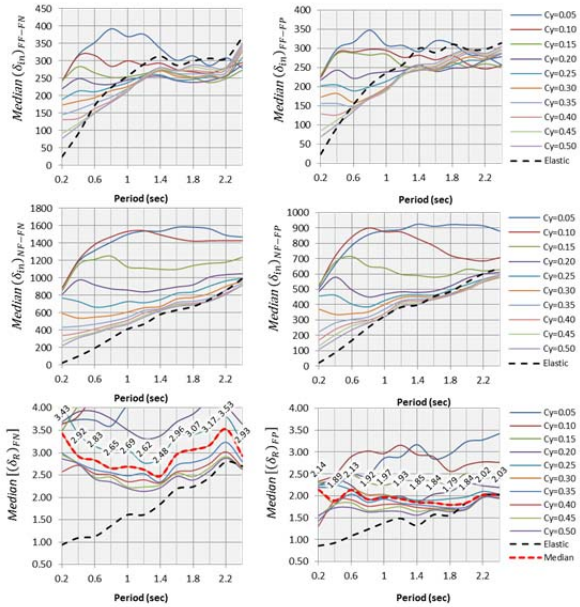

Figure B - 9: Median values of maximum displacement demands and inelastic displacement demand ratio (IDDR) In Terms of strength characteristics | Link:NLT#4 | ζ=%2.0 | EQL=3 | SYS#3 | Mf/Ms=0.25 | Kf/Ks=4

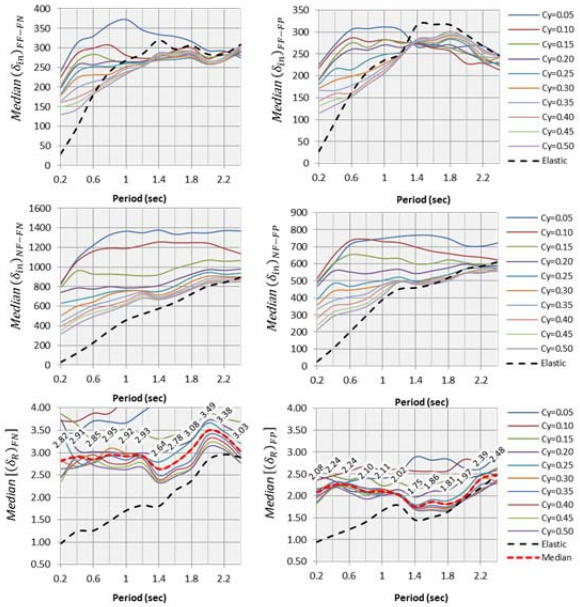

Figure B - 11: Median values of maximum displacement demands and inelastic displacement demand ratio (IDDR) In Terms of strength characteristics | Link:NLT#4 | ζ=%2.0 | EQL=4 | SYS#2 | Mf/Ms=0.15 | Kf/Ks=4

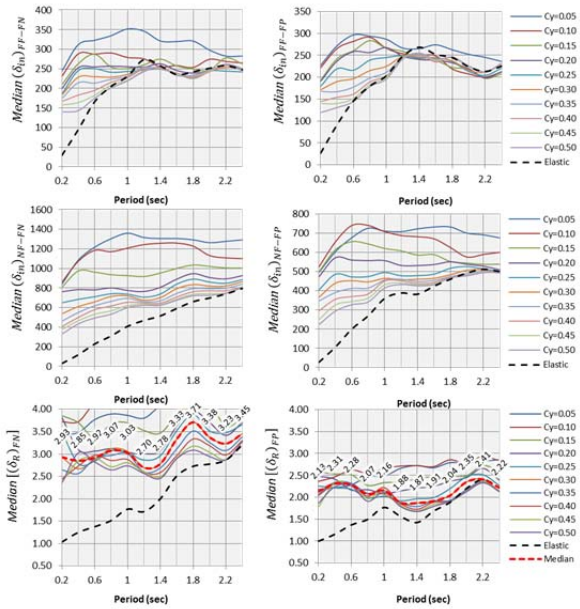

Figure B - 10: Median values of maximum displacement demands and inelastic displacement demand ratio (IDDR) In Terms of strength characteristics | Link:NLT#4 | ζ=%2.0 | EQL=4 | SYS#1 | Mf/Ms=0.15 | Kf/Ks=2

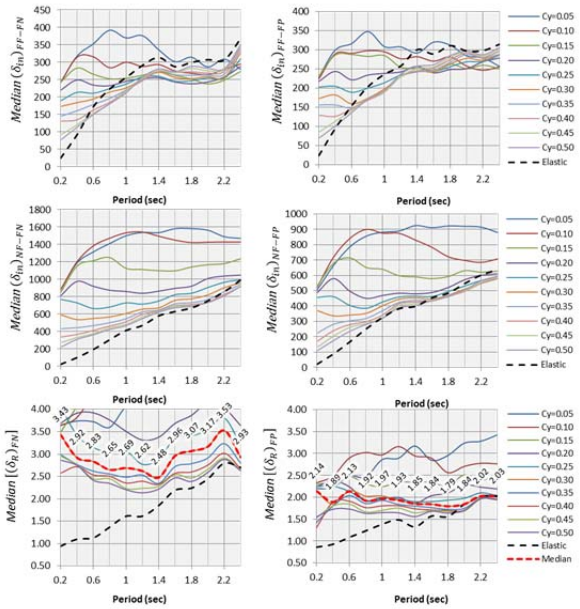

Figure B - 12: Median values of maximum displacement demands and inelastic displacement demand ratio (IDDR) In Terms of strength characteristics | Link:NLT#4 | ζ=%2.0 | EQL=4 | SYS#3 | Mf/Ms=0.25 | Kf/Ks=4

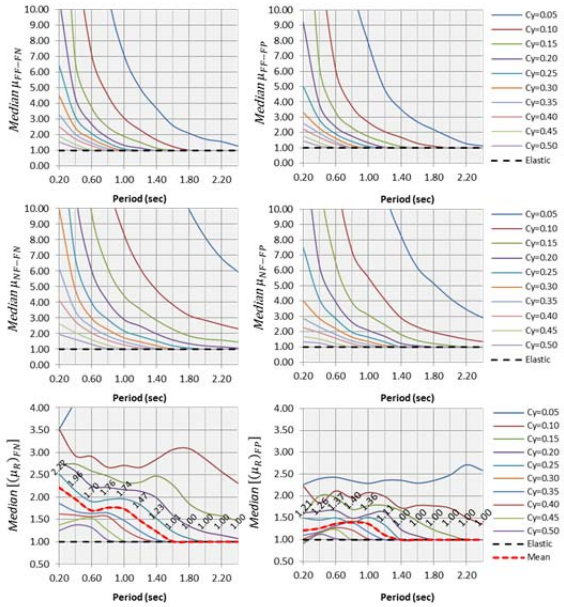

Figure B - 13: Median values of maximum ductility demand and ductility demand ratio (DDR) in Terms of strength characteristics | Link:NLT#4 | ζ=%2.0 | EQL=1 | SYS#1 | Mf/Ms=0.15 | Kf/Ks=2

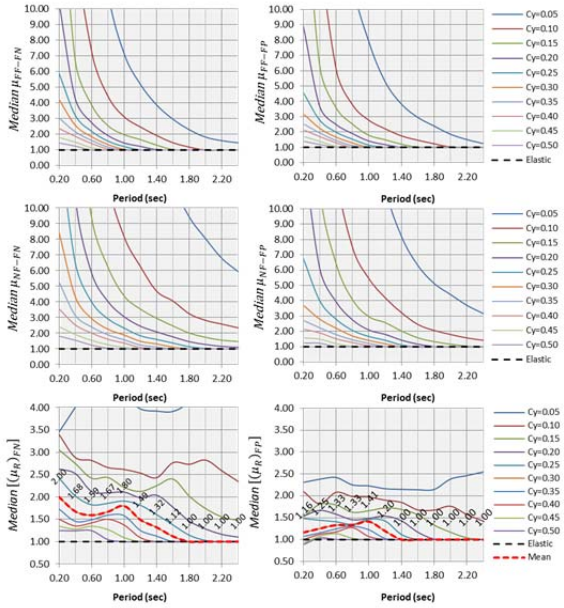

Figure B - 14: Median values of maximum ductility demand and ductility demand ratio (DDR) in Terms of strength characteristics | Link:NLT#4 | ζ=%2.0 | EQL=1 | SYS#2 | Mf/Ms=0.15 | Kf/Ks=4

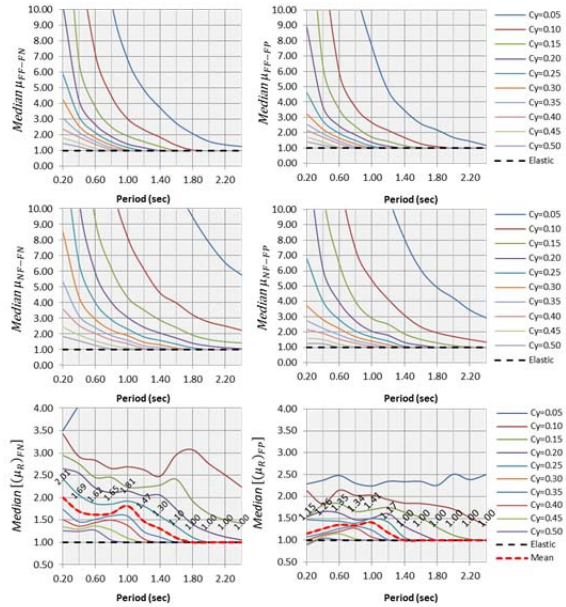

Figure B - 15: Median values of maximum ductility demand and ductility demand ratio (DDR) in Terms of strength characteristics | Link:NLT#4 | ζ=%2.0 | EQL=1 | SYS#3 | Mf/Ms=0.25 | Kf/Ks=4

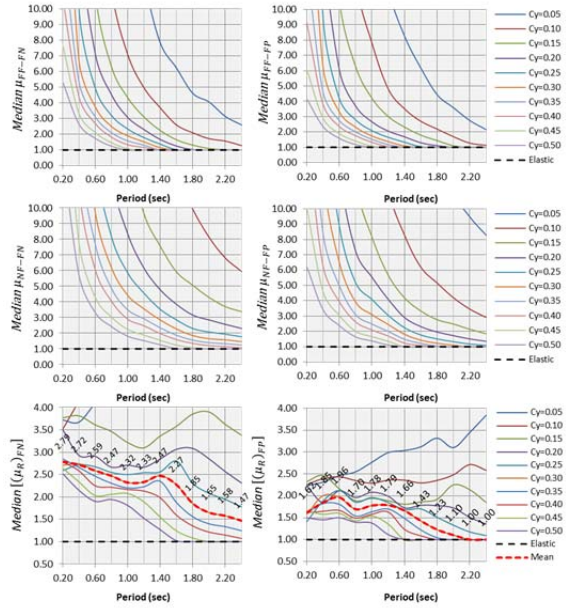

Figure B - 16: Median values of maximum ductility demand and ductility demand ratio (DDR) in Terms of strength characteristics | Link:NLT#4 | ζ=%2.0 | EQL=2 | SYS#1 | Mf/Ms=0.15 | Kf/Ks=2

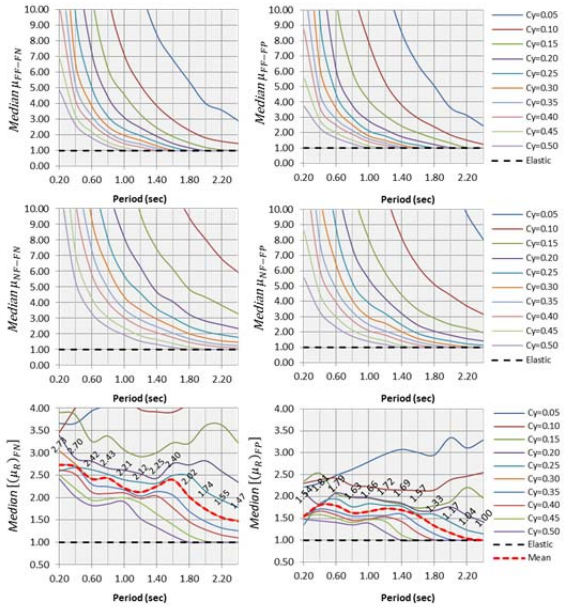

Figure B - 17: Median values of maximum ductility demand and ductility demand ratio (DDR) in Terms of strength characteristics | Link:NLT#4 | ζ=%2.0 | EQL=2 | SYS#2 | Mf/Ms=0.15 | Kf/Ks=4

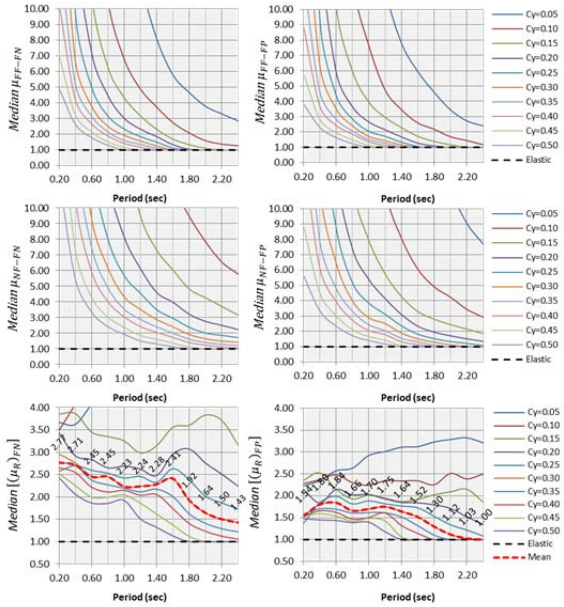

Figure B - 18: Median values of maximum ductility demand and ductility demand ratio (DDR) in Terms of strength characteristics | Link:NLT#4 | ζ=%2.0 | EQL=2 | SYS#3 | Mf/Ms=0.25 | Kf/Ks=4

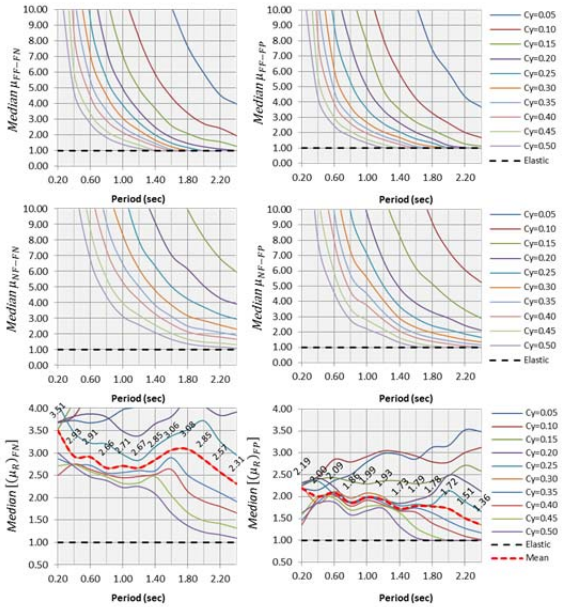

Figure B - 19: Median values of maximum ductility demand and ductility demand ratio (DDR) in Terms of strength characteristics | Link:NLT#4 | ζ=%2.0 | EQL=3 | SYS#1 | Mf/Ms=0.15 | Kf/Ks=2

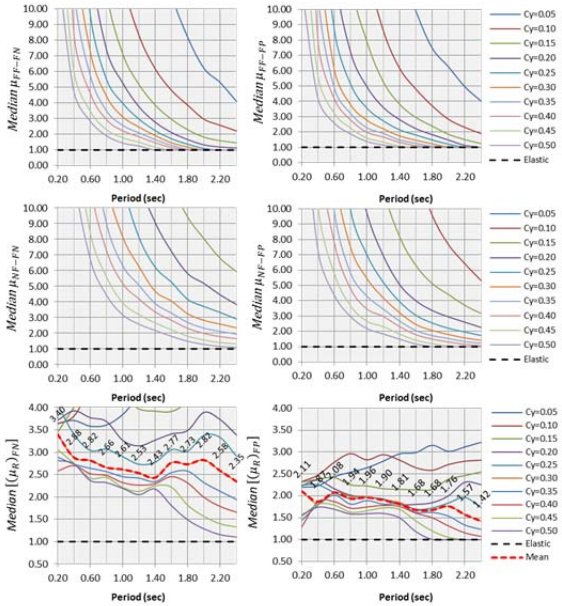

Figure B - 20: Median values of maximum ductility demand and ductility demand ratio (DDR) in Terms of strength characteristics | Link:NLT#4 | ζ=%2.0 | EQL=3 | SYS#2 | Mf/Ms=0.15 | Kf/Ks=4

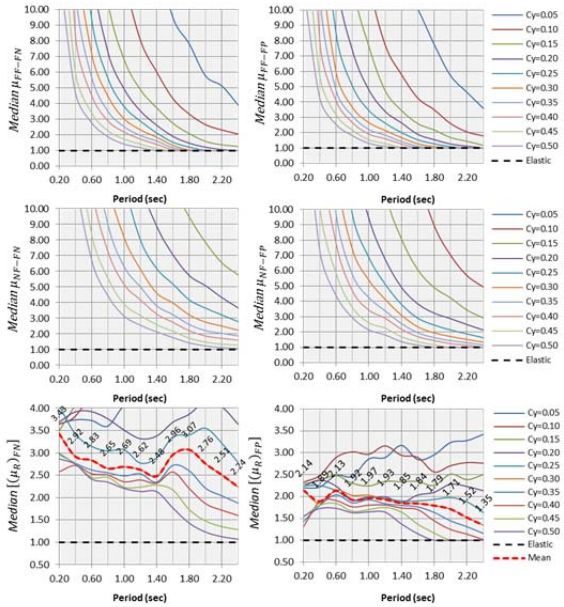

Figure B - 21: Median values of maximum ductility demand and ductility demand ratio (DDR) in Terms of strength characteristics | Link:NLT#4 | ζ=%2.0 | EQL=3 | SYS#3 | Mf/Ms=0.25 | Kf/Ks=4

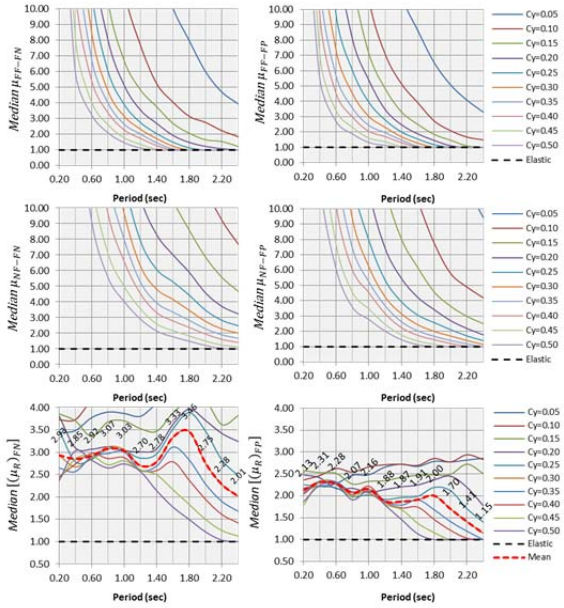

Figure B - 22: Median values of maximum ductility demand and ductility demand ratio (DDR) in Terms of strength characteristics | Link:NLT#4 | ζ=%2.0 | EQL=4 | SYS#1 | Mf/Ms=0.15 | Kf/Ks=2

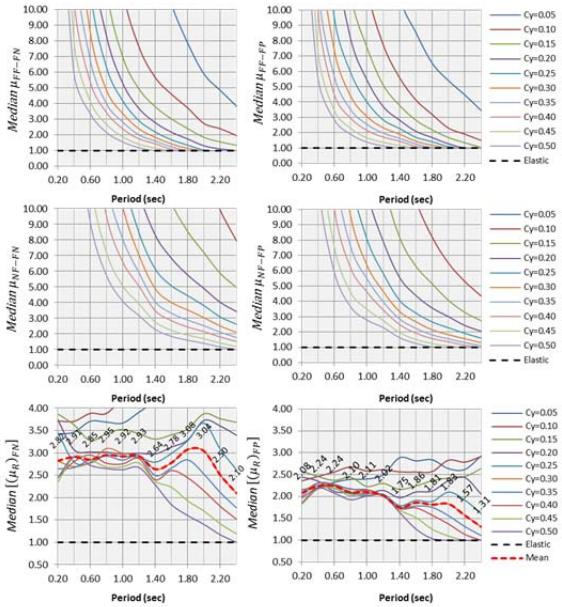

Figure B - 23: Median values of maximum ductility demand and ductility demand ratio (DDR) in Terms of strength characteristics | Link:NLT#4 | ζ=%2.0 | EQL=4 | SYS#2 | Mf/Ms=0.15 | Kf/Ks=4

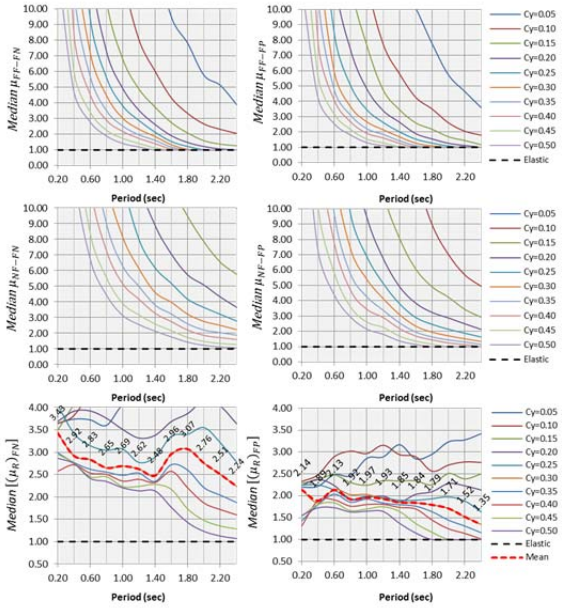

Figure B - 24: Median values of maximum ductility demand and ductility demand ratio (DDR) in Terms of strength characteristics | Link:NLT#4 | ζ=%2.0 | EQL=4 | SYS#3 | Mf/Ms=0.25 | Kf/Ks=4

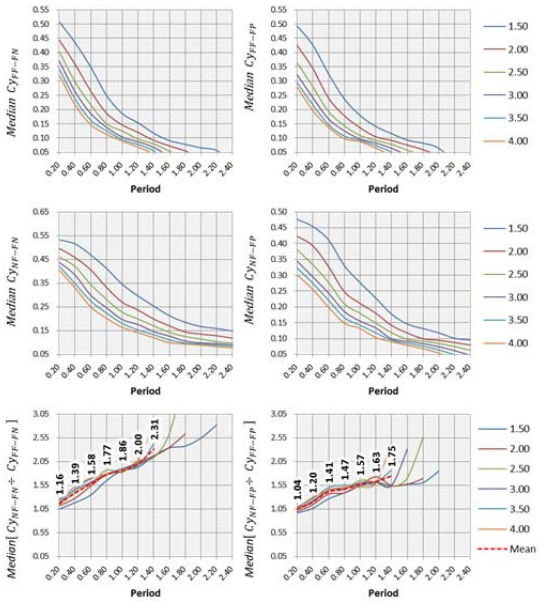

Figure B - 25: Median values of yield capacity demand and yield capacity demand ratio (YCDR) in Terms of target ductility | Link:NLT#4 | ζ=%2.0 | EQL=1 | SYS#1 | Mf/Ms=0.15 | Kf/Ks=2

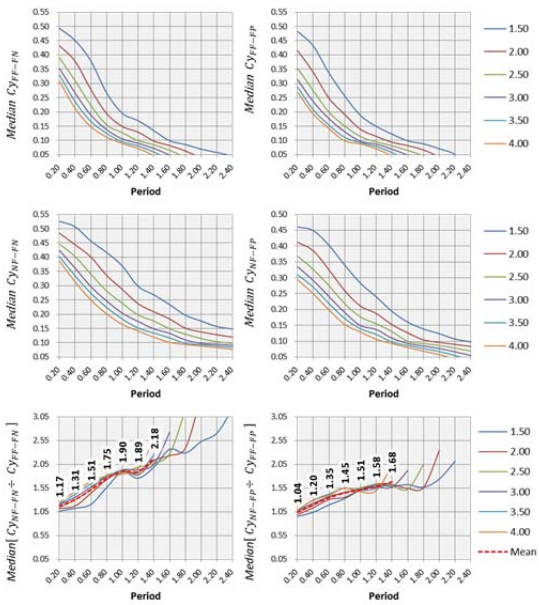

Figure B - 26: Median values of yield capacity demand and yield capacity demand ratio (YCDR) in Terms of target ductility | Link:NLT#4 | ζ=%2.0 | EQL=1 | SYS#2 | Mf/Ms=0.15 | Kf/Ks=4

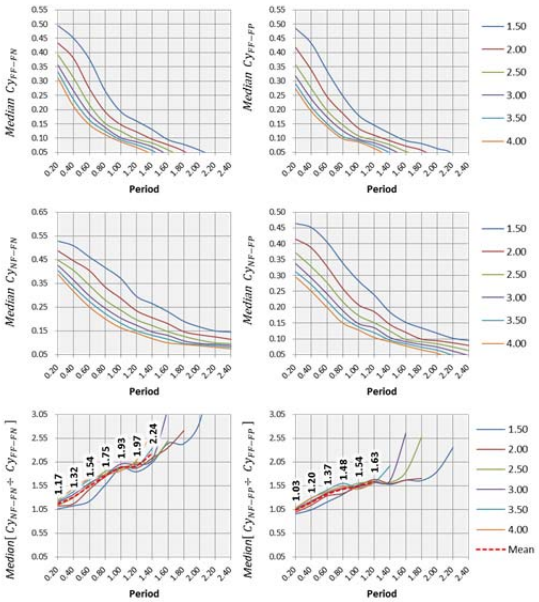

Figure B - 27: Median values of yield capacity demand and yield capacity demand ratio (YCDR) in Terms of target ductility | Link:NLT#4 | ζ=%2.0 | EQL=1 | SYS#3 | Mf/Ms=0.25 | Kf/Ks=4

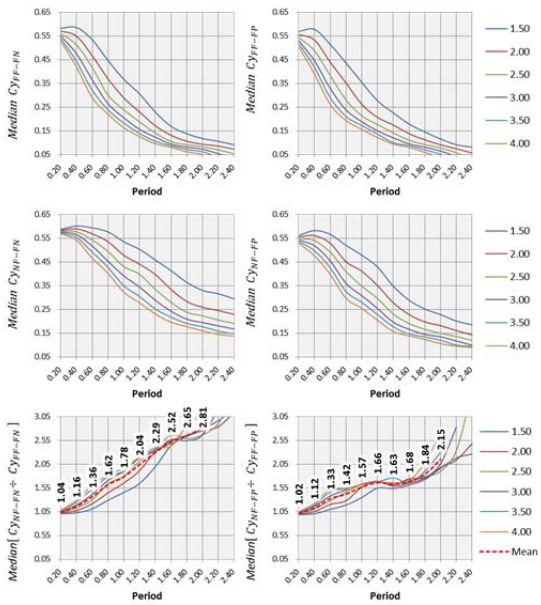

Figure B - 28: Median values of yield capacity demand and yield capacity demand ratio (YCDR) in Terms of target ductility | Link:NLT#4 | ζ=%2.0 | EQL=2 | SYS#1 | Mf/Ms=0.15 | Kf/Ks=2

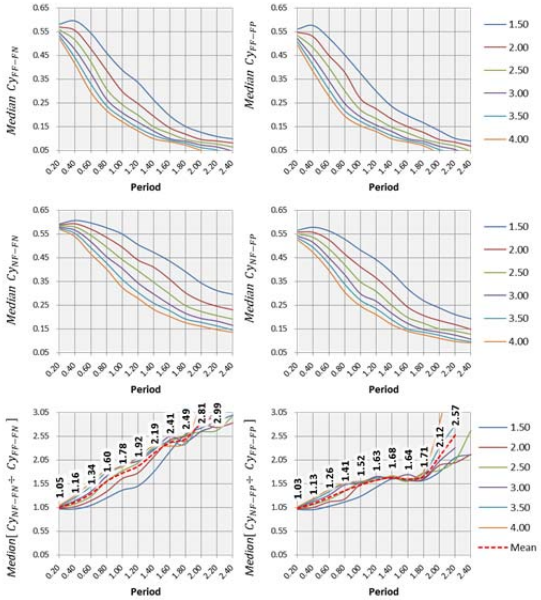

Figure B - 29: Median values of yield capacity demand and yield capacity demand ratio (YCDR) in Terms of target ductility | Link:NLT#4 | ζ=%2.0 | EQL=2 | SYS#2 | Mf/Ms=0.15 | Kf/Ks=4

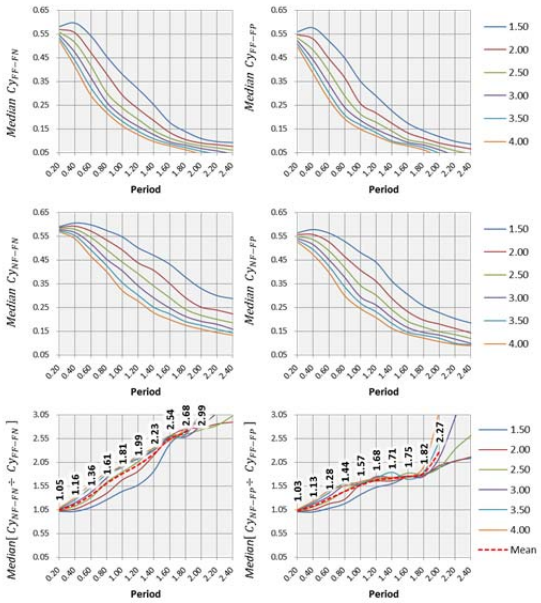

Figure B - 30: Median values of yield capacity demand and yield capacity demand ratio (YCDR) in Terms of target ductility | Link:NLT#4 | ζ=%2.0 | EQL=2 | SYS#3 | Mf/Ms=0.25 | Kf/Ks=4

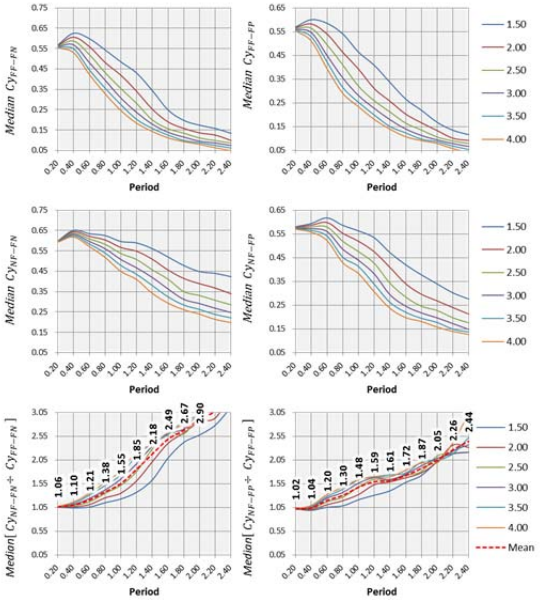

Figure B - 31: Median values of yield capacity demand and yield capacity demand ratio (YCDR) in Terms of target ductility | Link:NLT#4 | ζ=%2.0 | EQL=3 | SYS#1 | Mf/Ms=0.15 | Kf/Ks=2

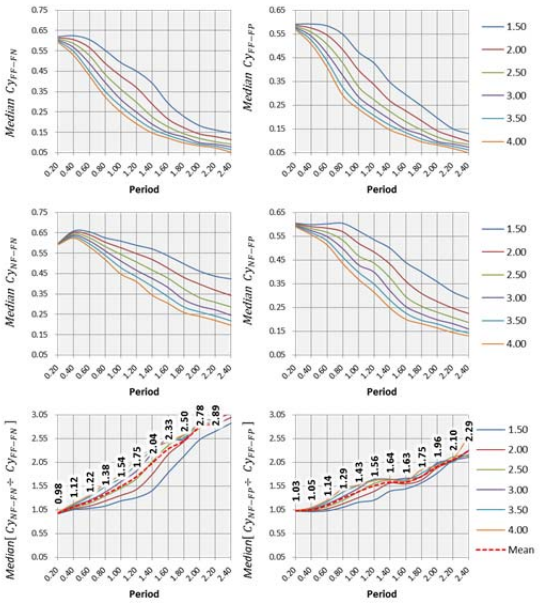

Figure B - 32: Median values of yield capacity demand and yield capacity demand ratio (YCDR) in Terms of target ductility | Link:NLT#4 | ζ=%2.0 | EQL=3 | SYS#2 | Mf/Ms=0.15 | Kf/Ks=4

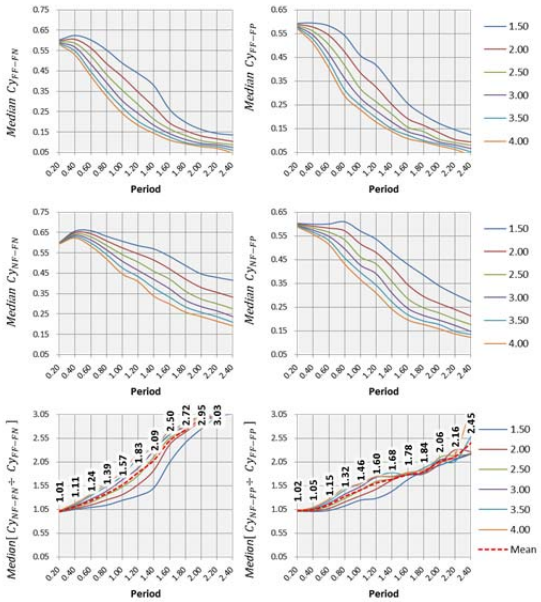

Figure B - 33: Median values of yield capacity demand and yield capacity demand ratio (YCDR) in Terms of target ductility | Link:NLT#4 | ζ=%2.0 | EQL=3 | SYS#3 | Mf/Ms=0.25 | Kf/Ks=4

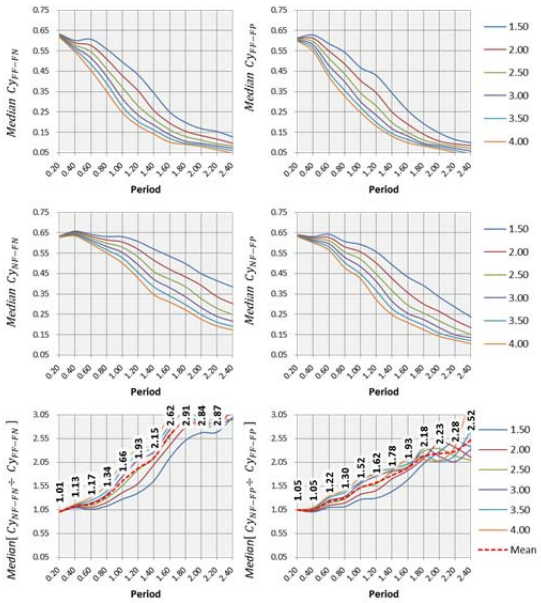

Figure B - 34: Median values of yield capacity demand and yield capacity demand ratio (YCDR) in Terms of target ductility | Link:NLT#4 | ζ=%2.0 | EQL=4 | SYS#1 | Mf/Ms=0.15 | Kf/Ks=2

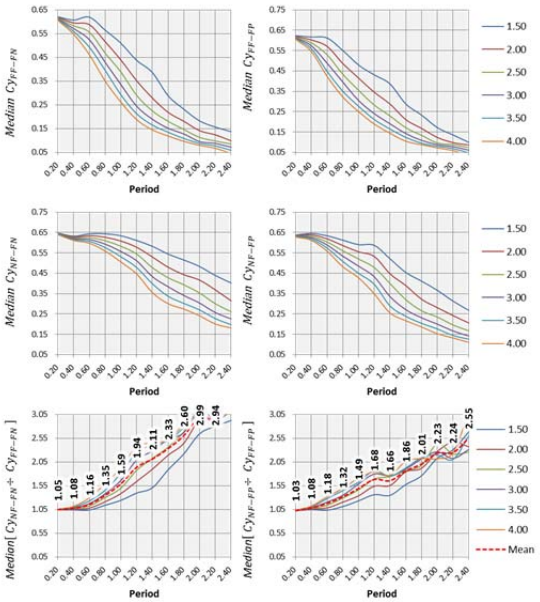

Figure B - 35: Median values of yield capacity demand and yield capacity demand ratio (YCDR) in Terms of target ductility | Link:NLT#4 | ζ=%2.0 | EQL=4 | SYS#2 | Mf/Ms=0.15 | Kf/Ks=4

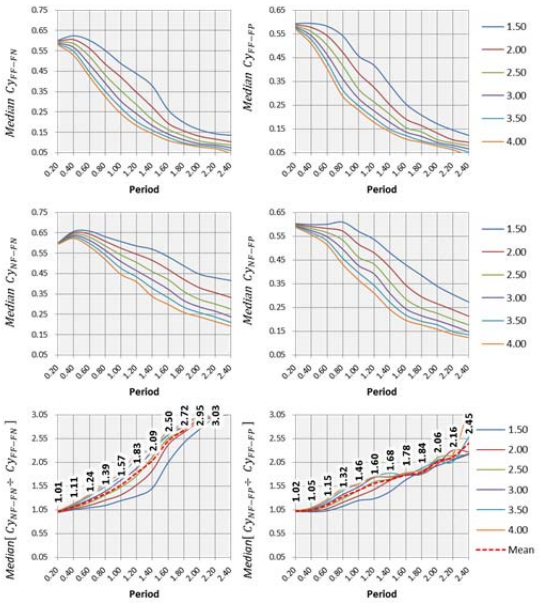

Figure B - 36: Median values of yield capacity demand and yield capacity demand ratio (YCDR) in Terms of target ductility | Link:NLT#4 | ζ=%2.0 | EQL=4 | SYS#3 | Mf/Ms=0.25 | Kf/Ks=4

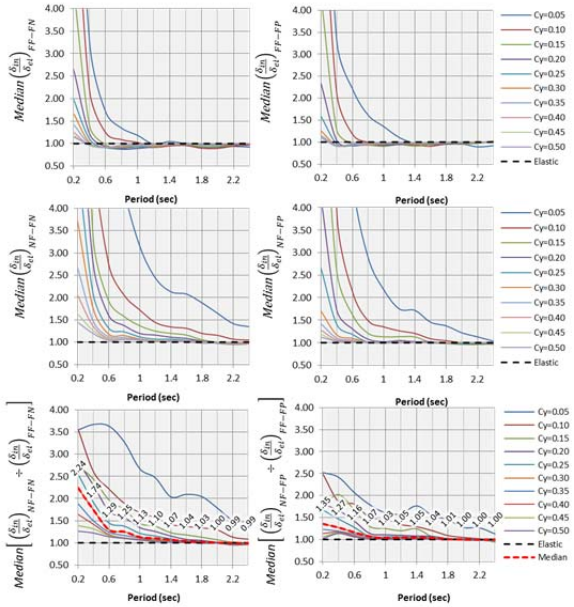

Figure B - 37: Median values of maximum inelastic to elastic displacement demand and maximum inelastic to elastic displacement demand ratio in terms of strength characteristics | Link:NLT#4 | ζ=%2.0 | EQL=1 | SYS#1 | Mf/Ms=0.15 | Kf/Ks=2

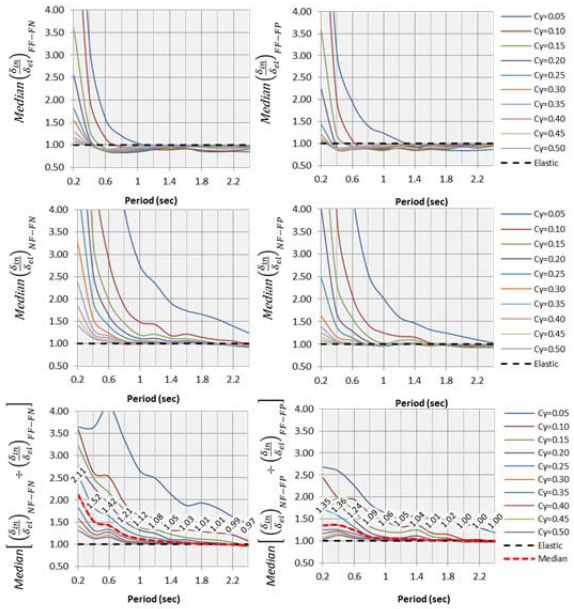

Figure B - 38: Median values of maximum inelastic to elastic displacement demand and maximum inelastic to elastic displacement demand ratio in terms of strength characteristics | Link:NLT#4 | ζ=%2.0 | EQL=1 | SYS#2 | Mf/Ms=0.15 | Kf/Ks=4

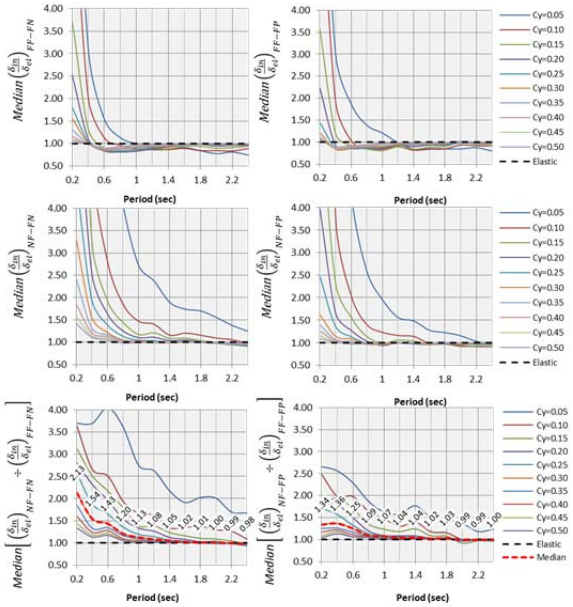

Figure B - 39: Median values of maximum inelastic to elastic displacement demand and maximum inelastic to elastic displacement demand ratio in terms of strength characteristics | Link:NLT#4 | ζ=%2.0 | EQL=1 | SYS#3 | Mf/Ms=0.25 | Kf/Ks=4

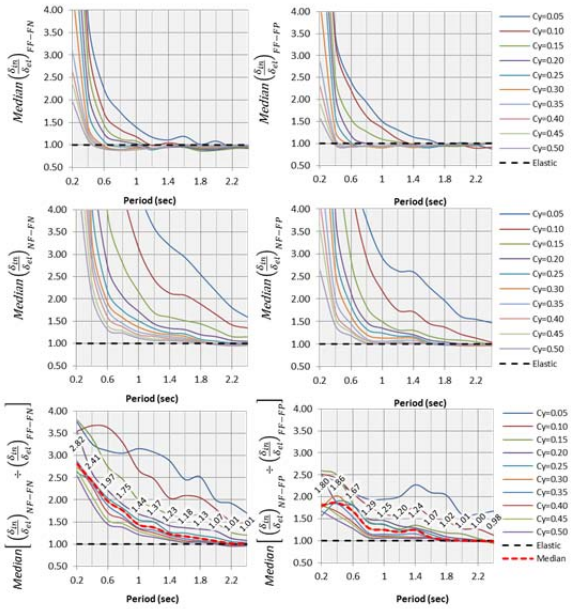

Figure B - 40: Median values of maximum inelastic to elastic displacement demand and maximum inelastic to elastic displacement demand ratio in terms of strength characteristics | Link:NLT#4 | ζ=%2.0 | EQL=2 | SYS#1 | Mf/Ms=0.15 | Kf/Ks=2

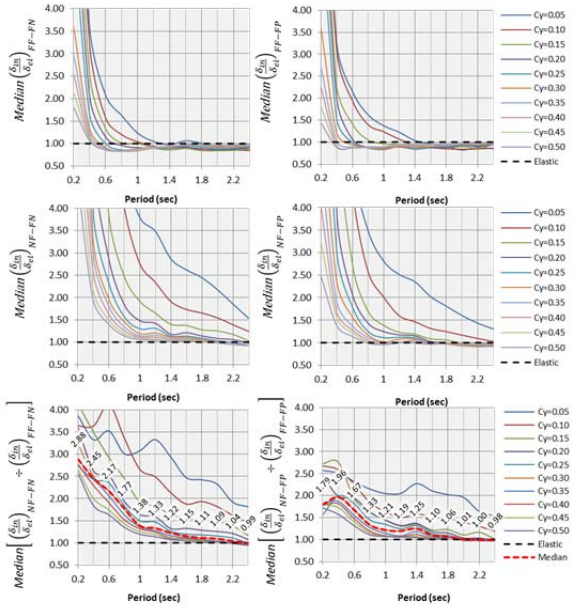

Figure B - 41: Median values of maximum inelastic to elastic displacement demand and maximum inelastic to elastic displacement demand ratio in terms of strength characteristics | Link:NLT#4 | ζ=%2.0 | EQL=2 | SYS#2 | Mf/Ms=0.15 | Kf/Ks=4

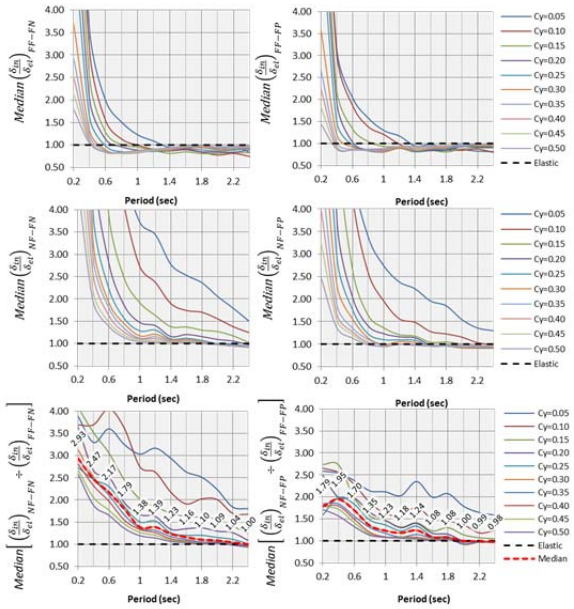

Figure B - 42: Median values of maximum inelastic to elastic displacement demand and maximum inelastic to elastic displacement demand ratio in terms of strength characteristics | Link:NLT#4 | ζ=%2.0 | EQL=2 | SYS#3 | Mf/Ms=0.25 | Kf/Ks=4

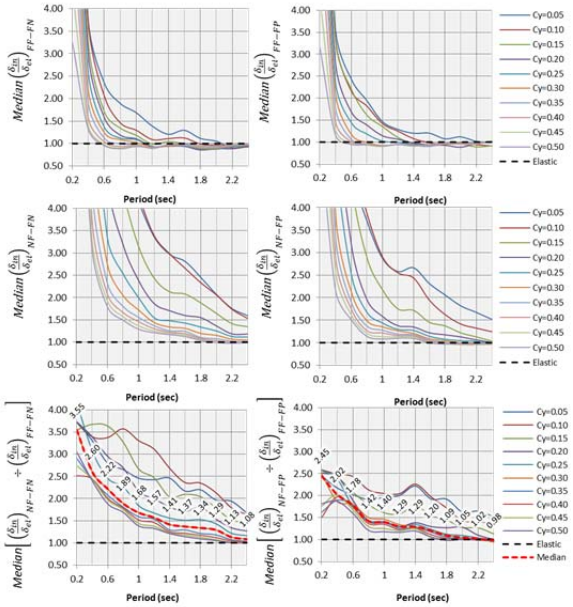

Figure B - 43: Median values of maximum inelastic to elastic displacement demand and maximum inelastic to elastic displacement demand ratio in terms of strength characteristics | Link:NLT#4 | ζ=%2.0 | EQL=3 | SYS#1 | Mf/Ms=0.15 | Kf/Ks=2

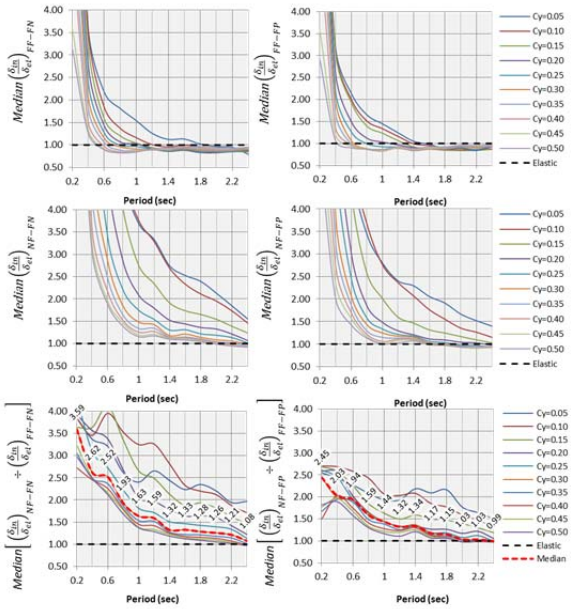

Figure B - 44: Median values of maximum inelastic to elastic displacement demand and maximum inelastic to elastic displacement demand ratio in terms of strength characteristics | Link:NLT#4 | ζ=%2.0 | EQL=3 | SYS#2 | Mf/Ms=0.15 | Kf/Ks=4

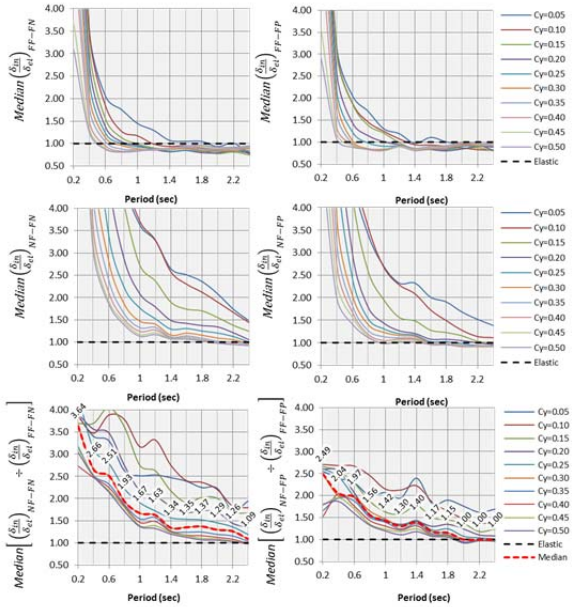

Figure B - 45: Median values of maximum inelastic to elastic displacement demand and maximum inelastic to elastic displacement demand ratio in terms of strength characteristics | Link:NLT#4 | ζ=%2.0 | EQL=3 | SYS#3 | Mf/Ms=0.25 | Kf/Ks=4

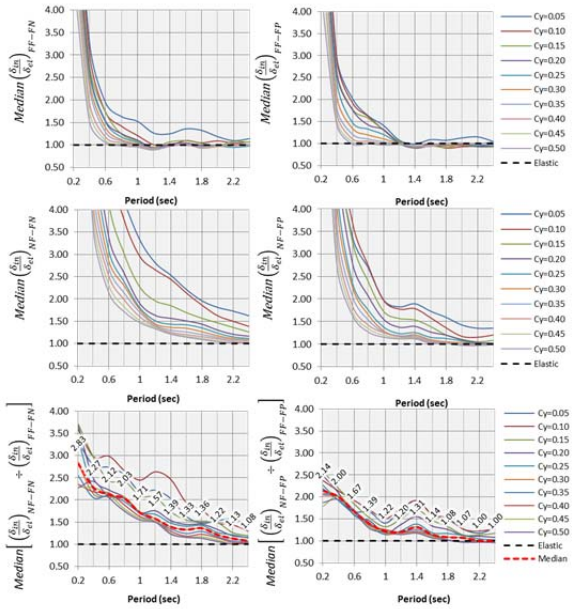

Figure B - 46: Median values of maximum inelastic to elastic displacement demand and maximum inelastic to elastic displacement demand ratio in terms of strength characteristics | Link:NLT#4 | ζ=%2.0 | EQL=4 | SYS#1 | Mf/Ms=0.15 | Kf/Ks=2

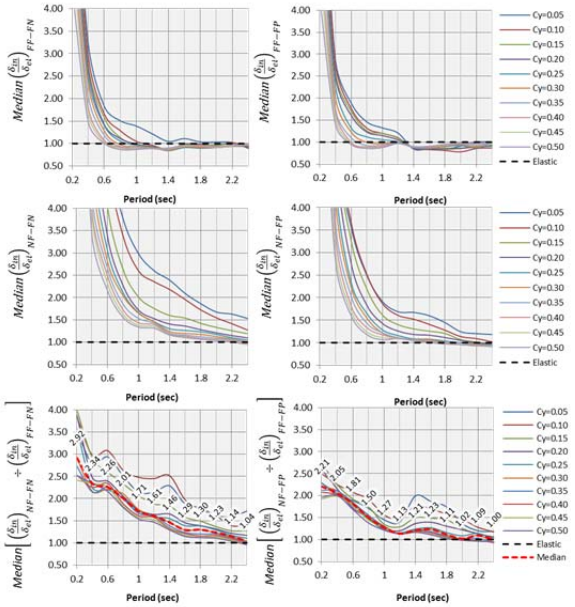

Figure B - 47: Median values of maximum inelastic to elastic displacement demand and maximum inelastic to elastic displacement demand ratio in terms of strength characteristics | Link:NLT#4 | ζ=%2.0 | EQL=4 | SYS#2 | Mf/Ms=0.15 | Kf/Ks=4

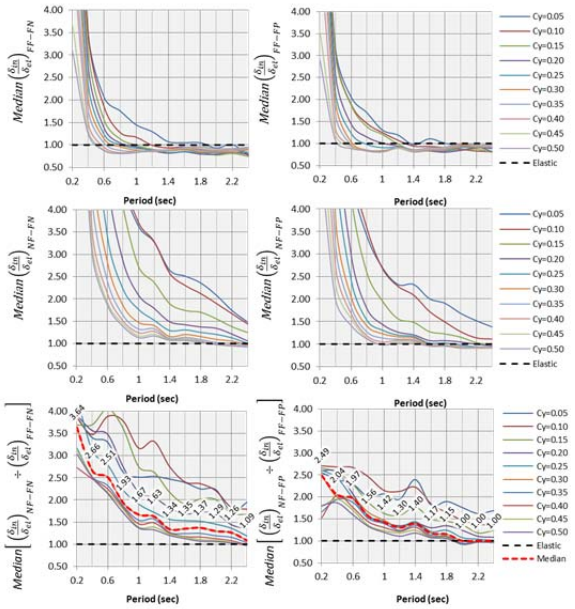

Figure B - 48: Median values of maximum inelastic to elastic displacement demand and maximum inelastic to elastic displacement demand ratio in terms of strength characteristics | Link:NLT#4 | ζ=%2.0 | EQL=4 | SYS#3 | Mf/Ms=0.25 | Kf/Ks=4

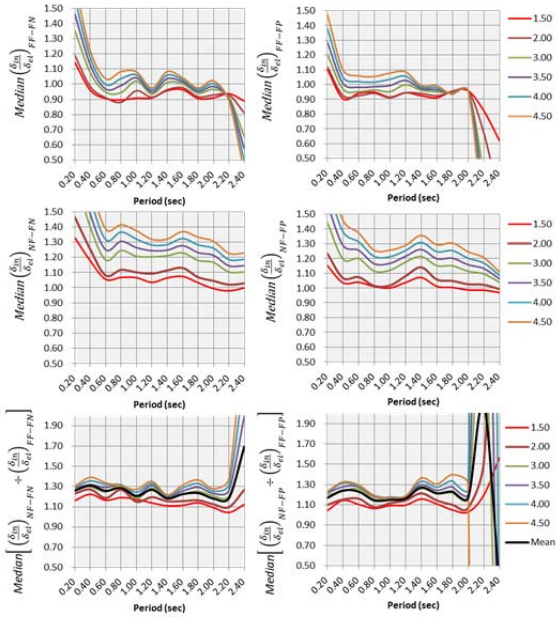

Figure B - 49:Median Values of “Maximum Inelastic To Elastic Displacement Demand” and “Maximum Inelastic To Elastic Displacement Demand Ratio” | Link:NLT#4 | ζ=%2.0 | EQL=1 | SYS#1 | Mf/Ms=0.15 | Kf/Ks=2

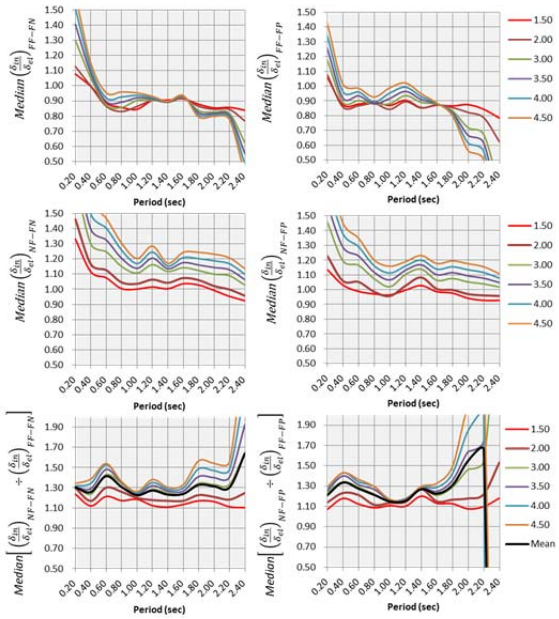

Figure B - 50:Median Values of “Maximum Inelastic To Elastic Displacement Demand” and “Maximum Inelastic To Elastic Displacement Demand Ratio” | Link:NLT#4 | ζ=%2.0 | EQL=1 | SYS#2 | Mf/Ms=0.15 | Kf/Ks=4

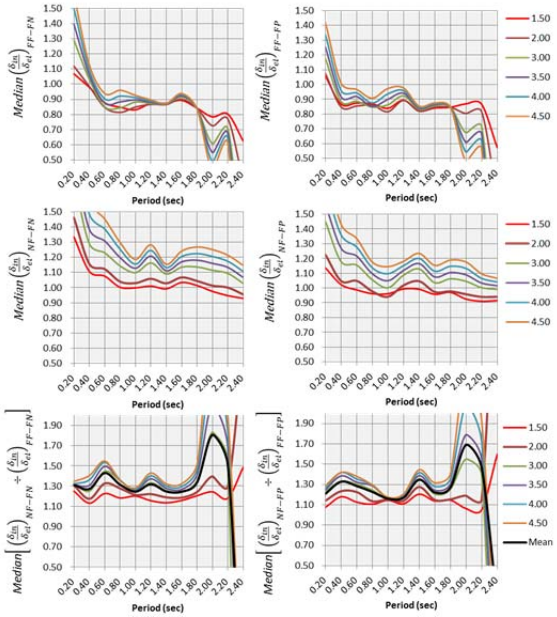

Figure B - 51:Median Values of “Maximum Inelastic To Elastic Displacement Demand” and “Maximum Inelastic To Elastic Displacement Demand Ratio” | Link:NLT#4 | ζ=%2.0 | EQL=1 | SYS#3 | Mf/Ms=0.25 | Kf/Ks=4

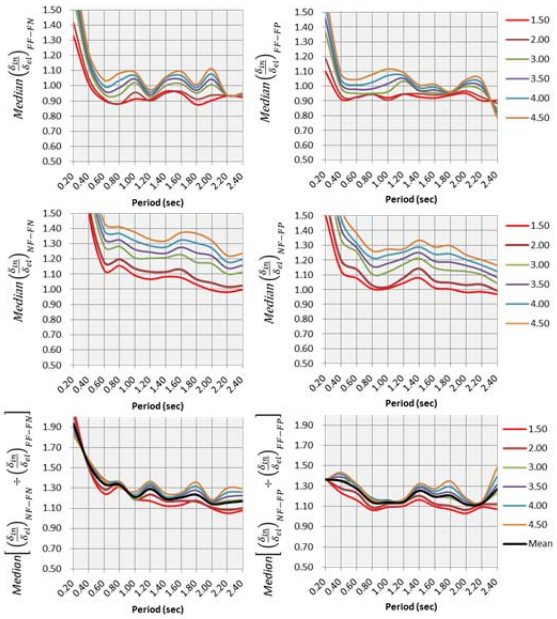

Figure B - 52:Median Values of “Maximum Inelastic To Elastic Displacement Demand” and “Maximum Inelastic To Elastic Displacement Demand Ratio” | Link:NLT#4 | ζ=%2.0 | EQL=2 | SYS#1 | Mf/Ms=0.15 | Kf/Ks=2

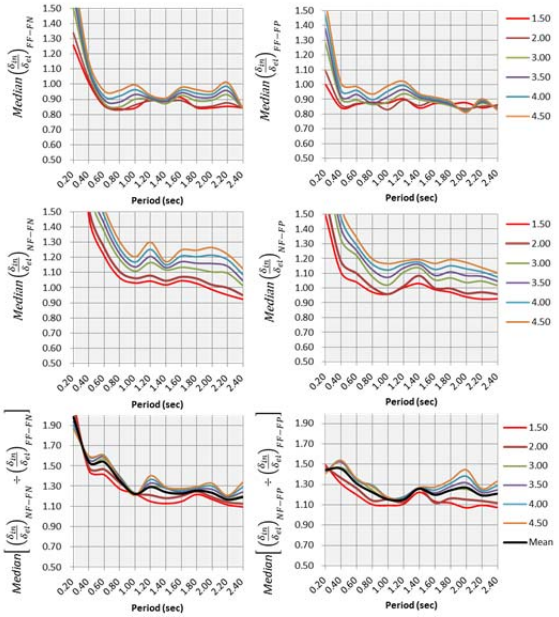

Figure B - 53:Median Values of “Maximum Inelastic To Elastic Displacement Demand” and “Maximum Inelastic To Elastic Displacement Demand Ratio” | Link:NLT#4 | ζ=%2.0 | EQL=2 | SYS#2 | Mf/Ms=0.15 | Kf/Ks=4

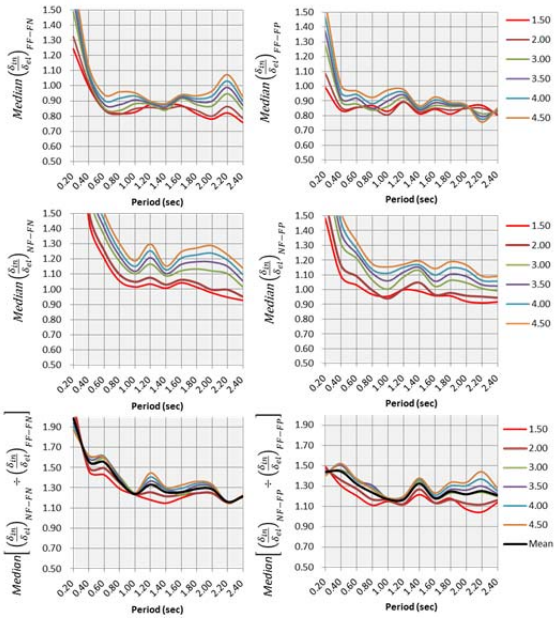

Figure B - 54:Median Values of “Maximum Inelastic To Elastic Displacement Demand” and “Maximum Inelastic To Elastic Displacement Demand Ratio” | Link:NLT#4 | ζ=%2.0 | EQL=2 | SYS#3 | Mf/Ms=0.25 | Kf/Ks=4

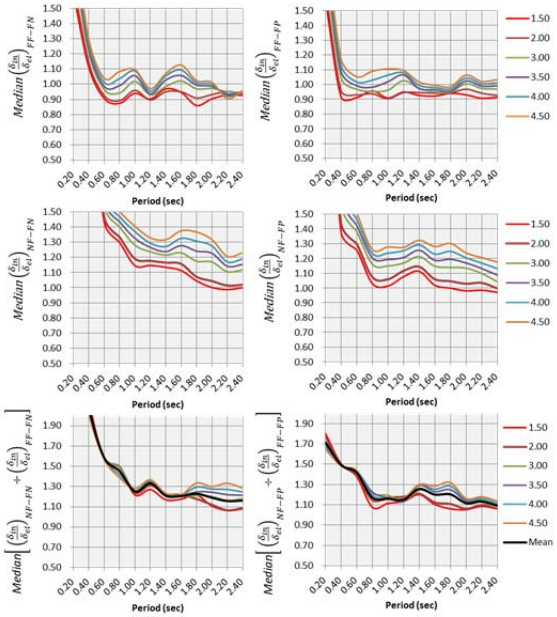

Figure B - 55:Median Values of “Maximum Inelastic To Elastic Displacement Demand” and “Maximum Inelastic To Elastic Displacement Demand Ratio” | Link:NLT#4 | ζ=%2.0 | EQL=3 | SYS#1 | Mf/Ms=0.15 | Kf/Ks=2

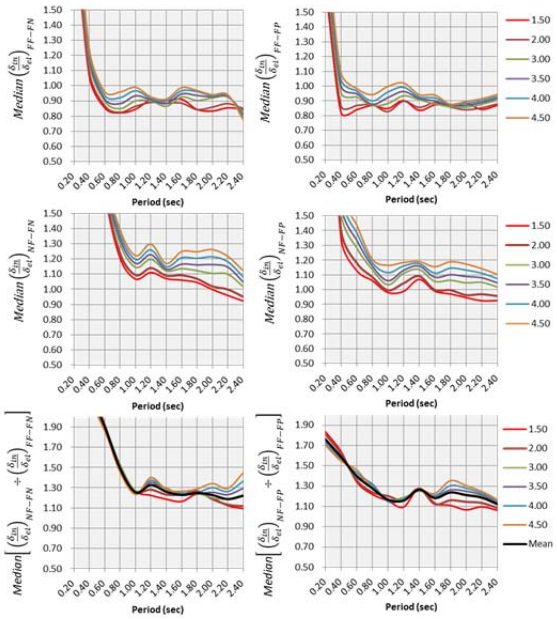

Figure B - 56:Median Values of “Maximum Inelastic To Elastic Displacement Demand” and “Maximum Inelastic To Elastic Displacement Demand Ratio” | Link:NLT#4 | ζ=%2.0 | EQL=3 | SYS#2 | Mf/Ms=0.15 | Kf/Ks=4

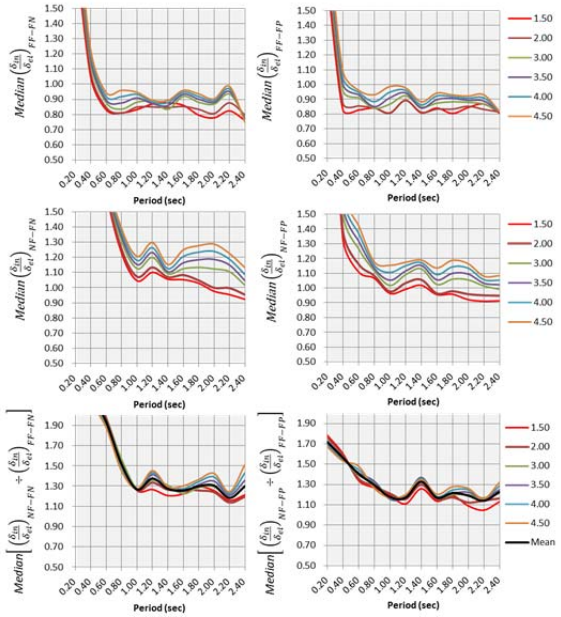

Figure B - 57:Median Values of “Maximum Inelastic To Elastic Displacement Demand” and “Maximum Inelastic To Elastic Displacement Demand Ratio” | Link:NLT#4 | ζ=%2.0 | EQL=3 | SYS#3 | Mf/Ms=0.25 | Kf/Ks=4

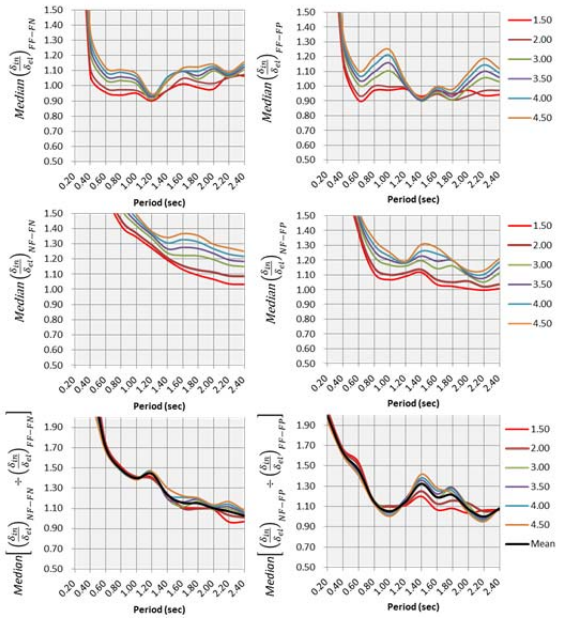

Figure B - 58:Median Values of “Maximum Inelastic To Elastic Displacement Demand” and “Maximum Inelastic To Elastic Displacement Demand Ratio” | Link:NLT#4 | ζ=%2.0 | EQL=4 | SYS#1 | Mf/Ms=0.15 | Kf/Ks=2

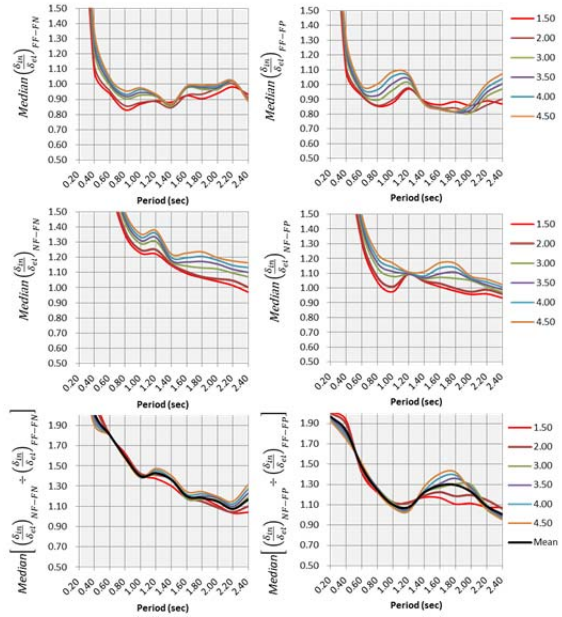

Figure B - 59:Median Values of “Maximum Inelastic To Elastic Displacement Demand” and “Maximum Inelastic To Elastic Displacement Demand Ratio” | Link:NLT#4 | ζ=%2.0 | EQL=4 | SYS#2 | Mf/Ms=0.15 | Kf/Ks=4

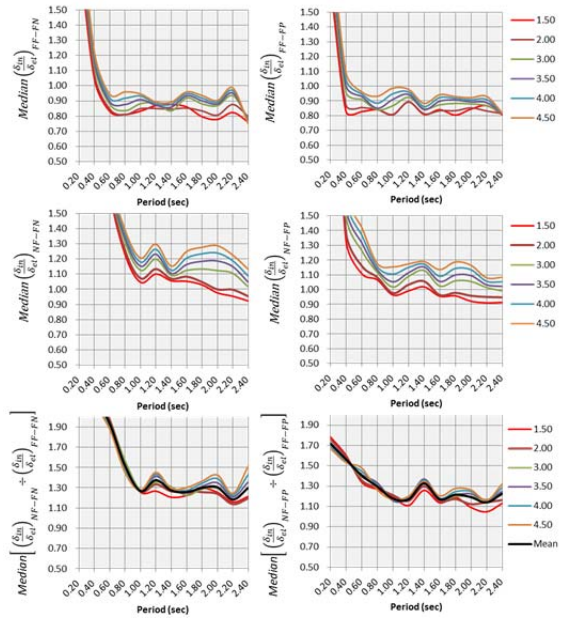

Figure B - 60:Median Values of “Maximum Inelastic To Elastic Displacement Demand” and “Maximum Inelastic To Elastic Displacement Demand Ratio” | Link:NLT#4 | ζ=%2.0 | EQL=4 | SYS#3 | Mf/Ms=0.25 | Kf/Ks=4

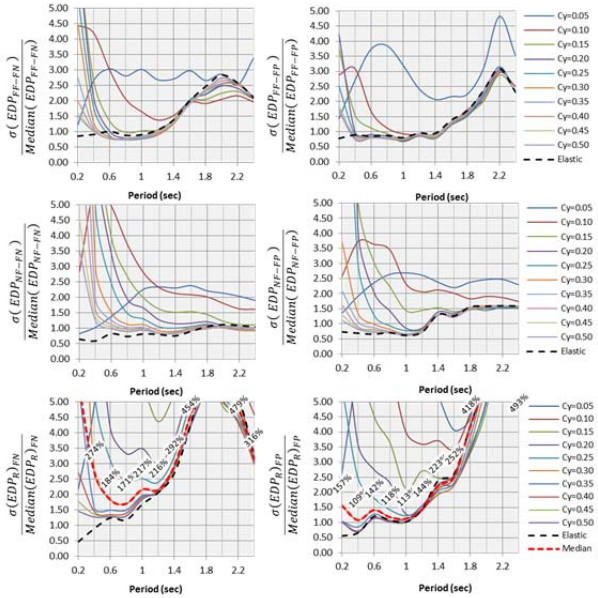

Figure B - 61:COV Values of “EDP” and “IEDP Ratio” In Terms of strength characteristics | Link:NLT#4 | ζ=%2.0 | EQL=1 | SYS#1 | Mf/Ms=0.15 | Kf/Ks=2

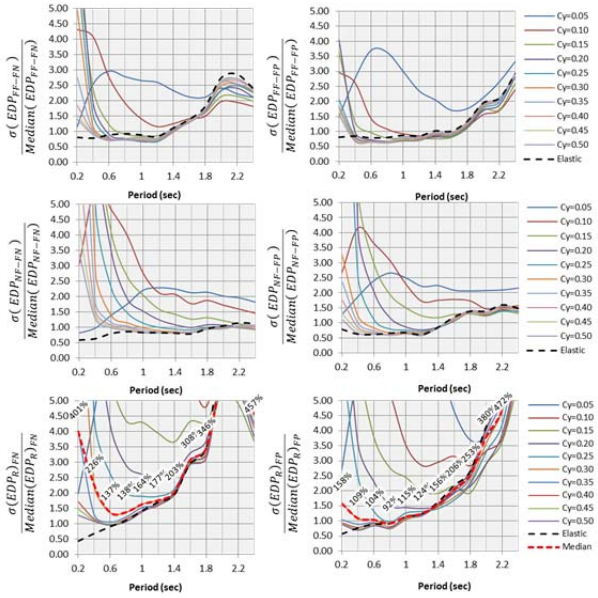

Figure B - 62:COV Values of “EDP” and “IEDP Ratio” In Terms of strength characteristics | Link:NLT#4 | ζ=%2.0 | EQL=1 | SYS#2 | Mf/Ms=0.15 | Kf/Ks=4

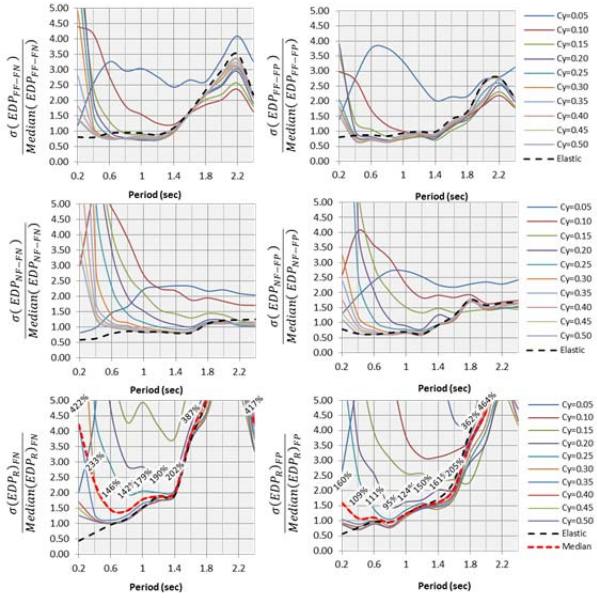

Figure B - 63:COV Values of “EDP” and “IEDP Ratio” In Terms of strength characteristics | Link:NLT#4 | ζ=%2.0 | EQL=1 | SYS#3 | Mf/Ms=0.25 | Kf/Ks=4

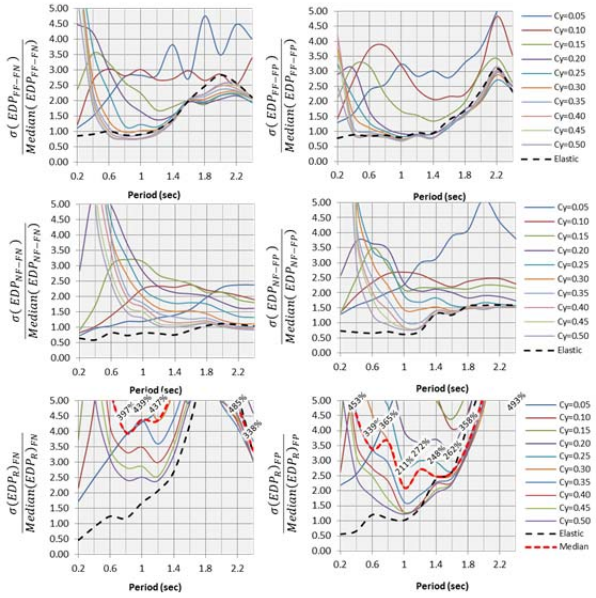

Figure B - 64:COV Values of “EDP” and “IEDP Ratio” In Terms of strength characteristics | Link:NLT#4 | ζ=%2.0 | EQL=2 | SYS#1 | Mf/Ms=0.15 | Kf/Ks=2

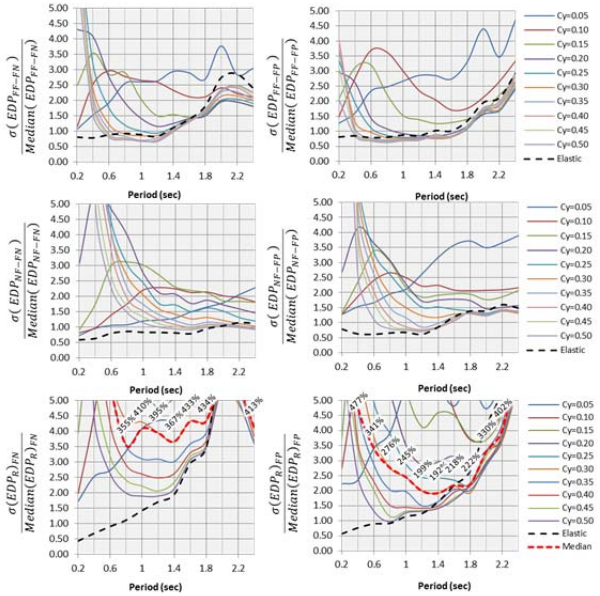

Figure B - 65:COV Values of “EDP” and “IEDP Ratio” In Terms of strength characteristics | Link:NLT#4 | ζ=%2.0 | EQL=2 | SYS#2 | Mf/Ms=0.15 | Kf/Ks=4

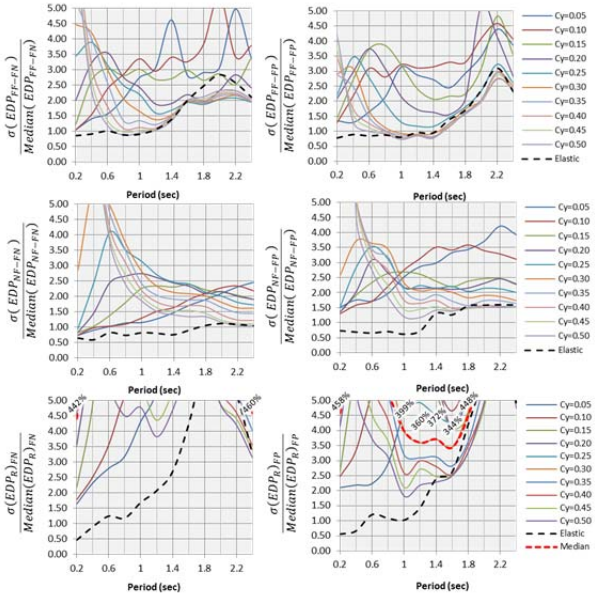

Figure B - 67:COV Values of “EDP” and “IEDP Ratio” In Terms of strength characteristics | Link:NLT#4 | ζ=%2.0 | EQL=3 | SYS#1 | Mf/Ms=0.15 | Kf/Ks=2

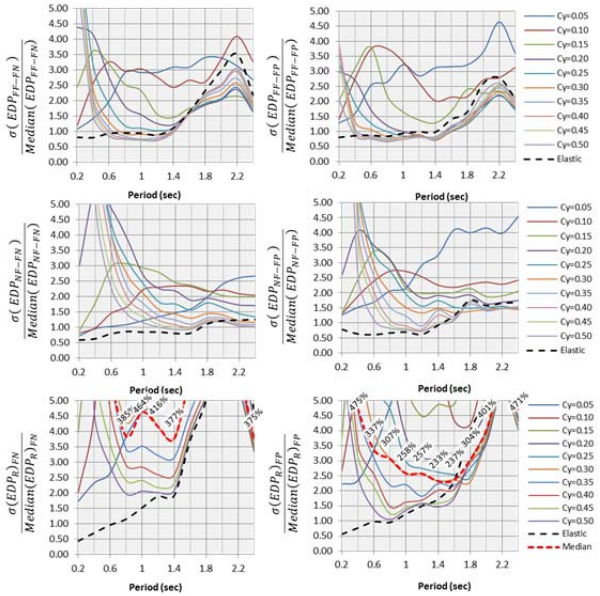

Figure B - 66:COV Values of “EDP” and “IEDP Ratio” In Terms of strength characteristics | Link:NLT#4 | ζ=%2.0 | EQL=2 | SYS#3 | Mf/Ms=0.25 | Kf/Ks=4

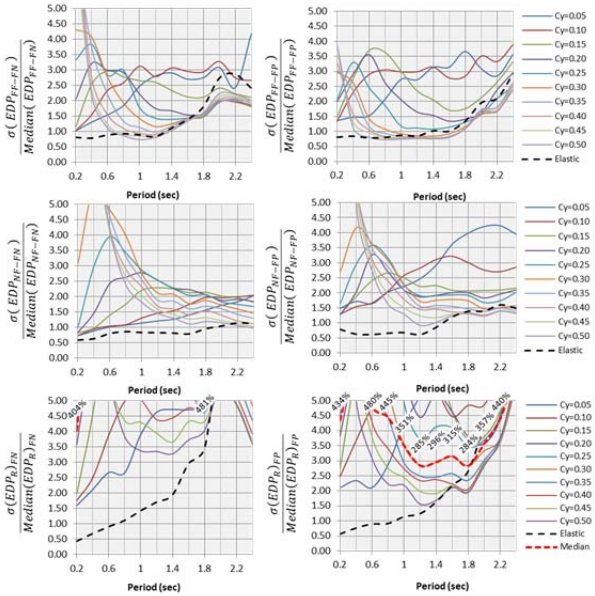

Figure B - 68:COV Values of “EDP” and “IEDP Ratio” In Terms of strength characteristics | Link:NLT#4 | ζ=%2.0 | EQL=3 | SYS#2 | Mf/Ms=0.15 | Kf/Ks=4

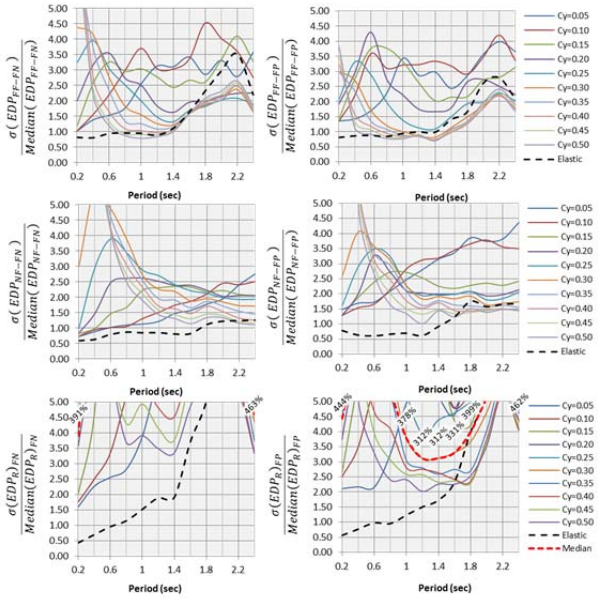

Figure B - 69:COV Values of “EDP” and “IEDP Ratio” In Terms of strength characteristics | Link:NLT#4 | ζ=%2.0 | EQL=3 | SYS#3 | Mf/Ms=0.25 | Kf/Ks=4

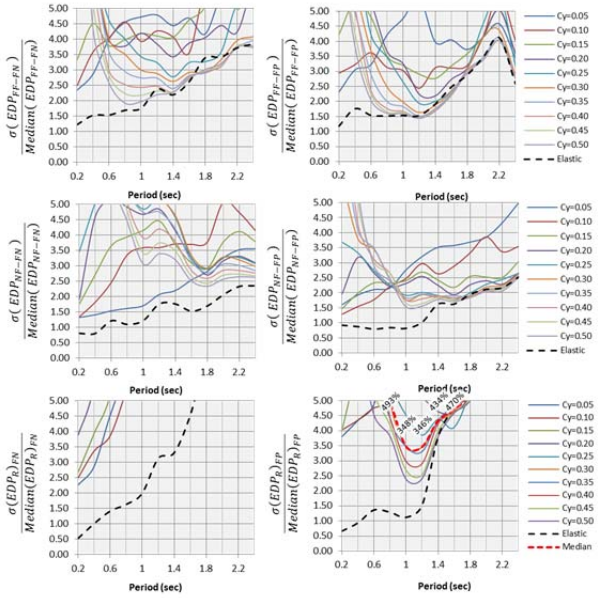

Figure B - 70:COV Values of “EDP” and “IEDP Ratio” In Terms of strength characteristics | Link:NLT#4 | ζ=%2.0 | EQL=4 | SYS#1 | Mf/Ms=0.15 | Kf/Ks=2

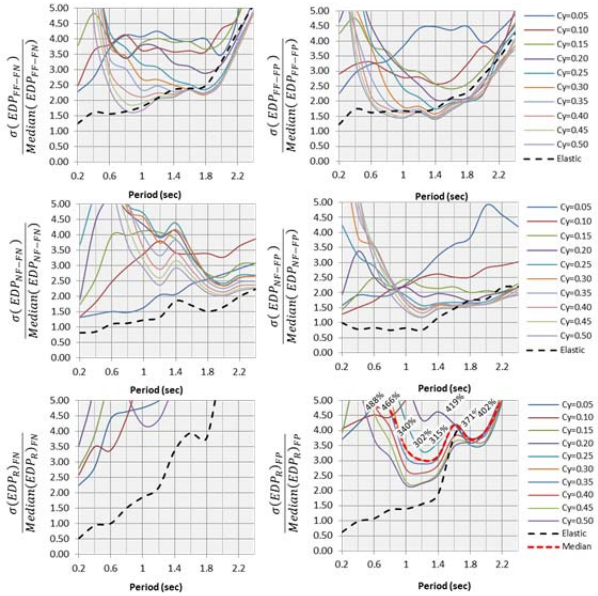

Figure B - 71:COV Values of “EDP” and “IEDP Ratio” In Terms of strength characteristics | Link:NLT#4 | ζ=%2.0 | EQL=4 | SYS#2 | Mf/Ms=0.15 | Kf/Ks=4

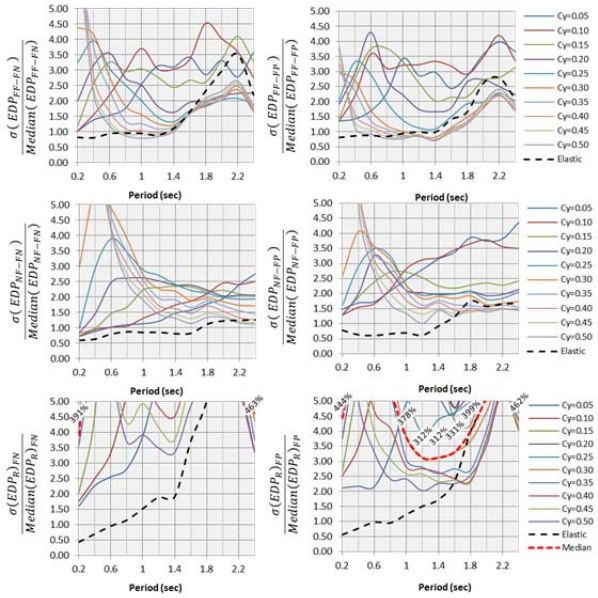

Figure B - 72:COV Values of “EDP” and “IEDP Ratio” In Terms of strength characteristics | Link:NLT#4 | ζ=%2.0 | EQL=4 | SYS#3 | Mf/Ms=0.25 | Kf/Ks=4

Appendix C – overview of response of a representative SDOF system and results of sensitivity analysis of SDOF systems

Appendix C.1 Overview of response of a representative SDOF system

As previously mentioned the main finings of this research are presented in a statistical context; namely, using each EDP's mean (or median) supplemented by their dispersion values. While having knowledge about statistical distribution of results is very useful for predicting probable EDP of interest, yet it cannot give a good insight into variability of responses.

Thus, to better illustrate variability of the results with respect to different system characteristics, results of analysis of a SDOF model with elastic period of vibration of 0.6 Sec and strength characteristic of %20, subjected to a NF GM and its FF GM counterpart is determined and discussed in this section.

Notes:

1. Backbone curves used for T_e=0.6 Sec and C_y=%20, are identical to what presented in Appendix A.
2. For pulse-like NF GM, NGA#171, and for ordinary FF GM, NGA#169, (both originated form Imperial Valley-06, 1979 earthquake) were used – see Table C-1.

Table C-1: Properties of selected NF GM and its FF counterpart used for analysis of a representative SDOF system

	NGA#171	NGA#169
Magnitude	6.53	6.53
Vs30	186 m/s – Site Class "C"	274.50 m/s – Site Class "C"
Closest Distance	0.07 (km)	22 (km)
PGA	0.31 (g)	0.285 (g)
PGV	7900 (cm/Sec)	29.75 (cm/Sec)
PGD	1300 (cm)	16.67 (cm)

3. Results are presented only for FN component of the input motion

Appendix C.1.1 *Time history displacement response of representative SDOF*

Figure C-1 depicts time history displacement response of a SDOF system as described in previous section due to NGA#171 and NGA#169 (Imperial Valley-06,

1979). Results are presented for all five types of backbone curves as detailed in Appendix E.1.

Observations:

- As it is evident form Figure C-1 the maximum displacement demand for NF GMs could be highly sensitive to the selected inelastic model.
- The NF displacement demand for the first 4.0 Sec is identical amongst NLT#2 to NLT#5; however, it is slightly different for NLT#1. This shows how response of the structure in one direction can effect the response of the structure in the other orthogonal direction when the properties in two horizontal orthogonal directions are coupled.
- The main source of difference in maximum displacement response is when the direction of displacement reverses at about 4.0 Sec; this is essentially when the main input energy begins to rise. From this point the effect of early yielding is well evident in response of NLT#4 & NLT#5 when one compares them with response of NLT#2 and NLT#3.
- Finally when at about 6.0 Sec from beginning of the record, displacement direction reverses again, the effect of load reversal protocol defined in nonlinear link properties, effects the residual displacement. Residual displacement is highly dependent on the backbone curve and the reversal load pattern and can vary significantly. [1]

[1] This shows that for practical projects being designed based on a NLTHA which is using a few input motions, a very accurate estimate of backbone curves and their load reversal pattern is crucial.

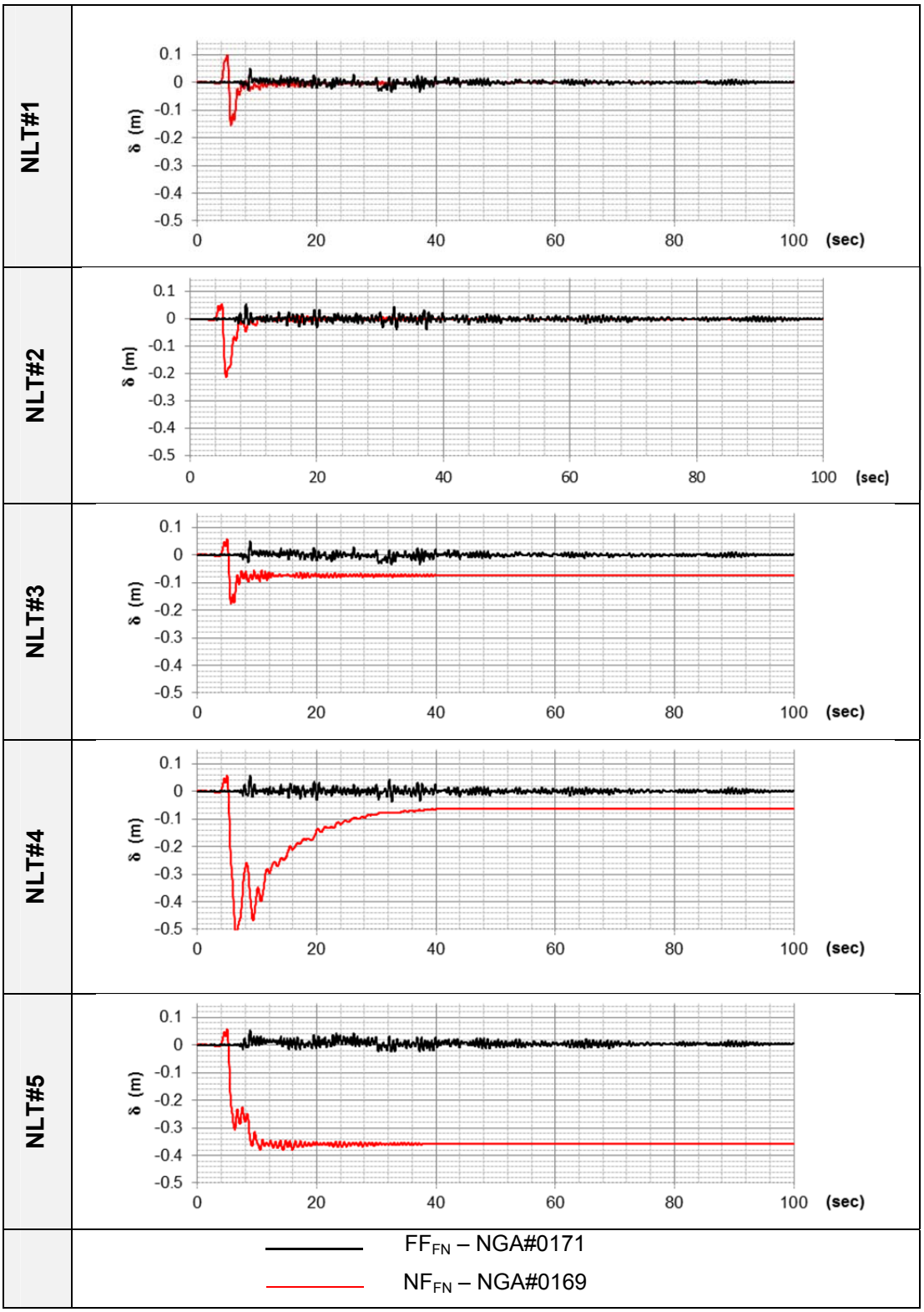

Figure C-1: Displacement TH for Imperial Valley-06, 1979 in FN direction (Te = 0.6 sec due to FN component of NGA#171 and NGA#169, Imperial Valley-06, 1979 earthquake

Appendix C.1.2 ***Hysteresis response of representative SDOF***

Figure C-2 shows the hysteresis behaviour of each oscillating system as described in Appendix C.1.1 for the displacement demand time histories as shown in Figure C-1.

Observations:

- Hysteresis behaviour of all types of nonlinear links show significant numbers of excursion due to FF – NGA#0169, although associated with relatively small displacement amplitudes. This shows that while each excursion might not cause significant damage, yet the cumulative effect of small damages in reality might cause severe problems.
- Almost none of the excursions of FF – NGA#0169 run into negative stiffness zone; hence the effect of unloading pattern is not captured in FF GM – NGA#0169, responses.
- Hysteresis behaviour of all types of nonlinear links show relatively few numbers of excursions due to NF – NGA#0171; however, all associated with relatively large displacement amplitudes.
- The effect of backbone shape and unloading pattern is well evident on maximum displacement demands of NF – NGA#0171, mainly because response of the structure due to that input motion well (passes Δ_d and) run into negative stiffness zone of backbone curves.
- Since the system experiences large displacements (beyond Δ_d), response of the system is very sensitive to the inelastic model which is used to simulate nonlinear behaviour of the structure.

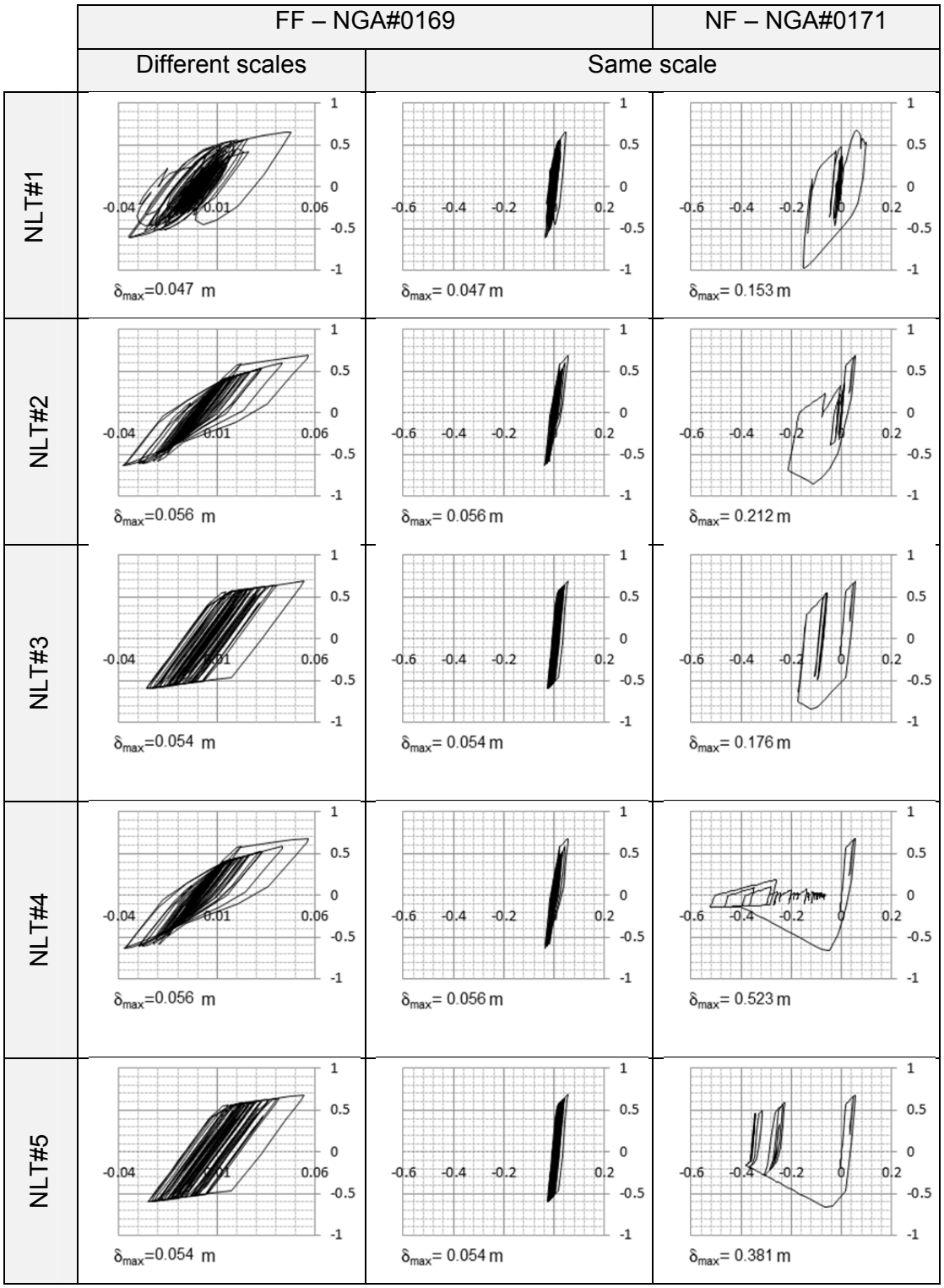

Figure C-2: Hysteresis behaviour of NLT#1 to 5 - SDOF systems with T_e=0.6 sec and C_y=%20 due to FN component of NGA#171 and NGA#169, Imperial Valley-06, 1979 earthquake

Appendix C.1.3 ***Energy History of representative SDOF***

Figure C-3 shows the history of input energy, hysteritically dissipated energy, visoelastically dissipated energy, and kinematic/strain energy for the same SDOF system, as described in Appendix C.1, subjected to FF – NGA#0169 & NF – NGA#0171 GMs.

For brevity, results are only presented for NLT#4 and NLT#5.

Observations:

- Table C-2 summarizes the magnitude of Input Energy and the proportions of hysteritically, and viscously damped energies.
- From Table C-2 one can infer that FF – NGA#0169, imposes much more energy into the system (about %50 more than its NF GM counterpart)
- For both systems, i.e. NLT#4 and NLT#5, the ratio of hysteretic energy to input energy is some %77 ($\pm$ %10).

Table C-2: summary of energy analysis

		Modal Damping Energy	Hysteretic Energy	Input Energy	Unit
NLT#4	FF – NGA#0169	0.16	0.53	0.69	Mega Joule
		23%	77%	100%	Unitless
	NF – NGA#0171	0.08	0.35	0.43	Mega Joule
		18%	82%	100%	Unitless
NLT#5	FF – NGA#0169	0.19	0.43	0.62	Mega Joule
		30%	70%	100%	Unitless
	NF – NGA#0171	0.07	0.34	0.41	Mega Joule
		16%	84%	100%	Unitless

- Table C-3 lists A) the time instances when the bulk of energy is imposed into the system, and B) the rate of input energy; when the rate of input energy is defined as $\frac{E_{95}-E_5}{T_{95}-T_5}$, where:

  E_{95}: %95 of total input energy

  E_5: %5 of total input energy

$T_{95} - T_5$: duration that input energy reaches from %5 to %95 of total input energy.

Table C-3 shows that %90 of input energy ($E_{95} - E_5$) of:

- FF – NGA#0169: is imposed in about 50 Sec (between ~8 to ~58 Sec of vibration), and
- NF – NGA#0171: is imposed in about 6.2 Sec (between ~4.1 to ~10.3 Sec of vibration).

- Main energy content of FF – NGA#0169 is imposed to the system very gradually, however, Main energy content of NF – NGA#0171 is imposed to the system very rapidly.
- By comparing content of Table C-3 and Table C-2 one can infer that although the input energy due to NF – NGA#0171 is about %60 of that due to FF – NGA#0169, yet the rate of input energy due to NF – NGA#0171 is more than %500 of that due to FF – NGA#0169.

Table C-3: summary of arrival time of Input Energy and its rate in Terms of input energy per Sec

		T-%5 E_I	T-%95 E_I	Rate of Input Energy
NLT#4	FF – NGA#0169	8.05 sec	58.40 sec	13.64 kJ/Sec
	NF – NGA#0171	4.10 sec	10.35 sec	69.36 kJ/Sec
NLT#5	FF – NGA#0169	7.85 sec	54.95 sec	13.13 kJ/Sec
	NF – NGA#0171	4.10 sec	10.25 sec	66.86 kJ/Sec

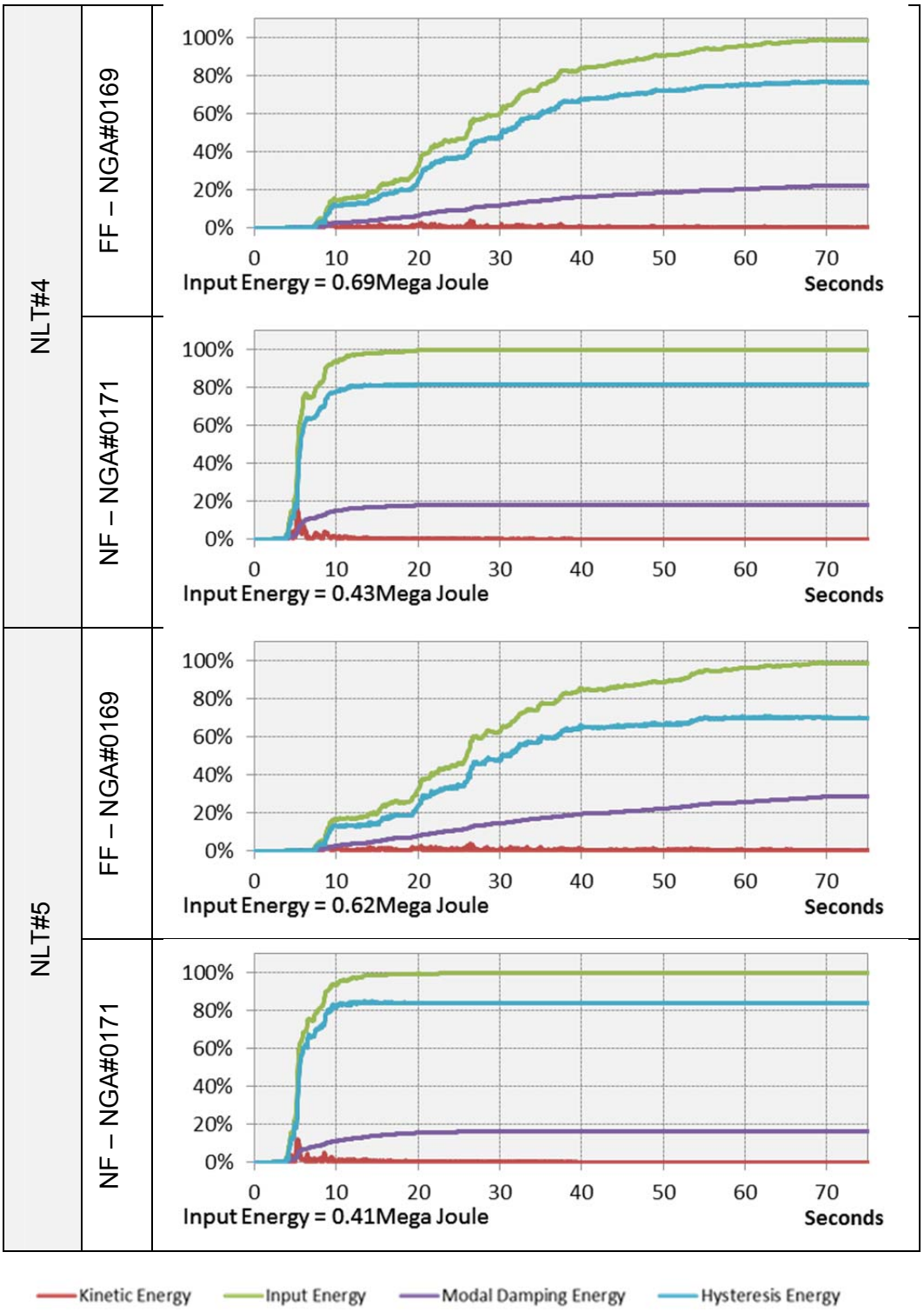

Figure C-3: Input Energy, Modal Damping Energy, Kinetic Energy and Hysteretic Damping Energy (Normalized to total Input Energy) due to FN component of NGA#171 and NGA#169, Imperial Valley-06, 1979 earthquake

Appendix C.1.4 *Summary of observations for a representative SDOF system*

- Effect of backbone curves and unloading/reloading paths are much more pronounced when larger displacements take place (especially in the beginning of the input motions - the typical case for NF GMs).
- Nonlinear response of the structures to the FF GMs is associated with several small excursions, while nonlinear response of the structures to the NF GMs is associated with a few very large excursions.
- Large excursions due to the NF GMs in the beginning of vibration can cause significant degradation in both stiffness and strength; this in turn result in a much softer system (with much longer period) which is more susceptible to the effect of long-period pulses of NF GMs. This phenomenon is more obvious when one considers the fact that long-period pulses usually continue after initiation of degradations (elongation of equivalent period) especially for short period structures.
- Rate of input energy of the NF GMs are (generally) considerably more than that of FF GMs, hence for the NF GMs the main part of imposed energy should be dissipated in a relatively short period of time; in turn, this requires significant displacement to allow for dissipation of such a huge energy flux in one or a very few cycles of excursion.

Appendix C.2 Sensitivity analysis for maximum displacement demand spectra and IDDR

In Appendix C.2.1 to Appendix C.2.4 we briefly discuss results of sensitivity analysis performed on EDPs and EDP.Ratios of interest with respect to variation of important parameters as noted in section 3.3.

Appendix C.2.1 *Effect of hysteresis model on maximum displacement demand and IDDR:*

By comparing Figure A-1 to Figure A-13 of Appendix A (and similar ones when data base becomes available) one may conclude that:

a) for reasonably designed structures (based on today's state of practice; i.e. Cy≥~%20 in FN direction and Cy ≥~%10 in FP direction):

i) properties of backbone curves and load reversal patterns can significantly influence the magnitude of expected displacement demand for both NF and FF GMs, both in FN and FP directions (specially for shorter period ranges); however,

ii) despite dependency of magnitude of expected maximum displacement demand on properties of backbone curves, IDDR, remains almost unchanged; this is irrespective of selected hysteresis model (i.e. properties of backbone curves, influence the magnitude of expected displacement demands; for both NF and FF GMs with the same rate hence, the ratio of those two values remains unchanged),

b) for relatively weak structures (Cy≤~%15 in FN direction and Cy <~%10 in FP direction), IDDR of the system increases as i) degree of degradation increases, and ii) level of residual strength decreases.

For reasonably strong structures designed based on current design codes and guidelines, choice of backbone curve and load reversal pattern would similarly effect magnitude of expected maximum displacement demand for both the FF and the NF GMs; hence it has nominal effect on IDDR.

By comparing Figure A-66 to Figure A-78 of Appendix A (and similar ones when data base becomes available) one may conclude that:

c) for structures with Te≥0.6 sec, dispersion of IDDRs in both FN and FP directions are almost independent to selected properties of backbone curves and load reversal patterns (hysteresis model),

d) for structures with Te≤0.6 sec, dispersion of IDDR increases as degree of degradation increases and level of residual strength decreases. As a rule of thumb, the modified CV of IDDR linearly varies from %100 to about %400 when T_e varies from 0.6 Sec to 0.2 Sec. It is of note that this anomaly in dispersion is partially due to unbounded response of structures to some input motions.

For the standard structures with Te≥0.6 sec, modified CV of IDDR is almost independent to the selected hysteresis model.

Appendix C.2.2 ***Effect of system (modal) damping on maximum displacement demand and IDDR***

By comparing Figure A-1 to Figure A-13 with Figure A-79 to Figure A-91 of Appendix A (and similar ones when data base becomes available) one may conclude that:

e) The expected displacement demand for both NF and FF GMs - in both FN and FP directions - becomes less jagged as ζ increases; this phenomenon is particularly noticeable for the spikes that usually happens for relatively weak structures,

f) The expected displacement demands are in general reduced slightly as ζ increases; this effect diminishes as structure experiences more nonlinear excursions (i.e. energy dissipation through hysteretic behaviour dominates),

g) The IDDR values are reduced slightly, however the effect is so nominal that one may argue IDDR is almost independent to the system damping ratio. As one may expect, reductions are more obvious around the peaks/spikes in short period range.

Albeit, system damping ratio in general reduces the expected maximum displacement demands for both the FF and the NF GMs, it has almost the same effect on maximum displacement responses due to both FF and NF GMs; hence, it has no to nominal influence on IDDR values.

Appendix C.2.3 ***Effect of input motion intensity on maximum displacement demand and IDDR***

By comparing Figure A-1 to Figure A-13 and Figure A-151 to Figure A-163 of Appendix A (and similar ones when data base becomes available) one may conclude that:

h) Expected displacement demands are increased as the intensity level increases.

i) Due to nonlinear response of the structure, in general, the incremental rate of expected displacement demand is less than the rate of increment of input motion intensities

j) The incremental rate of expected displacement for the NF GMs is more than that for the FF GMs. This effect is much more pronounced in shorter period range. Hence, IDDR increases as intensity level is increases.

Appendix C.2.4 ***Effect of pairing method on maximum displacement demand and IDDR***

Trend of expected maximum displacement demands due to suite of "Linearly scaled GMs" (to match a target response spectrum) is in general very similar to that due to suite of "PGA matched GMs"; however, matching to a UHRS resulted in much more uniform IDDR with respect to elastic periods of vibrations. That is to say, the IDDR determined for suite of "Linearly scaled GMs" is much more uniform (complete with less slope/flatter) than that determined for suite of "PGA matched GMs".

As a rule of thumb, for reasonably designed structures (i.e. Cy≥%20~%25 in FN direction, and Cy ≥%10~%15 in FP direction) one can expect that:

k) for longer period range - let's say T_e=2.4 sec: IDDR of "Linearly scaled GMs" are about %20 less than those of of "PGA matched GMs"; and

l) for shorter period range - let's say T_e=0.2 sec: IDDR of "Linearly scaled GMs" are about %20 more than those of "PGA matched GMs".

Appendix C.3 Sensitivity analysis for maximum ductility demand spectra and DDR

In Appendix C.3.1 to Appendix C.3.4 we briefly discuss results of sensitivity analysis performed on DDRs and DDR.Ratios of interest with respect to variation of important parameters as noted in section 3.3.

Appendix C.3.1 *Effect of hysteresis model on maximum ductility demand and DDR:*

By comparing Figure A-14 to Figure A-26 of Appendix A (and similar ones when data base becomes available) one may conclude that:

m) Properties of backbone curves and load reversal patterns has slight influence on the magnitude of expected ductility demands for both NF and FF GMs, and in both FN and FP directions. However, the influence of backbone curves and load reversal patterns are almost equivalent for both NF and FF GMs; thus,

n) DDR, is almost independent to selected hysteresis models; nonetheless, dependency of DDR to selected hysteresis model increases as elastic period of vibration of the system and strength characteristic of the system decreases.

Appendix C.3.2 *Effect of system (modal) damping on maximum ductility demand and DDR*

Effect of system damping on Maximum Ductility Demand and DDR is very similar to what was observed for maximum displacement demands and IDDR. Refer to section Appendix C.2.2.

Appendix C.3.3 *Effect of input motion intensity on Maximum Ductility Demand and DDR*

By comparing Figure A-14 to Figure A-26 and Figure A-92 to Figure A-104 of Appendix A (and similar ones when data base becomes available) one may conclude that:

o) Expected ductility demands are increased as the intensity level increases.

p) The incremental rate of expected ductility demands for the NF GMs is more than that for the FF GMs. This effect is much more pronounced in shorter period ranges.

Appendix C.3.4 *Effect of pairing method on maximum ductility demand and DDR*

The maximum ductility demands trend for “Linearly scaled GMs” is in general very similar to trend of “PGA matched GMs”; however, matching to a UHRS resulted in more uniform DDR which in general is less than that for PGA matched GMs.

Appendix C.4 Sensitivity analysis for strength spectra and YCDR

Note: in this subsection “Yield Capacity Demand” stands for” “Yield Capacity Demand, required for achieving some specific target ductility”.

Appendix C.4.1 *Effect of hysteresis model on yield capacity demand and YCDR*

By comparing Figure A-27 to Figure A-39 of Appendix A (and similar ones when data base becomes available) one may conclude that:

q) Properties of backbone curves and load reversal patterns have insignificant influence on Yield Capacity Demand values; this is valid for both NF and FF GMs; and in both FN and FP directions.

r) Similarly, variation of backbone curves and load reversal patterns have insignificant effect on YCDR (associated with a specific target ductility).

Appendix C.4.2 *Effect of system (modal) damping on yield capacity demand and YCDR*

By comparing Figure A-27 to Figure A-39 with Figure A-105 to Figure A-117 of Appendix A (and similar ones when data base becomes available) one may conclude that:

s) The expected Yield Capacity Demand for both NF and FF GMs and in both FN and FP directions, are slightly reduced as ζ increases; this is due to the fact that more energy is damped through system (modal) damping, hence less energy is required to be damped through hysteresis behaviour of the system.

t) Although increment of system damping results in reduced Yield Capacity Demand, yet the rate of reduction of Yield Capacity Demand for both NF and FF GMs are very similar; thus, YCDR is almost independent to the system damping values.

Appendix C.4.3 ***Effect of input motion intensity on yield capacity demand and YCDR***

By comparing Figure A-27 to Figure A-39 with Figure A-105 to Figure A-117 of Appendix A (and similar ones when data base becomes available) one may conclude that:

u) As the intensity level of input motions increases, expected Yield Capacity Demand increases too.

v) As the intensity level of input motions increases, expected Yield Capacity Demand for the very short period structures approaches a single point which is almost equivalent to the capacity required to keep the structure elastic (note, inelastic displacement for very short period structures are almost unbounded, hence, the capacity which allows for a ductility of 8 or less, should be very close to the capacity required to keep the structure elastic. For more information in this regard see section 4.2.4).

w) The incremental rate of strength spectrum due to increasing intensity of input motions for the NF GMs is almost equivalent to that for the FF GMs. Hence, YCDR is almost independent to the earthquake intensity level.

Appendix C.4.4 *Effect of pairing method on yield capacity demand and YCDR*

Trend of expected Yield Capacity Demand for “Linearly scaled GMs” to match a target response spectrum is in general very similar to that of “PGA matched GMs”; however, similar to what mentioned for ductility demand, matching to a UHRS resulted in much more uniform YCDR with respect to elastic periods of vibrations. That is to say, although YCDR determined for both “Linearly scaled GMs” and “PGA matched GMs” start form about unity for very short period structures and linearly varies with respect to the elastic period of vibration.

The slope (tangent value) of an equivalent linear function of YCDR for “Linearly scaled GMs” is about %80 of that determined for “PGA matched GMs”.

Appendix C.5 Sensitivity analysis of “maximum inelastic to elastic displacement demand” and “maximum inelastic to elastic displacement demand ratio”

Appendix C.5.1 *Effect of hysteresis model on ratio of $\frac{\delta_{inelastic}}{\delta_{elastic}}$ for the NF GMs to $\frac{\delta_{inelastic}}{\delta_{elastic}}$ for the FF GMs*

By comparing Figure A-40 to Figure A-52 of Appendix A (and similar ones when data base becomes available) one may conclude that properties of backbone curves and load reversal patterns have insignificant influence on trend or amplitudes of $\frac{\delta_{inelastic}}{\delta_{elastic}}$ determined for the NF GMs and $\frac{\delta_{inelastic}}{\delta_{elastic}}$ determined for the FF GMs; and also almost nominal influence on the ratio of $\frac{\delta_{inelastic}}{\delta_{elastic}}$ for the NF GMs to $\frac{\delta_{inelastic}}{\delta_{elastic}}$ for the FF GMs.

Appendix C.5.2 *Effect of system (modal) damping on ratio of $\frac{\delta_{inelastic}}{\delta_{elastic}}$ for the NF GMs to $\frac{\delta_{inelastic}}{\delta_{elastic}}$ for the FF GMs*

By comparing Figure A-40 to Figure A-52 and Figure A-118 to Figure A-130 of Appendix A (and similar ones when data base becomes available) one may conclude that:

x) due to presence of more viscose energy dissipation, less hysteresis energy dissipation is required; hence structures see less inelastic deformation. As a result the ratio of $\frac{\delta_{inelastic}}{\delta_{elastic}}$ for both the FF and the NF GMs becomes unbounded at shorter periods (fewer short period structures experience instability condition),

y) for moderate to long period ranges, the ratio of $\frac{\delta_{inelastic}}{\delta_{elastic}}$ for the NF GMs to $\frac{\delta_{inelastic}}{\delta_{elastic}}$ for the FF GMs is unchanged and is almost equal to unity,

z) for elastic period of vibrations less than 0.6 Sec the trend of ratio of $\frac{\delta_{inelastic}}{\delta_{elastic}}$ for FF GMs and $\frac{\delta_{inelastic}}{\delta_{elastic}}$ for the NF GMs remains unchanged; nonetheless, the amplitudes are less pronounced for higher damping ratios. Thus, in general, it seems that for short period structures, underestimation of damping ratio could result in overly conservative values for $\frac{\delta_{inelastic}}{\delta_{elastic}}$.

Appendix C.5.3 ***Effect of input motion intensity on ratio of $\frac{\delta_{inelastic}}{\delta_{elastic}}$ for the NF GMs to $\frac{\delta_{inelastic}}{\delta_{elastic}}$ for the FF GMs***

By comparing Figure A-40 to Figure A-52 and Figure A-118 to Figure A-130 of Appendix A (and similar ones when data base becomes available) one may conclude that as intensity level increases:

aa) ratio of $\frac{\delta_{inelastic}}{\delta_{elastic}}$ for the NF GMs to $\frac{\delta_{inelastic}}{\delta_{elastic}}$ for the FF GMs increases,

bb) in general increment of intensity level can increase possibility of instability of the system; thus, $\frac{\delta_{inelastic}}{\delta_{elastic}}$ becomes unbounded at longer period ranges.

Appendix C.5.4 ***Effect of pairing method on ratio of $\frac{\delta_{inelastic}}{\delta_{elastic}}$ for the NF GMs to $\frac{\delta_{inelastic}}{\delta_{elastic}}$ for the FF GMs***

The ratio of $\frac{\delta_{inelastic}}{\delta_{elastic}}$ for the NF GMs to $\frac{\delta_{inelastic}}{\delta_{elastic}}$ for the FF GMs trend for "Linearly scaled GMs" is in general very similar to that for "PGA matched GMs"; however, matching to a UHRS resulted in more uniform $\left(\frac{\delta_{inelastic}}{\delta_{elastic}}\right)_{NF-GMs}$ and $\left(\frac{\delta_{inelastic}}{\delta_{elastic}}\right)_{FF-GMs}$. Also amplitudes of $\frac{\delta_{inelastic}}{\delta_{elastic}}$ for both NF and FF GMs were less for "Linearly scaled GMs" in compare with the similar for "PGA matched GMs".

It is of note that while the effect of pairing is not that obvious for not-amplified input motions, it is more noticeable for higher intensity (amplified) input motions.

Appendix D – Overview of response of a representative 2DOF system and results of sensitivity analysis of 2DOF systems

Appendix D.1 Overview of response of a representative 2DOF system

Similar to what was mentioned in Chapter 3, since statistical representation of each EDP might not be very useful in understanding of variation of EDPs for different structures, in this section we study seismic behaviour of a given structure with respect to variation of dynamic characteristics of the structure, due to an individual input motion.

To achieve this goal, the same results, detailed in Appendix C for a fixed base structure is replicated here, except:

- the effect of FFS is added into the mathematical model using the simplified method proposed in Chapter 5 while α is set to %15 and β is set to 2.0,
- structural system properties (above foundation) are similar to those presented in Appendix C; however for brevity results of systems denoted as NLT#2 and NLT#3 are not presented (for details of dynamic properties of the selected structures refer to Appendix C),
- The same input motions that were used in Appendix C are used for determination of response of the structure with flexible basis (for details of input GMs refer to Appendix C).

In summary: for consideration of effects of FFS along with NF-effects, the same models used in Appendix C were modified by adding some linear springs and discrete masses to the base of the structures; result of THNLA of the new 2DOF models are compared with the same for the fixed base structures (presented in Appendix C), and detailed in the following subsections.

Appendix D.1.1 *Time history displacement response of representative 2DOF systems*

Figure D-1 depicts time history displacement response of a 2DOF system with $Te = 0.6\,sec$, $Cy = \%20$, $\propto = \%15$, and $\beta = 2.0$ due to NGA#171 and NGA#169 (Imperial Valley-06, 1979); for NLT#1, NLT#4 and NLT#5 inelastic models as detailed in Appendix D.1.

Observations:

- While consideration of base flexibility cause no adverse effect on nonlinear displacement demands due to FF GMs, it can greatly increase nonlinear displacement demands due to the NF GMs.

  This observation essentially endorses the hypothesis noted in Chapter 1, i.e. ignoring FFS where the structure might get exposed to some long-period pulses due to NF-effects could be un-conservative for some special cases/input motions.
- Effect of FFS on maximum displacement demand for the NF GMs could be highly sensitive to the selected inelastic model.

  The adverse effects of FFS on maximum displacement demands due to the NF GMs increase as effective period of structures (due to degradation effects) increases. That is to say:
  - for NLT#1, which is a bilinear inelastic model with no degradation property, the increase in displacement demand (due to consideration of effects of FFS) is insignificant for both NF and FF GMs,
  - for NLT#4, which is a Quadri-linear model with cyclic (but no in-cycle) stiffness degradation, the displacement demand increases about %15 for the FF GMs and about %30 for the NF GMs, when effects of FFS are accounted for, and
  - for NLT#5, which is a Quadri-linear model with in-cycle and cyclic strength and stiffness degradation, the displacement demand increases nominally for FF GMs, but significantly (about %200) for the NF GMs , when effects of FFS are accounted for.

Obviously these results are determined for a single system with some specific inelastic properties, and some specific foundation mass and stiffness ratio; thus they cannot be generalized to all structures, however, these results show how individual system's response could vary with respect to the dynamic properties of the system.

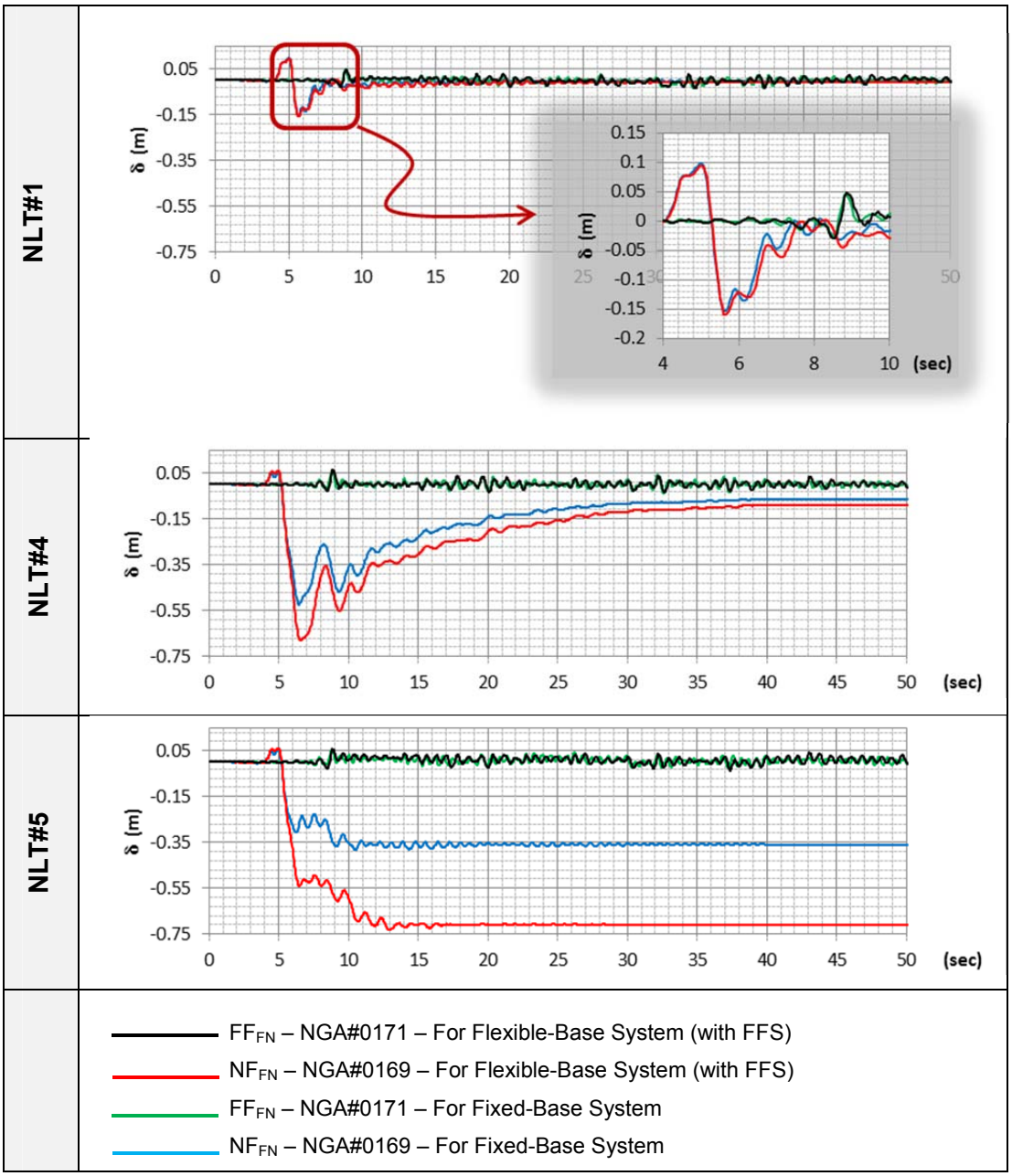

Figure D-1: Displacement TH for Imperial Valley-06, 1979 in FN direction (Te = 0.6 seconds) due to FN component of NGA#171 and NGA#169, Imperial Valley-06, 1979 earthquake, for both Fixed-base and Flexible-base conditions

Appendix D.1.2 *Hysteresis response of representative 2DOF systems*

Figure D-2 shows the hysteresis behaviour of each oscillating system as described in Appendix E for the displacement demand time histories as shown in Figure D-1

for the flexible base structures along with hysteresis behaviour of the same structures when the base is fixed (as shown in Figure C-2).

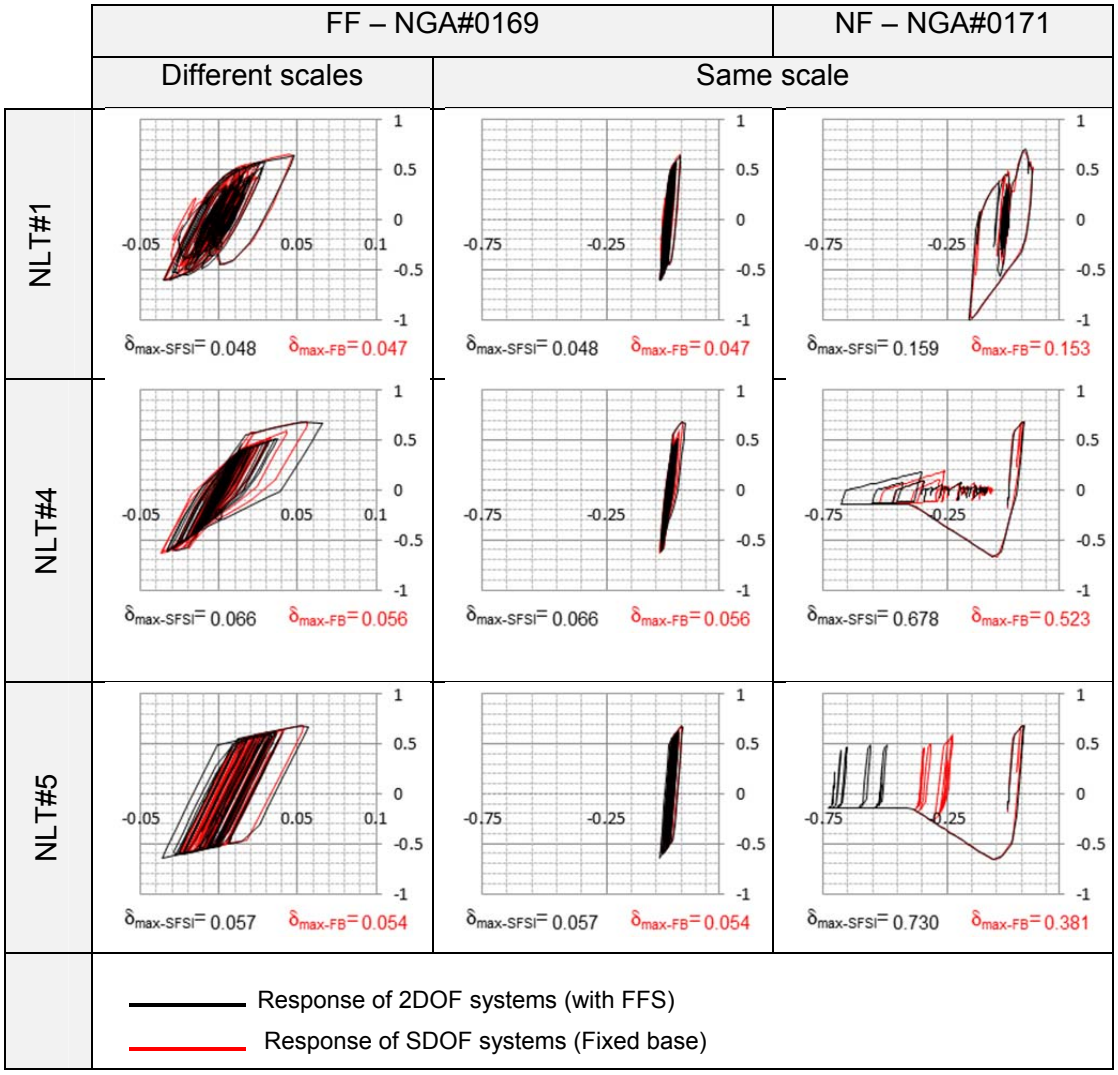

Figure D-2: Hysteresis behaviour of NLT#1, NLT#4 and NLT#5 – for a 2DOF systems and a SDOF with T_e=0.6 sec and C_y=%20, ∝ = %15 , and β=2.0 due to FN component of NGA#171 and NGA#169, Imperial Valley-06, 1979 earthquake

Observations:

- All results mentioned in Appendix C.1.2 for fixed base structures are valid and can be extended to their corresponding flexible structure. Additionally:

- In general (when effects of FFS are considered by mean of adding some flexibility to the base of the system) hysteretic pattern for NF and FF GMs remains almost unchanged.
- The main inelastic displacement of the structures due to the NF GMs still happens in a few big excursions associated with the long-period pulse of the NF GMs. As flexibility of the base increases and the period of the structure gets closer to the period of the pulse signal associated with the NF GMs, the adverse effect of the NF GMs on inelastic displacement demand of the structure increases.
- Thus, generally speaking, FFS effects may amplify adverse effects of the NF GMs on displacement demand of the structures.

Appendix D.1.3 ***Energy history of representative 2DOF system***

Figure D-3 shows the history of input energy, hysteritically dissipated energy, visoelastically dissipated energy, and kinematic/strain energy of the 2SDOF system, along with the same for their corresponding fixed base structures as detailed in Appendix C.1.3.

Observations:

- All results mentioned in Appendix C.1.3 for the fixed base structures are valid and can be extended to their corresponding flexible structure.

  Additionally:
- While the trend and the rate of input energy is almost independent of base flexibility, the magnitude of input energy, hysteritically dissipated energy, viscoelastically dissipated energy, and kinematic/strain energy is somewhat dependent on effects of FFS.

  That is to say:
  - for the NF GMs, the magnitude of input, hysteretically damped, viscously damped, and kinetic energy, are almost independent to the base flexibility,

- for FF GMs: when FFS effects are included in the modeling, the magnitude of input, hysteretically damped, viscously damped, and kinetic energy could be as much as 1.3 times of those when the structure is fixed base; nonetheless., the proportion of hysteretically damped, viscously damped, and kinetic energy to input energy is almost unchanged.

Appendix D.1.4 ***Summary of observations for representative 2DOF system***

- FFS has nominal to no adverse effect on nonlinear displacement demand due to the FF GMs; however, FFS can greatly increase nonlinear displacement demand due to the NF GMs
- The main adverse effect of FFS on displacement demand of the structures due to the NF GMs is manifested in a big excursion associated with response of the structure to the long-period pulse of the NF GMs. This effect can be interpreted as imposing more damage to the superstructure.
- FFS has almost no effect on input energy due to the NF GMs, however it can moderately increase the magnitude of input energy due to FF GMs; thus, ignoring FFS in analysis can result in underestimation of accumulative damage (proportional to input energy) due to FF GMs.

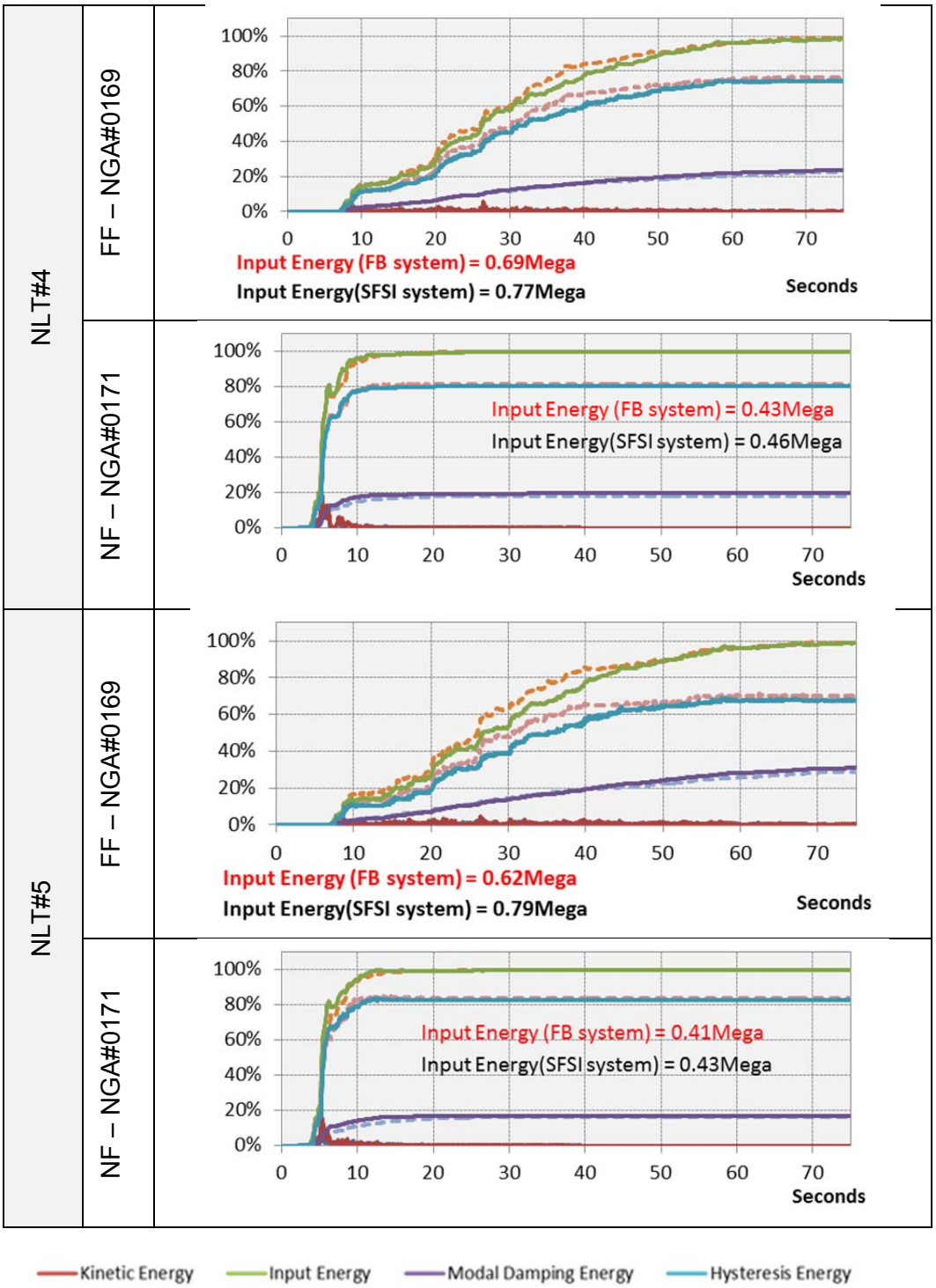

Note: solid lines are results of flexible base system, and dash-lines are results of fixed base systems

Figure D-3: Input Energy, Modal Damping Energy, Kinetic Energy and Hysteretic Damping Energy (Normalized to total Input Energy) due to FN component of NGA#171 and NGA#169, Imperial Valley-06, 1979 earthquake

Appendix E – detail of inelastic discrete link models

Appendix E.1 NLT#1; a bilinear model with stress hardening, and coupled properties in two horizontal directions

This model is proper for consideration of nonlinear response of the structures when P-Δ effects are insignificant, i.e. when product of the column axial dead load and its maximum estimated lateral deflection is less than 20% of the column plastic moment (Caltrans SDC).

For the purpose of FEM modeling, a SAP2000 built-in discrete plasticity model, “hysteretic isolator plasticity“ was used.

Hysteretic isolator plasticity is a biaxial hysteretic model that has coupled plasticity properties for its two orthogonal shear deformations (equivalent to structural lateral capacity in two horizontal directions). Biaxial hysteretic coupled plasticity properties for the two shear deformations in this model is based on the hysteretic behavior proposed by Wen (1976), as formulized per equation E-1:

$$\begin{cases} f_2 = R_2 \times K_{e1} \times d_2 + (1 - R_2) \times F_{y2} \times z_2 \\ f_2 = R_2 \times K_{e1} \times d_2 + (1 - R_2) \times F_{y2} \times z_2 \end{cases} \qquad \text{E-1}$$

Where:

K_{e2} and K_{e3} are the elastic spring constants in each horizontal direction

F_{y2} and F_{y3} are the yield forces = Varies from %5W to %50 W

R_2 and R_3 are the ratios of post-yield stiff nesses to K_{e2} and K_{e3} = 10%

z_2 and z_3 are velocity/displacement dependent internal variables which effect the sharpness of corner of bilinear hysteresis curve (for further information about formulation of z_2 and z_3 refer to SAP2000 analysis manual).

Figure E-1 shows a family of backbone curves associated with a series of strength characteristics (Cy) for the bilinear NLT#1 models.

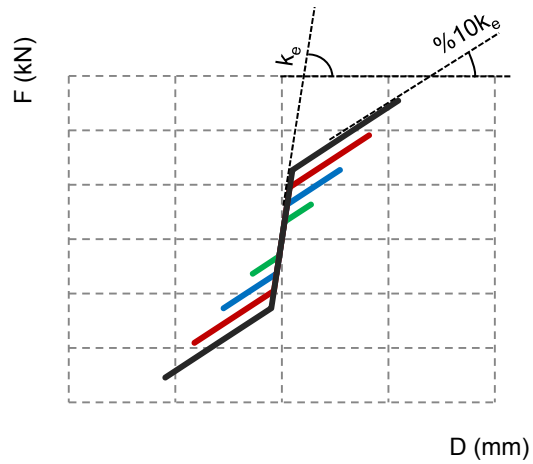

Figure E-1: typical family of backbone curves associated with a series of strength characteristics (Cy) for NLT#1 models

To show hysteresis properties of the NLT#1 link plasticity models, an increasing sawtooth displacement controlled loading, as depicted in Figure E-2, was applied in one direction on a NLT#1 link element defined for a system with elastic period of vibration of 0.60 Sec and strength characteristic (C_y) of %20 (This model is identical to what is denoted as NL-39 in chapter 4).

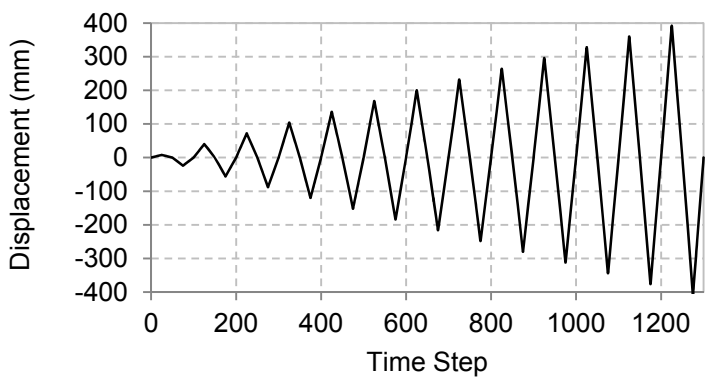

Figure E-2: displacement controlled loading protocol used for verification of hysteresis behaviour of discrete nonlinear models used in this project

To offset the dynamic effects the system damping was set to 0.99 and then internal forces were monitored. Figure E-3 shows the hysteresis behaviour of abovementioned NLT#1 link element (T= 0.6 Sec & C_y = %20) under the displacement controlled loading protocol as shown in Figure E-2.

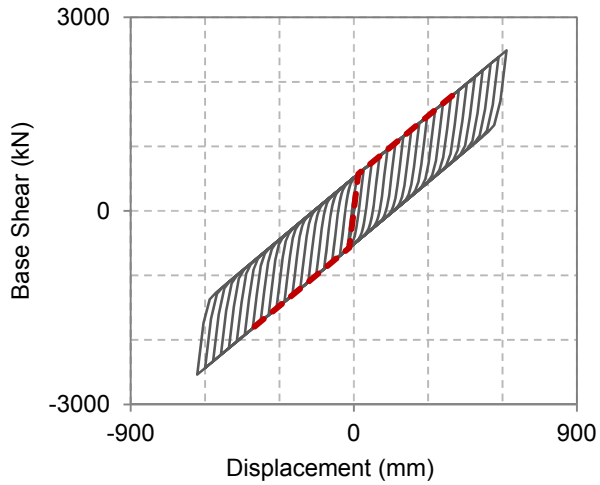

Figure E-3: hysteresis behaviour of a NLT#1 link - defined for a system with elastic period of 0.6 Sec and strength characteristic of %20

Appendix E.2 NLT#2; a multi-linear model with consideration of stress hardening and in-cycle strength and stiffness degradation

NLT#2 is a multi-linear model with consideration of %10 post yield stress hardening, which ends at 6×Δy and follows with a %5 negative stiffness ratios. This model allows for cyclic stiffness and strength degradations.

Figure E-4 depicts a family of backbone curves associated with a series of strength characteristics for the multi-linear NLT#2 models.

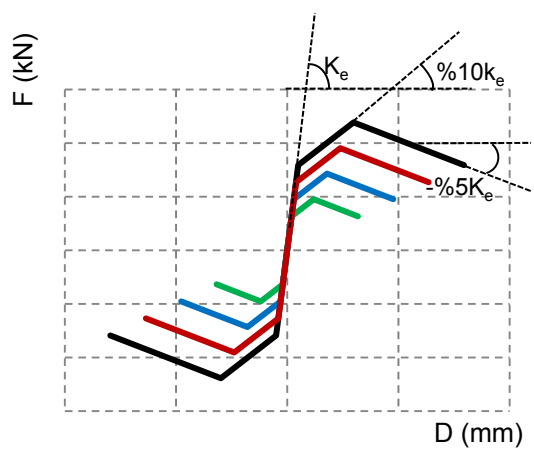

Figure E-4: typical family of backbone curves associated with a series of strength characteristics (Cy) for NLT#2 models

Example for determining properties of a representative NLT#2 backbone curve: displacement-capacity boundary (backbone curve) of a representative NLT#2 model with elastic period of 0.6 Sec, elastic stiffness of 32 MN/m, and strength characteristic of %20 could be defined as below:

- $K_e = 32000\ kN/m \rightarrow \begin{array}{l} K_s = +\ \%10\ K_e = +\ 3200\ kN/m \\ K_t = -\ \%5\ K_{se} = -\ 1600\ kN/m \end{array}$
- $T = 0.6\ sec \rightarrow m = K \times (\frac{T}{2\pi})^2 = 32000\,\frac{kN}{m} \times \left(\frac{0.6\ sec}{2\pi}\right)^2 = 292\ tonne$
- $W = m \times g = 2860\ kN \rightarrow f_y = 0.2 \times W = 572\ kN$
- $\Delta_y = \frac{f_y}{K_e} = 18mm \rightarrow \Delta_d = 6 \times \Delta_y = 108mm$
- $f_d = f_y + 5\,\Delta_y \times \%10\ K_e = 859\ kN$

Hence, force deformation backbone curve for abovementioned model with elastic period of 0.6 Sec and strength characteristic of 0.2 is:

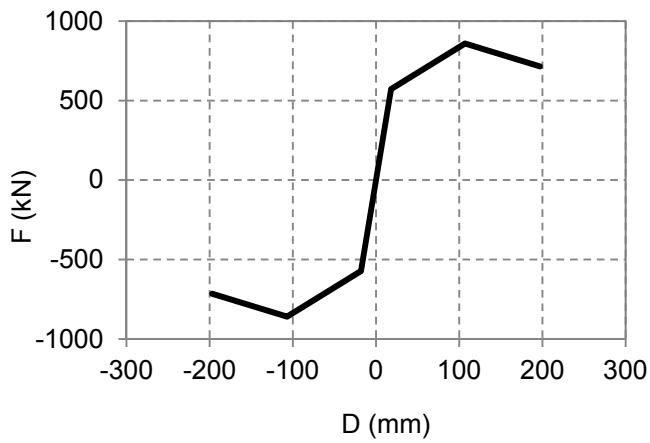

Δ	-197	-107	-18	0	18	107	197
F	-715	-859	-572	0	572	859	715

Figure E-5: displacement-capacity boundary/backbone curve of a representative NLT#2 model (equivalent to NL-39 in chapter 4)

For modeling of NLT#2 links, a SAP2000 built-in discrete plasticity model, named "Multi-Linear Pivot Hysteretic Plasticity model" (developed based on the Multi-Linear Takeda model, but enhanced with some additional parameters to control the

degrading hysteretic loops) was used for modeling of NLT#2 family of discreet nonlinear elements. [1]

The Multi-Linear Pivot Hysteretic Plasticity model is capable of synthesizing cyclic stiffness/strength degradation as well as pinching effects which are typically produced by opening of cracks when substantial displacement is imposed on reinforced concrete structures. The formulation of Multi-Linear Pivot Hysteretic Plasticity models allows for unloading and reverse loading excursions to always reach the capacity boundary; however, the unloading and reverse loadings path is always directed toward specific points, called pivot points, in the force-deformation plane. For more information refer to SAP2000 analysis manual.

To show hysteresis properties of NLT#2 family of discreet nonlinear elements, and see how degradation and pinching effects are captured, the same displacement controlled loading protocol as depicted per Figure E-2 was applied to a NLT#2 link element defined for a system with elastic period of vibration of 0.60 Sec and strength characteristic (C_y) of %20; again system damping was set to 0.99 and the system's internal forces were monitored. Figure E-6 shows the NLT#2 - Pivot/Takeda plasticity model response due to aforementioned displacement controlled loading.

[1] It is shown by other researchers that results of NLTHA of structures using Takeda plasticity model, developed for modeling of nonlinear response of concrete structures due to cyclic loadings, can very well predict the dynamic response of a concrete bridge column subjected to seismic excitation (Chin, Hsiung, et al. 2002).

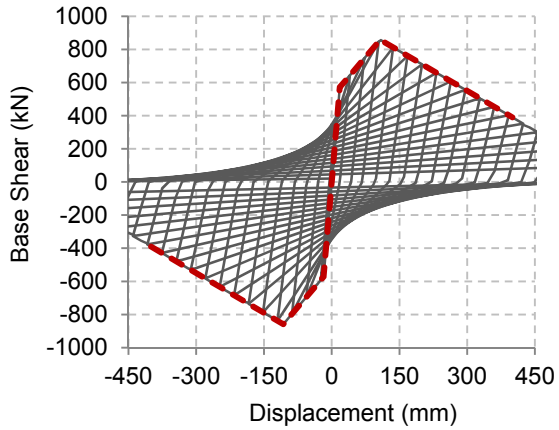

Figure E-6: hysteresis behaviour of a NLT#2 link - defined for a system with elastic period of 0.6 Sec and strength characteristic of %20

Appendix E.3 NLT#3: a multi-linear model with consideration of stress hardening, in-cycle and cyclic strength and stiffness degradation

NLT#3 is very similar to NLT#2, except NLT#3 family of nonlinear elements accounts for cyclic and in-cycle strength and stiffness degradation, which intends to approximate the hysteretic behavior of structures in which lateral stiffness and lateral strength decrease when subjected to cyclic reversals.

In this model, magnitude of strength and stiffness degradation is a function of maximum displacement in previous cycles as well as a function of dissipated hysteretic energy.

In-cycle degradation may be used to approximately reproduce the hysteretic behavior of structures in which P-Δ effects that occurs in a single cycle (in-cycle). In general in-cycle degradation due to negative stiffness can lead to dynamic instability of the structural model under certain conditions. For more information refer to chapter 4.

Conversely, cyclic degradation which is mainly appropriate for poorly detailed reinforced concrete structures which sustain extensive damages due to load reversals; may cause some extra degradation of strength in subsequent cycles of deformation (this is in addition to in-cycle degradation mainly due to P-Δ effect).

To show hysteresis properties of the of NLT#3 family of discreet nonlinear elements, the same displacement controlled loading protocol as depicted in Figure

E-2 was applied to a representative NLT#3 link element defined for a system with elastic period of vibration of 0.60 Sec and strength characteristic (C_y) of %20.

Figure E-7 shows the internal force of the representative NLT#3 as detailed above for Figure E-2's loading protocol.

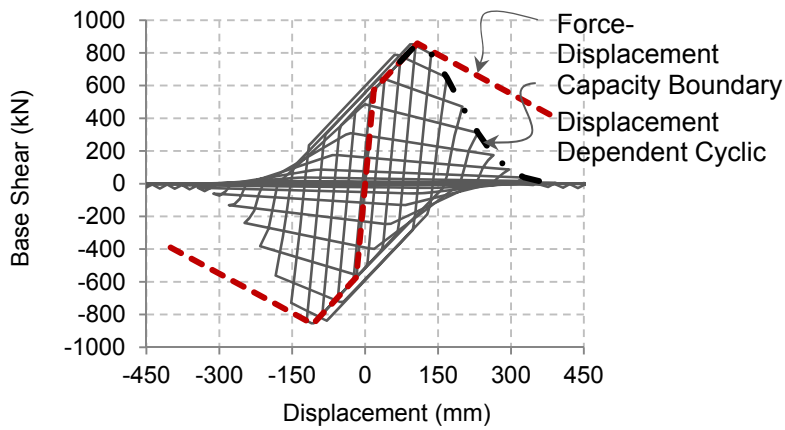

Figure E-7: hysteresis behaviour of a NLT#3 link - defined for a system with elastic period of 0.6 Sec and strength characteristic of %20

It is of note that for modeling of NLT#3 links, a SAP2000 built-in discrete plasticity model which is originally formulated based on kinematic hardening behavior of material is used. Hence, the force-displacement capacity boundary does not remain static and degerades (move inward) as a result of cyclic large strains (in some cases, it is also possible for the boundary to move outward due to cyclic strain hardening) which in turn results in an apparent cyclic degradation. This phenomenon is denoted on Figure E-7 as "Displacement Dependent Cyclic Envelope".

Appendix E.4 NLT#4; a multi-linear model with consideration of stress hardening and cyclic strength and stiffness degradation complete with some residual strength

NLT#4 is very similar to NLT#2, except that its backbone is associated with some %20F_y residual strength, which in turn allows for nonzero capacity at large displacements and some numerical advantages with ductility demands are significant; furthermore, NLT#4 negative stiffness starts at 3 × Δ_y (as opposed to NLT#2, which its negative stiffness starts at 6 × Δ_y).

Figure E-8 depicts a family of backbone curves associated with a series of strength characteristics for the multi-linear NLT#4 models. As one can see this family of backbone curves are very similar to those of Figure E-4, except for the residual strength Plato at tail of the curve and the displacement where the negative stiffness starts.

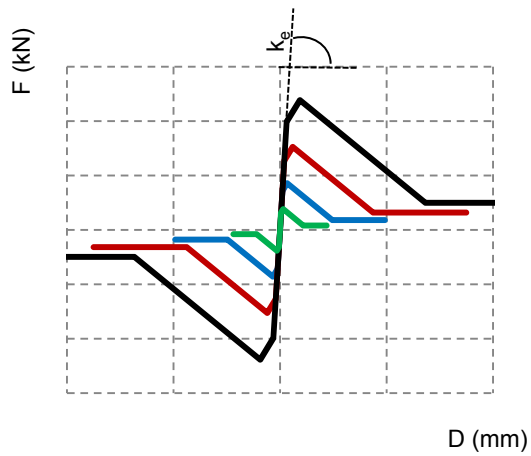

Figure E-8: typical family of backbone curves associated with a series of strength characteristics (Cy) for NLT#4 and NLT#5 models

Again, SAP2000 built-in discrete plasticity model, "Multi-Linear Pivot Hysteretic Plasticity model", is used for modeling of NLT#4 family of discreet nonlinear elements. Figure E-9 shows hysteresis response of NLT#4 for the displacement controlled loading protocol as depicted per Figure E-2 when the elastic period of vibration of the systems is 0.60 Sec and strength characteristic (C_y) of the system is %20.

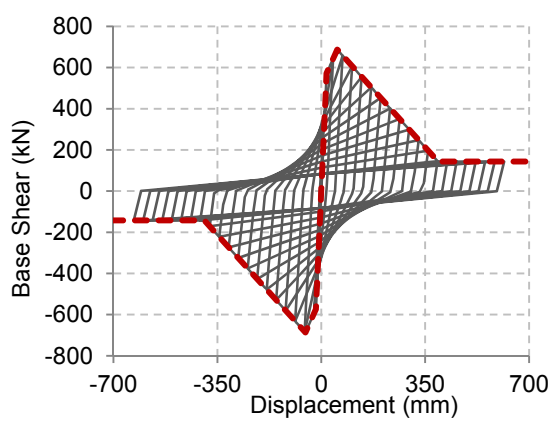

Figure E-9: hysteresis behaviour of a NLT#4 link - defined for a system with elastic period of 0.6 Sec and strength characteristic of %20

Appendix E.5 NLT#5; a multi-linear model with consideration of stress hardening, cyclic and in-cycle strength and stiffness degradation, complete with some residual strength

NLT#5 is very similar to NLT#3, except that its backbone is associated with some %20F_y residual strength; also, NLT#4 negative stiffness starts at $3 \times \Delta_y$ (as opposed to NLT#2, which its negative stiffness starts at $6 \times \Delta_y$).

Family of backbone curves for NLT#5 is similar to that for NLT#4 as depicted in Figure E-8.

Modeling of NLT#5 was done using the same SAP2000 built-in discrete plasticity model that used for modeling of NLT#3; refer to section Appendix E.3 for more information.

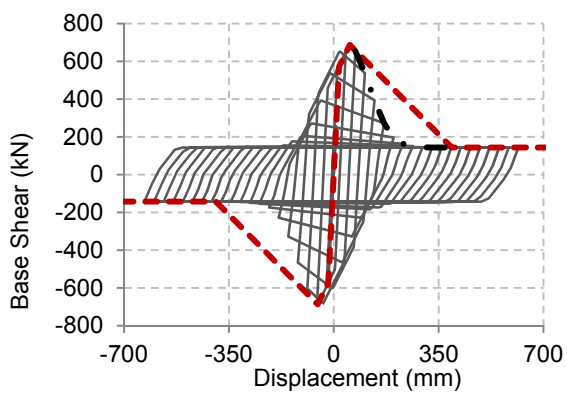

Figure E-10: hysteresis behaviour of a NLT#5 link - defined for a system with elastic period of 0.6 Sec and strength characteristic of %20

Appendix F – PGA matched GMs

Appendix F.1 Screening methods for classifying GMs as pulse-like (NF) or ordinary (FF) GMs, and properties of the selected NF GMs

In the past many researchers have developed libraries of Forward Directivity NF GMs using visual or qualitative selection techniques (e.g., Mavroeidis and Papageorgiou, 2003; Someville, 2003; Akkar et al., 2005). However, lately Baker and Shahi proposed a more quantitative method which uses wavelet analysis to identify the NF pulses within a velocity time history of a GM and extracts it if such is of interest.

Baker and Shahi's proposed method uses a filtering technique, called pulse indicator, which scores the GMs in Terms of their likelihood of being a pulse-like GM in a variety of orientations. Their scoring and filtering procedure in summary consists of:

Step#1: Decomposing the velocity time history signal into non-stationary functions using the wavelet transform function which is somewhat analogues to Fourier transform. Figure F-1 shows the main wavelets that Baker and Shahi used for decomposing GMs.

It is of note that every one of the employed mother wavelets (as presented per Figure F-1) consists of a symmetric double sided pulse which mainly signify the directivity pulses; hence, due to shape of employed wavelets this technique is unable to identify any Fling Step pulse within a NF GM signal as it cannot be represented by any assembly of the proposed mother wavelets as used in Baker and Shahi's routine.

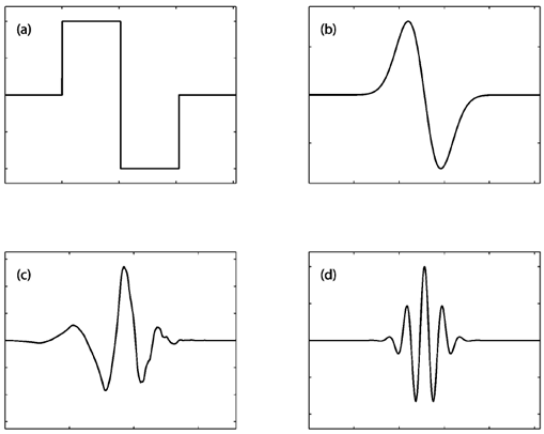

Figure F-1: Common mother wavelets used for wavelet analysis: (a) Haar wavelet, (b) Gaussian wavelet of order 1, (c) Daubechies wavelet of order 4, and (d) Morlet wavelet.

Step#2: Selecting the wavelet which has the most dominant amplitude and enhancing its shape by adding up a few more wavelets (which have close periods and arrival times, to those of the dominant wavelet.

Step#3: Running the selected/extracted wavelet assembly through a threefold qualification criterion to assure the dominant energy content of the extracted wavelet (in compare with the rest of the motion); the threefold qualification criterion consists of:

Pulse Indicator criterion: a predictor of the likelihood that a given record is pulse-like; the Pulse Indicator equation, determined through a logistic regression analysis, is formulated as per equation F-1:

$$Pulse\ Indicatior = \frac{1}{1 + e^{-23.3+14.6(PGV\ Ratio)+205(Energey\ Ratio)}} \qquad \text{F-1}$$

Where:

PGV ratio = the peak ground velocity (PGV) of the residual record divided by the original record's PGV,

Energy ratio = the energy of the residual record divided by the original record's energy [1]

Records with Pulse Indicator scores above 0.85 are classified as pulse-like GMs and, records with Pulse Indicator scores below 0.15 are classified as ordinary records.

1. The pulse arrival time criterion: This criterion intends to ensure that the pulse starts before a significant portion of the original ground motion's Cumulative Squared Velocity (CSV) is observed (i.e. 10% of

[1] Energy Ratio is computed as the Cumulative Squared Velocity of the signal, which is equivalent to sum of the squared discrete wavelet coefficients

pulse total CSV to happen before the original ground motion reaches 20% of its CSV).

2. The peak Ground Velocity Criterion: This criterion indicates that the absolute amplitude of the velocity pulse needs to be large enough, i.e. not less than 30 cm/s.

Given the difference between Forward Directivity and Fling step pulses it was desirable that this research independently accounts for each of them, however after consideration of limited number of available recorded NF GMs associated with Fling Step pulses, and dominance of energy content of Forward Directivity pulses in compare with Fling Step pulses (when both have the same pulse amplitude)[1], eventually only Forward Directivity NF GMs were selected and used in this project.

Appendix F.2 Suite of "PGA matched GMs"

Although this method of matching sounds rudimentary, yet it is a very robust pairing technique as it inherently preserves all unique properties of each NF GM as well as properties or its FF GM counterpart. Namely, in this method the GMs (rotated to Fault-Normal and Fault-Parallel directions) are paired and used for NLTHA with no further amplitude or frequency content manipulation. Section Appendix F.3 details some of the limitations associated with amplitude or frequency manipulation/scaling approaches.

For selection of PGA matched GMs, three different databases were used and their proposed NF GM libraries were compared to make sure a very comprehensive yet reliable set of NF GMs (and their FF GM counterparts) is selected. The three different databases used for selection of PGA matched GMs are:

1. PEER Ground Motion Database
2. Selecting and Scaling Earthquake Ground Motions for Performing Response-History Analyses - NIST GCR 11-917-15 report, available online.

[1] It is of note that energy content of a pulse is directly related to its damaging effect.

3. Jack Baker's research group, online available resources on the topic of "Quantitative classification of pulse-like ground motions" (Mainly Baker and Shahi work, in 2007)

In the course of GM selection, care was exercised to select the NF GMs which are collectively recognized as pulse-like NF GM by all above parties/databases; hence, we have a broad consensus about validity of them as being pulse-like NF GM.[1]

It is of note that the first database (i.e. PEER) only accounts for shallow crustal earthquake and the latter database only recognizes the forward directivity pulses in fault normal direction; hence, by virtue of selecting from overlapped subset of these two databases, the selected PGA matched GMs are only originated from crustal earthquakes, and are only associated with forward directivity effects in fault normal direction.

Appendix F.3 Selection criteria for "PGA matched GMs"

The main criteria were set to allow for selection of pairs of PGA matched GMs in a way that:

a) both members of a pair (one NF and one FF GM) are originated form a single event, and
b) both selected GMs have very close PGA magnitudes,
c) the NF GM set is collectively identified as NF pulses-like GMs by all three different sources/databases, as named in section Appendix F.2.

To enhance the quality of selected NF GMs, three more selection criteria were added which account for:

[1] While Bake and Shahir's proposed technique for selection of pulse like GMs is very efficient (and now is widely accepted by industry, i.e. adopted by NIST GCR 11-917-15 report) yet one can argue that this method is not very reliable as it uses a continuous likelihood functions to produce a binary decision about a record being pulse-like. to offset such an argument; for selection of NF GMs due diligence was exercised to make sure selected NF pulse-like GMs are recognized as pulse-like by all reliable references.

- only events with Mw greater than or equal to 6.0,
- closest distance to rupture plane less than 30 km,
- pulse periods greater than or equal to 1.2 Sec.

The reason for adding the last bullet criterion was that unlike long-period velocity pulses, the velocity pulses with periods shorter than 1.2 Sec are not very clean and visually distinguishable pulses, as they seem very much alike the rest of the velocity signals; thus one might question validity of them as being recognized as NF-pulses. This argument is well evident by comparing Figure F-2 which shows the original NGA record # 1853 along with its associated 0.7 sec extracted velocity pulse with Figure F-3 which shows NGA record # 1483 along with its associated 6.3 sec extracted velocity pulse. It is of note that by this subjective selection criterion a series of GMs which might have effected the response of short to moderate period structures are now excluded from the pool of identified NG-GMs. Nonetheless, one might argue that short period pulses are usually associated with weak to moderate earthquakes; hence, a) their effect could be trivial and b) majority of them are already excluded from the pool of identified NG-GMs by virtue of using the first bullet criterion (i.e. M_w limitation).

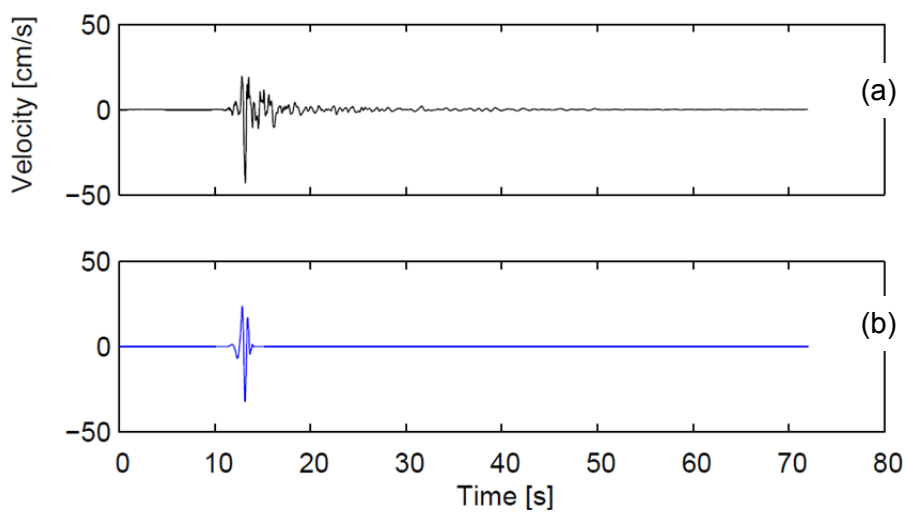

Figure F-2: NGA record # 1853, 2000 Yountville, Napa Fire Station #3, Pulse Period = 0.7 s and PGV = 43 cm/s – (a) recorded motion, (b) extracted pulse (courtesy of Baker's research group)

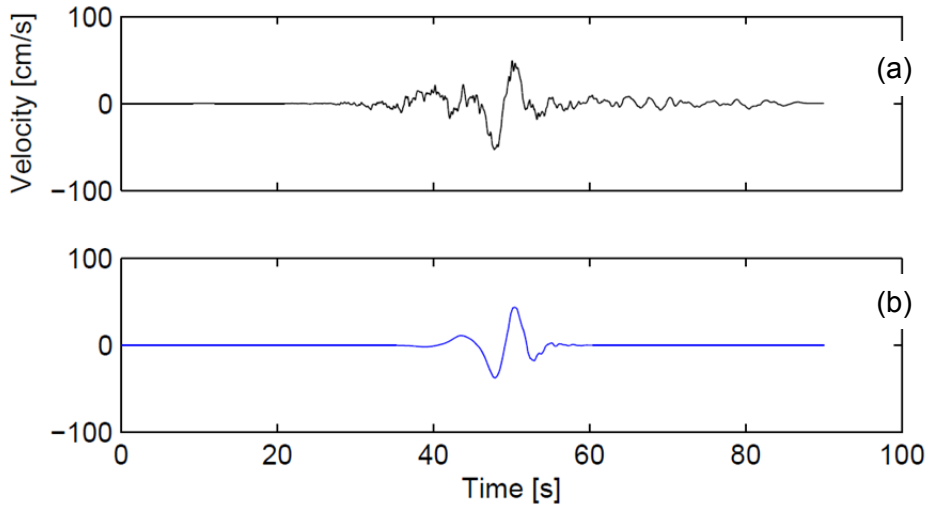

Figure F-3: NGA record # 1483, 1999 Chi-Chi, Taiwan, TCU040, Pulse Period = 6.3 sec and PGV = 53 cm/s – (a) recorded motion, (b) extracted pulse (courtesy of Baker's research group)

Appendix F.4 Selected PGA matched GMs

Each of the three databases named in section Appendix F.2 recognizes different sets of GMs as pulse-like NF GMs; the main source of this discrepancy is due to using different techniques for identifying pulse-like GMs.

NIST GCR 11-917-15 reports a total of 88 pulse-like NF GMs, the fewest number of them in compare with the other two databases (i.e. Baker in Bulletin of the Seismological Society of America, October 2007, listed 91 pulse-like GMS); we started our NF GM selection by applying selection filtering criteria as noted in section Appendix F.3 (i.e. pulse period, magnitude, and site to fault distance limitations) to NIST GCR 11-917-15 report GM library; as a result the list of pulse-like NF GM was down from 88 to 68; of those 68 remaining NF GMs, 14 of them were not recognized as pulse-like GMs by PEER ground motion database; thus, it resulted in total of 54 GMs recognized as pulse-like NF GM by both NIST GCR 11-917-15 report and PEER ground motion database. For three of these 54 remaining NF GMs, no good matching FF GM was found (PGA matching). Hence, again the list was down to 51 GMs. Finally to make sure that selected NF GMs are widely recognized as pulse-like ground motions, the selected list was cross checked with the list of pulse-like GMs identified by Baker research group in 2007, listed in their flatfile available at "Summary results for pulse-like ground motions" (http://www.stanford.edu/~bakerjw/pulse-classification/Pulse_like%20records.xls).

As a result of this cross check, 10 more NF GMs which were only associated with Fault-Parallel pulses (i.e. no Fault-Normal Pulse) were deleted from the list and the list of selected pulse-like NF GMs was again reduced to 40 NF GMs.[1]

Table F-1 summarizes the PGA matched NF GMs along with their FF counterparts. The average M_w for selected PGA matched GMs is 7.1 and the Coefficient Of Variation (COV) of M_w over the entire range of selected GMs is about 7%.

Out of 40 selected PGA matched NF GMs, 15 of them are associated with both Fault-Normal and Fault-Parallel pulses, and the rest only has Fault-Normal pulses.

Appendix F.5 Pulse periods for PGA matched NF GMs:

Median value of periods of Fault-Normal pulses is about 4.11 Sec with an average of 5.35 Sec and a coefficient of variation of some 68%. Similarly, median value of periods of Fault-Parallel pulses is about 3.51 Sec with an average of 4.45 Sec and a coefficient of variation of some 71%.

[1] List of 10 NF GMs associated with Fault-Parallel pulses, but with no Fault-Normal pulses, identified by both PEER database and NIST GCR 11-917-15 report as pulse like GMs, are: NGA# 722, 763, 764, 765, 767, 803, 1148, 1492, 1501, 1602.

Table F-1: List of PGA matched NF and FF GMs

					NF GMs			FF GMs		
#	Event	Event	Mw	Fault Type	NGA #	Dist	Vs30	NGA #	Dist	Vs30
1	Imperial Valley-06	1979	6.53	SS	159	0.65	274.5	165	7.29	274.5
2	Imperial Valley-06	1979	6.53	SS	171	0.07	186.21	169	22.03	274.5
3	Imperial Valley-06	1979	6.53	SS	178	12.85	162.94	162	10.45	231.2
4	Imperial Valley-06	1979	6.53	SS	181	1.35	203.22	164	15.19	659.6
5	Imperial Valley-06	1979	6.53	SS	182	0.56	210.51	189	9.64	338.6
6	Irpinia, Italy-01	1980	6.9	N	292	10.84	1000	288	22.56	500
7	Morgan Hill	1984	6.19	SS	459	9.86	663.31	458	11.54	221.8
8	N. Palm Springs	1986	6.06	RV-OBL	529	4.04	345.419	540	6.04	345.4
9	Superstition Hills-02	1987	6.54	SS	723	0.95	348.69	725	11.16	207.5
10	Loma Prieta	1989	6.93	RV-OBL	766	11.07	270.84	809	18.51	714
11	Cape Mendocino	1992	7.01	RV	828	8.18	712.822	829	14.33	311.8
12	Landers	1992	7.28	SS	900	23.62	353.63	864	11.03	379.3
13	Northridge-01	1994	6.69	RV	1013	5.92	628.99	963	20.72	450.3
14	Northridge-01	1994	6.69	RV	1045	5.48	285.93	1082	10.05	308.6
15	Northridge-01	1994	6.69	RV	1050	7.01	2016.13	1052	7.26	508.1
16	Northridge-01	1994	6.69	RV	1051	7.01	2016.13	1087	15.6	257.2
17	Northridge-01	1994	6.69	RV	1063	6.5	282.25	999	37.36	349.4
18	Northridge-01	1994	6.69	RV	1084	5.35	251.24	1080	13.42	557.4
19	Northridge-01	1994	6.69	RV	1085	5.19	370.52	1077	26.45	336.2
20	Northridge-01	1994	6.69	RV	1086	5.3	440.54	952	18.36	545.7
21	Chi-Chi, Taiwan	1999	7.62	RV-OBL	1182	9.77	438.19	1201	14.82	378.8
22	Chi-Chi, Taiwan	1999	7.62	RV-OBL	1244	9.96	258.89	1504	0.64	433.6
23	Chi-Chi, Taiwan	1999	7.62	RV-OBL	1476	28.05	[426]	1236	37.48	366.2
24	Chi-Chi, Taiwan	1999	7.62	RV-OBL	1480	19.84	[495]	1281	47.16	514.8
25	Chi-Chi, Taiwan	1999	7.62	RV-OBL	1481	25.44	[229]	1535	13.08	424.2
26	Chi-Chi, Taiwan	1999	7.62	RV-OBL	1486	16.74	465.55	1183	40.44	210.7
27	Chi-Chi, Taiwan	1999	7.62	RV-OBL	1489	3.78	487.27	1198	10.97	544.7
28	Chi-Chi, Taiwan	1999	7.62	RV-OBL	1493	5.97	454.55	1246	18.04	223.2
29	Chi-Chi, Taiwan	1999	7.62	RV-OBL	1494	5.3	460.69	1536	11.6	212.7
30	Chi-Chi, Taiwan	1999	7.62	RV-OBL	1505	0.32	487.34	1520	18.16	680
31	Chi-Chi, Taiwan	1999	7.62	RV-OBL	1510	0.91	573.02	1521	8.88	680
32	Chi-Chi, Taiwan	1999	7.62	RV-OBL	1511	2.76	614.98	1512	8.2	443
33	Chi-Chi, Taiwan	1999	7.62	RV-OBL	1515	5.18	472.81	1495	6.36	447.8
34	Chi-Chi, Taiwan	1999	7.62	RV-OBL	1519	7	[562]	1211	39.02	574.7
35	Chi-Chi, Taiwan	1999	7.62	RV-OBL	1528	2.13	[504]	1186	34.18	560.3
36	Chi-Chi, Taiwan	1999	7.62	RV-OBL	1529	1.51	714.27	1184	19.96	549.6
37	Chi-Chi, Taiwan	1999	7.62	RV-OBL	1530	6.1	494.1	1208	24.11	442.1
38	Chi-Chi, Taiwan	1999	7.62	RV-OBL	1548	13.15	599.64	1292	63.43	259
39	Chi-Chi, Taiwan	1999	7.62	RV-OBL	1550	8.29	[538]	1541	12.4	493.1
40	Chi-Chi, Taiwan-03	1999	6.2	RV	2627	14.66	614.98	2622	16.46	624.9

Appendix F.6 Peak ground velocities of PGA matched GMs:

Table F-2 summarizes the variation of PGV for 40 x PGA matched NF GMs and 40 x PGA matched FF GMs in both Fault-Normal and Fault-Parallel directions.

Table F-2: summary of PGV of selected suite of PGA matched GMs

		PGV (cm/Sec)				
		Median	Average	COV	Max	Min
NF GM	Fault-Normal	78.06	35.31	45%	190.67	35.37
	Fault-Parallel	52.68	36.39	69%	237.76	13.85
FF GM	Fault-Normal	32.30	17.97	56%	91.71	7.56
	Fault-Parallel	31.89	17.65	55%	96.37	8.12

Appendix A summarizes the properties of the "PGA matched GMs" and provides more information about individual selected GMs

Appendix F.7 Qualification of "PGA matched GMs "

Likewise any other pairing techniques, PGA Matching as detailed in section Appendix G.1 has its own pros and cones; for example:

1. Selection process is extremely easy and needs no numerical/signal processing.
2. Selected GMs need no amplitude or frequency adjustment; and the native GMs would be directly used as input to NLTHA-FE models
3. Since native GMs are used for numerical analysis, calculated responses of the structures are the closest ones to the real responses have the structure been exposed to the real event/GMs.

And some of its cons are:

1. Having equivalent PGA's for a pair of NF and FF GMs doesn't guarantee that the response spectrum of those GMs have similar shapes or magnitudes over the entire range of periods of interest; indeed, such a scenario is almost impossible to happen in reality.
2. Similarly the average response spectrum of selected NF GMs most probably won't match the shape or magnitude of average response spectrum of their FF GM counterparts.

3. The effect of soil stiffness / site class on recorded input motions is totally ignored in this process; despite the fact that the frequency content or amplitude of a NF GM or its FF counterpart might have been significantly affected by site specific properties. Table F-3 summarizes the site class, where selected PGA matched GMs were recorded, in Terms of shear wave velocity in the upper 30 meters of the soil. It is of note that the variation of site class from record to record is significant.

Table F-3: Summary of shear wave velocity in the upper 30 meters of the site where selected PGA matched GMs were recorded

	$Vs_{30})_{NF\ GMs}$	$Vs_{30})_{FF\ GMs}$	$\frac{Vs_{30})_{NF-GMs}}{Vs_{30})_{FF-GMs}}$
Median	523	421	138%
Average	388	148	106%
COV	74%	35%	77%
Max	2016	714	600%
Min	163	208	31%

Table F-4: Summary of "PGA MATCHED GMS"

NGA#	Earthquake Name	Year	Fault-Normal				Fault-Parallel			
			PI	PGV (cm/Sec)	Pulse	Tp (Sec)	PI	PGV (cm/Sec)	Pulse	Tp (Sec)
159	Imperial Valley-06	1979	100%	54.38	1	2.3	11%	19.76	0	0.95
171	Imperial Valley-06	1979	100%	115.04	1	3.35	97%	27.3	0	4.56
178	Imperial Valley-06	1979	100%	41.1	1	5.24	100%	45.44	1	3.07
181	Imperial Valley-06	1979	100%	111.87	1	3.84	100%	64.72	1	2.58
182	Imperial Valley-06	1979	100%	108.82	1	4.23	94%	44.53	1	4.45
292	Irpinia, Italy-01	1980	94%	41.5	1	3.09	99%	45.51	1	3.45
459	Morgan Hill	1984	100%	35.39	1	1.24	92%	13.85	0	1.21
529	N. Palm Springs	1986	100%	73.63	1	1.38	15%	29.35	0	0.89
723	Superstition Hills-	1987	100%	106.75	1	2.28	84%	49.67	0	3.57
766	Loma Prieta	1989	98%	45.67	1	1.72	93%	27.6	0	1.62
828	Cape Mendocino	1992	92%	82.1	1	3	98%	60.74	1	0.95
900	Landers	1992	100%	53.23	1	7.5	0%	25.02	0	2.69
1013	Northridge-01	1994	100%	77.11	1	1.65	100%	40.75	1	2.79
1045	Northridge-01	1994	100%	87.75	1	2.41	100%	74.75	1	2.18
1050	Northridge-01	1994	87%	50.4	1	0.5	1%	19	0	1.09
1085	Northridge-01	1994	100%	116.56	1	3.49	100%	78.36	0	1.69
1086	Northridge-01	1994	100%	122.72	1	3.11	1%	54.67	0	1.62
1182	Chi-Chi, Taiwan	1999	97%	64.71	1	2.63	0%	42.69	0	1.11
1244	Chi-Chi, Taiwan	1999	100%	85.45	1	4.77	100%	108.7	0	4.92
1476	Chi-Chi, Taiwan	1999	100%	62.34	1	6.45	10%	37.32	0	6.43
1480	Chi-Chi, Taiwan	1999	100%	62.43	1	5.4	100%	48.05	1	6.36
1481	Chi-Chi, Taiwan	1999	100%	50.86	1	6.96	100%	45.69	1	7.78
1486	Chi-Chi, Taiwan	1999	100%	43.96	1	8.58	97%	28.05	0	7.16
1489	Chi-Chi, Taiwan	1999	99%	44.82	1	11.83	2%	57.31	0	9.09
1493	Chi-Chi, Taiwan	1999	100%	41.9	1	12.94	9%	42.35	0	9.22
1494	Chi-Chi, Taiwan	1999	100%	60.92	1	10.47	11%	39.57	0	9.27
1505	Chi-Chi, Taiwan	1999	100%	191.15	1	12.17	100%	236.56	1	11.3
1510	Chi-Chi, Taiwan	1999	100%	88.44	1	5.15	5%	38.12	0	8.45
1511	Chi-Chi, Taiwan	1999	92%	63.73	1	3.98	14%	63.17	0	5.11
1515	Chi-Chi, Taiwan	1999	95%	56.12	1	9.18	3%	49.36	0	8.97
1519	Chi-Chi, Taiwan	1999	100%	53.67	1	9.04	57%	43.24	0	5.47
1528	Chi-Chi, Taiwan	1999	100%	68.39	1	10.04	99%	53.05	1	6.55
1529	Chi-Chi, Taiwan	1999	97%	106.57	1	9.72	97%	77.56	1	3.81
1530	Chi-Chi, Taiwan	1999	100%	62.18	1	8.26	7%	28.03	0	7.81
1548	Chi-Chi, Taiwan	1999	100%	78.66	1	9.01	86%	48.25	1	10.36
1550	Chi-Chi, Taiwan	1999	100%	51.82	1	10.33	100%	51.33	1	7.91
1051	Northridge-01	1994	100%	107.07	1	0.9	76%	50.37	0	0.48
1063	Northridge-01	1994	100%	167.2	1	1.23	99%	62.71	1	3.01
1084	Northridge-01	1994	92%	130.27	1	3.48	82%	93.3	0	1.63
2627	Chi-Chi, Taiwan-	1999	100%	59.35	1	0.91	98%	19.47	0	1.19
		Sum	-	-	40	-		-	15	-
		Median	-	64.22	-	4.105	-	45.6	-	3.69
		Average	99%	78.15075	-	5.344	63%	52.13175	-	4.56875
		COV	3%	45%	-	68%	68%	69%	-	69%
		Max	-	191.15	-	12.94	-	236.56	-	11.3
		Min	-	35.39	-	0.5	-	13.85	-	0.48

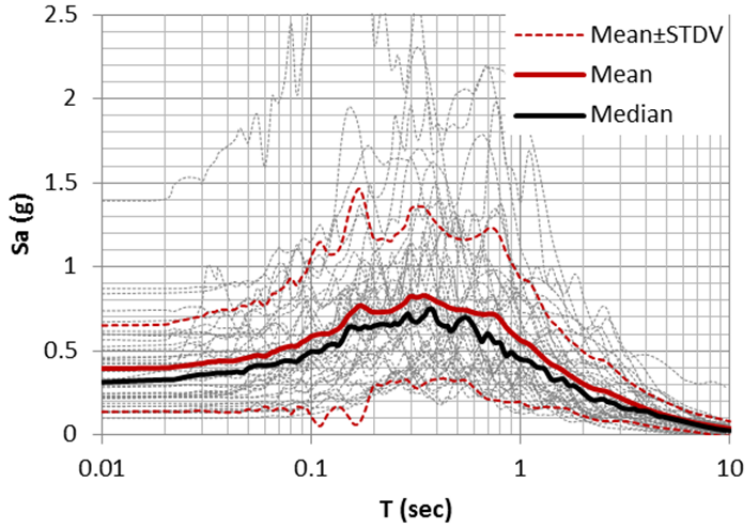

Figure F-4: 5% Damped Response Spectrum of Fault-Normal Components of 40 x PGA matched NF GMs

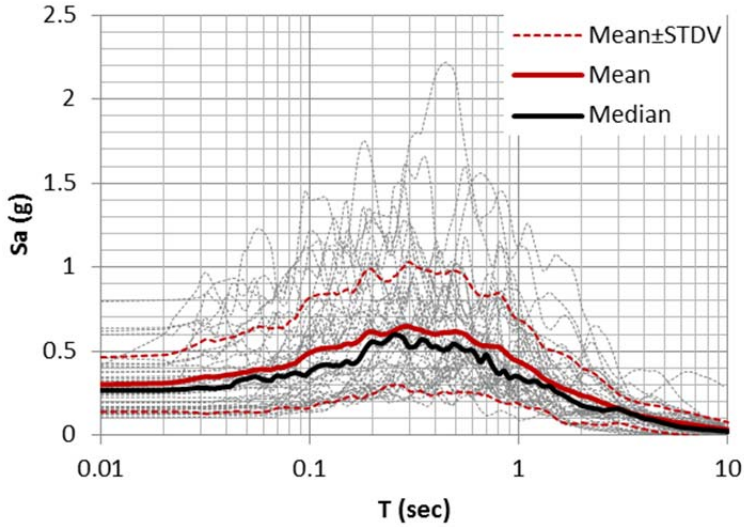

Figure F-5: 5% Damped Response Spectrum of Fault-Parallel Components of 40 x PGA matched NF GMs

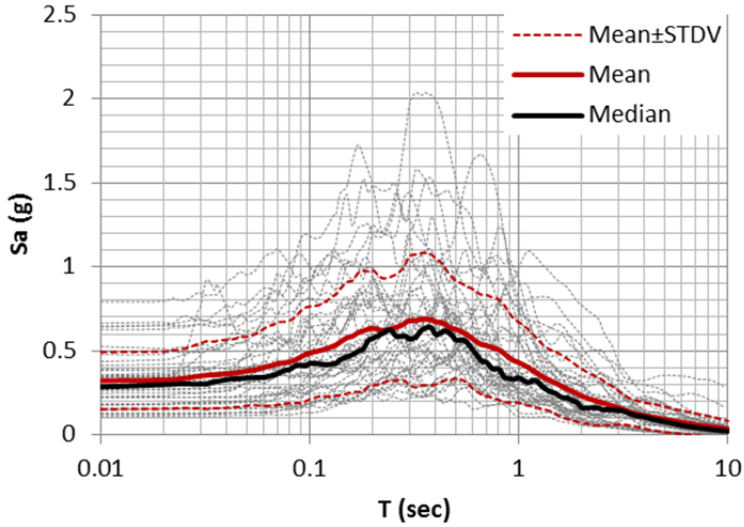

Figure F-6: 5% Damped Response Spectrum of Geometric Mean of Horizontal Components of 40 x PGA matched NF GMs

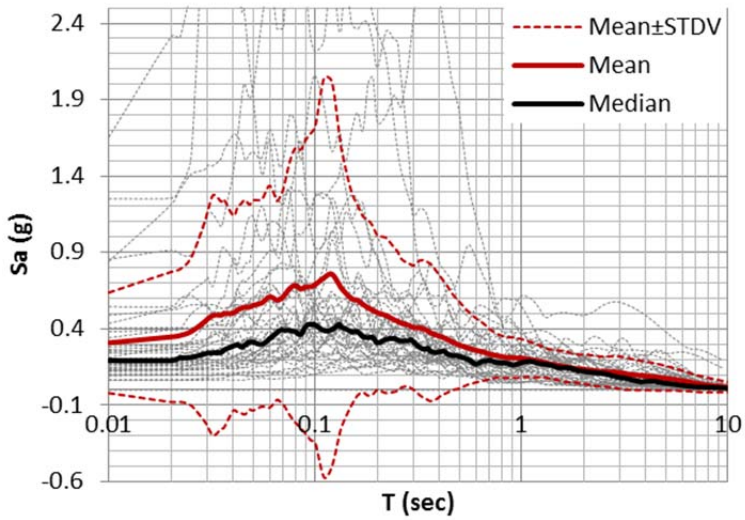

Figure F-7: 5% Damped Response Spectrum of Vertical Components of 40 x PGA matched NF GMs

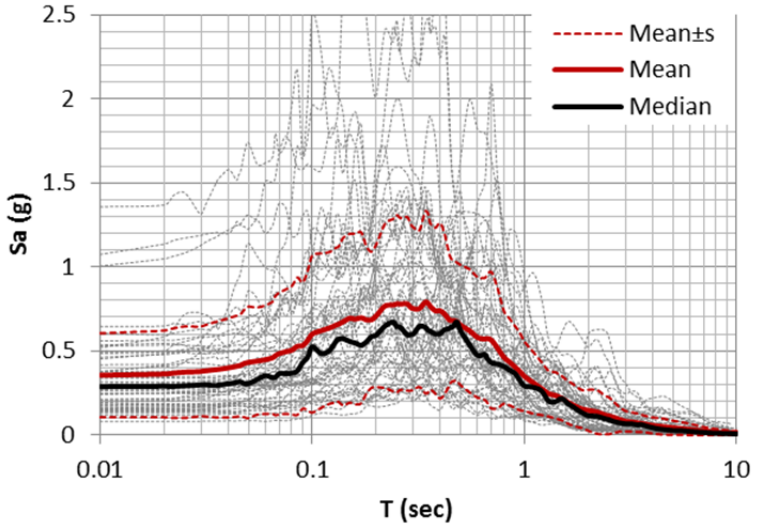

Figure F-8: 5% Damped Response Spectrum of Fault-Normal Components of 40 x PGA matched FF GMs

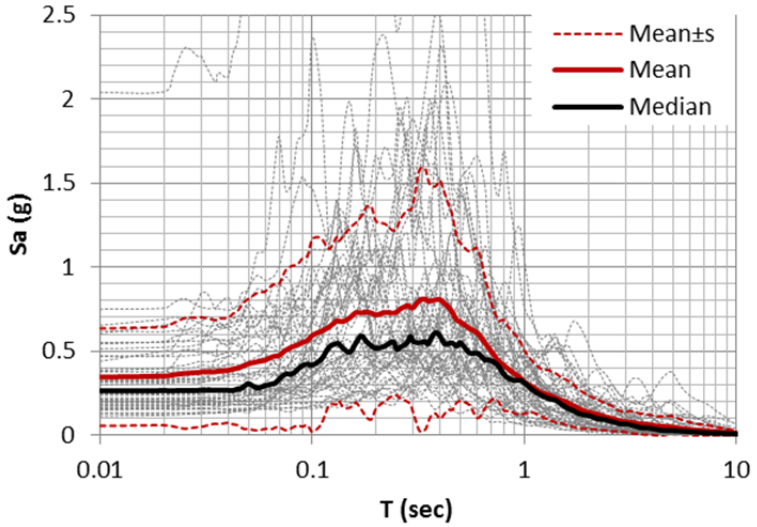

Figure F-9: 5% Damped Response Spectrum of Fault-Parallel Components of 40 x PGA matched FF GMs

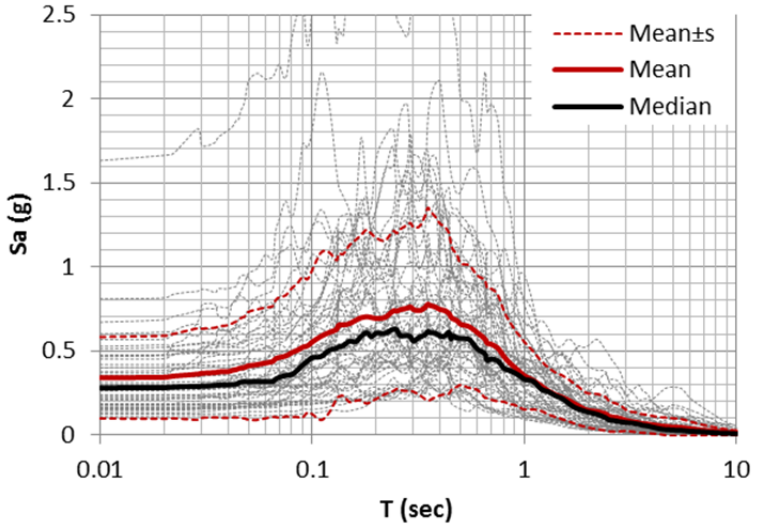

Figure F-10: 5% Damped Response Spectrum of Geometric Mean of Horizontal Components of 40 x PGA matched FF GMs

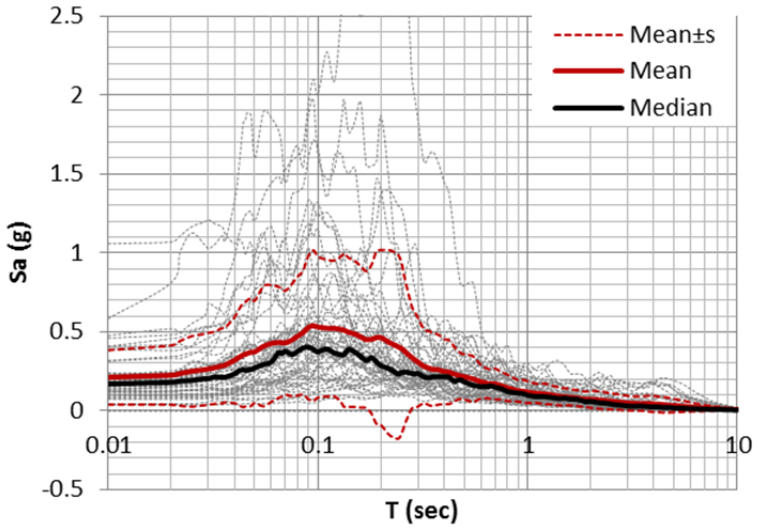

Figure F-11: 5% Damped Response Spectrum of Vertical Components of 40 x PGA matched FF GMs

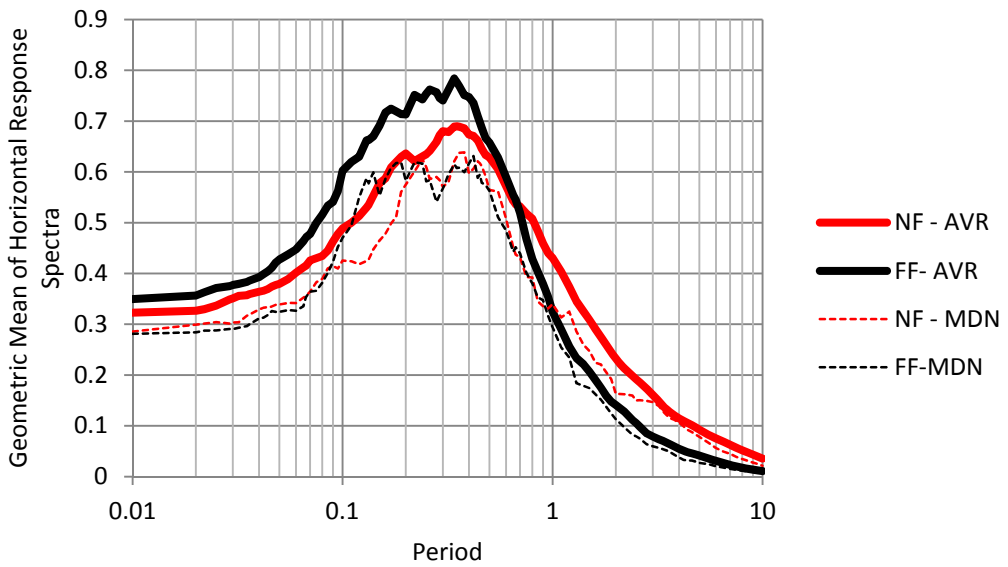

Figure F-12: Comparison of 5% Damped Response Spectrum of FF and NF GMs

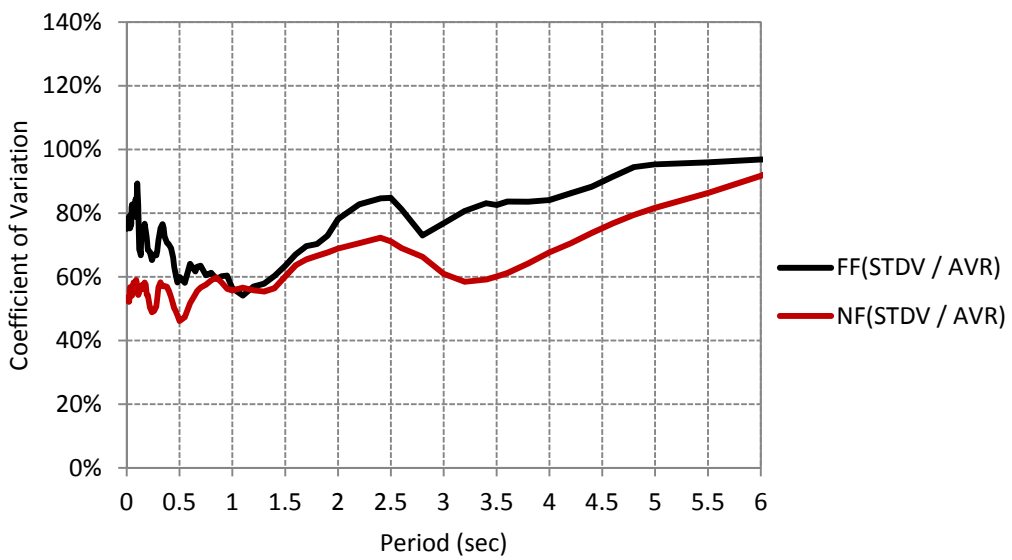

Figure F-13: Dispersion of 5% Damped Response Spectrum of FF and NF GMs

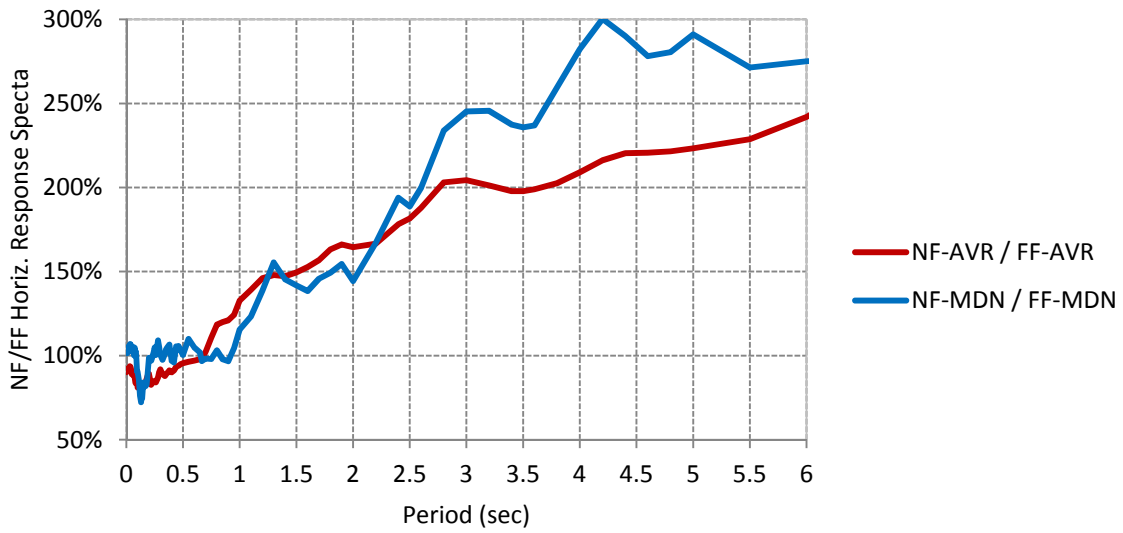

Figure F-14: Comparison of 5% Damped Response Spectrum of FF and NF GMs

Appendix G – Linearly scaled GMs

Selected Set of “Linearly scaled GMs”

(30 near-fault and 30 ordinary ground motions linearly scaled to UHARS of Vancouver, BC)

- Used PEER Ground Motion Database for selection of:
  - 30 NF ground motions associated with long period velocity pulses
  - 30 FF ground motions
- Linearly matching to a target response spectrum (1/2475yrs UHARS of Vancouver, Bc)

Appendix G.1 Suite of “linearly scaled GMs”

As mentioned in section 3.3.1.1, to allow for selection of a comparable suite of NF and FF GMs one may decide to scale them all to a baseline, e.g. a target response spectrum.

It is of important note that although this pairing technique is **NOT** recommended for practical projects(refer to section Appendix G.4-Qualification of “linear scaling “for the NF GMs) it is yet presented here for pure academic reasons to allow for investigating the effect of different pairing techniques on the final results.

The NBCC2010 code based %5 damped UHRS with 2% probability of exceedance in 50 years, determined for a reference ground conditions (Site Class C) in Vancouver, BC was set as the baseline (target spectrum) for selecting NF and FF GMs. See Figure G-1.

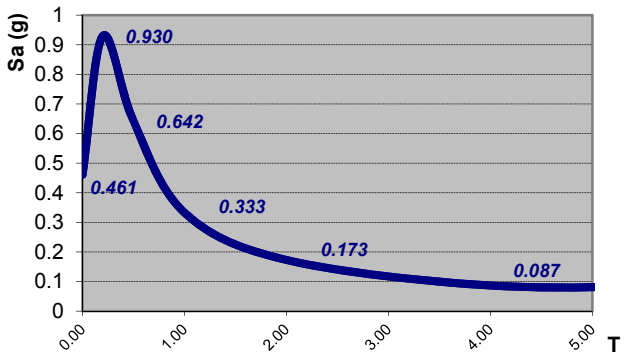

Figure G-1: 1/ (2475 yrs) UHRS - For Site Class "C" in Vancouver

Matching to this target spectrum could be done either in frequency domain or in time domain; respectively called spectrally matching and linear scaling procedures. Spectrally matching procedure involves manipulating the original ground motion by means of decomposing it to a series of harmonic excitations and tweaking the phase angle and the amplitudes of each decomposed component to reach to the best fit to the target spectrum. While this process can retain the general shape of the original GM, yet the frequency content of the spectrally matched GMs could be widely different from what is in original GMs. Obviously such a phenomenon is much more pronounced when NF GMs (associated with strong long-period velocity pulses) are matched to a smoothed response spectrum which does not explicitly account for particularities of the NF GMs. Conversely, linear scaling of recorded

motions to match the target spectrum is a very effective and simple approach, which preserves the frequency content of the original ground motions. As such, the linear scaling method for scaling of selected GM response spectra to the target spectra was used to allow for preservation of frequency content of the ground motions.

The linear scaling factor for each GM was determined in a way to minimize the Mean Squared Error (MSE) between the spectra of the scaled records and the target spectrum over the period range of interest (0.15sec to 2.0sec). The MSE procedure was applied to the geometric mean of the two horizontal components (FN and FP) for calculation of scale factors for each GM in data base and finally the GMs were ranked and selected based on their scaled MSE. Obviously this approach results in selection of records that have spectral shapes that are similar on average to the target response spectrum over the period range of interest, however individual spectra fluctuates about the target response spectrum.

The MSE, used in selection of GMs, is defined as:

$$MSE = \frac{\sum_i w(Ti)\,\{ln\left[SA_{trarget}\,(Ti)\right] - ln\,[\,f\ \times\ SA_{record}\,(Ti)]\}^2}{\sum_i w(Ti)}$$

Where, f is the linear scale factor applied to the entire response spectrum, and $w(Ti)$ is a weight function that assigns relative weights to different parts of the period range of interest to emphasize the importance of each part of period range of interest.

The determined scale factors applied as a uniform scale factor to all three components of ground motion, so the relative amplitude of different components remains unchanged.

Appendix G summarizes the properties of the “Linearly scaled GMs” and provides more information about individual selected GMs.

Appendix G.2 Selection criteria for “linearly scaled GMs”

PEER Ground Motion Database was used for selection of 30 x NF GMs (associated with long period velocity pulses), and 30 x FF GMs, while both suites were linearly scaled to closely match the target spectrum as described in section Appendix G.1

Below is a summary of filtering criteria used for selection of “Linearly scaled GMs”:

- The moment magnitude for both suites of the NF GMs and their FF GM counterparts are more than 5.8, and less than 8.
- No limitation for fault mechanisms.
- No limitation for strong motion duration (duration is defined as the time needed to build up between 5 and 95 percent of the total Arias intensity).
- No limitation for Joyner-Boore distance;
- The closest distance to rupture plane, for the NF GMs is less than 20km; and for FF GMs is more than 25km
- V_{30} is more than 360m/s (This criterion is set to exclude the GMs recorded on soft soils.
- The period dependent weight factor is 1.0 for any period between 0.15 to 2.0 Sec and 0 for any period above 10 Sec. Weight factor between 0 to 0.15 Sec and 2 to 10 Sec varies linearly with respect to 10^T when T is period of vibration.

Appendix G.3 Selected linearly scaled GMs

Based on selection criteria detailed in section Appendix G.2 a suite of 30xFF GMs and a suite of 30xNF GMs, rotated to Fault-Normal and Fault-Parallel directions, were selected and linearly matched to the target spectrum. All ground motions were selected using PEER Ground Motion Database.

Summary of selected 30xLinearly Scaled NF GMs is presented in Table G-1. Similarly, summary of selected 30xLinearly Scaled FF GMs is presented in Table G-2.

Figure G-2 depicts the geometric mean and arithmetic mean horizontal response spectra of selected linearly scaled NF GMs. Horizontal response spectrum of each individual member of suite of linearly scaled NF GMs is determined based on geometric mean of Fault-Normal and Fault-Parallel Components of that individual GM. Similarly Figure G-3 depicts the geometric mean and arithmetic mean horizontal response spectra of selected linearly scaled FF GMs. The shaded areas on Figure G-2 and Figure G-3 shows the period range of interest which used for scaling purposes.

Table G-1: Summary of selected 30 x linearly scaled NF GMs

NGA#	Scale Factor	Pulse	Event	Year	Mag	Mechanism	Rrup (km)	Vs30 (m/s)
77	54%	FN Pulse	San Fernando	1971	6.61	Reverse	1.8	2016.1
292	113%	FN & FP Pulse	Irpinia- Italy-01	1980	6.9	Normal	10.8	1000
496	157%	FP Pulse	Nahanni- Canada	1985	6.76	Reverse	4.9	659.6
568	82%	FN & FP Pulse	San Salvador	1986	5.8	Strike-Slip	6.3	545
779	53%	FN & FP Pulse	Loma Prieta	1989	6.93	Reverse-Oblique	3.9	477.7
802	103%	FN Pulse	Loma Prieta	1989	6.93	Reverse-Oblique	8.5	370.8
803	112%	FN & FP Pulse	Loma Prieta	1989	6.93	Reverse-Oblique	9.3	370.8
825	53%	FP Pulse	Cape Mendocino	1992	7.01	Reverse	7	513.7
828	72%	FN & FP Pulse	Cape Mendocino	1992	7.01	Reverse	8.2	712.8
879	71%	FN Pulse	Landers	1992	7.28	Strike-Slip	2.2	684.9
983	59%	FN Pulse	Northridge-01	1994	6.69	Reverse	5.4	525.8
1013	90%	FN & FP Pulse	Northridge-01	1994	6.69	Reverse	5.9	629
1050	149%	FN Pulse	Northridge-01	1994	6.69	Reverse	7	2016.1
1085	61%	FN Pulse	Northridge-01	1994	6.69	Reverse	5.2	370.5
1086	61%	FN Pulse	Northridge-01	1994	6.69	Reverse	5.3	440.5
1148	256%	FP Pulse	Kocaeli- Turkey	1999	7.51	Strike-Slip	13.5	523
1182	103%	FN Pulse	Chi-Chi- Taiwan	1999	7.62	Reverse-Oblique	9.8	438.2
1193	132%	FP Pulse	Chi-Chi- Taiwan	1999	7.62	Reverse-Oblique	9.6	427.7
1202	129%	FN Pulse	Chi-Chi- Taiwan	1999	7.62	Reverse-Oblique	12.7	555.2
1486	256%	FN Pulse	Chi-Chi- Taiwan	1999	7.62	Reverse-Oblique	16.7	465.6
1489	131%	FN Pulse	Chi-Chi- Taiwan	1999	7.62	Reverse-Oblique	3.8	487.3
1493	180%	FN Pulse	Chi-Chi- Taiwan	1999	7.62	Reverse-Oblique	6	454.6
1494	170%	FN Pulse	Chi-Chi- Taiwan	1999	7.62	Reverse-Oblique	5.3	460.7
1499	221%	FN Pulse	Chi-Chi- Taiwan	1999	7.62	Reverse-Oblique	8.5	495.8
1510	120%	FN Pulse	Chi-Chi- Taiwan	1999	7.62	Reverse-Oblique	0.9	573
1511	94%	FN Pulse	Chi-Chi- Taiwan	1999	7.62	Reverse-Oblique	2.8	615
1515	144%	FN Pulse	Chi-Chi- Taiwan	1999	7.62	Reverse-Oblique	5.2	472.8
1528	139%	FN & FP Pulse	Chi-Chi- Taiwan	1999	7.62	Reverse-Oblique	2.1	504.4
2457	265%	FN Pulse	Chi-Chi- Taiwan-03	1999	6.2	Reverse	19.6	427.7
2627	167%	FN Pulse	Chi-Chi- Taiwan-03	1999	6.2	Reverse	14.7	615
Average	127%	-	-	-	7.1	-	7.43	628.31
COV	49%	-	-	-	7%	-	61%	63%
Max	265%	-	-	-	7.62	-	19.6	2016.1
Min	53%	-	-	-	5.8	-	0.9	370.5

Table G-2: Summary of selected 30 x linearly scaled FF GMs

NGA#	Scale Factor	Pulse	Event	Year	Mag	Mechanism	Rrup(km)	Vs30(m/s)
40	800%	None	Borrego Mtn	1968	6.63	Strike-Slip	129.1	442.9
135	745%	None	Santa Barbara	1978	5.92	Reverse-Oblique	27.4	438.3
357	366%	None	Coalinga-01	1983	6.36	Reverse	34	376.1
746	431%	None	Loma Prieta	1989	6.93	Reverse-Oblique	53.6	391
762	290%	None	Loma Prieta	1989	6.93	Reverse-Oblique	39.5	367.6
910	481%	None	Big Bear-01	1992	6.46	Strike-Slip	[41.9]	379.3
942	326%	None	Northridge-01	1994	6.69	Reverse	36.8	550
975	595%	None	Northridge-01	1994	6.69	Reverse	53.9	446
1015	426%	None	Northridge-01	1994	6.69	Reverse	51.9	405.2
1046	570%	None	Northridge-01	1994	6.69	Reverse	85.5	405.2
1190	539%	None	Chi-Chi- Taiwan	1999	7.62	Reverse-Oblique	50.5	478.3
1191	582%	None	Chi-Chi- Taiwan	1999	7.62	Reverse-Oblique	64.2	486.5
1281	321%	None	Chi-Chi- Taiwan	1999	7.62	Reverse-Oblique	47.2	514.8
1325	510%	None	Chi-Chi- Taiwan	1999	7.62	Reverse-Oblique	83.3	649.2
1812	623%	None	Hector Mine	1999	7.13	Strike-Slip	84.9	370.8
2107	434%	None	Denali- Alaska	2002	7.9	Strike-Slip	50.9	963.9
2113	590%	None	Denali- Alaska	2002	7.9	Strike-Slip	54.8	382.5
2115	533%	None	Denali- Alaska	2002	7.9	Strike-Slip	126.4	376.1
2253	713%	None	Chi-Chi- Taiwan-02	1999	5.9	Reverse	46.6	389.8
2940	704%	None	Chi-Chi- Taiwan-05	1999	6.2	Reverse	88.2	478.3
2946	634%	None	Chi-Chi- Taiwan-05	1999	6.2	Reverse	59.8	544.7
2952	765%	None	Chi-Chi- Taiwan-05	1999	6.2	Reverse	67.7	680
2982	408%	None	Chi-Chi- Taiwan-05	1999	6.2	Reverse	80.3	366.2
3025	732%	None	Chi-Chi- Taiwan-05	1999	6.2	Reverse	40.7	642.7
3027	462%	None	Chi-Chi- Taiwan-05	1999	6.2	Reverse	57.2	501.4
3202	727%	None	Chi-Chi- Taiwan-05	1999	6.2	Reverse	52.8	714.3
3224	800%	None	Chi-Chi- Taiwan-05	1999	6.2	Reverse	59.2	424
3283	794%	None	Chi-Chi- Taiwan-06	1999	6.3	Reverse	72.3	432.9
3471	503%	None	Chi-Chi- Taiwan-06	1999	6.3	Reverse	26.3	573
3472	383%	None	Chi-Chi- Taiwan-06	1999	6.3	Reverse	25.9	615
Average	560%	-	-	-	6.72	-	60.38	492.87
COV	28%	-	-	-	10%	-	43%	27%
Max	800%	-	-	-	7.90	-	129.10	963.90
Min	290%	-	-	-	5.90	-	25.90	366.20

Figure G-4 shows the ratio of geometric mean and arithmetic mean horizontal lastic response spectra of the selected linearly scaled NF GMs to those of linearly scaled FF GMs. Figure G-4 intends to illustrate the relative expected response of an elastic system (which its response is governed by response of the first mode ovf vibration) due to each of selected sets of linearly scaled GMs.

For detailed properties of selected linearly scaled GMs refer to Appendix G.

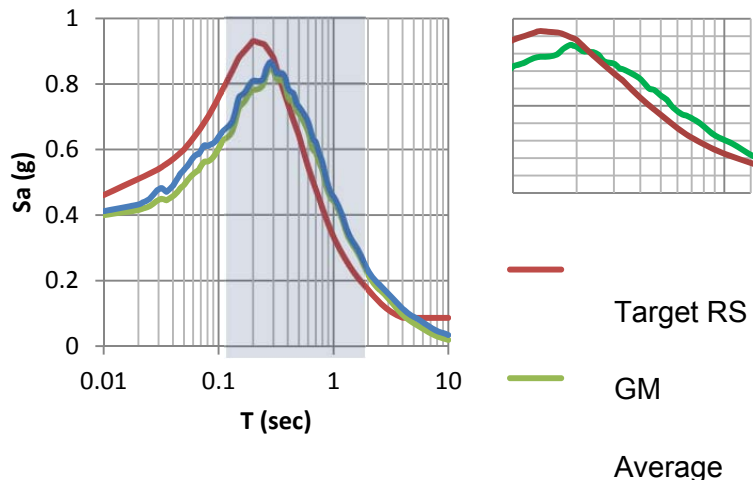

Figure G-2: Geometric Mean and Arithmetic Mean Horiz. Response Spectra for the NF GMs

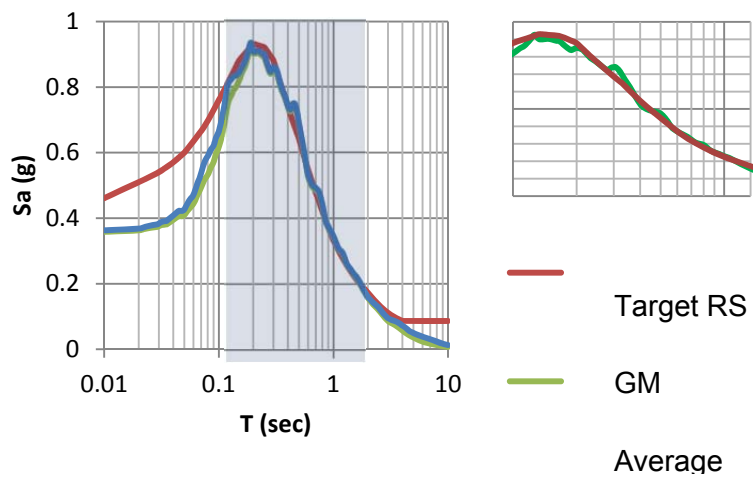

Figure G-3: Geometric Mean and Arithmetic Mean Horiz. Response Spectra for FF GMs

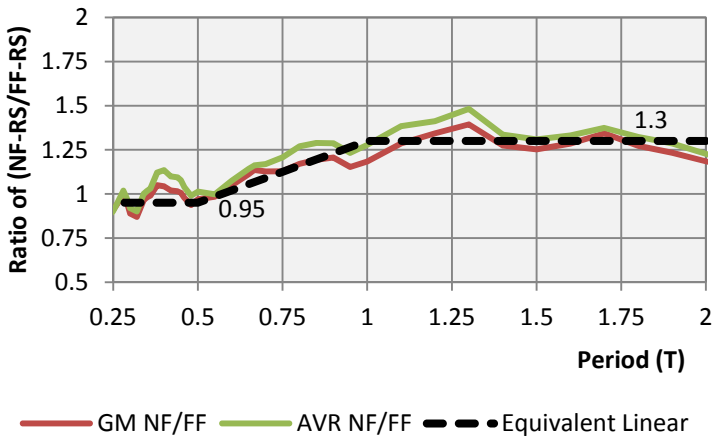

Figure G-4: Ratio of Geometric Mean and Arithmetic Mean Horiz. Response Spectra of linearly scaled NF GMs to linearly scaled FF GMs for Period Range of Interest

Appendix G.4 Qualification of "linear scaling "for the NF GMs

Similar to what mentioned in section Appendix G.1 , linear scaling to the target response spectrum has its own pros and cones. Some of its pros are:

1. Implemented of this approach is very simple and straightforward,
2. The selection routine is readily available as the algorithm is inbuilt in PEER database interface,
3. The process allows for a good match over a broad range of periods; hence responses of structures due to each set of selected GMs could be compared over the entire range of periods of interest,

and some of its cons are:

1. The process of scaling to a single target spectrum doesn't differentiate between Fault-Normal and Fault-Parallel components of the NF GMs. to accurately characterize near fault ground motions, it is required to specify separate response spectra for the Fault-Normal and Fault-Parallel components of the NF GMs; then one can select the NF GMs based on a weighted average of MSE for two horizontal components.
2. One of the big caveats in this approach is that the scoring process for selection of GMs is based on minimizing each GMs' MSE by way of applying a scale factor to it. However, applying a scale factor is equivalent to

considering a hypothetical new GM which its energy content is different from the original GM. This inherently means that we are considering a scenario earthquake which is originated from a similar source but either its site to source distance is different or the M_w of its source event is different (or both). Nonetheless, each of these factors (i.e. site to source distance or M_w) can influence the period of the NF strong velocity pulses. In another word, although by virtue of scaling we implicitly account for a different distance to fault or M_w (or both); we do not accordingly consider a change in the pulse period for the scaled NF GM. In summary: while linear scaling method is widely acceptable for ordinary GMs, it can significantly jeopardize the unique properties of each NF GM and make the validity of the results somewhat questionable.

3. The strong long-period pulses associated with NF GMs inherently amplify their elastic response spectra over a narrow period range in vicinity of the pulse periods. Now, if this pulse period falls within the period range of interest it is almost impossible to achieve a good match to target spectrum as the linearly scaled response of the NF GM systematically surpasses the target spectrum in vicinity of the pulse period and falls below it for the remaining period range of interest. See Figure G-2 and Figure G-4.

It is of note that Carballo and Cornell (2000) showed that inelastic response is nonlinearly related to the intensity of the input motions, i.e. the intensities higher than the target spectrum produce disproportionately larger inelastic demands. Therefore, the median inelastic response of the scaled NF GMs for the pulse period range (where their elastic responses systematically exceed the target spectrum) could be skewed toward the higher values, while an opposite trend is expected for the rest of period range of interest. In another word if one compares the inelastic response of the linearly scaled NF GMs with those of linearly scaled FF GMs (which tightly match the target spectrum for the entire period range of interest) they may overestimate the NF effects around the pulse period and vice versa for the rest of period range of interest.

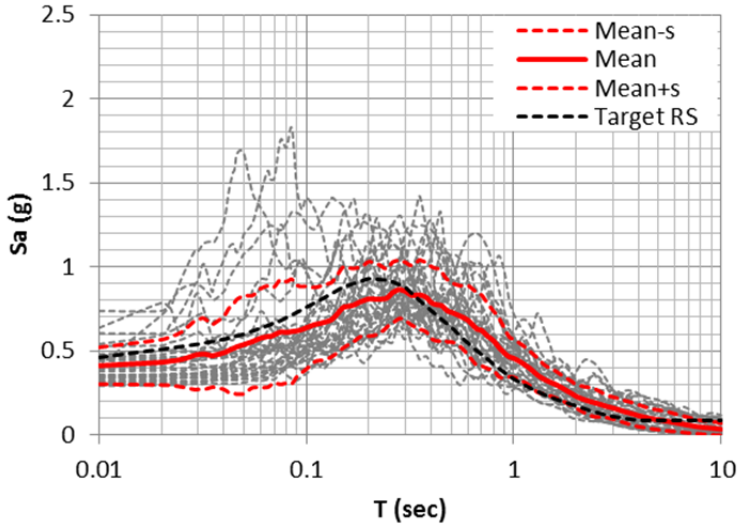

Figure G-5: 5% Damped Response Spectrum of Fault-Normal Component of 30 x linearly scaled NF GMs

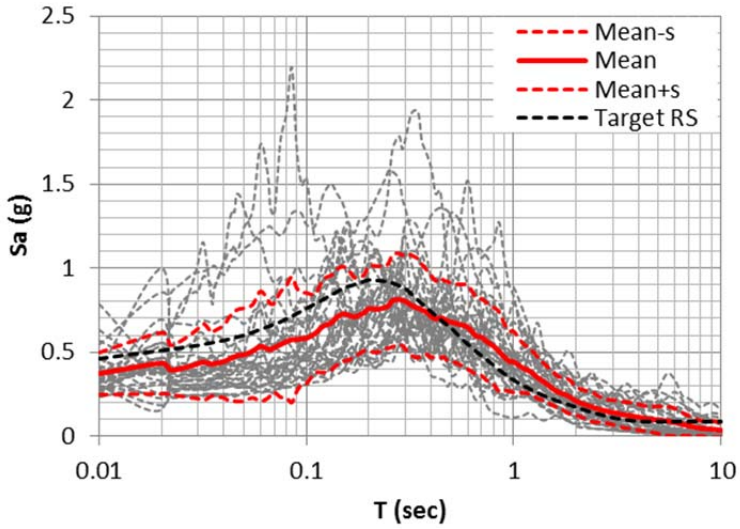

Figure G-6: 5% Damped Response Spectrum of Fault-Parallel Component of 30 x linearly scaled NF GMs

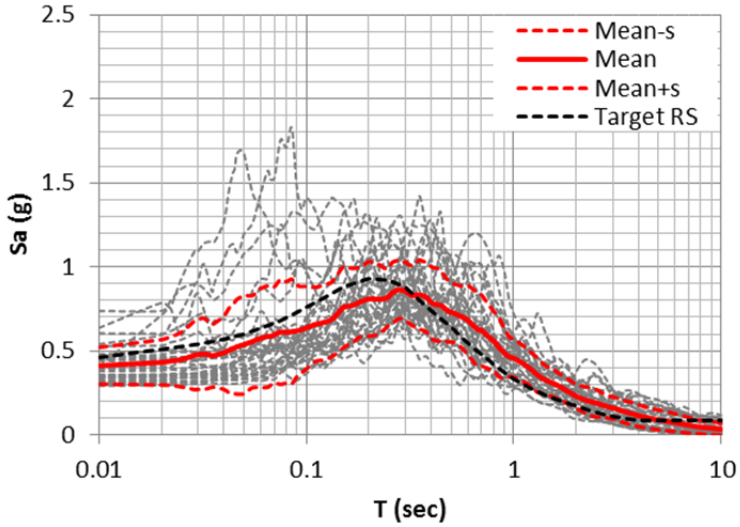

Figure G-7: 5% Damped Response Spectrum of Geometric Mean of Horizontal Components of 30 x linearly scaled NF GMs

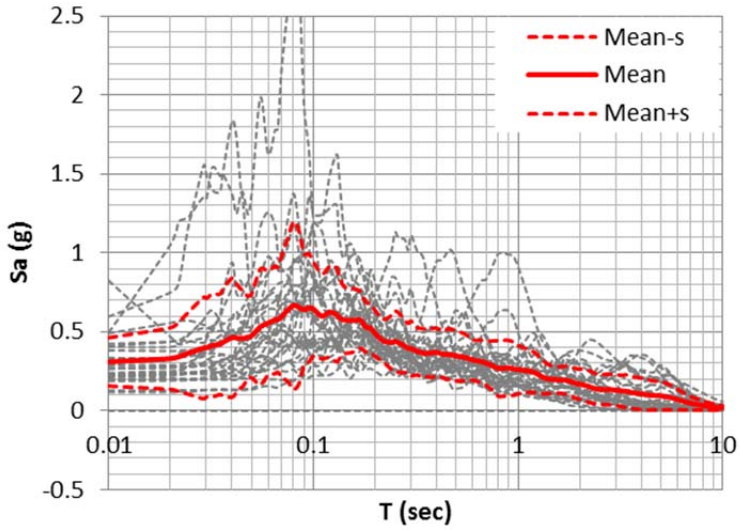

Figure G-8: 5% Damped Elastic Response Spectrum of Vertical Components of 30 x linearly scaled NF GMs

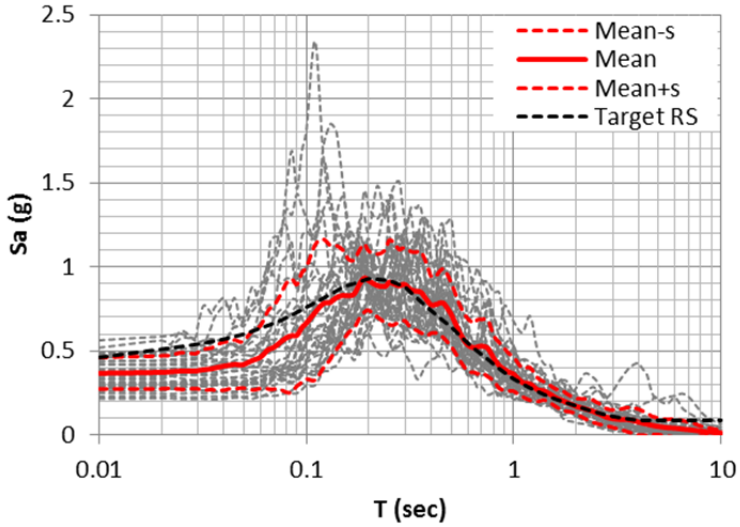

Figure G-9: 5% Damped Response Spectrum of Fault-Normal Component of 30 x linearly scaled FF GMs

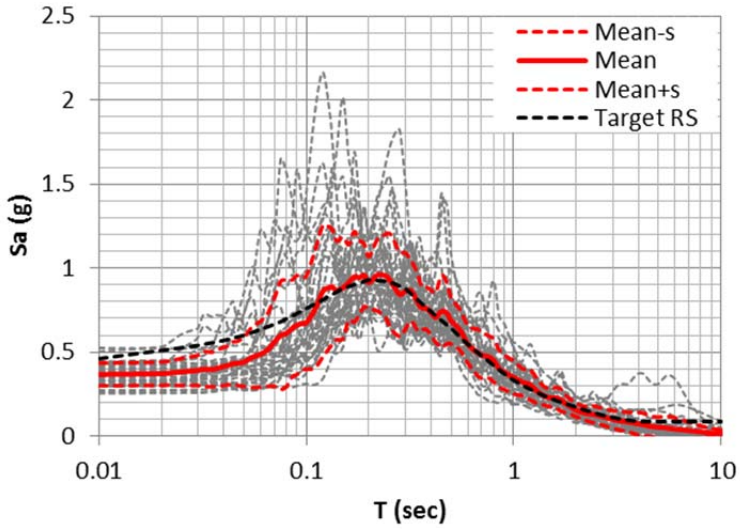

Figure G-10: 5% Damped Response Spectrum of Fault-Parallel Component of 30 x linearly scaled FF GMs

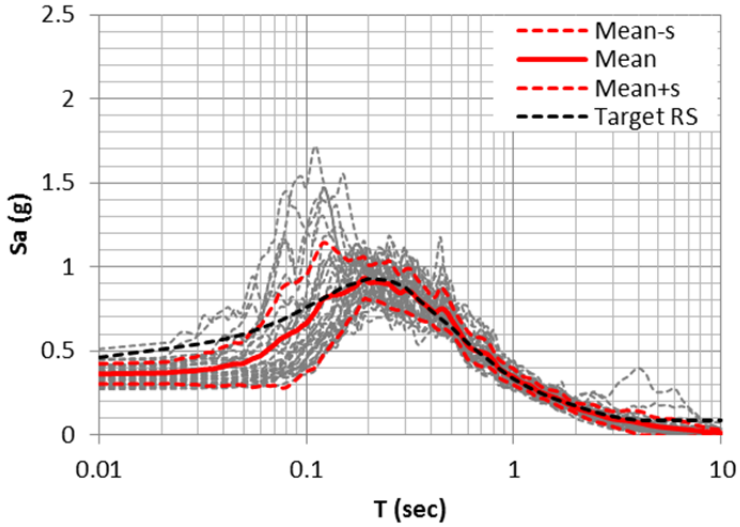

Figure G-11: 5% Damped Response Spectrum of Geometric Mean of Horizontal Components of 30 x linearly scaled FF GMs

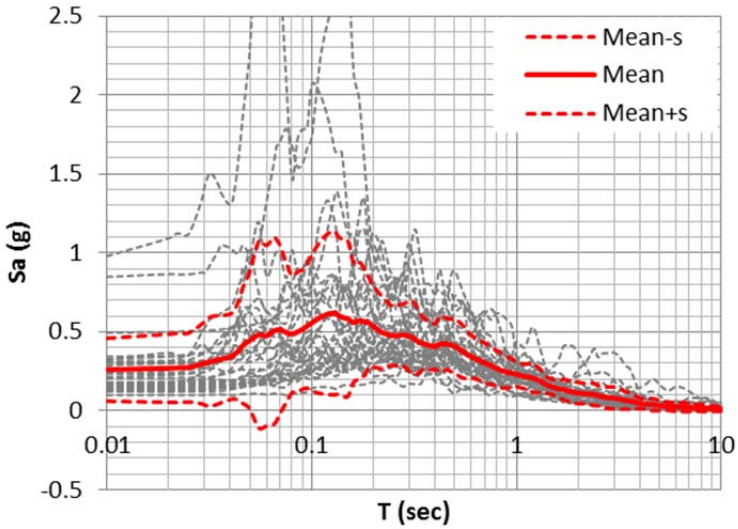

Figure G-12: 5% Damped Response Spectrum of Vertical Components of 30 x linearly scaled FF GMs

Appendix H - Signal analysis and details of the selected PGA matched GMs

General

This appendix summarizes:

- the properties of the original rotated Near-Fault ground motion as were extracted from PEER website - depicted with red color in following graphs.
- the properties of the “filtered” rotated Near-Fault ground motion as detailed per point “a”- depicted with blue color on following graphs.
- the properties of the “baseline corrected ” filtered ground motions as detailed per point “b”- depicted with blue color on following graphs.

The Butterworth Filter Function was used as a low frequency pass filter for processing Near-Fault ground motions to extract the low frequency content of the native rotated Near-Fault ground motions and filter out the high frequency content of Near-Fault ground motions out. Butterworth filter functions and equations are based on Analog Electronics By L.K. Maheshwari M.M.S. Anand. For more details refer to the following section.

It is of note that in some cases filtering caused an accumulative error/deviation from the displacement baseline over duration of strong ground motion. This error/deviation from the base line monolithically builds up due to integration process over the time domain. Although, the effect of this error on filtered acceleration ground motions and their corresponding elastic response spectra is negligible, yet a 3rd order polynomial baseline correction process was utilized to make the filtered inputs more realistic. Since none of the selected Near-Fault input ground motions shows significant residual displacement at the end its duration (corresponding to fling effects), this approach deemed to be appropriate; hence, the resultant signal deemed to be a proper representative of low frequency content of Near-Fault Ground motions. Note, that base line correction would have been accounted for any filing effect (residual displacement) if the original Near-Fault input ground motion would have showed such a phenomenon.

Butterworth filter amplitude response:

The Butterworth filter is a maximally flat response within the pass-band, with no response ripples (as is the case in many other forms of RF filter).

Figure H2-1, depicts the proposed Butterworth filter magnitude with a low-pass frequency of 0.5 Hz as used for processing Near-Fault ground motions in this project.

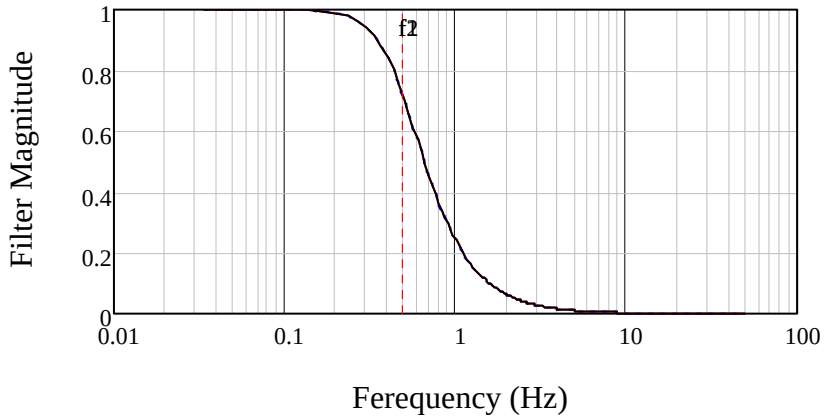

Figure H2-1: the proposed Butterworth filter for a low-pass frequency of 0.5 Hz

Legend/color code for all figures in this appendix:

Original Near Field Ground Motion as extracted from PEER

Filtered Ground Motions with a low-pass frequency of 0.5 Hz

Baseline corrected filtered Ground Motions (low-pass frequency of 0.5 Hz)

Ground Motion: 0159-IMPVALL.H-AGR

1 - NF-0159-IMPVALL.H-AGR-FN.ACC Intervals = 0.01 Sec Duration = 28.36 Sec
H1 for rotation: IMPERIAL VALLEY 10/15/79 2316, AGRARIAS, 003 (UNAM/UCSD STATION 6618)
H2 for rotation: IMPERIAL VALLEY 10/15/79 2316, AGRARIAS, 273 (UNAM/UCSD STATION 6618)

2 - NF-0159-IMPVALL.H-AGR-FP.ACC Intervals = 0.01 Sec Duration = 28.36 Sec
H1 for rotation: IMPERIAL VALLEY 10/15/79 2316, AGRARIAS, 003 (UNAM/UCSD STATION 6618)
H2 for rotation: IMPERIAL VALLEY 10/15/79 2316, AGRARIAS, 273 (UNAM/UCSD STATION 6618)

3 - NF-0159-IMPVALL.H-AGRDWN.AT2 Intervals = 0.01 Sec Duration = 28.36 Sec
IMPERIAL VALLEY 10/15/79 2316, AGRARIAS, DWN (UNAM/UCSD STATION 6618)

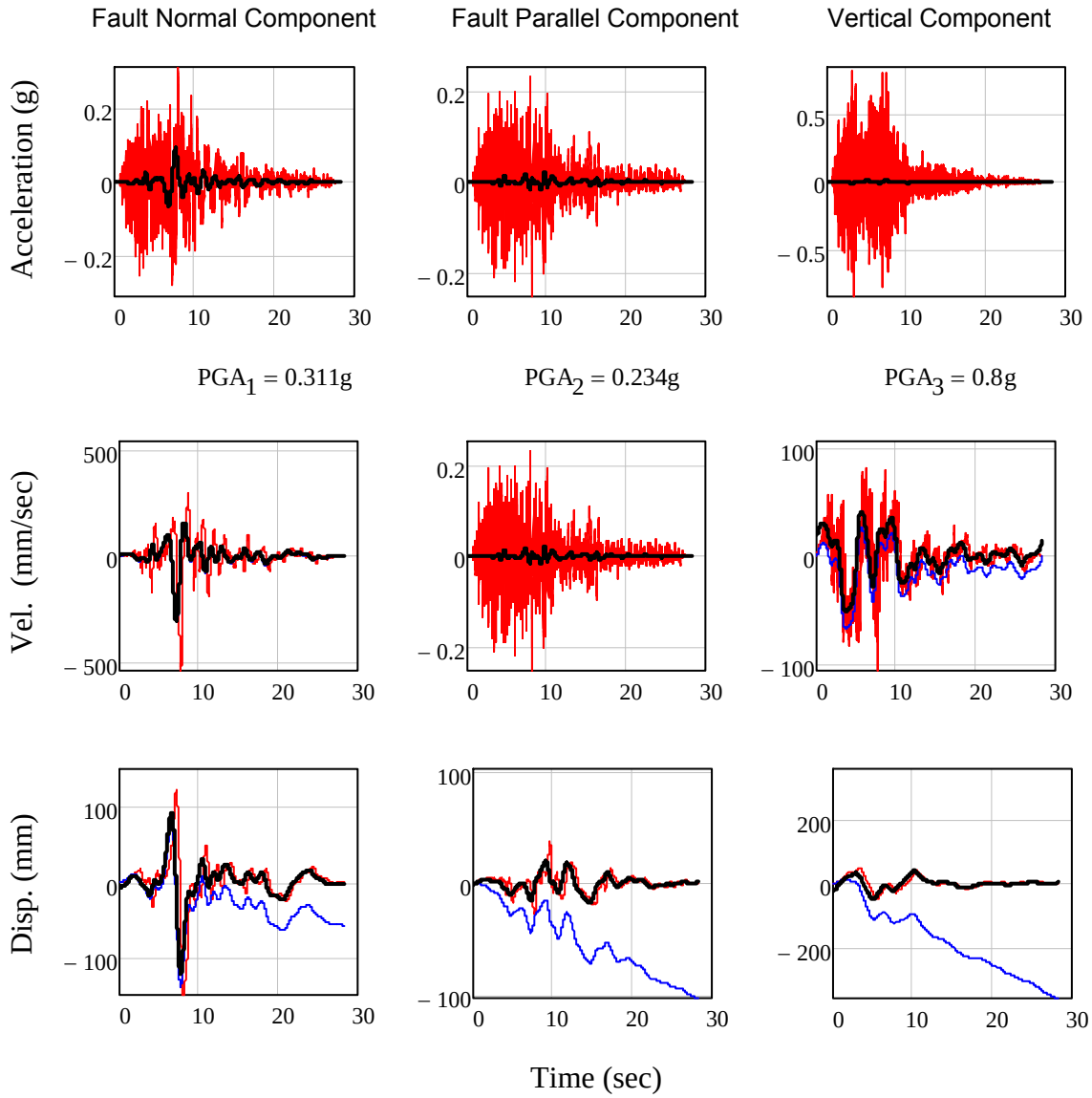

FFT of Input, filtered & Baseline Corrected GMs

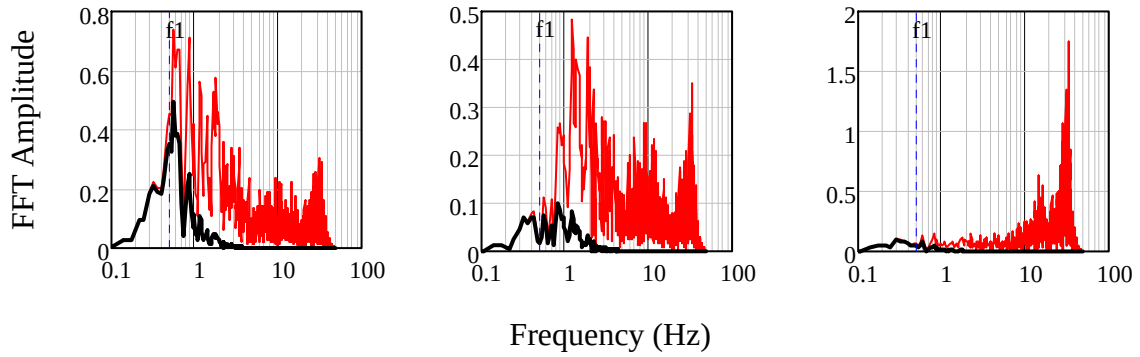

Elastic %5 Damped Response Spectra

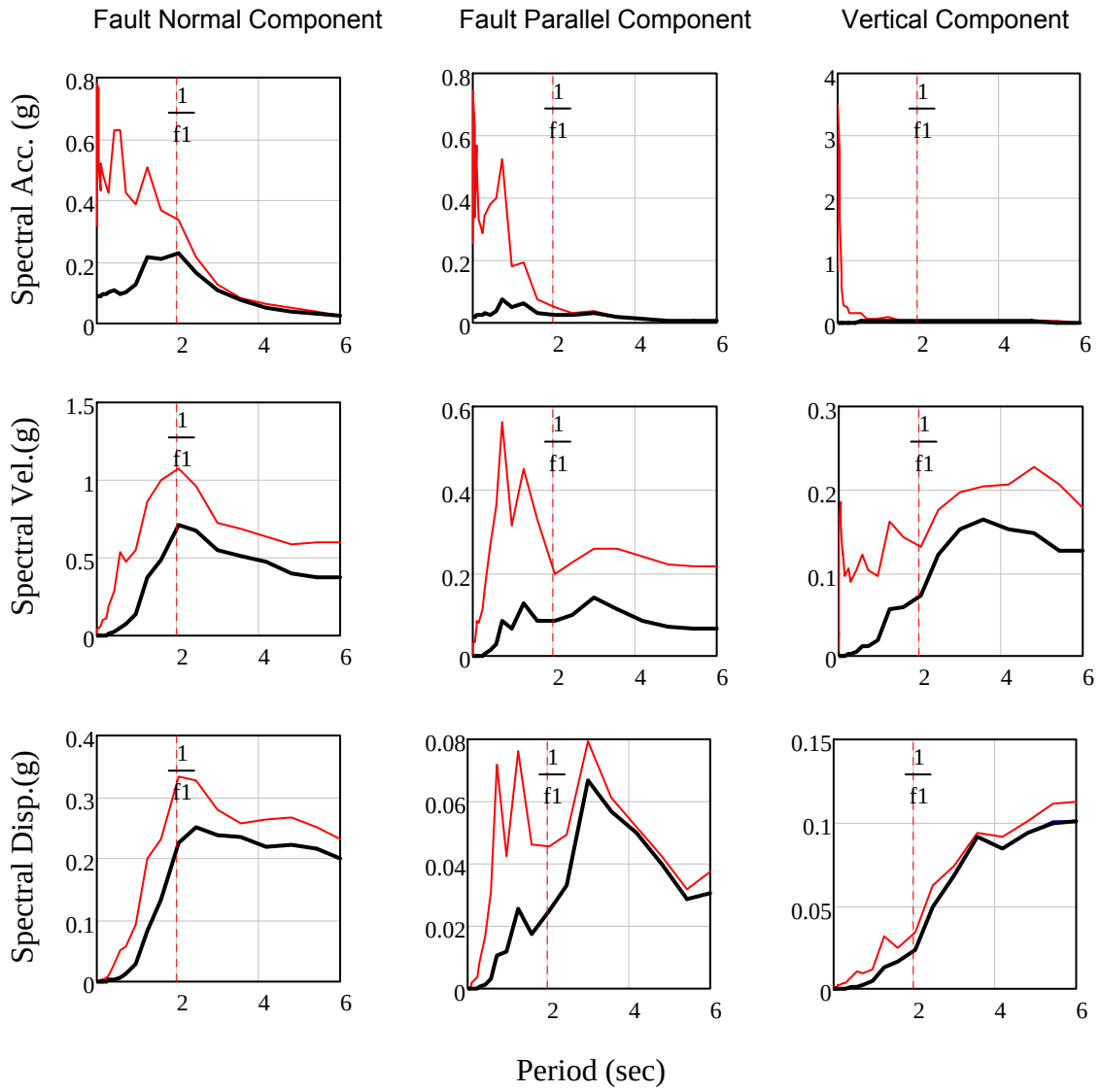

Ground Motion: 0171-IMPVALL.H-EMO

1 - NF-0171-IMPVALL.H-EMO-FN.ACC Intervals = 0.005 Sec Duration = 39.985 Sec H1 for rotation: IMPERIAL VALLEY 10/15/79 2316, EC MELOLAND OVERP FF, 000 (CDMG STATION 5155) H2 for rotation: IMPERIAL VALLEY 10/15/79 2316, EC MELOLAND OVERP FF, 270 (CDMG STATION 5155)

2 - NF-0171-IMPVALL.H-EMO-FP.ACC Intervals = 0.005 Sec Duration = 39.985 Sec H1 for rotation: IMPERIAL VALLEY 10/15/79 2316, EC MELOLAND OVERP FF, 000 (CDMG STATION 5155) H2 for rotation: IMPERIAL VALLEY 10/15/79 2316, EC MELOLAND OVERP FF, 270 (CDMG STATION 5155)

3 - NF-0171-IMPVALL.H-EMO-UP.AT2 Intervals = 0.005 Sec Duration = 39.985 Sec IMPERIAL VALLEY 10/15/79 2316, EC MELOLAND OVERP FF, UP

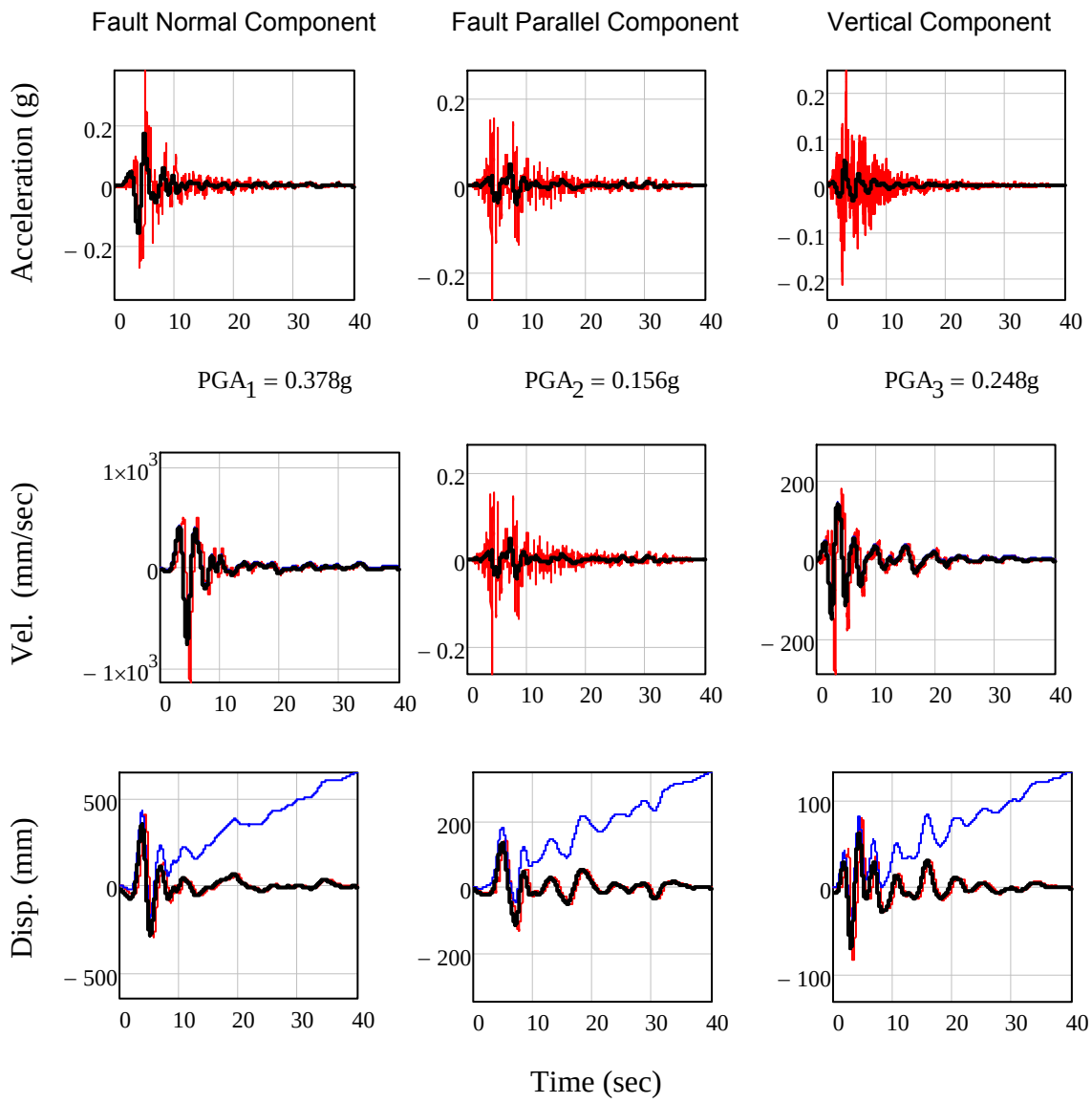

FFT of Input, filtered & Baseline Corrected GMs

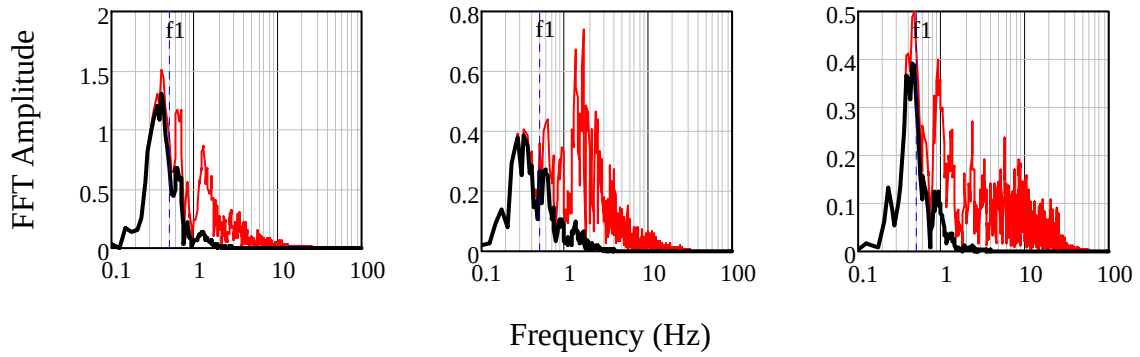

Elastic %5 Damped Response Spectra

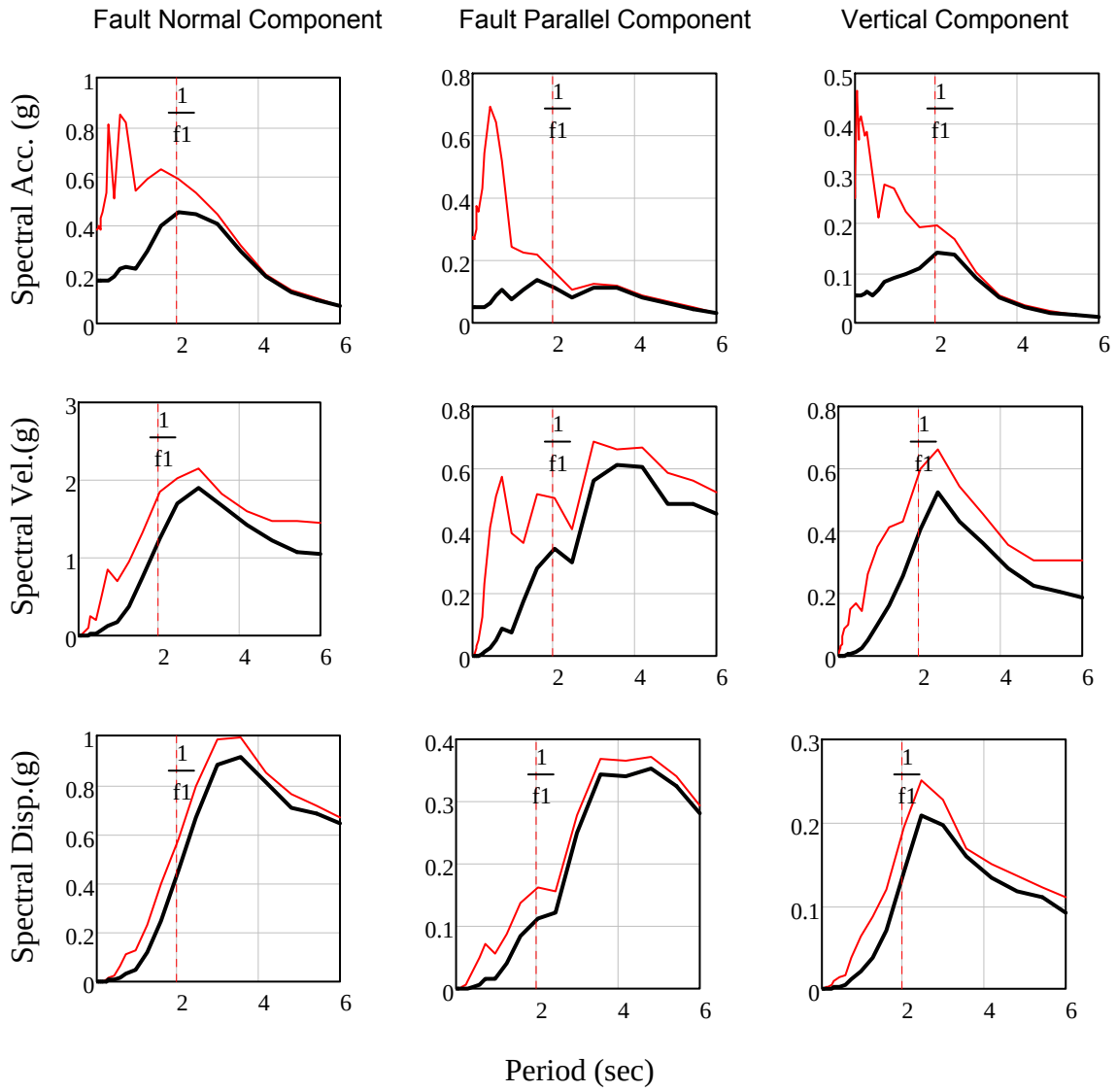

Ground Motion: 0178-IMPVALL.H-E03

1 - NF-0178-IMPVALL.H-E03-FN.ACC Intervals = 0.005 Sec Duration = 39.545 Sec H1 for rotation: IMPERIAL VALLEY 10/15/79 2316, EL CENTRO ARRAY #3, 230 (USGS STATION 5057) H2 for rotation: IMPERIAL VALLEY 10/15/79 2316, EL CENTRO ARRAY #3, 140 (USGS STATION 5057)

2 - NF-0178-IMPVALL.H-E03-FP.ACC Intervals = 0.005 Sec Duration = 39.545 Sec H1 for rotation: IMPERIAL VALLEY 10/15/79 2316, EL CENTRO ARRAY #3, 230 (USGS STATION 5057) H2 for rotation: IMPERIAL VALLEY 10/15/79 2316, EL CENTRO ARRAY #3, 140 (USGS STATION 5057)

3 - NF-0178-IMPVALL.H-E03-UP.AT2 Intervals = 0.005 Sec Duration = 39.545 Sec IMPERIAL VALLEY 10/15/79 2316, EL CENTRO ARRAY #3, UP (USGS STATION 5057)

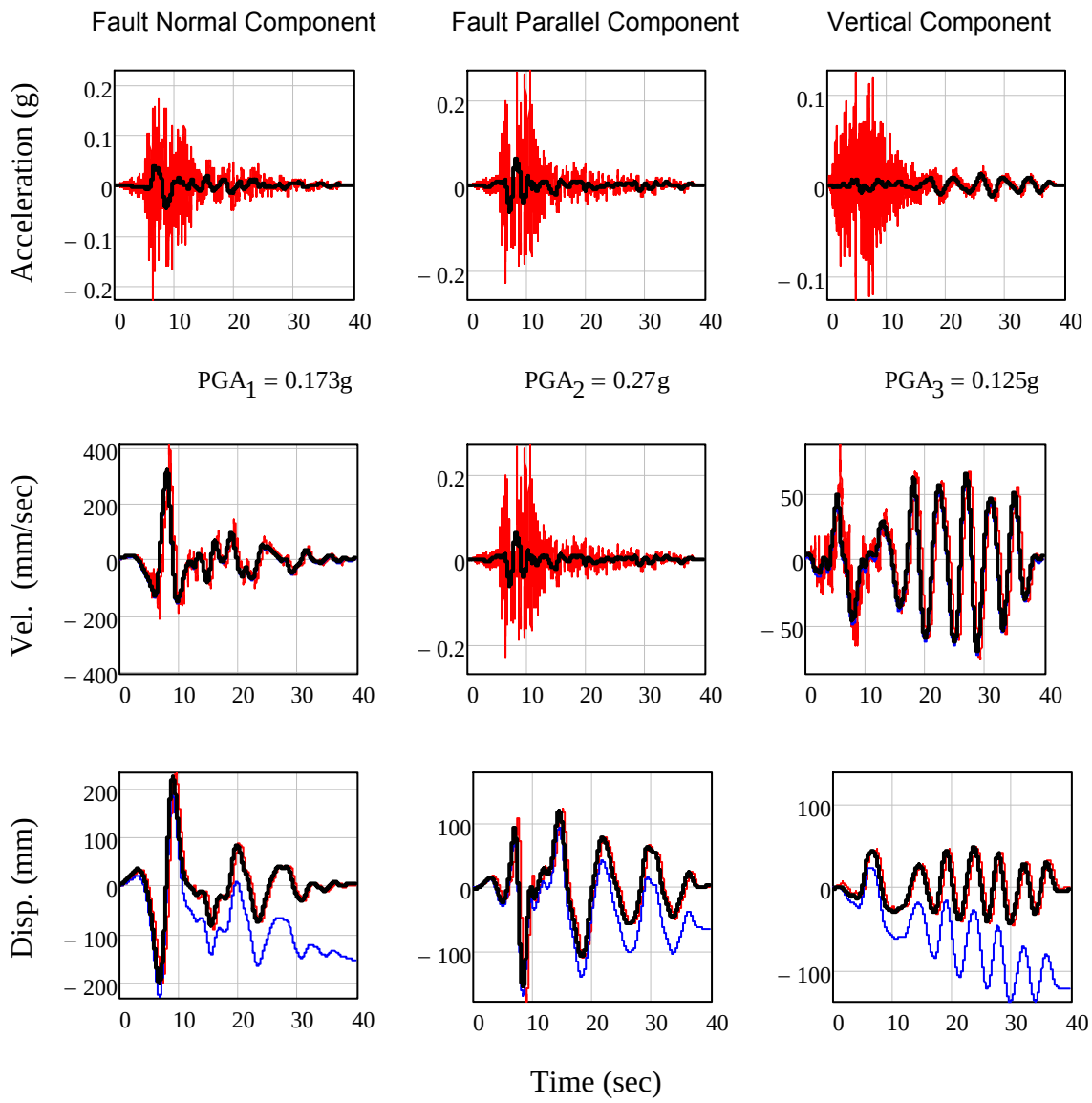

FFT of Input, filtered & Baseline Corrected GMs

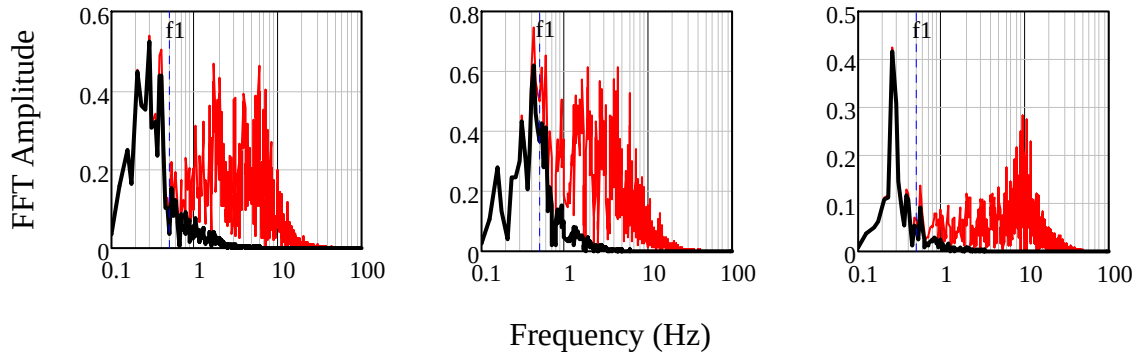

Elastic %5 Damped Response Spectra

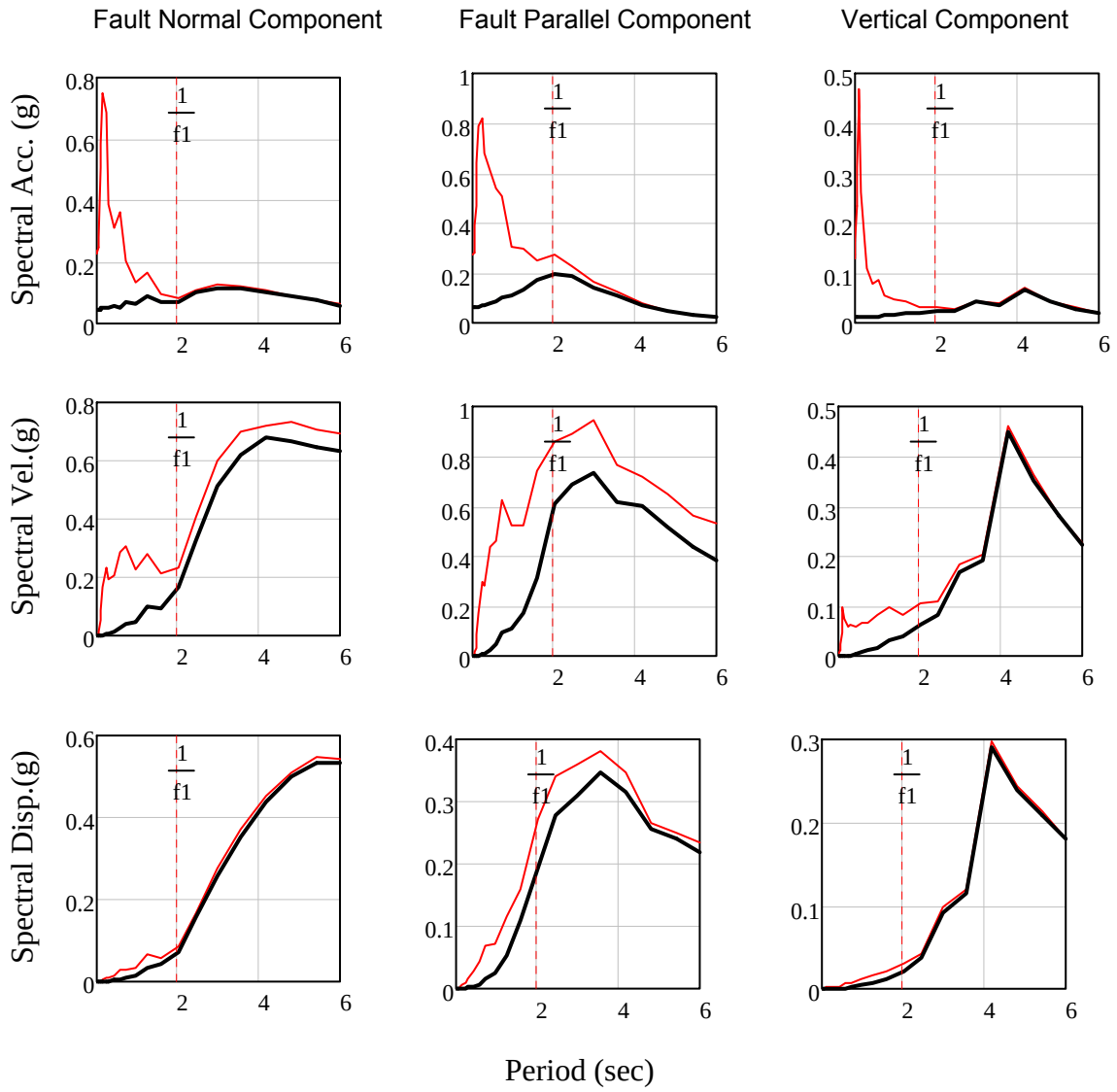

Ground Motion: 0181-IMPVALL.H-E06

1 - NF-0181-IMPVALL.H-E06-FN.ACC Intervals = 0.005 Sec Duration = 39.035 Sec H1 for rotation: IMPERIAL VALLEY 10/15/79 2316, EL CENTRO ARRAY #6, 230 (CDMG STATION 942) H2 for rotation: IMPERIAL VALLEY 10/15/79 2316, EL CENTRO ARRAY #6, 140 (CDMG STATION 942)

2 - NF-0181-IMPVALL.H-E06-FP.ACC Intervals = 0.005 Sec Duration = 39.035 Sec H1 for rotation: IMPERIAL VALLEY 10/15/79 2316, EL CENTRO ARRAY #6, 230 (CDMG STATION 942) H2 for rotation: IMPERIAL VALLEY 10/15/79 2316, EL CENTRO ARRAY #6, 140 (CDMG STATION 942)

3 - NF-0181-IMPVALL.H-E06-UP.AT2 Intervals = 0.005 Sec Duration = 39.035 Sec IMPERIAL VALLEY 10/15/79 2316, EL CENTRO ARRAY #6, UP (CDMG STATION 942)

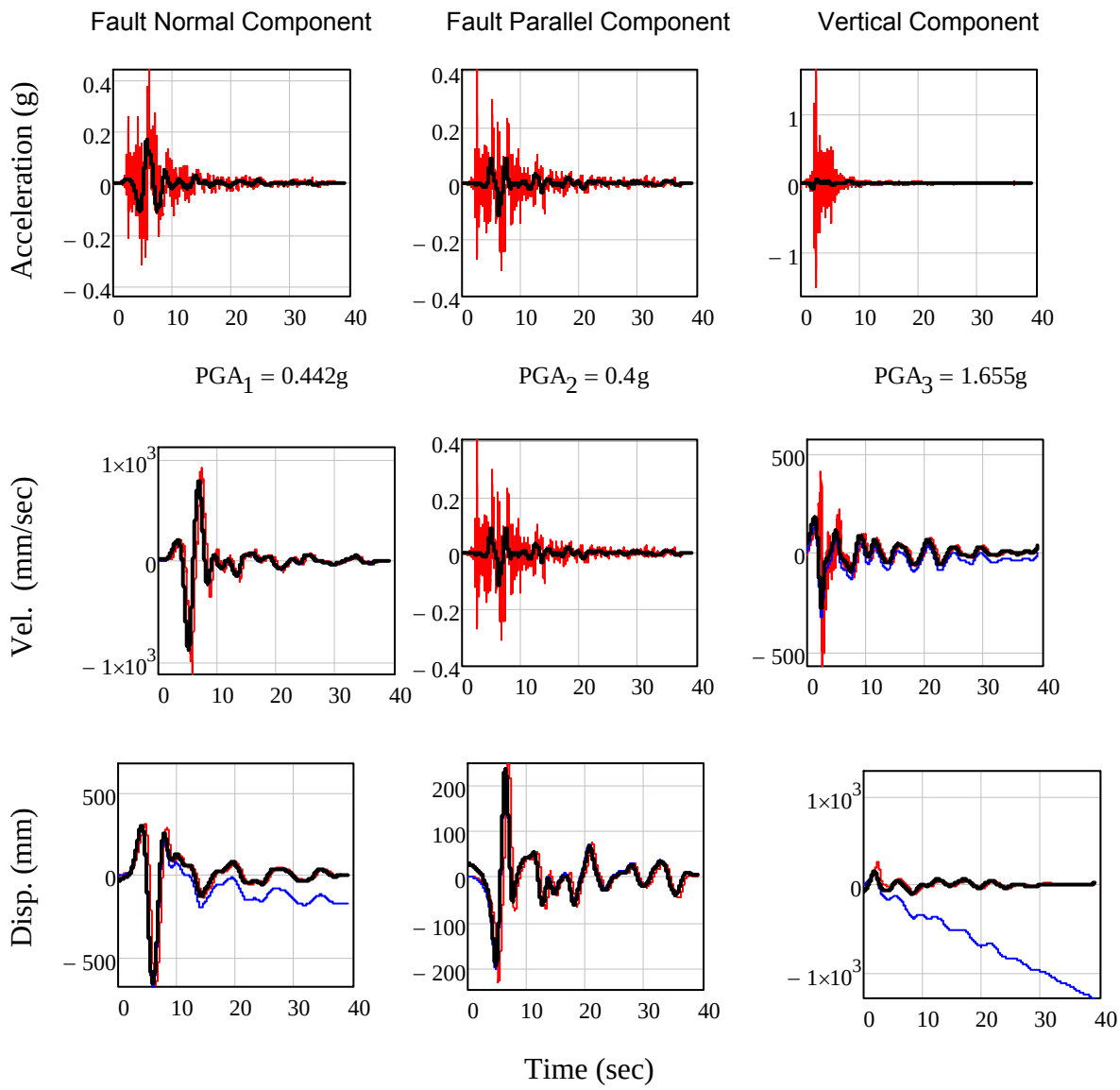

FFT of Input, filtered & Baseline Corrected GMs

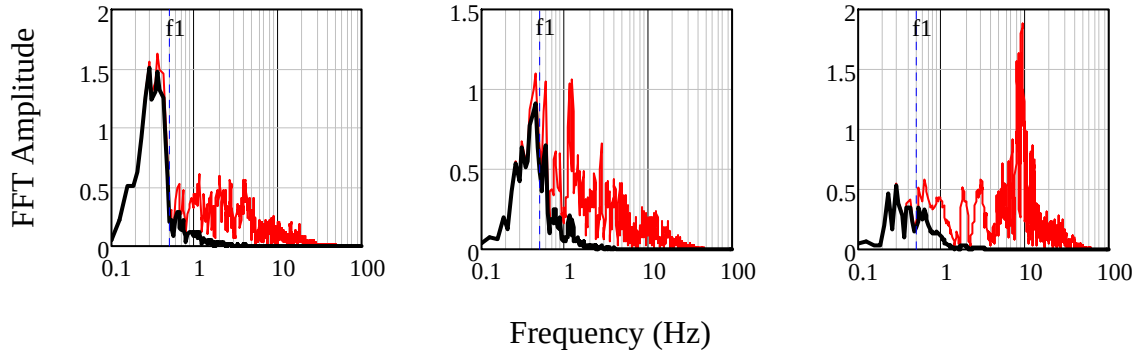

Elastic %5 Damped Response Spectra

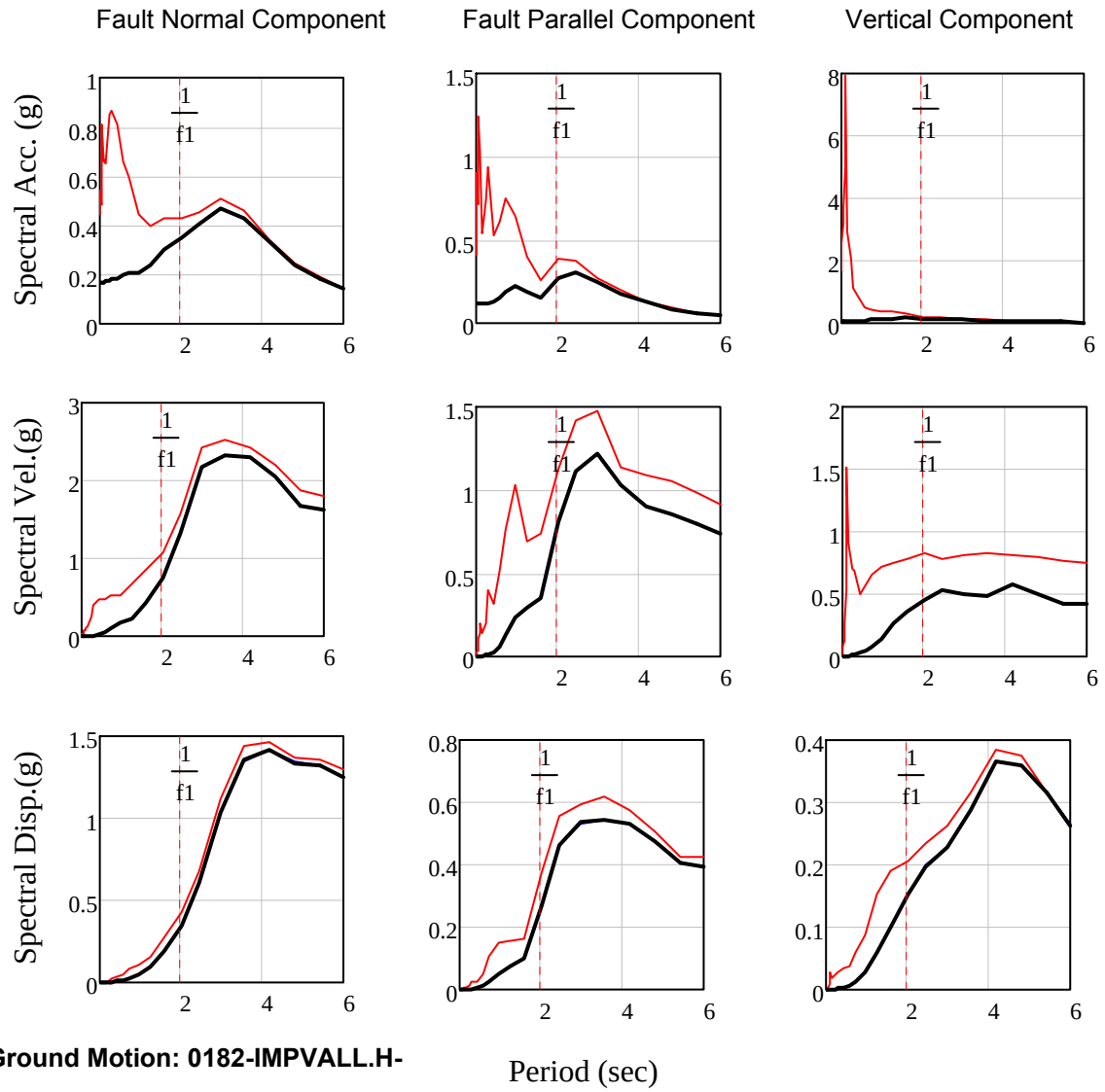

Ground Motion: 0182-IMPVALL.H-